UNIVERSITY OF SOUTHAMPTON

TECTONOSTRATIGRAPHIC ANALYSIS OF THE NORTHERN EXTENT OF THE OCEANIC EXOTIC TERRANE, NORTHWESTERN HUELVA PROVINCE, SPAIN.

A thesis submitted for the degree of
Doctor of Philosophy

by

Christopher Philip Eden

Department of Geology
Faculty of Science
University of Southampton
January 1991

UNIVERSITY OF SOUTHAMPTON

ABSTRACT

FACULTY OF SCIENCE

GEOLOGY

Doctor of Philosophy

TECTONOSTRATIGRAPHIC ANALYSIS OF THE NORTHERN EXTENT OF THE OCEANIC EXOTIC TERRANE, NORTHWESTERN HUELVA PROVINCE, SPAIN.

by Christopher Philip Eden

The Iberian Peninsula has recently been recognised as a composite of many different 'suspect terranes' that have been amalgamated within a complex mosaic forming the southern limb of the European Hercynian Arc. In the SW of the Iberian Peninsula continental collision between two of these suspect terranes, the Ossa Morena Zone to the north and the South Portuguese Zone, resulted in thrust stacking and imbrication of several distinct tectonic units. South of Aroche in northwest Huelva Province, this thrust stack is recognised as a series of slices of six different lithological units. The Beja-Acebuches Amphibolites, a thin unit of basic rocks considered to represent a dismembered ophiolite, occurs in the footwall of the Ossa Morena Zone and has been subjected to ductile deformation. In the immediate footwall of the Beja-Acebuches Amphibolites, a thrust stack, consisting of the Peramora Mélange, Cumbres de Los Ciries and Alajar Formations has experienced a low P/high T metamorphic event that produced syn-kinematic andalusite and cordierite porphyroblasts.

The Peramora Mélange Formation is a newly identified unit of oceanic mélanges, containing blocks of amphibolite and metasediments. Sources for these exotic blocks are considered, both from field data and geochemical analysis, to be the Beja-Acebuches Amphibolites and the high grade rocks of the Ossa Morena Zone, that lie structurally above and to the north. The Cumbres de Los Ciries Formation is a monotonous unit of quartz-mica schists considered to represent a distal foreland basinal deposit. Along strike, in the mica-schists of the Alajar Formation, blocks of exotic material, including marble and serpentinite are observed. All these formations have undergone intense ductile deformation, medium to high grade greenschist/lower amphibolite polymetamorphism and syn-kinematic recrystallisation of constituent mineral assemblages.

In contrast the La Giralda Formation and the Puerto Cañon Formation, although intensely thrusted and folded, retain many original sedimentological features of a deep marine turbiditic association. Both of these formations have suffered low grades of greenschist facies metamorphism. The La Giralda Formation is a distal association of slaty mudstones and mature medium grained arenites, while the Puerto Cañon Formation is a more proximal association containing lithoclasts of volcanic material suggesting partial provenance from a basic source.

All boundaries between the tectonostratigraphic units are tectonic, a feature that makes correlation of deformation events across them difficult. Three phases of deformation are recognised across the region, however, their spatial and temporal relationship with respect to dated events is poorly constrained. A model for the deposition of these sedimentary formations within a foreland basin setting is proposed.


1cm

ACKNOWLEDGEMENTS

Research was funded by N.E.R.C. grant number GT4/87/103. Thanks and gratitude must be exetended to many people who have helped to make this project an interesting and enjoyable learning experience. On the academic side Dr. Jim Andrews, who initiated the project, has contributed a wealth of experience and enthusiasm and has sacrificed many handfuls of hair during the editing of the thesis. I am grateful to Dr. Uve Geise of Aachen University for providing geochemical data from the Beja-Acebuches Amphibolites. The project benefitted immeasurably from discussions with many members of the academic staff of Southampton University including Andy Barker, Ian Croudace, Steve Roberts, Rex Taylor, Dave Sanderson and Dr. Dave Peacock. Bob Nesbitt is thanked for facilitating access to equipment. The efforts of the technical staff: Bob, John, Robin, Dave S, Stan, Posy, Frances, Lola and Anthea are also gratefully acknowledged. Particular thanks must go to Barry and Dean for the speedy execution of photographic work. Post graduates, new and old, have provided much needed light entertainment and I am especially grateful to Jacko (el completamente Loco), Colin, Roberto and Marta, Paul, Jim, Steve, Cathy, Nicky, Rob, and everyone who knows me! Phil Lake provided me with a valuable initiation into the Spanish Way and Marcos and Lorena kept the flavour of Spain alive for me (¡Abolemos todo!). Tom, Andrea, Mulu and Steve deserve a special mention for sharing a room with me during the heady days of my second year. The tedium of night time working was alleviated by the company of Pius, Mulu, Ibrahim and Rahim. I also thank Simon, Trevor, Jochan and Mark for accompanying me on many lunchtime trots that kept me sane (well, as sane as possible..)

For my friends in Aroche: el trabajo en España fue una experiencia inolvidable, debido especialmente a la amabilidad de las gentes de Aroche: ¡para ellos escribiré en español! En primer lugar, quisiera mencionar a Agueda, quien me enseño a bailar 'sevillanas' y me mantiene informando acerca de la vida en Aroche, un pueblo que significa mucho para mi. Antonio Cuaresma y Marisa me proporcionaron comidas interminables sin pedir nada a cambio y Antonio me enseño mucho lugares de interés. A él tengo que decirle que 'este proyecto ha sido casi tan difícil como que los ingleses dejen el Peñon! Manolo y Concha me ofrecieron la hospitalidad de su casa, la cual acepté frecuentemente. Algunos más me hicieron sentir Aroche como mi casa incluyendo a José y Adrian, los amables dueños del bar Lopez (un lugar que visité a menudo, con su suculente 'pescado a la plancha'); Lorenza y Juana, Lorenzo, Marcelina y Alejandro, cuya Vente se couvirtió en mi casa. Recordaré siempre la amistad y hospitalidad de Pepe Castilla y Ana y mi invitación para que vengan a inglaterra continúa en pie. A toda la gente de Aroche, un saludo afectuoso y os agradezco de todo corazón que abrierais vuestras puertas a éste loco inglés.

Asímismo, pasé muchas horas espléndidas discutiendo sobre geología con Ana Crespo, Miguel Orozco, Cecilio Quesada, Tomás Oliveira y el grupo de geólogos Portugueses. Las tapas y cervecitas tendrán por siempre un significando muy especial. Miguelito (el loco de la Jara), me ahorró mucho tiempo y casi salvó mi vida. Él fué quien me enseño los 'Fabulosos Mármoles de Alajar' por primera vez y pasamos muchos buenos momentos pescando en Los Picos.

My mother and father provided me with love, understanding and financial support during lean times for which I am thankful and I am eternally grateful to Oonagh who not only provided moral bolstering but also acted as editor, hatchet person, and companion. This work is for them.

Contents List:

Chapter 1: Introduction.

1.1 Introduction.

The Iberian Peninsula forms the southern branch of the Ibero-Armorican Arc (Fig 1.1). Lotze (1945) subdivided the Peninsula into distinct geotectonic zones which Julivert *et al.* (1974) related to the Hercynian foldbelt (Fig. 1.2). In general terms material of Carboniferous and Devonian ages predominate in the 'external' zones ie the Cantabrian and South Portuguese Zones (Julivert 1974) whilst Lower Palaeozoic and Precambrian rocks predominate in the others. The Cantabrian and South Portuguese Zones are characterised by low grade metamorphism while in the 'internal' zones high grade amphibolite and granulite facies metamorphic rocks are common and extensive granitic plutonism occurs.

Recently Quesada (*in press*) proposed a subdivision based on the 'terrane' concept (Fig. 1.2). This classification differs noticeably from the scheme outlined above; the Iberian Peninsula is divided into several distinct terranes, each of which displays contrasting stratigraphic, structural and metamorphic elements and each of which is bounded by major structural discontinuities.

<table>
<tr><th>Julivert et al. (1974)</th><th colspan="2">Quesada (in press)</th></tr>
<tr><td>- Cantabrian Zone</td><td rowspan="2">- Northern imbricate margin
- Allochthonous Oceanic Exotic Terranes</td><td rowspan="3">Iberian Terrane</td></tr>
<tr><td>- West Asturian Leonese Zone</td></tr>
<tr><td>- Central Iberian Zone</td><td>- Parautochthonous core</td></tr>
<tr><td>- Ossa Morena Zone</td><td>- Southern imbricate margin</td><td></td></tr>
<tr><td>- South Portuguese Zone</td><td colspan="2">Exotic oceanic terrane
South Portuguese Terrane</td></tr>
</table>

Table 1.A Comparison between the Zonal and Terrane subdivision of the Iberian Peninsula.

Because of wide differences in evolutionary style, these units are considered to represent suspect terranes with respect to the Iberian Terrane which comprises the greatest area of the Iberian Peninsula. Both systems of classification are compared in Table 1.A. Within the context of the present study it is significant that the South Portuguese Zone is separated into two terranes; the Oceanic Exotic Terrane and the South Portuguese Terrane. In the following sections the term 'Oceanic Exotic Terrane' refers to the area within which the study area is located, while the term 'Ossa Morena Zone' is used to refer to the area located immediately to the north of the study area.

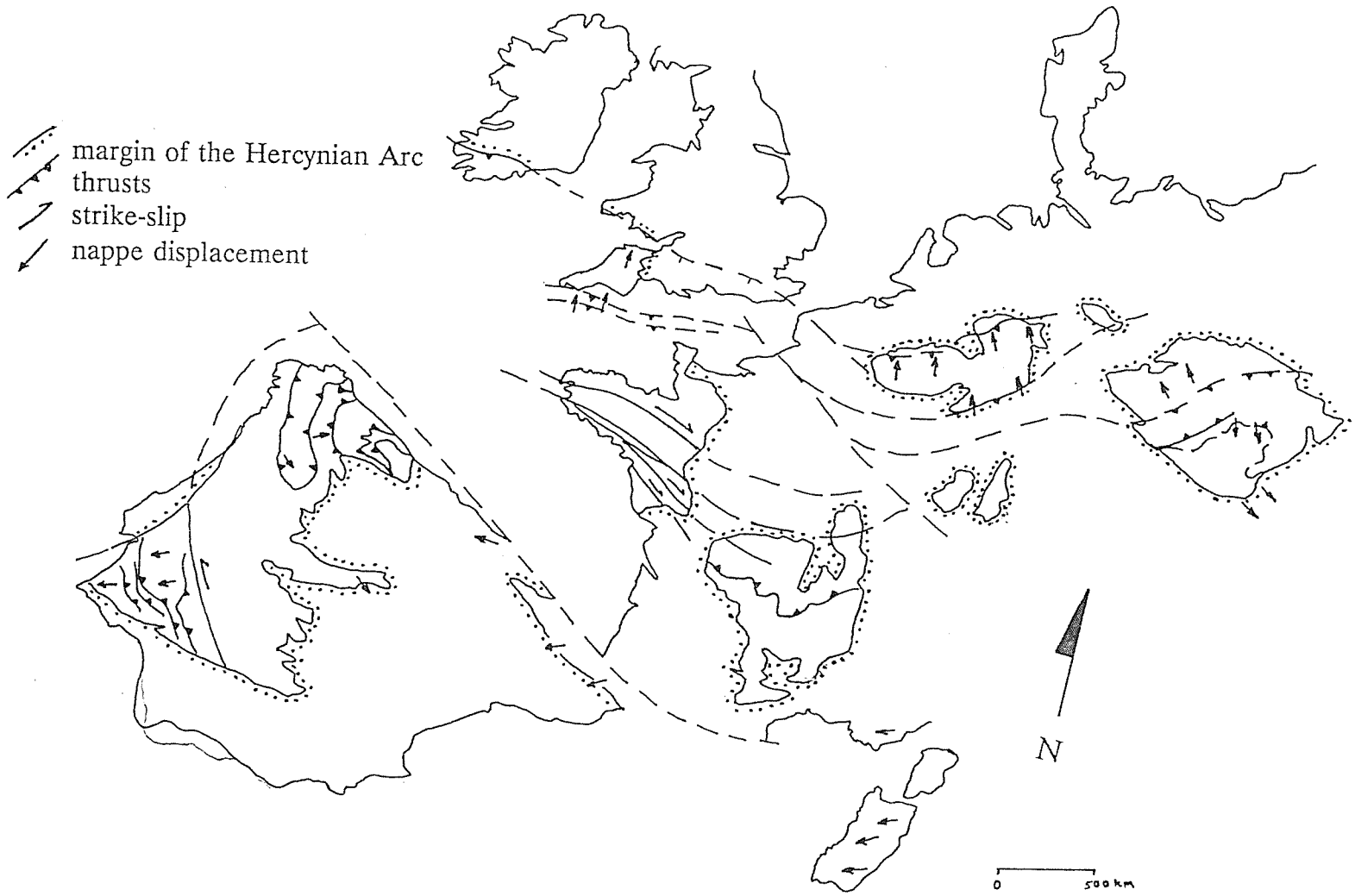

Figure 1.1 Location of Iberia in relation to the Hercynian belt of Europe (partly after Barnes & Andrews 1986; Matte 1986; Frank & Engel 1983).

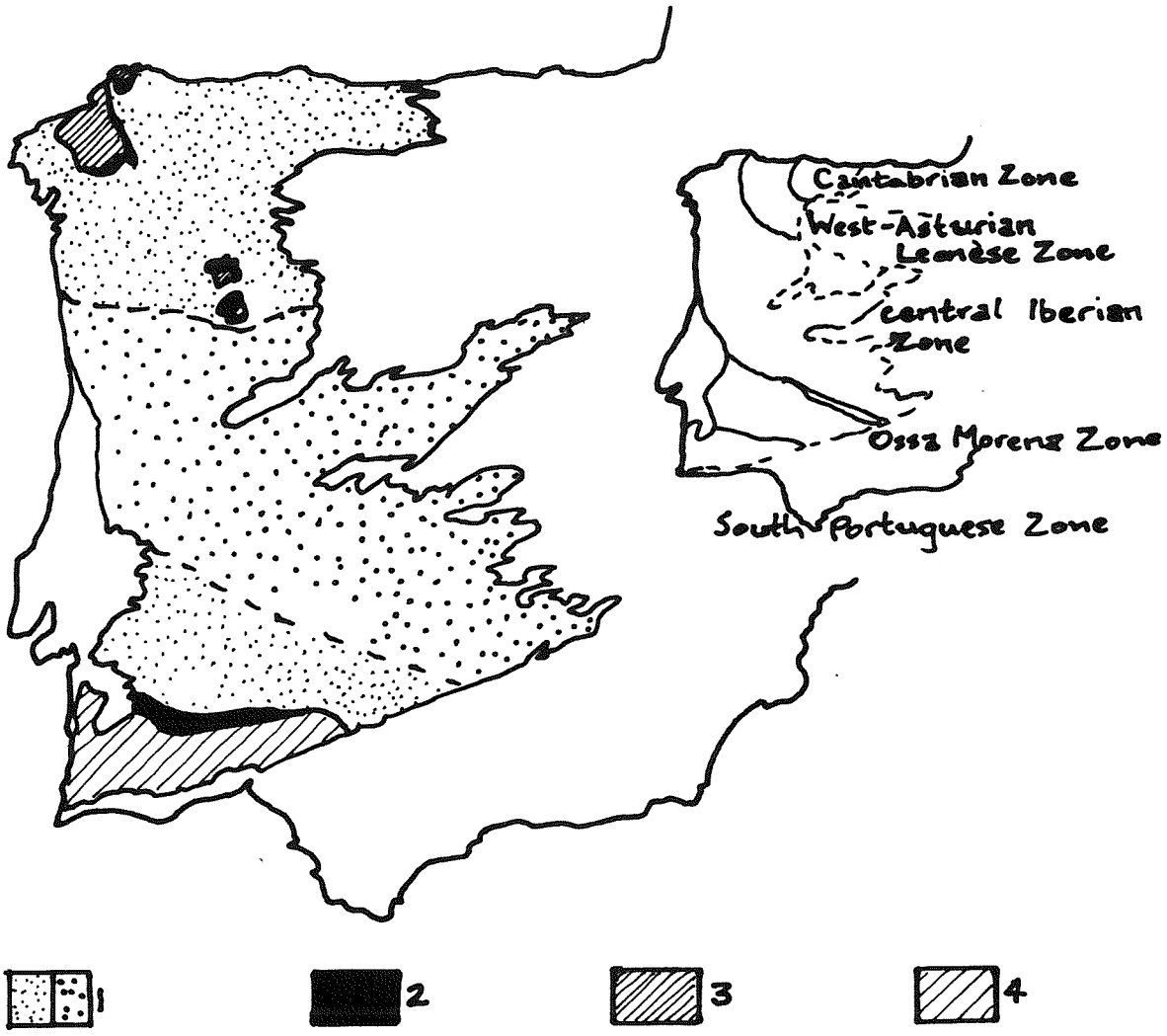

1. Iberian Terrane
a imbricated margins
b parautochthonous core

2. Oceanic exotic terranes

3. NW continental exotic terranes

4. SW Portuguese suspect terrane

Figure 1.2 Terrane subdivision of Iberia (a) compared with the zonal subdivision of Julivert *et al.* (1974).

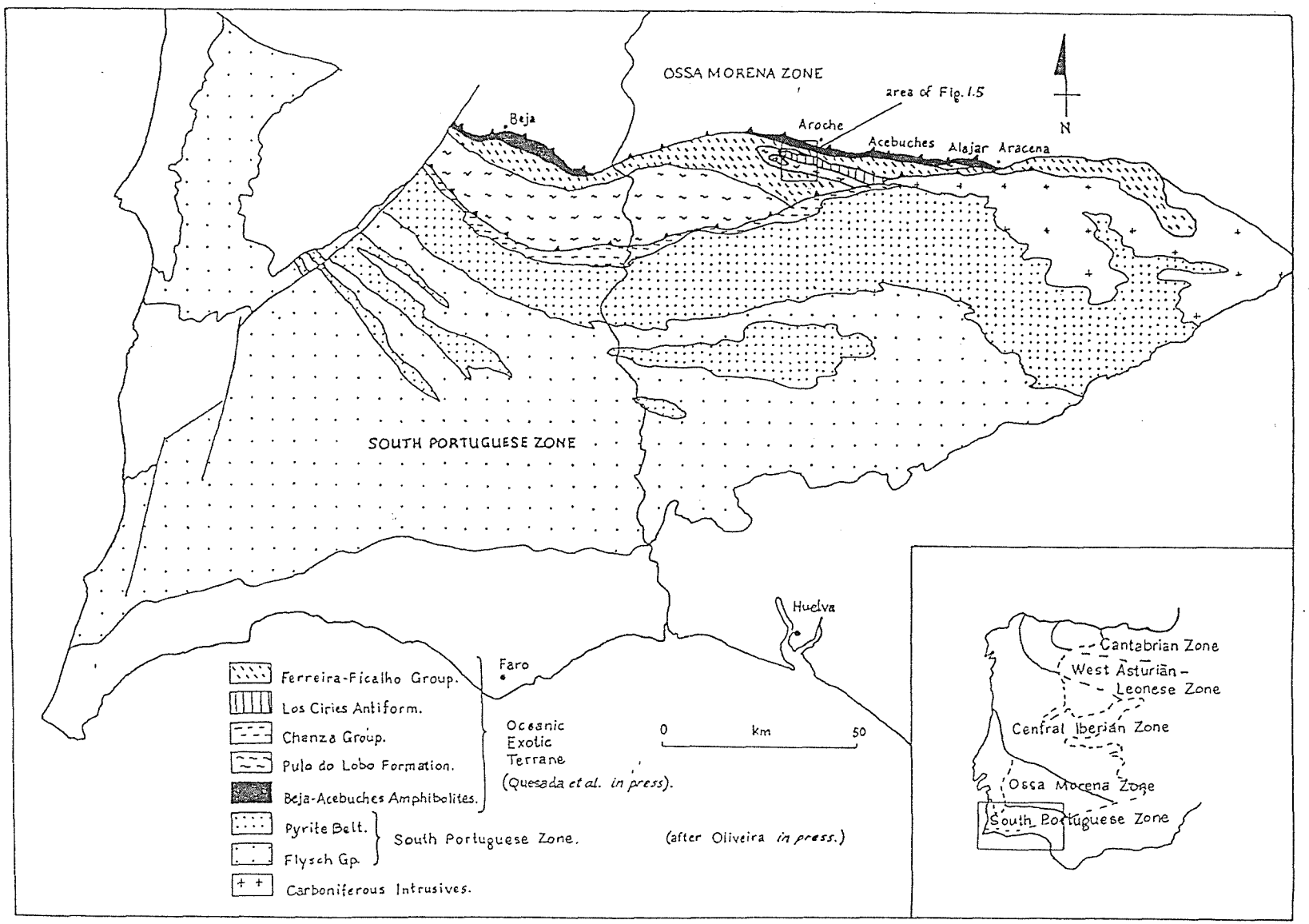

Figure 1.3 Geology of the Southwestern Iberian Peninsula (partly after Quesada *et al in press.* and Oliviera *in press*)

1.2 Location

The study area and its position with respect to the regional geology is shown in Fig. 1.3. It is located immediately south of the boundary between the Ossa Morena Zone and the Oceanic Exotic Terrane. In the study area (Fig. 1.4), the Ossa Morena Zone is represented by a Precambrian to Lower Palaeozoic metamorphic complex (the Aracena Massif) while the Oceanic Exotic Terrane is represented by a sequence of Upper Palaeozoic metasediments. The contact between these two suspect terranes is marked by the Beja-Acebuches Amphibolites, an exotic terrane with oceanic crustal affinities (Muñha 1983). Fig. 1.4 illustrates the local geology with respect to the geology of the Aracena Massif.

Field work was concentrated mostly to the south of Aroche (Fig. 1.5), situated in the northwest of Huelva Province in Andalusia, southern Spain. Aroche is about 150kms to the NW of Sevilla and is reached by the N433 which winds across the Sierras de Aracena, Giralda and Aroche in the Sierra Morena range. The field area is accessed by an unpaved road which runs for about 20kms south from Aroche, via El Mustio and eventually joins the H-120 leading into Cabezas Rubias. The rugged terrain is punctuated by strike-parallel ridges and deep valleys delineating the quartz-mica schists of the Cumbre de Los Ciries Formation and supports isolated farmhouses, many of which are now derelict. These ridges and valleys surround the low land area of the Los Ciries Antiform (Fig. 1.5). This structure has a southwestward dipping axial plane as shown in the cross section Fig. 1.5.

Field mapping was carried out on a scale of 1:25 000 and concentrated mostly on road and river sections. Geological boundary mapping has previously been done by the Spanish Geological Survey (Instituto de Geología y Minero de España) and is represented on sheets 916: Aroche and 917: Aracena (Apalategui *et al.* 1983, 1984). Throughout the text, grid references quoted are taken from 1:25 000 topographic maps published by the Dirección General del Instituto Geográfico Nacional. For localities to the south of Alajar grid references are taken from the 1:50 000 topographic maps published by the Servicio Geográfico del Ejército (1955) as recent maps for the area are, as yet, unobtainable. Grid references are quoted using the last two digits of each map reference grid and are supplemented by two further numbers, thus locating each point to the nearest ten metres. Thus GR 8023 0175, the grid reference for Venta Romero in Aroche is abbreviated from $^{6}8023\ ^{42}0175$.

The main amount of time allocated to field work was spent studying the geology to the south of Aroche. Five days in the first field season (October 1987) was spent in Alajar and this was supplemented by a further two or three days in the second field season (March-June 1988).

1.3 Stratigraphy and Previous Research

1.3.1 The South Portuguese Zone

This zone has been the subject of increased study since the publication of geological maps concerning the geology of the Spanish sector (Apalategui *et al.* 1983, 1984) which have elucidated

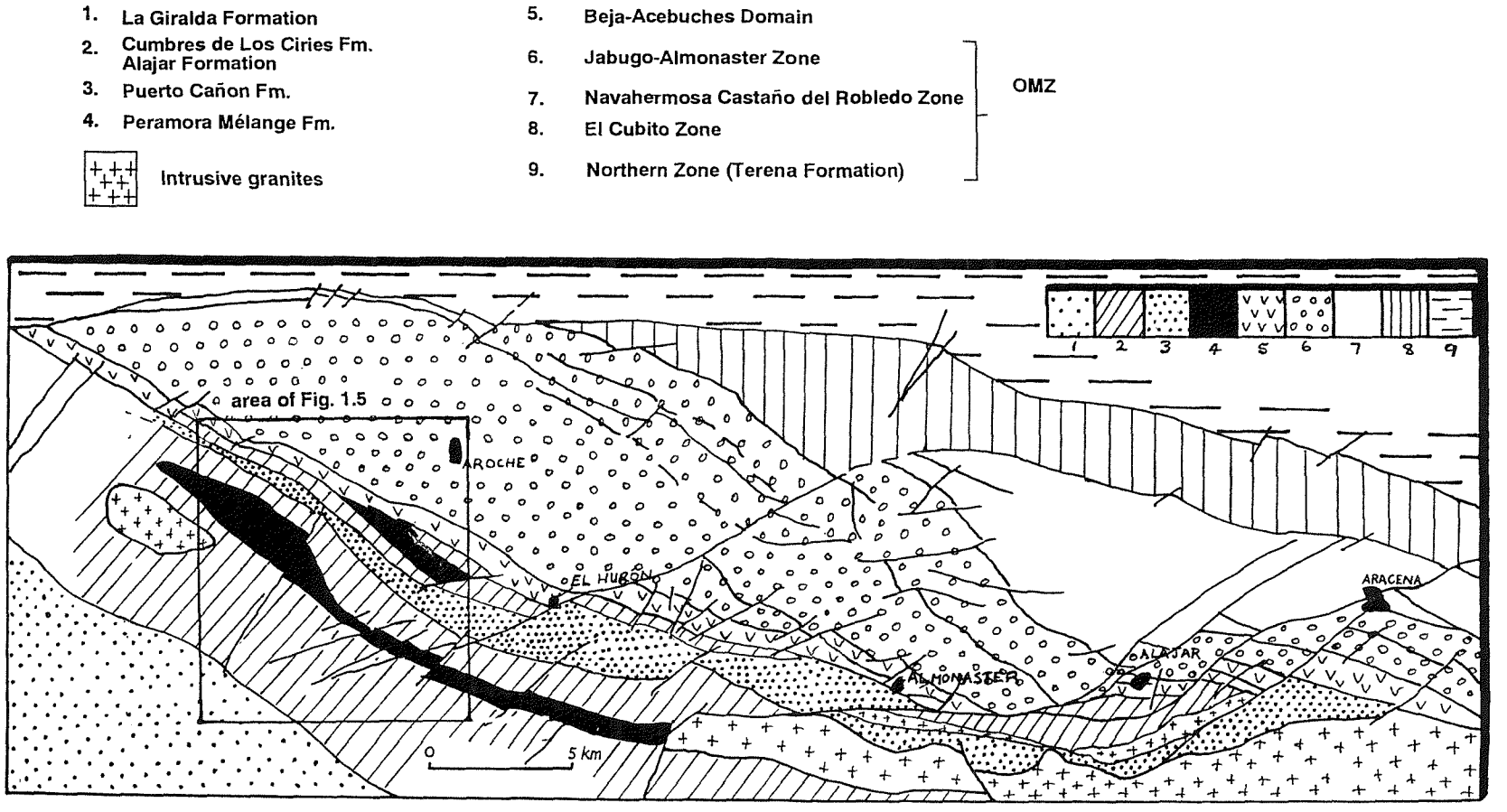

Figure 1.4 The Aracena Massif and its relationship to the geology within the northern extent of the Oceanic Exotic Terrane (Partly after Bard 1969; Apalategui 1983, 1984; Crespo-Blanc 1989).

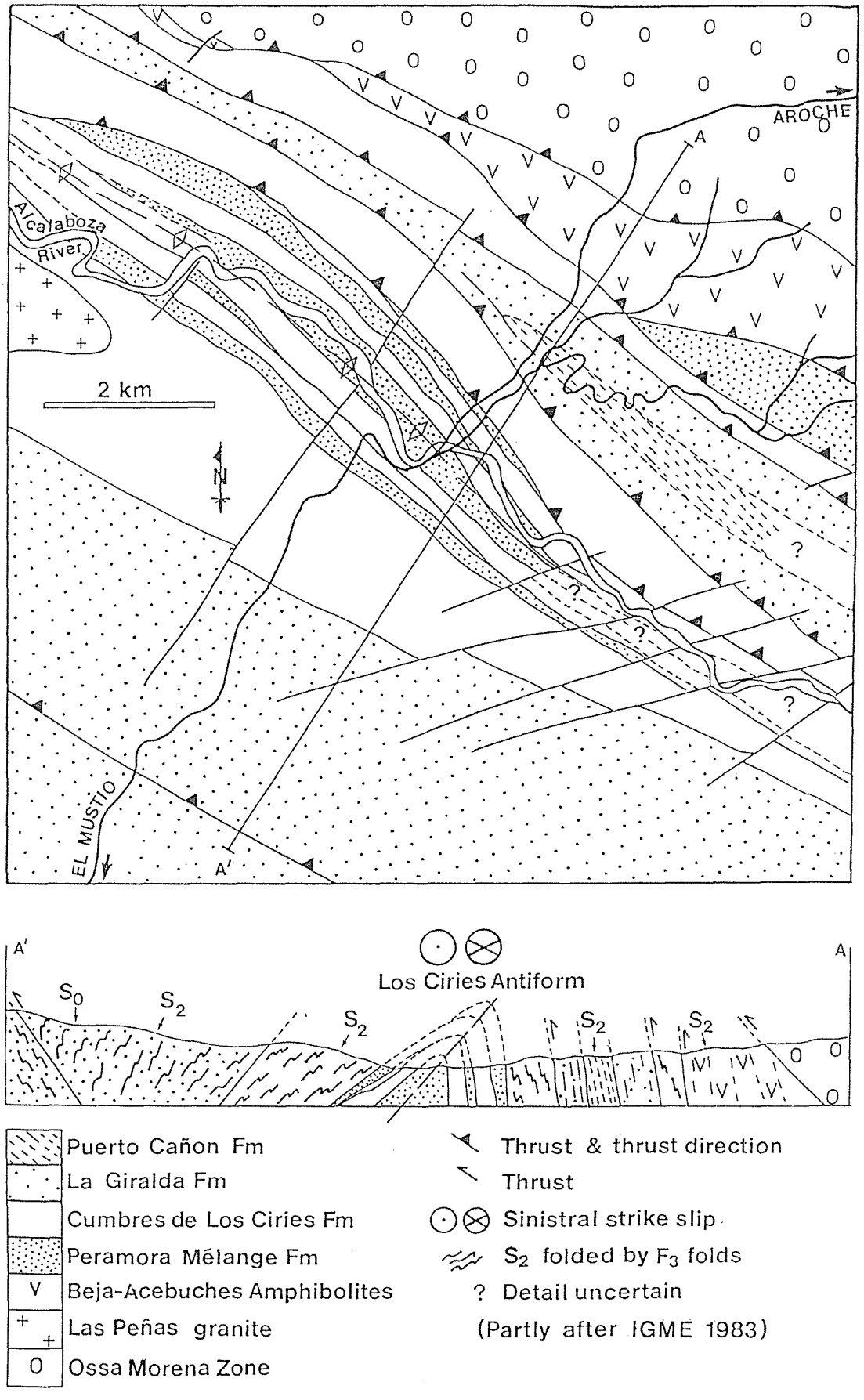

Figure 1.5 Geology of the principal study area located to the south of Aroche. The cross-section illustrates geological relationships.

geological relationships and posed significant questions of interpretation. On the Portuguese side of the border, structural and lithological relationships are well documented. Recent contributions by Oliveira and co-workers have established a stratigraphic framework which has provided the basis for subsequent work. The scheme proposed by Oliveira *et al.* (1985) is shown in Figure 1.6. Five geological domains are recognised within the South Portuguese Zone.These are:

(a) Beja-Acebuches Ophiolite.

(b) Pulo do Lobo Antiform.

(c) Pyrite Belt.

(d) Baixo Alentejo Flysch Group.

(e) SW Portugal (Bordeira and Aljezur Antiforms).

1.3.1.a *The Beja-Acebuches Amphibolites.*

This unit outcrops along the boundary between the Ossa Morena Zone and the South Portuguese Zone (Fig. 1.3, 1.4 & 1.5). It extends for some 100kms spanning the length of the Sierra Morena and is no wider than 1500m at its widest extent. It consists of basic rocks that display metamorphic grades up to granulite facies on the northern margin ranging rapidly to greenschist facies southwards. Internal organisation has been interpreted as representing an overturned and dismembered ophiolite (Bard 1977; Munha *et al.* 1986, Ribeiro *et al.* 1987; Oliveira *in press*).

Crespo-Blanc & Orozco (1988) demonstrated the existence of a sinistral ductile shear zone, the South Iberian Shear Zone (SISZ), which is focused within the Beja-Acebuches Amphibolite. Shearing is accompanied by development of two stretching lineations that are orientated from NNW-SSE to WNW-ESE respectively. The latter is associated with intense mylonitisation and recrystallisation of the amphibolites and affects the whole sequence (Munha *et al.* 1989), perhaps being related to ophiolite obduction towards the NW.

Radiometric dates recently obtained from amphiboles within the Beja-Acebuches Amphibolites (Dallmeyer and Quesada 1990) yield Ar^{40}/Ar^{39} cooling ages of c.340 Ma.

1.3.1.b *Oceanic Exotic Terrane.*

This terrane forms the focus of the present study (Fig. 1.3 & 1.4). It has previously been defined as the northernmost expression of the South Portuguese Zone (Schermerhorn 1971, Oliveira *in press*). The region has, until recently, been termed the Pulo do Lobo Antiform, a name reflecting the presence of lithologically similar sedimentary formations on the northern and southern flanks of a core of quartz-mica schists (the Pulo Formation). The term 'antiform' is misleading as recent investigations (Ribeiro & Silva 1983, Silva *et al. in press*, Lake *thesis in prep*) have shown that the whole area comprises a series of stacked thrust sheets, which makes conclusions concerning the relationships between the various formations tenuous.

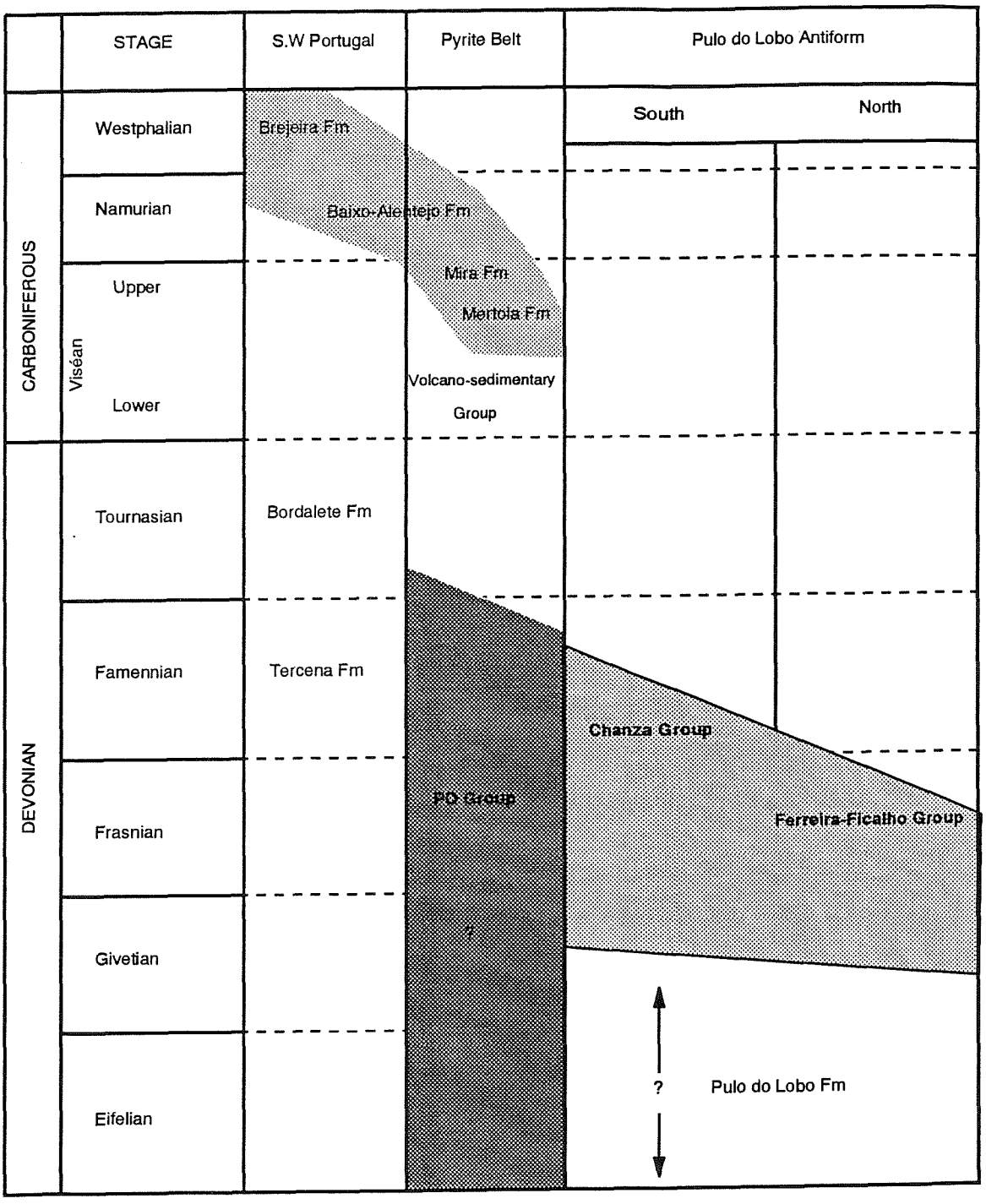

Figure 1.6 Stratigraphy of the South Portuguese Zone. (after Oliveira *et al.* 1986)

The Oceanic Exotic Terrane has been subdivided (Munha *et al.* 1986, Oliveira *in press*) on the basis of structural and lithological criteria into several distinct units (Fig. 1.3). These are:

A - The Pulo do Lobo Formation

B - The Ferriera - Ficalho Group (north).

C - The Chanza Group (south).

A - *The Pulo do Lobo Formation* (Pfefferkorn 1968)

This is the lowest unit in the succession. It consists of quartz-mica schists and quartzite horizons with minor intercalations of felsic volcanics (Oliveira *in press*) and has a maximum outcrop width of some 20kms. All of this material has been strongly deformed and the sheared fine grained matrix supports augen of quartz ('exudation quartz veinlets' Schermerhorn (1971)) and rare blocks of basic material. The depositional environment of this formation remains uncertain as original sedimentary structures have been obliterated. Recently, however, this formation has been recognised as part of an exotic suspect terrane due to its oceanic character (Munha 1986, Quesada *in press*). Late felsic dykes that cross-cut the regional foliation, may be related, on a larger scale, to the formation of the Iberian Pyrite Belt located to the south (Fig. 1.3) (Oliveira *in press and pers. comm.*).

B - *The Ferreira-Ficalho Group.*

This Group occurs on the northern margin of the Oceanic Exotic Terrane (Fig. 1.3). It is composed of a series of flysch - type sediments that accumulated within a basin to the south of the Ossa Morena Zone (Oliveira *in press*). The sediments consist of variably deformed and metamorphosed slates, arenites and tuffs with minor intrusives. Distinction between the formations within this group has previously been made on structural as well as lithological criteria, however, only the upper part of the Horta da Torre Formation has been dated (spores and acritarchs) as being Upper Palaeozoic in age (Oliveira *et al.* 1986). Three formations are recognised (Fig. 1.6):

- The Ribeira de Limas Formation.
- The Santa Iria Formation.
- The Horta da Torre Formation.

The Ribeira de Limas Formation consists of a series of fine grained siltstones and intercalated arenites. The boundary between this formation and the underlying Pulo Formation is considered to be conformable (Oliveira *in press*).

The Santa Iria Formation (Carvalho *et al.* 1976) unconformably overlies both the Pulo do Lobo Formation and the Ribeira de Limas Formation. It consists of a turbiditic sequence of slaty mudstones, medium to coarse grained arenites and minor tuffites.

Horta da Torre Formation (Oliveira *et al.* 1986). This formation overlies the Santa Iria Formation and consists of a series of fine grained dark phyllites with intercalations of massive quartzite. Spores and acritarchs extracted from the upper part of these rocks within the Portugal yield ages of lower to middle Famennian (Oliveira *et al.* 1986) inferring that they are the youngest formation recognised within the Ferreira-Ficalho Group.

C - *The Chanza Group.*

This Group (Fig. 1.6) occurs on the southern margin of the Oceanic Exotic Terrane (Fig. 1.3). Three formations have been identified within this group, a feature used to suggest that these are the southern equivalents of the Ferreira-Ficalho Group to the north (Schermerhorn 1971; Carvalho 1976; Oliveira (*in press*); Silva 1989). All the formations have a terrigenous character:

The Atalaia Formation composed of slaty mudstones and sandstones.

The Gafo Formation consisting of greywackes, siltstones and shales. This formation is approximately 650 metres thick and includes intercalated acid and basic dyke suites.

The Repressa Formation is mainly composed of siliceous siltstones, shales and quartzwackes. It too has a considerable thickness, of some 1100 metres.

Age relations are as yet unclear because of a lack of fossil material. Southward diachroneity, related to southward progradation, is observed throughout the South Portuguese Zone and extrapolating from this relationship it is assumed that the Gafo and Repressa Formations may be slightly younger than their northern counterparts and are thus Upper Famennian to Lower Tournasian in age (Oliveira *in press*).

1.3.1.c *The Pyrite Belt.*

The Pyrite Belt is underlain by the Phyllite-Quartzite (PQ) Formation, which consists of phyllites, siltstones, quartzwackes and dark shales (Fig. 1.3 & 1.6). Shales and slates, some of which have been dated as Late Givetian (Lake *et al.* 1988), are frequently interbedded with lenses of limestone which yield a fauna of cephalopods, trilobites and conodonts giving a Middle to Upper Famennian age (Boogard 1963; Boogard and Schermerhorn 1980, 1981). The PQ Formation is considered to have accumulated during the Upper Devonian in a large epicontinental sea that was affected firstly by pre-Famennian compression and subsequently by extension during the Upper Famennian - Middle Viséan (Oliveira *in press*, Silva *et al. in press*); this last phase resulting in the formation of grabens and half grabens.

The Volcano-Sedimentary (VS) Complex (Schermerhorn 1971), conformably overlying the PQ Formation consists of bimodal volcanics that interfinger with purple shales, siltstones and rare limestones. The thickness of the VS Complex ranges from 100m to >500m according to distance from

the volcanic centres (IGME 1984-sheet 937, Oswin 1986, Oliveira *in press*) and is dated, by conodonts and cephalopods, as Upper Famennian/Lower Upper Viséan (Boogard 1963; Oliveira 1983).

1.3.1.d *The Baixo Alentejo Flysch Group.*

This Group of turbiditic sedimentary rocks is composed of sandstones, shales, siltstones and greywackes ranging in age from Upper Viséan in the north to Lower Westphalian in the south (Fig. 1.3). Three formations are recognised (Schermerhorn & Stanton 1969, Oliveira *et al.* 1979, Ribeiro *et al.* 1987): the Mértola Formation, the Mira Formation, and the Brejeira Formation, the latter consisting of sediments ranging from mature sandstones to immature greywackes. Southward progradation in this Group is indicated both by a decrease in volcanic fragments, indicating a northern provenance, and by southward younging, as demonstrated by macrofossils (Oliveira *in press*).

1.3.1.e *SW Portugal.*

Here shallow water sedimentary rocks, mainly sandstones and shales, predominate. The oldest formation, the Tercenas Formation, is of Famennian age while fauna, including goniatites, trilobites and corals, give an age of middle Tournasian to late Namurian for the Carrapateira Group (Oliveira *et al.* 1985). Oliveira (*in press*) envisages the flysch sediments of SW Portugal developing in a southwestward prograding sedimentary basin which evolved in response to collision occurring to the north.

1.3.2 The Ossa Morena Zone.

The Ossa Morena Zone, which forms the southern margin of the Iberian Terrane (Quesada *in press*) is bounded to the north by the Central Iberian Zone and to the south by the South Portuguese Zone (Fig. 1.2b). The oldest rocks that occur within this terrane are Precambrian. They crop out in the core of two antiforms, the Portalegre - Badajoz - Córdoba antiform and the Olivenza Monesterio antiform (Fig. 1.7a) which are contained within the trend of the Hercynian foldbelt. The Precambrian strata can be subdivided, according to temporal position with respect to tectonic events that punctuated the late Precambrian, into pre-orogenic and syn-orogenic successions (Quesada *in press*). Both of these successions are interpreted as being consistent with a phase of rifting of continental crust, formation of oceanic crust and then a protracted period of stasis which allowed the accumulation of graphitic pelites and quartzites (the Serie Negra) that occurs widely across the Ossa Morena Zone.

The Cambrian, which outcrops within and to the north of the Badajoz -Córdoba shear zone (Fig.1.7b), begins with a basal conglomerate that lies unconformably on the Precambrian. This is followed by a sequence of shallow water platformal deposits including a carbonate facies dated as Lower Cambrian (Zamarreño & Debrenne 1977). Above the carbonates is a thick sequence of

terrigenous material that has yielded Lower to Middle Cambrian fauna (Lotze 1956, Bard 1964).

The Ordovician, Silurian and Devonian are variably represented throughout the zone although there are many problems in resolving the stratigraphic zonation of the former two, due to lack of good palaeontological control. Within the Ordovician, conglomerates with intercalated arenites and quartzites have been identified and these are overlain by terrigenous material with minor carbonates. The Silurian is represented by a horizon of black slates rich in graptolites, making it relatively easily identified. To the north of the study area the Devonian is represented by a succession of slates and greywackes, the Terena Formation (Pushman 1967), deposited unconformably upon the Ordovician and Silurian. This flyschoid formation has been dated as Frasnian to Lower Viséan (Boogaard 1963, Boogaard and Vázquez 1981).

The Carboniferous has been well documented throughout the Iberian Peninsula. Traditionally it has been divided into three main sequences separated by unconformities (Julivert *et al.* 1984, Crespo-Blanc 1989), as summarised below:

(a) A Culm-type sequence of turbiditic character, containing basic volcanic rocks. This has been dated as Dinantian in age and has a thickness of several hundred meters.

(b) A coal-bearing sequence that can be subdivided into two: 1. A paralic sequence of Upper Viséan - Namurian age. 2. A limnic Westphalian sequence possibly deposited in an intramontane environment.

(c) An almost undeformed post-tectonic Stephanian molasse sequence also deposited in intramontane basins.

There appears to be a certain amount of stratigraphic as well as structural diachroneity within these sediments in that they become progressively younger towards the NE (Quesada *et al. in press*).

Deformation within the Ossa Morena Zone has had a protracted history, lasting from late Precambrian to Upper Palaeozoic. This has resulted in a very complicated structural framework and a wedge-shaped partitioning of the region (Apalategui *et al. in press*). Structures are generally verging towards the SW. These are the result of interference between an early phase of deformation which has been reactivated by late Palaeozoic deformation. This has reorientated the main structures into parallelism with the main Hercynian trend, the structures of which display a general southwesterly vergence. Recently Apalategui *et al.* (*in press*) have divided the Ossa Morena Zone into linear NW - SE trending belts each of which display distinct structures (Fig. 1.7b).

1.4 Regional Setting of the Spanish Hercynides

The Devonian and Carboniferous rocks of the Southern Iberian Peninsula form the southern flank of the Ibero-Armorican Arc which extends from Iberia, through SW England, to northern Europe (Fig. 1.1). There are many features which suggest that similar processes were occurring in

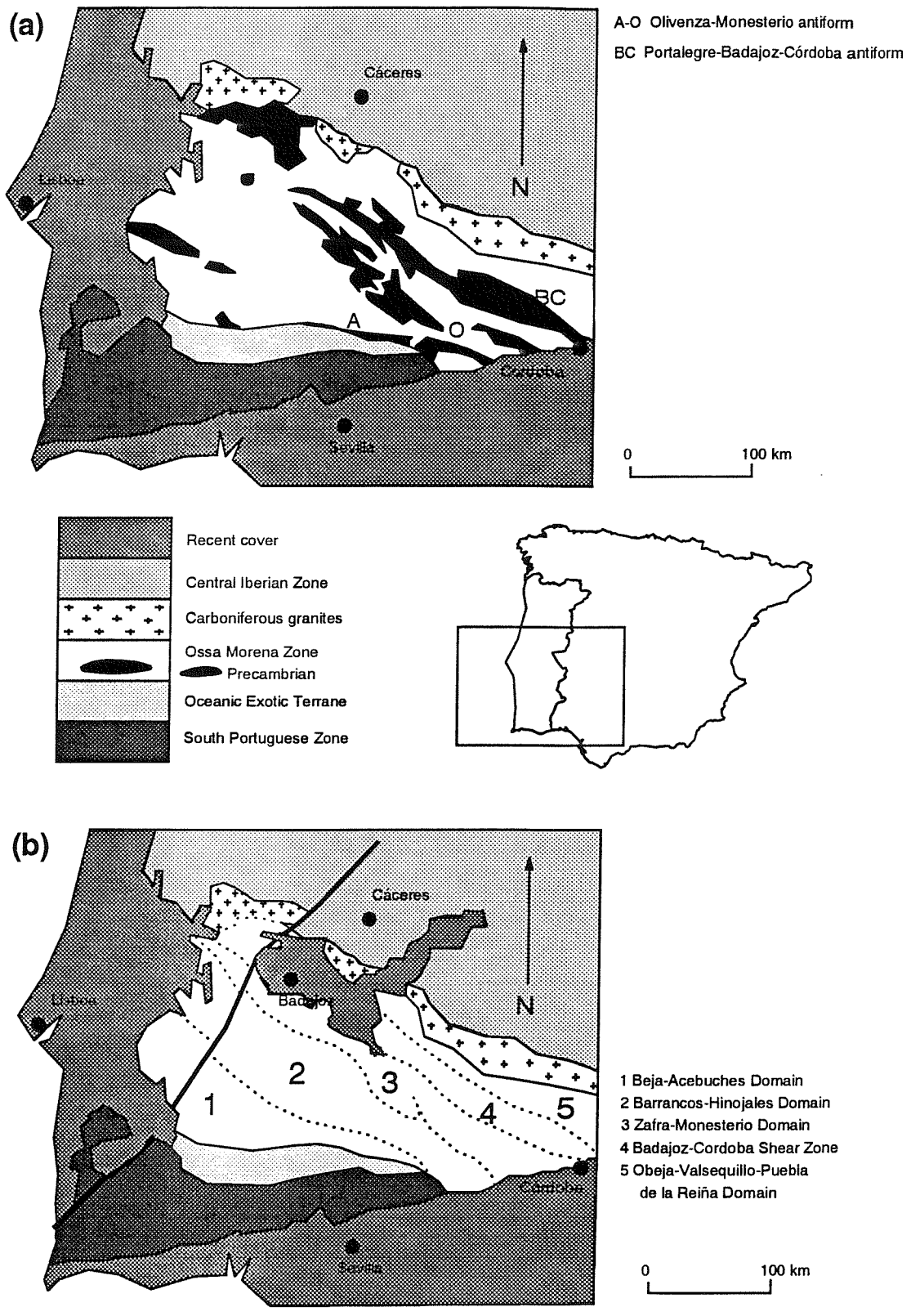

Figure 1.7 (a) Stratigraphy and (b) Structure of the Ossa Morena Zone (Apalategui *et al. in press*).

these widely separated regions. These include:

- The polarity of metamorphism and deformation which decreases towards the SW in SW Iberia and northwards in northern Europe.

- The southwestward vergence of structures reflecting the northerly vergence seen in northern Europe. - Major episodes of bimodal volcanism which occurred throughout the Upper Devonian and extended into the Lower Carboniferous, resulting in the formation of the Iberian Pyrite Belt.

- The presence of suture zones marked by the Beja-Acebuches Amphibolites in SW Iberia and the Lizard Complex in SW England.

- A similarity in stratigraphy.

- A similar Upper Devonian/Lower Carboniferous age for the extensive flysch deposits.

The structure of the South Portuguese Zone has previously been described in both 'thin-skinned' and 'thick-skinned' tectonic models (Bard 1971; Carvalho 1972; Riding 1974; Schermerhorn 1975; Vegas & Muñoz 1976; Routhier *et al.* 1980; Munha 1983; Matte 1983; Ribeiro & Silva 1983; Andrews *in press*; Silva *et al. in press*). The general consensus (Matte & Burg 1981; Matte 1986; Crespo-Blanc 1989; Quesada *in press*; Silva *et al. in press*) is that the present geometric arrangement of formations resulted from oblique closure of a mid-Devonian ocean basin. Many different geotectonic interpretations have been applied to the evolution of this region, ranging from an intracontinental orogen (Schermerhorn 1975) to an oblique strike-slip mobile belt (Badham 1982; Andrews *in press*). There is a marked polarity of all geological elements: structure is dominated by folding and thrusting with southwesterly vergence; metamorphism ranges from lower greenschist facies within the Oceanic Exotic Terrane, through prehnite-pumpellyite facies in the Pyrite Belt (Schermerhorn 1975), to very low grade anchimetamorphic or negligible metamorphism in the extreme southwest of Portugal (Munha 1983); rocks become younger towards the SW (Oliveira *et al.* 1986 and *in press*). A marked structural discontinuity exists between the Oceanic Exotic Terrane and the Pyrite Belt; the former displays three distinct cleavage forming phases of deformation whilst the latter shows two, becoming only one in SW Portugal (Silva et al. *in press*).

The depocentre of the Pyrite Belt sediments was probably within a prograding basin, or basins, that formed between the South Portuguese Zone and the Ossa Morena Zone. Oliveira (*in press*), proposes three distinct deformational events that governed the geometry of these basins: a pre-Famennian collision between the Ossa Morena Zone and South Portuguese Zone, an Upper Famennian to Middle Viséan extensional regime, when terrigenous and volcanogenic sediments were deposited, and an Upper Viséan compressional regime that gave rise to syn-orogenic flysch deposits.

1.5 Objectives

The objectives of this study are:

(a) To clarify structural relationships across the boundary between the Ossa Morena and South Portuguese Zones.

(b) To characterise the environment of deposition of the sedimentary rocks within the Oceanic Exotic Terrane.

(c) To investigate provenance of the formations identified using geochemistry. (d)

To detail metamorphic characteristics of the rocks within the structural framework.

(e) To develop a model for the geotectonic evolution of the area and to integrate this into the broad framework of the Hercynian Orogeny.

Chapter 2 - Lithostratigraphy

Abstract

Field work has identified six lithologically distinct formations preserved as a folded imbricate thrust stack on the boundary between the Ossa Morena Zone and the South Portuguese Zone. One formation, the Peramora Mélange Formation, consisting of blocks and phacoids of material ranging from metasediments to amphibolites, has not been identified in previous work, either in Spain or Portugal. Amphibolite blocks predominate within this formation and on this basis it is classified as an oceanic mélange. These formations are marine in character although many of the primary sedimentological features have been reworked and obliterated during tectonic deformation. The La Giralda Formation is the thickest of the sedimentary sequences seen in the study area. On the basis of palynology the youngest formations are dated as extending from the Givetian to the earliest Famennian.

2.1 Introduction.

Six lithostratigraphic formations, which provide the basis for both lithological and structural mapping, are identified. Field names rather than established names are used in descriptions to avoid confusion with earlier definitions (Chapter 1). The formations identified are (Fig. 1.4):

A - The Puerto Cañón Formation.

B - La Giralda Formation.

C - The Cumbres de Los Ciries Formation.

D - The Alajar Formation.

E - The Peramora Mélange Formation.

F - The Beja-Acebuches Amphibolites.

The local formations tabulated above can be loosely correlated with those defined by previous workers in the area and with formations recognised by Crespo-Blanc (1989) who mapped lithologies within and to the south of the Sierra de Aracena (Fig. 2.1). Crespo-Blanc identified four sedimentary formations: The Orthoquartzite Formation; The Flyschoid Formation; The Quartz-schist Formation and the Sierra de Las Bañas Formation. The two former formations are considered to have a gradational contact which is marked by an alternation of phyllites and greywackes, and have been affected by a single major phase of deformation. The Quartz-schist Formation, consisting of an alternation of quartz-schists and micaceous metaquartzites, and the meta-turbidites of the Sierra de Las Bañas Formation have, however, been exposed to three major deformation phases and are separated from the overlying formations by a tectonic contact.

Giese *et al.* (1988) described several formations from south of Almonaster La Réal and obtained spores and acritarchs that yielded an Upper Famennian age (Fig. 2.1). They correlate the formation from which the spores were obtained with the Santa Iria formation (Carvalho *et al.* 1976,

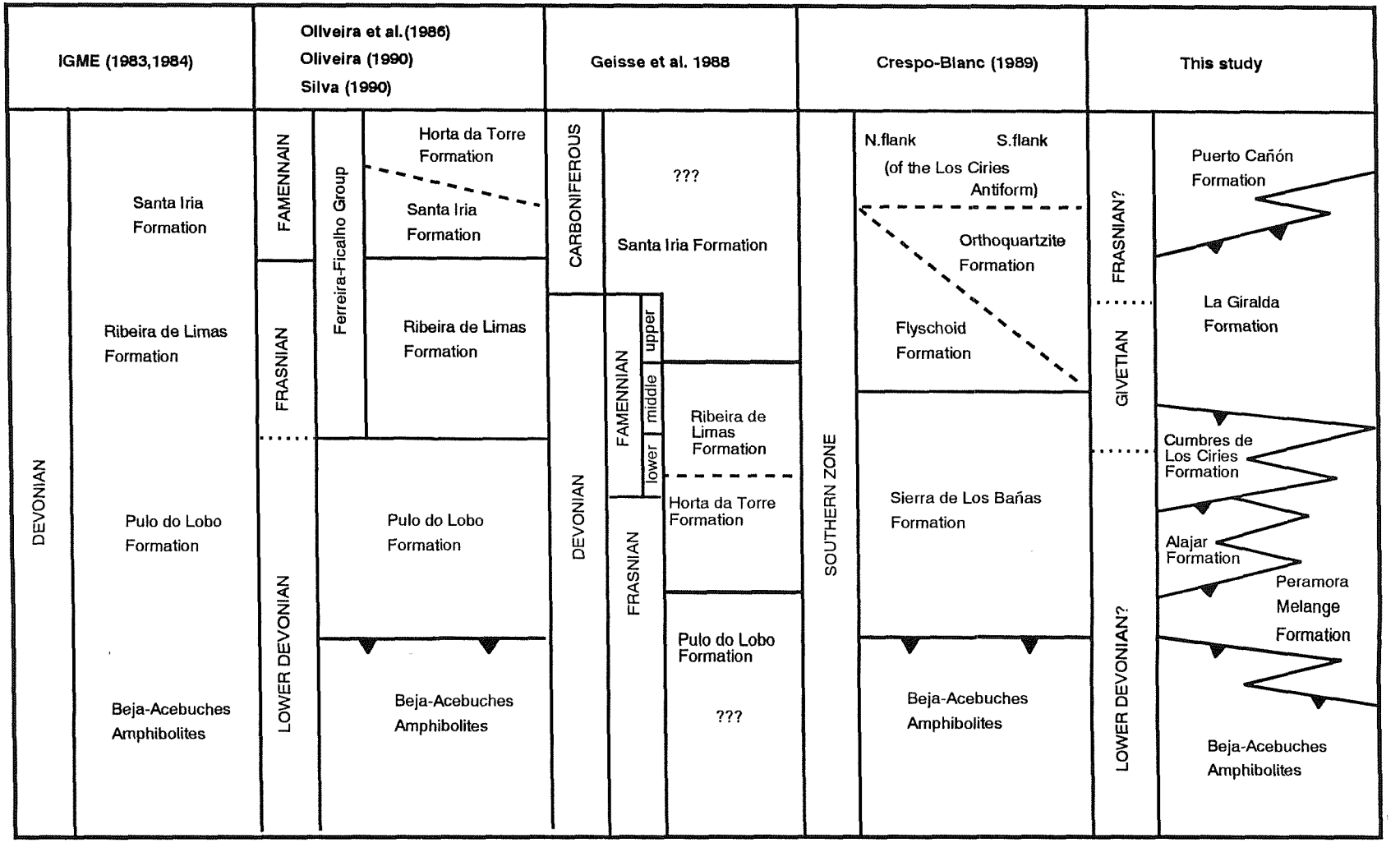

Figure 2.1 Comparison of stratigraphy between that used in the present study with those used by previous workers in the area.

Oliveira 1983) and argue that these dates place the Santa Iria Formation above the Horta da Torre Formation (Oliveria *et al.* 1986) which, they suggest is a lateral facies transition of the Ribeira de Limas Formation.

A correlation between formations identified in previous studies with those of the present study is proposed in Fig. 2.1. It has been argued (Apalategui *et al.* 1983, Oliveira *et al.* 1986, Crespo-Blanc, 1989) that the lithostratigraphic association comprises a normal succession, however, field work during the present study indicates that the boundaries between all the formations listed above are probably tectonic although deformation, manifested primarily by the presence of a strong NW dipping regional schistosity, has obliterated all pre-existing lithostratigraphic contacts. With the exception of the data discussed above, ages for units within the succession are as yet poorly constrained and in this study a tectonostratigraphic approach is preferred, the lithological units being grouped according to their position in the structural nappe pile.

2.2 Sedimentology.

The sedimentary sequences identified are all marine in nature, an assumption based on the presence of turbidites from which acritarchs have been recovered (Lake *thesis in prep.*). The sedimentary facies are grouped following the classification adopted by Pickering *et al.* (1989) for deep water deposits and are defined on the basis of textural criteria, bed thickness, internal organisation and composition. Four main facies classes exist: chaotic deposits (Facies C), sandstones (Facies S), mudstone and sandstone couplets (Facies M) and fine grained siltstone and siltstone/mudstone couplets (Facies F). These are further subdivided into organised and disorganised. Sedimentological features in all of the facies identified have been extensively modified due to deformation and metamorphism.

2.2.1 Facies C - ***Chaotic deposits.*** (approximating to Facies Class F, Pickering *et al.* 1989). This facies consists of chaotic mixtures of sediments that were emplaced by large-scale downslope mass movement. The character of these deposits ranges from isolated clasts of material to large rafts of discontinuous quartzite which are matrix supported. The interstitial matrix is recrystallised and often highly sheared, although the clasts themselves may be relatively undeformed, ranging from angular to flattened. Rapid lateral and vertical transition between lithologies occurs. Exotic clasts range in size from pebbles to large rafts (up to 50m in length) of exotic material.

2.2.2 Facies S - ***Sandstone.*** (Facies Class B, Pickering *et al.* 1989). Beds within this facies are poorly defined and the matrix is recrystallised, giving a very pure quartzite in which sedimentary structures are absent. The beds are assumed to have consisted of sand grade material.

2.2.3 Facies M - *Mudstone and sandstone couplets.* (Facies Class C, Pickering *et al.* 1989). This class can be separated into organised and disorganised categories on the presence or absence of internal structures.

2.2.3.1 Facies M_D - *disorganised mudstone/sandstone couplets.* (Facies C1, Pickering *et al.* 1989). Silt and clay sized fractions are characteristic of this facies. The maximum grain size is in the range of fine to coarse sand (up to 3mm grain size). Bounding surfaces between the beds are generally well defined. Internal sedimentary structures are absent although silty mud clasts may occur in varying proportions. Some beds may support rafts of sandstone or mudstone within them.

2.2.3.2 Facies M_O - *organised mudstone/sandstone couplets.* (Facies C2, Pickering *et al.* 1989). This facies shows marked normal grading and a Bouma sequence may be well developed. Beds can vary from less than 5cm to greater than 15m in thickness.

2.2.4 Facies F - *fine grained siltstone and siltstone/mudstone couplets.* (Facies Class D, Pickering *et al.* 1989). These deposits form over a large area in the study area and comprise very fine grained sediments that are dominated by silts and muds. Sands may contribute up to 20% of the volume. Once again two sub-facies, based on internal organisation, are recognised.

2.2.4.1 Facies F_D - *disorganised fine grained material.* These occur as variably thick beds of essentially structureless siltstone and mudstone in which bedding and grading is ill defined or absent.

2.2.4.2 Facies F_O - *organised fine grained material.* This facies occurs as either discrete beds or as interlaminated units of mud and silt. Also included are intercalated organic rich muds. Normal grading from coarse to fine units is common.

2.3 Stratigraphy.

Fig. 2.2 shows the distribution of the various formations and summarises structural relationships. This map also locates the type sections of the Puerto Cañón Formation, the Cumbres de Los Ciries Formation and the Peramora Mélange Formation along the Alcalaboza River which flows through the low land area of the Los Ciries Antiform (Fig. 1.5) and is surrounded by the highland areas dominated by the Cumbres de Los Ciries Formation.

2.3.1 The Puerto Cañón Formation.

This formation comprises a narrow belt of turbidites exposed south of Aroche [GR 7581 9810] and also to the south of Alajar [GR 0465 9155]. No base to this formation is identified as contact between this and the underlying formations is considered to be tectonic. The maximum width of outcrop is >150m. Several sedimentary facies are represented: (i) a fine grained mudstone facies (Facies M_D), (ii) a fine grained silty facies (Facies F_O), (iii) a coarser grained immature arenaceous

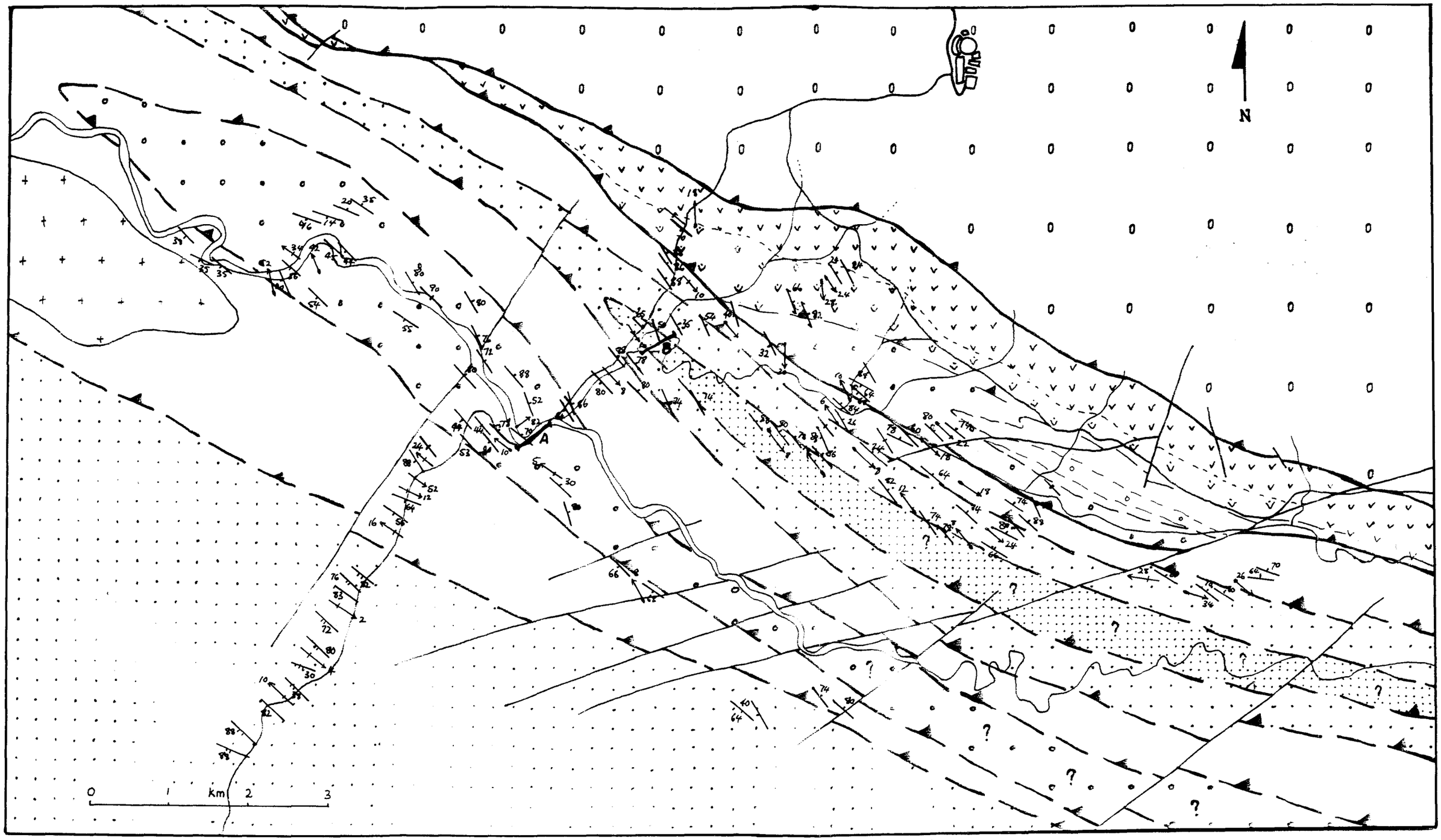

Figure 2.2 Geology of the area to the south of Aroche together with summarised structural data.

A - Peramora Mélange / Cumbres de Los Ciries type section B - Puerto Cañón Formation type section

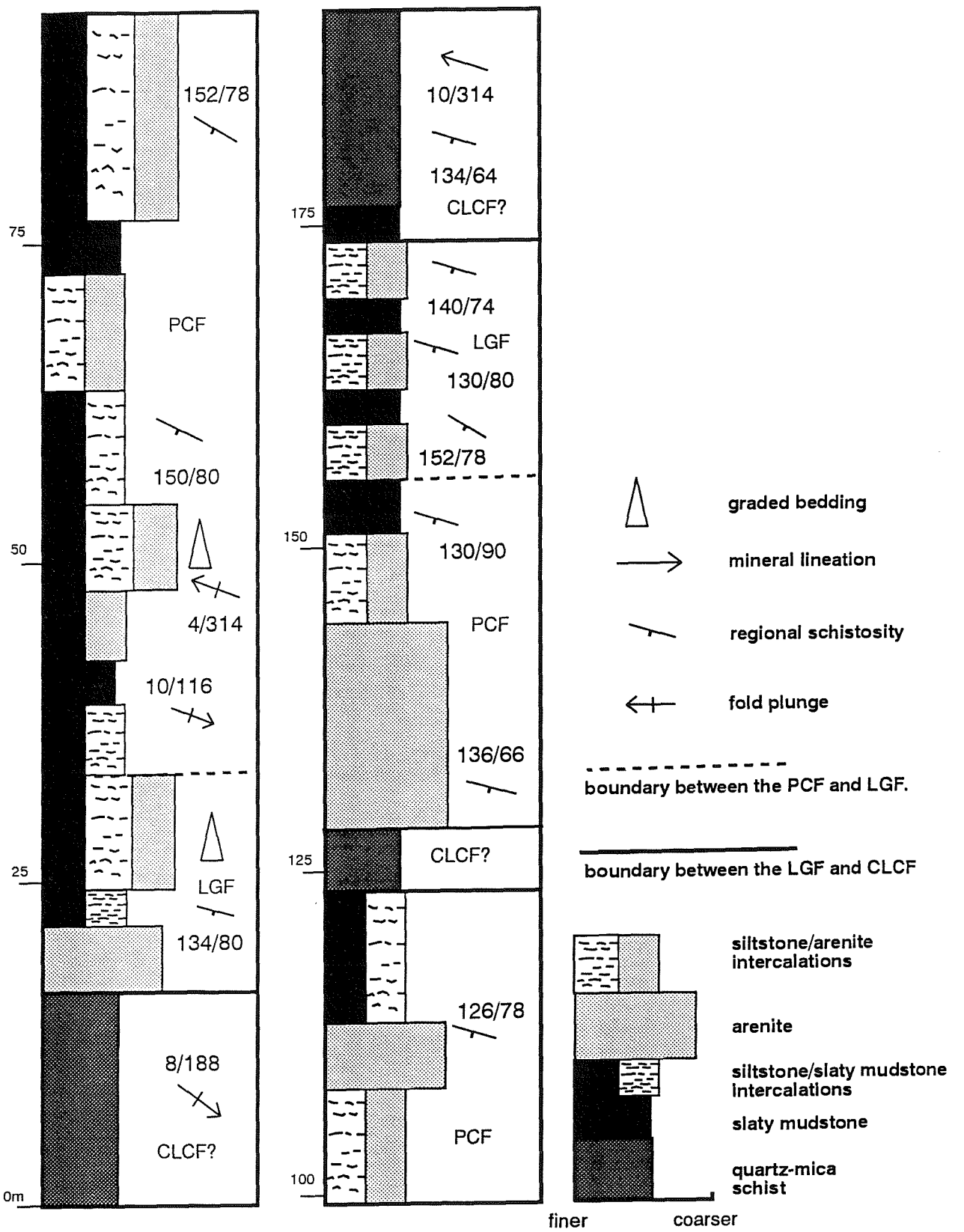

Figure 2.3 Log of the type section for the Puerto Cañon Formation

Figure 2.4
(A) Folded intercalated fine grained silty mudstones and light grey siltstones of the Puerto Cañon Formation from the Alcalaboza River [GR 7635 9790].

(B) Medium grained arenites and fine grained siltstone intercalations of the Puerto Cañon Formation which have a well developed bedding parallel cleavage.

(C) Thin section from the Puerto Cañon Formation, south of Alajar [GR 0465 9155] illustrating the immaturity of these metasediments. An igneous clast with randomly orientated plagioclase and amphibole is surrounded by finer grained quartz, biotite and plagioclase.

(D) Thin section from the Puerto Cañon Formation south of Aroche [GR 7655 9765] illustrating immaturity of the metasediments. This sample has polymetamorphic quartz grains and lithic clasts which have been orientated within the matrix. A weak pressure solution cleavage is marked by orientated flakes of biotite.

(E) and (F) are examples of the La Giralda Formation. These two photographs show centimetric intercalations of fine grained silty mudstones and light grey siltstones.

(G) Thin section from a shear zone within the Alajar Formation (sample 7928 [GR 1410 9430]). The sample shows intense grain size reduction and quartz ribbons characteristic of a mylonite.

(H) Exotic marble block from within the Alajar Formation located to the south of Alajar [GR 0640 9270].

(I) Disc-shaped quartzite phacoid from the Alajar Formation on the flanks of the Sierra de Los Picos. This particular phacoid has a pointed nose.

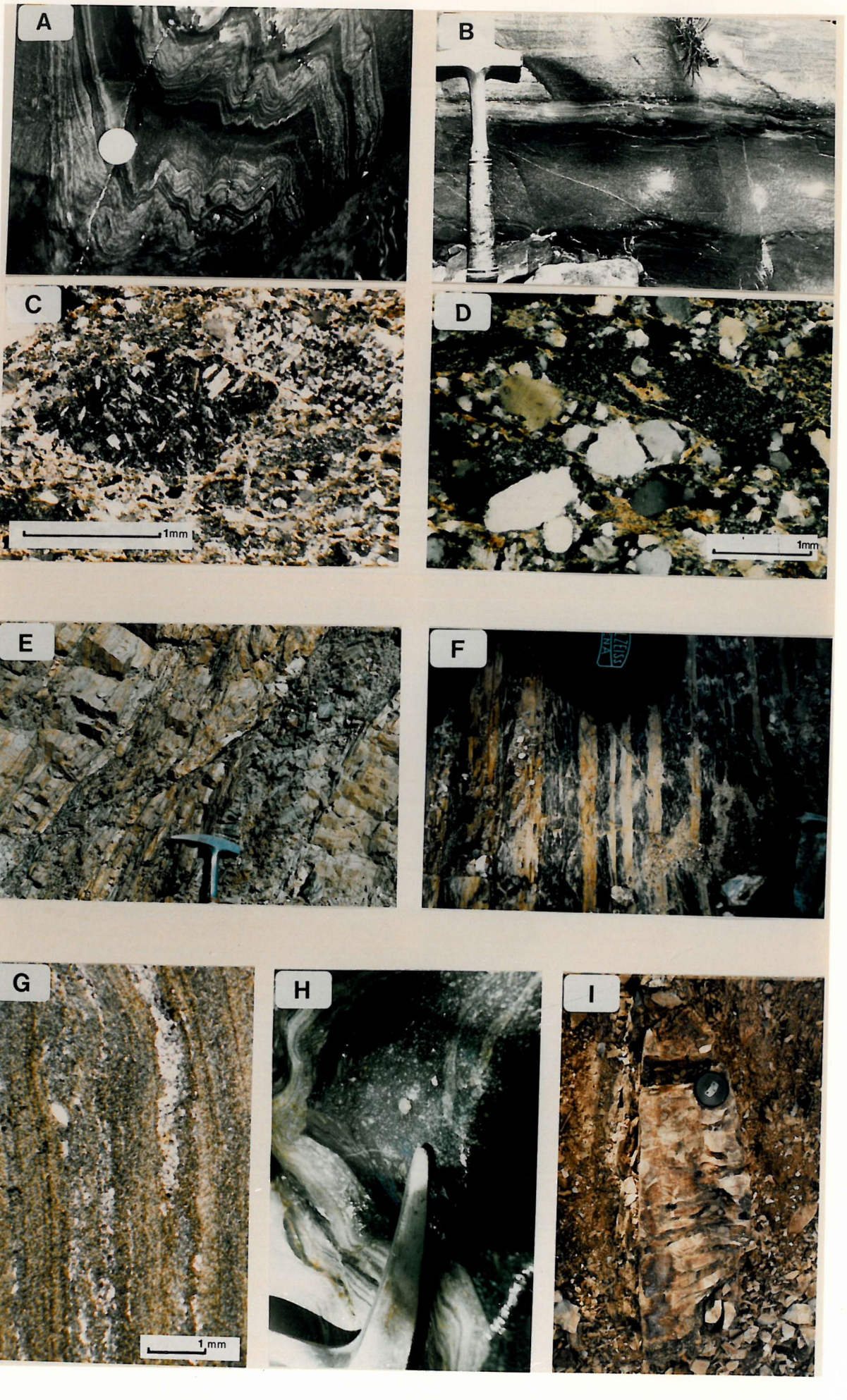
A
B
C
1mm
D
1mm
E
F
G
1 mm
H
I

facies (Facies M_D). Fig. 2.1 shows that this formation is thought to correlate with the Santa Iria Formation (Oliveira *et al.* 1979) possibly placing it within the Frasnian or Famennian.

The type section occurs south of Aroche along the Alcalaboza river extending from [GR 7659 9760] to [GR 7680 9775]. Fig. 2.3 summarises the salient features: fine grained slaty mudstone and coarse grained immature (up to 0.5cm grain size) arenites are found in close association forming intercalations that range from centimetres to metres in thickness. Fine grained mudstone beds possess a pervasive cleavage and have suffered brittle boudinage while coarse grained layers, although sometimes weakly deformed, often show no fabric. Coarse grained units are composed of rounded to sub-rounded grains, up to 0.5cm in diameter, of volcanic fragments and lithic clasts while quartz exists both as original and as polymetamorphic grains. Low grade metamorphism, resulting in the growth of muscovite mica along foliation planes, has been accompanied by pressure solution creating embayments within the quartz, leaving intragranular sutures of mica and opaque minerals. Petrographic analysis of material from south of Alajar [GR 0465 9155] (Fig. 1.4) shows that the coarser grained material has a considerable pyroclastic component. Clasts include igneous fragments, consisting of aggregates of randomly orientated plagioclase crystals, and polymetamorphic quartz grains (Fig. 2.4C & D). These have been orientated with their long axes parallel to the plane of schistosity, emphasised by development of mica. Fine grained units can be subdivided into dark coloured muddy horizons and lighter coloured silty horizons (Facies F_O) and often rip-up clasts of one type are found in the other (Facies M_D). The former are highly cleaved and are extremely friable. In one locality [GR 7675 9768] a massive unit of homogenous greywacke ≈20m in width is exposed, while in other places thin layers (≤5cm) of black mudstone are repeatedly interleaved with fine grained grey coloured silty layers (Fig. 2.4A & B). The sedimentological association of fine grained slates and silts, together with coarser grained arenites and greywackes is consistent with development of the C-D-E subdivisions of the Bouma sequence. Transport processes resulting in this type of deposit are thought to be by means of mud rich, very high density turbidity currents or fluidised sand-mud debris flows (Pickering *et al.* 1989).

Only one sample collected from this formation has yielded an age. Sample 8139 is a fine grained black slaty mudstone [GR 7603 9825]. It has yielded the palynomorph *G.lemurata* which ranges from earliest Givetian to early Famennian (Fig. 2.13). This would place it as the same age as the underlying La Giralda Formation.

2.3.2 The La Giralda Formation.

This flysch dominated unit outcrops on either side of the Los Ciries Antiform (Apalategui *et al.* 1983) (Fig. 2.4E & F) and is composed of arenites and fine grained siltstones intercalated with black slaty mudstones together with minor tuffaceous layers. These lithologies occur in layers that vary from several metres to several centimetres in thickness and graded beds are common.

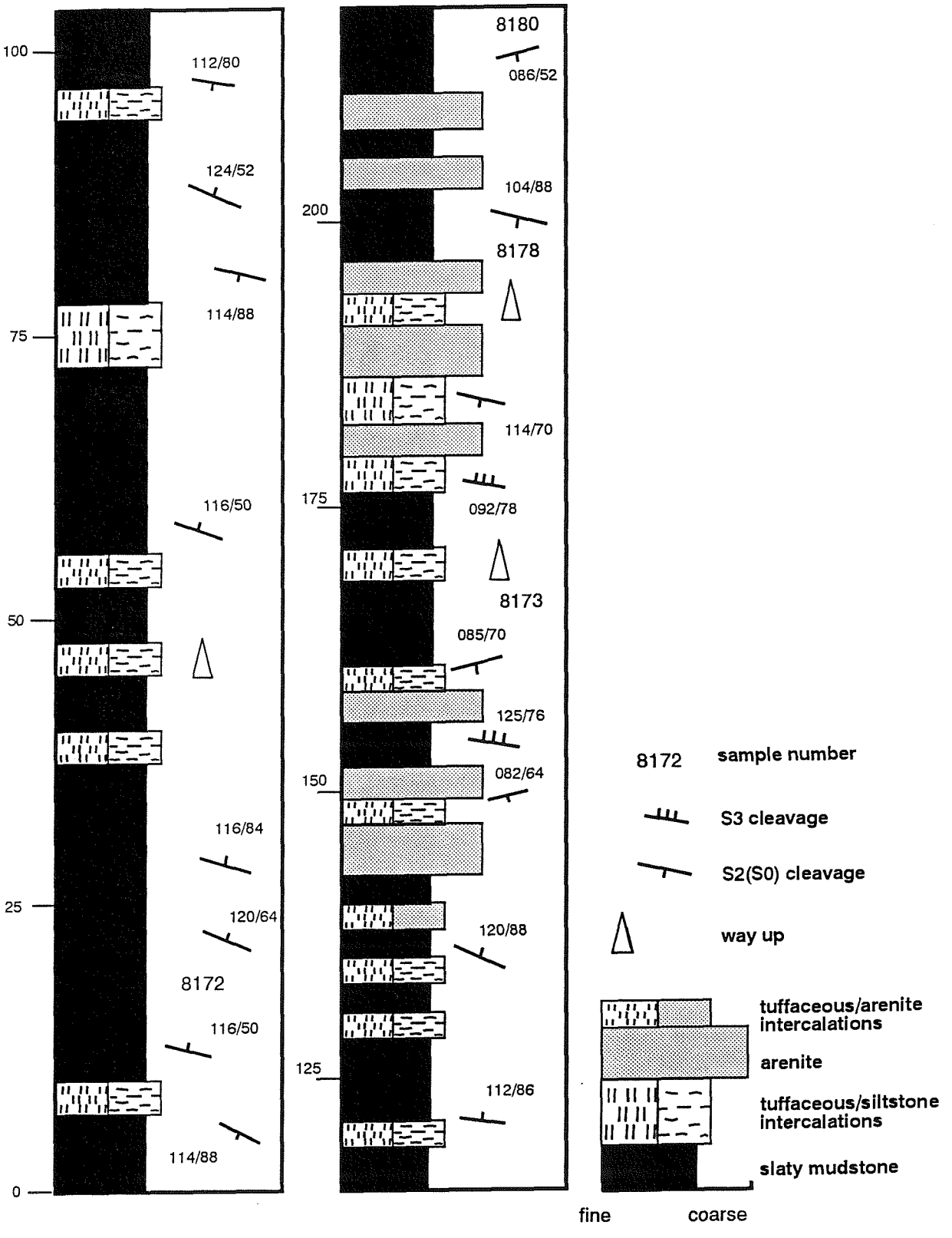

Figure 2.5 Graphic log to illustrate the type section of the La Giralda Formation.

Modification by lower greenschist facies regional metamorphism has overprinted an original sedimentary fabric, however, the fine grained character and maturity of the original sediments remains clear.

The type section (Fig. 2.5) begins at [GR 7195 9403] on the Aroche-El Mustio road and here slaty mudstone predominates. Fig. 2.4F illustrates that characteristic of the formation is the intercalation of fine grained siltstones, mudstones and arenites, together with tuffaceous bands, interleaved on a centimetric to decicentimetric scale.

Two lithological associations are described: (a) massive arenites (Facies S), (b) fine grained slaty mudstones, siltstones (Facies F_O and F_D) and tuffaceous material (Facies M_D).

2.3.2.1 *Massive arenites (Facies S).*

These are exposed throughout the length of the section but nowhere have sediments with a grain size fraction coarser than 5mm been recognised. Thin section (Fig. 3.18A - D) illustrates that the arenites are mainly composed of quartz grains (showing undulose extinction and deformation lamellae) with accessory feldspar (generally plagioclase), tourmaline and zircon. Biotite, muscovite and chlorite may occur as detrital minerals but are also present as secondary minerals, forming along cleavage planes. Essential minerals are supported in a fine grained phyllosilicate matrix which has been modified by low grade metamorphism. Pre-metamorphic maturity is suggested by a heavy mineral population consisting mainly of zircon with lesser amounts of heavily weathered tourmaline. Zircon is present in grains (up to 50μm) that range in shape from rounded to euhedral. The latter crystals are frequently zoned and may have been derived from air fall as they lack indications of significant post-depositional transport.

Original sedimentary features have been strongly modified by regional folding and thrusting with concomitant pervasive cleavage formation. Pressure solution has removed material, creating embayments in quartz and leaving the remaining grains elongate parallel to schistosity. It has also resulted in the formation of intergranular sutures of insoluble material, mainly mica and opaque minerals.

2.3.2.2 *Fine grained slaty mudstones, siltstones (Facies F_O and F_D) and tuffaceous material (Facies M_D).*

Fine grained slaty mudstones and siltstones form the main part of this formation. They have been extensively modified by tectonic deformation, recording at least three cleavage forming phases. Slaty mudstones form black, homogenous intercalations which are associated with both lighter coloured silty layers and green, tuffaceous layers often alternating on a centimetric scale.

The tuffaceous bands can be up to several meters in thickness and have a characteristic green colour. They have a fine grained matrix supporting a population of euhedral quartz and feldspar

crystals that can reach up to 5mm in diameter. Thin section shows that they consist mainly of fine grained phyllosilicate minerals with quartz and plagioclase as inclusions. There is a well developed foliation which is deflected around these larger grains. Chlorite and muscovite are present as late stage alteration products.

The slates consist of monotonous black, fissile material with a strong cleavage, and often have crystals of pyrite developed within the foliation whereas slaty mudstones are highly cleaved and readily decompose. Intercalation of these different lithologies can sometimes be used to infer younging directions.

It is from these latter lithologies that spore yielding samples have been collected. In using samples such as these for dating purposes it must be remembered that analysis and interpretation is heavily constrained by several factors: the polydeformational history that affected the area, lack of any clear sedimentological control, and poor exposure. However, despite these qualifying constraints age ranges can be determined by using parameters such as inception of taxa, last occurrence of taxa, non-occurrence of zonal species and relative abundance of taxa (Lake *thesis in prep*). All of these parameters may also be affected by influences such as palaeoenvironmental variation, palaeoclimate, sedimentological control, or reworking. The samples were collected mostly within the La Giralda Formation, although one sample was collected to the north of the Los Cires Antiform within the Puerto Cañon Formation (Fig. 2.6).

Five main age ranges are defined extending from Basal Givetian to Early Famennian. Sample 8139 contains the spore *G. lemurata*, as do most of the samples from the area, and this spore only indicates the relatively broad range of Basal Givetain to Early Famennian (Fig. 2.7). Sample 8151, 8178 and 8182 all yield a similar stratigraphic range of Late Givetian to Early Famennian. This is defined by the presence of *Contagisporites optivus*. The presence of *Cristatisporites triangulatus* and *Cristatisporites inusitatus* may indicate a Mid to Late Givetian age and the upper stratigraphic limit for these samples is placed within the Early Famennian. Sample 8173 contains *Retusotriletes rugulatus*, a spore that is charateristic of the Eifelian to Early Givetian. It has an upper stratigraphic limit of Mid to Late Frasnian. In this sample the lower limit is interpreted from the presence of *C. triangulatus*. Samples 8028, 8156, 8180, 8200 and 9134 are all dated as extending from Mid or Late Givetian to earliest Famennian on the basis of spore evidence alone. These dates are supplemented, however, by the presence of two acritarch species (*Maranhites cf gallicus* and *M. perplexus*) which further constrain the maximum age to Early - Late Frasnian (Fig. 2.7).

A further sample, collected from the east of Almonaster La Réal, and thought be from rocks that correlate with the Horta da Torre Formation of Portugal (Oliveira *et al.* 1986), is dated as being of Late Frasnian to Early Fammenian age on the basis of a combination of *G. Lemurata* and *C.inusitatus*, together with *D. mucronatus*. The latter species is first documented from the top of the Frasnian and this constrains the sample to latest Frasnian - earliest Famennian.

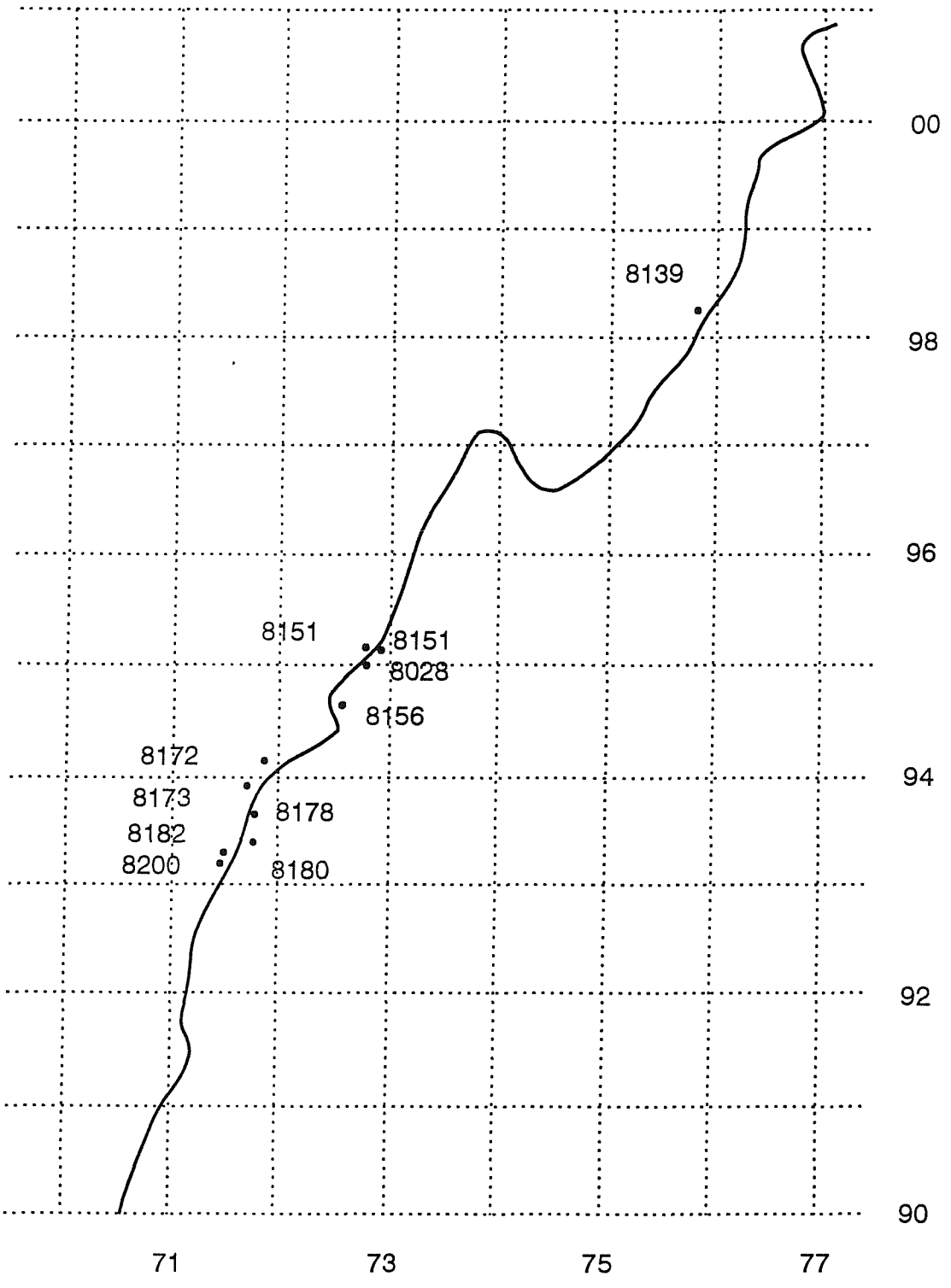

Figure 2.6 Location of samples which yielded spores along the Aroche El Mustio Road. These are generally from thin, fine grained, dark brown coloured slatey mudstone beds.

Figure 2.7 Summary table of the main index palynomorphs obtained from samples along the Aroche-El Mustio section. Sample B197 is taken from the east of Almonaster la Réal from within rocks that correlate with the La Giralda Formation.

2.3.3 The Cumbres de Los Ciries Formation.

The Cumbres de Los Ciries Formation consists of a monotonous sequence of quartz-mica schists intercalated with minor discontinuous quartzites, which have been extensively modified by polyphase tectonism and metamorphism. Strength of deformation has obliterated any indication of sedimentary history and nowhere are sedimentary structures preserved.

There is a marked topographic change as the boundary between this formation and the neighbouring Peramora Mélange Formation is crossed. The topography of the Cumbres de Los Ciries Formation and the overlying La Giralda Formation is characterised by strike-parallel ridges, and deep valleys which form along faults that criss-cross this rugged terrain. This formation can be correlated with the Pulo do Lobo Formation (Pfefferkorn 1968). No dates have as yet been extracted from these rocks either in Spain or in Portugal but their style of deformation and metamorphic characteristics has led previous workers (Oliveira *et al.* 1979) to assign them to the basement of the South Portuguese Zone.

The type section for this formation is located in the core of the Los Ciries Antiform where it is imbricated with the Peramora Mélange Formation (section 2.3.5) (Fig. 2.8). For descriptive purposes this formation is subdivided into three lithological units: (a) quartz-mica schists, (b) discontinuous interbedded quartzites and clasts of exotic material, (c) welded quartz-mica schists.

2.3.3.1 *Quartz-mica schists.*

These rocks crop out both to the north and south of the Los Ciries Antiform (Apalategui *et al.* 1983) and are imbricated with the Peramora Mélange Formation in the core of the Los Ciries Antiform (Fig. 1.5). The lithology is characterised both by a strong regional foliation and by the presence of attenuate quartz augen (Fig. 2.9A & D). They are composed of essential quartz, muscovite and biotite. Quartz displays features consistent with ductile strain including dynamic recrystallisation, sutured grain boundaries, deformation bands and quartz ribbons, whereas mica is present as stringers forming S-C structures (Chapter 3). Mineral paragenesis is consistent with mid-greenschist facies metamorphism. Accessory minerals include plagioclase feldspar (albite), zircon, tourmaline and apatite while chlorite forms as a late stage mineral replacing the micas. Although intense recrystallisation has occurred a fine grained mud-rich lithology is inferred which may approximate to Facies F_D.

2.3.3.2 *Interbedded quartzites.*

These occur in discontinuous layers (up to 2m thick) and form a minor component of the formation. They are often present as highly strained quartz-mylonites. Grain size is generally fine although this has been modified by the formation of complex cleavages (Fig. 3.15G & H and frontispiece) all of which have been folded during D_3 deformation. Extensive recrystallisation has

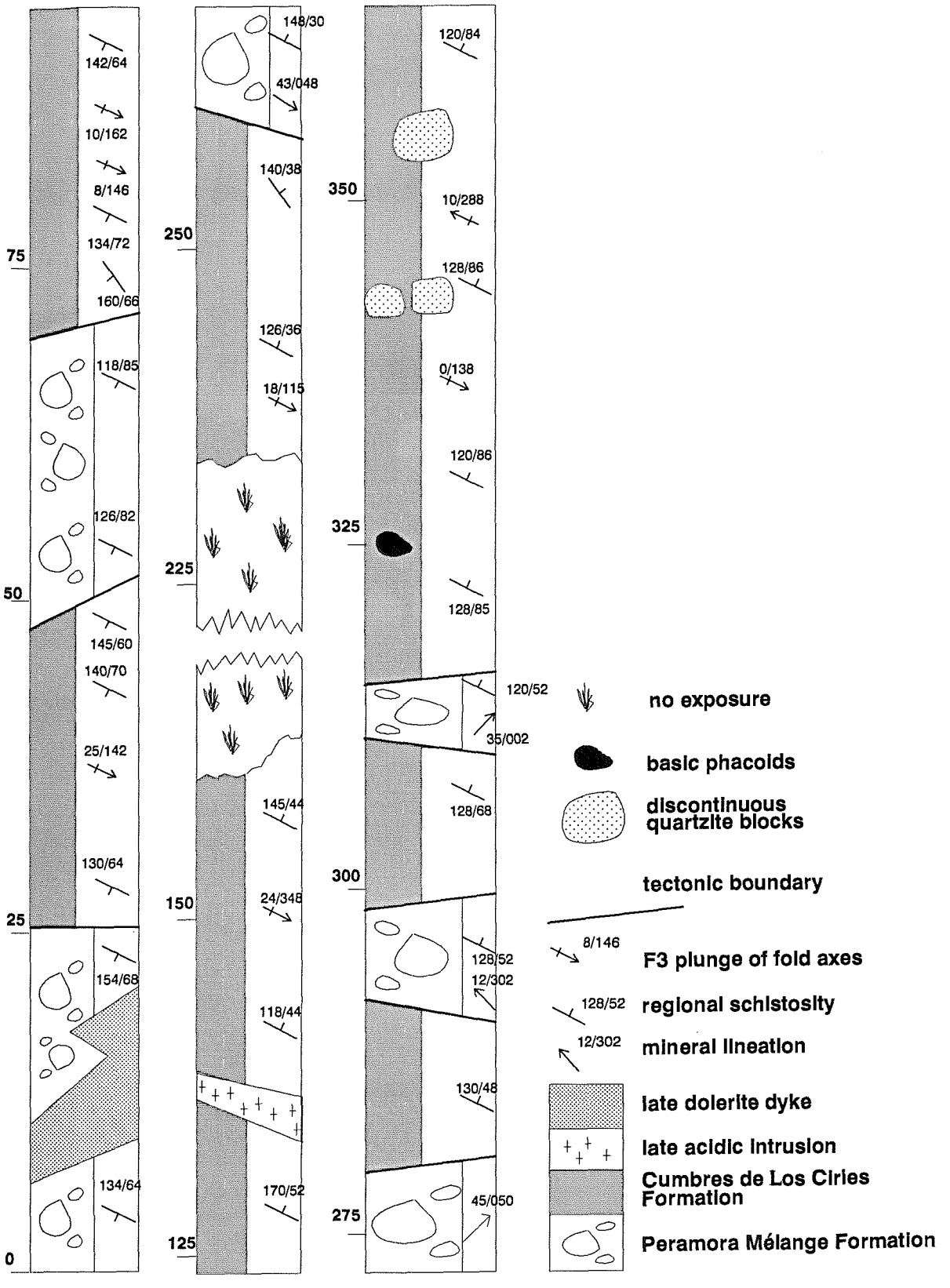

Figure 2.8 Graphic log illustrating the type section for both the Cumbres de Los Ciries Formation and the Peramora Mélange Formation.

Figure 2.9
(A) Attenuated quartz augen and intense steeply dipping schistosity of the Cumbres de Los Ciries Formation on the northern limb of the Los Ciries Antiform [GR 7580 9780].

(B) Blue-grey quartzite clast within the matrix of the Cumbres de Los Ciries Formation [GR 7745 9765].

(C) Well developed mineral lineation in the Cumbres de Los Ciries Formation on the northern border of the Northern Metasedimentary Domain, immediately juxtaposed against the Beja-Acebuches Amphibolites [GR 7635 9910].

(D) Hand sample (8210) [GR 7640 9905] from the boundary between the Beja-Acebuches Amphibolites and the Cumbres de Los Ciries Formation to illustrate the nature of the intense S_{N2} schistosity.

(E) S_{A2} foliation plane in the Beja-Acebuches amphibolites consisting of coarse amphibole and plagioclase [GR 7640 9855].

(F) Compositional banding within the Beja-Acebuches Amphibolites to the north of Almonaster la Réla [GR 9480 9370].

(G) and (H) Thin sections from the Beja-Acebuches Amphibolites (El Hurón) showing the equilibrium textures and poikilitic texture [GR 9172 9660].

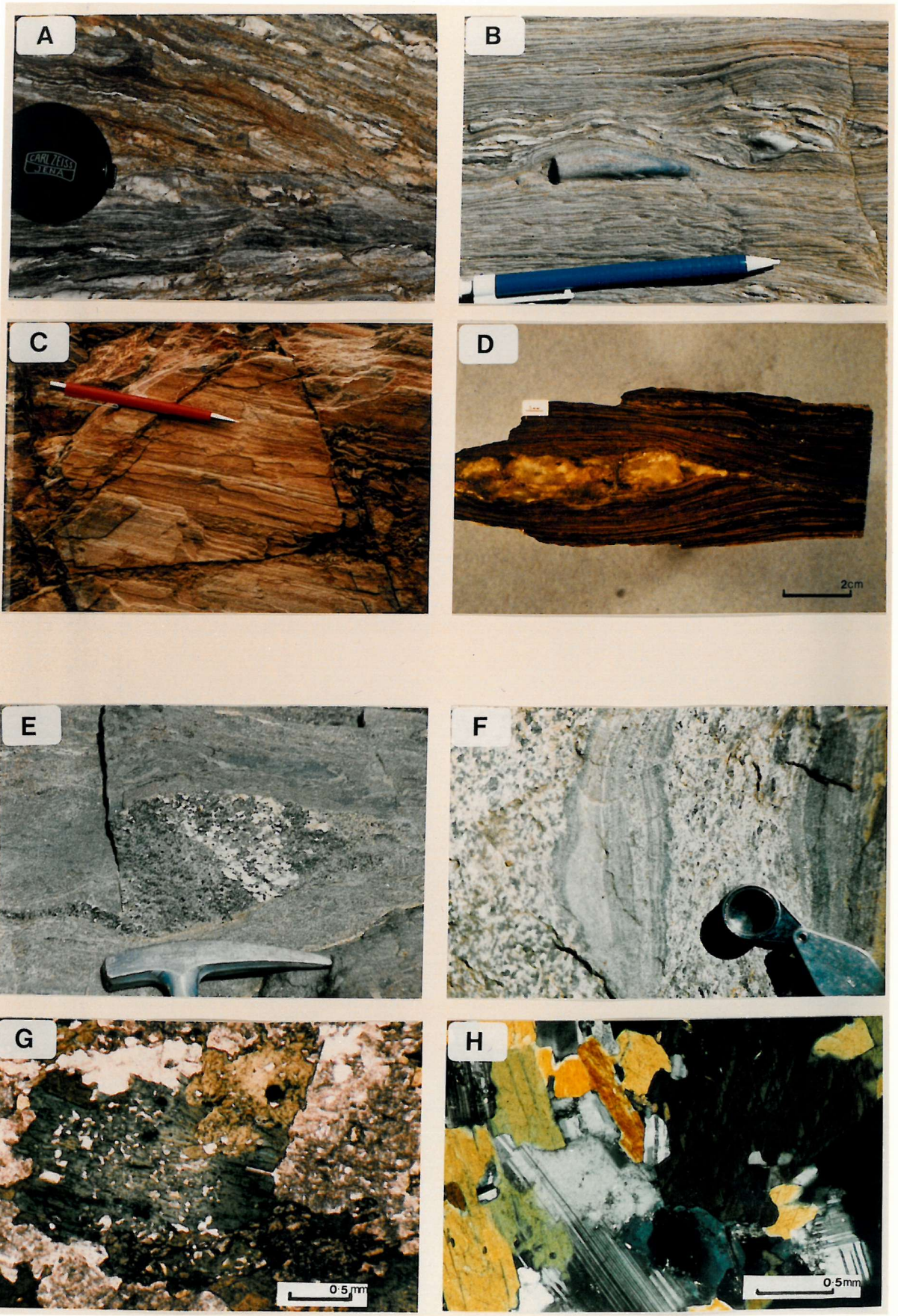
A
CARL ZEISS JENA
B
C
D
2cm
E
F
G
0·5mm
H
0·5mm

destroyed the original sedimentary fabric. Quartz ultramylonites occur on the southern margin of the section, present as lenses of millimetrically foliated quartzite (Chapter 3 - Southern Metasedimentary Domain).

Exotic clasts also occur around which the regional foliation is deflected. They consist of basic phacoids ranging in size from small pebbles to decicentimetric clasts.

2.3.3.3 *Welded quartz-mica schists.*

Exposures of these rocks occur along the banks of the Alcalaboza River [GR 8073 9667] at the confluence with the Barranco del Ciego (Fig. 2.9A - D). Here the rocks exhibit a well developed foliation and lineation. Andalusite is visible both as orientated porphyroblasts forming as part of a lineation plunging sub-horizontally to the NW-SE, and randomly orientated porphyroblasts contained within the plane of foliation. Other metamorphic minerals include garnet and cordierite but these are seldom visible in hand specimen.

Thin section (Fig. 3.14C, D, F) shows a well developed foliation and S-C structures indicative of sinistral shear. Quartz ribbons and mica fish are contained within this foliation with aggregates of accessory minerals such as tourmaline and zircon located along grain boundaries. Andalusite grows within the fabric as elongate porphyroblasts with inclusions of quartz, although no earlier fabric is defined. Garnet truncates both mica and quartz grains (Chapter 5) and analysis by electron microprobe shows that it is composed mainly of almandine with lesser proportions of spessartine.

2.3.4 The Alajar Formation.

This formation, which lies outside the main study area (Fig. 2.10a. For location see Fig. 1.4), is exposed south of the village of Alajar [GR 0550 9450]. Criteria used for its definition are (a) a matrix of fine grained phyllite (Facies F_D) enclosing (b) variably sized phacoids of very pure orthoquartzites strongly attenuated parallel to strike (Facies S).

The formation is observed along a well exposed section which extends south from Alajar for some 2kms following the course of the Barranco de Alajar (Fig. 2.10a and Fig. 2.11). Immediately to the south of the village there is a complex zone of tectonic mélange (the Nivel-Mezcla of Crespo-Blanc 1989) with a thickness of several tens of metres. It consists of angular blocks of diorite, amphibolite, high grade gneisses, diopside bearing marbles and marbles that carry large nodules of wollastonite. The contact between this horizon and the Beja-Acebuches Amphibolites is an abrupt tectonic contact with the amphibolites outcropping in the footwall. The amphibolites themselves are mainly fine grained with coarser bands that become less important to the southwest. The Alajar Formation becomes dominant south of a line approximately following latitude 37°52'N. Primarily the rocks consist of fine grained phyllites with massive orthoquartzites easily identifiable making a prominent feature of upright blocks across the Sierras of Los Picos and Giralda striking at 090° (Fig.

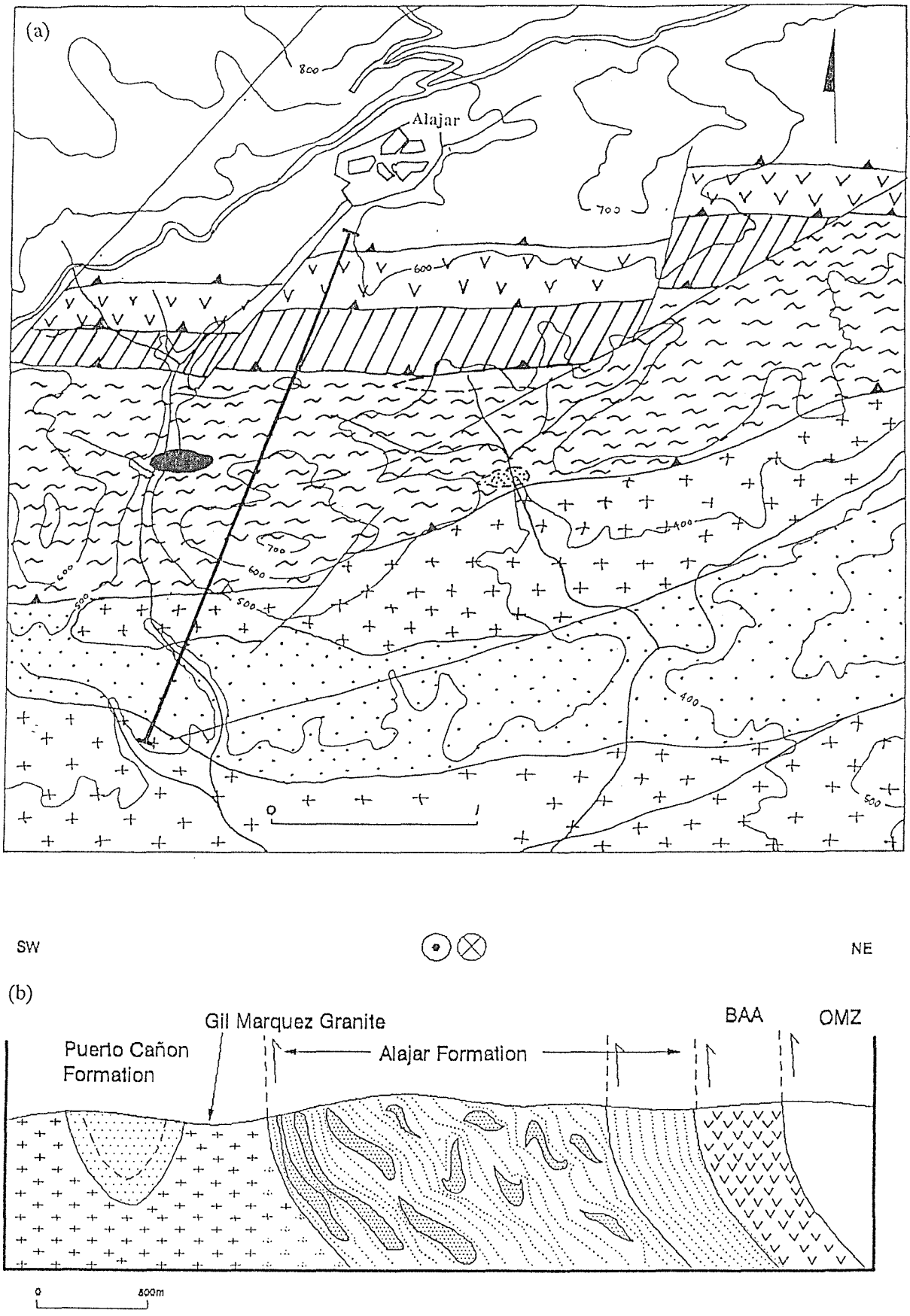

Figure 2.10 (a) Geology to the south of Alajar
(b) Cross section along the line indicated in (a).

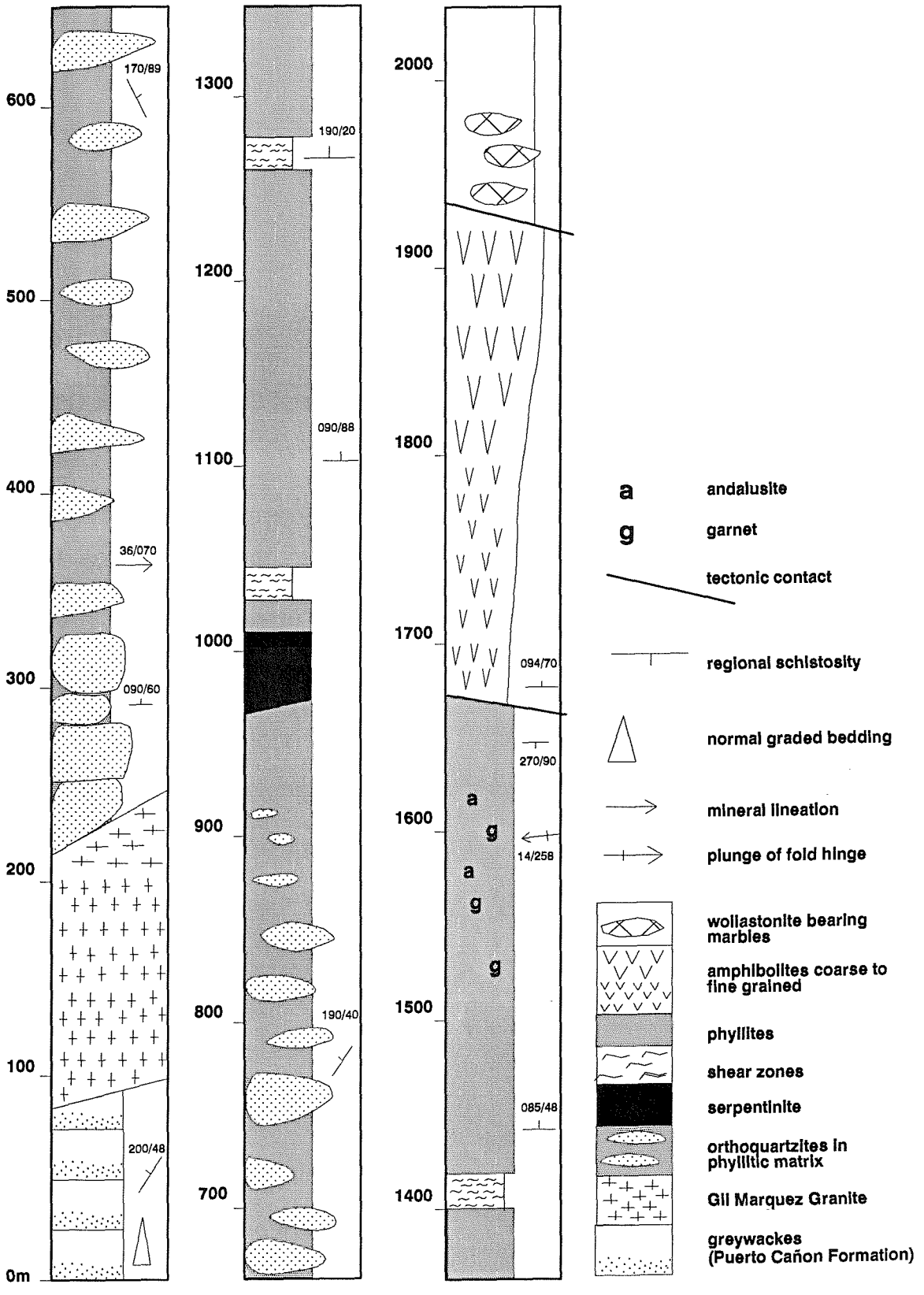

Figure 2.11 Graphic log across the Alajar Formation and the Beja-Acebuches Amphibolites to the south of Alajar.

3.3A). Continuing south the massive quartzites form continuous beds. Internally, however, they lack sedimentary features and have been reorientated into a sub-vertical attitude by shortening. Another feature, observed along this section, is the presence of thin bands of buff coloured, fine grained mylonites which form shear zones up to 15m thick (Fig. 2.4G). These zones of mylonitisation mark intra- as well as inter-formational ductile thrusts that occurred late in the deformational history. Sub-parallel to latitude 37°51'N the Alajar Formation is truncated by an intrusive igneous body, the Gil Marquez Granite (Bard 1969). This was intruded at a late stage in the deformation history as the margins display alignment of constituent minerals with the regional schistosity while internally the igneous fabric is undeformed (Crespo-Blanc 1989).

Three lithologies are described: (a) the phyllitic matrix, (b) massive orthoquartzites, (c) rare exotic material.

2.3.4.1 *The fine grained matrix.*

This is the dominant lithology of the Alajar Formation forming as a fine grained phyllitic matrix which alternates in colour between buff and black. It consists of ribbon quartz, muscovite, biotite and chlorite, the latter minerals being aligned within the plane of schistosity. Accessory minerals include rounded detrital tourmaline, zircon and minor apatite. Along the contact with the Beja-Acebuches Amphibolites, garnet and andalusite are observed occurring as syn-kinematic minerals. Microstructurally the matrix is similar to that of the Cumbres de Los Ciries Formation.

2.3.4.2 *The massive orthoquartzites (Facies S).*

These are composed of almost pure quartz with minor amounts of feldspar (plagioclase and orthoclase), together with muscovite and biotite mica. Colour varies from white to grey although occasionally black lenses are observed, sometimes associated with sulphide mineralisation. No recognisable sedimentary features such as graded bedding or flow direction indicators are recognised and they may represent dismembered fragments of original bedding. Size of individual lenses varies considerably from thin centimetric quartzite pebbles to phacoids that are greater than 30m strike-parallel length, the larger ones being generally sigmoidal in shape while the smaller ones are disc-shaped with either stubby or pointed noses (Fig. 2.4I).

2.3.4.3 *Exotic enclaves.*

Also located within this formation are rare, isolated blocks of exotic material. Three particular occurrences are observed. The first is a block of serpentinised ultramafic material measuring some 30-50 metres in length and with a width of up to 10 metres. It consists of an homogenous dark green serpentinite cropping out at [GR 0420 9275] (Fig. 2.10a) entirely enveloped within the fine grained matrix described above. A thin attenuated continuation of material that has

been altered to talc can be followed laterally for approximately 40m. Colourless to pale serpentine (65% modal proportion) has a fibrous pattern in crossed polars; magnesite (25%), a colourless low relief magnesium carbonate has high birefringence. Other minerals include iddingsite, tremolite, and opaque minerals. Whole rock geochemical analysis (appendix 2) shows that the rock consists of 41.84% MgO, 42.38% SiO_2, 9.41% Fe_2O_3. High Cr (1383 ppm) indicates that opaque minerals may include chrome spinel whereas high Ni (1919 ppm) is consistent with alteration of olivine to serpentine. The parent rock was therefore originally of dunitic composition. Subsequent to the discovery of this ultramafic phacoid several other similar phacoids have been located by a mapping programme carried out by the University of Aachen. These appear to lie along strike from the example mentioned above and describe a line of ultramafic material possibly describing a structural discontinuity (Giese *pers. comm.*).

Along strike from this ultramafic phacoid is an exposure of dark grey material [GR 0610 9300] previously identified by Apalategui *et al.* (1983 sheet 917 - Aracena) as an outlier of the Beja-Acebuches Amphibolite. This exposure consists of fragmented blocks of amphibolite and rare clasts of chert that may correlate with the Peramora Mélange Formation, described below. It is bounded on its northern border by an ≈10m wide zone of mylonites that form a thrust contact, parallel to the regional foliation, with the Alajar Formation. The blocks have been severely flattened and this makes recognition of their original shape difficult.

The third occurrence of exotic material is exposed along strike from the massive quartzites of the Sierra de Los Picos (Kühner *pers. comm.*). The exposure is composed of blocks of marble, entirely contained within the Alajar Formation and located about 10 metres north of the Gil Marquez granite (Fig. 2.10a - [GR 0640 9270]). These are impure carbonates which, in their turn, enclose blocks of quartzite. The matrix is multicoloured, ranging from white to black. Thin section demonstrates that grain size varies from fine to coarse, clasts of quartz are common. Calcite is the main carbonate and serpentine occurs as a pore filling mineral. Chlorite is present as a late stage mineral forming from the alteration of fine grained argillaceous material within the matrix.

2.3.5 The Peramora Mélange Formation.

This formation, which has not previously been described along the southern margin of the Ossa Morena Zone, is exposed along two belts: (a) the Los Ciries Antiform (Fig.2.2); (b) south of, and immediately juxtaposed against, the Beja-Acebuches Amphibolites. The main criterion for the definition of this formation is the identification of exotic blocks and phacoids within a sedimentary and volcaniclastic association corresponding to Facies C outlined above.

The matrix of the mélange is fine grained, recrystallised and has a distinctive green/blue colour that grades into grey on water-worn exposures. It consists predominantly of varying proportions of hornblende-actinolite-plagioclase-epidote and quartz, however, in some exposures the

matrix is dominated by phyllosilicate minerals. No original bedding is seen and the matrix and blocks are preserved as a chaotic association. Fig. 2.12A - I illustrates that the phacoids range from greywacke to fine grained metasediments, to large blocks of amphibolite.

2.3.5.1 *The Los Ciries Antiform.*

Exposure occurs along the banks of the Alcalaboza River extending southwestwards from the bridge at Peramora [GR 7498 9704] provides an extensive section across the hinge of the Los Ciries Antiform (Fig. 2.2). Here it can be seen that the Peramora Mélange Formation is structurally imbricated with the Cumbres de Los Ciries Formation within a folded imbricate thrust stack.

Fig. 2.12A -I illustrates representative blocks found in this formation. They consist mostly of quartzite and amphibolite, with a lesser proportion being composed of blocks of greywacke and fine grained metasediment. They are highly flattened within the regional schistosity although infrequently they retain an angular aspect (Fig. 2.12D & E). The matrix of the mélange is fine grained with a blue/green colour and is strongly foliated. Dominant matrix minerals are actinolite, visible as small light brown to green laths, and plagioclase occurring as small interlocking crystals, rarely showing lamellar twinning. Accessory minerals include small crystals of clinozoisite, and small crystals of quartz. Epidote and chlorite occur as late stage minerals.

Several localities are important in defining this formation:

1. [GR 7500 9720] Near the bridge at Peramora. (a) Large phacoids of amphibolite with strongly deformed internal foliation and flattened concordant to the external foliation. These range in size up to 5m in length. (b) Angular blocks of greywacke(?) contained within the recrystallised matrix (Fig. 2.12D & E). These are frequently spotted with rounded porphyroblasts of cordierite(?) that do not extend into the matrix. Clast size ranges from <2cm up to 25cm. (c) Attenuated clasts of red coloured siliceous chert. These are aligned parallel to the foliation and are frequently associated with rotated K-feldspar clasts. These 'flame' structures range in size from 3cm to 20cm and possess a sigmoidal internal foliation. (d) In the river bed there are attenuated, discontinuous blocks of fine grained quartzite. These are up to 50cm in length and have a light grey colour.
2. [GR 7452 9675]. Foliation parallel phacoids (up to 5m in length) around which the foliation deflects. These are composed predominantly of amphibolite blocks. In this locality there are numerous blocks within the fine grained matrix.
3. [GR 7420 9735]. Samples 9095-9103 were collected from this locality and clearly demonstrate the nature of the mélange. (a) sample 9095 is fine grained and green coloured. In thin section small clasts (>1cm) are visible. These are composed of uniformly sized crystals of amphibole, plagioclase, zoisite and small needles of actinolite ± quartz. Mineral orientation within these clasts is random, as opposed to the external foliation which is strongly orientated. (b) 9096, 9097, 9098 are red coloured and form as boudins within the main foliation. Thin section shows they are composed of

Figure 2.12
(A) Blocks of greywacke that have been strongly flattened in the matrix of the Peramora Mélange Formation. The matrix of the mélange has a characteristic green-blue colour [GR 7015 9920].

(B) Small clast of amphibolite contained within the matrix of the Peramora Mélage Formation along the Barranco del Ciego [GR 8110 9665].

(C) Rounded blocks of meta-gabbro within a fine grained matrix of dark grey fine grained mudstone. This sample is from the Alcaboza River [GR 8090 9640].

(D) and (E) Angular blocks of quartzite within the blue-green matrix of the Peramora Mélange Formation [GR 7490 9685] around which the S_{N2} foliation has been deflected.

(F) Thin section from the Peramora Mélange Formation showing complex isoclinal folding of an early schistosity.

(G) Blocks of foliated amphibolite contained within a fine grained dark grey coloured siltstone. These blocks are exposed in the hinge of an eastward plunging fold at [GR 7920 9755].

(H) Small clast of amphibolite which has been been flattened within the matrix of the Peramora Mélange Formation [GR 7030 9925].

(I) Clasts of metasediment with an early dark grey lamination (bedding?). Aslo visible on this exposure are porphyroblasts of andalusite around which the S_{N2} foliation is deflected. On the margins of the exposure the blocks become extremely flattened [GR 8140 9685].

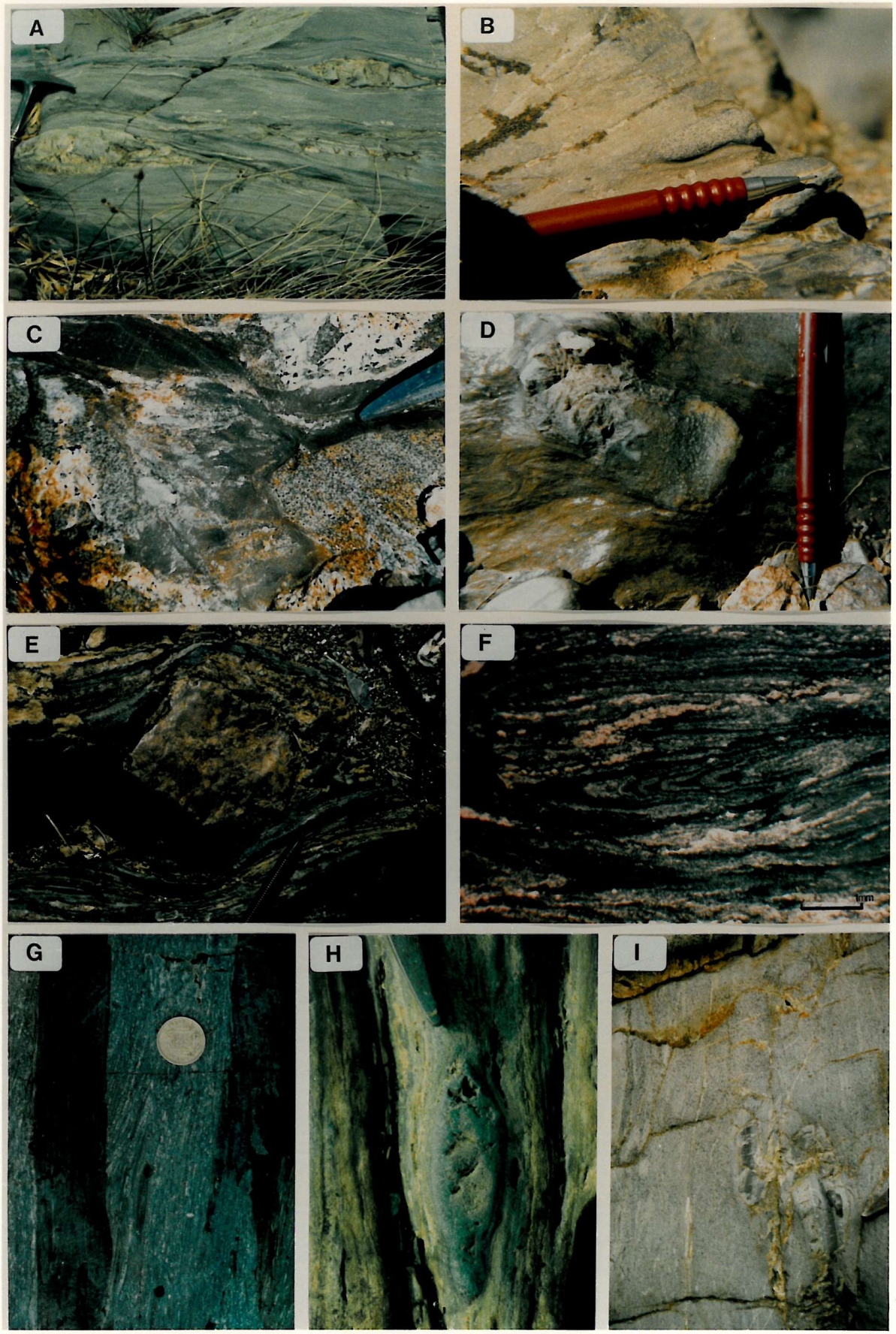
A
B
C
D
E
F
1mm
G
H
I

similar material as 9095. (c) 9099 is a fine grained quartzite with uniform grain size and within which ribbon quartz is developed. Quart c-axes are strongly aligned. (d) 9103 is from a quartzite boudin (≈20cm in length) and displays advanced quartz deformation fabrics (serrated grain boundaries, sub-grain development). In thin section it consists of quartz and large crystals of zoisite orientated with their long axes parallel to the foliation. Hand sample shows that the quartzite is black, grading into translucent in places.

2.3.5.2 *The Alajar mélange.*

This enclave is exposed immediately to the south of a thrust marked by an ≈10 metre wide zone of high strain mylonites [GR 0665 9305] (Fig 2.10a). Blocks include siliceous and amphibolitic material while the matrix varies in colour from dark grey to dark green and is fine grained. It supports a strong foliation although a mineral stretching lineation is not well developed. Dominant matrix minerals are actinolite and plagioclase with accessory quartz, epidote, Fe-Ti opaque minerals and zoisite.

2.3.5.3 *River sections.*

Streams cut perpendicular across strike (Fig. 2.2) and present a series of cross sections through the Peramora Mélange Formation as well as parts of the Beja-Acebuches Amphibolite and Cumbres de Los Ciries Formation. Two river sections are considered: (i) El Ciego, (ii) Rioja.

(i) Barranco del Ciego (Fig. 2.13). This river section extends from [GR 8140 9725] to [GR 8090 9640], trending approximately 060° passing through horses of sheared quartz-mica schist and mélanges. It flows from north to south across the Beja-Acebuches Amphibolites, the quartz schists of the Cumbres de Los Ciries Formation, and onto the Peramora Mélange Formation before joining the main northwestward flowing Alcalaboza River. The northern contact with the Beja-Acebuches Amphibolites is marked by a thin (≈3m) shear zone. The eastern continuation of the Peramora Mélange Formation was not investigated during the present study but the geological map by IGME (Apalategui *et al.* 1983) depicts it as being truncated by a brittle 060° trending fault located south of El Hurón. The rocks in this section show: (a) a well developed stretching lineation, (b) clear evidence for the chaotic nature of the mélange with lateral facies changes, and (c) sharp contacts between the Cumbres de Los Ciries Formation and the Peramora Mélange Formation. Examples of field relationships are shown in Fig. 2.12A,B,C,D,E,G,H. The principal features are: (i) [GR 8135 9680]: blocks that are flattened within the foliation (Fig. 2.12I). These consist of phacoids made up of fine grained metasediments each possessing an earlier schistosity (bedding?) which has been reorientated into the plane of the later foliation. This exposure represents a change in facies within the mélange. These sediments remain chaotic and in this sense approximate to Facies C. They are,

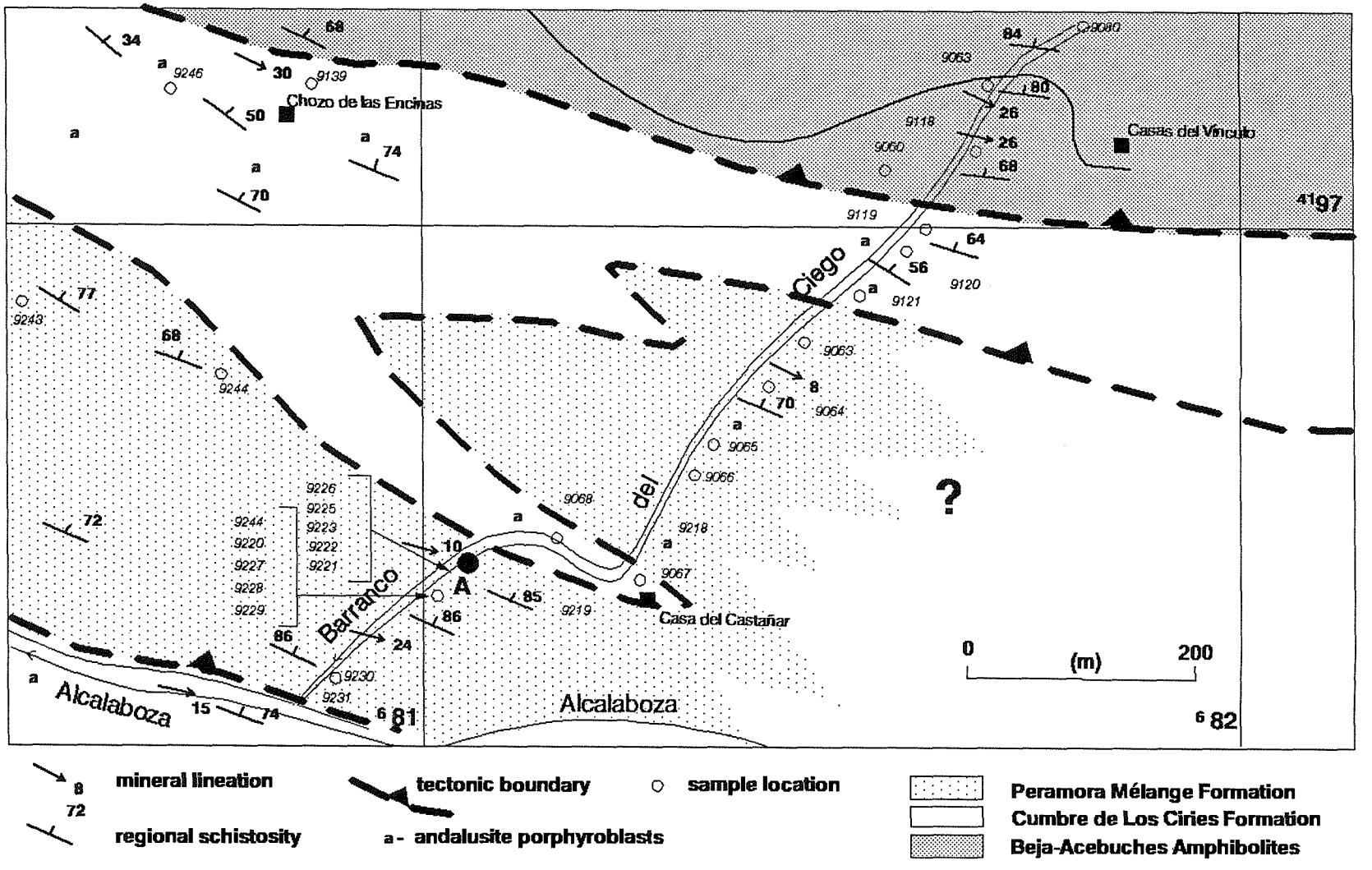

Figure 2.13 Barranco del Ciego section

however, composed of different clast types within a fine grained pelitic matrix. Cordierite porphyroblasts up to 1mm are commonly developed within the matrix. Clasts and phacoids such as these are common along this section: (ii) [GR 8145 9697]. A large phacoid (≈ 5m in length) of black quartzite is, once again, aligned parallel to the regional foliation. (iii) [GR 8125 9660]. A clear boundary between a sliver of Cumbres de Los Ciries-type lithology and Peramora Mélange-type lithology (Fig. 3.5G). The matrix of the former displays the characteristic schistose sheen and quartz augen, while the latter is composed of blocks that often display randomly orientated crystals of amphibole and plagioclase. The boundary between the two lithologies is clearly seen and is strongly welded. (iv) [GR 8108 9663]. Small clasts of cherty material preserved within a red siliceous horizon and rotated into parallelism with the regional schistosity. (v) [GR 8103 9658]. A small clast of amphibolite wholly contained within a fine grained matrix (Fig. 2.12B).

Samples 9221, 9225, were collected at locality A (Fig. 2.13). Sample 9221 has a fine grained matrix with a blue/green colour in hand specimen. In thin section (Fig. 3.14G) it is composed of essential hornblende, actinolite and plagioclase with quartz, epidote and opaque minerals occurring as minor components. Colourless actinolite forms within the fine grained matrix as small elongate crystals orientated parallel to the foliation, and also as grains within feldspar ribbons. Plagioclase (andesine to bytownite) forms both as small matrix crystals and as aggregates contained within the matrix. In the latter case they have well developed deformation twins and there is evidence of brittle fracturing of the crystals. Quartz is present in small quantities. Also contained within the matrix are larger clasts of colourless amphibole which have a high relief compared to plagioclase. Chemically, the amphiboles are transitional between actinolite and hornblende (appendix 5). Chlorite occurs both as a primary mineral and as a late stage mineral replacing the amphibole. In the former case it forms as small green laths in the matrix, orientated parallel to the foliation. The mineral assemblage of this rock is thus hornblende-actinolite-plagioclase (An_{40}- An_{60})-epidote-chlorite-quartz with the opaque minerals chromite and ilmenite forming as amorphous accessory phases.

Sample 9225 consists of a small block of amphibolite encased in a fine grained matrix that is composed of very fine grained actinolite, plagioclase, phyllosilicates (biotite) and quartz. Accessory epidote minerals (zoisite, clinozoisite and epidote) occur together with opaque minerals. In hand specimen it is clearly seen that the amphibolite clast occurs as a discrete block (Fig. 2.12B), however in thin section the margins of the clast are diffuse and entrained within the matrix suggesting diminution of grain size during deformation. Actinolite together with hornblende are the main matrix minerals. These occur as a mesh of colourless to tan elongate crystals preserved parallel to the main foliation. Within the matrix of the amphibolite clast the amphibole consists of hornblende and actinolite, while microprobe analysis of plagioclase from stratigraphically similar rocks show that they are mainly andesine to labradorite. A relict granoblastic texture within the clast, which has been reorientated during deformation, is preserved. Flattening has resulted in rotatation of individual

grains and imposed a weak foliation. Late stage alteration of the plagioclase to sericite has occurred and chlorite is present also as a late stage mineral. Other clasts of amphibolite are highly flattened within the foliation; some have been attenuated and individual clasts of plagioclase have been released into the matrix (Fig. 3.14G).

Green coloured horizons (Fig. 3.5E) are abundant along the Barranco del Ciego section. A thin section of this material shows that it consists of hornblende, actinolite, plagioclase and epidote with sphene and opaque minerals as accessories. The mineral assemblage and the basic geochemistry (appendix 2) suggests that the original deposit may have been volcaniclastic in nature. These green coloured horizons are set in a dark grey, fine grained matrix composed of actinolite, hornblende and plagioclase.

(ii) Barranco de Rioja.

This river section (Fig. 2.14) extends from [GR 8025 9787] to [GR 7908 9726] and here too blocks and clasts of exotic material are common. The section is especially important with respect to the development of a mylonitic fabric (Chapter 3). At one exposure [GR 7922 9758] a D_3 fold plunges gently to the east. Within the foliation, and folded around the F_3 fold hinge, blocks of amphibolite are preserved within a fine grained phyllosilicate-rich matrix (Fig 2.12G). These blocks possess an early folded fabric clearly demonstrating that the mélange was generated post D_1. A further example, which clearly demonstrates the existence of amphibolite clasts within a fine grained muddy matrix, is observed at the end of the section. In this example the meta-igneous blocks are rounded, and deformation is minimal.

Along strike from the Barranco de Rioja, [GR 7879 9735], is a large enclave of alternating coarse grained gabbros and fine grained basalts (Fig. 3.5A). This association consists of steeply dipping sheets orientated parallel to strike. Coarse grained igneous material such as this is seen in a number of places along the boundary of the Beja-Acebuches Amphibolites and the Cumbres de Los Ciries Formation. This particular enclave of coarse/fine grained meta-igneous material may represent a large phacoid of sheeted dyke complex removed from its original position and rotated into parallelism with the regional schistosity during shearing.

2.3.6 The Beja-Acebuches Amphibolites.

These rocks have been the subject of several studies. Apalategui *et al.* (sheet 916-Aroche 1983) describe this sequence in terms of grain size being coarse grained in the north becoming fine grained southwards. Crespo-Blanc (1989) attributes grain size reduction to a major ductile shearing event (The South Iberian Shear Zone) that accompanied retrogressive metamorphism from amphibolite facies to greenschist facies. The transition between coarse and fine grained amphibolite is gradual, occurring over several tens of metres, but is complicated by cross cutting veins and dykes

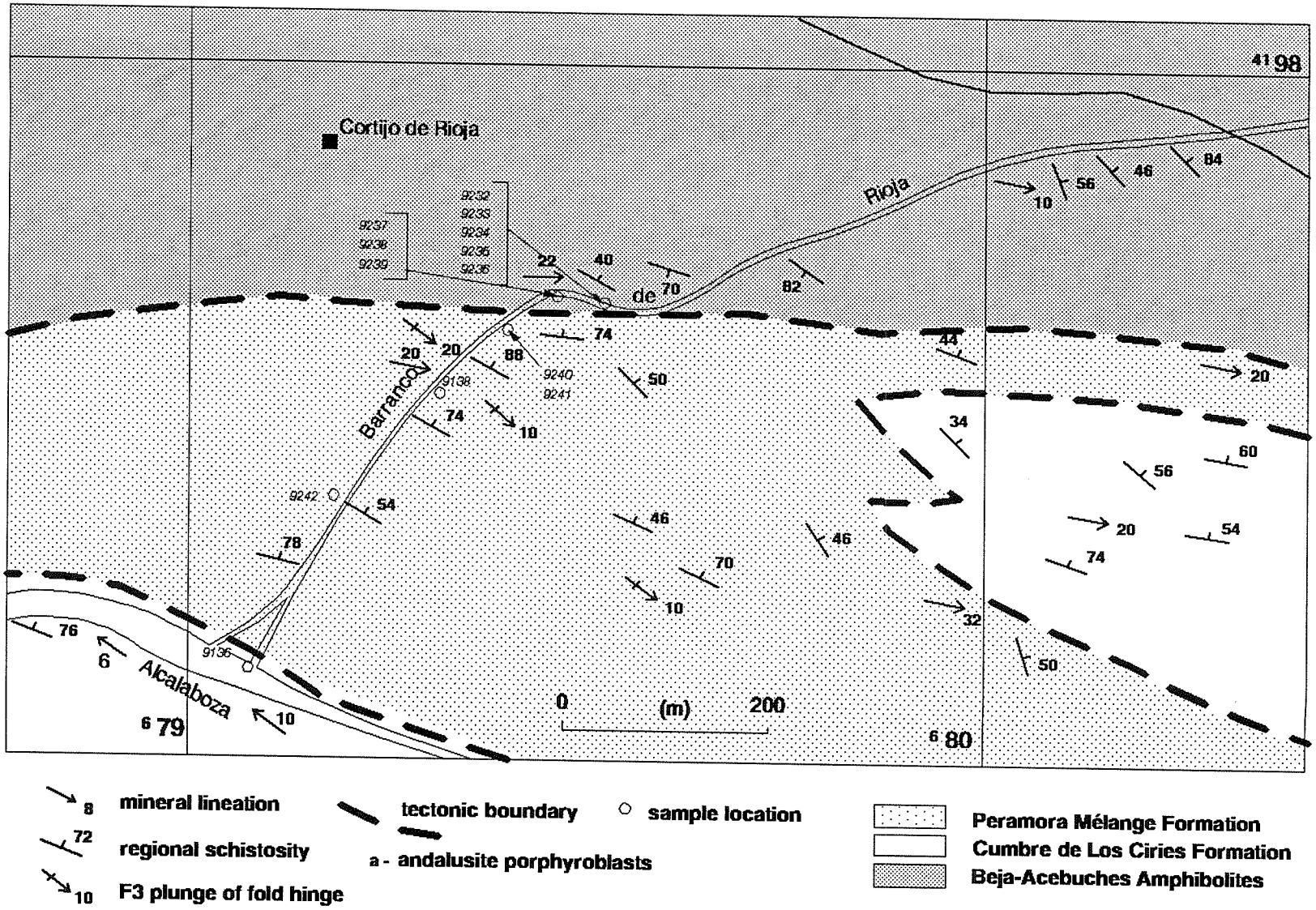

Figure 2.14 Barranco de Rioja section.

of acidic material which have been subjected to high strain and are now preserved as mylonites.

The coarse grained amphibolites are dark coloured with lighter foliation-parallel lenses of plagioclase feldspar. Often the rock has a banded appearance due to the alternation of plagioclase and amphibole rich layers which emphasise a strong regional schistosity dipping towards the NW. The fine grained amphibolite has the same proportion of amphibole and plagioclase as the coarse grained amphibolite although it may have been retrogressed to greenschist facies with the amphibole being predominantly composed of actinolite. Epidote minerals become increasingly important in the fine grained amphibolites.

2.3.6.1 *El Hurón [GR 8435 9664].*

This locality is situated on the northern margin of the coarse grained amphibolite. It is difficult to define consistent banding because the rocks have suffered extensive late stage brittle deformation, although in selected samples (generally preserved in the wall rocks of the deserted village of El Hurón) the original banding is observed. This compositional banding, defined by dark and light coloured intercalations, is caused by a predominance of plagioclase feldspar or amphibole respectively and all rock types possess a strong schistosity caused by the alignment of minerals into the S plane. Within this association several types of amphibolite exist: (i) coarse grained melanocratic amphibolites, (ii) coarse grained leucocratic amphibolites and (iii) fine grained dark coloured amphibolites.

(i) Coarse grained melanocratic amphibolites.

These are composed of essential hornblende (50-55%), with small inclusions of quartz and plagioclase, and plagioclase (40-45%) with a granoblastic texture; the boundaries between crystals generally form triple junctions indicating an equilibrium assemblage (Fig. 2.8H). Abundant small grains of magnetite and ilmenite also occur. Plagioclase composition ranges from An_{50}-An_{70}. Sphene is a common accessory mineral forming euhedral crystals along crystal boundaries or, less frequently, as small inclusions within the hornblende. Other accessory minerals include apatite and opaque minerals. Secondary alteration affects these rocks mostly in the form of sericitisation of the plagioclase and chlorite rarely forms as a late stage mineral.

(ii) Coarse grained leucocratic amphibolites (Fig. 2.8F).

This rock type has a predominance of plagioclase (often 70-80%) with a composition of An_{50}-An_{60}. Once again the rocks possesses a granoblastic equilibrium texture and a strong mineral orientation. Plagioclase is frequently altered to sericite.

(iii) The fine grained dark coloured amphibolites (Fig. 2.8E & F and Fig. 3.3H).

These are in close association with the coarse grained amphibolites and may represent dykes that were originally basaltic in nature. In thin section they are composed of fine, equigranular amphibole (50-55%) and plagioclase (40-45%), and possess a well defined mineral orientation.

2.3.6.2 *Puerto Cañón [GR 7755 9905].*

This locality provides clear evidence of disruption of the amphibolites after the imposition of an L-S foliation (Fig. 3.3). The dominant coarse grained amphibolite is cross cut by both basic and acidic dykes injected during sinistral shearing. Basic dykes are predominantly composed of mafic minerals with crystals of plagioclase entrained in the foliation. The acidic dykes are granitic in composition with essential quartz, potassium feldspar and biotite. Plagioclase, zircon, apatite and opaque minerals occur as accessory minerals. There is a myrmekitic texture between vermicular quartz and feldspar indicating that temperature was relatively high during the breakdown of feldspar. The rock has a well developed S-C structure visible in exposure indicating that intrusion of the acidic magma occurred pre- or syn-deformation.

2.3.6.3 *Aroche Section [GR 7682 0000] - [GR 7635 9920].*

On the northern boundary of the Beja-Acebuches Amphibolites coarse grained amphibolite is tectonically juxtaposed against granites, marbles and quartzo-feldspathic gneisses of the hanging wall rocks of the Ossa Morena Zone. The contact is visible as a thrust that has resulted in disruption and brecciation of the amphibolite. An early foliation is preserved within blocks of amphibolite that are suspended within a foliated granitic matrix. In thin section the coarse grained amphibolite is composed of essential amphibole and plagioclase and these are contained within a well developed S-schistosity. Movement direction is indicated in both the amphibolite and the granite by a mineral lineation defined by the orientation of plagioclase, quartz and amphibole within the plane of foliation.

Throughout this section there are a number of cross cutting dykes that are themselves foliated. These are mainly acidic in composition, consisting of quartz, alkali feldspar, muscovite, biotite and accessory tourmaline, apatite, opaque minerals and zircon, although towards the southern end of the section several gabbroic lenses occur. These acidic dykes are possibly related to the granite that is in thrusted contact with the northern boundary of the amphibolites. Associated with them are thin (10cm wide) vein arrays of aplitic dykes that consist mainly of quartz and feldspar. These too disrupt the foliation seen in the amphibolites and often contain small (up to 5cm) xenoliths of amphibolite [GR 7670 0063]. At this locality a 5m thick, light coloured rock marks a shear zone within which the minerals have been stretched parallel to the main foliation forming quartz ribbons.

Towards the southern boundary of the amphibolites, where they are juxtaposed against the underlying quartz-schists, the rocks become predominantly fine grained due to syn-kinematic grain size reduction. This transition is accompanied by the development of a well defined mineral stretching

lineation contained within the regional schistosity.

2.4 Summary.

(A) The Puerto Cañon Formation consists of a narrow belt of sedimentary rocks located in the immediate footwall of the Beja-Acebuches Amphibolites. It is composed of an association of immature coarse grained arenites and fine grained mudstones and siltstones. Only one clear set of structures is preserved, this is a bed parallel cleavage with associated tight mesoscopic folds. Its relationship with the structurally underlying formations is uncertain, due to a certain similarity in structural style, and it has been suggested (Crespo-Blanc, 1989) that on the basis of the lithological and structural variations as described above, this formation may be, or was originally, in unconformable contact with them, although nowhere can this contact be seen. An alternative interpretation is that the Puerto Cañon Formation represents a facies variation of the La Giralda Formation. The main argument against this is that lithologies within the Puerto Cañon Formation are sufficiently different to have experienced a completely different sedimentary history ie immature turbidites and coarse grained arenites indicate a more proximal source for sediments than is seen within the La Giralda Formation. Therefore similarities in the deformational history (Chapter 3) may indicate later deposition within the same stress regime. A single sample collected from this formation yields a basal Givetian to early Famennian age.

(B) The La Giralda Formation consists of fine grained sedimentary rocks composed of arenites, slaty mudstones, siltstones and tuffaceous material. Low grade metamorphism (up to biotite grade) has affected all lithologies within the sedimentary pile and deformation has resulted in reorientation of beds with concommitant destruction of sedimentary fabrics, although where present, graded bedding predominantly indicates normal younging. A marine environment of deposition is inferred by a turbiditic succession within which acritarchs are found. Zircon crystals extracted from the sediments indicate that sediment supply may have been both from volcanic and terrigenous sources. Palynomorphs recovered from black slates within the section (Lake *thesis in prep*) place this formation in the late Givetain to early Frasnian stages. Sparse spore preservation, together with the fine grained nature of the lithologies, indicates a distal provenance possibly within a relatively deep marine foreland basin.

(C) The Cumbres de Los Ciries Formation forms a thick sequence of quartz-mica schists ranging from 5-10 kms in outcrop width. Sedimentary features have been entirely overprinted although the phyllosilicate rich nature of the rock indicates that the protolith must have been composed predominantly of fine grained mud. Rounded accessory tourmaline and zircon may suggest the presence of a detrital component from a granitic source. Contained within the foliation are fragmented quartzites, phacoids of basic material and thin layers of mylonitised quartzite. These may exhibit up to three cleavages.

A narrow belt of low-pressure/high-temperature metamorphism exists on the southern boundary between the Beja-Acebuches Amphibolites and the Cumbres de Los Ciries Formation.

The regional association of arenites and, later in the sedimentary history, arenites and marine mudstones (La Giralda Formation), would suggest that the sedimentary environment was deep water marine, dominated by a background sedimentation of fine grained clastic material into which turbidites were periodically introduced. Fragmented quartzites suggest that the original sediment was possibly deposited as a basinal mud with periodic influxes of coarser grained sand-rich sediments.

(D) The Alajar Formation is defined on the basis of massive, erosion-resistant sigmoidal and lensoid orthoquartzite blocks which are enveloped within a fine grained phyllitic to schistose matrix, and rare exotic material, including an ultramafic phacoid, marble and amphibolitic blocks. There are two distinct sedimentary associations: a distal mud/silt facies and a more proximal sandstone facies. Sedimentologically, both the matrix and the quartzite phacoids represent deposits that must have been mature. The fine grained phyllite may originally have been deposited either as a distal deep water mud within an oceanic basin or on a starved continental margin. The quartzites may in turn represent periodic influxes of mature sands as grain flow deposits that accumulated close to the continental margin. An oceanic environment is inferred by their close proximity to oceanic crust, however, no graded bedding or other sedimentary features are apparent. Garnet and andalusite occur as syn- to post-deformational porphyroblasts within the fine grained matrix on the northern boundary of the formation, juxtaposed against the Beja-Acebuches Amphibolites.

Several methods of emplacement of the exotic enclaves are possible. These enclaves may be a response to tectonism, introduced along fault planes that developed during structural evolution (Saleeby 1984). Alternatively they may have a sedimentary origin, being part of a mélange that developed during collision between the Ossa Morena Zone and the South Portuguese Zone. In the latter situation one might expect to find more occurrences of similar enclaves. Intense flattening suffered by all the exotic phacoids, coupled with high strain seen across the region as a whole points towards a combination of the two hypotheses, ie they represent blocks introduced into a receiving basin by the shedding of debris, and have subsequently been reworked by tectonic processes. A possible source for the marble blocks may be the high grade marbles which crop out in the hanging wall of the Ossa Morena Zone. This infers that the high grade material of the Jabugo Almonaster Zone was thrust over the amphibolites, shedding debris as thrusting progressed. However, this hypothesis is limited by the rarity of high grade material present within the Alajar Formation. A possible source for the ultramafic material may be the overthrusting Beja-Acebuches Amphibolites although, once again, the rarity of similar material may make this suggestion tentative.

(E) The Peramora Mélange Formation occurs as a volumetrically significant formation consisting of large phacoids, varying in composition from quartzites through to amphibolites. These

are contained within a fine grained matrix. The formation has been identified both to the south of Alajar and south of Aroche and imbrication with the Cumbres de Los Ciries Formation indicates a complex structural and metamorphic history. It is suggested here that the Peramora Mélange Formation may have been deposited during southward obduction of oceanic crust and was subjected to post-depositional deformation. Several facies are recognised within this formation, ranging from chaotically deposited blocks within a fine grained basic matrix, to blocks of metasediment preserved in a phyllosilicate rich matrix. In all cases, however, the matrix has been recrystallised during post-emplacement metamorphism. The association of blocks of the size described within a basic matrix suggests a considerable volcaniclastic input that was fed by a basic source. Such a source may be represented by the Beja-Acebuches Amphibolites. The occurrence of metasedimentary clasts within a pelitic matrix is more problematic. These latter deposits are proportionally less well represented than the basic material and may have been derived from a marginal source, although obliteration of sedimentary structures during deformation, as well as modification during metamorphism, makes any interpretation as to a source, tentative.

The final tectonic episode to affect the region was a period of minor igneous activity. During this time both acid and basic igneous rocks were intruded cutting across the regional schistosity. Similar rocks seen in Portugal are believed to represent feeder dykes to the Iberian Pyrite Belt volcanics (Oliveira *in press*). Undeformed basic dykes occur in the core of the Los Ciries Antiform cross-cutting the foliation. They can be up to 5m in width and have a random mineral orientation (mainly amphibole and plagioclase). Acidic dykes are also seen in the core of the Los Ciries Antiform and throughout the Aroche-El Mustio section although these have been almost completely weathered to clay minerals.

Chapter 3: Structure.

Abstract

Docking between the Ossa Morena Zone and the South Portuguese Zone resulted in imbrication of different lithotypes. Discussion concentrates on the domains that together comprise the Oceanic Exotic Terrane. These are the Beja-Acebuches Amphibolite Domain, the Northern Metasedimentary Domain, the Alajar Domain, the Central and the Southern Metasedimentary Domains. The Alajar Domain, located outside the main study area is correlated along strike with the Northern Metasedimentary Domain. These domains comprise a folded imbricate thrust stack. Micro- and macrostructures are consistent with sinistral strike-slip ductile shear within an overall transpressive regime. Three clear phases of deformation are observed in the Central Metasedimentary Domain, the first and second phases producing pressure solution cleavages while the third is related to strike normal shortening with only local cleavage production.

3.1 - Introduction

Throughout the Pulo do Lobo Antiform three discrete fabrics are dominant (Silva 1989, Oliveira *in press*). These include two early pervasive cleavages, S_1 and S_2 that have been folded by F_3 folds. Crespo-Blanc (1989) argued that all the elements are contained within a continuum of a single phase of deformation where contrasting units were assembled within a single tectonic mosaic during the Hercynian orogeny.

Six distinct structural domains (Fig. 3.1) are defined within and adjacent to the Oceanic Exotic Terrane:

A. The Aracena metamorphic Domain.

B. The Beja-Acebuches Amphibolite Domain.

C. The Northern Metasedimentary Domain.

D. The Alajar Domain (Fig. 2.8).

E. The Central Metasedimentary Domain.

F. The Southern Metasedimentary Domain.

These structural domains are separated by major discontinuities, the boundaries approximating to those of lithological formations. The most significant boundary is that separating the Ossa Morena Zone from the Oceanic Exotic Terrane which is preserved as a ductile shear zone paralleling the Beja-Acebuches Amphibolites. A formational boundary is seen in the hinge of the Los Ciries Antiform where the Peramora Mélange Formation and the Cumbres de Los Ciries Formation are juxtaposed as imbricate tectonic slices, a process that may have occurred during docking between the Ossa Morena Zone and the South Portuguese Zone.

Lack of marker horizons, together with intense strain induced grain size reduction and

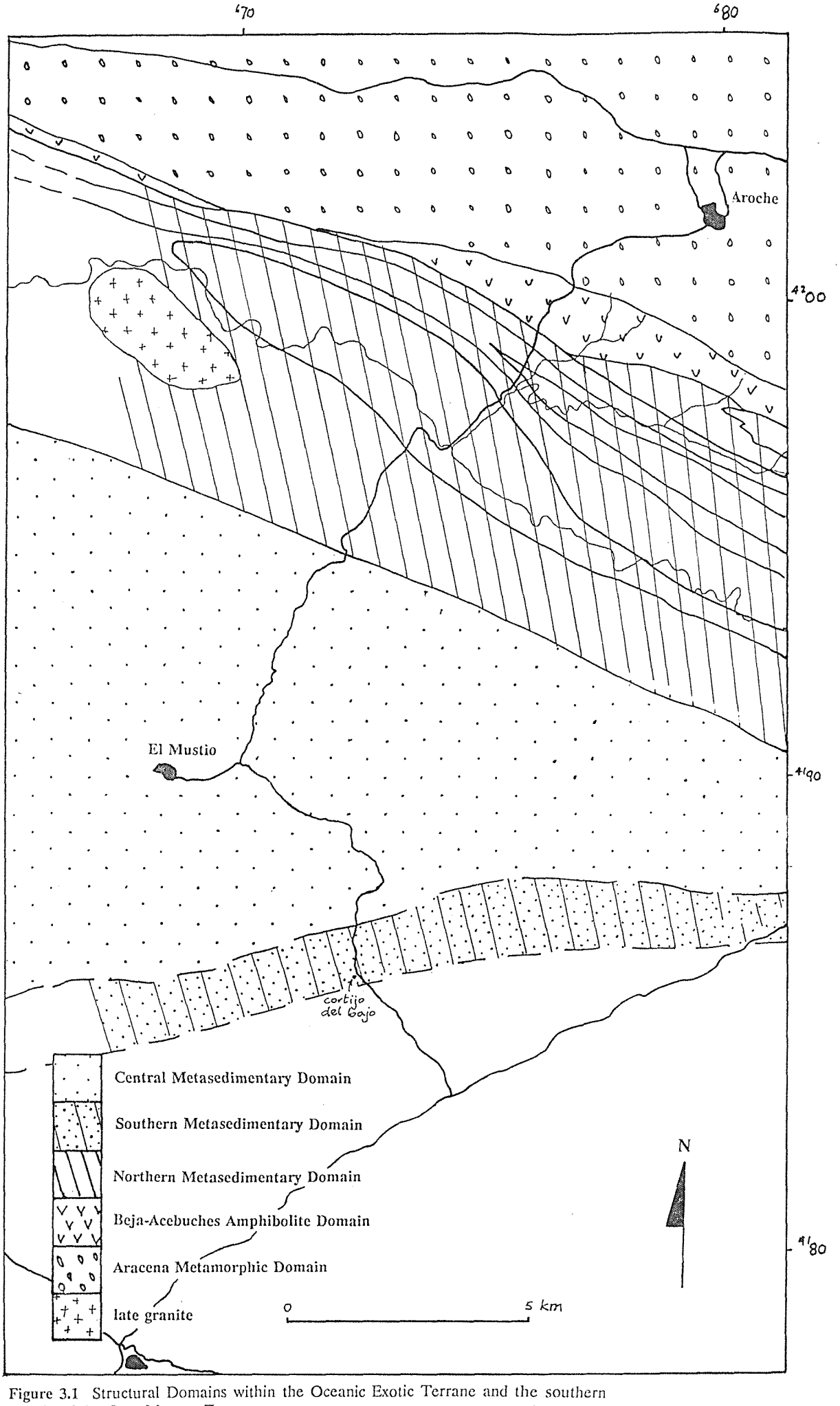

Figure 3.1 Structural Domains within the Oceanic Exotic Terrane and the southern margin of the Ossa Morena Zone.

recrystallisation related to ductile deformation, make it difficult to quantify the strain. Field data and macrostructural analysis suggest that considerable strike slip movement may have occurred. The main aims of this chapter are to:

(a) Describe the structure and deformational styles within domains.

(b) Assess the relationship of ductile deformation within the Beja-Acebuches Amphibolites to that observed in contiguous units.

(c) Propose mechanisms of juxtaposition of the various units within a transpressive regime.

Correlation of deformation events across tectonic boundaries is complicated by lithological variation, consequently the nomenclature used throughout the text is designed to separate deformational events recognised within each domain (Fig. 3.2).

3.2 The Aracena Metamorphic Domain.

The Aracena Metamorphic Domain lies to the north of the study area and is only briefly described to appraise the regional framework. Three sub-domains are identified: the El Cubito Zone (Bard 1969), the Navahermosa-Castaño del Robledo Zone and the Jabugo - Almonaster Zone (Fig. 1.4). Crespo-Blanc (1989) describes three phases of deformation which developed under differing metamorphic conditions. In the El Cubito Zone and the Navahermosa-Castaño del Robledo Zone the first deformation is seen as a syn-metamorphic foliation associated with SW verging isoclinal folds that formed during greenschist facies metamorphism. The first foliation in the Jabugo-Almonaster Zone, however, is axial planar to a SSW verging overturned antiform developed under granulite facies conditions. The regional second foliation is accompanied by retrograde metamorphism in the Jabugo-Almonaster Zone and a notable increase of ductile deformation towards the boundary with the Navahermosa-Castaño del Robledo Zone. The vergence and younging directions within the Jabugo-Almonaster Zone are consistent with the development of a synformal anticline, the southern limb of which has been 'detached' during the formation of a tectonic mélange which delineates the northern border of the Beja-Acebuches Amphibolites. The third phase of deformation, which may have occurred during Upper Viséan to Middle Westphalian times (Silva *et al. in press*), was accompanied by low grades of metamorphism and widespread upright chevron folding together with pressure solution cleavage. During this phase the main antiform of the Aracena Massif was formed and the earlier structures were steepened to their sub-vertical orientation.

3.3 The Beja-Acebuches Amphibolite Domain.

This unit partly contains the regionally significant tectonic boundary, the South Iberian Shear Zone (Crespo-Blanc & Orozco 1988), and may correspond to the suture between the Ossa Morena Zone and the Oceanic Exotic Terrane. The South Iberian Shear Zone is marked by a thick belt of mylonites which transports the Aracena Metamorphic Domain southwards over the younger Oceanic Exotic

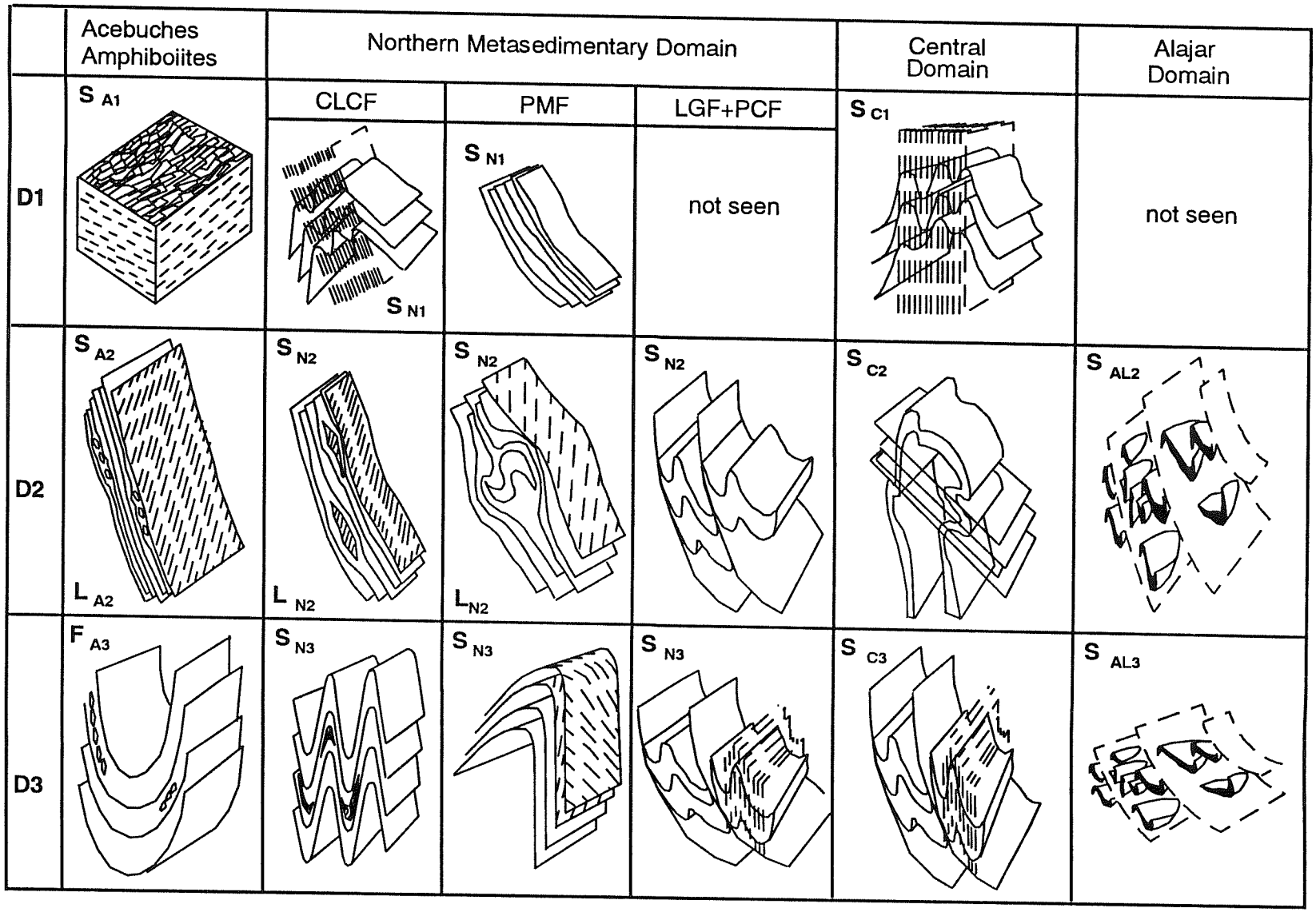

Figure 3.2 Correlation between structural elements identified within the Beja-Acebuches Domain and Oceanic Exotic Terrane.

Terrane. High temperature/low pressure metamorphism evolved into retrogressive greenschist facies, the latter accompanying the main phase of ductile deformation along the shear zone (Crespo-Blanc 1989). Principal structural features (Apalategui *et al.* 1983; Crespo-Blanc & Orozco 1988; Crespo-Blanc 1989), include: (a) in the coarse grained amphibolites there is a well developed L-S fabric that becomes an L-fabric southwards. This fabric corresponds to the regional mylonitic schistosity, S_m, that contains a stretching lineation, L_e (Crespo-Blanc 1989), (b) a late phase of folding, (c) sinistral NE-SW faults displacing all units.

During the present study fieldwork was concentrated in several places: south of Alajar [GR 9480 9370], SW of Aroche [GR 7680 9995], east of Almonaster la Real [GR 9535 9470], and between El Hurón [GR 8435 9664] and Puerto Cañón [GR 7638 9925] (Fig. 1.4).

Two main phases of deformation are observed throughout the amphibolites. In this study these are labelled D_{A1} and D_{A2} to differentiate them from deformational events observed in other domains (Fig. 3.2). The first phase of deformation, D_{A1}, is recognised as a foliation within the coarse grained amphibolites, observed north of Almonaster la Real, [GR 9535 9470], at the northernmost end of the Aroche section, at El Hurón and below the Cortijo del Puerto Cañón [GR 7755 9905]. It consists of an S-foliation composed of amphibole and plagioclase that has been reorientated by subsequent deformational events, a feature that obscures any consistency in its orientation. The nature of this foliation is clearly seen at [GR 7638 9925] (Fig. 3.3C & F). Here, the early foliation has been reorientated by the intrusion of acid and basic dykes. This phase of deformation is thus difficult to measure.

North of Almonaster la Real (Fig. 1.4) two different lithologies form a distinct banding up to several centimetres thick. Quesada *pers. comm.* and Crespo-Blanc (1989) suggest that these represent intrusive sheets associated with an oceanic dyke complex. The dykes have been modified by recrystallisation to form L-S tectonites and in places have been disrupted by faulting. Fragments of banded amphibolite are only locally preserved. At El Hurón several different lithologies occur (Fig. 3.3H) including coarse and fine grained mafic rocks, as well as fine grained plagioclase rich material. Fabrics preserved within lacunae of less deformed material, which include randomly orientated amphibole and plagioclase as well as granoblastic embayment textures, may represent an original igneous texture.

In places, syn-kinematic acid and mafic dykes intrude the amphibolites. At a river exposure near Puerto Cañón [GR 7638 9925] the dykes truncate an early fabric that is preserved within fragmented blocks of amphibolite (Fig. 3.3C-F). The dykes are orientated at a steep angle to the ambient foliation. S-C structures and rotated foliation (Fig. 3.3D) within the acidic dykes, and sheared plagioclase porphyroclasts within the basic dykes indicate sinistral shear parallel to the dyke margins (Fig. 3.3E). Fig. 3.4a shows that the sheared dykes are orientated at varying angles to the regional foliation. They may form as a set of conjugate Riedel shears with complimentary P shears within the overall

Figure 3.3

(A) Sierra de Los Picos, south of Alajar. This photograph illustrates the large strike-parallel quartzite phacoids which are supported within a sheared fine grained phyllitic matrix. (N - S is left to right of the photo respectively)

(B) Boundary between the Ossa Morena Zone and the Beja-Acebuches Amphibolites south of Alajar [GR 7675 9990]. The granites of the Ossa Morena Zone are thrust over the amphibolites with the production of a tectonic mélange.

(C) Feathered edge of a sherared basic dyke which cross-cuts amphibolite blocks. The blocks possess an early foliation and the dykes also possess a well developed schistosity. [GR 7755 9905].

(D) Intensely sheared acidic material cross-cutting an early foliation in amphibolite at Puerto Cañon [GR 7755 9905].

(E) Sinistrally sheared plagioclase porphyroblasts within a basic dyke. [GR 7755 9905].

(F) Chaotically disrupted blocks of amphibolite at Puerto Cañon [GR 7755 9905] which possess an early foliation. The cross-cutting acidic dykes are also foliated.

(G) Strong mineral lineation in the Beja-Acebuches Amphibolites at in the Beja-Acebuches Amphibolites at Almonaster la Réal marked by attenuated plagioclase and amphibole [GR 9480 9370].

(H) Beja-Acebuches Amphibolites at El Hurón [GR 8435 9660] showing the intensely sheared nature of bands of intercalated melanocratic and leucocratic material.

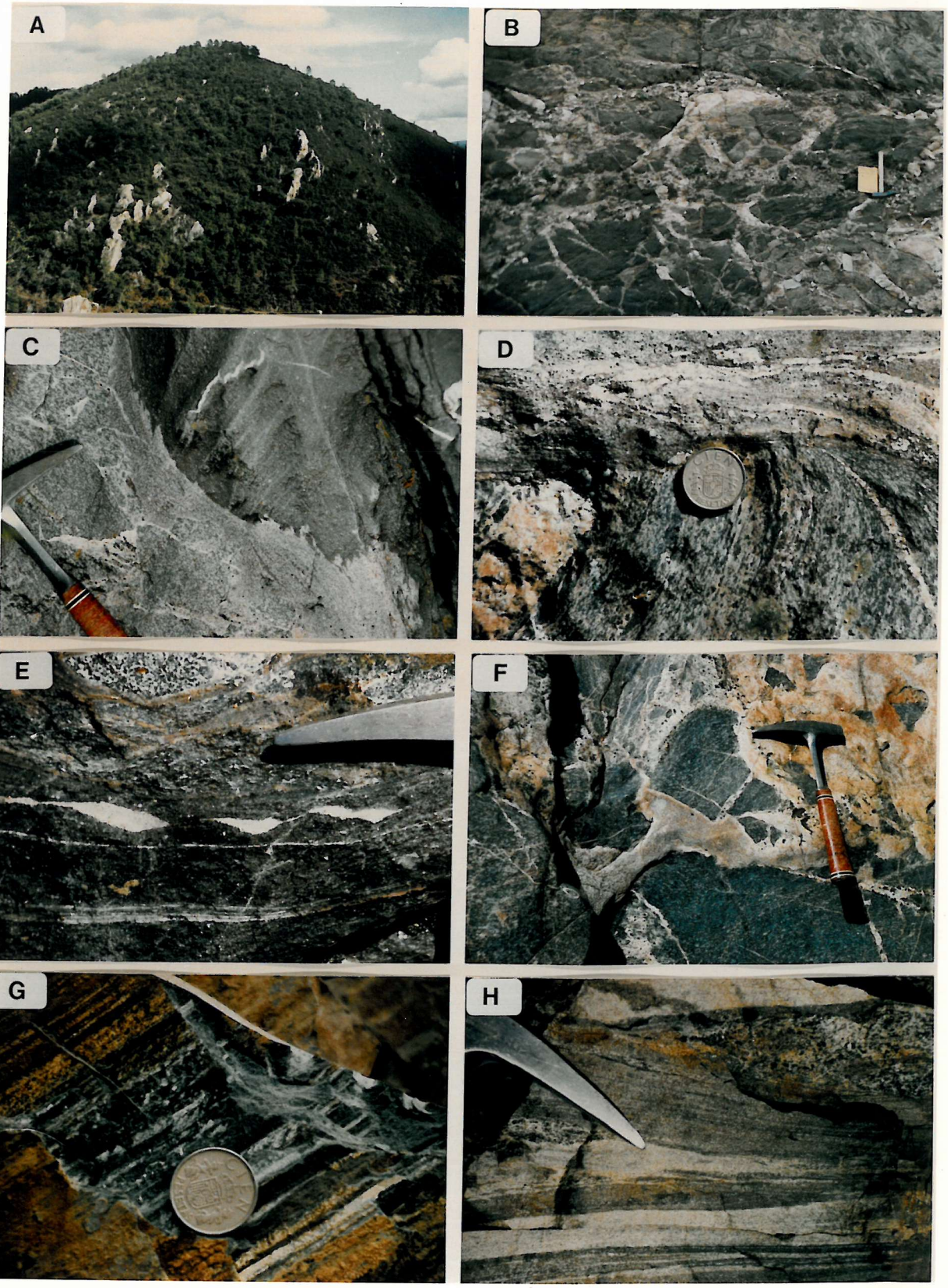
A
B
C
D
E
F
G
H

Figure 3.4

(a) Beja -Acebuches Amphibolites, southern margin. Contours: S_{A2} - foliation, • L_{A2} - mineral lineation, o F_{A3} - plunge of F_3 fold axes, + discrete shears. [GR 7635 9970 - 7630 9915].

(b) Los Ciries Antiform. S_{N2} - regional foliation, • L_{N2} - mineral lineation, o F_{N3} plunge of fold axes.

(c) Foliation and lineation from the Alcalaboza River, Barranco del Ciego and Barrance de Rioja. Contours: S_{N2} foliation, • L_{N2} - mineral lineation, o F_{N3} - fold axial plunge.

(d) Regional foliation within the Alajar Domain and mineral lineation observed on quartzite phacoids. + S_{AD2} regional foliation, • L_{AD2} - mineral lineation.

(e) +: F_{C3} fold axial planes and •: F_{C3} fold plunges from the Central Metasedimentary Domain. [GR 7350 9550 - 7255 9454].

(f) Bedding (S_o) parallel schistosity (S_{C2}) from the Central Metasedimentary Domain. Grid references as in (e).

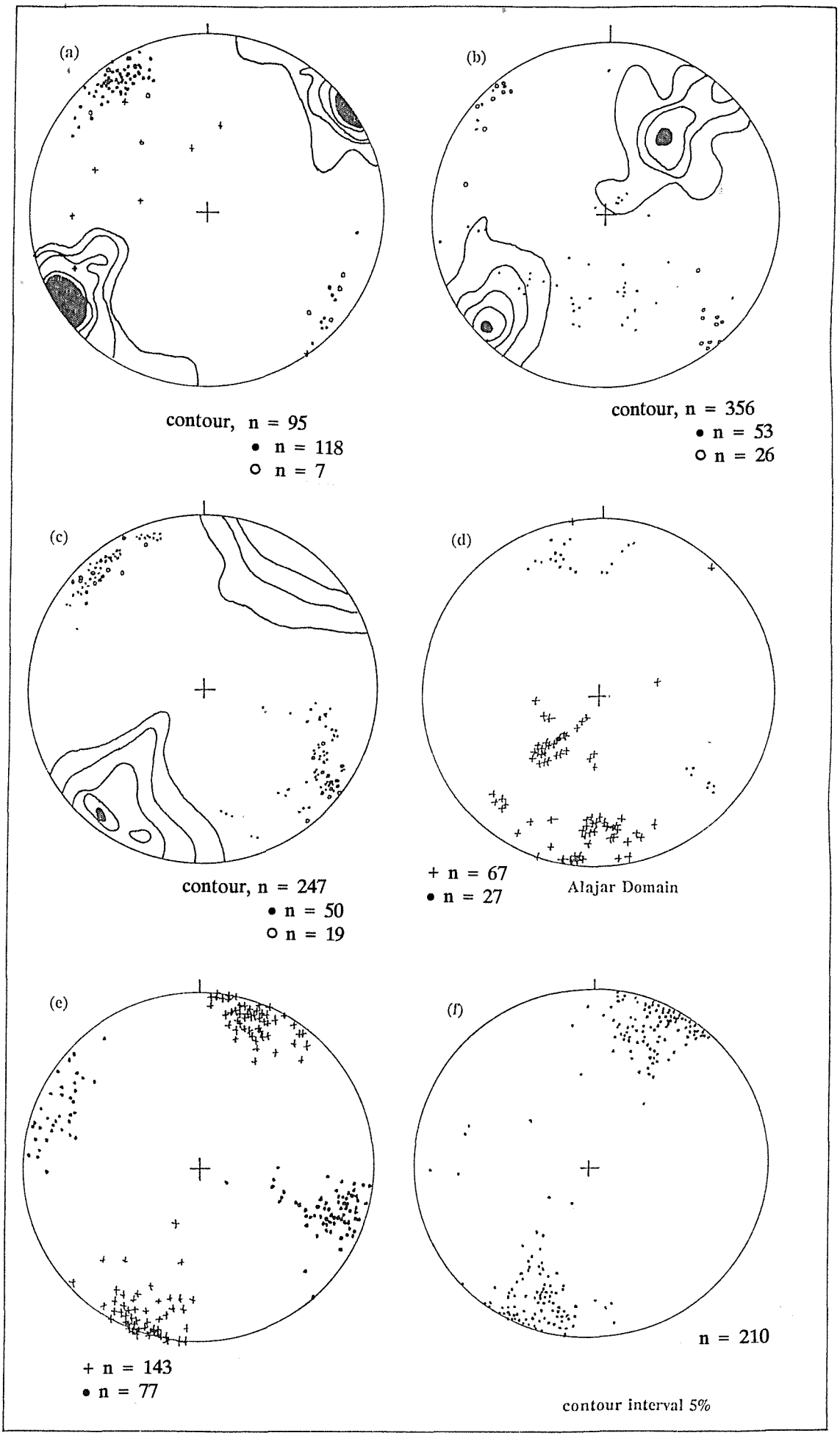
(a)
contour, n = 95
• n = 118
o n = 7
(b)
contour, n = 356
• n = 53
o n = 26
(c)
contour, n = 247
• n = 50
o n = 19
(d)
+ n = 67
• n = 27
Alajar Domain
(e)
+ n = 143
• n = 77
(f)
n = 210
contour interval 5%

sinistral regime (Fig. 3.4a). In attempting to formulate a kinematic explanation for these structures it has to be remembered that D_3 folding may have reorientated them.

At the northern end of the Aroche section [GR 8435 9664] the Beja-Acebuches Amphibolites are overthrust by granite and high grade rock of the Ossa Morena Zone (Fig. 3.3B). The foliation within both the granite and the amphibolite (S_{A2}) is steeply dipping with a strike parallel NW/SE shallowly plunging mineral lineation (Fig. 3.4a). The main D_{A2} foliation within the Beja-Acebuches Amphibolite Domain is an S_{A2} schistosity (Fig. 3.4a) that has subsequently been folded by an F_{A3} phase of folding. S_{A2} is observed as an LS-fabric that evolves in places to a strong L-fabric within which there are accumulations of plagioclase and amphibole. A sub-horizontal mineral lineation, composed of plagioclase and amphibole and consistent with strike-slip deformation (Fig. 3.3G), is contained within the S_{A2} schistosity.

A late phase of deformation, D_{A3}, affecting the amphibolites consists of minor folding which generated folds with axial planar surfaces dipping towards the NE, and with fold hinges plunging subhorizontally at low angles (Fig. 3.4a).

3.4 The Northern Metasedimentary Domain.

This domain includes part of the La Giralda Formation, Peramora Mélange Formation, part of the Cumbres de Los Ciries Formation and all of the Puerto Cañon Formation. The domain has been subjected to significant non-coaxial ductile deformation synchronous with metamorphism ranging from epidote-amphibolite-facies in the Peramora Mélange Formation to lower greenschist facies in the La Giralda and Puerto Cañon Formations (Chapter 5). Imbrication is clearly exposed in the hinge of the Los Ciries Antiform, where tectonic wedges of Cumbres de Los Ciries and Peramora Mélange are juxtaposed with strongly welded contacts (Fig. 1.5). These contacts are also exposed along the Barranco del Ciego section (Fig. 3.5G). Deformational events in this domain are labelled with a subscript 'N' (Fig. 3.2).

3.4.1 First Deformation (D_{N1}).

The earliest deformation (D_{N1}) is recognised only in the Cumbres de Los Ciries Formation. An early recognised as an early schistosity (S_{N1}) is composed of biotite, muscovite and recrystallised quartz, preserved within lenses bounded by planes of a later schistosity. The lenses occur on meso- and microscopic scales and are orientated parallel to S_{N2}. In discontinuous quartzite layers, S_{N1} is visible as a pressure solution cleavage appearing as impersistent millimetric to centimetric microlithons orientated obliquely to S_{N2} (Fig. 3.6), becoming poorly defined and eventually lost in regions of high strain (S_{N2}). The S_{N1} schistosity is often isoclinally folded and accompanied by extreme flattening (Fig. 3.6). The enveloping surfaces correspond to the XY plane of the strain ellipsoid.

Figure 3.5

(A) Sheeted dyke complex at [GR 7880 9740] showing clear relationships between fine and coarse grained meta-igneous sheets. The dotted line is parallel to the dyke margins.

(B) Shear bands in the welded quart-mica schists of the Cumbres de Los Ciries Formation indicating sinistral shear [GR 7937 9710]. Shearing is accompanied by an intense sub-horizontal mineral lineation.

(C) Extensional foliation boudinage seen on the banks of the Barranco del Ciego [GR 8105 9665]. The boudin consists of a closely spaced schistosity within which an early S_{N1} is preserved.

(D) An example of an intrafolial fold from the Barranco del Ciego [GR 8105 9665]. The early schistosity has been truncated by a later schistosity (S_{N2}).

(E) Intrafolial fold within the Peramora Mélange Formation [GR 8105 9660] showing extension in the upper limb and shortening in the lower limb.

(F) Asymmetric feldspar porphyroclast in the matrix of the Peramora Mélange Formation within the Los Ciries Antiform [GR 7495 9701] showing an element of sinistral shear.

(G) Boundary between structural horses of Peramora Mélange Formation and Cumbres de Los Ciries Formation (left and right of the photograph respectively). This example is seen in the Barranco del Ciego [GR 8125 9660].

(H) Lens-shaped quartzite phacoid entirely contained within a marble matrix in the Alajar Formation [GR 0640 9270].

(I) Sigmoidal shaped quartzite phacoid within a sheared phyllitc matrix. These quartzite bodies range up to 30m in length and have an intensely sheared fabric.

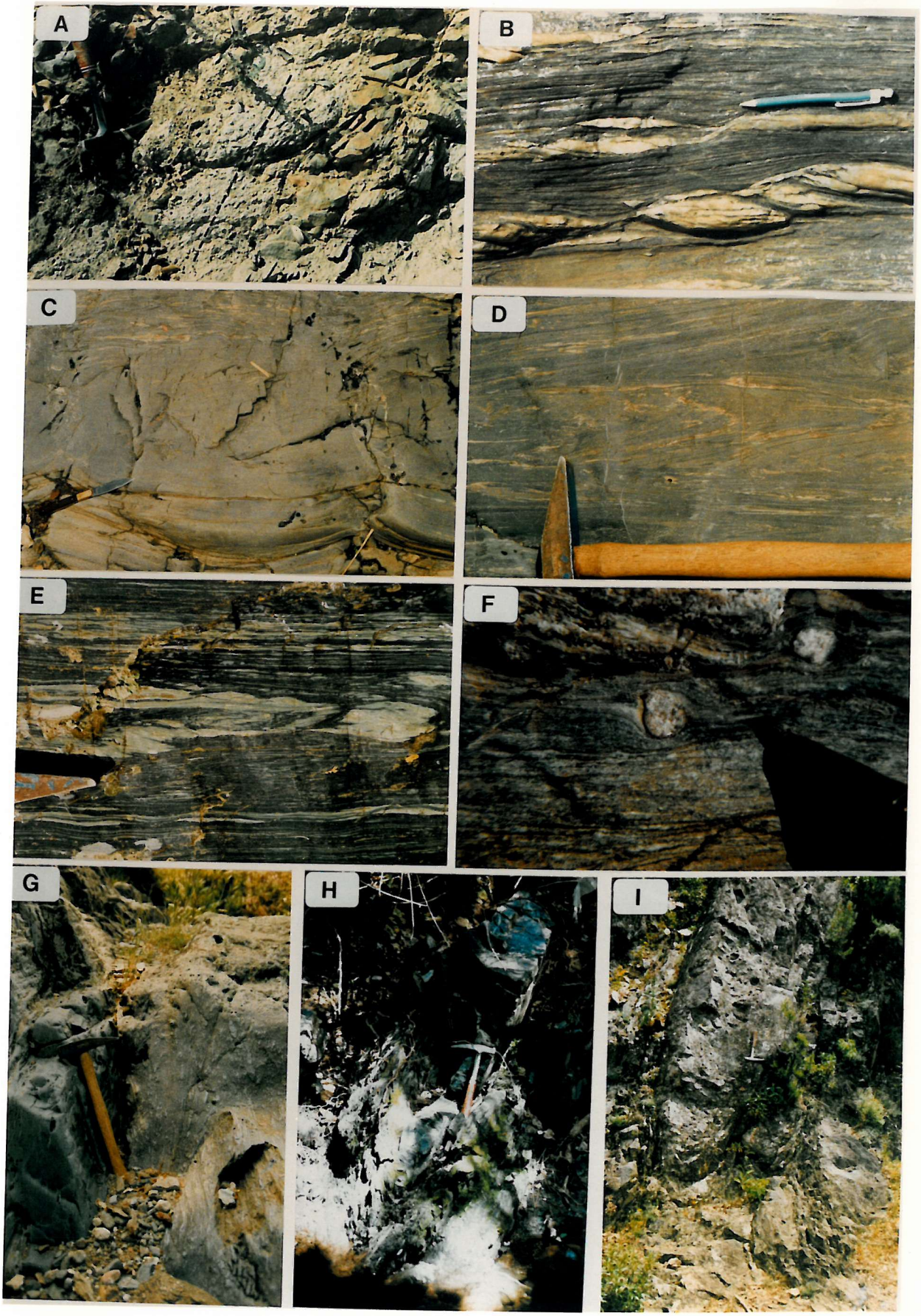
A
B
C
D
E
F
G
H
I

Figure 3.6 Field relationships between S_{N1} and S_{N2} in the Cumbres de Los Ciries Formation within the Northern Metasedimentary Domain.

(a) S_1 orientated obliquely to S_2 within the Cumbres de Los Ciries Formation.

(b), (d) and (f) Clasts of quartzite which retain an early S_{N1}. Ribbon quartz in the surrounding matrix also indicates high strain.

(c) Relict pods of quartz-mica schist preserving an early S_{N1} around which S_{N2} is deflected. These pods have the same composition as the matrix.

(e) Clast of green, basic material preserving an S_{N1} schistosity which is truncated by S_{N2}.

(g) and (h) Quartzite clasts within the sheared quartz-mica schist matrix. An early cleavage has been truncated by S_{N2}.

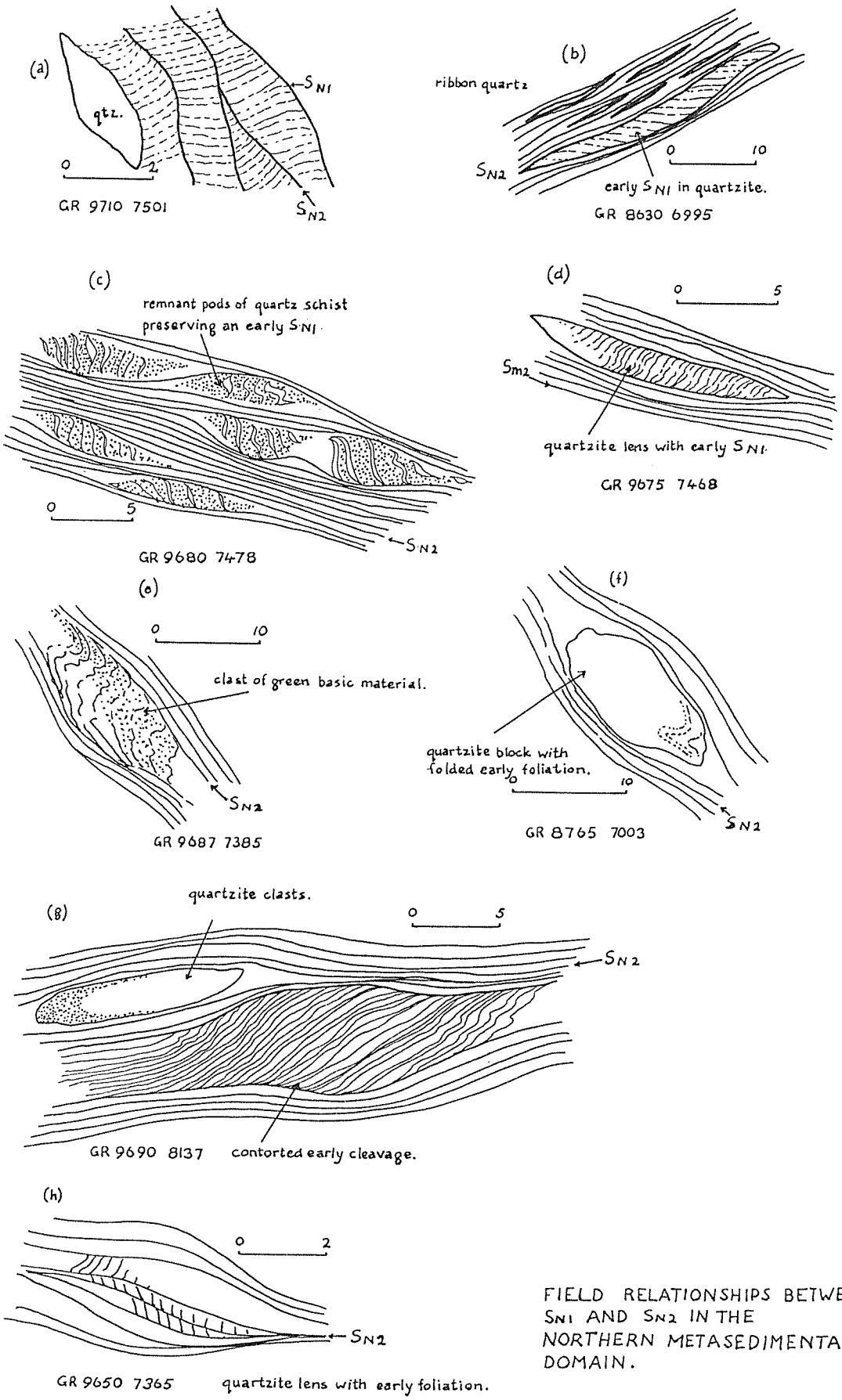

FIELD RELATIONSHIPS BETWEEN S_{N1} AND S_{N2} IN THE NORTHERN METASEDIMENTARY DOMAIN.

Figure 3.6

3.4.2 Second Deformation (D_{N2}).

Within both the Peramora Mélange and the Cumbres de Los Ciries Formations, D_{N2} represents a phase of high strain, an event that may possibly correspond to shearing within the Beja-Acebuches Amphibolites (Fig. 3.2). A steeply dipping schistosity, S_{N2}, forms part of the regional fabric and is seen on a larger scale extending from the Aracena Massif into Portugal (Crespo-Blanc & Orozco, 1988; Crespo-Blanc, 1989; Silva *et al. in press*). In the northern part of this domain S_{N2} is accompanied by a strong mineral lineation (Fig. 3.4C) and is folded by tight F_{N3} folds overturned to the SW with axial planes dipping steeply towards the NE. The S_{N2} cleavage is usually pervasive although locally it anastomoses around lacunae of lower strain (Fig. 3.6). In the Cumbres de Los Ciries Formation this cleavage consists of quartz grains, biotite and muscovite mica flakes.

3.4.2.1 *Mineral lineation.*

South of the boundary between the Beja-Acebuches Amphibolites and the Northern Metasedimentary Domain there is a well defined mineral lineation, which is associated with the South Iberian Shear Zone (Fig. 3.4C). Elsewhere it is variably developed and its orientation is frequently rotated by several degrees across closely spaced foliation planes. Exposures along the Alcalaboza river [GR 8070 9645] display features consistent with sinistral shearing such as shear bands and S-C structures. Here the lineation plunges sub-horizontally and consists of recrystallised quartz, mica flakes and andalusite rods.

In places the schistosity is well defined but a mineral lineation is not eg in the core of the Los Ciries Antiform where a lineation is poorly developed (Fig. 3.4b). The mineral lineation becomes less well defined away from the contact with the Beja-Acebuches Amphibolites, and south of the Alcalaboza River is absent, although recrystallisation and a strong regional foliation suggests that strain remained high throughout the domain.

The variable orientation of the mineral lineation can be ascribed to either to variation within the same schistosity forming event, or subsequent folding during F_{N3}. Reorientation of mineral lineations has been attributed to the anastomosing character of the mylonitic schistosity (Carreras & Casas 1987), and its subsequent reworking within the same shearing event. Early foliations are progressively replaced and reorientated by later ones (Bell and Hammond 1984). The growth of porphyroblasts, or pre-existing porphyroclasts, can provide a perturbation around which the schistosity is deflected (Bell 1981, 1985), creating areas within which strain fluctuates.

The effects of later folding depend on the pre-folding orientation of the mineral lineation. If parallel or sub-parallel to the later fold axis, then a lineation will vary little from its original attitude (Fig.3.7a). If, however, the original lineation is oblique to the direction of shortening the lineation will rotate into a new orientation (Fig. 3.7b). The lineation shown in Fig. 3.4C is sub-parallel to the F_{N3} fold axes suggesting the former case. Fig. 3.4c shows data for the regional foliation and associated lineation from the barrancos de Rioja, Ciego and Alcalaboza (located in Figs. 2.11 & 2.12).

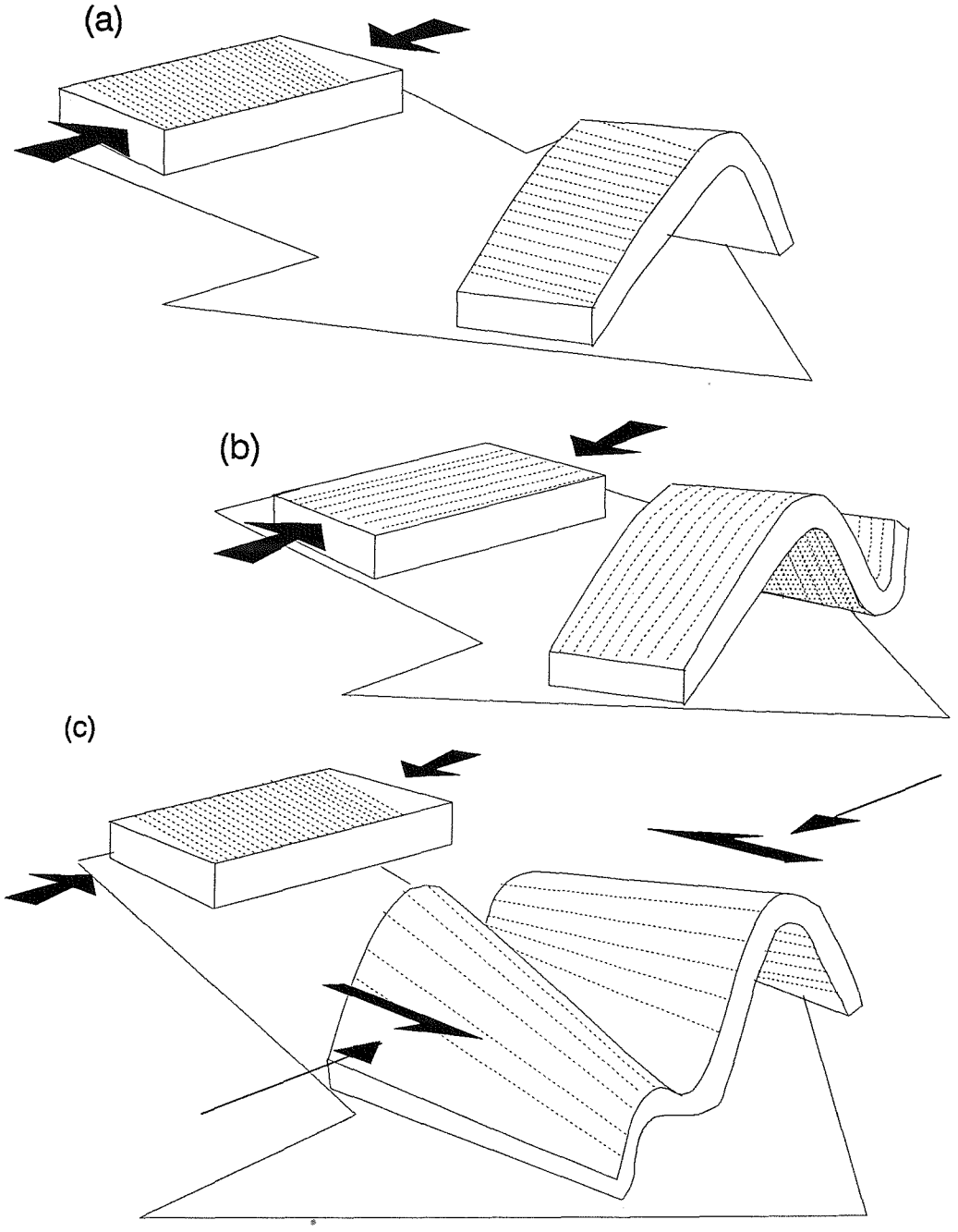

Figure 3.7 Effects of folding on a pre-existing mineral lineation. (a) shows the case when the mineral lineation is orientated parallel to the fold axial plane, (b) shows the lineation orientated normal to compression and (c) shows a lineation affected by components of both strike-slip and normal compression.

The foliation here is orientated sub-vertically although there is a maximum indicating that most of the planes measured dip steeply towards the northeast. The mineral lineation describes a bimodal spread of data indicating that it plunges sub-horizontally. F_{N3} fold axes also plunge subhorizontally both to the northeast and southwest. This relationship may occur if folding was accompanied by a component of strike-slip (Fig. 3.7c).

Locally, reorientation of the lineation can clearly be attributed to folding of a pre-existing anisotropy. The scatter of data points from the Los Ciries Antiform may be due to F_{N3} folding of earlier anisotropies (Fig. 3.4b).

3.4.2.2 *Intrafolial folds.*

These are clear indicators of ductile non-coaxil strain which occurs within the Northern Metasedimentary Domain. Fig. 3.5D [GR 8105 9665] shows an example of an intrafolial fold. A later schistosity anastomoses around the fold and truncates the fold limbs, effectively isolating it within it within the deforming matrix. Another example is observed at [GR 8104 9663] (Fig. 3.5E) where a green epidote-rich layering defines an intrafolial fold which has been strongly attenuated parallel to the foliation. Fig. 3.8 shows several folds preserved as lacunae around which S_{N2} is deflected and within which the fold axial plane is parallel to the schistosity. The anastomosing S_{N2} often truncates the early foliation isolating lacunae within the newly developing fabric and this early fabric may correspond to S_{N1} (Fig. 3.2).

Asymmetric folds and sheath folds which resemble syn-mylonitisation folds are frequently recognised in mylonite zones (Carreras *et al.* 1977, Bell 1978, Cobbold & Quinquis 1980, Bell & Hammond 1984, White *et al.* 1986; Holdsworth 1990). These phenomena are often attributed to perturbations that arise due to variations in rheological parameteres such as strain rates, deformation mechanisms, metamorphism and anisotropy. Local flow perturbation (Fig. 3.9) gives rise to local flow vorticity gradients and the production of localised distortions in the strain field. Holdsworth (1990) reasons that the resulting change in rate of shear parallel to the flow direction may locally generate zones of compression and extension causing buckle folds (Fig. 3.5D) and shear bands (Fig. 3.5E) respectively.

3.4.2.3 *Relict low strain lacunae.*

Lenses, varying in scale from porphyroblasts to metre sized phacoids, of less deformed rock are often observed within the regional schistosity. In the Peramora Mélange examples range from small scale intrafolial folds (Fig. 3.5D) to the preservation of a fragment of sheeted dyke complex, the margins of the individual sheets being parallel with the penetrative fabric [GR 7880 9740] and (Fig. 3.5A). Field relationships of the latter example are obscured by lack of exposure although its immediate juxtaposition against quartz-mica schists, exhibiting features consistent with high strain,

FIGURE 3.8

(a) Folded intrafolial fold observed in the Barranco de Rioja [GR 8195 9690]. All the following examples are from the Peramora Mélange Formation in the Northern Metasedimentary Domain.

(b) An early, S_{N1}, foliation truncated by a later foliation, S_{N2}, from the Barranco de Rioja [GR 8155 9655].

(c) Phacoid of quartzite that preserves an early schistosity around which S_{N2} is deflected, [GR 8130 9660].

(d) Early foliation (S_{N1}) that has been intensely reorientated within the S_{N2} schistosity, [GR 7975 9775].

(e) and (f) are further examples of an early cleavage that has been reorientated by D_{N2} deformation. [GR 7975 9755] and [GR 8060 9725] respectively.

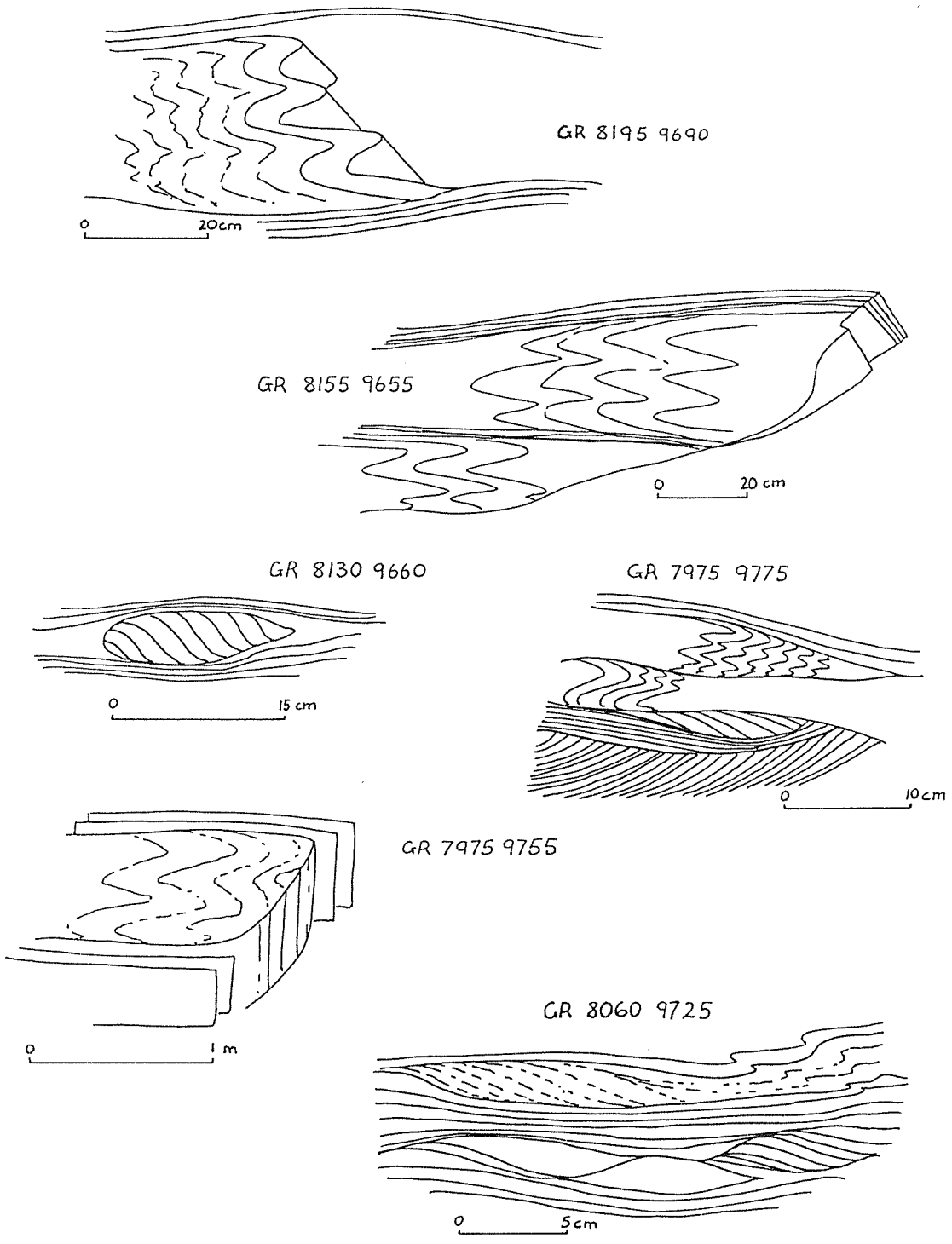

CLEAVAGE RELATIONSHIPS OBSERVED IN THE NORTHERN METASEDIMENTARY DOMAIN (PERAMORA MÉLANGE FORMATION).

Figure 3.8

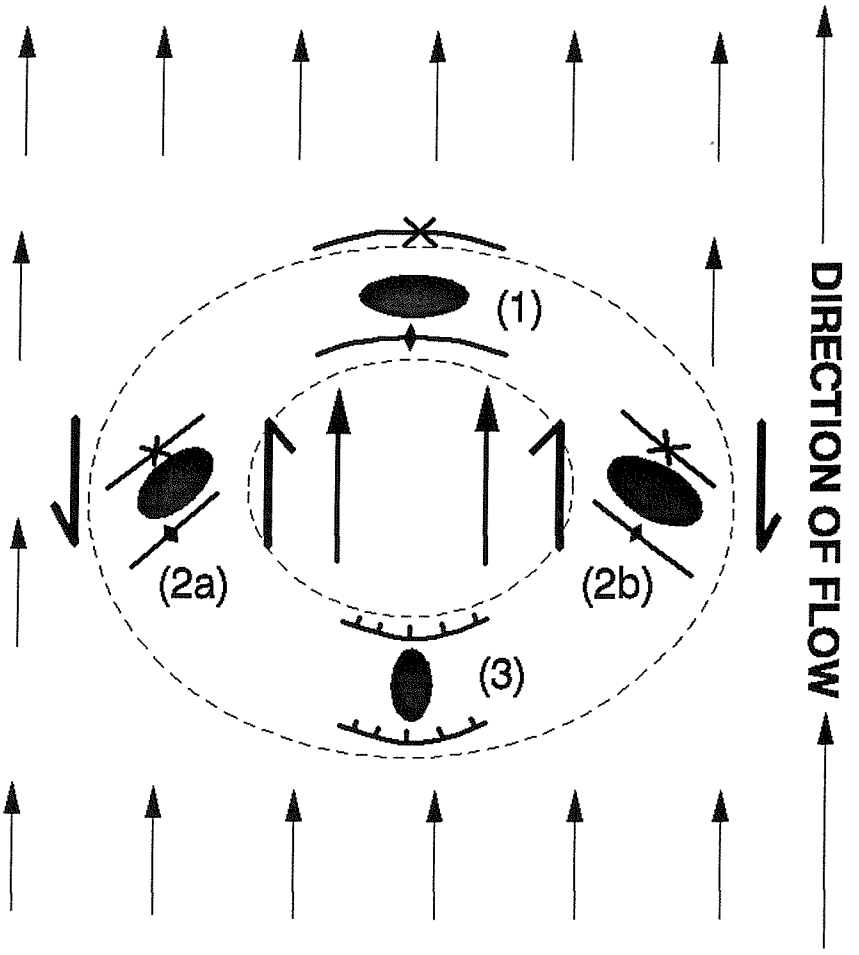

(1) Folds overturned in the flow direction (sheath folds)

(2) Oblique, asymmetric folds (A=Z-folds, B=S-folds)

(3) (a) Shear bands dipping in the flow direction
(b) extensional foliation boudinage

Figure 3.9 Structures associated with a vorticity gradient within a flowing rock mass. Folds and sheath folds, shear bands, and extensional foliation boudinage as well as lacunae of low strain may all form due to differential flow rates.

suggests that internally the phacoid retained low strain values during post-emplacement shearing and reorientation within the D_{N2} ductile deformation regime. This form of strain partitioning may occur due to ductility contrasts between different lithotypes (Ramsay & Graham 1970; Ramsay 1980; Simpson 1983; Gapais *et al.* 1987; White 1988). In this example the large phacoid of sheeted dyke may have acted as a competent block within the ductilely deforming environment.

3.4.2.4 *Shear sense indicators*

These are common within both the Cumbres de Los Ciries Formation and the Peramora Mélange Formation (Fig. 3.10).

(i) Shear bands, S-C structures and extensional foliation boudinage.

Two types of S-C structures are found within the Cumbres de Los Ciries Formation and the Peramora Mélange Formation resulting from a dominantly sinistral shear régime. These are termed type I (*sensu* Berthé *et al.* 1979) and type II (*sensu* Lister & Snoke 1984). They are well developed along the Alcalaboza river [GR 7960 9695], where they are defined by lenses of quartz (Fig. 3.5B) which vary in length from 2 - 50 centimetres. Quartz has been remobilised as shearing progressed with small 'fish' breaking off from the main lens and becoming isolated within the matrix (Fig. 3.5B). Shear bands show varying stages of development, from quartz ribbons to thick quartz veins. Also included in this category of shear indicators is foliation boudinage (Platt & Vissiers 1980; Hanmer 1986), an example of which is observed at [GR 8105 9665] (Barranco del Ciego - Fig. 3.5C). Within this particular example a closely spaced cleavage (S_{N2}) modifies an earlier foliation (S_{N1}) that has been truncated and reorientated (Fig. 3.11) indicating sinistral shear. Fragments of the host rocks within the boudin necks are supported in a quartz matrix.

The generation of shear bands has been discussed above (Platt 1983, Holdsworth 1990, Platt & Vissiers 1980) (Fig. 3.9), and are thought to arise due to perturbations in the anisotropy that develops during mylonitisation, caused by a local change in the orientation of the axes of the strain ellipsoid (White *et al.* 1980). They may represent the final phase of ductile deformation in a shear zone as temperature and pressure fall, possibly forming within a semiductile regime (Passchier, 1984; Shimamoto 1989). Extensional foliation structures may also have developed at a late stage in the mylonitisation event (Platt & Vissiers 1980; Malaveille & Lacassin 1988) (Fig. 5.9).

(ii) Asymmetric augen structures.

This category of indicator includes clasts, porpyroclasts and porphyroblasts which are recognised by the distribution of the S_{2N} fabric around more resistant augen (Lister & Price 1978; Van de Drissche & Brun 1987; Malaveille 1987). One example is a σ-type feldspar porphyroclast from the Los Ciries Antiform [GR 7495 9701] (Fig. 3.5F). Here the mineral lineation plunges down

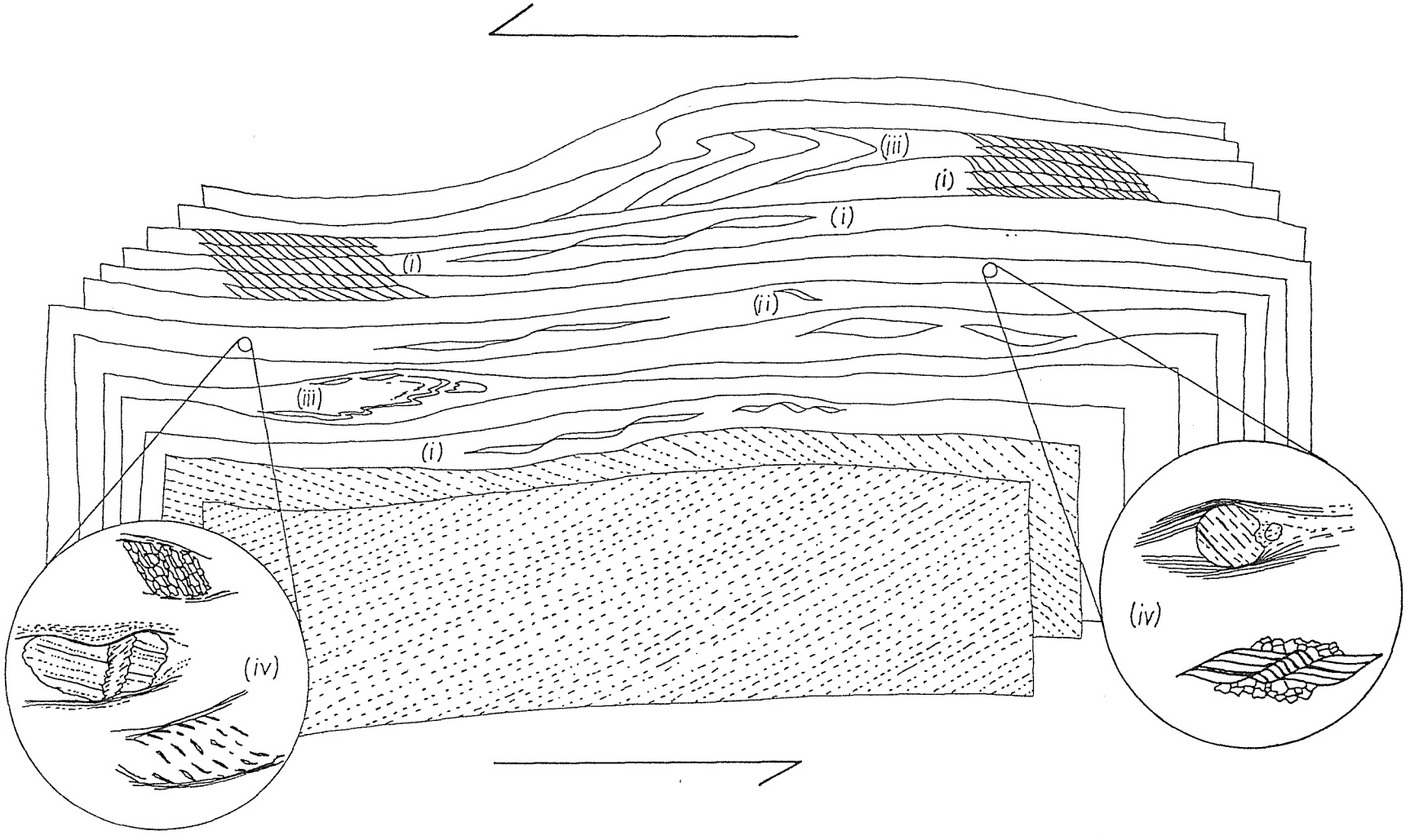

Figure 3.10 Summary of shear sense indicators seen in the Northern Metasedimentary Domain. (i) shear bands, (ii) asymmetric feldspar porphyroclasts, (iii) intrafolial folds, (iv) microstructures.

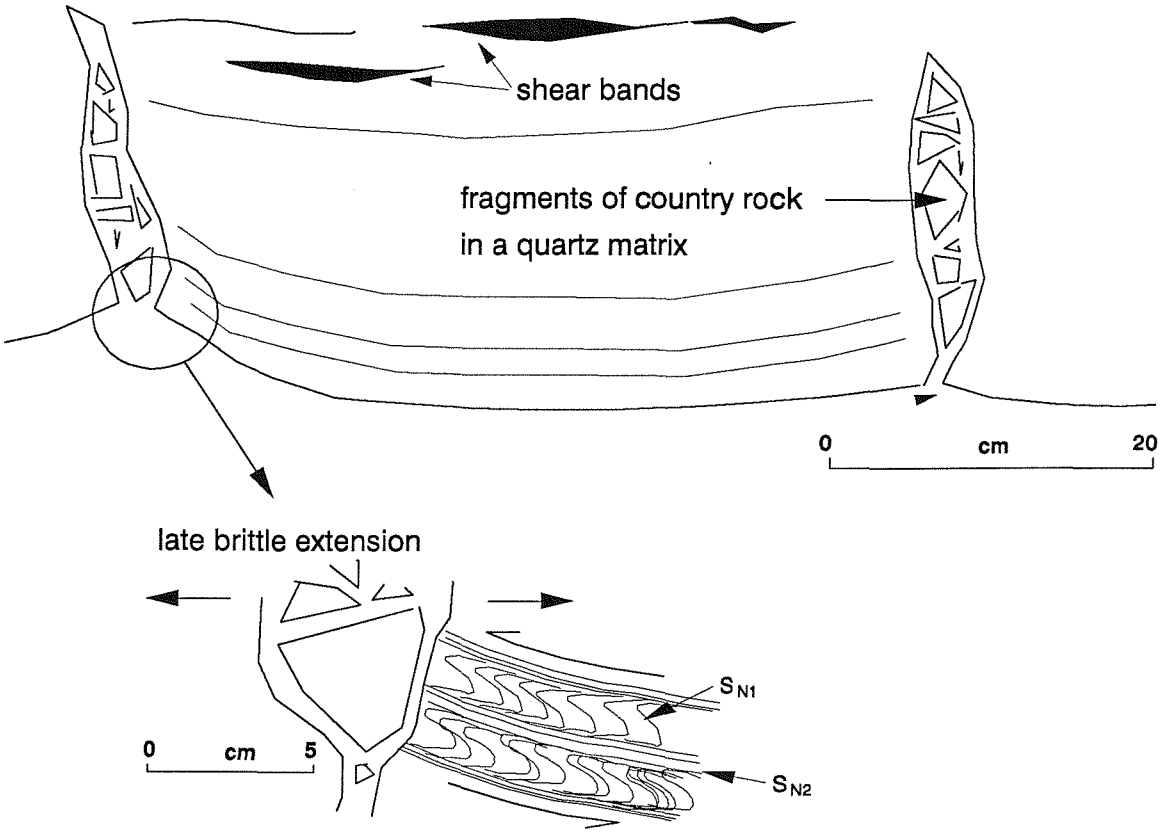

Figure 3.11 Extensional foliation boudinage seen in the Barranco de Rioja [GR 8105 9665].

dip (Fig. 2.4b). The inference is that two directions of movement are recorded by this kinematic indicator (Fig. 3.12B). One interpretation is that sinistral ductile strike-slip occurred first and the resultant foliation was subsequently folded during D_{N3} with the production of a down-dip mineral lineation accompanying top to the north shear, an event which obliterated any indication of an earlier lineation. The strain ellipsoid shown in Fig. 3.12A therefore corresponds to F_{N3}.

Fig. 3.12C [GR 7493 9700] shows a δ-type plagioclase porphyroclast (*sensu* Passchier & Simpson 1985), located within the XZ plane of the strain ellipsoid, indicating dextral movement (Law *et al.* 1986; Takagi & Ito 1988). This type of indicator shows that while the majority of kinematic indicators give a sinistral sense of displacement, locally there are areas where a dextral sense is inferred.

(iii) Folds and sheath folds.

Folds which infer a sense of shear are commonly seen within the Northern Metasedimentary Domain (Fig. 3.5E [GR 8104 9663]). This fold is defined by a green, epidote rich layer, each limb displaying a different deformation history; the lower limb has been shortened, with concomitant folding, while the upper limb has been extended and boudinaged. These features may be attributed to folding and subsequent transposition of an earlier fabric (possibly bedding) that was initially orientated obliquely to the flow direction.

Transposition of an early fabric is clearly demonstrated within an isolated tectonic wedge of Cumbres de Los Ciries type material mapped between [GR 8085 9745] and [GR 8050 9700]. This wedge is entirely located within the Peramora Mélange Formation continuing east into the Barranco del Ciego, but is not seen further west in the Barranco de Rioja (Fig. 2.2). In this locality several centimetric folds illustrate transposition of the schistosity (Hobbs *et al.* 1976) (Fig. 3.13).

These observations are consistent with the occurrence of strike-slip non-coaxial deformation. It is clearly demonstrated that early fabrics have been transposed and reorientated throughout the shearing event.

3.4.2.5 Microstructures related to D_{N2}

Thin sections from the Peramora Mélange Formation were generally cut parallel to the mineral lineation within the XZ plane. Quartz exhibits the following microstructures: (a) sub-grain development, (b) neocrystallisation (Fig. 3.14A), (c) sutured grain boundaries, (d) undulose extinction, (e) deformation lamellae, (f) preferred crystallographic fabric, and (g) ribbons. Sutured grain boundaries indicate dynamic recrystallisation and grain boundary migration (Knipe & Law 1987; Drury & Humphreys 1988) which eventually leads to new grain development (Fig. 3.14B). Ribbon quartz (Fig. 3.14D) commonly occurs in areas where strain values are high (White *et al.* 1980) e.g. sample 9117 [GR 7313 9555]. These relationships are clearly developed in sample 9117 (Fig. 3.16G & H and

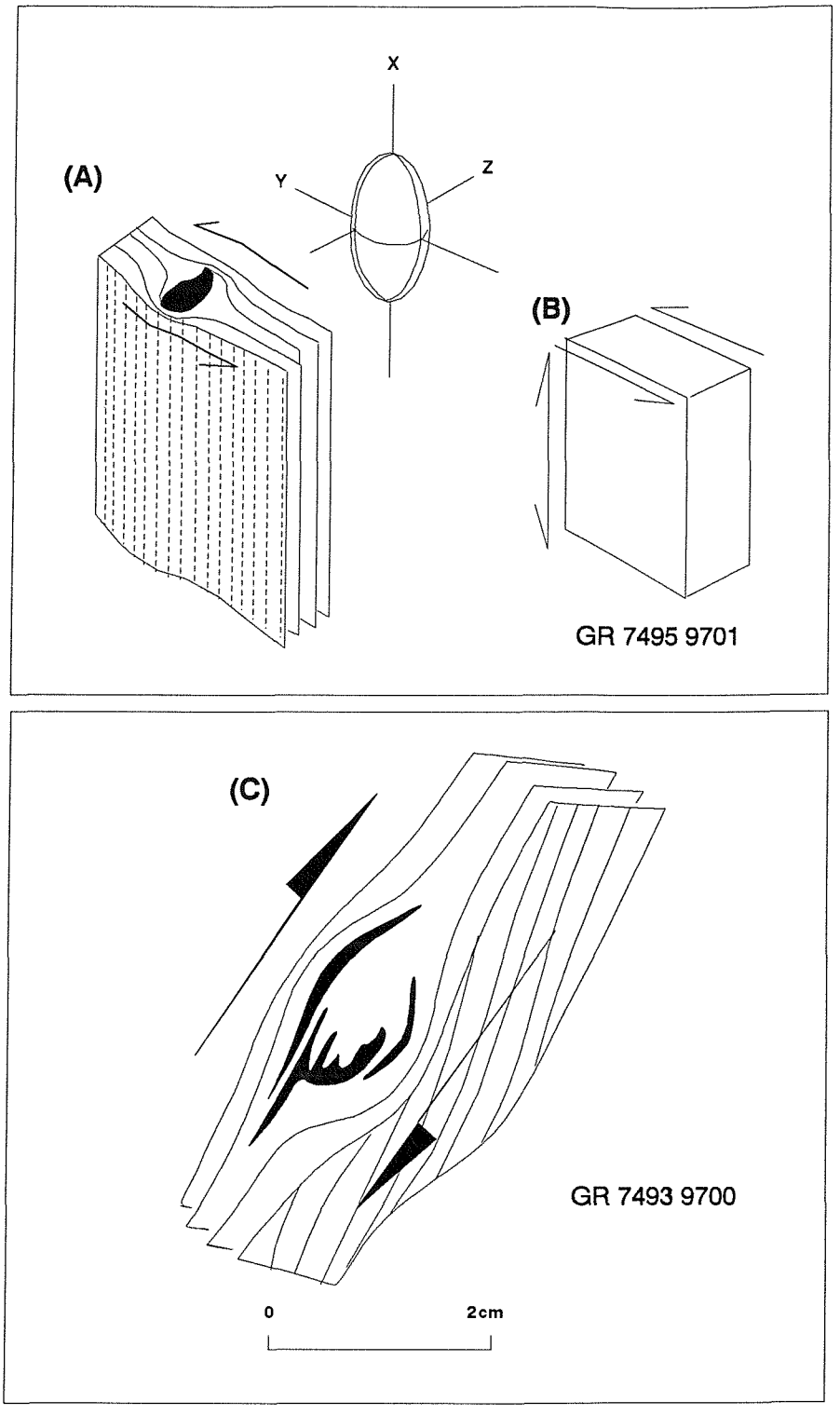

Figure 3.12 (A) Kinematic indicator in the Los Ciries Antiform. Two phases of deformation are observed, both strike-slip and dip-slip corresponding to two directions of movement (B). (C) illustrates a dextrally rotated feldspar porphyroclast in the Los Ciries Antiform.

FIGURE 3.13

(a), (b), (c) and (d) Examples of transposed schistosity within the Northern Metasedimentary Domain [GR 8060 9725]. The schistosity consists of andalusite bearing quartz-mica schist while the transposed layering is composed of fine grained white to buff coloured pelites.

(e) Transposed dark grey coloured slaty mudstone layer observed in the bed of the Alcalaboza river [GR 7790 9770]. This example clearly indicates sinistral strike-slip deformation with extension on teh upper fold limb and shortening on the lower limb.

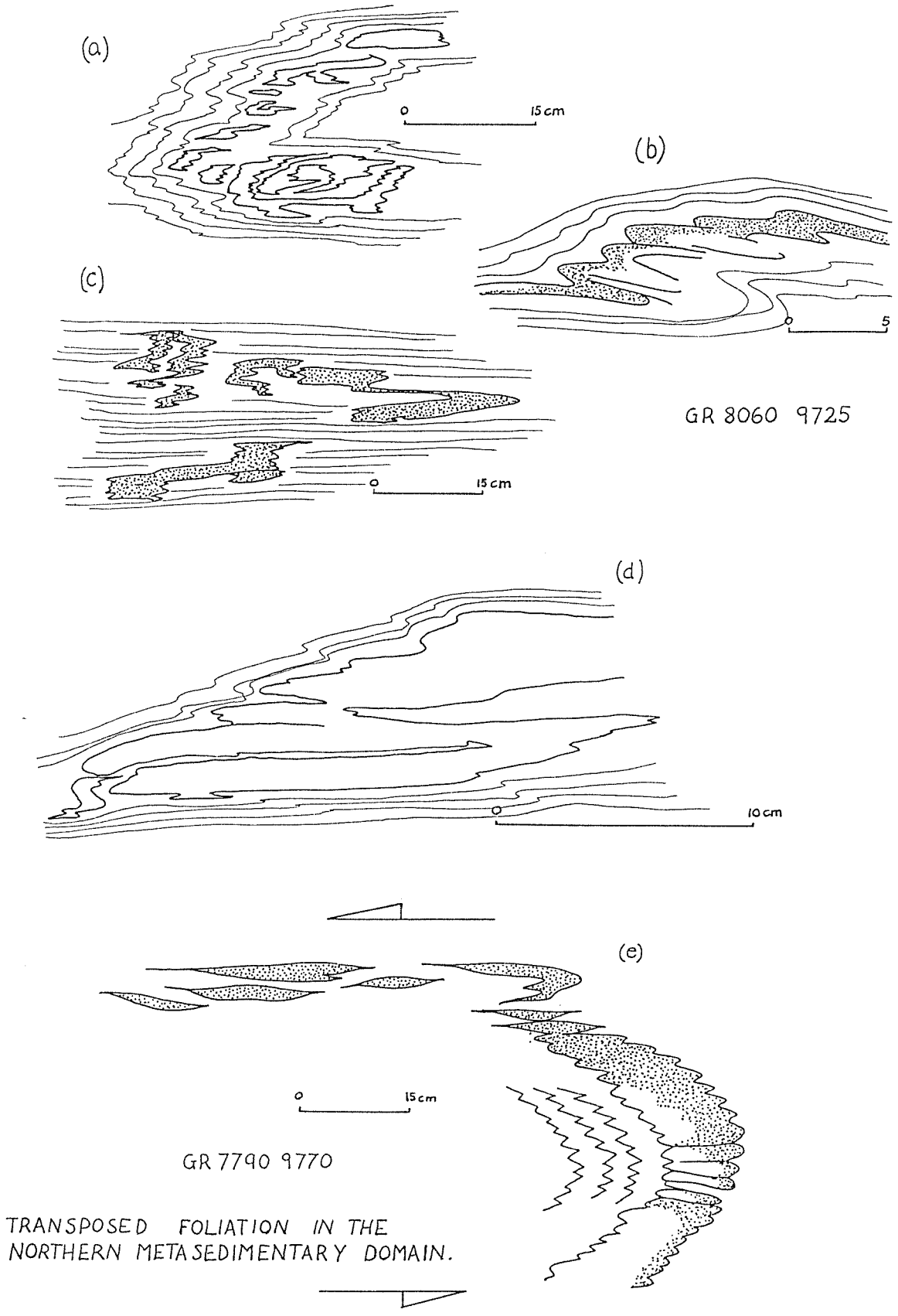
(a)
0
15 cm
(b)
5
GR 8060 9725
(c)
0
15 cm
(d)
10 cm
(e)
0
15 cm
GR 7790 9770
TRANSPOSED FOLIATION IN THE
NORTHERN METASEDIMENTARY DOMAIN.

Figure 3.13

FIGURE 3.14

(A) Strain free quartz grains displaying Y-shaped equilibrium boundaries within a lens of recrystallised quartz, around which an intense mylonitic foliation is developed (sample 8014).

(B) Formation of sub-grains in quartz, sample 7039.

(C) Sample 9262 [GR 7470 9685] taken from the contact between horses of Cumbres de Los Ciries Formation and Peramora Mélange Formation, shows elongation of quartz and mica grains displaying differences in the attitude of the mica grains within the lens, with respect to that outside the lens.

(D) Dynamic recrystallisation and grain size reduction resulting in diminution of quartz grains and mica fish (sample 7035 Alajar Formation [0460 9150] x2.5).

(E) Sample 9061 [GR 8150 9705] shows brittle fragmentation of a cordierite porphyroblast. S_{N2} is deflected around the crystal which displays sector trilling. Mica crystals and quartz aggregates bridge the fragments, indicating low strain rates.

(F) Sample 9136 [GR 7910 9730]. S-C structures in quart-mica schist.

(G) Relict amphibole and plagioclase (sample 9102 [GR 7495 9705] from the Peramora Mélange Formation x2.5). This example shows a strong mylonitic foliation which consists of actinolite, plagioclase and quartz.

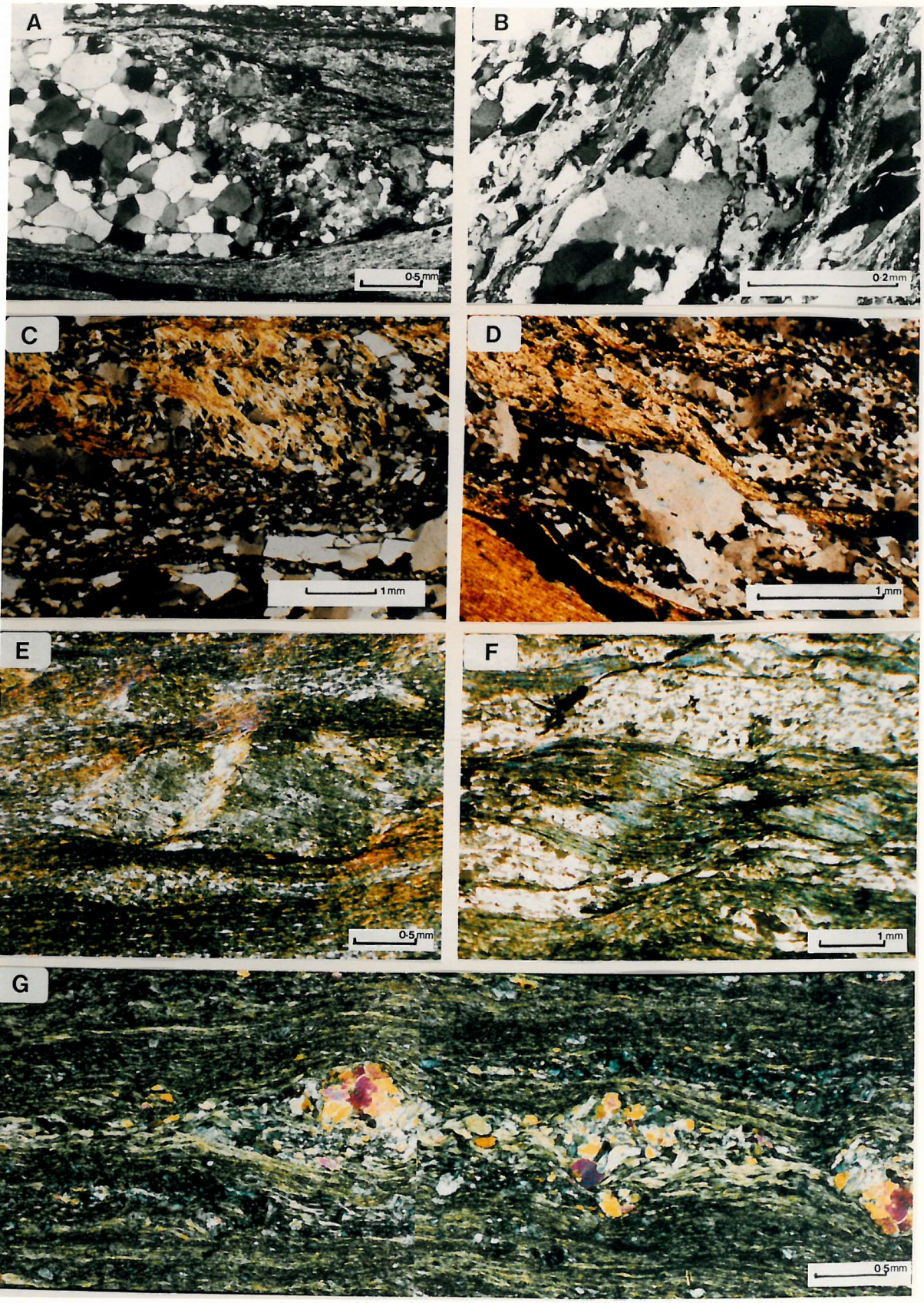
A
0·5 mm
B
0·2 mm
C
1 mm
D
1 mm
E
0·5 mm
F
1 mm
G
0·5 mm

frontispiece). In this sample S_{N1} is deflected into the S_{N2} pressure solution cleavage indicating top to the southwest shear during D_{N2}, while D_{N3} folded the earlier fabrics into their present sub-vertical orientation (Fig. 3.4b).

Tullis *et al.* (1973) attributed changes in the deformation state of a quartzite to varying conditions of temperature, strain and strain rate (Table 3.A). Simpson (1985) reviewed textures associated with deformation across the brittle-ductile transition and pointed out that under lower greenschist facies conditions ductile deformation of quartz is accompanied by kinking in biotite and fracturing in feldspar and amphibole.

A. Low T (≈250-500°), low strain, fast strain rate	Narrow deformation bands. Basal deformation lamellae. No recrystallisation.
B. Moderate T (≈500-700°C), low strain rates	Recovery and recrystallisation. Some deformation lamellae. New grains at boundaries of original grains. Undulose extinction of old grains. Sutured boundaries.
C. High T (>800°C)	Complete or near complete recrystallisation. Ribbon quartz.

Table 3.A Summary of changes in deformation within quartzites during varying conditions of temperature, strain and strain rate (after Tullis *et al.* 1973).

Complete whole rock ductility is achieved under middle to upper greenschist facies conditions; and no evidence remains for brittle deformation at epidote-amphibolite conditions. Large strain-free grains with Y-shaped triple junctions are an indication of crystallisation during the late stages of deformation (Fig. 3.14A). Applying the observations of Tullis *et al.* (1973) and Simpson (1985) to the microstructural textures discussed above would suggest that deformation occurred within a temperature range between 500°- 800°C.

3.4.2.6 *Microstructure of samples collected on the northern boundary of the Northern Metasedimentary Domain.*

The Northern Metasedimentary Domain has been affected by medium temperatures and low pressure metamorphism (Chapter 5) coincident with high strain. Strike-slip deformation is dominated by non-coaxial shear, with concomitant production of a strong mineral lineation contained within the regional schistosity (S_{N2}). In the footwall of the Beja-Acebuches Amphibolites the Cumbres de Los Ciries Formation consists of quartz-mica schist with porphyroblasts of andalusite, cordierite and garnet developed within the foliation (Fig. 3.14E). Biotite is extensively recrystallised and modified with the

formation of mica 'fish', with individual fish being linked by fine grained necks (Fig. 3.14D). They often define S-C structures (Fig. 3.14F) with mica being concentrated in the C-plane, and as such fall within type II S-C mylonites (Lister & Snoke 1984, O'Brien *et al.* 1987). Inclusions in cordierite often define a preferred orientation within porphyroblasts which represent an earlier schistosity. The presence of sector twinning (Kitamura & Yamada, 1987) indicates that these porphyroblasts grew at a later stage than the ealier schistosity and that subsequent modification during high strain gave rise to local dextral shear (Fig. 5.8E).

In the Peramora Mélange Formation relict crystals of hornblende and plagioclase form aggregates around which the foliation is deflected. Both amphibole and plagioclase indicate sinistral shear during deformation (Fig. 3.14G), which probably occurred under lower to medium greenschist facies metamorphism (Simpson 1985).

The core of the Los Ciries Antiform is characterised by knife-sharp imbrication of thin slivers of the Peramora Mélange Formation and the Cumbres de Los Ciries Formation. The microstructural features seen in both the Permaora Mélange lithologies and the Cumbres de Los Ciries-type material are similar to those described above although here low pressure, high temperature porphyroblasts are absent. Kinematic indicators which include the reorientation of mica grains are common (Fig. 3.14C).

3.4.3 Third Deformation.

D_{N3} in the Northern Metasedimentary Domain is dominated by irregular, NE verging tight overturned folds and chevron folds formed by shortening perpendicular to the plane of S_{N2}. F_{N3} fold axial surfaces are orientated parallel to the S_{N2} schistosity with interlimb angles ranging from 50° to 60° (Fig.3.4b and Fig. 3.15). Chevron folding of the main schistosity within the Cumbres de Los Ciries Formation occurs on all scales from meso- to microscale (Fig. 3.16G).

The Los Ciries Antiform was also formed during D_{N3}. Parasitic folds on both limbs indicate overall vergence to the NE, ie opposite to the general SW trend of fold vergence across the belt. The main S_{N2} foliation, which defines the limbs of the fold, is asymmetrically orientated around the fold hinge (Fig. 3.4b and 3.15) with the northern limb dipping ≈75° to the NE and the southern limb dipping at 40-50° towards the SW, giving an interlimb angle for the Los Ciries Antiform of ≈70°. S_{N3} is not developed anywhere within the Los Ciries Antiform. An interpretation for development of the Los Ciries Antiform must account for, (a) parasitic fold vergence (dominantly towards the NE), (b) fold axial planes steeply dipping to the SW with hinges plunging sub-horizontally (Fig. 3.4b), (c) reorientation of the L_{N2} mineral lineation (Fig. 3.4b), (d) transport direction of adjacent structural domains, indicated by fold vergence, to the SW. An interpretation that accounts for these features is that the Los Ciries Antiform formed above a blind backthrust (Dunne & Ferrill 1988) associated with southwestward directed thrusting (Fig. 3.15).

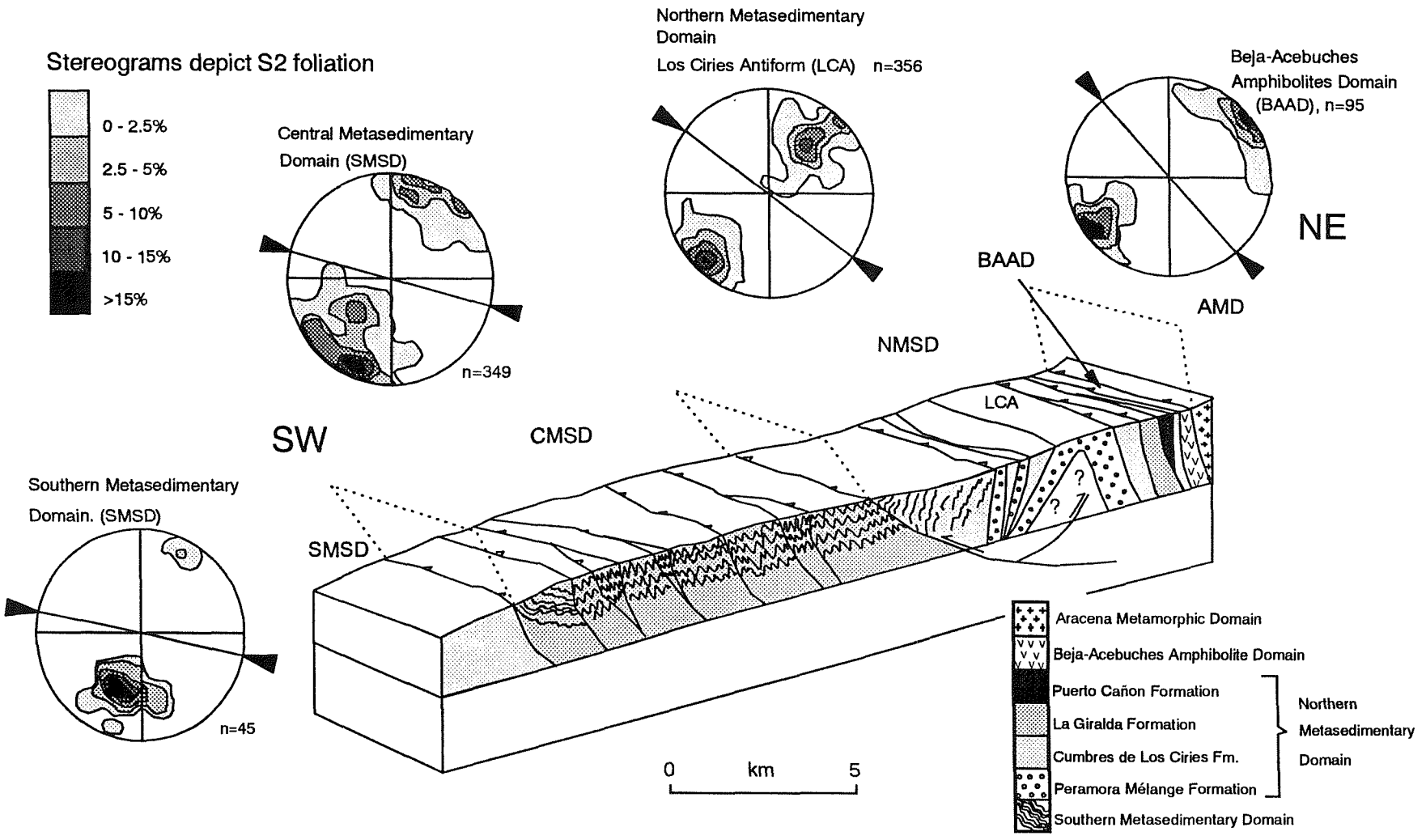

Figure 3.15 Cross section across the Oceanic Exotic Terrane illustrating the relationship between structural domains identified. The stereograms depict the regional S_2 schistosity.

3.4.4 The Puerto Cañón Formation and the La Giralda Formation.

These two formations lie on the northern limb of the Los Ciries Antiform being exposed in the bed of the Alcalaboza river and along the road section between [GR 7610 9833] and [GR 7585 9810]. Here, they consist of fine grained slates and phyllites interbedded with medium grained turbidites. Upright, mesoscopic folds with tight interlimb angles occur that correspond to F_{N3} (Fig. 3.17a) while graded bedding indicates that the folds face upwards. Along the River Alcalaboza section [GR 7640 9800 - 7685 9775] early deformation in both formations produced intrafolial folds (Fig. 3.16E) and ductile attenuation of the fine grained slate layers (Fig. 3.16C), and this was accompanied by the formation of an intense bedding parallel cleavage. Sinistral strike-slip produced extensional boudinage of fine grained slate layers with quartz-filled necks (Fig. 3.16A & B). In some examples a later component of compression operated parallel to the boudin axes resulting in a quartz infill (Fig. 3.16A). In places thin slate beds, originally extended with the creation of quartz filled necks, have been folded and crenulated (Fig 3.16D).

The La Giralda Formation occurs in both the Northern Metasedimentary Domain and the Central Metasedimentary Domain. However, the style of deformation differs markedly between the two domains. A clear early cleavage, such as is observed in the Central Metasedimentary Domain (section 3.6.1), is absent within the La Giralda Formation in the Northern Domain, while sedimentary features such as bedding and way up criteria are frequently preserved. Sinistral ductile deformation is observed, generally in fine grained dark coloured slaty mudstone layers. In places these have been folded and the bedding has been transposed (Fig. 3.13e). The regional foliation observed in the Puerto Cañón and the La Giralda Formations has been folded by a later phase of deformation (here labelled D_{N3}). This may have resulted in a steepening of earlier fabrics (Fig. 3.17).

Preservation of sedimentary structures, and lower metamorphic grades observed in these formations than in the juxtaposed Peramora Mélange and Cumbres de Los Ciries Formations (section 5.3), suggest high structural levels of deformation.

3.5 The Alajar Domain.

The Alajar Domain represents an along strike equivalent of the Northern Metasedimentary Domain (Fig. 1.4). Structural events in this domain are designated with the subscript 'AL' (Fig. 3.2).

3.5.1 Ductile strike slip deformation, D_{AL1}.

The S_{AL1} fabric is characterised by quartz recrystallisation, grain size reduction and mica fish (Fig. 3.14D). Style of imbrication in this domain contrasts with that observed in the Northern Metasedimentary Domain; here 15m thick shear zones characterise horse boundaries marking both intraformational discontinuities and interformational contacts (cross section in Fig. 2.8). These shear zones consist of buff coloured fine grained mylonitic material that weathers easily into uniform

FIGURE 3.16

(A) Foliation boudinage within a fine grained slaty mudstone layer [GR 7630 9775]. This structure shows two phases of extension. The first phase created the boudin while the secnd phase faulted a quartz vein that formed parallel to the boudin axis.

(B) Angular boudins of fine grained slaty mudstone intercalated with fine grained grey siltstone. The individual boudins are separated by quartz necks [GR 7630 9775].

(C) Strong ductile deformation within a slate layer in the Puerto Cañon Formation. The slaty mudstone layer has been intensely attenuated and is emphasised by quartz.

(D) Thin slaty mudstone layers intercalated with light grey coloured silt layers. These layers display at least two phases of deformation. The first phase resulted in boudinage of the layers with the formation of quartz filled boudin necks while the second phase crenulated the boudinéd layers.

(E) Tight isoclinal interfolial fold within a fine grained light grey siltstone layer [GR7630 9770].

(F) Shear bands defined by quartz augen that are joined by thin attenuated necks. In the top of the photograph there is a 1.5cm thick band of andalusite. These andalusite bands are sinsitally sheared in places.

(G) and (H) thin section and hand sample of a discontinuous quartzite from the Cumbres de Los Ciries Formation in the Northern Sedimentary Domain (sample 9117 [GR 7325 9615]). The sample displays three phases of deformation. The first is a contorted cleavage, S_{N1}, which is ductilely sheared between the sub-vertical S_{N2} cleavage. F_{N3} folding was accompanied by dutile deformation of the earlier cleavages, opening of dilation jogs and flexural slip duplexes.

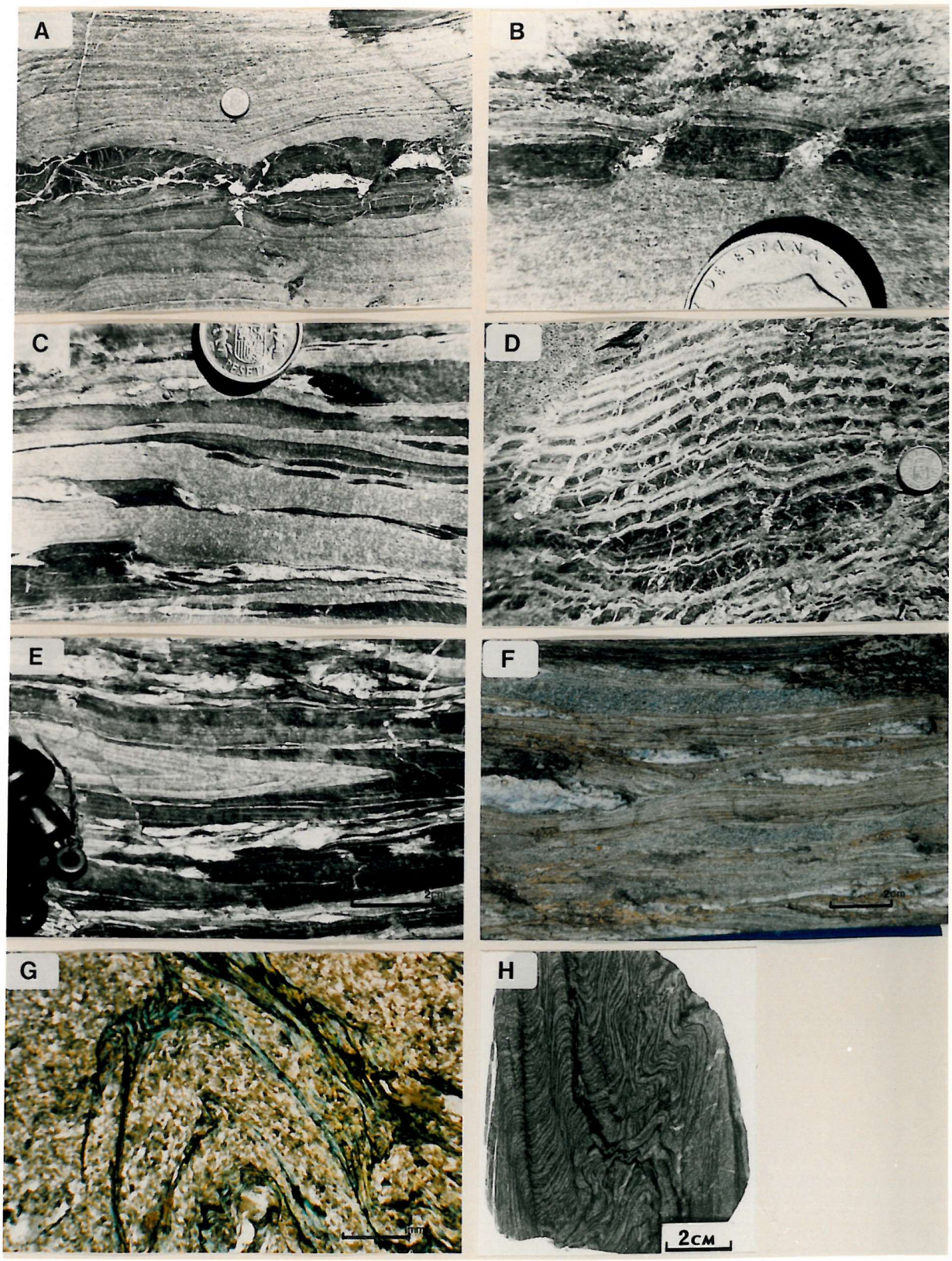
A
B
C
D
E
F
G
H
2cm
2cm
1mm
2CM

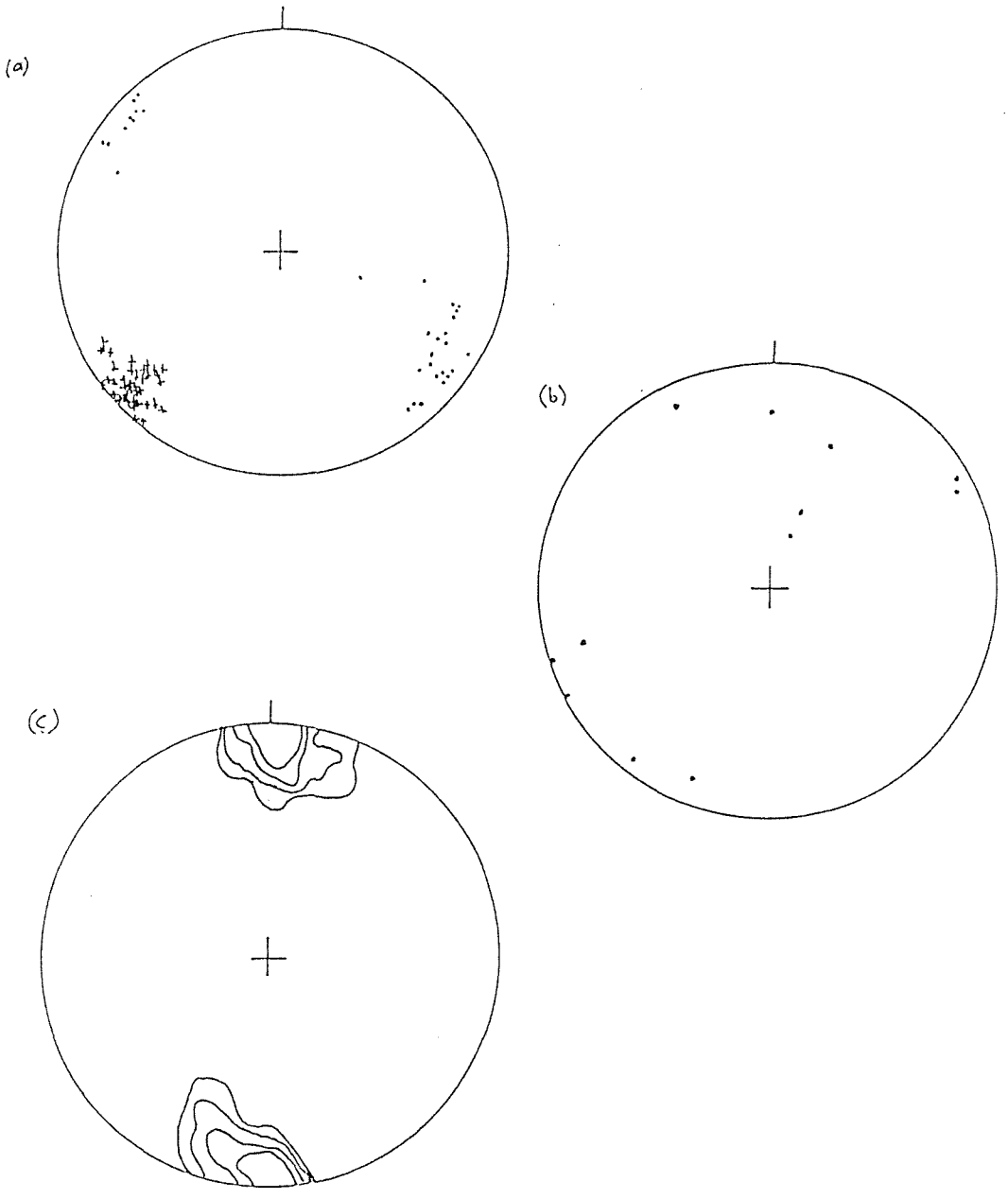

Figure 3.17 (a) Stereogram structural elements from the Puerto Cañon Formation [GR 7640 9800 - 7685 9775]. + FN2 - dip of fold axial surface, n=38.

(b) Small scale thrusts within the Central Metasedimentary Domain measured along the detailed section illustrated in Fig. 3.20. The data indicate that D_{N3} thrusts are both southwesterly and northwesterly dipping. Rarely preserved slikensides indicate down-dip movement. • D_{N3} - thrust surfaces, n=12.

(c) S_0/S_{C2} foliation from the northern end of the section illustrated in Fig. 3.28. [GR 7005 9865 - 7015 8865]. contour - 5%

centimetre sized cubes (Fig. 2.4G). A sub-horizontal stretching lineation, which has been folded during F_{AL2}, is strongly developed in these sheared rocks. Crenulation of the mylonitic fabric occurred at a later stage, possibly during F_{AL3}. Lens-shaped to sigmoidal quartzite bodies, varying in scale from pebble size (<5cm) to >30 metres in length (Fig. 3.4A and Fig. 3.5I), are attenuated parallel to strike.

Structural measurements from the matrix and the quartzite phacoids are shown in Fig. 3.4d. In the fine grained matrix the foliation, consisting of recrystallised biotite, chlorite, muscovite and quartz aggregates, dips towards the NE. A down dip mineral lineation, which may have been reorientated by folding during compression normal to strike, is weakly developed on the quartzite lenses. Removal of the effects of folding suggests a NW-SE trend to the stretching lineation.

Similarities between the Northern Metasedimentary Domain and the Alajar Domain include: (a) D_{AL1} ductile deformation may have obliterated most of the sedimentary structures. Microstructures are consistent with deformation within a ductile non-coaxial regime (Tullis *et al.* 1973; Simpson, 1985), (b) strike-slip deformation occurs, (c) D_{AL2} folding has resulted in a steepening of the regional foliation, and (d) imbrication is observed in both the Alajar and Northern Metasedimentary Domains.

3.6 The Central Metasedimentary Domain.

Rocks within this domain (Fig. 3.1 and Fig. 3.15) belong to a single formation, the La Giralda Formation, which forms an extensive area of flysch sediments dominated by fine grained turbidites affected by lower greenschist facies metamorphism (Chapter 5, section 5.3). Deformation events in this domain are labelled with the subscript 'C' (Fig. 3.2).

Differences between this domain and the structurally overlying domains include: (a) ductile deformation in the Northern Metasedimentary Domain has obliterated most of the sedimentary structures; in the Central Metasedimentary Domain many primary sedimentary stuctures are preserved, (b) in the Central Metasedimentary Domain three distinct fabrics are observed; an early S_{C1} cleavage is clearly defined throughout. Structural elements of this domain are illustrated in Fig. 3.2 and Fig. 3.15.

3.6.1 First and second deformation (D_{C1}/D_{C2}).

D_{C1}, manifest as a complex schistosity, S_{C1}, is often present as a crenulated mica-rich plane which may be rotated into parallelism with S_{C2} (Fig. 3.18B & C). Crenulation of this cleavage is a ubiquitous feature and a consistent orientation is not observed. This makes it difficult to measure. Mesoscopic F_{C1} folds are not observed. S_{C2} is observed regionally mainly as a bedding parallel pressure solution schistosity (Fig. 3.18A), but is often orientated oblique to bedding. Cleavage development varies according to lithology; in slates it is a pervasive slaty cleavage while in coarser

FIGURE 3.18

(A) Sample 8069 [GR 7250 9455]. This sample shows an isoclinal fold in fine grained siltstone intercalated with a coarser grained arenite layer. Folding is accompanied by an axial planar cleavage in the fine grained siltstone which is not evident in the arenite. In the coarser grained layer a bedding parallel cleavage is observed.

(B) Sample 8148 [GR 7005 9625]. An F_{C3} fold in a fine grained siltstone showing three clear phases of deformation. The early cleavage is contorted and truncated by a bedding parallel pressure solution cleavage. All these cleavages have been folded with slip occurring along the S_{C2} cleavage with the formation of fexural slip duplexes.

(C) Sample 8150 [GR 7000 9620] shows an early S_{C1} cleavage in a fine grained siltstone which has been rotated by the formation of a late pressure solution cleavage, S_{C2}.

(D) Sample 8091 [GR 7115 9240] is an example of a folded layer in a fine grained siltstone with the formation of a fine grained siltstone with the formation of flexural slip duplexes and a weak axial planar cleavage.

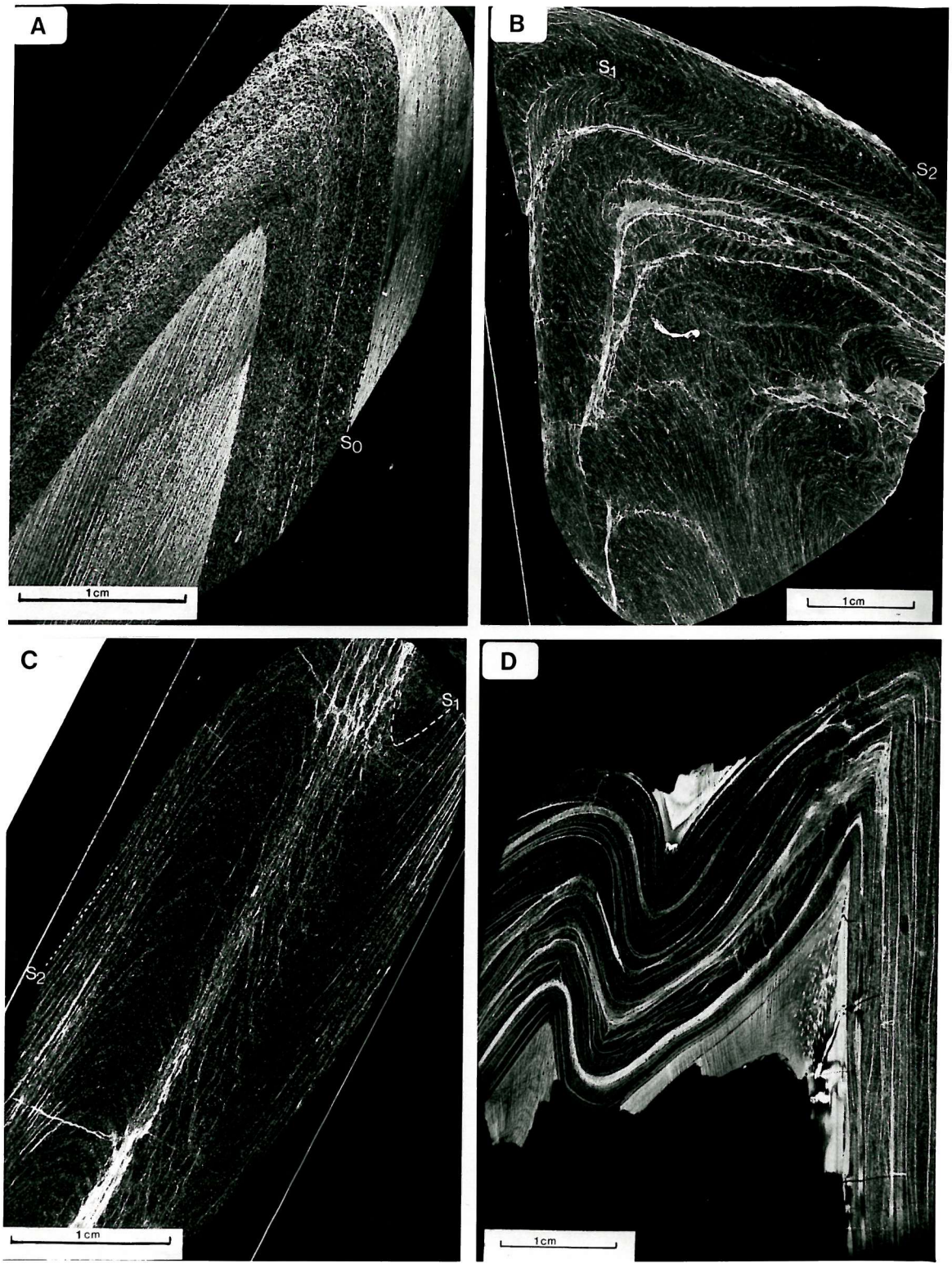
A
S_0
1 cm
B
S_1
S_2
1 cm
C
S_1
S_2
1 cm
D
1 cm

Figure 3.19 La Giralda Formation

(A) Hand sample of a quartzite ultramylonite (sample 8192 [GR 7005 8730]. In thin section the quartz c-axes show strong alignment indicating top to the south shear. The foliation is accompanied by a weakly developed down-dip mineral lineation. The sample is from the southern end of the section illustrated in Fig. 3.27.

(B) Open, cylindrical fold in a normally graded quartz arenite layer. The fold is located at the northeastern end of the section illustrated in Fig. 3.27.

(C) Fine grained siltstone displaying three phases of deformation each delineated by mica growth. [GR 7010 8970].

(D) Fragmented blocks of foliated fine grained siltstone [GR 7305 9545] located within the zone of disruption on the thrusted boundary between the Northern Metasedimentary Domain and the Southern Metasedimentary Domain.

(E) Folded D_2 thrust above vertically orientated southwestward younging beds [GR 7145 9315].

(F) F_{N4} folded fine grained siltstone and mudstone intercalations [GR 7030 8970].

(G) F_{N3} chevron folding of fine grained siltstones within the Central Metasedimentary Domain [GR 7000 8050].

(H) Kink band in fine grained siltstone beds within the Central Metasedimentary Domain [GR 7000 8945].

(I) F_{C3} fold in the Central Metasedimentary Domain within fine grained silty mudstone and slaty mudstone intercalations. The fold in the lower half of the photograph is cylindrical while the folded bedding in the upper half of the photograph has been disrupted with the right hand limb being sheared out [GR 7210 9410].


A
5 mm


B


C
1 cm


D


E


F


G

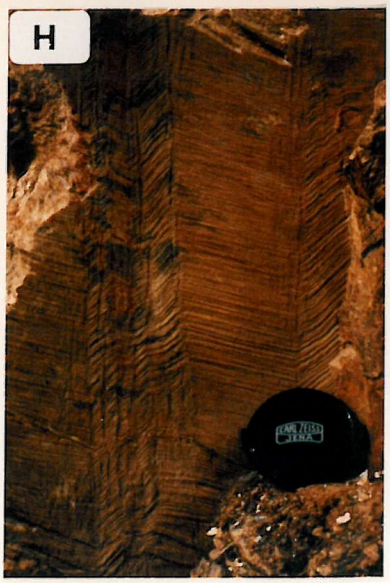
H

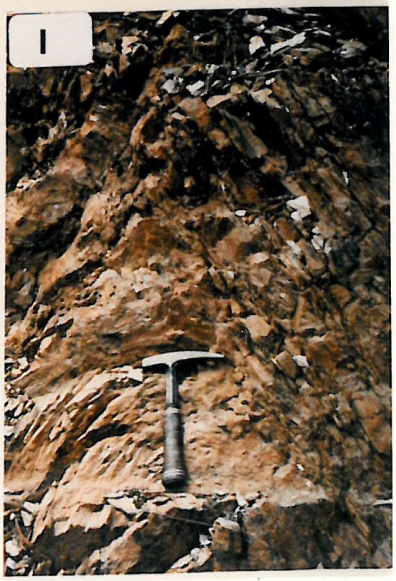
I

grained arenites it is a penetrative or spaced pressure solution cleavage. In tuffaceous horizons the cleavage is a spaced pressure solution cleavage deflected around clasts of euhedral plagioclase. Mesoscopic F_{C2} folds are not observed but S_{C2}, which is often sub-parallel to S_0, reflects F_{C3} folding and dips NE/SW (Figs. 3.4e & f).

3.6.2 Late Deformation ($F_{C3} \pm S_{C3}$ and F_{C4}).

Folds and thrusts of this event are of microscopic to regional scale. D_{C3} thrusts vary orientation (Fig. 3.17b) and are often accompanied by slickensides and sheared out fold limbs (3.19I). Localised development of an S_{C3} cleavage displays lithological dependence (Fig 3.18D). F_{C3} fold axial surfaces range in dip from sub-vertical to north-easterly dipping, while F_{C3} fold plunges are sub-horizontal (Fig. 3.4e). Along the Aroche - El Mustio section extensive disruption by numerous thrusts has occurred and no consistent facing direction can be measured. Locally, however, upward facing folds occur (Fig. 3.19B). In profile folds vary in shape from gentle (interlimb angle 180°-120°) to tight (≤30°) and range from parallel to similar classes, a feature that is dependent both on local strain intensity and lithological variation (Ramsay & Huber 1987).

D_{C4} is only locally visible, occurring as a crenulation of F_{C3} fold axial planes, best seen in plan view (Fig. 3.19F [GR 7075 8990]). F_{C4} fold axial planes are orientated oblique to the regional foliation and are steeply dipping, trending ≈170° to 180° (Fig. 3.28). They generally have steeply plunging fold hinges and may have been generated during a late D_{C4} phase of sinistral strike slip movement (Fig. 3.28).

3.6.3 D_{C1}, D_{C2} and D_{C3} field relationships.

Several examples from the section are used to illustrate the structural meso- and micro-scale relationships of within the Central Metasedimentary Domain.

A detailed example comes from a strike perpendicular section [GR 7150 9323] - [GR 7138 9305], which is dominated by strike parallel thrusts (Fig. 3.20, the section is located in Fig. 3.21). The rocks here are homogenous green arenites, intercalated with thin beds of slate within which way-up is determined by gradual changes from coarse (<1mm) to fine grained rocks. A deflected cleavage within fine grained slates is also used to infer way-up. S_{C1} is variably preserved in this section; in places the cleavage is strongly deformed and may be rotated into parallelism with S_{C2} which exists both as a bedding parallel and bedding oblique cleavage (Fig. 3.20). S_{C3} is only locally developed and is lithology dependent, best developed in fine grained slates. These relationships are well demonstrated in an F_{C3} fold at 100 metres from the beginning of the section [GR 7138 9313]. Here, S_{C1} is preserved, as a contorted cleavage, within S_{C2} cleavage planes which are orientated obliquely to bedding. Locally, S_{C3} cuts across both of these and is orientated sub-vertically (Fig. 3.21b). Younging relationships demonstrate that this F_{C3} fold is inverted, SW facing. It is separated from

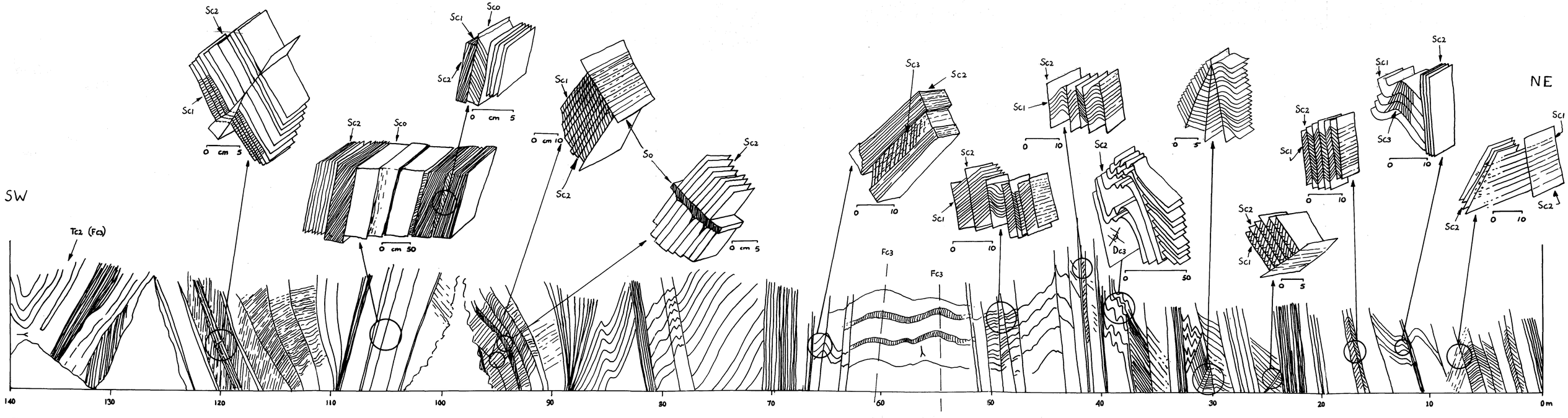

Figure 3.20 detailed section from Aroche - El Mustio road.

vertical exaggeration x2.

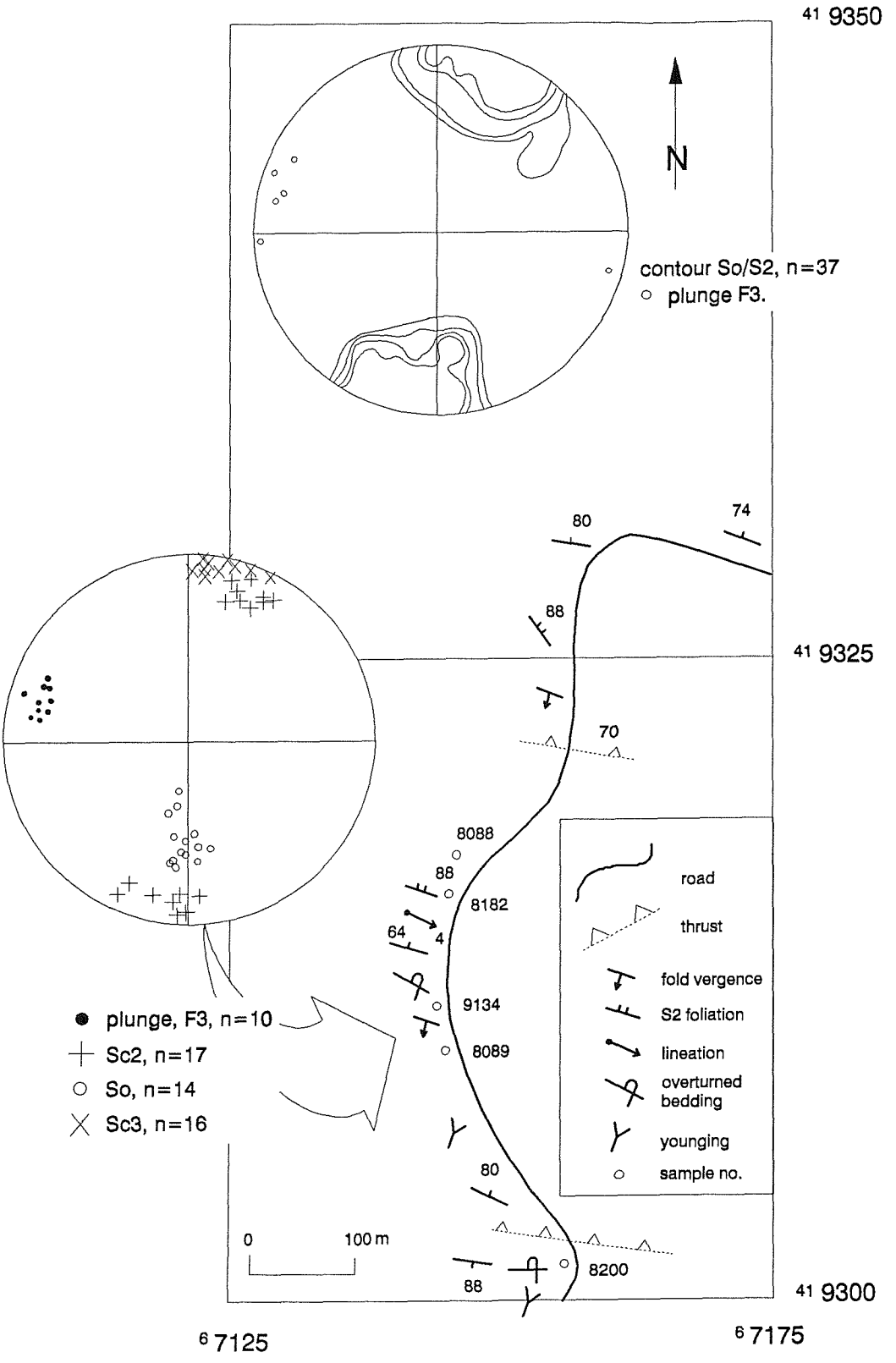

Figure 3.21 Location of the detailed section illustrated in Fig. 3.20. The diagram also shows structural data from along this section.

the next thrust package by a zone of highly deformed slates. Along this section the orientation of S_{C2} is generally sub-parallel to S_0 and F_{C3} fold axial planes are sub-vertical (Fig. 3.21a). F_{C3} folds plunge at shallow angles sub-horizontally. The variable plunge of the fold axes may be interpreted by shortening normal to strike which was accompanied by a component of strike-slip (Fig. 3.7c).

At [GR 7138 9304] an isolated F_{C3} fold lies above vertical beds. Grading in the beds below the fold indicates younging towards the SW while the fold itself is a downward facing syncline. A folded thrust surface is postulated to interpret this relationship (Fig. 3.20).

A further example of cleavage/bedding relationships comes from [GR 6995 9803] (Fig. 3.22). In this locality a fine grained arenite is interbedded with a fine grained phyllitic horizon. Small scale NE verging, F_{C3} cylindrical folds are formed within the arenite layer while irregular chevron folds are formed within the phyllite, a consequence of ductility contrasts between lithologies. The S_{C1}/S_{C2} cleavage/bedding intersection is folded around the hinge of the F_{C3} fold. Kink banding (Fig. 3.19H) also occurs in the same locality forming in rocks possessing a strong anisotropy. Kink band width varies from centimetric to decicentimetric and the kink band axis dips 68° to the NE on a strike of 100°, cross cutting an earlier cleavage. Kink bands may result from late stage compression parallel or nearly parallel to the dominant plane of schistosity (Ramsay & Huber 1987) and may accommodate additional strain by slip along cleavage planes (Verbeek 1978).

3.7 The Southern Metasedimentary Domain.

This domain is located immediately to the north of the Pyrite Belt, from which it is separated by a structural discontinuity (Apalategui *et al.* 1983) (Fig. 3.1). Here, the rocks consist of minor discontinuous quartzite mylonites within a matrix of quartz-mica schists similar to the Cumbres de Los Ciries Formation. A down dip mineral elongation lineation is weakly developed (Fig. 3.28c). The quartzite mylonites occur as discontinuous elongate blocks that measure up to ≈1m in length and have a width of up to 50cm (Fig. 19A). Microstructures, such as alignment of quartz axes, together with the rare development of a mineral lineation suggest transport direction to the SW. In hand samples e.g. 8192, recrystallised quartz has a uniformly fine grained matrix which displays features such as sutured crystal edges and alignment of c-axes, the products of intense dynamic recrystallisation. Although furthest from the main suture between the Ossa Morena Zone and the Oceanic Exotic Terrane, this zone demonstrates higher levels of strain than the other zones described.

3.8 Boundaries between formations.

Apaletegui *et al* (1983, 1984) and Crespo-Blanc (1989) describe many boundaries between lithological formations and structural domains as conserving primary stratigraphic relationships. However, in this study only abrupt tectonic boundaries are recognised.

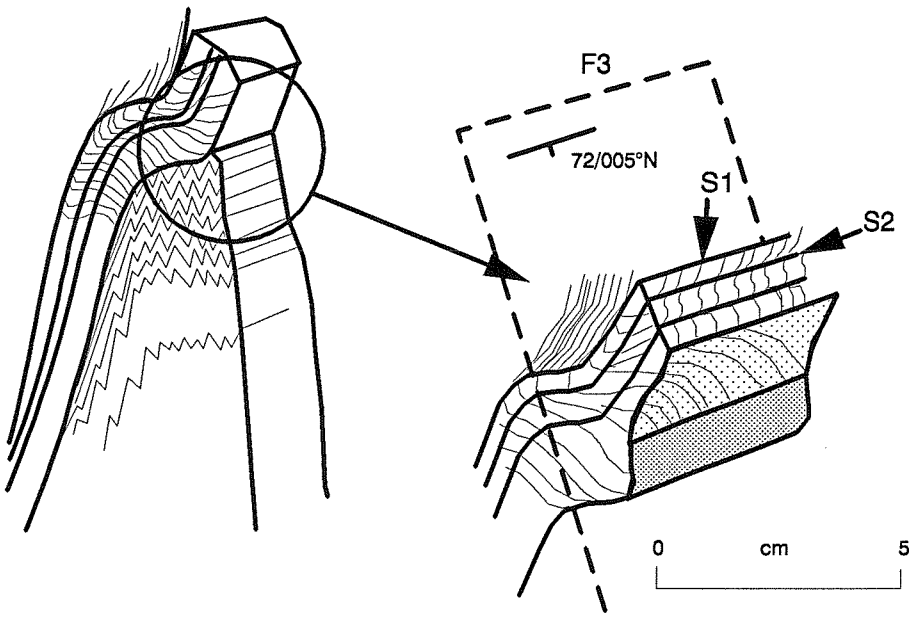

Figure 3.22 An example of lithology dependence during shortening within the Central Metasedimentary Domain. The medium grained arenite layers form open, cylindrical folds while the fine grained siltstone layers are chevron folded. These folds are further illustrated in Fig. 3.19G.

3.8.1 Boundary between the Beja-Acebuches Amphibolites and the Cumbres de Los Ciries Formation at Puerto Cañon.

This boundary is clearly seen along the Aroche-El Mustion road section ([GR 7630 9920] to [GR 7635 9905]) (Figs. 3.23 & 3.24) and also along the banks of the Alcalaboza river west of Puerto Cañon [GR 7965 9695]. Within fine grained amphibolites there are minor strike parallel F_{A3} folds with sub-horizontal axes. As the boundary is approached lenses of coarser grained gabbroic material occur [GR7635 9925] and these crop out directly along strike from basic dykes seen in exposure at Puerto Cañon [GR 7755 9905]. These gabbroic lenses are later foliation concordant bodies injected during D_{A2}. The footwall to the amphibolites in the road section is dominated by quartz-mica pelitic schists of the Cumbres de Los Ciries Formation. These are characterised by the presence of syn-kinematic andalusite, around which the foliation is deflected, and a well developed mineral lineation (Fig. 3.24c). Further south, away from the suture zone, andalusite becomes randomly orientated within the S_{N2}-surfaces of the quartz-mica schists.

The nature of the early schistosity, S_{A1}, observed in the Beja-Acebuches Amphibolites is unclear due to overprinting during ductile deformation, D_{A2}. It may represent an early phase of deformation related either to on-ridge generation of ocean crust or to obduction, although any interpretation as to its origin must, of necessity, be tentative.

In Portugal the progression from coarse grained amphibolites, through fine grained amphibolites to sediments with a pelitic character has been used to suggest that the Beja-Acebuches Amphibolites represent an inverted ophiolitic sequence (Oliveira *et al.* 1986, Munha *et al* 1986, 1989). However, the intensity of ductile shearing that has now been recognised (Crespo-Blanc 1989) has bought into question stratigraphic evidence of way-up and this hypothesis remains uncertain.

3.8.2 The boundary between the Northern Metasedimentary Domain and the Central Metasedimentary Domain.

The boundary between the Central Metasedimentary Domain and the Northern Metasedimentary Domain consists of a 500 metre wide zone of disruption. The boundary may be seen on the Aroche-El Mustio road beginning at [GR 7345 9620] and continuing for approximately 1 km to the southwest (Fig. 3.23b and Fig. 3.25). At approximately 100m from the NE end of the section the quartz-mica schist gives way to interbedded fine grained argillites and siltstones dipping steeply to the SW. S_{C1}, S_{C2} and F_{C3} fabrics and folds are clearly developed at this point (Fig. 3.26A, B, and C). Within the quartz schists there are numerous blocks which deflect the foliation, some are composed of quartzite and others are basic in composition. No way up indicators are seen in this part of the section. At approximately 500m the foliation and fold axial surfaces begin to shallow out (Fig. 3.25D & 3.26). A 50m wide zone of chaotic disruption is observed (Fig. 3.26D - locality E in Fig. 3.25) within which there are large blocks of foliated siltstone (Fig. 3.26D - locality D Fig. 3.25).

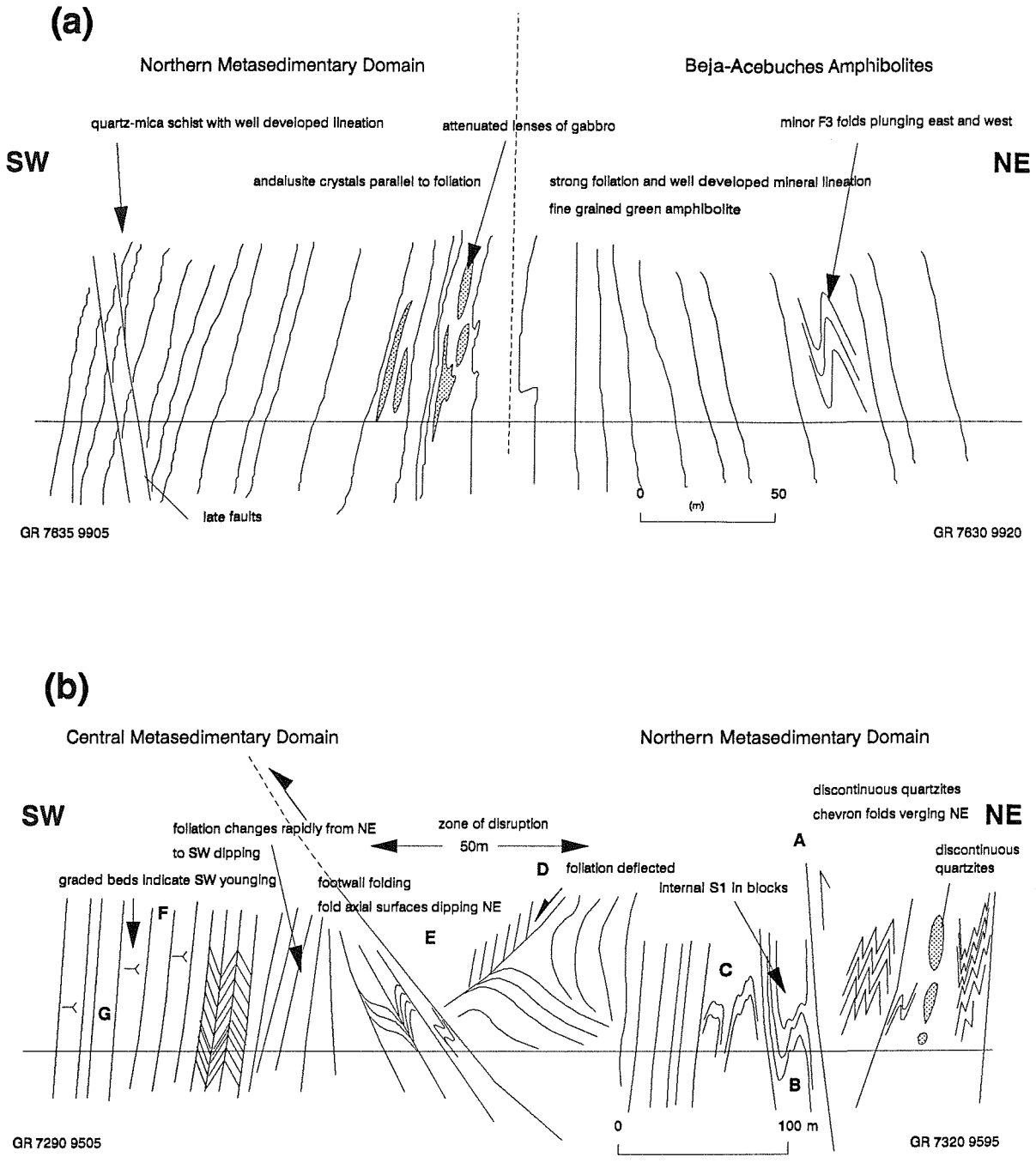

Figure 3.23 Boundaries between (a) the Beja-Acebuches Amphibolites and the Northern Metasedimentary Domain, and (b) contact between the Northern and Central Metasedimentary Domains.

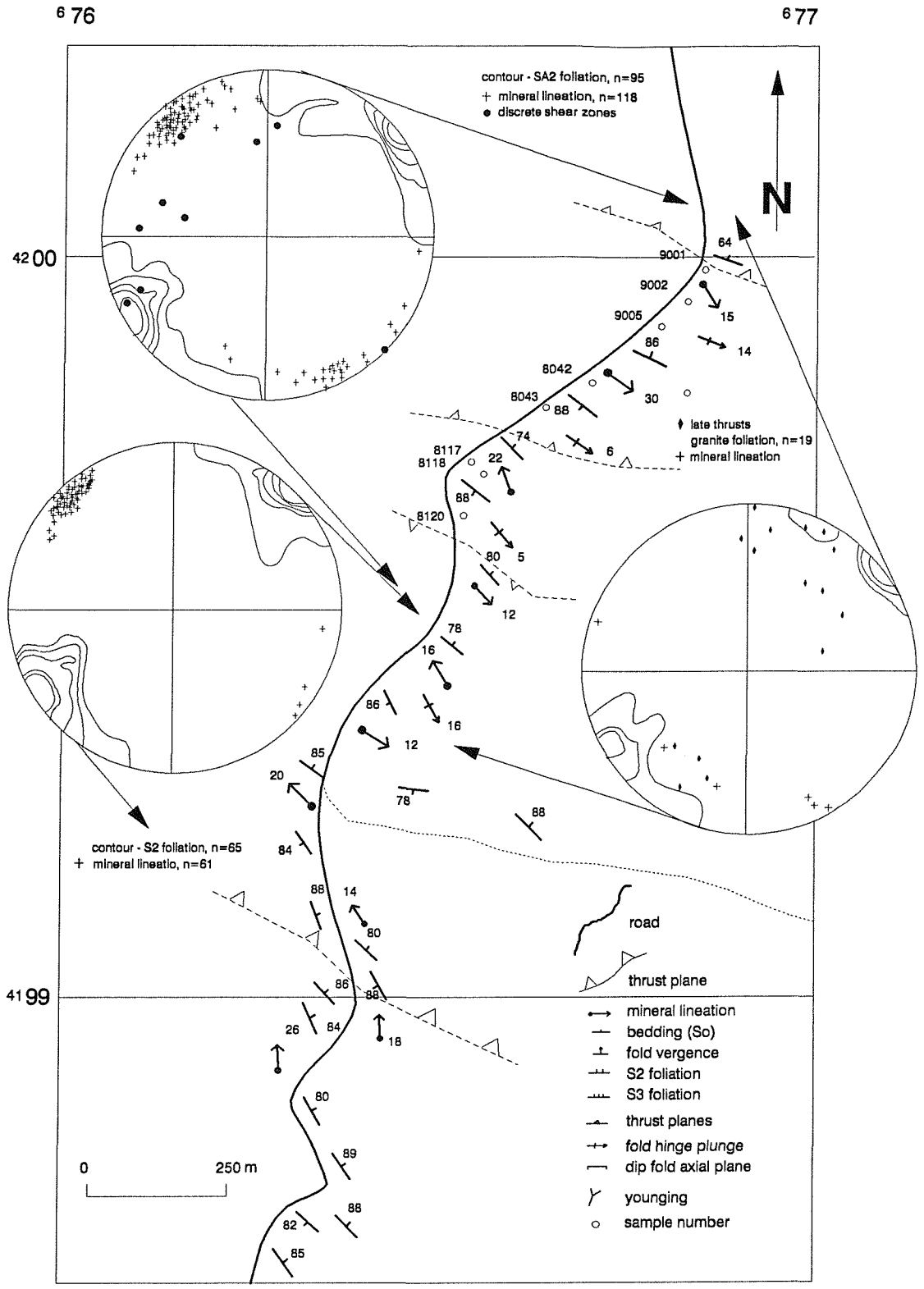

Figure 3.24 Boundary between the Beja-Acebuches Amphibolites and the Northern Metasedimentary Domain.

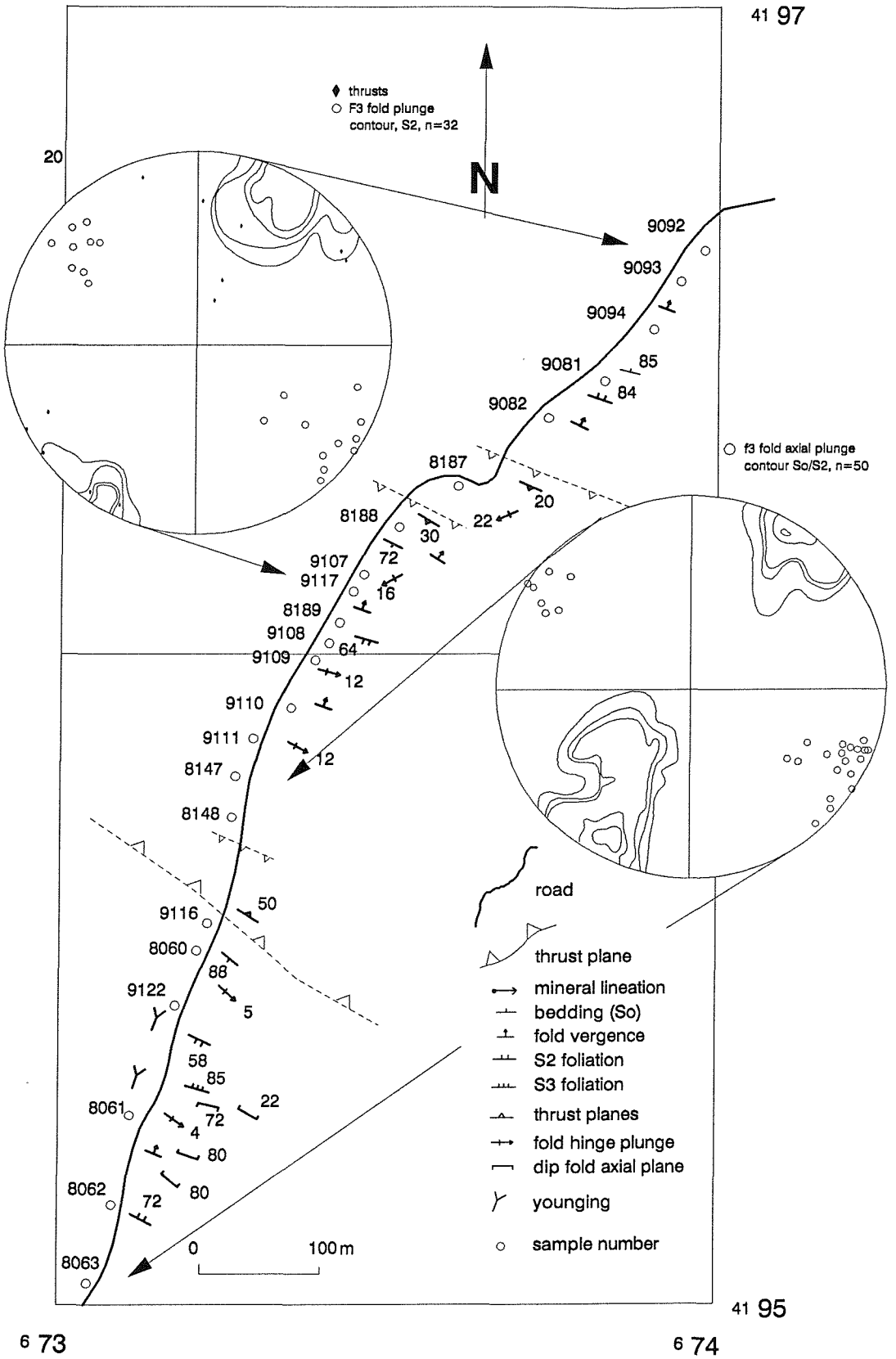

Figure 3.25 Boundary between the Northern Metasedimentary Domain and the Central Metasedimentary Domain.

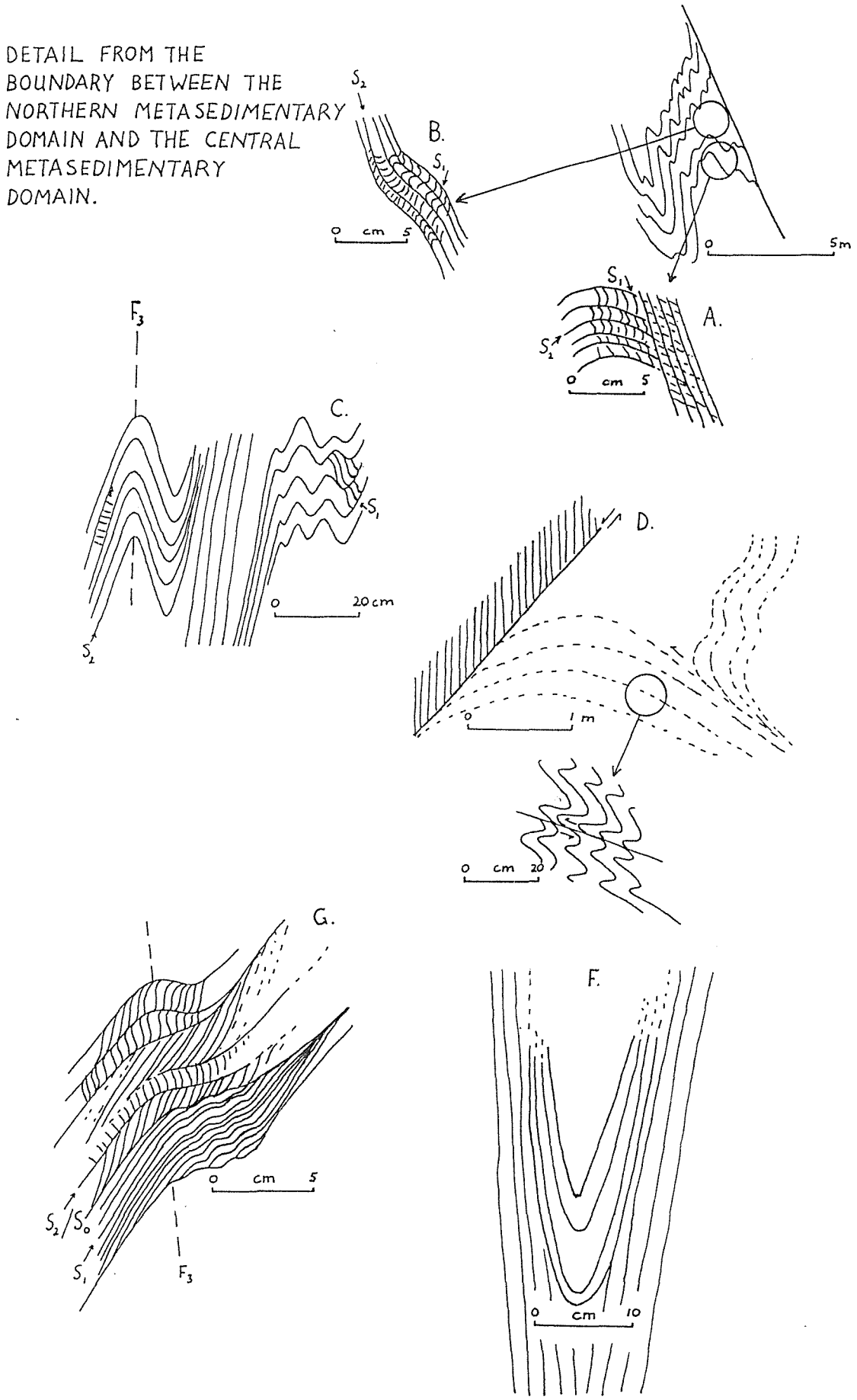
DETAIL FROM THE BOUNDARY BETWEEN THE NORTHERN METASEDIMENTARY DOMAIN AND THE CENTRAL METASEDIMENTARY DOMAIN.
S2
B.
S1
0 cm 5
0 5m
S1
A.
S1
0 cm 5
F3
C.
S1
0 20 cm
S2
D.
0 1 m
0 cm 20
G.
0 cm 5
S2/S0
S1
F3
F.
0 cm 10

Figure 3.26

Beyond this point the foliation dips gently to the NE then rapidly steepens to the SW. S_{C1} is rarely preserved and S_{C2} is often orientated oblique to S_{C0}. Graded bedding here indicates younging predominantly towards the SW. One tight fold (F_{C3}?), which has a sub-vertical fold axial plane and an interlimb angle of ≈30°(Fig. 3.26F - locality F Fig. 3.25), is located ≈150m to the southwest of the zone of disruption.

3.8.3 Boundary between the Southern Metasedimentary Domain and the Central Metasedimentary Domain.

This boundary is marked by an apparent increase in the bulk strain southwards over approximately 500m. A schematic section, based upon field measurements, extends northeastwards for some 700 metres from [GR 7010 8780] (Fig. 3.27 and Fig. 3.28). It begins in intensely deformed quartz-mica schists of the Southern Metasedimentary Domain within which the foliation and the fold axial planes dip consistently to the NE (Fig. 3.28). F_{S3} chevron folds verge predominantly towards the SW (Fig. 3.28). Within the schist matrix discontinuous blocks of quartzite ultramylonites (Fig. 3.18A), which have a mylonitic fabric concordant to the external foliation and support a weak, rarely preserved down-dip mineral lineation, are located. Fine grained sandstone units are interbedded with the schists and increase in proportion towards the north, eventually becoming dominant beyond 300m. These usually display younging up to the NE, and F_{C3} folds become more open and cylindrical. Apalategui *et al.* (1983, 1984) consider this intercalation of lithologies to be sedimentary in origin. However, contrasting metamorphic grades (up to mid-greenschist facies in the Southern Metasedimentary Domain; lower greenschist facies in the Central Metasedimentary Domain) and structural styles (ultramylonites in the Southern Metasedimentary Domain and normally graded bedded sedimentary rocks in the Central Metasedimentary Domain) are more consistent with tectonic juxtaposition.

3.9 Summary.

In general, at least three phases of deformation affect the Oceanic Exotic Terrane and Beja-Acebuches Amphibolites (Fig. 3.2). D_1 is locally preserved in lenses as a deformed cleavage, S_{N1}, in the Northern Metasedimentary Domain and the Central Metasedimentary Domain whilst D_{N2} represents a phase of sinistral ductile deformation, giving rise to a pervasive schistosity (S_{N2}). During D_2 several features developed that are common to the Beja-Acebuches Amphibolite Domain, the Northern Metasedimentary, the Southern Metasedimentary Domains and Alajar Domain but are absent in the Central Metasedimentary Domain. These features include:

(a) A strong regional foliation striking NW -SE and now dipping steeply, mainly to the NE.

(b) A sub-horizontal mineral lineation, well defined in the fine grained amphibolites of the Beja-Acebuches Amphibolites and the rocks of its immediate footwall in the Northern Metasedimentary

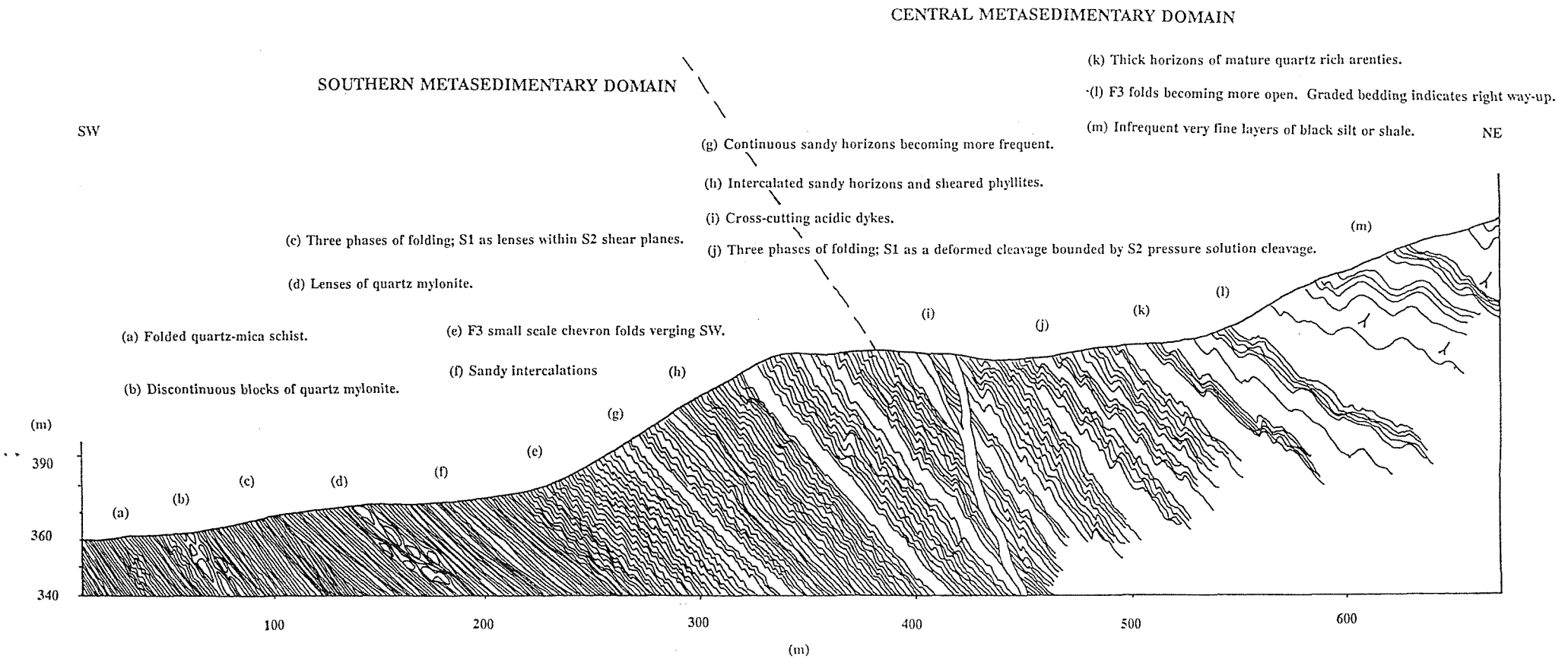

Figure 3.27 Schematic section of the boundary between the Central Metasedimentary Domain and the Southern Metasedimentary Domain.

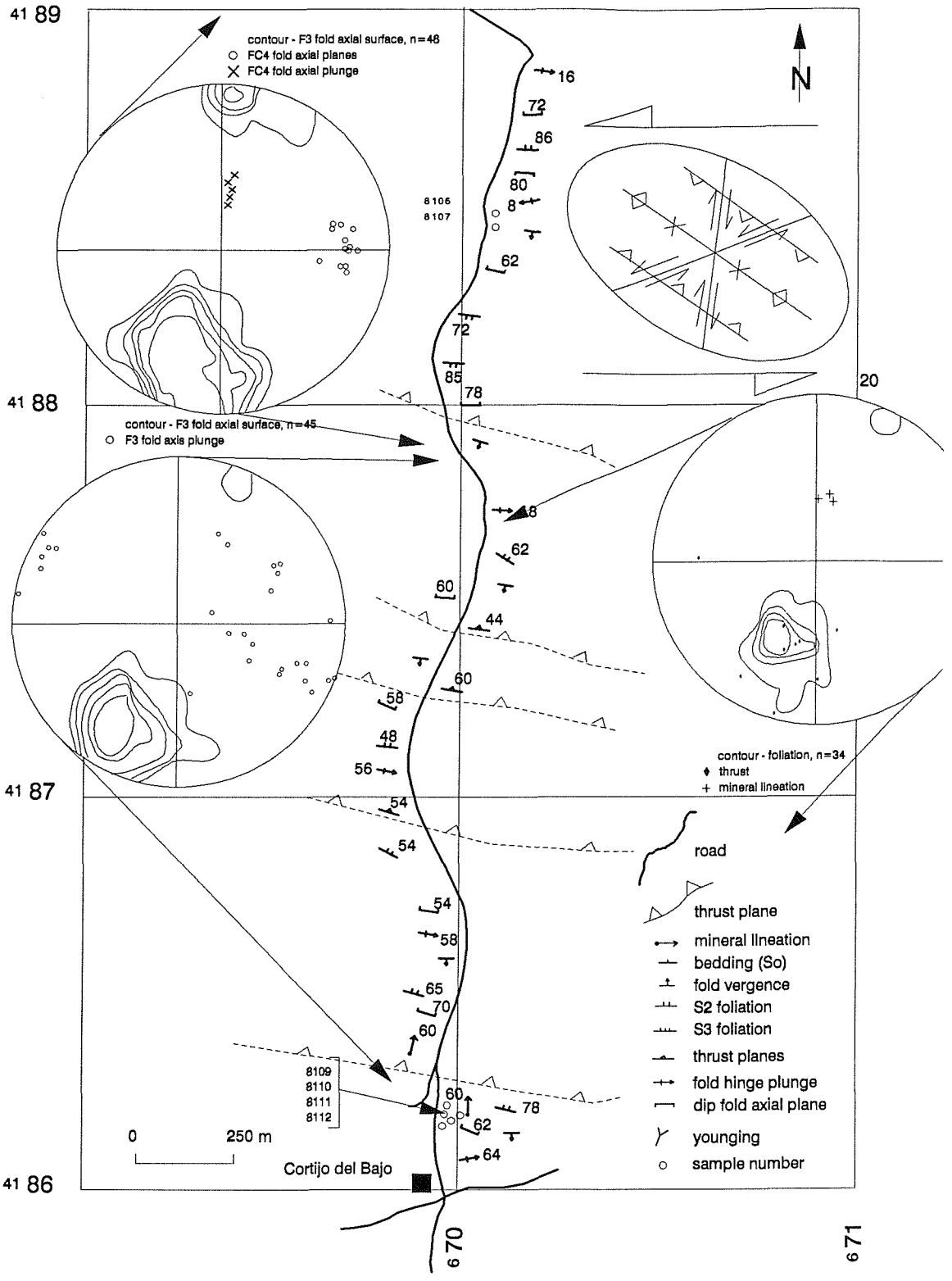

Figure 3.28 Boundary between the Central Metasedimentary Domain and the Southern Metasedimentary Domain.

	Beja-Acebuches Domain	**Northern Metasedimentary Domain**	**Alajar Domain**	**Central Metasedimen -tary Domain**	**Southern Metasedimen -tary Domain**
D_1	L-S fabric on northern boundary with the Aracena Massif.	S_{N1} locally preserved in lenses in the Cumbres de Los Ciries Formation.	not observed.	S_{C1} preserved as a highly deformed fabric.	not observed
D_2	grain size reduction; strong sinistral mylonitic fabric (S_{A2}).	strong mylonitic fabric (S_{N2}); sinistral ductile deformation; imbrication.	strong regional fabric; ductile deformation imbrication.	S_{C2} pressure solution cleavage truncates earlier schistosity; D_2 thrusts.	S_{S2} fabric, ultramylonite s, both dip-slip and strike-slip displacement.
D_3	NE-SW shortening (F_{A3}).	NE-SW shortening producing chevron folds and formation of the Los Ciries Antiform (F_{N3}).	folding of D_{AL2} thrusts.	F_{C3} folds verging mainly towards the SW; locally S_{C3}; D_{C3} thrusts, SW directed.	chevron folds verging SW (F_{S3}).
D_4	not observed.	not observed.	not observed.	D_{C4} due to shortening parallel to F_{C3} fold hinges.	not observed.

Table 3.B Summary of deformational features in the structural Domains.

domain, and variably developed in the core of the Los Ciries Antiform.

(c) Formation of meso- and microscale kinematic indictors, the majority of which display sinistral strike-slip movement.

During the second phase of deformation the Northern Metasedimentary Domain and the Beja-Acebuches Amphibolite Domain were imbricated to form a complex of horses accumulated during thrust strike-slip deformation.

The major structural elements of the Central Metasedimentary Domain are (Table 3.B):

(a) Four phases of deformation: S_{C1} is a contorted cleavage between S_{C2} pressure solution cleavage planes and these fabrics are folded by F_{C3} folds. F_{C4} occurs only locally.

(b) Both D_{C2} and D_{C3} are characterised by thrusts. Dominant transport direction is towards the SW as indicated by fold vergence, facing direction and orientation of fold axial planes. F_{C3} fold hinges form perpendicular to this direction.

D_{N3} in the Northern Metasedimentary Domain produced chevron folds in the Cumbres de

Los Ciries Formation and also formed the Los Ciries Antiform. Strike-slip was accompanied by a component of normal movement such that the overall movement vector was that of oblique (transpressive) motion between domains (Sanderson & Marchini 1984). This is shown by the sub-horizontal E-W orientation of the mineral stretching lineation, orientation of F_{N3} fold hinges, generally perpendicular to the transport direction, and the dip of F_{N3} fold axial planes, which are generally dipping steeply to the NE.

3.10 Late Hercynian brittle faulting.

The study area is cut by numerous faults, clearly seen on the aerial photographs, that offset the different formations (Figs. 1.5, 2.2 and 3.29). These form part of a system of faults described in detail in Simancas (1983, 1984), Apalategui *et al.* (1983, 1984), Crespo-Blanc (1989) and the 1:200 000 map of Portugal (Ribeiro *et al.* 1987). They will only be briefly described here.

Several sets of fractures are recognised: (a) NW-SE and E-W faults. These are the most important sets and include brittle faults separating the Beja-Acebuches Amphibolites from the Northern Metasedimentary Domain. (b) Faults that trend approximately N60°E cross cutting the faults in the previous category. These are associated with a N-S trending fault set.

The orientation of these faults is consistent with a sinistral shear regime. The 060° trending faults can be interpreted as Riedel shears. They must have been generated at higher crustal levels than earlier ductile sinistral which suggests that tendency for strike-slip movement along the belt was long lived, spanning uplift from low structural levels to high levels. The age of the main fracture system is considered to be Stephanian or later as they cross-cut granitic plutons of Upper Carboniferous age (Simancas 1983).

3.11 Discussion.

The S_1 cleavage, preserved as discontinuous lenses within S_2 planes, has been interpreted as representing a phase of recumbent folding related to nappe emplacement (Oliveira 1988; Crespo-Blanc 1989; Silva *et al. in press*). Fonseca (*pers. comm*) relates the S_1 schistosity to northward tectonic transport, possibly associated with ophiolite obduction, although this phenomenon may be locally represented in a less deformed lacunae of fragmented ocean crust. No such observations are made either to the south of Aroche or Alajar. Field observations and microstructural analysis suggest that a regional significance placed upon the early schistosity must account for reworking during subsequent structural overprinting and as such it may simply represent an early mylonitic fabric which has been reorientated during subsequent mylonite forming events. In this respect D_{N1} and D_{N2} represent a single deformation sequence and can be regarded as separate events in descriptive terms only.

Boundaries between various structural domains within the Oceanic Exotic Terrane have previously been considered to retain primary sedimentary characteristics (Apalategui *et al.* 1983, 1984,

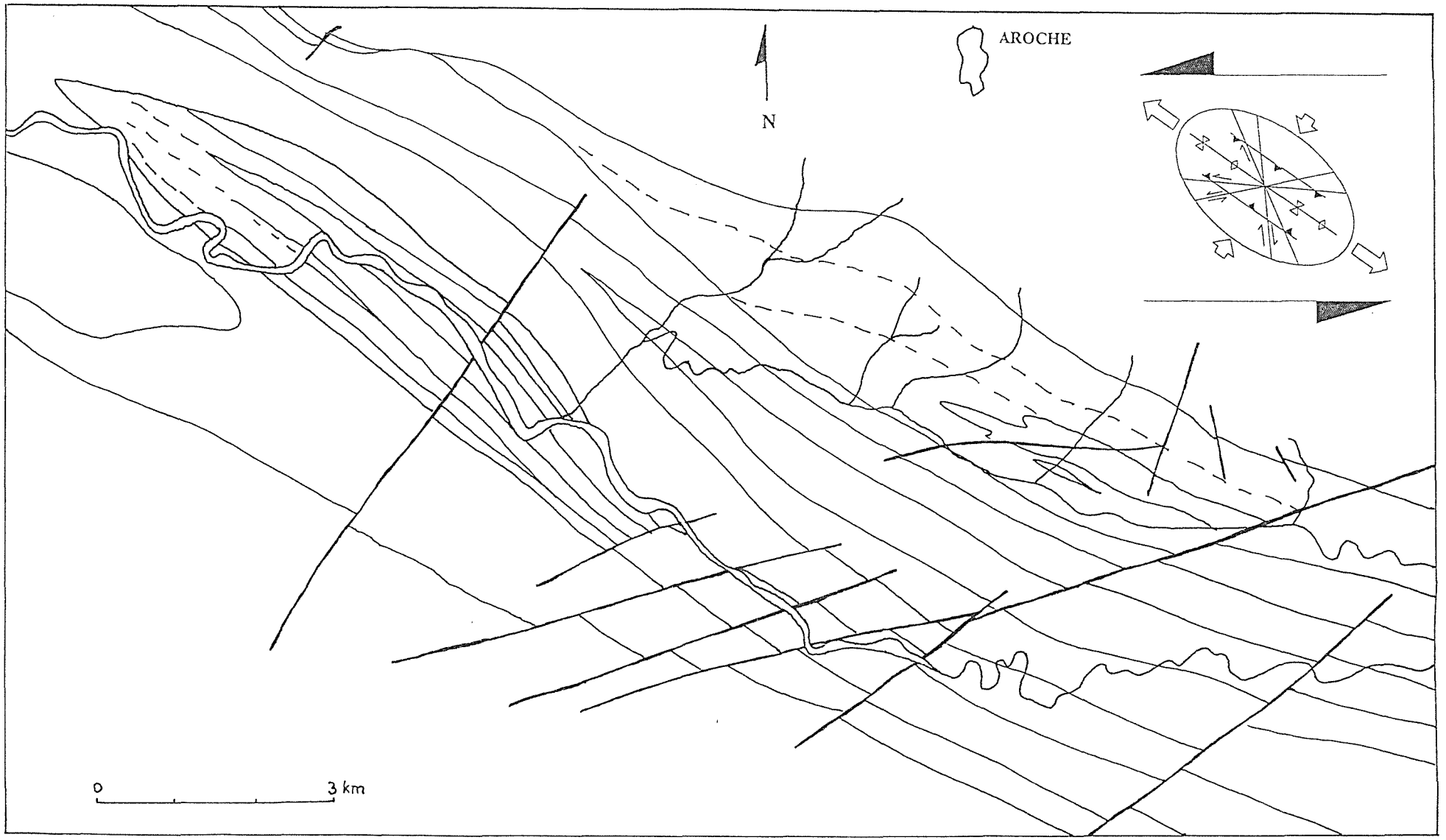

Figure 3.29 Late faults in the Aroche area cross cutting the earlier regional fabrics.

Crespo-Blanc 1989). Main features highlighted during this study that support interformational tectonic contacts include: firstly, imbrication between units with different structural and metamorphic characteristics; secondly, variation in apparent strain over relatively short distances, and thirdly the rarity of sedimentary structures in any of the formations identified. Three boundaries are considered:

(a) The boundary between the Beja-Acebuches Amphibolites and the Northern Metasedimentary Domain. This boundary is characterised by distinct lithologies on either side of the contact (amphibolites to the north and quartz-mica schists imbricated with mélanges to the south) and marked by a strong mylonitic foliation and associated mineral lineation imposed during strike-slip ductile deformation (the South Iberian Shear Zone (Crespo-Blanc & Orozco 1988).

(b) The boundary between the Northern Metasedimentary Domain and the Central Metasedimentary Domain is defined by a zone of disruption that fragments quartz-mica schists of the Cumbres de Los Ciries Formation to the north and the La Giralda Formation to the south.

(c) The boundary between the Central Metasedimentary Domain and the Southern Metasedimentary Domain displays an apparent increase in strain southwards from the bedded arenites and siltstones of the La Giralda Formation to the strongly deformed quartz-mica schists withint the Southern Metasedimentary Domain. High strain in the latter formation is demonstrated by the occurrence of quartzite ultramylonites within strongly sheared phyllonites (Cortijo del Bajo).

Brittle deformation occurred at a late stage in the tectonic evolution giving rise to fault sets that can be classified as synthetic Riedel shears and complementary P shears. These brittle fault sets were formed during the final increments of strike-slip movement across the belt and probably occurred in the late Carboniferous.

Chapter 4: Geochemistry.

Abstract

This chapter analyses geochemical relationships within the study area. The geochemistry of the Beja-Acebuches Amphibolites is considered using a representative sample set from El Hurón. This suite is compared with both blocks and matrix from the Peramora Mélange Formation. Results indicate that an ophiolite, represented by the Beja-Acebuches Amphibolites in the hangingwall, supplied sediment both as blocks and pyroclastic debris to form the Peramora Mélange Formation in the footwall.

A sample set from the La Giralda Formation and the Cumbres de Los Ciries Formation is also examined. The fine grained nature of these sediments precludes framework analysis using point counting techniques and in this study geochemistry is used as a tool to relate the sediments to a possible source. Results indicate that the source consisted of basic and acidic components and signatures obtained are similar to those from sedimentary rocks of the northern margin of the Hercynian Arc. The sedimentary formations within the study area are mature and have a geochemical signature consistent with a Continental Arc/Active Margin.

4.1 Introduction.

The aims of the geochemical approach to the study area are to:

(a) compare the geochemistry of the Beja-Acebuches Amphibolites with the blocks and matrix of the Peramora Mélange Formation.

(b) characterise and distinguish, using major and trace element geochemistry, the Beja-Acebuches Amphibolites, the Peramora Mélange Formation, Cumbres de Los Ciries Formation and the La Giralda Formation in terms of tectonic setting.

(c) use geochemistry to define provenance.

The present geochemical study is based on 192 samples. Of these 26 samples were collected from the Beja-Acebuches Amphibolites, 17 from El Hurón [GR 8435 9664], and 35 samples from the Peramora Mélange Formation (17 samples from the matrix and 18 from exotic blocks) (Figs. 4.1 and 4.2). 22 samples from the Cumbres de Los Ciries Formation and 60 samples from the La Giralda Formation were analysed for both major and trace elements. Data from this study are compared with data from samples collected from west of Alajar (Giese 1990 - appendix 2) and sample localities are listed in appendix 1. Some of the samples were analysed for trace elements only as these are considered to be more reliable in provenance determinations.

Sampling was effected with a view to obtaining a random sample of all the formations in an arbitrary transect across the belt. The representative sample set collected from El Hurón consists of fresh, medium grained, homogenous amphibolites in which the constituent minerals, mainly hornblende and plagioclase, are of comparable grain size; material containing large crystals were avoided.

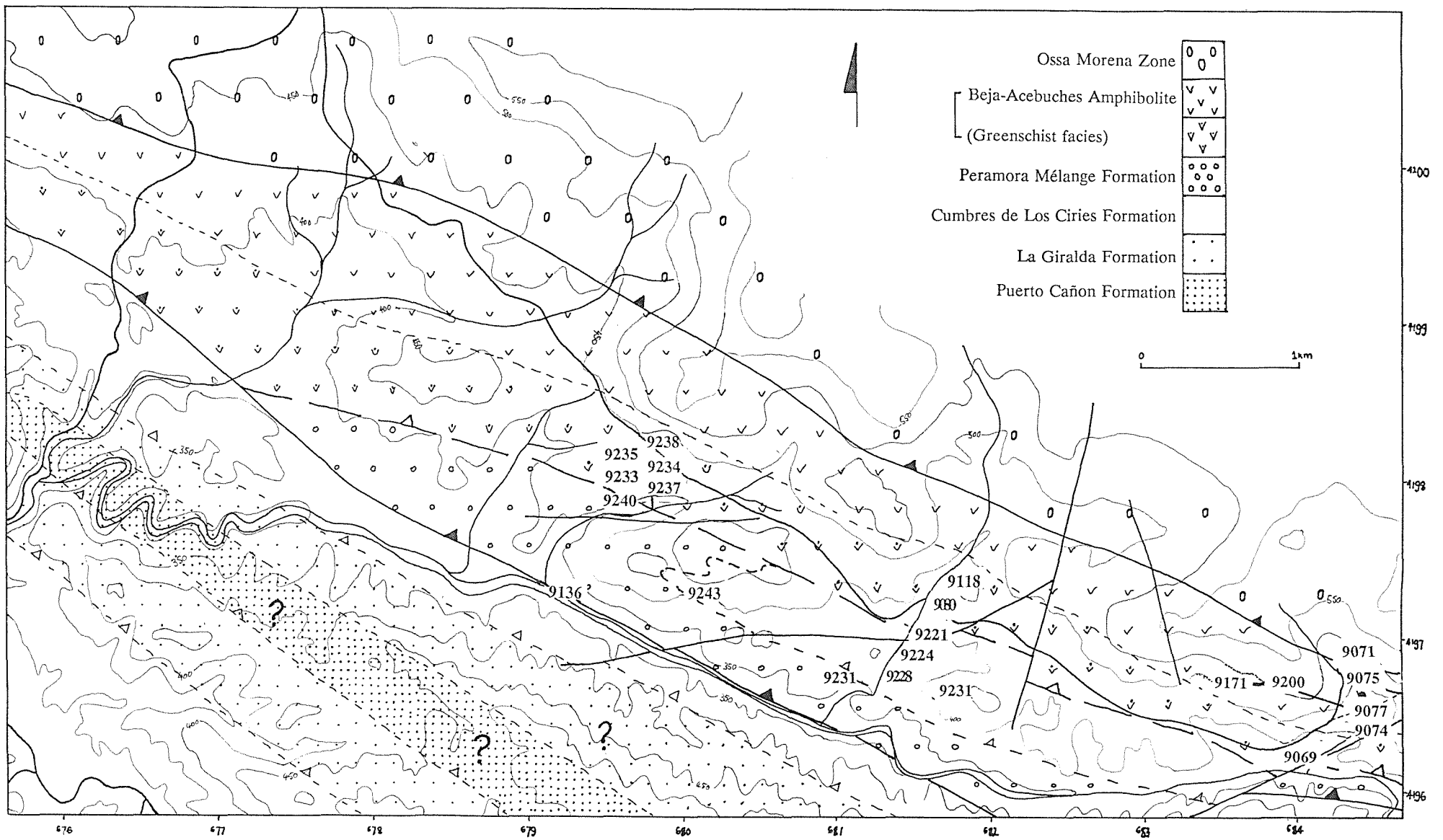

Figure 4.1 Map to locate geochemical samples used in this study.

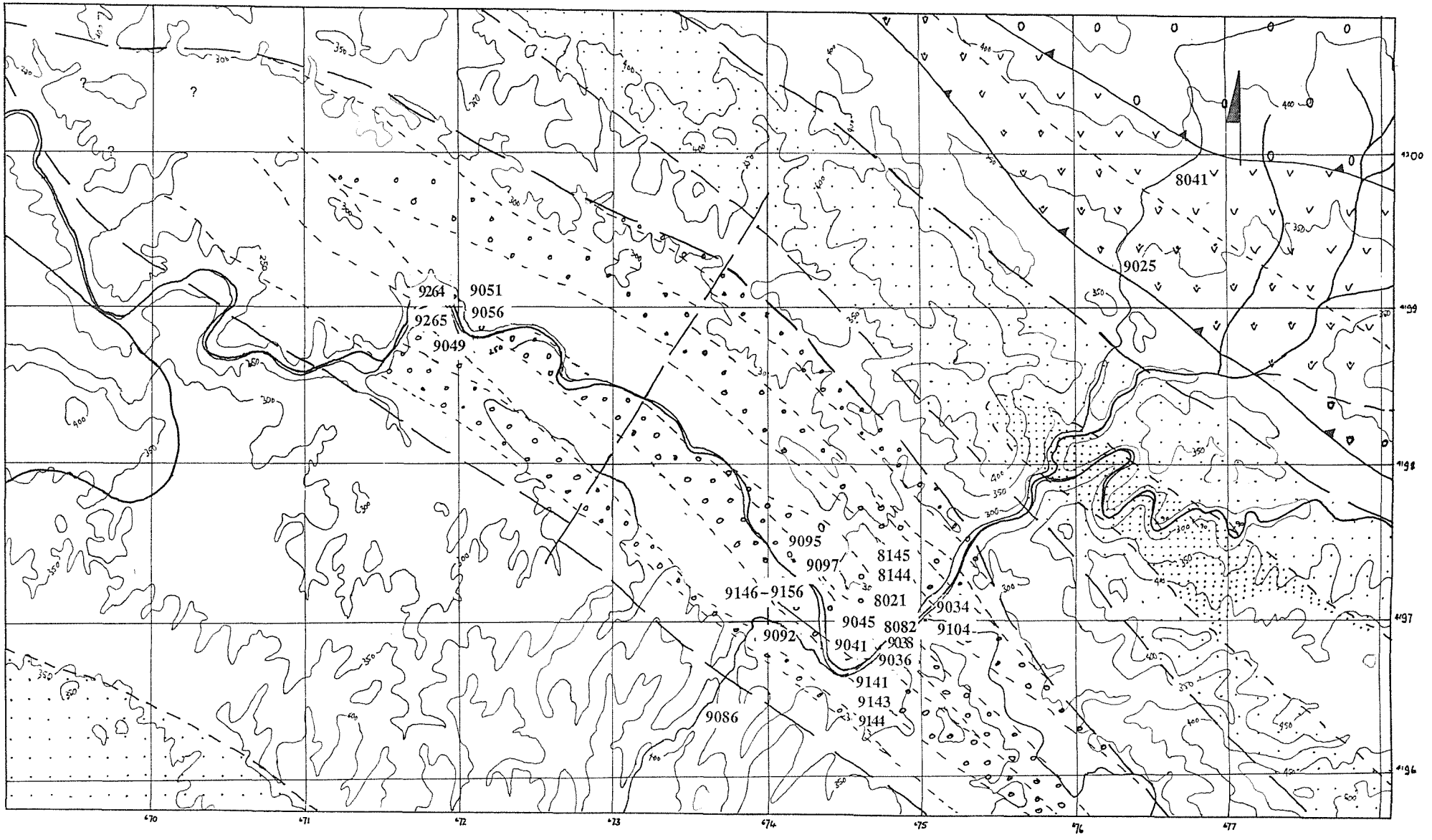

Figure 4.2 Map to locate the samples collected for geochemical analysis.

4.1.1 Previous work.

Geochemical studies, together with field observations (Bard & Moine 1979, Dupuy *et al.* 1979, Munha *et al.* 1986, 1989), have shown that the Beja-Acebuches Amphibolites may represent a dismembered ophiolite. Munha *et al.* (1986) working along strike from the study area in Portugal, used features such as internal lithological organization and metamorphic zonation to infer that the ophiolite was overturned. Both Munha *et al.* (1986) and Dupuy *et al.* (1979) identify the Beja Acebuches Amphibolites as being originally tholeiitic basalts. Munha *et al.* (1989) point out that the amphibolites display considerable variation in incompatible element concentrations, ranging from MORB-type (Mid Ocean Ridge Basalt) in the Acebuches area to arc-type tholeiites in the Beja area. They conclude from geochemical data that the dismembered ophiolite, represented by the Beja-Acebuches Amphibolites, and the sediments and volcanics of the Pulo do Lobo Formation, originated within the same ocean basin. This basin is thought to have been located somewhere between the Pyrite Belt and the Ossa Morena Zone. The mixed MORB - Island Arc geochemistry of the Beja-Acebuches Amphibolites is accounted for by ophiolite obduction synchronous with a spreading ridge/trench system active during docking between the Ossa Morena Zone and the South Portuguese Zone.

The Peramora Mélange Formation has not previously been recognised as a discrete formation and its discovery has significant implications for modelling the tectonic evolution of the basin. Geochemical analysis and provenance definition of the formation provide essential information for this model.

4.2 The Beja-Acebuches Amphibolites.

4.2.1 Petrography.

Bard (1969) identified four stratigraphically normal levels within the sequence of amphibolites. Level D (south, and hence the top of the sequence) consists of fine grained amphibolitic schists spotted by pre-kinematic plagioclase and with foliation planes delineated by boudinaged epidote. Level C is composed of banded amphibolites with local feldspar-rich layers. The mineralogy includes hornblende (richtero-tschermakite), oligoclase ± sphene ± epidote ± ilmenite and pyrite. Diopside is rarely seen. Level B consists of a medium to fine grained massive foliated amphibolite composed of andesine, hornblende ± diopside ± sphene ± ilmenite ± cummingtonite ± epidote. Level A is a heterogenous massive amphibolite with fine grained lenses crossed by coarse grained 'dioritic' amphibolites.

Studies by the Spanish Geological Survey carried out during the course of mapping of sheet 916 and 917 (Apalategui *et al.* 1983, 1984) identified coarse grained amphibolites that give way southwards to fine grained amphibolites. Actinolite and tremolite were noted in both fine and coarse grained amphibolites.

Crespo-Blanc (1989) details petrographic studies from various localities within the Beja-Acebuches Amphibolites and identifies the presence of pyroxene both as primary crystals and as relict grains within the coarse grained amphibolites in the northern margin of the belt. The presence of these relict grains is used to infer that granulite facies metamorphism may have affected the northern margin of the Beja-Acebuches Amphibolites. A major episode of shearing later affected the Beja-Acebuches Amphibolites, becoming stronger towards the south (Fig. 1.4 and Fig. 3.3) an event that accompanied retrogression of the high grade amphibolite facies complex to greenschist facies conditions.

In the present study 26 amphibolite samples were analysed for major and trace elements. Representative modal analyses are given in Table 4.A. A typical mineral assemblage consists of essential hornblende (blue-green pleochroic) and plagioclase (lab-olig), which has suffered minor secondary alteration to sericite, with accessory sphene, epidote and quartz. The main opaque mineral phase is ilmenite. Fig. 2.9H shows that the mineral assemblage is generally at equilibrium, with triple junctions between the crystals, little evidence of plagioclase deformation twins or brittle fracturing of the constituent mineral phases. Pyroxene was not present in the samples studied.

Sample	Hornblende	Plagioclase	Quartz	accessories (inc. opaques)
9025	57%	35%	2%	6% (5% sphene)
9177	60%	38%	0.5%	1.5%
9183	57%	40%	1%	2%
9184	60%	37%	0.5%	1.5%
9185	63%	34%	0.5%	1.5%
9186	57%	39%	2%	2%
9189	61%	35%	1%	2%
9190	61%	36%	1%	2%
9192	60%	38%	0.5%	15%

Table 4.A Representative modal analyses of samples from the Beja-Acebuches Amphibolites based on 500 points per sample.

4.2.2 Screening of samples from the Beja-Acebuches Amphibolites and the Peramora Mélange Formation.

Screening, to eliminate those samples considered to be too altered, was effected using the discrimination diagram of Pearce (1973, 1975) and Pearce et al. (1973, 1979, 1981) which use elements that are considered to be immobile and therefore independent of processes of alteration. Both Ti and Zr are normally in this category and Fig. 4.3a, indicates an overall MORB-type geochemistry for the majority of the samples. Fig. 4.3a shows the complete compositional range of arc lavas and the solid line separates fields of basic and ultrabasic rocks from intermediate and acid lavas. The diagram also classifies rocks into Volcanic Arc Lavas and Within Plate Lavas, discriminating between magma types

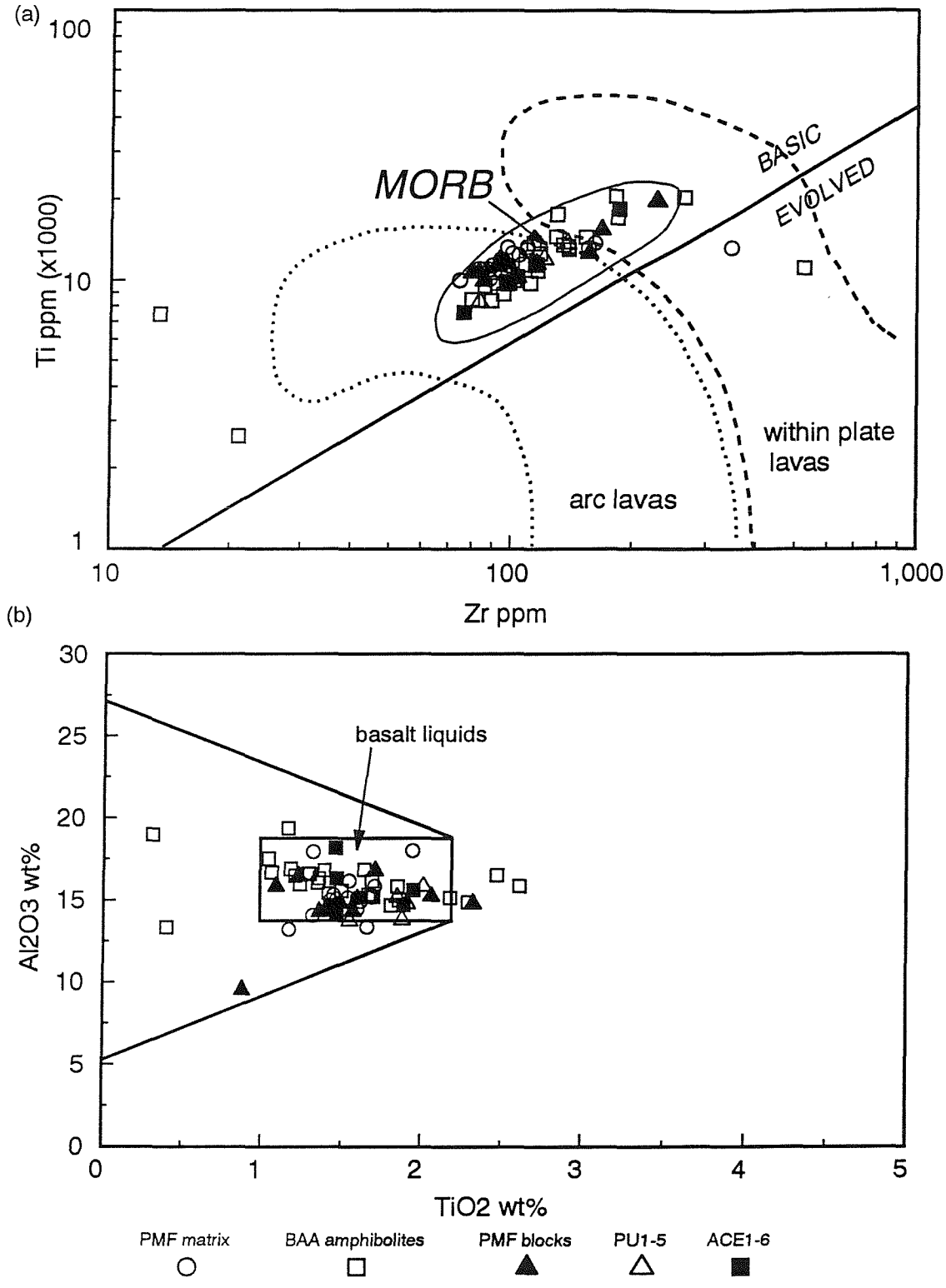

Figure 4.3 (a) Screening diagram using Zr vs Ti to check for samples considered too altered for use (after Pearce *in press*).

(b) Screening diagram using TiO_2 vs Al_2O_3.

on the basis of crystallising phases in the basic melt (olivine, pyroxene and feldspar), which do not affect the Ti/Zr ratios. However, once a Ti-bearing phase, such as an iron oxide begins to crystallise Zr continues to become enriched in the magma and the ratio decreases. Crystallisation of the oxide phase generally correlates with an increase in the SiO_2 content of the magma and thus the evolution from basic to acid magma coincides with a decrease in the Ti/Zr ratio. Another type of screening diagram uses the concentration of Al_2O_3 against TiO_2 (Fig. 4.3b). This diagram removes those rocks, such as cumulates, that deviate significantly from the true melt composition, and the majority of the basalts should occupy a well defined field. One consideration is that Al_2O_3 may have been mobilised during regional metamorphism. However, the samples from the study area (Fig. 4.3b), occupy the field of basalt liquids.

All the samples are thus of a general MORB-type character (Bard & Moine, 1979; Muñha *et al.* 1986). Samples from the Peramora Mélange Formation fall within this MORB field, a feature that is of considerable significance as these indications support field evidence that the mélange may be genetically related to the obducting oceanic crust. Three samples from the Beja-Acebuches Amphibolites and one from the Peramora Mélange Formation plot out of the MORB field and two of these plot out of the fields for basalts. This may be due to an enrichment or paucity of zircon in these samples. Several more samples are seen to deviate from the basalt liquids field in Fig. 4.3b, however, these may be due to the enhanced mobility of Al_2O_3 during deformation. These particular samples are treated with caution in the following diagrams.

4.2.3 Mobility of elements.

Many studies pertaining to the mobility of elements during regional metamorphism and metamorphism accompanying shearing have identified several elements that are commonly mobilised. Zirconium is generally taken to be immobile during processes such as sea floor weathering and low to medium grades of metamorphism (Pearce & Cann, 1973; Pearce & Nory, 1979; Moorhouse & Moorhouse, 1979; Wood *et al.* 1979). Zirconium has also been shown to vary systematically with igneous processes such as fractional crystallisation and partial melting. Element mobility can therefore be tested by comparison against this parameter (Barker, 1986).

Low Field Strength elements (Table 4.B) are known to be mobile during sea-floor alteration processes (Li 1981; Taylor 1988), therefore in the interpretation of basaltic volcanics high field strength 'immobile' elements such as TiO_2, P_2O_5, Zr, Y, Nb, and the rare earth elements (Table 4.B) have been used (Pearce & Cann, 1973; Floyd & Winchester 1975, 1978; Winchester & Floyd 1976, 1977; Pearce, 1975). However, other studies (Floyd & Winchester, 1983; Humphries & Thompson 1978; Ludden & Thompson, 1979) have shown that during some low-grade metamorphic conditions these elements may also be mobilised. Floyd & Winchester (1983) studied element mobility within meta-shear zones in Scotland and have pointed out that in high grade foliated or banded amphibolites,

	Low Field Strength Elements (LFS)						
element	Rb	K	Ba	Na	Sr		
radius/charge	1.47	1.33	1.67	0.97	0.37		
	High Field Strength Elements (HFS)						
element	Ga	Zr	Hf	Ti	P	Nb	Ta
radius/charge	0.21	0.20	0.20	0.17	0.15	0.14	0.14
	Rare Earth Elements (REE) + Y						
element	La	Ce	Nd	Eu	Er	(Y)	Yb
radius/charge	0.34	0.34	0.33	0.31	0.29	0.3	0.3

Table 4.B Incompatible trace element groupings (Sanders *et al.* 1980)

channelways for metasomitizing fluids may exist which can lead to alteration of the bulk chemistry of the rock. Extensive shearing and accompanying retrogression may also result in a change in the composition of a mafic rock as well as the abundance of the immobile elements. These authors used the abundance of TiO_2 as a crude fractionation index, and similarly the FeO^*/MgO ratio, although they report that this latter parameter is 'disturbed'. Several fractionation indices can therefore be used (TiO_2, Zr and the FeO*/Mgo ratio) to test for element mobility, however, for simplicity, only Zr is used in this study. Examples of mobility of elements in response to post-emplacement processes are given in variation diagrams shown in Fig. 4.4. Several features are apparent:

- A weak negative correlation between CaO and Zr lies along the clinopyroxene addition/removal vector, an indication of primary magmatic processes.

- There are strong positive correlations between P_2O_5, TiO_2 and Zr. These demonstrate well defined igneous trends which suggest that these elements were essentially immobile during metamorphism.

- There is a weak positive correlation, with a significant spread of the data for Na_2O and Fe_2O_3, a weak negative correlation for MgO and no correlation for Al_2O_3 or SiO_2. These latter elements may therefore have experienced some mobility during metamorphism.

4.2.4 Trace elements.

The role of trace elements in geochemical analysis is based on the partitioning of the elements between various mineral phases and melts during fractionation. The behaviour of some of the elements used in this study is summarised in Table 4.C (Green 1980). Fig. 4.5 shows selected trace elements plotted against Zr. There are strong positive correlations between Nb, Y, Ti and Zr, showing that these elements were essentially immobile and may be indicative of magma evolution; a weak negative correlation between Ni, Cr and Zr and no correlation between Sr and Pb suggesting significant mobility of these two elements during metamorphism. The weak negative correlation of Ni and Cr may indicate limited metamorphic mobility and/or possibly primary igneous processes.

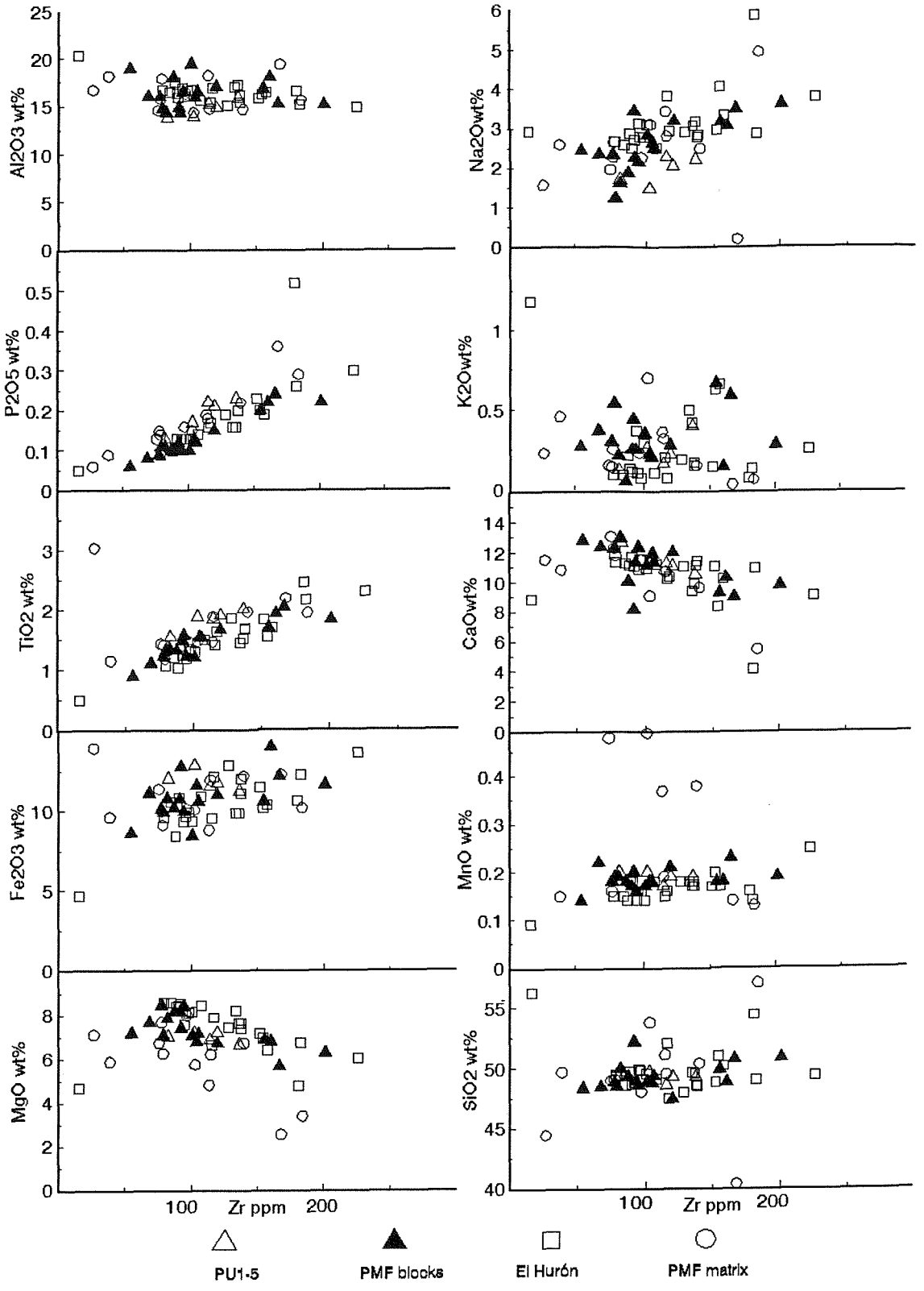

Figure 4.4 Discrimination diagrams of major elements in the El Hurón amphibolites and the Peramora Mélange Formation using Zr as the differentiation index.

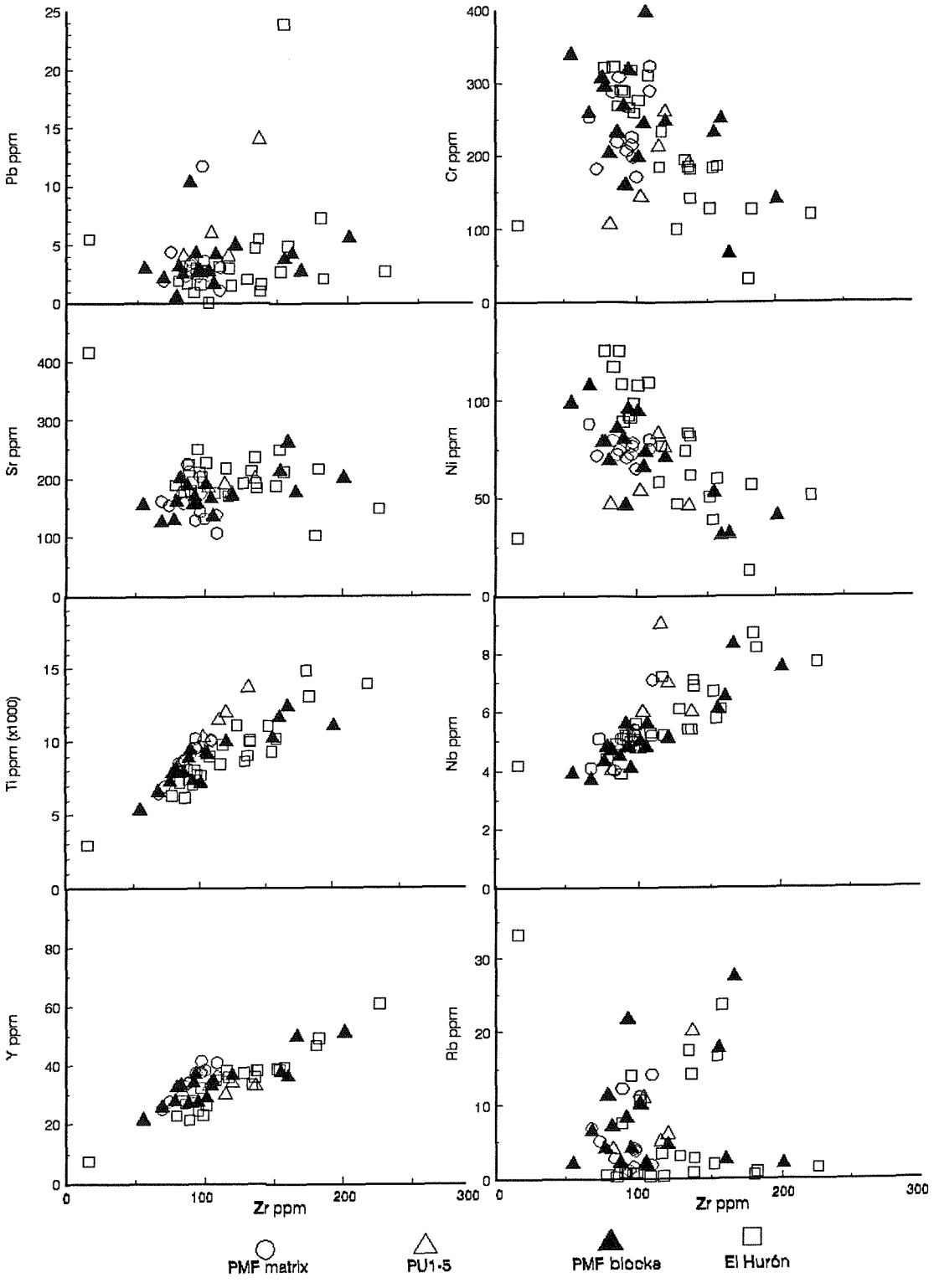

Figure 4.5 Discrimination diagrams of trace elements in the El Hurón amphibolites and the Peramora Mélange Formation using Zr as the differentiation index.

Ni, Cr	High values (up to Ni = 300ppm, Cr = 600ppm) may indicate derivation from mantle peridotite. Decrease in Ni suggests olivine fractionation, and Cr in Cr spinel or clinopyroxene fractionation.
V, Ti	Parallel behaviour indicates fractionation of Fe - Ti oxides (ilmenite or titanomagnetite), divergent behaviour indicates substitution into accessory phases such as sphene or rutile.
Zr	Generally incompatible and doesn't readily substitute into major phases. May substitute for Ti in accessory phases.
Ba, Rb	Both elements substitute for K in K-feldspar, hornblende and biotite.
Sr	Substitutes readily for Ca in plagioclase and for K in K-feldspar.

Table 4.C Summary of trace element behaviour in petrogenetic modelling (after Green 1980).

4.3 Geochemistry of the Beja-Acebuches Amphibolites and the Peramora Mélange Formation and relation to tectonic environment.

Many papers provide accounts for determining the tectonic setting of modern basaltic rocks and their ancient counterparts using major and trace element geochemistry (Pearce & Cann 1973; Floyd & Winchester 1975; Pearce 1973; Pearce & Noray 1979; Beccaluva *et al.* 1979; Tarney *et al.* 1980; Boyle 1986; Boryta & Condie 1990). Figs. 4.2 and 4.3 show that both K_2O and Rb are present in significantly low quantities. This agrees with petrographical observations that the mica content, into which both these elements are mainly partitioned, is low. The low percentage of K_2O is also a good indication that this element was relatively immobile; low Rb + K_2O is also typical for fresh N-type MORB (Viereck *et al.* 1989). Na_2O shows a weak positive trend with most of the samples falling within the range 1.81 - 3.07 wt% (average 2.44 wt% with a standard deviation of 0.63 (Le Maitre, 1976) which again suggests that this element was relatively stable during metamorphism. Total alkali content of the rocks may also confirm the nature of the original material. The Harker variation diagram, in which SiO_2 is plotted against total alkalis, (Fig. 4.6) shows that all the samples mostly plot in a tightly spaced group within the sub-alkalic field. Considering the mobility of SiO_2 this is somewhat surprising. However, it does demonstrate that the samples are consistent with previous observations with regards parentage, in that the rocks of the Peramora Mélange Formation closely parallel the compositions displayed by the Beja-Acebuches Amphibolites.

Many of these diagrams demonstrate clear evidence for fractional crystallisation during original differentiation processes. Both Ni and Cr show negative trends suggesting the precipitation of either olivine or clinopyroxene in the original magma. However, if either olivine or clinopyroxene were the main precipitating phases a greater amount of both Cr and Ni would be expected. The negative trend of Al_2O_3 as well as CaO (Fig. 4.4) vs Zr would suggest that plagioclase was a co-

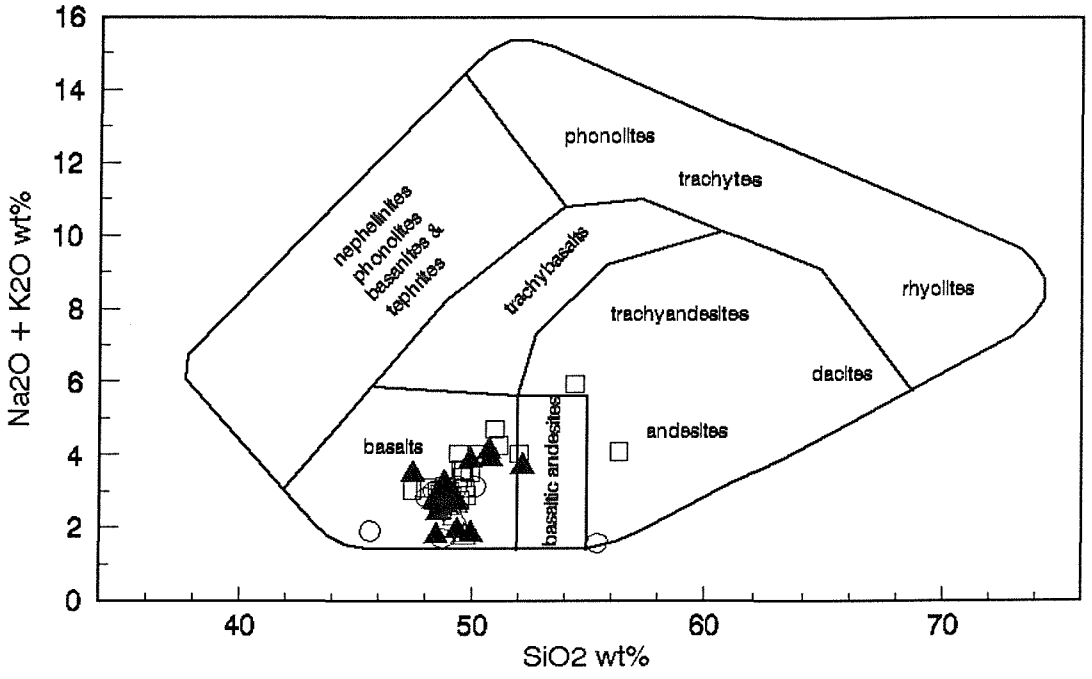

Figure 4.6 Basalt discrimination diagram using SiO_2 vs total alkali content.

existing precipitating phase. Major element variation plots against MgO (Fig. 4.7) indicate that both clinopyroxene and olivine may have been removed from the melt during fractional crystallisation.

Thus, there is ample evidence for magmatic differentiation preserved not only within the Beja-Acebuches Amphibolites but also within the exotic blocks found within the Peramora Mélange Formation. The matrix of the latter also retains a record of its parentage in that samples yield geochemical data identical with that obtained from both the amphibolites and the amphibolite blocks within the mélange.

Zr, Ti, TiO_2, P_2O_5 and Y have already been shown to be immobile. In Fig. 4.4 both P_2O_5 and Zr show a strong linear trend which indicates that both elements became enriched in the residual liquid during crystallisation of the magma. P_2O_5 is plotted against Zr (Fig. 4.8a) (after Pearce & Cann 1973) and in this diagram the samples fall within the tholeiitic field. This relationship is also shown in Fig. 4.8b (after Floyd & Winchester 1975) in which the ratio of Zr/P_2O_5 is plotted against TiO_2. No negative trend is apparent in the present study and this is interpreted as an indication that accessory minerals, such as apatite or zircon, either formed at a late stage in the crystallisation history or not at all.

4.3.1 The Zr - Ti/100 - Yx3 diagram.

The Zr - Ti/100 - Yx3 plot (Pearce & Cann 1973, Holm 1982, Prestvik 1982) uses the relative abundances of these elements to separate the samples into four sub-groups: Within-Plate Basalts (WPB), Low-K Tholeiites (LKT), Ocean Floor Basalts (OFB) and Calc-Alkaline Basalts (CAB). To facilitate comparison for this study, the samples have been separated into lithologically distinct groups (Fig. 4.9).

The matrix from the Peramora Mélange Formation (Fig. 4.9a,iii) display the greatest variation and are spread across three fields. This may reflect (a) that these rocks experienced a greater degree of element mobility during prograde metamorphism of the ambient matrix or, (b) primary variations within the source rocks, or (c) that the elements were redistributed during sedimentation. The Beja-Acebuches Amphibolites and the blocks within the Peramora Mélange Formation (Figs. 4.7i and 4.7ii respectively) are closely grouped in the Ocean-Floor Basalts to Low-K Tholeiite Fields.

4.3.2 The MnO - TiO2 - P2O5 diagram.

This plot (Fig. 4.9b, after Mullen 1983) distinguishes between five tectonic and petrogenetic environments, assuming that the fractionation of olivine at low f_{O2} is responsible for tholeiitic trends (Osborn 1959). These are: Ocean Island Tholeiites (OIT), Mid Ocean Ridge Basalts (MORB), Island Arc Tholeiites (IAT), Ocean Island Alkali Basalts (OIA) and Calc-Alkaline Basalts (CAB). MnO is removed from the melt in clinopyroxene as well as olivine, whereas TiO_2, although absent from

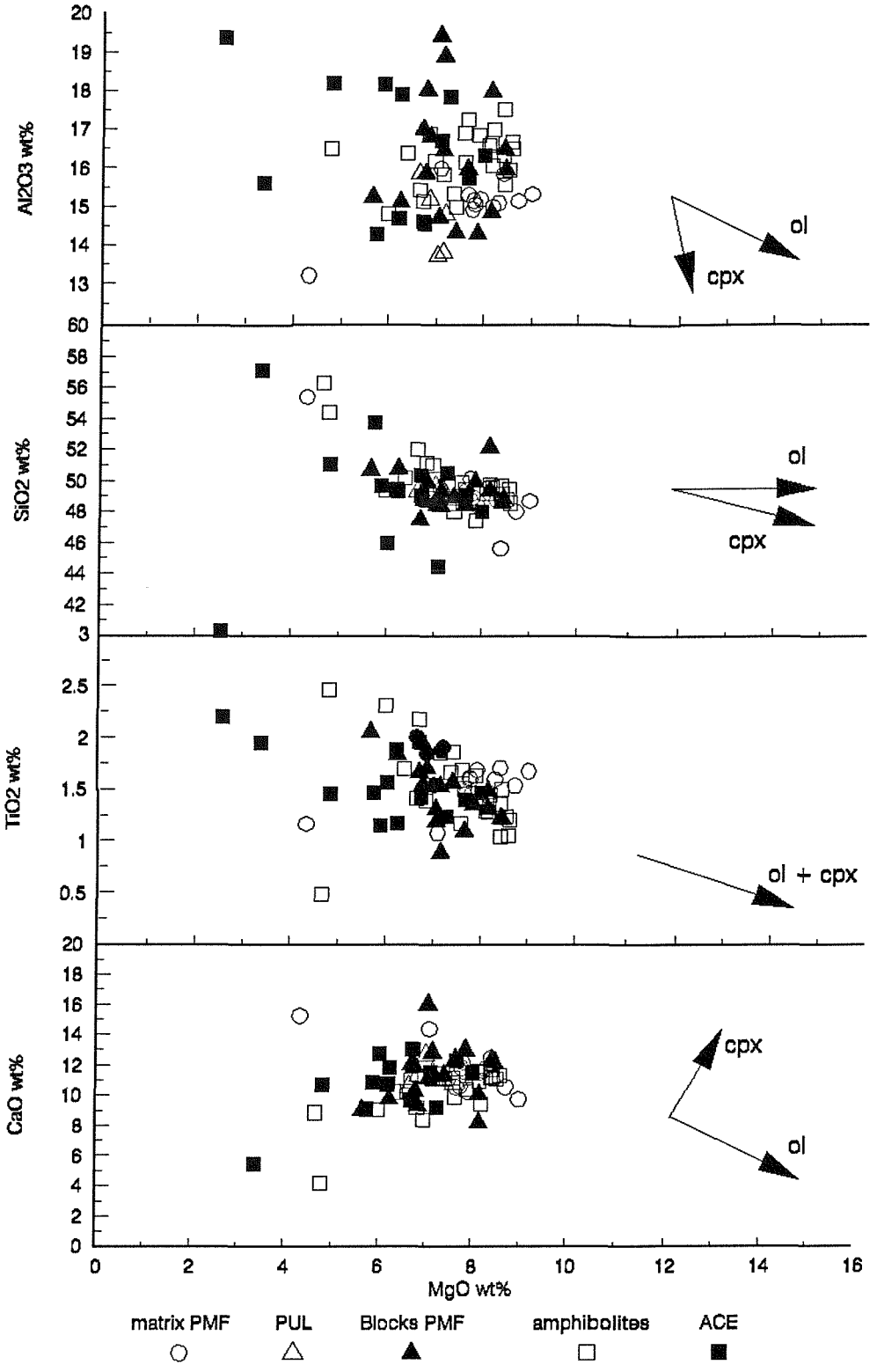

Figure 4.7 Discrimination diagrams illustrating that evidence of primary igneous processes is preserved. MgO is plotted against major elements and the evolution vectors of olivine (ol) and clinopyroxene (cpx) are illustrated.

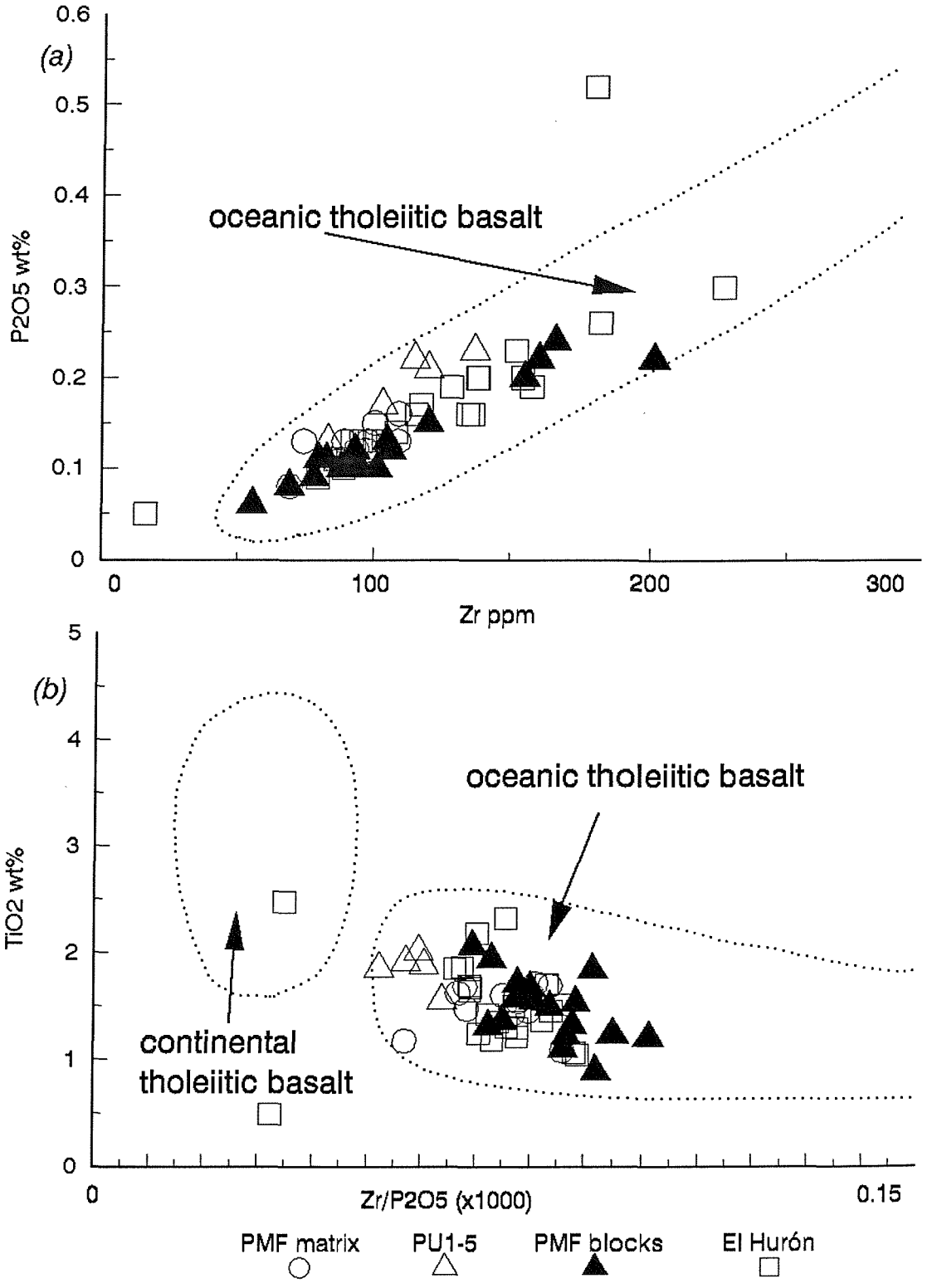

Figure 4.8 (a) Discrimination diagram showing field of Oceanic Tholeiitic Basalt using Zr vs P_2O_5.
(b) Discrimination between Oceanic Tholeiitic Basalt and Continental Tholeiitic Basalt using Zr/P_2O_5 and TiO_2.

olivine, is present in small amounts in both clinopyroxene and ilmenite. Metamorphism of original basalts results in incorporation of TiO_2 into the amphibole phase as well as in the accessory phases. P_2O_5 appears to relate to the extent of partial melting and to the initial composition of the magma (Mullen 1983).

All rock groups cluster between the MORB field and the Island Arc Tholeiite field (Fig. 4.9b).

4.3.3 The Nb - Zr - Y diagram.

Fig. 4.9c, (after Meschede 1986) separates the samples into five fields: N-type MORB (Normal-type MORB is that which constitutes the majority of ocean ridge basalts), P-type MORB (Plume MORB is recognised at within plate plumes), Within-Plate Tholeiites (WPT), Within-Plate Alkali Basalts (WAB) and Volcanic-Arc Basalts (VAB). The elements used in this discrimination diagram are all considered to be relatively immobile during fractionation processes and have been shown (section 4.2.4) to have retained this record with little alteration during metamorphism. The basic rocks analysed all plot within the MORB to Volcanic-Arc Basalt field with slight skew towards the latter.

4.3.4 Ti, Cr, Ni discrimination diagrams.

The elements Ti, Cr and Ni may be used to discriminate between Ocean Floor basalts (OFB) and Island Arc basalts (IAB). The data (Fig. 4.10) shows that the majority of the samples lie within the former field although some of the samples spread into the IAB field (Fig. 4.10a). Fig. 4.10b demonstrates that all rock groups lie close to the OFB/IAT boundary with some samples crossing into the IAT field.

4.3.5 Zr/Y vs Zr discrimination diagram.

This diagram (Fig. 4.11b, after Pearce & Norry 1979) is designed to discriminate between Ocean Island basalts, Mid Ocean Ridge basalts and Island Arc basalts. The samples from the study area for the most part occupy the area located in the MORB field with some spread into the Island Arc basalt field. This diagram illustrates that all samples are consistent with a MORB-type source.

4.3.6 Spider diagrams of elements.

Spider diagrams compare relative abundances of trace elements of samples. As previously described (section 4.2.4) several of the elements used in the construction of these diagrams may have been subject to a certain amount of post-emplacement mobilisation, in particular those elements located on the left of the diagrams. Fig. 4.12a shows a spider diagram for rocks from the study area. The data are also compared with an N-MORB trace element pattern and have been normalised with

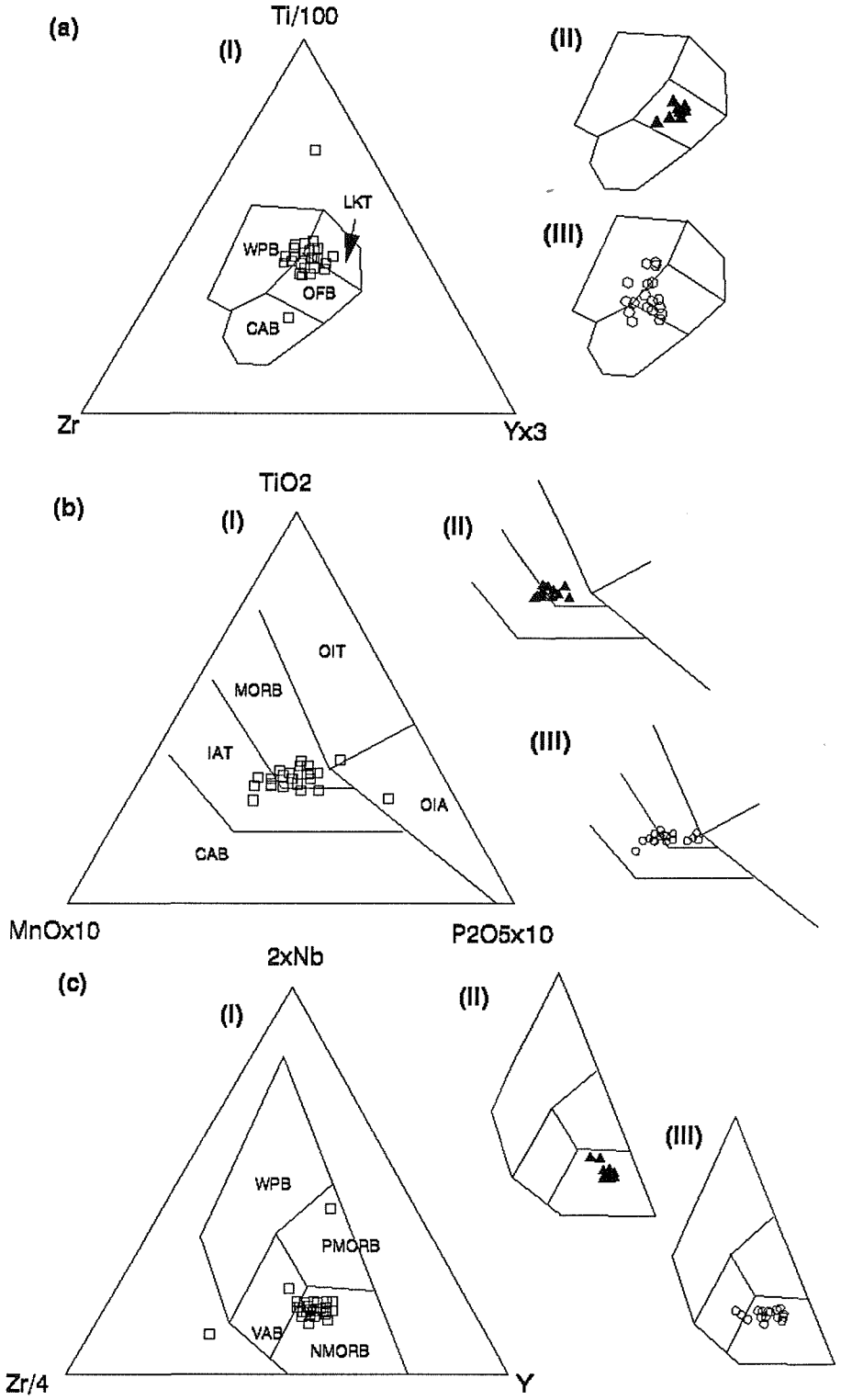

Figure 4.9 (a) Triangular diagram plotting Ti, Zr and Yx3 (after Pearce & Cann 1973).
(b) Diagram plotting TiO_2, MnO and P_2O_5 (after Mullen 1983).
(c) Triangular diagram plotting Nb, Zr and Y (after Meschede 1986).

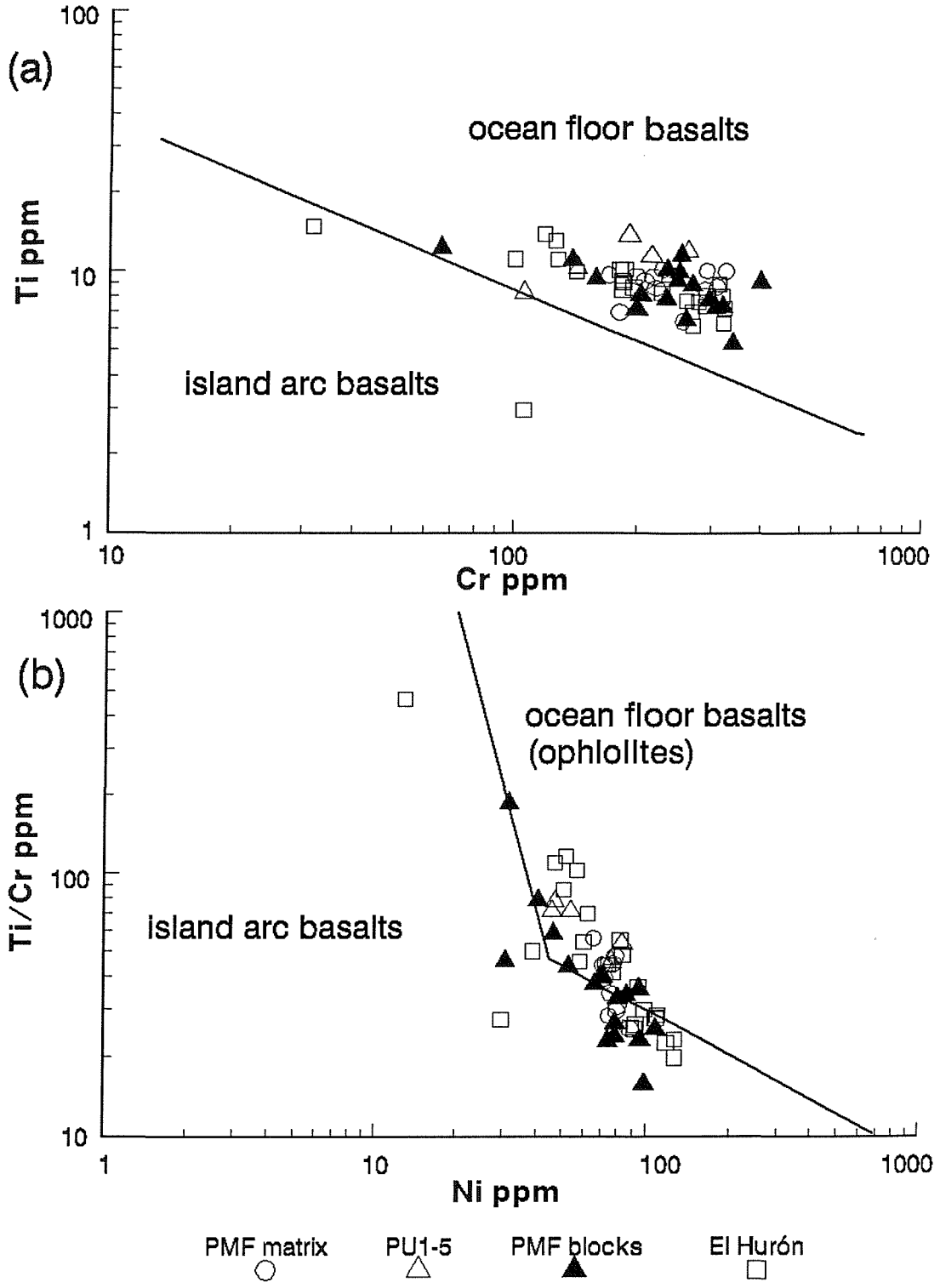

Figure 4.10 (a) Tectonic discrimination diagram using Cr vs Ti.
(b) Tectonic discrimination diagram using Ni vs Ti/Cr.

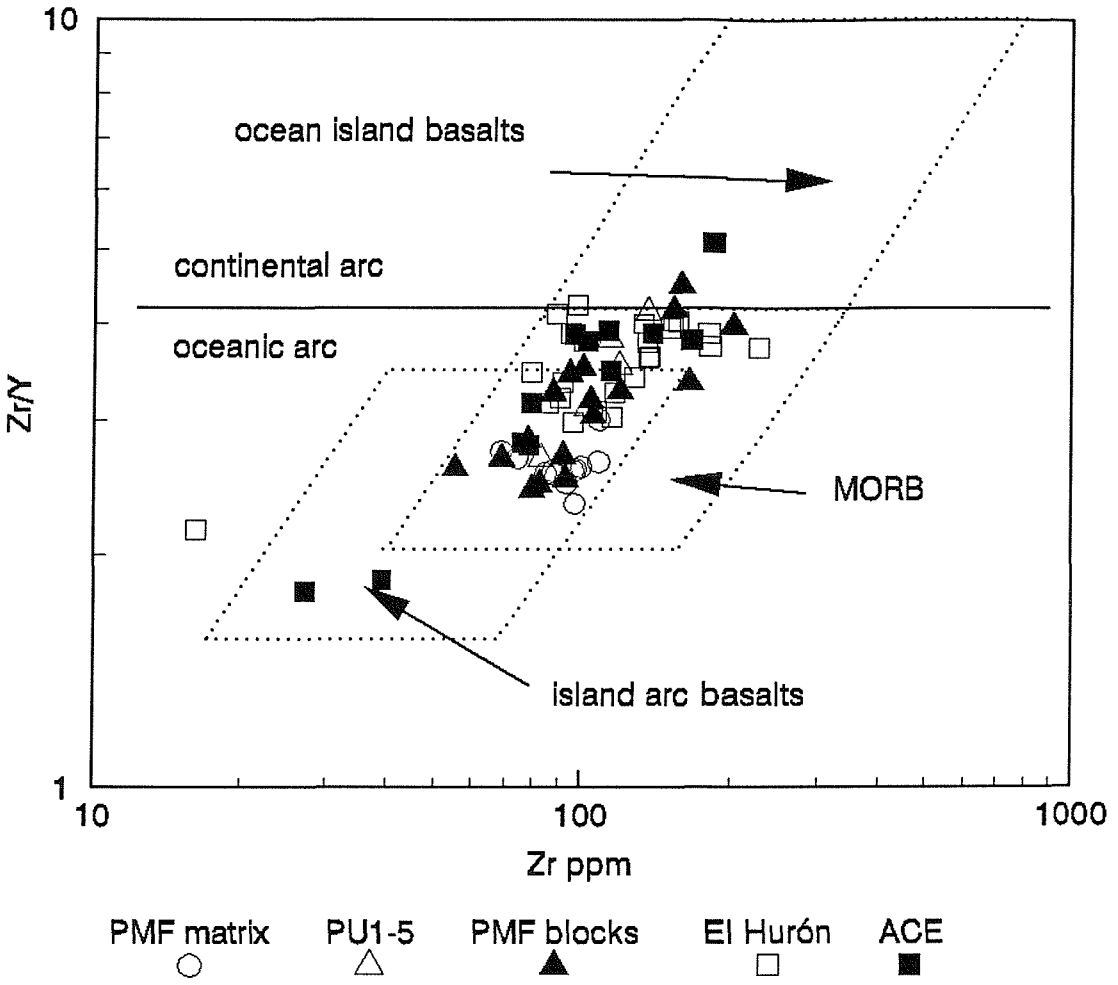

Figure 4.11 Basalt discrimination diagram to distinguish between oceanic arc and conitinental arc basalts using Zr and Y.

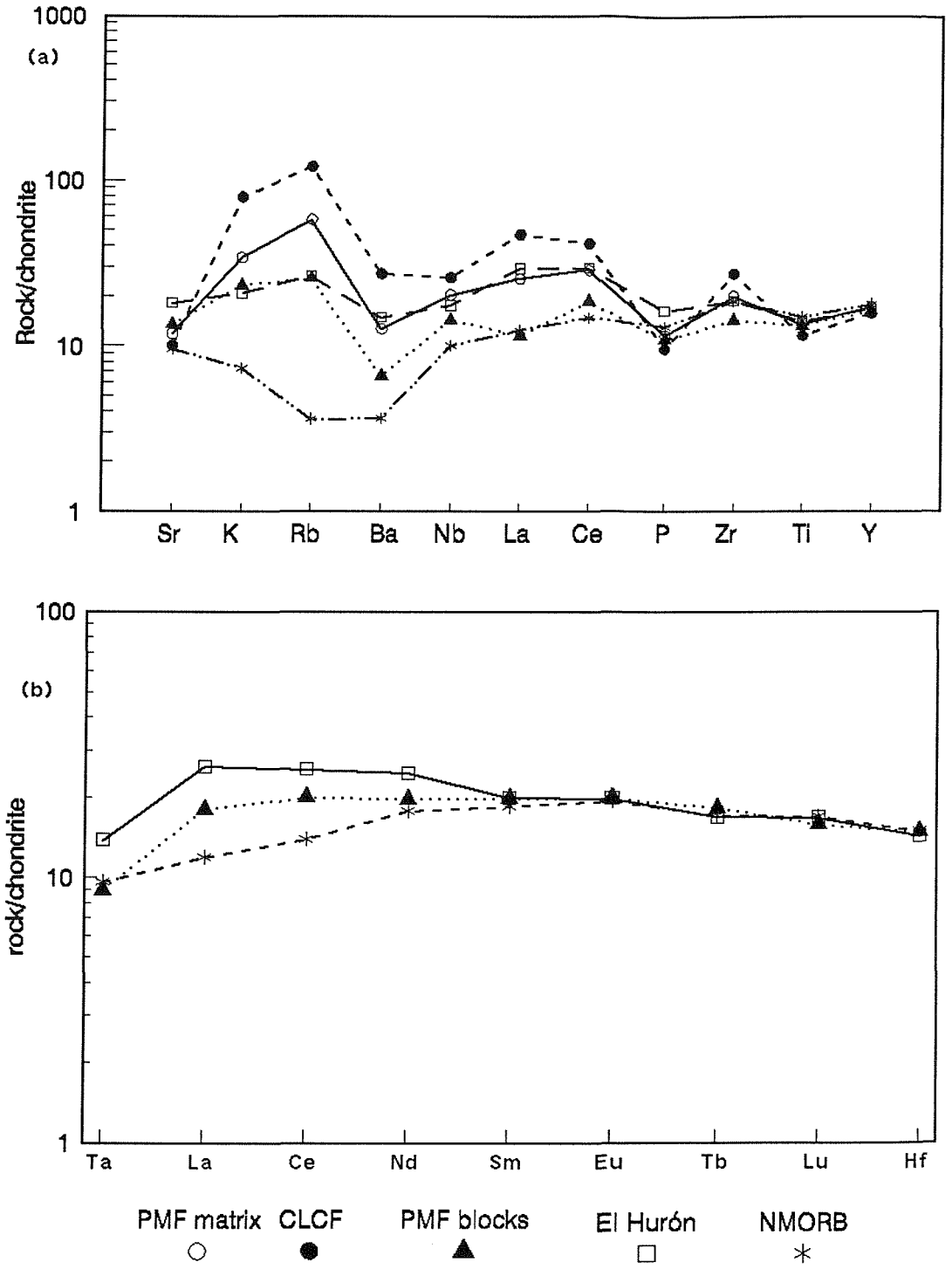

Figure 4.12 (a) Spider diagram of blocks within the Peramora Mélange Formation compared with averages from the El Hurón amphibolites, the Cumbres de Los Ciries Formation and NMORB.

(b) Spider diagram comparing averages from the Peramora Mélange Formation, The El Hurón amphibolites and NMORB.

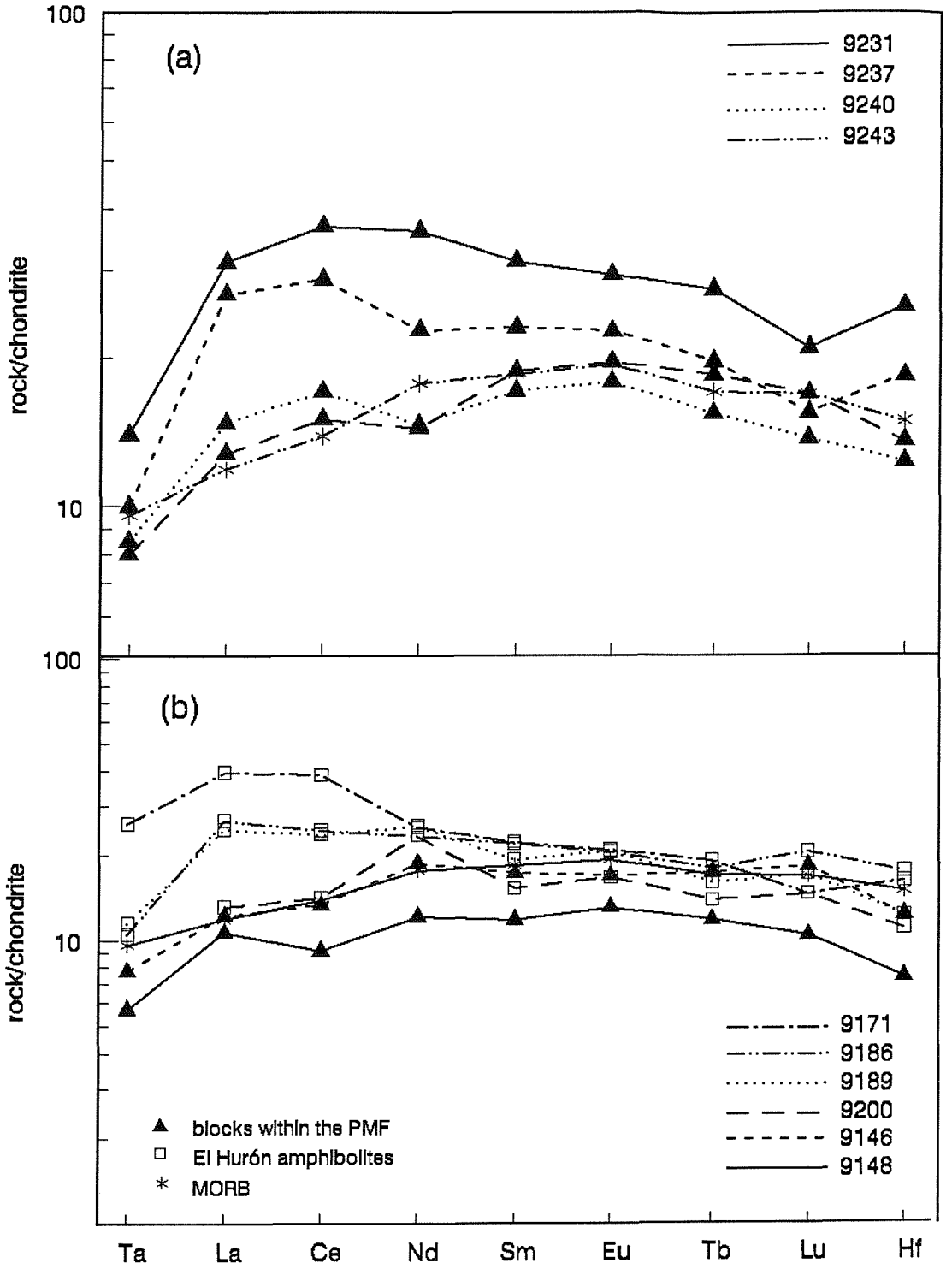

Figure 4.13 Averaged rare earth element patterns from six blocks from the Peramora Mélange Formation compared with four samples from the El Hurón amphibolites and MORB (Sun *et al.* 1979).

respect to chondrite values of the primitive mantle (Pearce 1973, 1975; Pearce & Noray 1979; Sun *et al.* 1979). The elements used are arranged in order of incompatibility from left to right across the diagram. The rock types represented include the matrix of the mélange, the blocks located within the matrix, samples from the Beja-Acebuches Amphibolites and an average of 22 samples taken from sediments of the Cumbres de Los Ciries Formation (appendix 2), which is in tectonic contact with these formations. The sediments of the Cumbres de Los Ciries Formation display the greatest variation in trace element abundance, possibly reflecting the greater amounts of syn-kinematic/metamorphic element mobility within them. There is an enrichment with respect to MORB in incompatible elements within all the lithotypes plotted. Compatible elements, positioned to the right of the diagram, parallel the relative abundances in NMORB suggesting a close association between MORB and the rock types analysed, possibly suggesting a genetic relationship.

Fig. 4.12b compares the average of six samples from the blocks within the Peramora Mélange Formation with four samples from the Beja-Acebuches Amphibolites of El Hurón, as well as with NMORB. Samples 9146, 9148, 9231, 9237, 9240 and 9243 are blocks that are found within the matrix of the Peramora Mélange Formation while samples 9171, 9186, 9189 and 9200 are from the El Hurón amphibolites. This diagram also includes rare earth element (REE), as well as Ta and Hf data analysed by INAA (appendix 3) which are normalised using chondrite abundances taken from Taylor & M^{c}Clennan (1985) and Sun & Nesbitt (1979). Once again there is a marked divergence between NMORB and the amphibolites at the incompatible end of the spectrum, although this becomes parallel at the less compatible end. Individual samples show a greater spread (Fig. 4.13). There is a close parallelism between the average for MORB and all the samples from the study area although there is a slight enrichment of all elements. Element patterns from the amphibolite blocks demonstrate the greatest amount of variation ranging from approximately ten (sample 9200) to thirty times chondrite (sample 9231). REE patterns are generally consistent with no obvious Eu anomaly (indicative of plagioclase partitioning), although the elements La, Ce, Nd, and Sm vary quite considerably with the former two displaying the greatest diversity. These results show that there is marked similarity between the amphibolite blocks found in the mélange and the samples representative of the Beja-Acebuches Amphibolites, once again supporting a genetic link between them.

4.4 Sedimentary geochemistry and provenance.

4.4.1 Introduction.

Identification of source rocks of the La Giralda Formation located south of the Aracena Massif would provide extra constraints for a model of erosion, deposition and terrane docking. It was originally intended that analysis of the fluorescence spectra of zircons would aid in provenance characterisation (Aoki 1984, Aoki *et al.* 1987) and several samples were processed for removal of the

heavy mineral populations. However, a small yield, with a mature assemblage consisting of minor amounts of rounded zircon and lesser amounts of tourmaline, revealed that in order to attempt a comprehensive analysis far more intensive sampling would be necessary. Since the sediments consist of uniformly fine grained basinal material that has been subjected to considerable amounts of structural reworking (Chapter 2 and 3), provenance studies concentrated on geochemical analysis as this can often reveal features that are obscured to the conventional provenance techniques (Wrafter & Graham 1989, Floyd *et al. in press*).

There are several advantages to the geochemical approach in provenance studies. Firstly, because of the fine grain size of the sediments, which range from slates to phyllites to fine grained arenites, there is a natural homogenisation of the elements, locked in fine mineral grains, being shed into the receiving basin, and these may thus be representative of the source rocks. A geochemical strategy therefore takes advantage of this natural 'averaging' of the constituent elements (Wightman 1986). Secondly, although the geochemistry of a rock reflects several processes (e.g. weathering and diagenesis) that result in the ultimate composition of that rock, certain elements such as Mg, Fe, Cr, Ni, and Ti are controlled mostly by the original composition of the source rocks (Wrafter & Graham, 1989). Thirdly, the grain size of the rocks, being so fine, precludes an exhaustive petrographic study; the elements that comprise the rock forming minerals, however, should still remain as part of the whole rock signature.

Fine grained samples were chosen specifically, (a) to determine if their geochemistry provides any indication of provenance, and (b) if this is the case to check if there exists any change in absolute abundance of major or trace elements away from the dismembered ophiolite thus relating sedimentation to a possible source. Tuffaceous horizons (<1m thick) throughout the sedimentary sequence are also discussed.

Samples of silty mudstones and low grade metamorphic siltstones were collected along the length of the Aroche-El Mustio section within the La Giralda Formation. The extent of the study area precluded comprehensive sampling, so a transect across strike was made. 60 samples (>1Kg) were collected and separated into several categories (appendix 2). Several samples were analysed for trace elements only as trace elements are considered to be less mobile, and hence more reliable in provenance studies (Taylor & M^{c}Clennan 1985; Wrafter & Graham 1989; Floyd *et al. in press*).

4.4.2 Mobility of elements in sedimentary rocks.

The nature of the source rock determines the original composition although this can be modified by several intermediate processes that occur between source and sink. Weathering, chemical and physical erosion, grain size, transportation, deposition and post-depositional processes, such as diagenesis and metamorphism, all modify mobile elements such as Na, Mg, K and Sr, whereas elements such as Zr, Ni and Ti tend to be concentrated in the heavy mineral fraction of the sediments

(Wronkiewicz & Condie 1987). Ni and Cr may be indicative of a basic source (Scultz-Dobrick, B. & Wedepohl, K.H. 1983; Wronkiewicz & Condie 1990) if they are in sufficiently high concentration, although they may be mobilised during diagenesis by becoming adsorped by clay minerals (M^{c}Clennan *et al.* 1990). The effects of grain size variation can be minimised by comparing sediments of similar grain size and sedimentary environment. Fine grained samples are better mixed than coarser grained samples, although trace elements tend to be enriched in muds relative to sands due to the dilution effects of quartz and calcite in the latter.

Variable degrees of weathering in the source area can affect alkali and alkaline earth elements; Rb and Ba are often fixed into the weathering profile by adsorption onto clays while smaller cations such as Na, Ca and Sr are severely leached from the weathering profile (M^{c}Clennan *et al.* 1990). Sawyer (1986) in a study of mid-upper greenschist/lower amphibolite facies metasediments (turbidites) notes that deposition was probably too rapid to allow significant weathering during transport, and much of the effects of chemical weathering were thus restricted to the source area. Nesbitt & Young (1982) reason that the dominant effect of weathering is the breakdown of feldspars to illite-type clays. Removal of Ca, Na and K by solution means that abundances of these elements, as compared with less easily removed elements can be used to measure the extent of chemical weathering. As aluminium is the least mobile element in feldspar they define a chemical index of alteration (CIA) which enables the intensity of weathering in source areas to be compared:

$$\mathbf{CIA = [Al_2O_3/(Al_2O_3 + CaO^* + Na_2O + K_2O)] \times 100} \qquad [4.1]$$

where CaO represents the CaO in silicates only.

In applying this equation to 60 samples from the study area the average is 83, ranging from 58 - 92, indicating that the source rocks were fairly heavily weathered prior to re-sedimentation and transport. In the determination of provenance it is therefore necessary to rely on elements that are least mobile during sedimentary processes. These include elements with a relatively short residence time in seawater such as the rare earth elements, the high field strength elements (Table 4.B), Th, Sc, Hf and Co (Table 4.D). The concept of residence time in sea water provides valuable insights into which elements will be most useful in provenance studies; those with low residence times and low sea water/upper crust partition coefficients (K_ySW) may be transferred almost quantitatively into sedimentary rocks (Li 1981; Taylor & M^{c}Clennan, 1985) (Fig. 4.14). Of particular use are Th, Y and the REE, although the latter have not been determined in the present study. Taylor and M^{c}Clennan (1985), who concentrated on fine grained terrigenous sedimentary rocks such as mudstones and shales in their analytical work, provide a comprehensive data base of comparative geochemistry for various sedimentary rocks.

Mobility of elements in low grade metapelites has been found to be relatively minor (Shaw

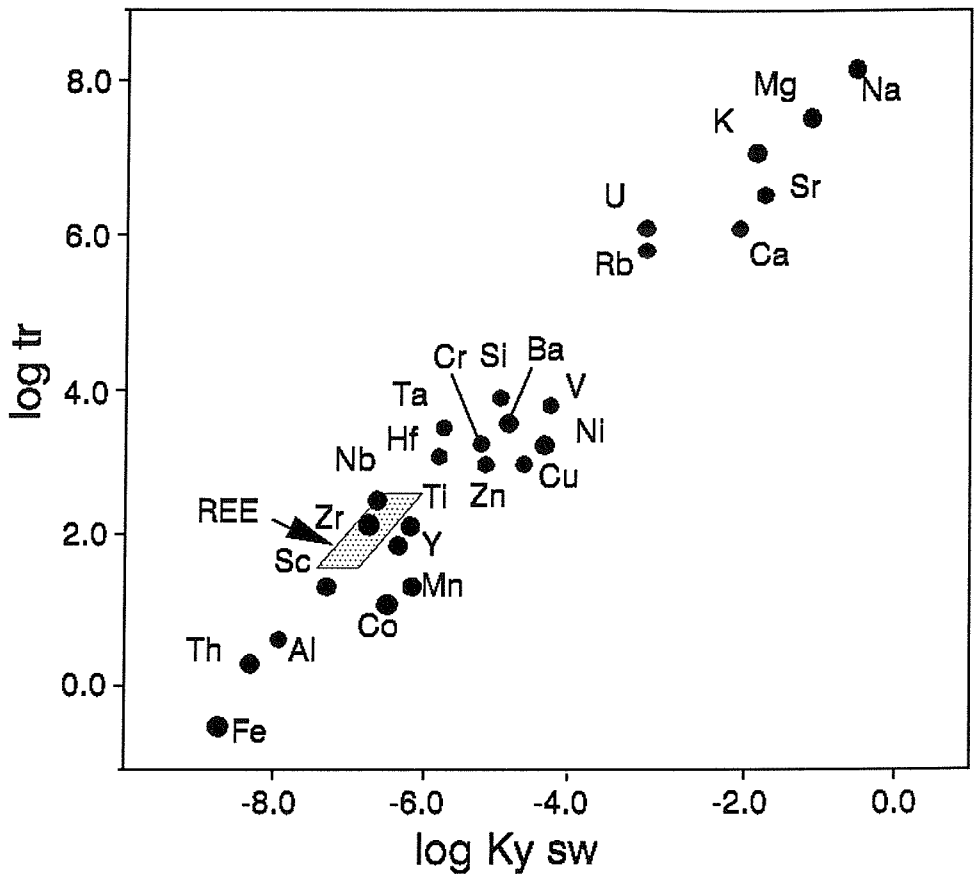

Figure 4.14 Mean residence time of elements in seawater (Taylor & M°Leannan 1982)

Na, K, Mg, Sr, Ca, Rb, U.	Highly mobile during processes of weathering and post sedimentation processes such as diagenesis and metamorphism. Little use in provenance studies.
Fe, Mn, Si, Cr, Ni, V, Pb.	May be mobile under reducing conditions or during diagenesis. May also be fixed onto clays. May provide limited insight into provenance.
Zr, Nb, Ti.	Immobile during sedimentary and post sedimentary processes. Generally concentrated in the heavy mineral fraction.
Th, Y, REE.	Immobile during sedimentation and concentrated in the clay fraction. These are considered to be the most useful in provenance studies.

Table 4.D - Summary of the geochemical behaviour of certain elements. Dashed line indicates those elements considered to be of use in provenance studies (Wrafter & Graham 1989; Floyd *et al* in press).

1954; Scultz-Dobrick, B. & Wedepohl, K.H. 1983) and as the metasediments in this study have been metamorphosed up to lower greenschist facies, metamorphism probably plays little part in changing the relative abundances of elements.

4.4.3 Petrography.

In order to compare geochemical variation within sedimentary associations it is neccessary to look at variations amongst lithotypes. A detailed description of these lithologies is found in Chapter 2, section 2.3.

4.4.3.a Mudstone.

Mudstones are mostly preserved as beds of slaty mudstones. They have been subjected to polyphase deformation that gave rise to three well developed cleavage traces. Bedding is seldom preserved as a planar feature and in isolation gives no indication way up. In hand sample they are fine grained and dark brown. Petrographic analysis is limited by the fine grain size of the samples although in some cases small quartz grains are visible. These rocks consist essentially of phyllosilicates, probably sericite and phengite. Vitrinite reflectance studies have shown that they have suffered lower greenschist facies metamorphism with temperatures in the order of <320°C (Chapter 5) and thus the clay minerals have probably been converted to white-mica.

4.4.3.b Siltstone.

These rocks differ from the mudstones by their pink or buff colour and 'gritty' texture. Thin sections occasionally demonstrate a minor population of larger quartz grains (up to 1mm), with long axes rotated into the plane of cleavage, and heavy minerals such as tourmaline or zircon. Matrix minerals include quartz, muscovite and biotite, with textural relationships revealing alignment of

phyllosilicates, a response to elevated temperatures during several phases of deformation.

4.4.3.c Tuffaceous horizons.

These are coarser grained than the siltstones or the mudstones with which they are closely associated, and have a characteristic green colour. The fine grained matrix consists of feldspar, quartz, mica and chlorite in which large (up to 0.5cm) euhedral crystals of plagioclase and quartz are present and are classified as crystal tuffs. They too have suffered deformation, metamorphism (at least to chlorite grade and probably higher) and post-depositional weathering, making field identification difficult (they can often be mistaken for arenites when weathering has removed some of the matrix minerals).

4.4.3.d Quartz-rich arenites.

These rocks comprise a mature mineral assemblage, consisting mostly of quartz with accessory zircon and tourmaline in the heavy mineral fraction. These too have suffered low grades of regional metamorphism and significant structural reworking.

4.4.3.e Quartz-mica schists.

Samples included in this group belong to the Cumbre de Los Ciries Formation (Chapter 2). They are composed of essential quartz and mica with metamorphic minerals including both muscovite and biotite, indicating that lower to mid greenschist facies conditions were reached. This metamorphic event occurred pre- to syn-kinematically as all the minerals present are preserved within the regional schistosity. Accessory minerals include plagioclase feldspar, zircon, tourmaline and apatite while chlorite forms as a late stage mineral replacing the micas.

4.4.4 Major element analysis.

Fig. 4.15 shows selected major elements of sediments plotted against yttrium, alongside samples from the Beja-Acebuches Amphibolites, the Cumbres de Los Ciries Formation and granitic samples from the Mina Fe in the Ossa Morena Zone (appendix 2). Granites cropping out in the hangingwall rocks of the Ossa Morena Zone were not collected during the present study. Fig. 4.15 shows the relative abundances of CaO, K_2O, MgO, MnO, TiO_2 and SiO_2. The data plots into consistent groups, with the Cumbres de Los Ciries Formation schists showing the greatest spread; field observations have determined metabasic clasts suggesting provenance of this latter formation, in part, was mafic. Slates of the La Giralda Formation have a high K_2O concentration possibly reflecting high mica content. In general, the grouping of the sediments appears to match the granitic rocks more closely than the amphibolites. A closer correlation of the sediments with the amphibolites is displayed by TiO_2 and P_2O_5. These two elements, mostly in apatite and opaque minerals, may

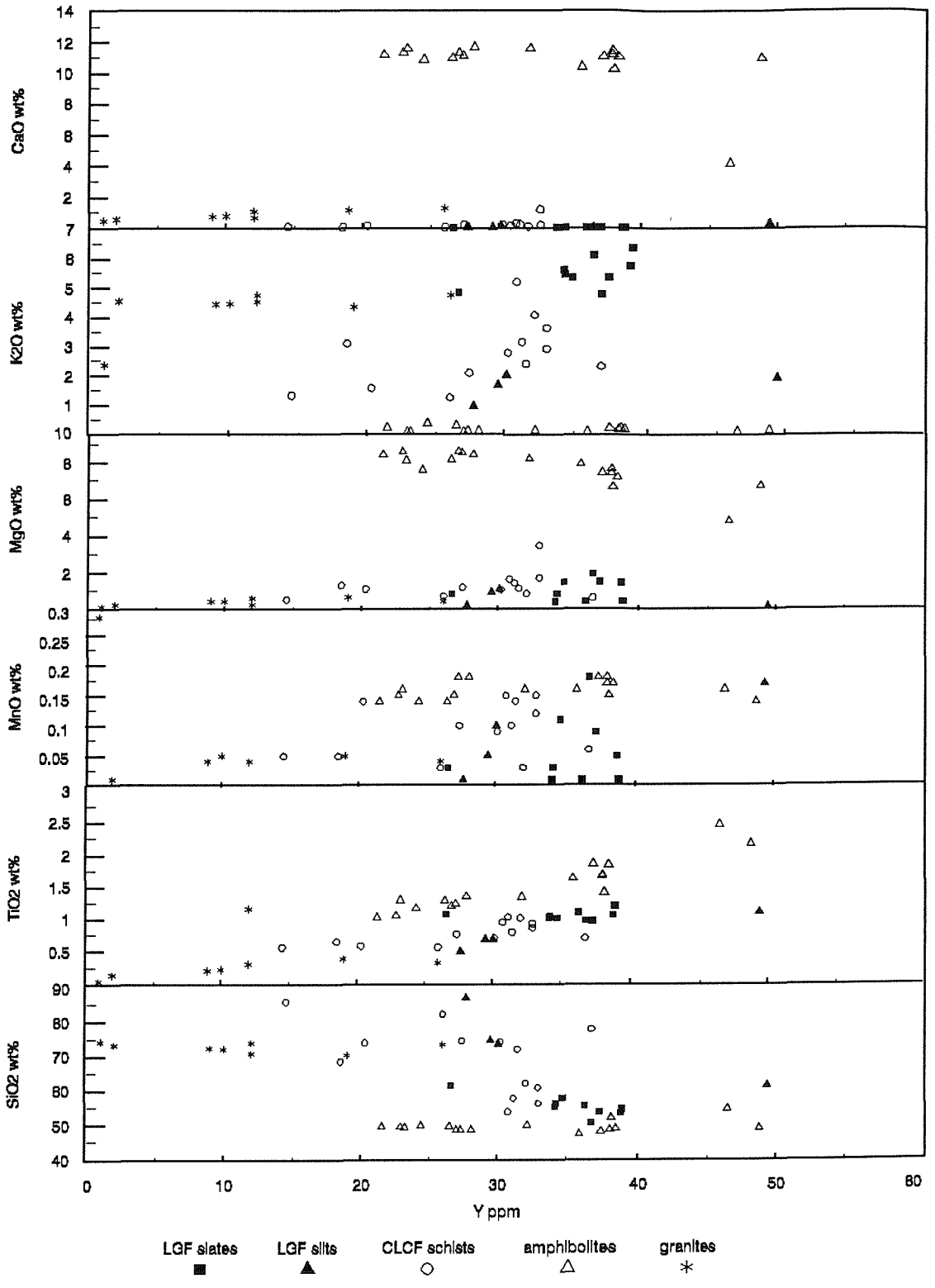

Figure 4.15 Bivariate discrimination diagrams for major elements against Y.

have had a basic provenance, such as the amphibolites. The data thus suggests that the sediments have affinties with both basic (the Beja-Acebuches Amphibolites?) and granitic components.

4.4.5 Trace elements.

The trace elements considered useful in provenance studies are Ti, Zr, Y, Th and U (Floyd & Leveridge, 1987) and trace element data for each of the rock groups identified are given in appendix 2. Relationships between elements are illustrated in Fig. 4.16. In all of these plots the data for the sediments generally falls between the amphibolites and the granitic material, particularly noticeable with Th, Ba and Nb. This may suggest mixing of sediments from both basic and acidic sources.

Sediments of the La Giralda Formation and Cumbres de Los Ciries Formation have a uniform K/Rb ratio, average 204.13, lying close to the ratio of 230 (Shaw 1968) for a typical differentiated magmatic suite (Fig. 4.17a) which suggests that the sediments have a significant component from an acidic source. The field for low grade metagreywackes (Caby et al. 1977) plots closely with the samples, most of which fall into the acid to intermediate field (Floyd & Leveridge, 1987) (Fig. 4.17a).

Binary plots for Cr/Nb and Ni/Nb are shown in Figs. 4.15b. The abundances of these elements from both acidic (granites from Mina Fe and Albaquerque in the Ossa Morena Zone) and basic sources (representative samples from the El Hurón amphibolites) are also plotted on these diagrams for comparison. Once again these show that the sediments, as well as the interbedded tuffaceous material, plot as intermediate in composition.

Of interest are the elements that plot against Cr (Fig. 4.18). Cr versus Ti for the sediments shows a positive correlation stemming from the acidic corner, while a negative correlation is described between Cr and Ti for the amphibolitic rocks. This positive trend, coupled with relatively high values of zirconium and intermediate values for Ni (Fig 4.16), would support the hypothesis that there was a significant acidic component and it would therefore seem reasonable that the material was derived from a mixed source.

The use of binary diagrams has been questioned as a meaningful discriminatory tool (Floyd *et al. in press*) as elements may be affected by sorting and heavy mineral content. As a result, data may spread across several fields in the discriminatory diagrams. Floyd *et al. (in press)* propose the use of upper continental crust-normalised multi-element patterns which they suggest can be used to more accurately compare sediments from different tectonic environments as well as showing the effects of mafic and heavy mineral input. In these diagrams the data are compared throughout with geochemical data from several areas including the Gramscatho and Giessen basins (Schultz-Dobrick & Wedepohl 1983, Franke & Engel 1982; Engel & Franke 1983; Floyd *et al.in press*), two areas that are considered to lie along strike from the study area as part of the northern continuation of the

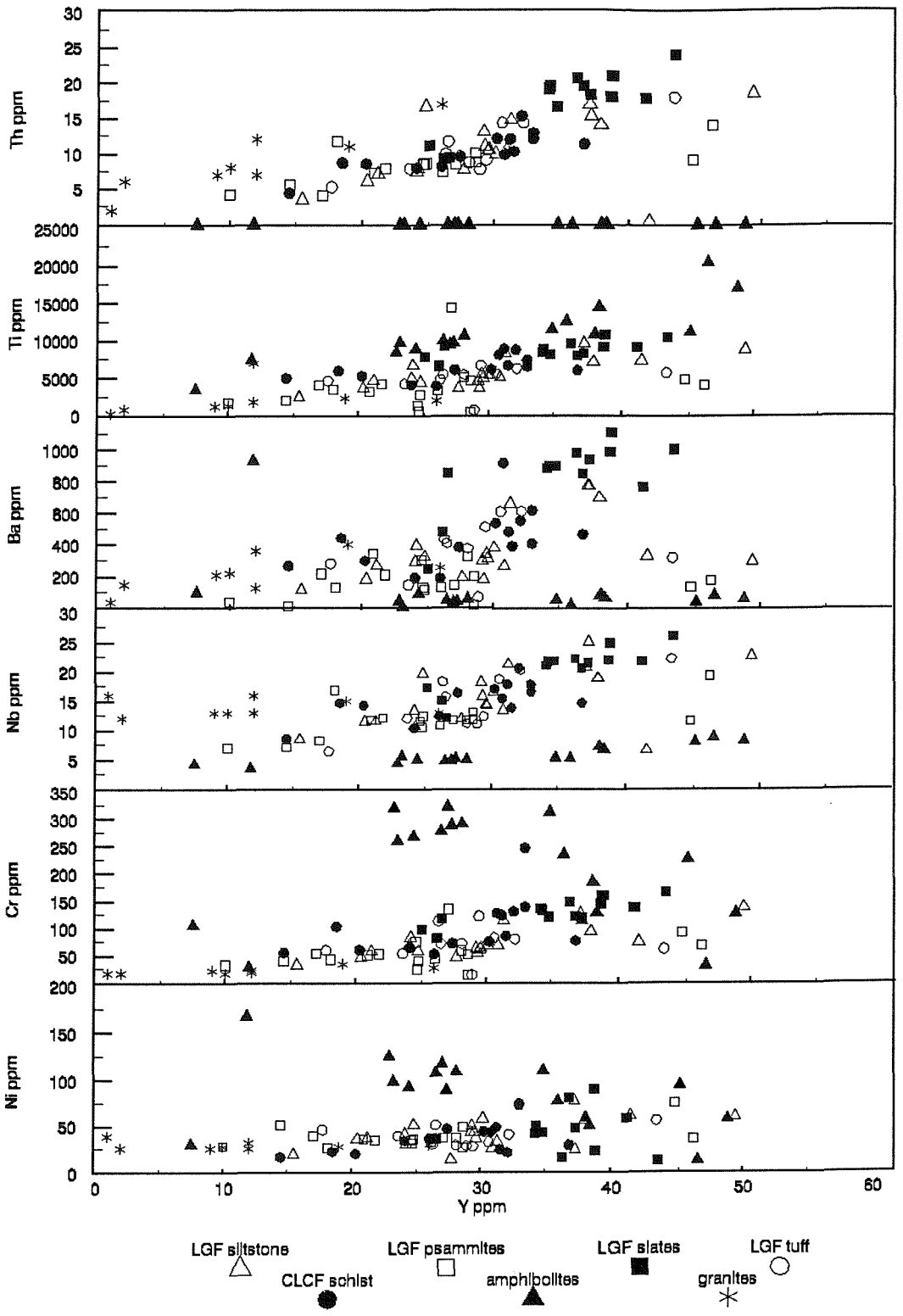

Figure 4.16 Bivariate discrimination diagrams for trace elements against Y.

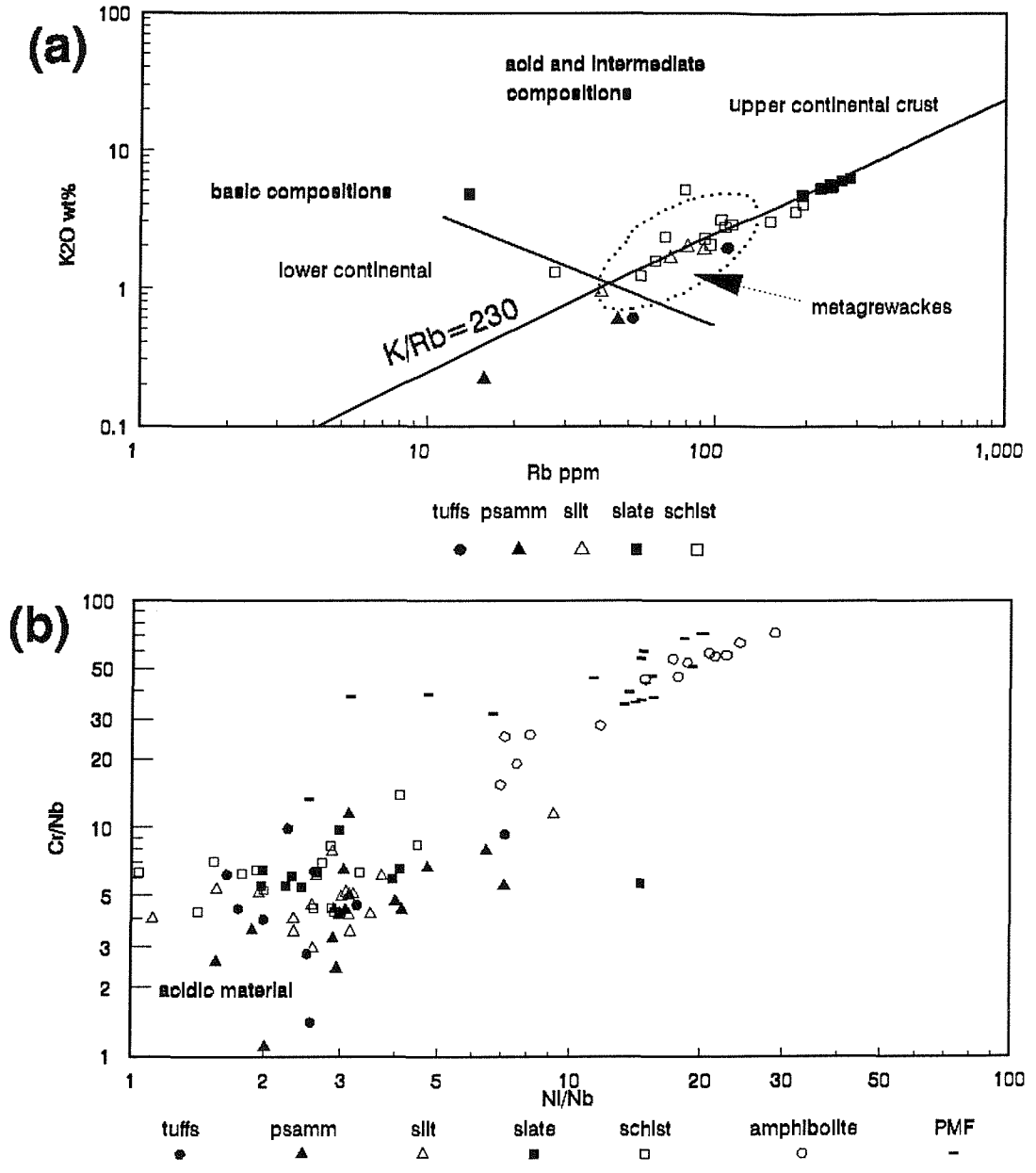

Figure 4.17 (a) Discrimination Rb vs K_2O.
(b) Discrimination diagram using Ni/Nb vs Cr/Nb.

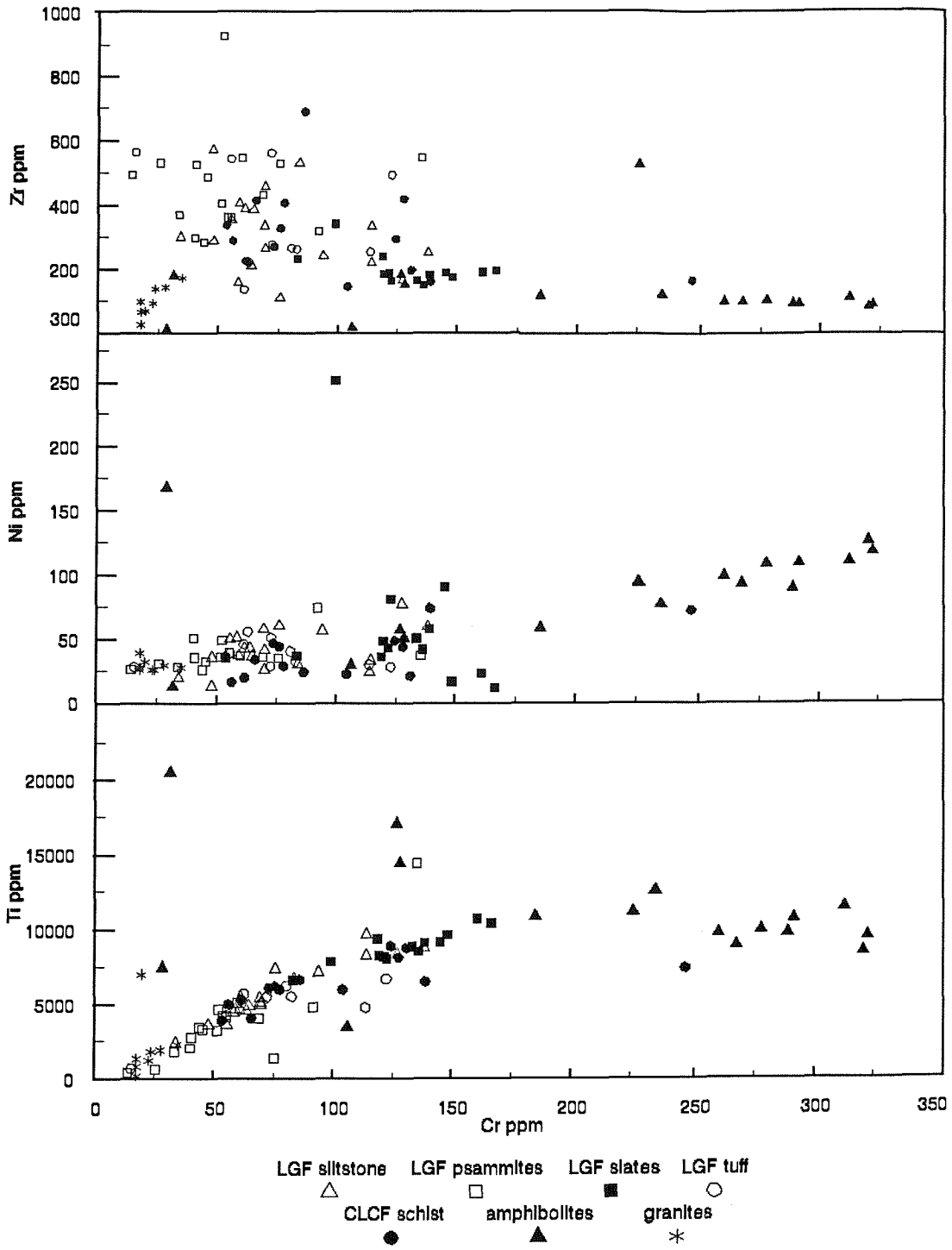

Figure 4.18 Cr ppm vs Ti, Ni, Zr ppm.

Hercynian Arc (Eden & Andrews, 1990).

Fig. 4.19 and 4.20 show multi-element diagrams for samples from both the Cumbres de Los Ciries Formation and the La Giralda Formation and compares them with averages from various tectonic settings and provenances, as well as greywackes from several tectonic environments. The elements are arranged (left to right) in order of increasing ocean residence time, comprising a more stable group (Th-Nb) and a more mobile group (Ni-Rb). Significant features of these diagrams are firstly, all the patterns show a negative Nb anomaly, a parameter that is typical of subduction related sedimentary sources (Floyd *et al. in press*). Secondly, positive V-Cr-Ni-Ti anomalies may indicate a mafic input.

Fig. 4.19a compares the slates and silts from the La Giralda Formation with the average granite from Mina Fe in the Ossa Morena Zone, and the El Hurón amphibolites. The plot shows that only the granites have lower V-Cr-Ni concentrations while all other elements have sub-parallel plots. One exception is Rb, which is considered to be highly mobile in sedimentary processes (Floyd *et al. in press*). Fig. 4.19b emphasises the V-Cr-Ni correlation, as NMORB is plotted in this diagram with the El Hurón amphibolites and the La Giralda arenites for comparison. The arenites have a lower V-Cr-Ni abundance although they are enriched in the more stable elements as compared to NMORB, displaying positive Ti-Zr-Y anomalies which may be consistent with the input of heavy minerals (mostly from zircon).

Fig. 4.19c compares the tuffaceous horizons from the La Giralda Formation with the granites and amphibolites. The plot for the tuffs falls between these two end members with the V-Cr-Ni concentrations describing a similar pattern to that seen in the amphibolites. The enrichment of stable elements as compared to both granites and amphibolites may suggest an intemediate signature.

Fig. 4.19d compares the schists of the Cumbres de Los Ciries Formation with the tuffaceous layers from the La Giralda Formation, the El Hurón amphibolites and the matrix of the Peramora Mélange Formation. These associations describe a paired pattern, with the amphibolites and Peramora Mélange Formation possessing relatively high V-Cr-Ni concentrations as compared with the Cumbres de Los Ciries Formation schists and the La Giralda Formation tuffs. All elements, with the exception of Rb, retain a parallelism from less stable to more stable elements.

Fig. 4.20a, b, c, and d compares samples from the La Giralda Formation and the Cumbres de Los Ciries Formation with averages from the Geissen and Gramscatho basins as well as with greywackes from various tectonic environments, and the average shale of Taylor & M$_c$Clennan (1985). Both the schists of the Cumbres de Los Ciries Formation and the slates of the La Giralda Formation are consistent with Continental Arc/Active Margin greywackes (CAAM) (Fig. 4.20d). All the metasediments analysed have similar profiles (Fig. 4.20a), a relationship that is emphasised when they are compared with the average shale and the Gramscatho and Geissen greywackes. These latter examples are identified as being erosive products of subduction-generated rocks containing both acidic

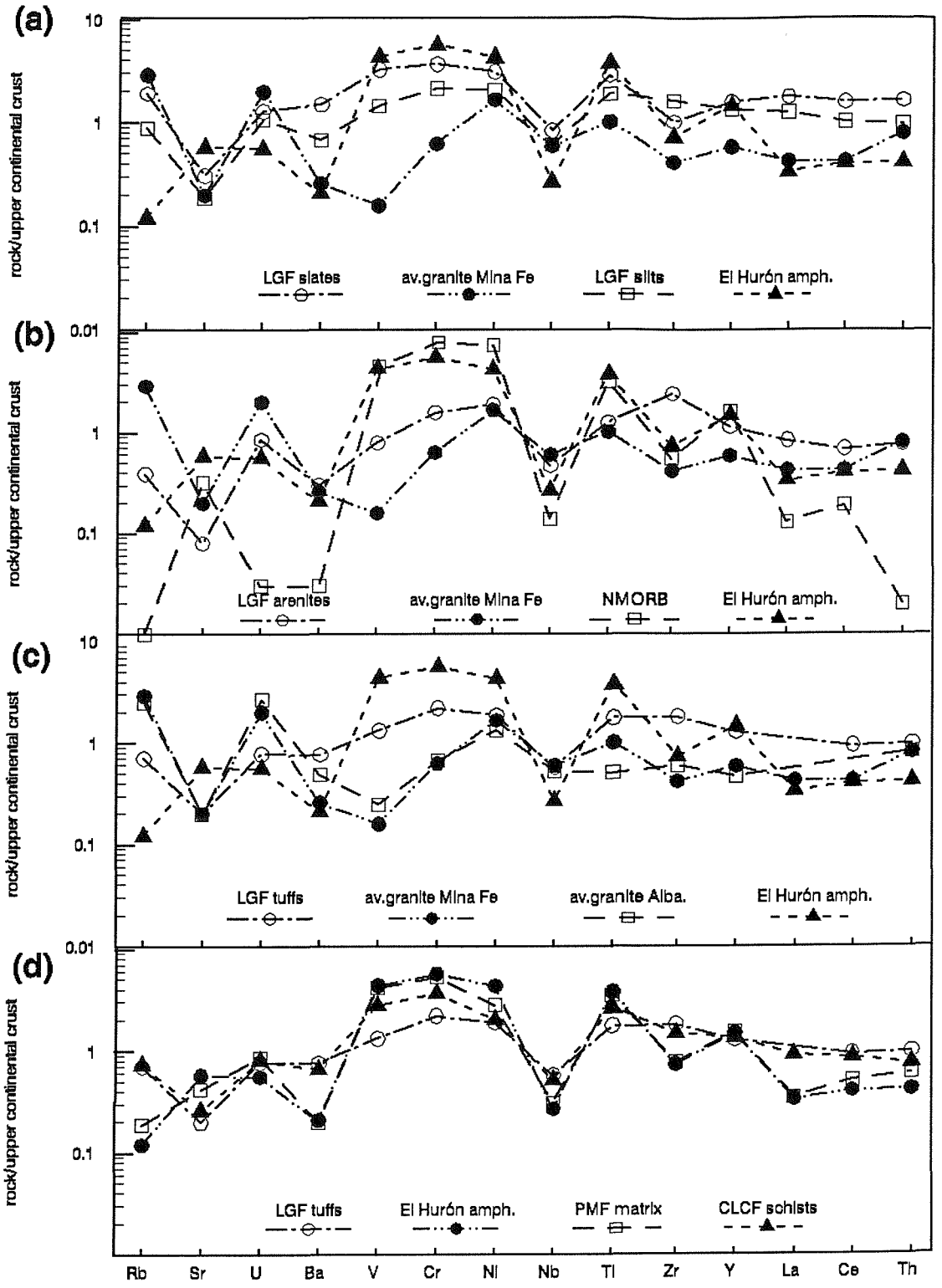

Figure 4.19 Multi-element Upper Continental Crust normalised spider diagrams to differentiate between tectonic environment in sediments and volcanics.

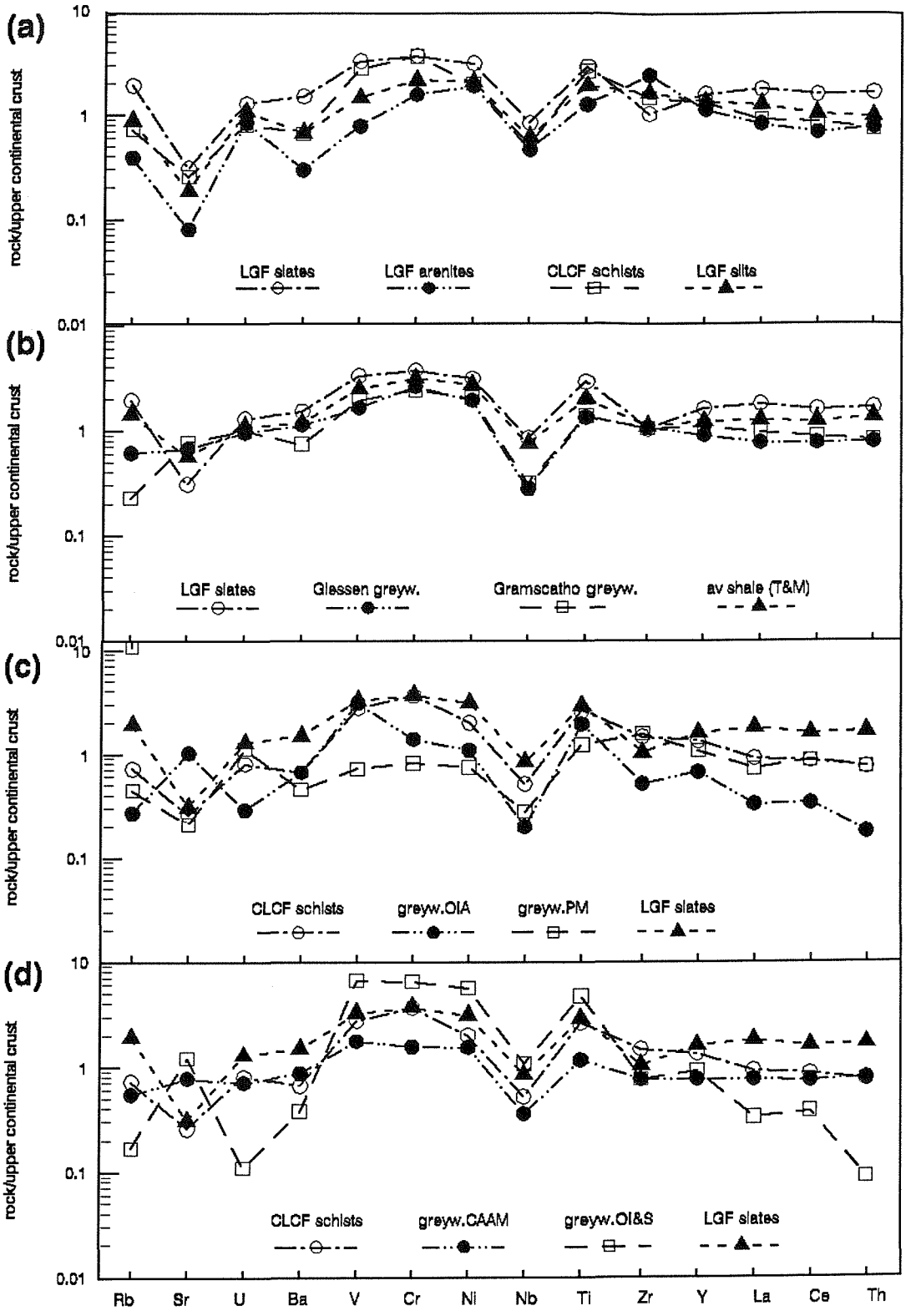

Figure 20 Multi-element spider plot comparing trace elements from the study area with greywackes from various tectonic environments.

and basic components (Floyd *et al. in press*, Schultz-Dobrick & Wedepohl 1983). The inference, therefore, is that the samples from the Oceanic Exotic Terrane are from a similar tectonic environment, being the product of erosion of both acidic and basic source areas.

4.5 Summary and conclusions.

1. The close correlation of selected major and trace elements with published data for oceanic crustal rocks indicates that element mobility was limited throughout the protracted structural evolution.

2. Geochemical data shows that the Beja-Acebuches Amphibolites located to the south of Aroche (El Hurón) give signatures similar to MORB-type basalts.

3. Geochemical data from both matrix and blocks of the Peramora Mélange Formation supports field evidence that they were derived from the Beja-Acebuches Amphibolites.

4. Spider diagrams reveal that the four data sets: amphibolite blocks in the mélange, matrix of the mélange, the El Hurón amphibolites and the sediments of the imbricated Cumbres de Los Ciries Formation, are all enriched with respect to incompatible elements, while compatible elements parallel plots for MORB. These data may suggest that the sediments were at least partly derived from a basic oceanic source, possibly the Beja-Acebuches Amphibolites.

5. Positive Ti-Zr-Y anomalies and high V-Cr-Ni anomalies suggest that the sediments of the Giralda Formation are of a mature type consistent with a Continental Arc/Active Margin, with inputs both from acidic and basic sources.

Chapter 5: Metamorphism.

Abstract

Several different metamorphic facies are identified throughout the Oceanic Exotic Terrane. On the southern margin of the Beja-Acebuches Amphibolites, rocks are retrogressed to greenschist facies. Prograde upper greenschist facies dominates in the Peramora Mélange Formation and these rocks are imbricated with greenschist facies metapelites of the Cumbre de Los Ciries Formation. The latter two formations are affected by a low pressure high temperature metamorphic event that produced andalusite and cordierite, a feature restricted to rocks immediately juxtaposed against the southern margin of the Beja-Acebuches Amphibolites. Vitrinite reflectance analysis carried out on samples from the La Giralda Formation indicate that lower greenschist facies conditions dominated within this formation during tectonic evolution.

5.1 Introduction.

This chapter presents the results of a detailed petrographic study of each metamorphic facies identified in the field (Figs. 5.1 & 5.2). Peak metamorphic assemblages attained during deformation are discussed.

5.1.1 Previous work on metamorphic processes.

Several studies have been conducted on metamorphic rocks within the Oceanic Exotic Terrane and within the South Portuguese Zone in general (Schermerhorn 1975). Munha (1983) describes four metamorphic zones within the South Portuguese Zone ranging from zeolite facies in SW Portugal (zone 1) and increasing in grade northwards to greenschist facies in the Pulo do Lobo Formation (zone 4) (Fig. 1.3). Data indicates a low-pressure metamorphic regime for the South Portuguese Zone with geothermal gradients of 40-50°C per km (Munha 1983). Munha *et al.* (1986), working in the Portuguese sector of the Beja-Acebuches belt, recognise an inverted metabasic sequence, the result of thrust stacking, which they consider to be an overturned oceanic complex. Index minerals within these rocks and their geochemistry lead to the delineation of an inverted metamorphic gradient within footwall rocks along the southern boundary of the Ossa Morena Zone Munha *et al.* (1986). Castro *et al.* (1987) note that the metamorphic grade within the Beja-Acebuches amphibolites increases rapidly both eastwards along strike and towards the north. Conditions range from zeolite-prehnite-pumpellyite facies in the west and south, through greenschist-amphibolite facies to granulite facies in the central and northern areas. The greenschist-amphibolite transition is considered to be consistent with temperatures of around 400-450°C and pressures not greater than ≈2Kb. Internal granulite facies rocks recrystallised at about 700°C (two-pyroxene geothermometry) within a low pressure metamorphic regime (Castro *et al.* 1987).

Bard (1969), presenting data from a petrographic traverse across the orogenic belt, considered not only the high grade rocks of the Aracena Massif but also the metabasites of the Beja-Acebuches

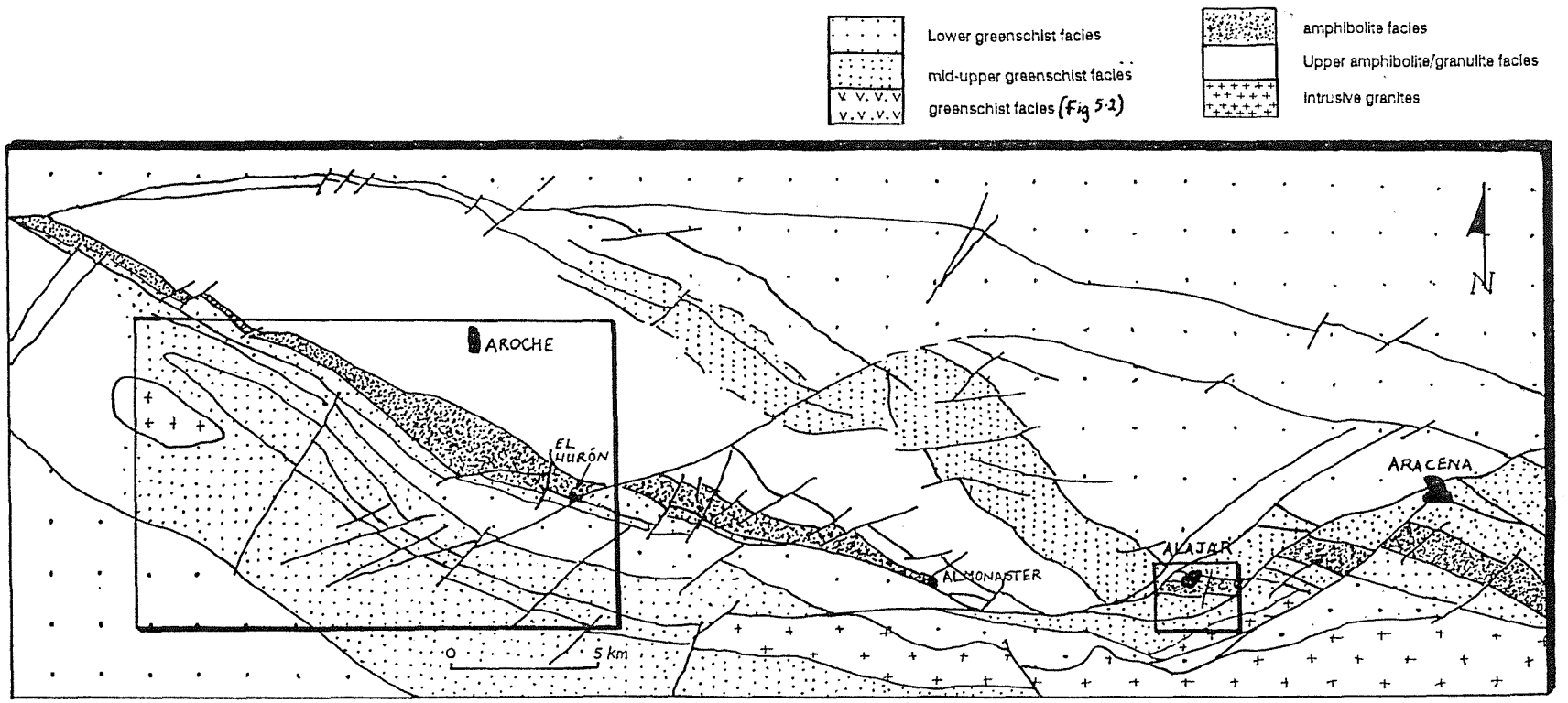

Figure 5.1 Metamorphic map of the Aracena Metamorphic Domain and contiguous Oceanic Exotic Terrane (partly after Bard 1969; Apalategui et al. 1983, 1984; Crespo-Blanc 1989). The study areas are shown in the insets.

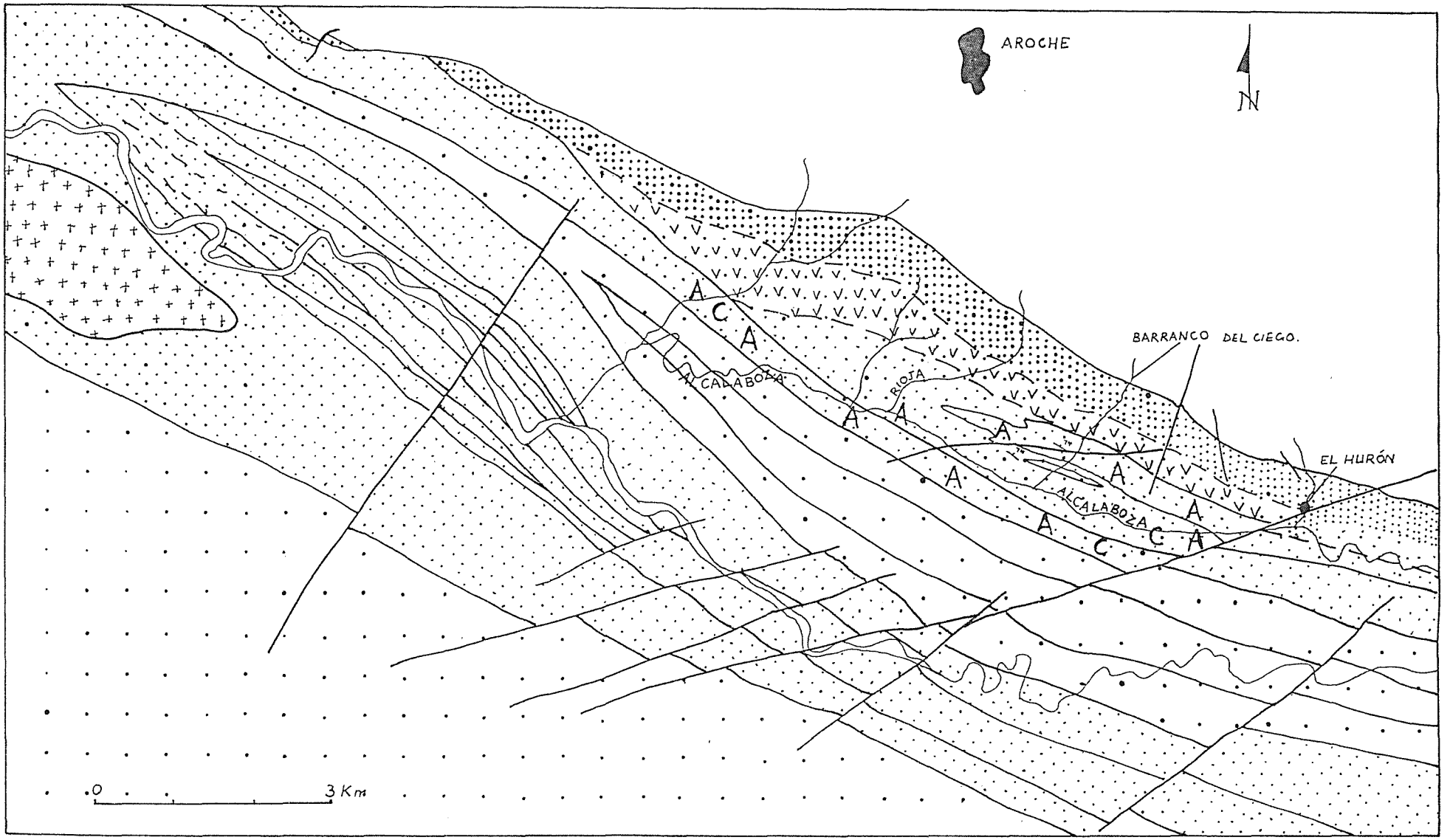

Figure 5.2 Metamorphic facies identified within the study area. Ornament as for Fig. 5.1. A - andalusite, C- cordierite.

Amphibolites. A progressive change is recorded south from the Aracena Massif, (a) in plagioclase composition (An >40 - An <12 with decreasing grade), (b) the optical property of hornblendes, and (c) the presence or absence of index minerals such as andalusite and cordierite within associated meta-pelites. In a study of 20 blue-green, green and brown hornblendes from the Beja-Acebuches Amphibolites, Bard (1970) concluded that increasing Ti and Al^{iv} in hornblendes, together with decreasing Al^{vi}, are dependent upon prograde metamorphism and he considered that the amphiboles formed during progressive low pressure metamorphism with an imposed geothermal gradient of up to 100°C per km. Subsequent studies by Crespo-Blanc (1989) and Crespo-Blanc & Orozco (1988) revealed the presence of a major shear zone (Fig. 1.1). Apparently high geothermal gradients are explained using a mechanism whereby a sharp decrease in metamorphic grade southwards from the Arecena Massif is due to retrogression and the introduction of fluids accompanying shearing (Kneller & Leslie 1984).

Crespo-Blanc (1989), working within and to the south of the Aracena Massif, describes mineral parageneses of the various formations. Several metamorphic zones are recognised with features including:

(1) the development of lower grade mineral assemblages coincident with the imposition of an intense mylonitic foliation.

(2) a range in metamorphic conditions within the Beja-Acebuches Amphibolites from high temperature amphibolite facies on the northern border with the Ossa Morena Zone through to high temperature greenschist facies on the southern border with the Sierra de Las Bañas Formation (the Cumbres de Los Ciries Formation of this study).

(3) mid-greenschist facies conditions in the Sierra de Las Bañas Formation.

Metamorphic grades within the Beja-Acebuches Amphibolites and sedimentary formations of the Oceanic Exotic Terrane within the footwall are thus relatively well documented. The present study further constrains metamorphic conditions within all the formations identified and relates them to kinematic evolution. In particular, metamorphic conditions within the Beja-Acebuches Amphibolites, the Peramora Mélange Formation and the Cumbres de Los Ciries Formation are discussed as the relationship between them is important to the construction of a model for tectonic evolution.

5.2 Metamorphic facies.

The main index minerals within each formation are summarised in Fig. 5.3. The diagram illustrates the extent of structural imbrication between the formations and shows firstly, how metamorphic index minerals vary according to lithology and secondly, that there is an apparent reduction of metamorphic grade towards the south.

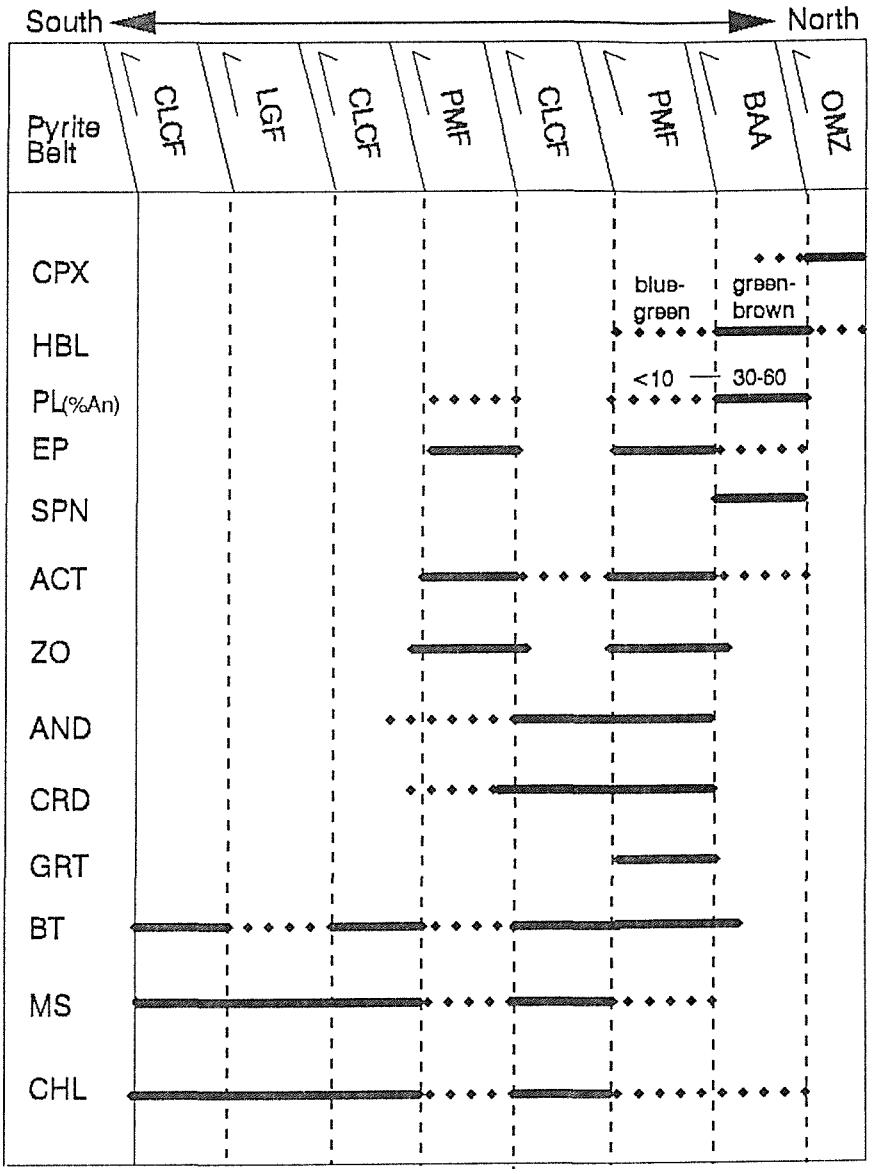

Figure 5.3 Summary diagram of metamorphic minerals in a section from north to south from the Beja-Acebuches Amphibolites to the Cumbres de Los Ciries Formation at its faulted contact with the Pyrite Belt.

5.2.1 The Beja-Acebuches Amphibolites.

A representative locality for this unit is El Hurón [GR 8435 9664], (Fig. 5.1) where fresh and generally coarse to medium grained fragmented amphibolites are observed. The amphibolites are composed of essential amphibole and plagioclase with accessory sphene and opaque minerals, mainly ilmenite (Table 4.A). Selected minerals from six samples were analysed by EDS microprobe at Manchester University (appendix 5). Table 5.A shows the main mineral assemblages observed.

hbl-plag(and-olig)-ilm ± diop	[5.1]
hbl-plag(and-olig)-ilm-ep	[5.2]
hbl-plag(and-byt)-ilm ± act	[5.3]
hbl-plag(ab-olig)-act-clz ± bte	[5.4]

Table 5.A Summary mineral parageneses observed in the Beja-Acebuches Amphibolites.

Assemblage [5.1] is rarely seen and diopside is present only in relict form or absent. This assemblage has previously been reported from the northern border of the Beja-Acebuches Amphibolites along the contact with the Ossa Morena Zone (Crespo-Blanc 1989) and, together with the presence of two pyroxenes, is taken as evidence for relict granulite facies metamorphism. Assemblages [5.2] and [5.3] are the main matrix forming assemblages, with actinolite often occurring as an accessory phase.

5.2.1.a *Amphibole*

Hornblende is the most common amphibole in the El Hurón amphibolites forming medium-sized (1-5mm) grains within a strong L-S schistosity (Fig. 5.8A). From Leake (1978) the standard amphibole formula for calcium-rich amphiboles is:

$$A_{(0-1)}B_2C_5T_8O_{22}(OH,F,Cl)_2$$

This is based on the assignment of specific elements to various sites, with the tetrahedral sites (T) being normally filled with Si and Al although Cr, Fe^{+3}, and Ti may be incorporated. (C) corresponds to the M1+M2+M3 sites and accommodates excess Al, Cr, Ti Fe^{+3}, Mg, Fe^{+2} and Mn while (B), M4 sites, use excess Fe^{+2}, Mn, Mg, Ca and Na. The A sites support any excess Na and all the K. Total A lies between 0 and 1. The separate components of Fe^{+3} and Fe^{+2} have not been determined in the present study and therefore all Fe is treated as Fe^{+2}. The ratio Fe^{+2}:Fe^{+3} is thus ∞ and it has been shown by Barker (1984) that the variability between these two elements alters the location on the compositional diagrams of Leake (1978) only slightly.

Using the calculations of Leake (1978), outlined above, all the amphiboles from the Beja-

Acebuches Amphibolites can be classified as calcic in composition. Where $(Ca+Na)_B > 1.34$, $Na_B < 1.67$ and $Ti < 0.50$ the amphiboles fall into the magnesio-hornblende through to actinolite fields (Fig 5.4a) and where $(Ca+Na) > 1.34$, $Na > 0.50$, $Ti < 0.50$ the amphiboles mostly fall into the edenite group (Fig. 5.5).

Possible edenite forming reactions are:

richterite + tremolite = anorthite + edenite + quartz (Bard 1970) [5.5]

albite + tremolite = edenite + quartz (Spear 1981) [5.6]

albite + actinolite = edenitic hornblende + quartz (Yardley 1989) [5.7]

Assemblage [5.6] has been noted, along with albite-anorthite pairs, in low grade amphibolites from the central Alps (Wenk 1979) demonstrating that edenite can form under a range of metamorphic facies, thus its use as an indicator of metamorphic grade is limited.

The composition of the majority of the amphiboles shown in Fig. 5.4a varies between actinolitic to magnesio-hornblende and shows a bimodal distribution of points indicating that a miscibility gap may exist between actinolite and magnesio-hornblende. No amphiboles were analysed as being tschermakitic in composition and this suggests that high amphibolite to granulite facies grades may not have been attained within this suite of rocks (Deer *et al.* 1966).

Changes in the pleochroic colour scheme of amphiboles are considered to be a reliable indicator of grade (Bard 1970, Binns 1965, Raase 1974). With increasing temperature the colour scheme (parallel to n_γ) changes from blue green (epidote-amphibolite facies), green (amphibolite facies), through greenish brown to brown in the upper amphibolite facies. In the samples from El Hurón the hornblendes vary from blue green through to green, suggesting that epidote-amphibolite to upper greenschist facies metamorphic conditions were attained.

Increase in Ti in amphiboles has been qualitatively used (*e.g.* Leake 1968, Bard 1970, Raase 1974) to characterise metamorphic grade. However, as all the samples analysed contain the opaque phases ilmenite and rutile, titanium is abundant within the system, thus ensuring that the amphiboles will be relatively saturated with respect to Ti. Histograms of the Ti content for the Beja-Acebuches Amphibolites in Fig. 5.6a indicate that the majority of data points fall within the amphibolite facies field. Some lower grade values are also recorded, possibly due to retrogression of hornblende to actinolitic hornblende. Observed values are consistent with pressure values of <5kb (Raast 1974).

5.2.1.b *Feldspar*

Samples from the Beja-Acebuches Amphibolites show well formed crystals of plagioclase in equilibrium with amphibole (Fig. 5.8A & Fig. 2.6H). Microprobe measurements of plagioclase were taken on the rims of the crystals as core regions often record compositional zoning, a feature not

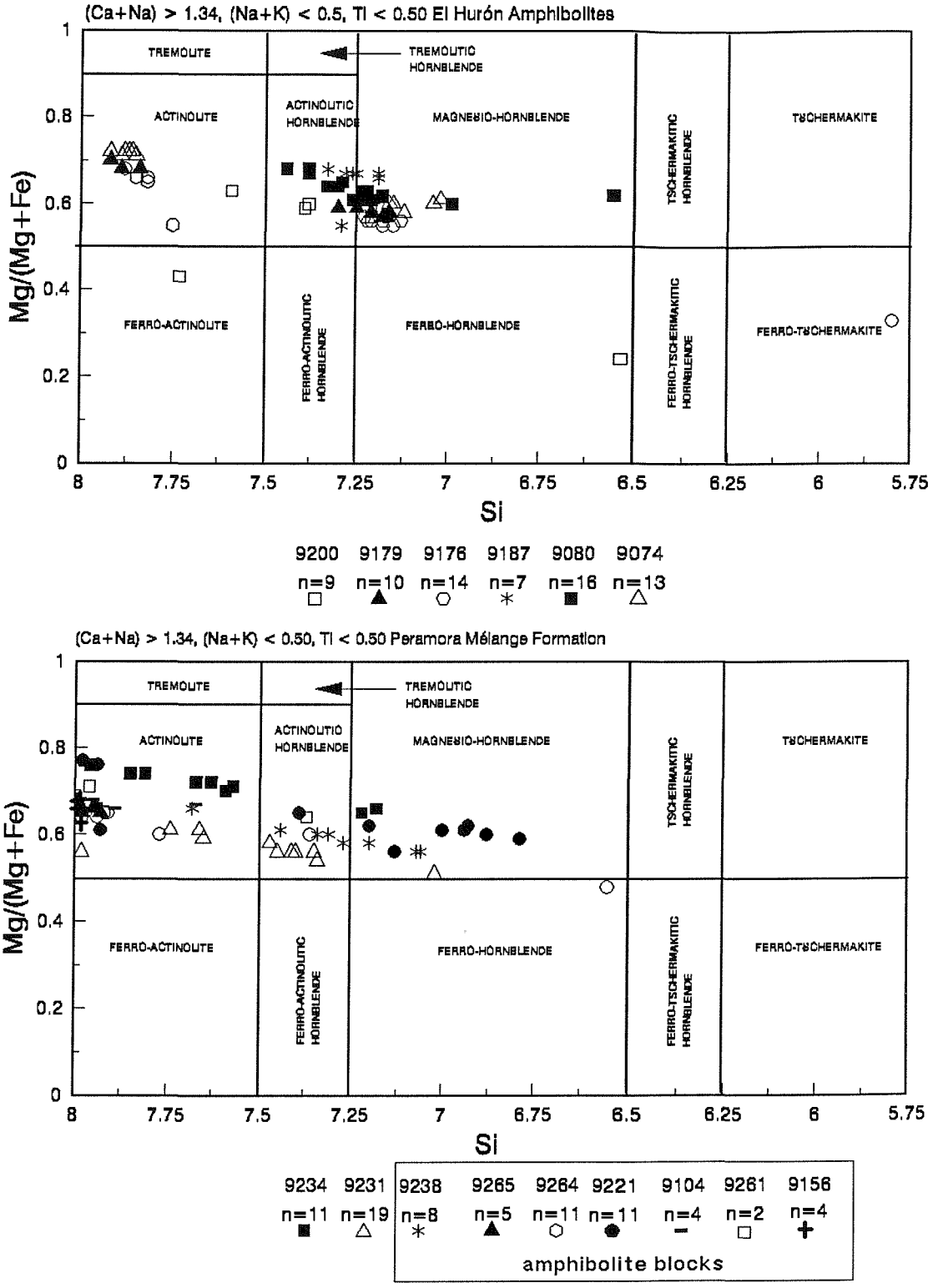

Figure 5.4 (a) Composition of calcic amphiboles from the Beja-Acebuches Amphibolites of El Hurón.
(b) Composition of calcic amphiboles from the Peramora Mélange Formation.

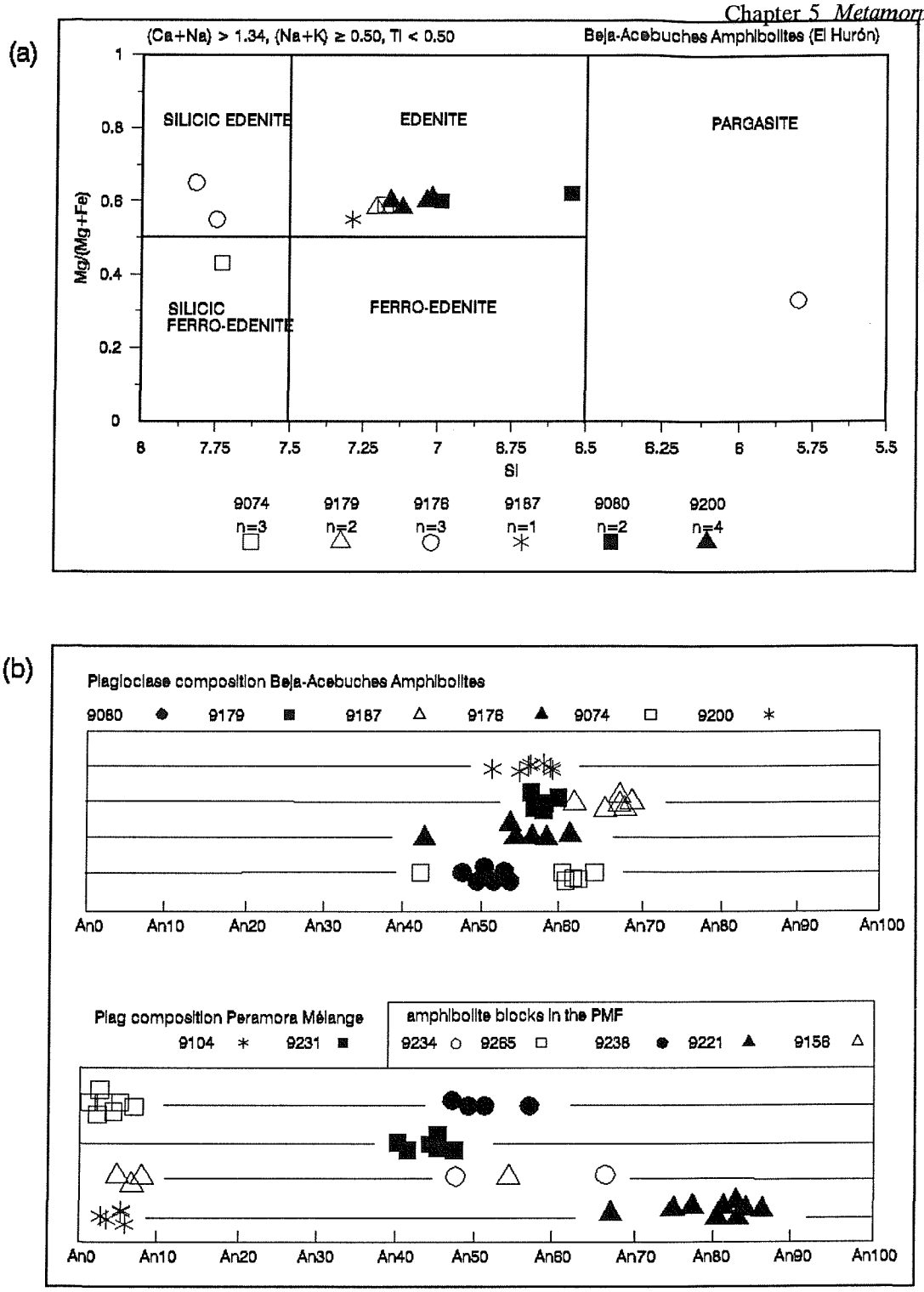

Figure 5.5 Composition of edenite amphiboles in the Beja-Acebuches Amphibolites from El Hurón.

Figure 5.7 (a) Composition of plagioclase from the Beja-Acebuches Amphibolites of El Hurón.
(b) Composition of plagioclase from the Peramora Mélange Formation.

observed optically in any of the samples studied. Zoning of feldspars within the Aracena Massif is clearly demonstrated, however, by Bard (1969) who shows that plagioclase from different areas within the metamorphic belt have different An contents. In any individual plagioclase crystal composition may range from as much as An_{58} in the core to An_{12} in the rim.

Fig. 5.7a shows plagioclase measurements from samples of the Beja-Acebuches Amphibolites. These form a well defined cluster with An content ranging from An_{40} to An_{70}, above the peristerite gap between albite and oligoclase (An_{3-20}). K_2O content ranges up to 0.6% wt% (appendix 5).

5.2.1.c *Epidote*

Epidote is commonly developed in samples from El Hurón, eg sample 9074 is a coarse grained amphibolite from El Hurón (Fig. 5.8A) in which plagioclase forms embayments within the amphibole. Hornblende displays a green to colourless pleochroic scheme and is commonly associated with colourless, high relief epidote. The assemblage hornblende-plagioclase(An_{40-70})-epidote is consistent with epidote-amphibolite facies metamorphism (Winkler 1979).

5.2.2 The Peramora Mélange Formation.

Specimens from the Peramora Mélange Formation were collected within the Los Ciries Antiform and along the banks of the barrancos of Rioja and Ciego (Fig. 5.2). Seven samples for analysis by EDS microprobe were collected from exotic amphibolite blocks and two from the matrix within which the blocks are located.

5.2.2.a *Amphibole*

The main mineral assemblage of the Peramora Mélange Formation consists of act-plag-ep-clz-chl-qtz ± cte (section 2.3.6). Amphiboles from the Peramora Mélange Formation plot for the most part in the actinolitic hornblende through to the actinolite fields (Fig. 5.4b), whereas amphiboles from the amphibolite blocks are nearly all located in the actinolite field with a greater spread of compositions than is observed in the Beja-Acebuches Amphibolites. A possible actinolite forming, prograde reaction is (Miyashiro 1973):

$$\underset{\text{chlorite (antigorite)}}{5(Mg, Fe)_5Si_2O_5(OH)_4} + 6CaCO_3 + 14\ SiO_2 = 3Ca_2(Mg, Fe)_5SiO_{22}(OH)_2 + CO_2 + 7H_2O \quad [5.8]$$
calcite quartz actinolite

Other possible reactions, which accounts for the formation of actinolite together with clinozoisite are given by Winkler (1979) and Yardley (1989):

pumpellyite + chlorite + quartz = clinozoisite + actinolite [5.9]

chlorite + calcite = epidote + actinolite + CO_2-H_2O [5.10]

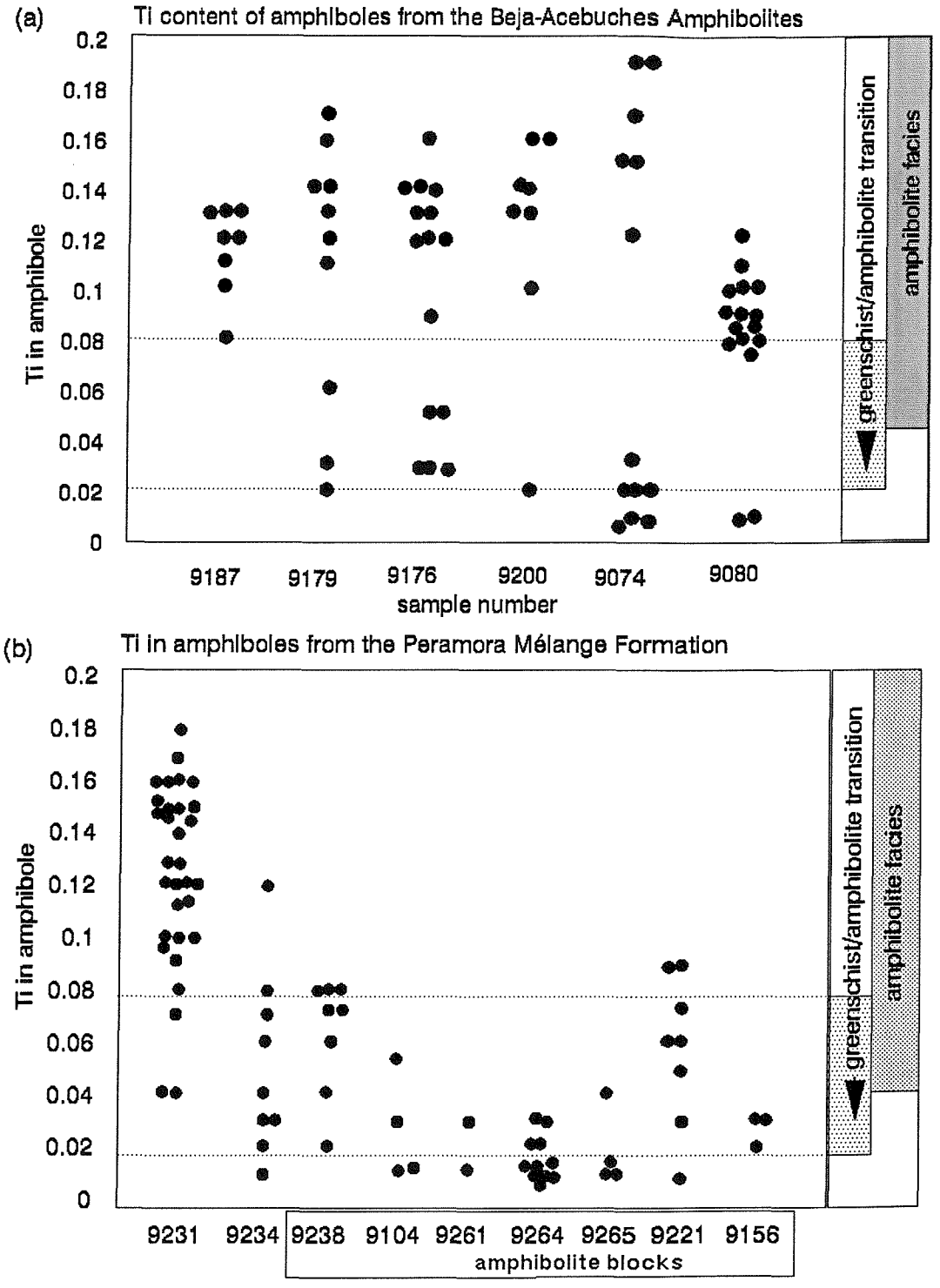

Figure 5.6 (a) Histograms of Ti content of amphiboles from the Beja-Acebuches Amphibolites of El Hurón.
(b) Histograms of Ti content of amphiboles from the Peramora Mélange Formation.

Figure 5.8

A. Amphibolite from El Hurón showing a high relief epidote porphyroblast overgrowing green-brown amphibole and plagioclase. Sample 9074 (x5)

B. Relict pleochroic amphibole (hornblende) in an amphibolite block in the Peramora Mélange Formation. Sample 9238 (x10)

C. Andalusite with the foliation, composed of phyllosilicates, deflected around it. Small porphyroblasts

D. Discrete block from within the matrix of the Peramora Mélange Formation. Large blades of clinozoisite and strain free crystals of plagioclase. Sample 9156 (x5)

E. Cordierite porphyroblast displaying sector trilling and with a fine grained phyllosilicate rich matrix deflected around it. Sample 9061 (x2.5)

F. Garnet (alm 60:spess 40) overgrowing an early fabric composed of biotite, muscovite and quartz. of muscovite overgrow the andalusite. Sample 9252 (x2.5) Sample 9136 (x10).

G. Cordierite porphyroblasts overgrowing an early fabric composed of quartz and phyllosilicates. Sample 9121 (x2.5)

H. Fragmented amphibole and plagioclase within a deformed block in the Peramora Mélange Formation (Barranco de Rioja). Small actinolite porphyroblasts are entrained from the large amphibole. Sample 9243 (x2.5)

These reactions define the boundary between very low grade metamorphic conditions and lower greenschist facies conditions.

Composition of actinolites from the study area (Fig. 5.4b) moves into the hornblende field as Al_2O_3 content increases. True actinolites have an Al_2O_3 composition of 3-4% (Deer *et al.* 1966). The occurrence of hornblende and actinolite in equilibrium within the same sample may indicate temperatures in the range of ≈450-600°C, ie in the field of the miscibility gap (Boyle 1986; Spear & Chenney 1989) between actinolite and hornblende; at temperatures above ≈600°C hornblende alone becomes the stable phase, although there also appears to be a continuous range of compositions present at higher grades, above ≈600°C (Misch & Rice 1975).

The Ti content of amphiboles from samples of the Peramora Mélange Formation is shown in Fig. 5.6b. Comparison with the Ti content of the Beja-Acebuches Amphibolites demonstrates that, in general, lower grades of metamorphism were attained in the Peramora Mélange Formation, the majority of data points falling in the greenschist/amphibolite transition zone. Sample 9231, which is from the matrix of the Peramora Mélange Formation, is an exception to this. In this sample amphiboles contain a higher than expected Ti content placing it within the amphibolite facies. Thin section demonstrates that the sample displays a strong alignment of interlocked plagioclase and amphibole. The sample was taken from a tectonic boundary between a unit of Peramora Mélange Formation and Cumbres de Los Ciries Formation and may have experienced higher grades of metamorphism during imbrication.

5.2.2.b *Plagioclase*

Samples from the Peramora Mélange Formation, both phacoids and matrix, are much finer grained than those from El Hurón. Plagioclase occurs as small uniform crystals and displays a bimodal spread of compositions from albite ($An_{<10}$) to labradorite (An_{50-70})(Fig. 5.7b); those from exotic blocks fall both in the field with low An contents and also with moderate to high An content. High values in the block material may represent a relict metamorphic phase inherited from the source rock while low values may indicate significant retrogression has occurred during overprinting.

5.2.2.c *Epidote Group Minerals.*

In the Peramora Mélange Formation both clinozoisite and epidote are commonly observed. In certain areas epidote occurs in abundance. In such cases it forms within green horizons that have been transposed within the regional schistosity. Clinozoisite is especially well developed in samples representative of the matrix where it forms both as small isolated crystals and as clusters of crystals up to 1mm in width. It also occurs as large crystals in some of the phacoids found within the mélange, eg sample 9156 (Fig.5.8D). Several possible reactions may result in the production of clinozoisite together with actinolite within basic rocks:

pumpellyite + chlorite + quartz = clinozoisite + actinolite [5.11]

pumpellyite + quartz = prehnite + clinozoisite + actinolite [5.12]

These reactions are consistent with prograde metamorphism at low grades. A typical metamorphic assemblage for greenschist facies is (Winkler 1979):

chlorite + zoisite/clinozoisite ± actinolite ± quartz ± albite [5.13]

This latter assemblage is commonly seen in samples from the matrix of the Peramora Mélange Formation.

Assemblage [5.16] and [5.17] (Table 5.B) are the main mineral assemblages for the matrix of the Peramora Mélange Formation. These assemblages generally consist of fine crystals of actinolite and actinolitic hornblende strongly orientated parallel to the foliation. Porphyroclasts of hornblende are strongly attenuated and may be accentuated by laths of chlorite (Fig. 5.8B). They are often rimmed by small needles of actinolite. Plagioclase is also present as porphyroclasts. Exotic amphibolite blocks within the matrix exhibit a complete gradation between relict igneous textures and a strongly deformed fabric.

5.2.3 The Beja-Acebuches Amphibolites and the Peramora Mélange Formation compared.

As established in 4.3, geochemical signatures for the Beja-Acebuches Amphibolites and the Peramora Mélange Formation suggest a genetic relationship. Amphibole (hornblende and actinolite), plagioclase and epidote are found in both units. Clinozoisite within the Peramora Mélange Formation may have been formed from the breakdown of a basic precursor, possibly calcic plagioclase. Epidote group minerals exist over a wide stability range under regional metamorphic conditions. For pressures between 4.5 - 6.5 kb the 'zoisite-in' curve lies between 350-370°C and has an upper limit of ≈670° at 6kb in the presence of quartz and H_2O (Liou 1985).

Sphene ($CaTiSiO_5$) and ilmenite ($FeTiO_3$) are common to both the El Hurón amphibolites and the Peramora Mélange Formation. In the former sphene often forms up to 6% of the assemblage with much smaller amounts visible in the Peramora Mélange Formation. Both minerals are of limited petrological use since they occur over a wide range of metamorphic conditions, sphene tending to be more stable at lower grades.

The absence of rutile, the high temperature TiO_2 polymorph occurring in high grade assemblages, is noticeable and may indicate a lowering of metamorphic conditions (Yardley 1989).

Chlorite forms as a late stage mineral and appears to be more stable within the lower grade assemblages of the Peramora Mélange Formation, where it develops as small crystals formed from the secondary alteration of hornblende. It becomes less evident within the higher grade assemblages

of El Hurón.

Element partitioning between amphibole and plagioclase can be used as a geothermometer (Spear 1981). The results from samples of both the El Hurón amphibolites and the Peramora Mélange Formation are plotted in Fig. 5.9. Miscibility gaps in amphiboles are represented by horizontal lines and those in feldspars as vertical lines, thus illustrating that as the composition of one parameter changes across the immisibility gap the other remains stable. Temperatures are shown to range between 530° and >700° in the El Hurón amphibolites while a greater spread of data is evident from minerals from the mélange matrix, with the lowest temperature being recorded by some exotic blocks. Spear (1981) emphasises the large errors in calculating $X_{Na(A)}$ and that temperatures obtained may be in error by as much as ±50°C. The technique was originally adapted for typical Barrovian sequences, and it may be that at lower pressure the hornblende-actinolite immiscibility gap is wider and persists to higher temperatures, a process that will change the shape of the contours. The temperatures obtained by analysis of minerals from the study area must therefore be viewed as estimates only, as more data is essential to provide stricter constraints.

A summary of the features observed in the Beja-Acebuches Amphibolites and the Peramora Mélange Formation and is given in Fig. 5.15a & b. Whilst the Beja-Acebuches Amphibolites, juxtaposed against the Northern Metasedimentary Domain, may have suffered retrogressive metamorphism to greenschist facies, the Peramora Mélange Formation probably suffered prograde metamorphism up to the greenschist/amphibolite facies transition. Retrogression in the former is shown by the development of actinolitic hornblende and epidote (after hornblende and tschermakite?), an assemblage that is consistent with temperatures >≈350°C (Barker 1990). Prograde metamorphism in the latter is indicated by Al-rich actinolite and intermediate plagioclase compositions, while retrogression in the amphibolite blocks contained within the Peramora Mélange Formation is shown by the actinolitic composition of the amphiboles as well as the albitic composition of plagioclase. Some of the blocks, eg sample 9221 retain features consistent with higher metamorphic grades than is seen in the enclosing matrix (Fig. 5.7 and 5.9). This may indicate preservation of higher grade mineral compositions inherited from the source rocks. As these blocks may have been derived from the Beja-Acebuches Amphibolites they were probably originally at amphibolite facies prior to incorporation within the mélange. Some samples from the matrix also indicate elevated temperatures (Fig. 5.7 and 5.9 sample 9231). This may be related to whole rock chemistry; the sample has a TiO_2 content of 1.83 wt%.

5.2.4 The Cumbres de Los Ciries and Alajar Formations and their relationship to the Peramora Mélange Formation.

A summary of the metamorphic assemblages observed is given in Table 5.B. Detailed descriptions of quartz-mica schists of the Sierra de Las Bañas Formation (the Cumbres de Los Ciries

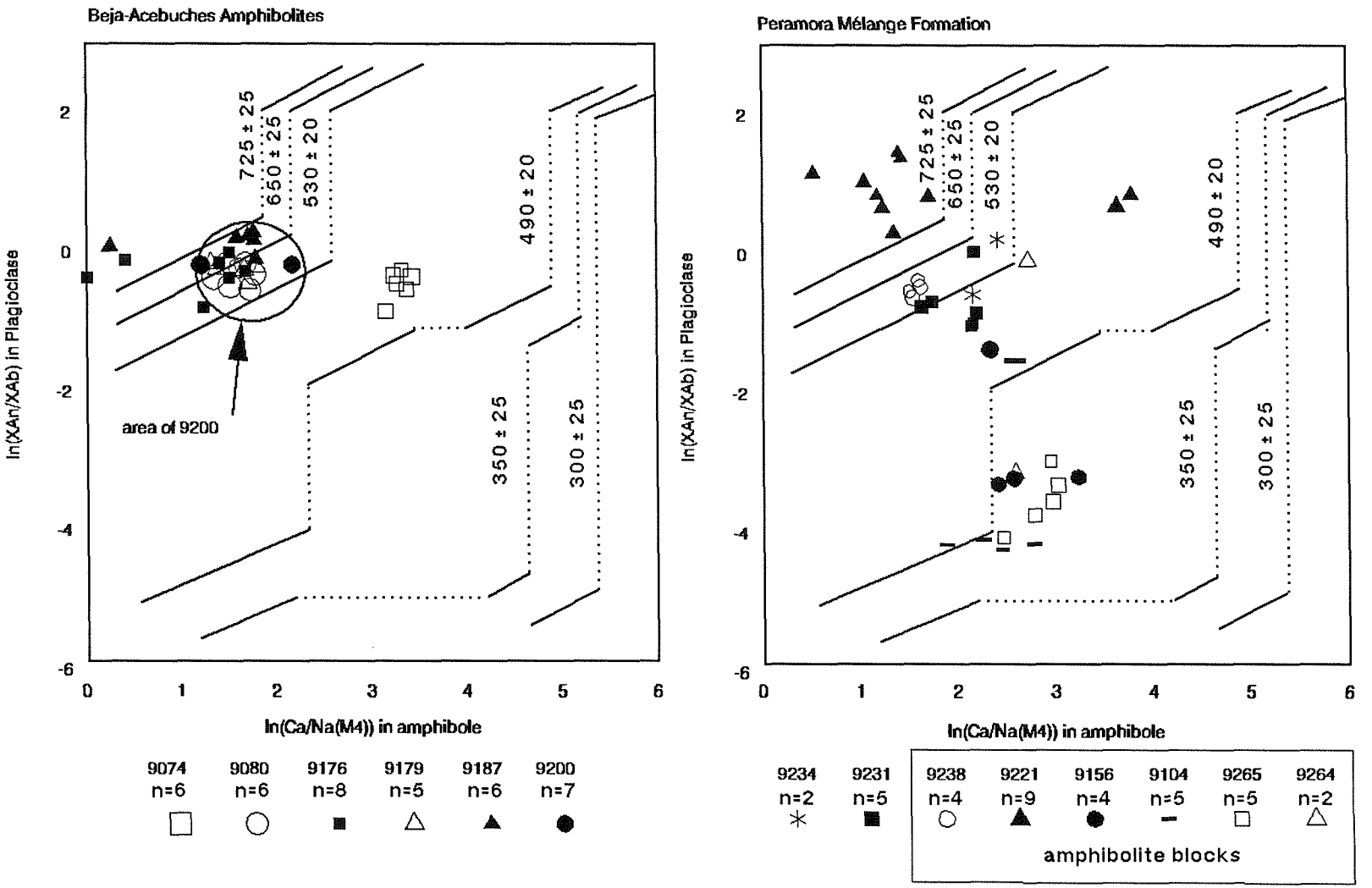

Figure 5.9 Geothermometer based on the Ca/Na content in amphiboles and An/Ab content in plagioclase.

qtz-bte-mus-and-chl ± cde ± gt	(CLCF)	[5.14]
qtz-bte-mus-cde ± and ± gt ± ortho	(CLCF)	[5.15]
act-actc hbl-plag($An_{<10-80}$)-ep-clz-chl ± cte	(PMF)	[5.16]
qtz-bte-mus-and ± cde ± gt ± plag	(CLCF)	[5.17]
qtz-bte-chl ± mus	(CLCF)	[5.18]
act-actc hbl-plag($An_{<10-80}$)-ep-clz ± bte ± mus	(PMF)	[5.19]
serp-magnes-tc ± cte	(AF)	[5.20]
qtz-mus-bte-chl ± plag(Ab-Olig)	(AF)	[5.21]
qtz-mus ± K-feld	(AF)	[5.22]

Table 5.B Summary mineral parageneses observed in the Cumbres de Los Ciries Formation, Alajar Formation and Peramora Mélange Formation.

Formation), are described by Crespo-Blanc (1989), and only representative examples of these parageneses are discussed here.

Mineral paragenesis [5.14] is characteristic of the rocks located on the southern border of the Beja-Acebuches Amphibolites in the Aroche section (Fig. 5.2).

5.2.4.a *Biotite, muscovite and chlorite*

Biotite, muscovite and chlorite occur as foliation parallel mica fish, reflecting the high strain that has affected the Cumbres de Los Ciries Formation and the Alajar Formation. Together, biotite and muscovite comprise 40-50% of the rock mass, probably forming according to the reactions (Winkler 1979):

phengite + chlorite = biotite + Al-richer chlorite + quartz [5.23]

phengite + chlorite + microcline = biotite + quartz + phengite with less Mg, Fe. [5.24]

Assemblage [5.18] is the most extensively developed paragenesis of the Cumbres de Los Ciries Formation. It occurs in the core of the Los Ciries Antiform and to the south of this structure (Fig. 5.2) within the Northern Metasedimentary Domain (Chapter 3). Greenschist facies conditions suitable for the formation of these minerals persisted throughout the structural evolution of the formation with the production of microlithons of phyllosilicates and quartz, now preserved in both the S_{N1} and S_{N2} schistosity.

[5.21] constitutes the main matrix forming assemblage of the Alajar Formation. Phyllosilicate minerals, including biotite, muscovite and chlorite exist as very fine grains that are strongly attenuated, forming mica fish and well developed S-C fabrics. An earlier foliation is not seen in this formation. Quartz displays well advanced deformation fabrics (Fig. 3.14D). Chlorite is developed not only as foliation parallel aggregates but also as fine grained mats replacing phyllosilicates. Accessory phases

include plagioclase (ab-olig), zircon, tourmaline and rare apatite.

Assemblage [5.22] occurs in the massive quartzites that are entrained within the matrix of the Alajar Formation. As stated in section 2.3.4 these form as massive sigmoidal lenses, consisting of up to 95% quartz with only accessory phyllosilicates and K-feldspar. During shearing they suffered extensive recrystallisation.

All the assemblages described above are consistent with an interpretation that greenschist facies persisted within the Cumbres de Los Ciries Formation and Alajar Formation, with the development of biotite, muscovite and chlorite, throughout the structural evolution of the Northern Metasedimentary Domain and the Alajar Domain. This resulted in the production of microlithons of phyllosilicates and quartz in the former domain and extensive recrystallisation in both domains.

5.2.4.b *Andalusite and cordierite*

Assemblage [5.14] occurs along a narrow belt immediately juxtaposed against the southern boundary of the Beja-Acebuches Amphibolites (Fig. 5.2). Andalusite occurs as syn-D_2 porphyroblasts with the phyllosilicate foliation deflected around them (Fig. 5.8C). Many of these porphyroblasts are fragmented and bridged by small elongate crystals of biotite and muscovite. An early cleavage is not preserved within the andalusite although abundant small inclusions of randomly orientated quartz and opaque minerals are frequently observed. Cordierite is infrequently developed in this assemblage but where it does occur it forms amorphous aggregates of dusty material now entirely altered to pinite.

Assemblage [5.17] is similar to [5.14]. Andalusite forms as a syn-D_2 mineral accompanied by the formation of biotite, cordierite and garnet, an association typical of low pressure/high temperature metamorphism (Yardley 1989). Mineral assemblages [5.15] and [5.16] are observed along the Barranco del Ciego (Fig. 5.2) where they form the matrix of the Peramora Mélange Formation. Assemblage [5.15] differs from [5.14] in containing well developed porphyroblasts of cordierite (up to 0.5mm - Fig. 5.8E). These porphyroblasts are clearly syn-kinematic and are associated with biotite which forms as small laths especially well developed in pressure shadow areas. Cordierite may enclose an early cleavage picked out by small inclusions of quartz and opaque minerals, although in some examples (eg 9121, Fig. 5.8G) it forms small porphyroblasts that replace an earlier quartz-rich matrix.

As noted above both cordierite and andalusite formed during ductile deformation. However, preservation of sector trilling, twins which do not appear to grow during active deformation (Putnis & Holland 1986; Kitamura & Yamada 1987), suggests that there may have been a period of little or no deformation before the formation of the intense regional foliation (Fig 5.8E). Deformation subsequent to porphyoblast growth has resulted in local fragmentation of andalusite and cordierite porphyroclasts (Fig. 3.16E).

Prograde metamorphism of pelites leads to the development of andalusite and cordierite,

possibly by the reactions (Harte & Hudson 1979):

$$\textbf{muscovite + chlorite + quartz = biotite + cordierite + } H_2O \quad [5.25]$$

$$\textbf{muscovite + chlorite + quartz = biotite + andalusite + } H_2O \quad [5.26]$$

Andalusite may also form in pelites at low pressures by the reaction:

$$\textbf{chlorite + muscovite + quartz = cordierite + andalusite + biotite + } H_2O \quad [5.27]$$

and this reaction represents the upper limit for chlorite in quartz-mica schists (Yardley 1989). In some samples muscovite grows randomly across andalusite porphyroblasts (Fig. 5.8C). This may be the result of retrogressive reactions, that occurred post formation of the andalusite, such as:

$$3Al_2SiO_5 + 2H_2O + 3(SiO_2 + K_2O) = \underset{\textbf{sericite}}{K_2Al_4Si_6Al_2(OH)_4O_2O} \quad [5.28]$$

The stability field of cordierite and andalusite is illustrated in fig. 5.10 (Yardley 1989). Cordierite tends to form in rocks with high X_{Mg} values increasing in proportion as temperature increases. The diagram illustrates that andalusite and cordierite may occur together at high temperatures and low pressures.

Andalusite occurs in the stability field delineated in fig. 5.10 & Fig. 5.14 although it may form under low grade conditions by the decomposition of pyrophyllite at ≈400°C. Harte & Hudson (1979) delineated a stability field for andalusite-cordierite-biotite at temperatures of between 570°- 665°C and pressures of 2 - 5.5kb although in their case study they used a very high P/T position for the Al_2SiO_5 invariant point. Miyashiro (1973) stated that at low pressures cordierite becomes stable at ≈450-500°C in association with quartz, muscovite, biotite and chlorite.

In rocks with higher Fe^{2+}/Mg ratios garnet and staurolite occur. The latter mineral is not seen in the belt although garnet with a composition of $[(Fe_{1.7}Mg_{0.15}Ca_{0.16}Mn_{1.0})Al_2Si_3)_{12}]$ (Fig. 5.8F and appendix 5) is seen as a late stage phase. This may suggest that pressures were towards the higher limit for the reactions illustrated above.

The assemblages discussed above indicate that a high P/low T metamorphic event resulted in the imposition of a metamorphic sole in the immediate footwall of the Beja-Acebuches Amphibolites. Metamorphic minerals accompanying this event probably overprint earlier metamorphic assemblages associated with regional metamorphism. The absence of any metamorphic minerals south of the Alcalboza River (Fig. 5.1) suggests that the metamorphic sole is inverted, becoming lower grade towards the south.

5.2.4.c *Serpentinite*

[5.20] is observed within an isolated exotic block of serpentinite measuring some 30m strike-parallel length and 10m wide and outcropping at [GR ^{7}0420 ^{41}9275] within the Alajar Domain. The block consists of essential serpentine and magnesite ($MgCO_3$) and has been altered on its margins to talc. The parent rock was originally dunitic in composition (section 2.3.4.3).

Metamorphism of ultramafic rocks occurs in the presence of variable amounts of H_2O and CO_2. These can be expressed in terms of X_{CO2} (Fig. 5.13, Johannes 1969). Relevant reactions are:

$$1 \text{ serpentine} + 1 \text{ magnesite} = 2 \text{ fosterite} + 2H_2O + 1 CO_2 \quad [5.29]$$
$$2 \text{ serpentine} + 3 CO_2 = 1 \text{ talc} + 3 \text{ magnesite} + 3 H_2O \quad [5.30]$$
$$1 \text{ serpentine} + 3 CO_2 = 2 \text{ quartz} + 3 \text{ magnesite} + 2 H_2O \quad [5.31]$$
$$1 \text{ serpentine} + 2 \text{ quartz} = 1 \text{ talc} + 1 H_2O \quad [5.32]$$
$$1 \text{ brucite} + 1 CO_2 = 1 \text{ magnesite} + 1 H_2O \quad [5.33]$$
$$4 \text{ quartz} + 3 \text{ magnesite} + 1 H_2O = 1 \text{ talc} + 3 CO_2 \quad [5.34]$$

The reactions listed above can occur over a relatively large temperature range although below 500°C (Fig. 5.11). At high values of X_{CO2} and temperatures greater than ≈500°C, fosterite, enstatite and anthophyllite become important (Winkler 1979). The assemblage seen in the field corresponds most closely to reaction [5.31], an assemblage that occurs between 350°-500°C at 2kb, rising to higher temperatures at greater pressures.

5.3 The La Giralda Formation and the Puerto Cañon Formation.

These two formations, (Fig. 5.2) have experienced lower grades of metamorphism than seen in the formations described above. The petrography of the Puerto Cañon Formation (section 2.3.1) shows that biotite, muscovite and chlorite grow as cleavage forming phases accompanying the main D_2 deformational event. In the La Giralda Formation in the Central Metasedimentary Domain (section 2.3.2) metamorphic minerals are poorly developed, forming mainly along cleavage planes. For this reason a suite of 30 samples from slate horizons within the La Giralda Formation were studied using vitrinite reflectance techniques, 17 of which have given productive results. Analysis was conducted on samples that either yielded palynomorphs or were located close to them and involved measuring the reflectivity of small fragments of polished vitrinite and palynomorphs.

The use of vitrinite reflectance studies in low grade terranes is well established (e.g. Clayton 1989), especially in the study of high rank metamorphism but there are several possible sources of error in any study of this sort, including the possibility of failure to recognise when material has been reworked. Vitrinite reflectivity may also be modified by oxidation of the host sediments.

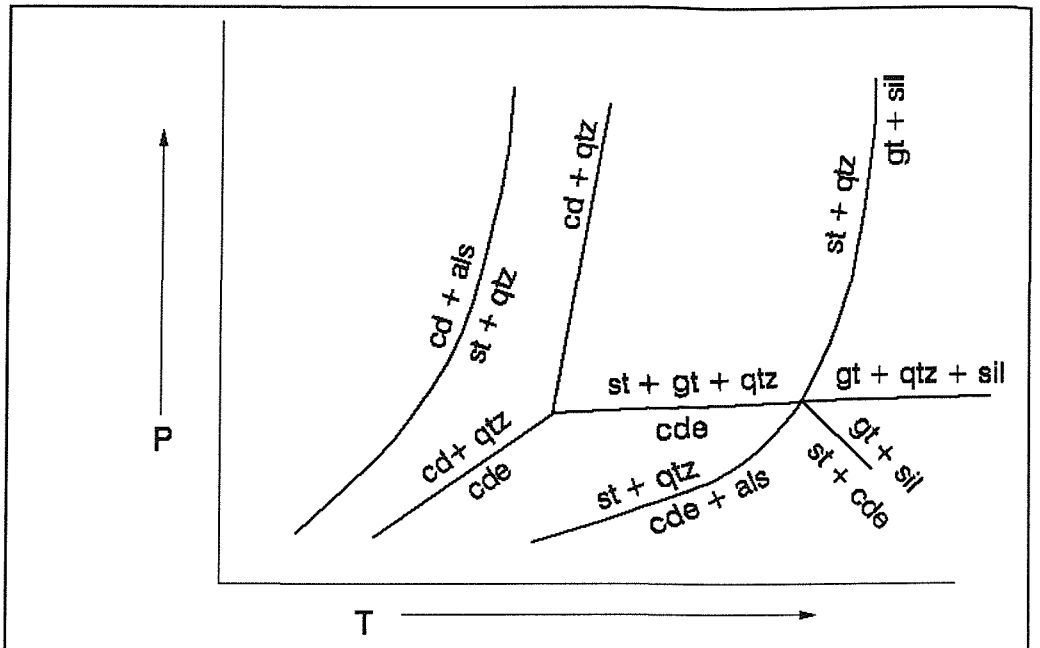

Figure 5.10 schematic P-T diagram to illustrate the effects of pressure and temperature on assemblages involving chloritoid, staurolite, Al-silicates, cordierite and garnet

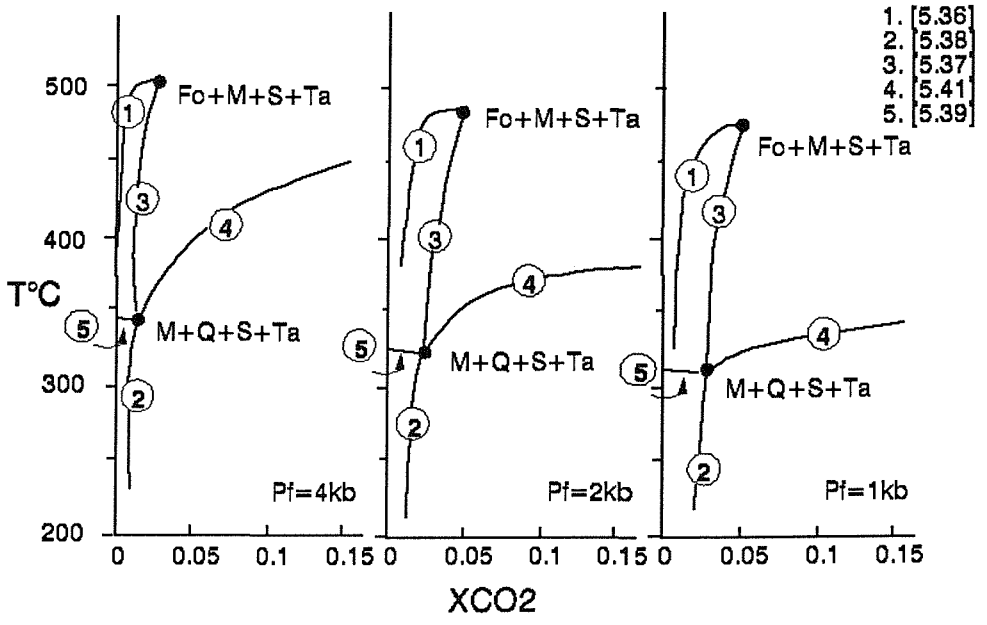

Figure 5.11 Isobaric equilibrium curves, reactions at low XCO2 (Johannes 1969)

sample number	no.	mean Rm	standard deviation	temperature (°C) (Barker & Pawlewicz (1986))
8072	86	4.2	1.4	289.3
8139	70	2.7	2.7	313.8
8151	91	5.9	1.4	327.4
8155.	84	4.6	1.3	300.2
8156	83	3.5	1.3	269.8
8163	94	3.8	1.4	276.8
8172	81	4.2	1.7	287.1
8173	92	3.4	1.7	262.1
8178	94	1.2	1.7	304.8
8180	81	4.6	1.8	297.1
8182	95	3.8	1.1	279.1
8186	91	2.4	1.3	222.7
8191	84	3.8	1.6	277.1
8200	79	4.9	2.1	300.4
9115	74	6.4	2	333.4
9116	70	6.5	1.9	335.9
9131	65	4.3	2	287.6

Table 5.C Temperature estimates from vitrinite reflectance after Barker & Pawlewicz (1986).

5.3.1 Results.

Preparation and analysis of the samples is described in appendix 4. Most of the samples analysed were collected from the Central Metasedimentary Domain although one sample (8139) was collected from the Puerto Cañon Formation on the northern limb of the Los Ciries Antiform (Fig. 5.12). Table 5.C shows the results obtained and also the interpreted palaeotemperatures. Histogram plots of measurements are shown in Fig. 5.13. Reflectance values were converted to temperature estimates using the time independent formula of Barker & Pawlewicz (1986):

$$T_{max} = \ln(Ro) + 1.4/0.0096$$

Vitrinite reflectance values recorded fall within a range of 1.2 - 6.5% (Fig. 5.12 and 5.13) and indicate a meta-anthracite rank (Teichmüller 1987) (appendix 4), with calculated temperatures from these results falling in the range of 230°-330°C. The histograms shown in Fig. 5.13 are in the main unimodal, suggesting that reflectivity is relatively consistent in the material measured (Knight 1990).

Measured mean Rm values are mostly higher the mean Rm% = 3 isotherm (Fig. 5.14) and may indicate that conditions reached lowermost greenschist facies.

5.4 Metamorphism along the boundary between the Ossa Morena Zone and the Oceanic Exotic Terrane.

5.4.1 *The Beja-Acebuches Amphibolites*

The presence of clinopyroxene on the northern boundary of the Beja-Acebuches Amphibolites (Bard 1969; Apalategui *et al.* 1983, 1984; Crespo-Blanc 1989) indicates that early in the structural evolution metamorphic conditions were high grade, possibly reflecting the close proximity of these rocks to the granulite facies complex of the Aracena Massif. This conclusion is supported by the presence of wollastonite bearing impure marbles that occur in the hangingwall rocks of the Jabugo Almonaster Zone, with the Beja-Acebuches metabasites in the immediate footwall. Wollastonite forms under a range of conditions, usually being restricted to contact metamorphic rocks although fluid chemistry has a strong control over its formation. At high X_{CO2} wollastonite is formed at high temperatures and low pressures (Yardley (1989).

Geochemical data suggests higher temperatures in the Beja-Acebuches Amphibolites than in the juxtaposed Peramora Mélange Formation. During the first phase of deformation high grade metamorphic assemblages may have been attained (Fig. 5.15a), possibly during thrusted juxtaposition between the Aracena Metamorphic Complex with the amphibolites at significant crustal depths. Lower grade assemblages which include epidote group minerals and actinolite resulted from retrogression (Fig. 5.14). These assemblages are restricted to the southern margin of the amphibolites where they are in contact with the Northern Metasedimentary Domain (Fig. 5.2). The third phase of deformation to affect this unit was accompanied by the growth of chlorite as metamorphic conditions achieved low greenschist facies.

5.4.2 *The Peramora Mélange Formation.*

The Peramora Mélange Formation shows characteristic assemblages of high grade greenschist/lower amphibolite facies necessitated by the stable coexistence of hornblende and actinolite, a reaction that begins to occur at around 500°C and at pressures of between 3 and 5.5kb in metabasic rocks (Winkler 1979) (Fig. 5.14). This is supported by the high Al_2O_3 content of actinolite which suggests conditions that reached upper greenschist to epidote-amphibolite facies (Deer, Howie & Zussman 1966). These assemblages may have developed during the second phase of deformation which corresponds to the main ductile shearing event (Fig. 5.15b). In the phyllosilicate-dominated facies within the Peramora Mélange Formation muscovite and biotite continued to grow during the last phases of deformation, accompanied by the growth of andalusite and cordierite on the southern boundary of the Beja-Acebuches Amphibolites (Fig. 5.15b). These minerals are not evident within the Los Ciries Antiform as the high T/low P metamorphism is highly localised along the contact with the Beja-Acebuches Amphibolites.

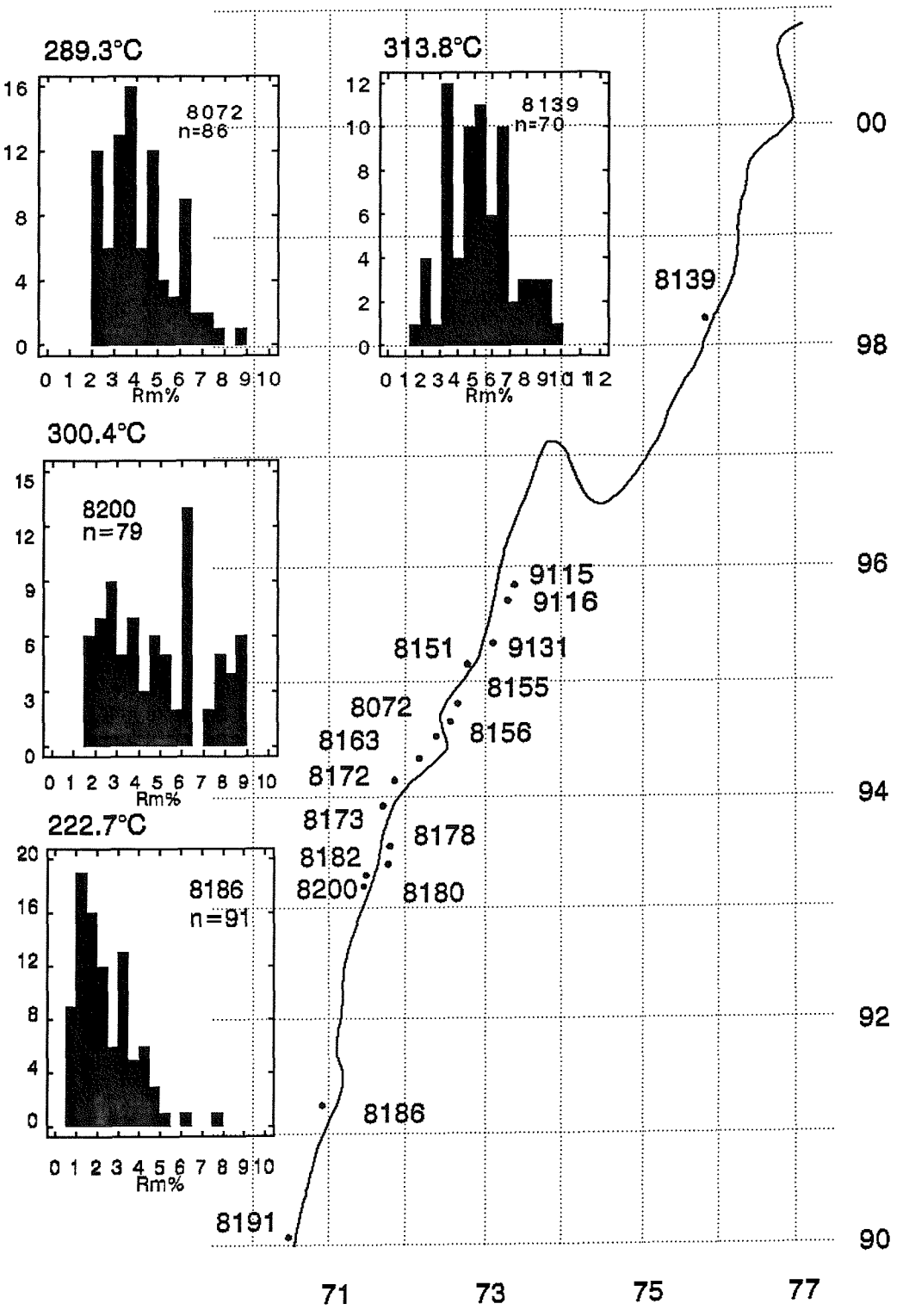

Figure 5.12 Location of samples for vitrinite reflectance analysis and selected histograms illustrating vitrinite reflectivity.

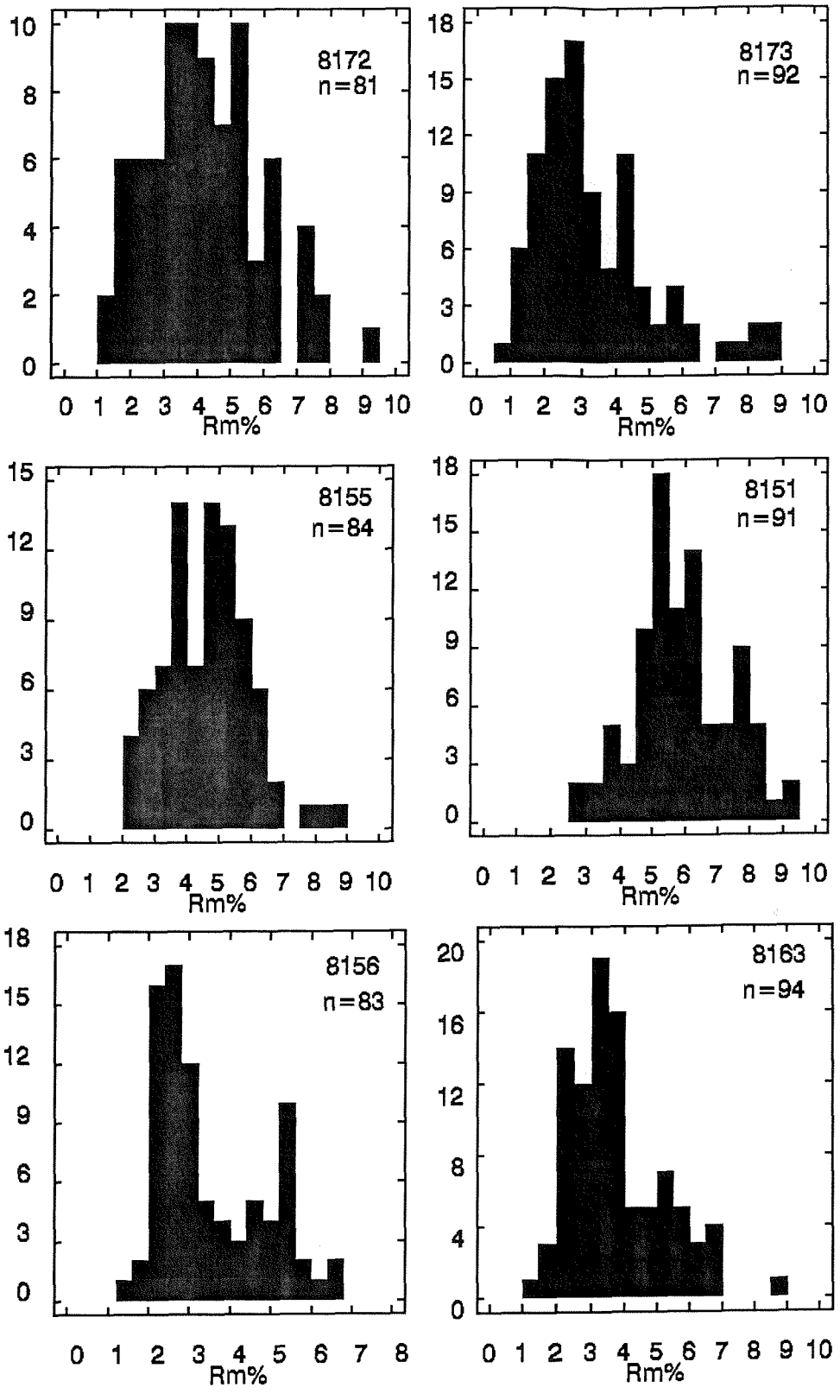

Figure 5.13 Vitrinite reflectance diagrams for palynomorph yielding samples from the La Giralda Formation.

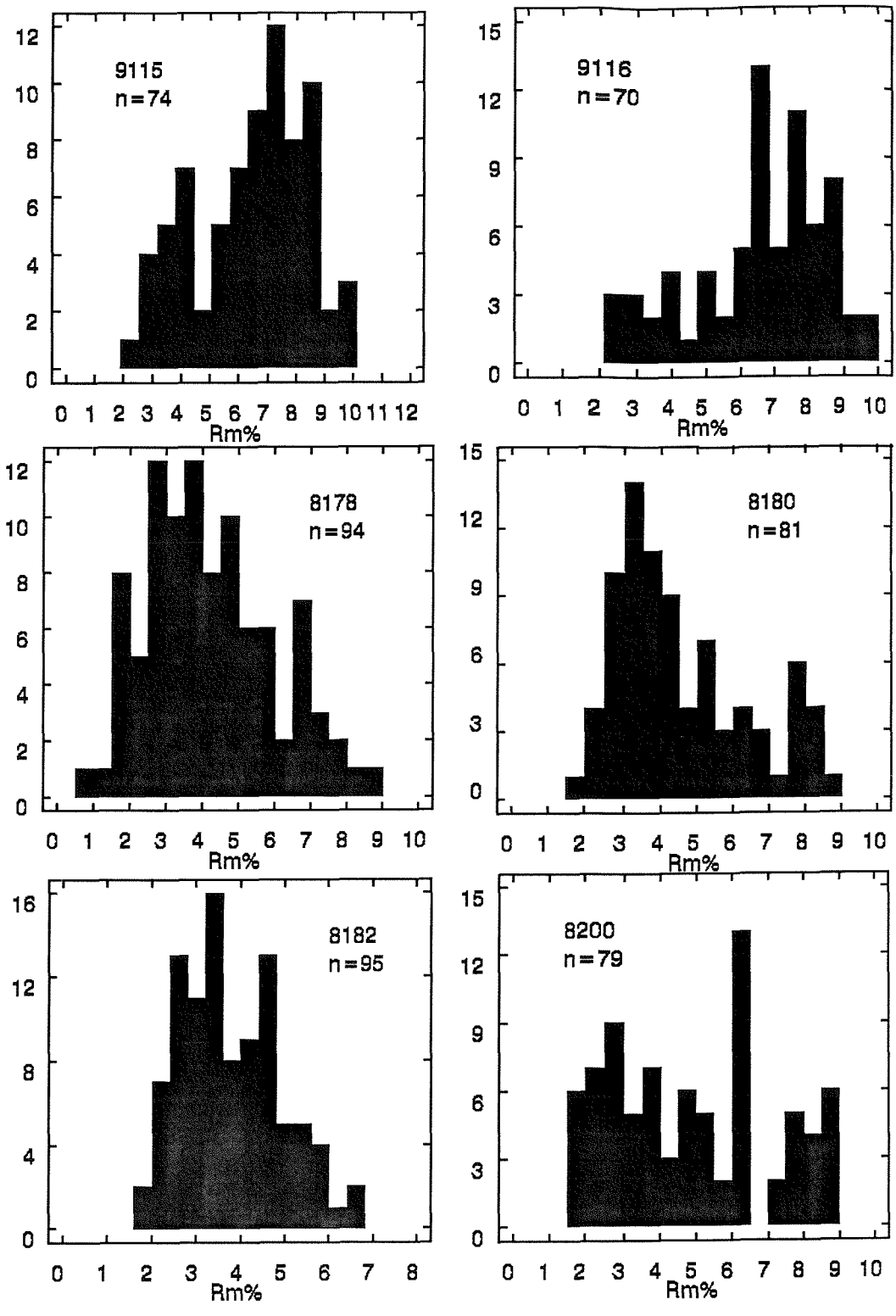
9115
n=74
9116
n=70
8178
n=94
8180
n=81
8182
n=95
8200
n=79
Rm%

5.4.3 *The Cumbres de Los Ciries and Alajar Formations.*

The Cumbres de Los Ciries Formation and the Alajar Formation are composed of similar metamorphic assemblages of quartz, biotite and muscovite. Pressure/temperature conditions of the metapelites close to the Beja-Acebuches Amphibolites are more closely constrained by the appearance of andulasite and cordierite which forms an inverted metamorphic sole beneath the ophiolite, with high temperature/low pressure metamorphic minerals becoming less abundant away from the contact and not appearing in the core of the Los Ciries Antiform. The earliest phase of deformation was accompanied by greenschist facies conditions that resulted in growth of biotite, muscovite and chlorite now preserved as microlithons truncated by the regional second phase schistosity, S_{N2}, (Fig. 5.15c). This latter phase gave rise to the strong regional schistosity which is composed of biotite, muscovite, quartz and chlorite, consistent with mid-upper greenschist facies conditions. During the third phase of deformation metamorphic conditions were significantly reduced, as folding of the earlier fabrics was unaccompanied by cleavage formation.

In the Alajar Formation an isolated outcrop of serpentinite indicates metamorphism at low grade greenschist facies. Assuming, say a pressure of 2kb, metamorphism of this phacoid occurred at a temperature between 325-475°C (Fig 5.14).

5.4.4 *La Giralda and Puerto Cañon Formations.*

Vitrinite reflectance analysis of vitrinite and palynomorphs from samples of the La Giralda Formation demonstrates that lowermost greenschist facies were reached. Petrographic analysis indicates that similar conditions were attained in the Puerto Cañon Formation (Fig. 5.15d). In both these formations metamorphism is of a significantly lower grade than observed in the Beja-Acebuches Amphibolites, Peramora Mélange Formation and Cumbres de Los Ciries Formation. One hypothesis for the cause of metamorphism recorded within these formations is that it may be due to the same thermal event that established the inverted metamorphic sole beneath the Beja-Acebuches Amphibolites. The inference is that low grades of metamorphism were attained that are related to ophiolite obduction with metamorphic conditions decreasing away from the hot ophiolite. However, a similar grade of metamorphism is observed in both the La Giralda Formation and Puerto Cañon Formation. If ophiolite obduction had occurred after deposition of these sediments then evidence of low pressure/high temperature metamorphism might be expected.

There is a decrease in maximum metamorphic conditions from high temperature amphibolite facies in the Beja-Acebuches Amphibolites, through upper and middle greenschist facies in the Peramora Mélange and Cumbres de Los Ciries Formations to lower greenschist facies in the Puerto Cañon and La Giralda Formations; a fall in temperature of up to 400°C over a horizontal distance of not more than four kilometres. The generation of such a complex metamorphic history is discussed in the model presented in Chapter 6.

1 - Rm% = 3 (Teichmuller, 1987)
2 - pure spessartine in (Hsu, 1968)
3 - (stp + ms) out ⇌ (bt + ms) in (Nitsch, 1970)
4 - chl + ms+ qtz ⇌crd + bt + Al2SiO5 + H2O (Harte & Hudson, 1979)
5 - pure almandine in (Hsu, 1968)
6 - transition zone actinolite⇌hornblende (Baker, 1990)
7 - Al2SiO5 triple point 583 C, 4.91kb (Powell & Holland 1984)

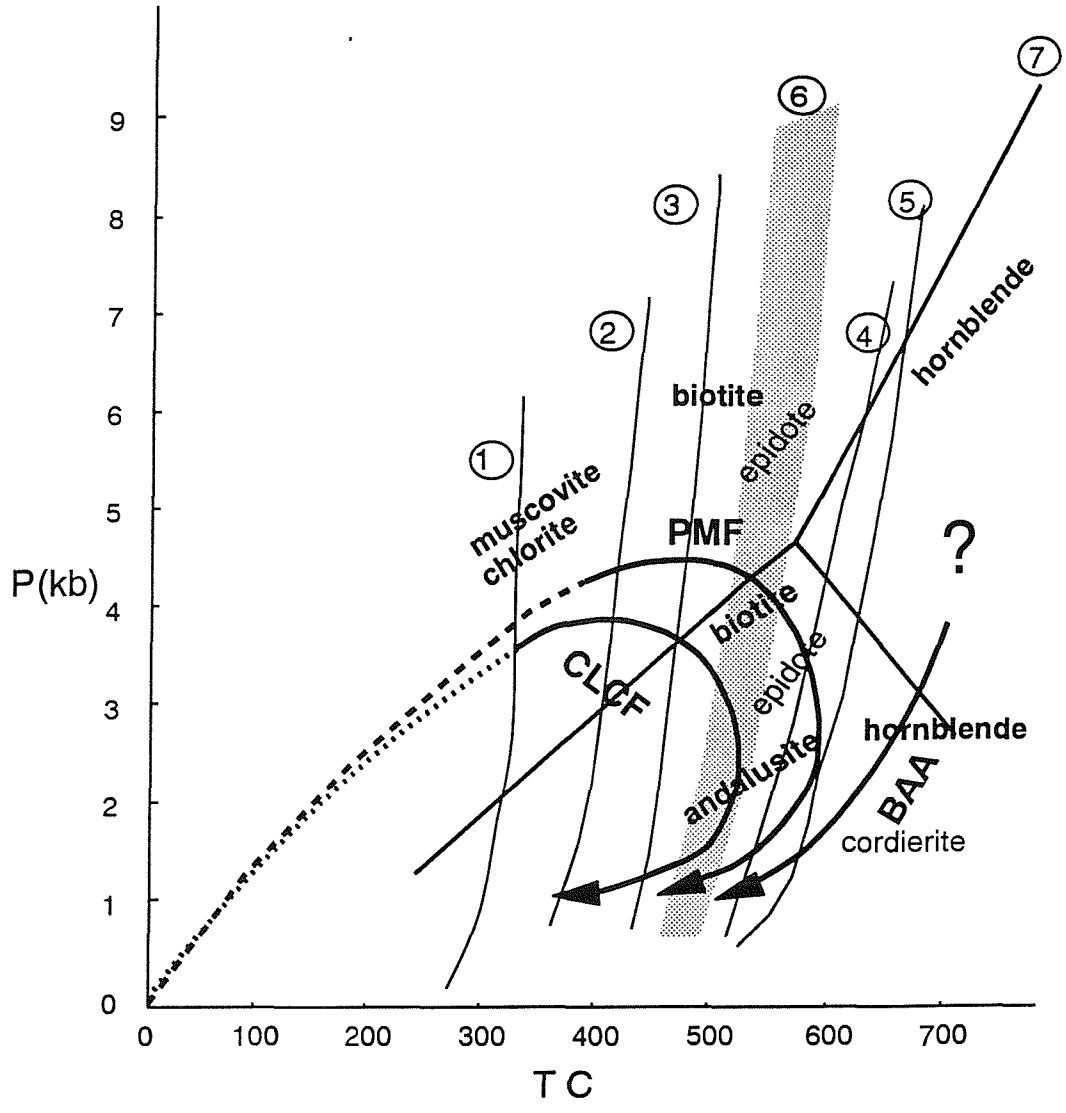

Figure 5.14 P-T-t path for the Beja-Acebuches Amphibolites, Cumbres de Los Ciries Formation and the Peramora Mélange Formation based on mineral parageneses, microprobe analysis and vitrinite reflectance.

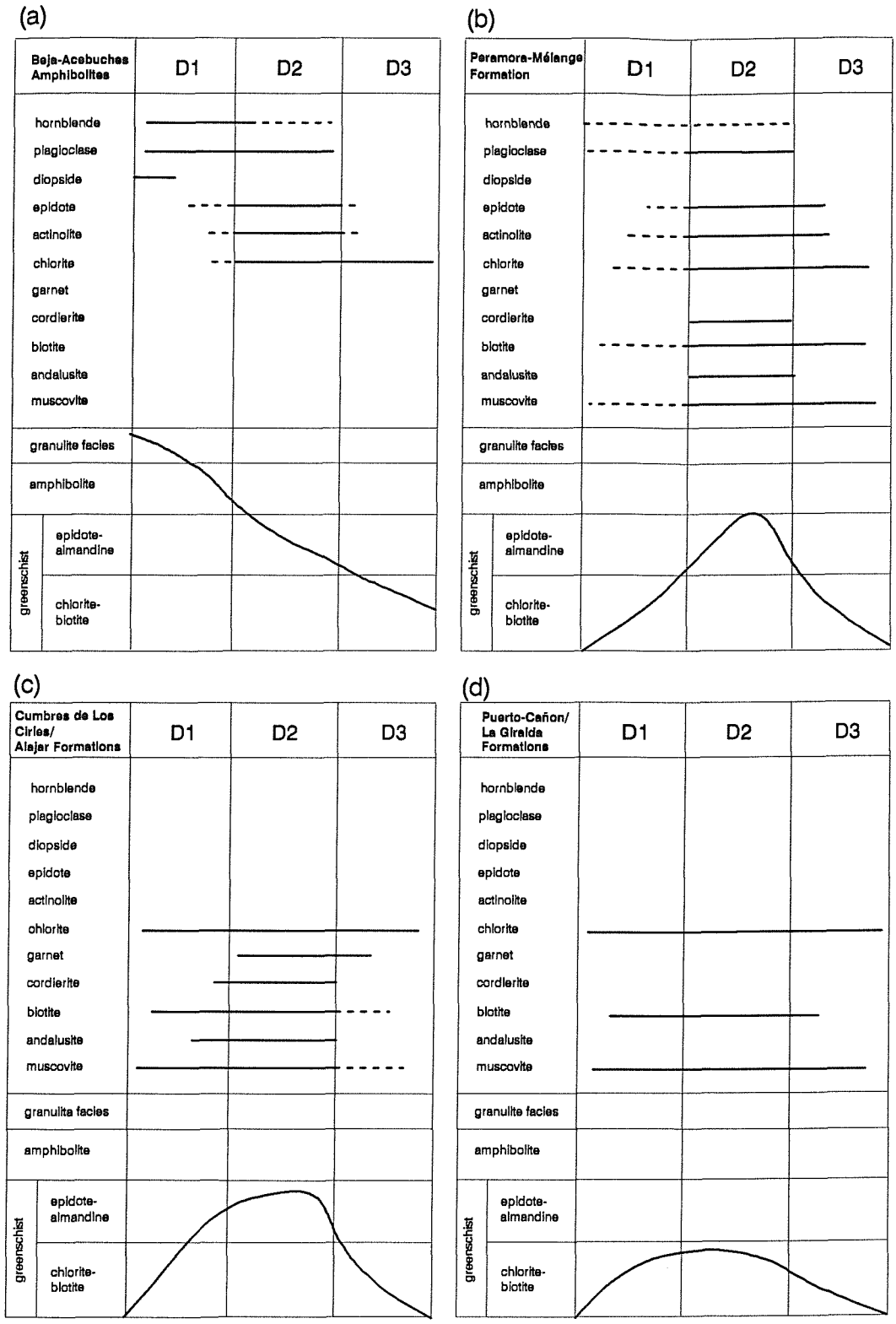

Figure 5.15 Schematic deformation/metamorphism diagrams for each of the formations identified in this study.

Chapter 6: A model for the evolution of the Oceanic Exotic Terrane

6.1 Introduction.

The geology of the SW Iberian Peninsula has previously been interpreted within a framework of both thin-skinned and thick-skinned tectonics (Chapter 1). Several important geological features constrain current models: (a) a suite of basic rocks that Munha *et al.* (1986) classify as a dismembered ophiolite ie the Beja-Acebuches Amphibolites, (b) early Carboniferous bimodal association of tholeiitic and alkalic volcanics with accompanying sulphide mineralisation (Munha 1979) that accumulated within an extensional tectonic regime, (the Iberian Pyrite Belt), (c) thick Upper Devonian/Lower Carboniferous sedimentary sequences which display diachroneity, younging towards the southwest (Julivert 1978; Oliveira *in press*), and (d) possible subduction related lower Carboniferous calc-alkaline plutonism in the southern part of the Ossa Morena Zone (Pacheco-Santos *et al.* 1985). There is a general consensus, however, that features observed are consistent with Upper Devonian/Early Carboniferous closure of an ocean basin with concomitant subduction and NE-SW shortening within an overall transpressive regime (Bard *et al.* 1973, Vegas & Muñoz 1976, Bard 1979, Oliveira 1980, Simancas 1983, Crespo-Blanc & Orozco 1988, Crespo-Blanc 1989, Oliveira *in press*, Silva *et al. in press*).

The Acebuches Amphibolites are considered to be an oceanic sequence on the basis of geochemical analysis and field observations. Munha *et al.* (1986) interpret the geochemical data as being transitional between MORB and island-arc suggesting formation in a small back-arc basin that may have been subducted soon after formation. In their model subduction occurred towards the northeast and is marked by the close association of basic metabasalts and acidic plutonism (Santos *et al.* 1988). The structurally underlying Pulo do Lobo and Ribeira de Limas Formations correspond to a subduction related accretionary wedge developed at the southern margin of the Iberian Terrane (Quesada *et al. in press*).

Direction of subduction, has been discussed by several authors with some arguing for southward subduction (Oswin 1986, Mata & Munha 1986) and others for northward subduction (Bard 1971, Carvalho 1972, Bard *et al.* 1973; Bard & Moine 1979, Vegas 1981; Simancas 1983, Ribeiro & Silva 1983, Ribeiro *et al. in press*). The present general consensus, however, is that limited northward dipping subduction occurred, a conclusion supported by features such as: (a) a strong southwesterly vergence of folds and a southwesterly directed transport direction, (b) the polarity of the diachroneity of sedimentary units in the South Portuguese Zone, (c) calcalkaline plutonism on the southern margin of the Ossa Morena Zone, (d) thrusting of the highly deformed Oceanic Exotic Terrane southwards over the less deformed Pyrite Belt successions, (e) locally preserved N-S mineral lineations within the Beja-Acebuches Amphibolites associated with ophiolite obduction (Fonseca *pers. comm.*), (f) high grade

metamorphic rocks preserved in the hinterland area of the Beja-Aracena Massif evolving to a low pressure/high temperature regime southwards, (g) an often quoted seismic section shot from Sagres to Elvas (Proedel *et al.* 1975) that infers sedimentary units lying above continental crust and supporting thin skinned tectonics within the South Portuguese zone.

Sinistral strike-slip movement is also recognised as a major element within the tectonic scenario. This is identified by (a) a strong steeply dipping regional west-east striking foliation that is accompanied by a sub-horizontal mineral lineation, (b) the existence of a major zone of ductile shear, the South Iberian Shear Zone (Crespo-Blanc & Orozco 1988, Crespo-Blanc 1989), (c) evolution of the Pyrite Belt sedimentary basins in an Upper Devonian/Early Carboniferous transpressional environment (Lake *et al.* 1988; Silva *et al. in press*, Quesada *et al. in press*).

The model presented below for the evolution of the Oceanic Exotic Terrane of the SW Iberian Peninsula is based on a regional study covering a small part of the belt. Within this area many geological features arise from a complex history of Palaeozoic terrane amalgamation. A model for the local development of the thrust belt is followed by a discussion of its generation within the scheme of late Devonian/early Carboniferous terrane amalgamation. Salient field observations, which impose constraints upon a model are summarised below and represented in Fig. 6.1.

6.2 Summary of data presented and discussed in Chapters 2-5.

6.2.1 *Facies and palaeoenvironments of the sedimentary formations.*

In the study area six formations are identified which occur together within a folded imbricate thrust stack. Each formation records a different tectonometamorphic history and is lithologically distinct. The Beja-Acebuches Amphibolites represent a dismembered ophiolite, coarse grained and of amphibolite facies in the north becoming fine grained and of greenschist facies in the south. This basic suite is strongly deformed and has a well defined regional schistosity accompanied by a sub-horizontal mineral lineation.

Identification of the Peramora Mélange Formation is critical in revising current models of tectonic evolution. The formation consists of tectono-sedimentary mélanges that were probably formed by a combination of processes including sedimentary mass wastage from the obducting ophiolite and tectonic underplating at the base of the Beja-Acebuches Amphibolites during overriding of the advancing thrust sheet. The mélanges are composed of blocks of amphibolite with lesser amounts of quartzite and greywacke. These phacoids are contained within a fine grained, recrystallised matrix which in places has a basic chemical composition. A block of sheeted dyke complex, consisting of intercalated fine grained basalts and coarse grained gabbros and measuring some tens of metres wide was possibly derived as a cohesive fragment from the obducting ophiolite. Matrix variations observed within the mélange range from a predominantly fine grained basic

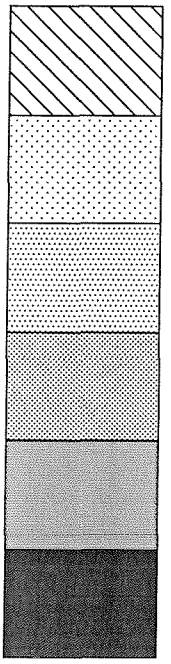

Puerto Cañon Formation

La Giralda Formation

Cumbres de Los Ciries Formation

Peramora Méiange Formation

Beja-Acebuches Amphiboiites

Ossa Morena Zone

● Low pressure/high temperature mineral assemblage

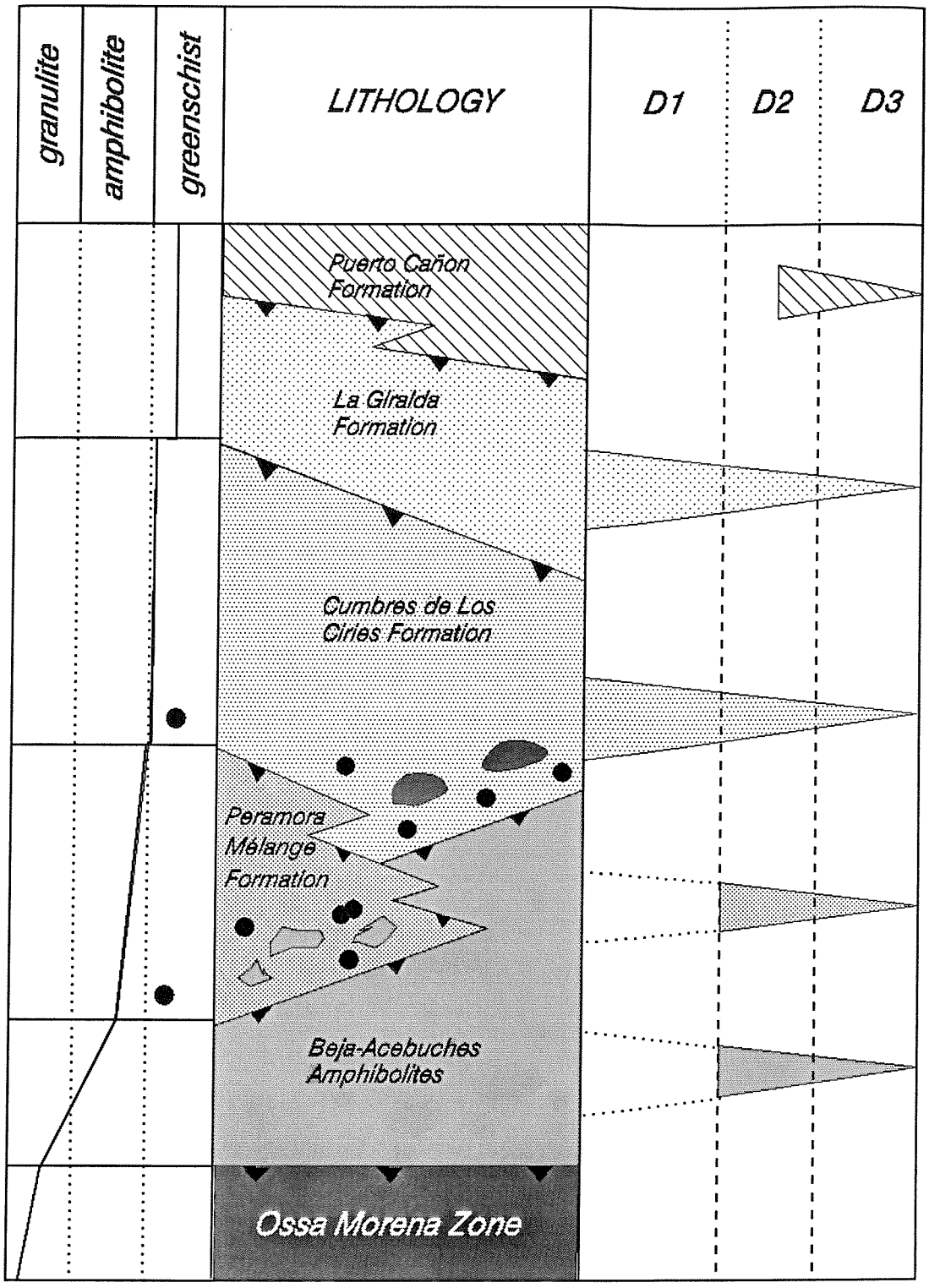

Figure 6.1 Tectonostratigraphic, structural and metamorphic summary of the various formations in the Aroche section.

amphibolite, that may originally have had a large volcaniclastic component, to a fine grained quartz-phyllosilicate schist. Syn-deformation low pressure/high temperature cordierite and andalusite occur within the latter in the immediate footwall of the Beja-Acebuches Amphibolites.

The Cumbres de Los Ciries Formation and the Alajar Formation appear to represent along strike facies variations and display many similarities. Both are composed of a thick sequence of intensely deformed quartz-mica schists which contain within their matrix rare occurrences of exotic clasts including serpentinite, marbles and, in the Aroche area, small blocks of basic material. Both formations also contain polydeformed discontinuous orthoquartzite blocks. In the Alajar area these occur as large foliation parallel 'fish' within a highly deformed fine grained matrix. Along strike the importance of these massive quartzite blocks diminishes and quartzites occur as smaller discontinuous blocks ranging in colour from grey to black. Decrease in block size may represent an along strike facies change where sedimentation in the Alajar area was periodically dominated by a quartz rich clastic input. In both formations, however, the quartzitic metasediments may represent recrystallised mature sediments which were originally fine grained and may have formed either as distal continental marginal sediments or as the distal representatives of an accretionary wedge. No proximal sediment protoliths are seen in either formation.

The La Giralda Formation forms an extensive metasedimentary unit, consisting of intercalated beds of siltstones, arenites and silty mudstones interpreted as a turbiditic sequence. Layers of tuffaceous material occur throughout as narrow beds. The formation crops out on both sides of the Los Ciries Antiform although on the northern limb it displays considerably higher strain. The fine grained mature sediments and the absence of proximal deposits, as well as the occurrence of rare, often poorly preserved spores which yield a Givetian-Famennian age (Chapter 2), again suggests a distal provenance.

The Puerto Cañon Formation occurs both in the Alajar and the Aroche areas. It consists of variably deformed fine-medium grained greywackes that display low grade metamorphism. Lithologies include silty mudstones, light coloured siltstones and coarse grained arenites that have a significant volcanic component represented by lithic clasts composed of amphibole and plagioclase as well as polymetamorphic quartz grains and lithic clasts of silt. The composition of these coarser horizons, together with the association of fine grained silty mudstones suggests a more proximal setting than the La Giralda Formation although, coarse grained conglomerates are absent. A single sample, collected from a fine grained silty mudstone layer, yielded a spore assemblage ranging between Lower Givetian - Lower Famennian suggesting deposition contemporaneous with that of the La Giralda Formation.

Consideration of the palaeoenvironment of deposition has to account for the fine grained nature of all the sedimentary formations. The Cumbres de Los Ciries Formation now consists of recrystallised quartz and mica which suggests that it was originally a fine grained muddy deep basinal

deposit fed periodically from a quartzo-feldspathic source. Blocks of high grade exotic material on the northern border suggest that it must have been fed by material from the hangingwall rocks of the Beja-Acebuches Amphibolites and the Jabugo-Almonaster Zone.

The Puerto Cañon Formation and the La Giralda Formation are also fine grained deposits, although these have medium grained components and are less mature. Lithic and igneous clasts are present. No exotic material exists within these deposits and no proximal deposits, such as conglomerates, are present. If these sedimentary formations were deposited in a subduction related environment, trench fill deposits might be expected. However, the absence of proximal material suggests that deposition of the Cumbres de Los Ciries, La Giralda and Puerto Cañon formations may have occurred on a foreland basinal plain.

6.2.2 *The differing structural domains*

Five structurally distinct domains are identified (Chapter 3) which comprise the components of an imbricate thrust stack. The Aracena Metamorphic Domain is represented by strongly deformed high grade granulite rocks of the Jabugo-Almonaster Zone (Crespo-Blanc 1989). This is composed of metasediments and meta-igneous rocks which have been thrust southwards over the Beja-Acebuches Amphibolites, from which they are separated by a thin tectonic mélange that contains blocks of high grade material derived from the Jabugo-Almonaster Zone. In the Aroche area the tectonic mélange contains blocks of ultra-basic material and granulites. This layer of disruption may also have provided a pathway for syn-kinematic granitic intrusions which display a strong foliation and associated lineation. The Beja-Acebuches Amphibolites are internally disrupted and display a foliation and lineation (D_{A1}) which, on the northern border, is disrupted and reorientated. This fabric rapidly evolves southward to a steeply dipping NW-SE striking foliation which has an associated sub-horizontal mineral lineation (D_{A2}). Imposition of the D_{A1} foliation preceded the intrusion of syn-kinematic acid and basic dykes, observed at Puerto Cañon and this syn-kinematic phase of sinistral, non-coaxial deformation generated the D_{A2} fabric.

The Beja-Acebuches Amphibolites are thrust SW over the Northern Metasedimentary Domain which is composed of several formations that display features consistent with deformation at different structural levels. Both the Peramora Mélange Formation and the Cumbres de Los Ciries Formation were deformed in a ductile regime dominated by sinistral strike slip which resulted in an intense anisotropy and the transposition of several (?) earlier fabrics. A pre-D_{N2} fabric is not observed in the Peramora Mélange Formation, a feature that may relate to its proximity to the overriding Beja-Acebuches ophiolite. D_{N1}, however, is clearly seen in the Cumbres de Los Ciries Formation away from the contact with the Beja-Acebuches Amphibolites as an early fabric truncated by the later regional foliation. A mineral lineation is variably developed; within the immediate footwall of the Beja-Acebuches Amphibolites where the rocks of the Peramora Mélange Formation and Cumbres

de Los Ciries Formation are strongly welded it is defined by a subhorizontal mineral lineation composed of actinolite and plagioclase in the former. Andalusite and phyllosilicates define the mineral lineation in the latter. In the core of the Los Ciries Antiform the mineral lineation is observed only in the Peramora Mélange Formation lithologies where it defines a variable plunge, possibly a result of reorientation during D_{N3}.

The La Giralda and Puerto Cañon Formations of the Northern Metasedimentary Domain are also strongly deformed within a sinistral non-coaxial regime. Deformation in these formations ranges from ductile to brittle as represented by transposed schistosity and brittle boudinage of silty mudstone intercalations. Graded bedding is often visible and in places lacunae of less deformed material occur. Such features suggest that deformation progressed at relatively high structural levels within a similar tectonic regime as the structurally lower formations.

D_{N3}, in all formations within the Northern Metasedimentary Domain is represented by shortening normal to the regional strike which produced tight chevron folds and thrusts directed predominantly towards the SW.

The Alajar Domain has many similarities with the Northern Metasedimentary Domain. A phase of intense non-coaxial ductile deformation, resulted in a strong regional schistosity and formed the lens shaped discontinuous quartzites of the Sierra de Los Picos and narrow ductile thrusts that form an anastomosing network concordant with the regional foliation occur. As these thrusts have subsequently been folded they are assigned to D_2. The main foliation is of a similar trend as is seen along strike in the Aroche area and the deformation event is therefore correlated with the second phase of deformation seen in the Cumbres de Los Ciries Formation.

The Central Metasedimentary Domain is composed entirely of rocks of the La Giralda Formation and has also undergone three main phases of deformation. The first phase, giving rise to a complex pressure solution cleavage, may represent early folding associated with the initiation of deformation across the domain. The second phase, represented by thrusts and the imposition of a bedding parallel pressure solution cleavage, is the result of continued strike normal/oblique compression. The third phase resulted in folding of earlier thrust surfaces, formation of chevron folds and the imposition of a locally developed fold axial planar cleavage. Fold vergence is generally SW although upright folds and folds associated with back-thrusting are common. The southward dipping fold axial plane of the Los Ciries Antiform was formed at this time.

Lithologies within the Southern Metasedimentary Domain correspond to the remainder of the Cumbres de Los Ciries Formation to the north. The phyllosilicate rich schists were intensely deformed and imbricated, on their northern boundary, with rocks of the Central Metasedimentary Domain. In this domain quartzite ultramylonites and a strong regional schistosity suggest high to very high strains. Fold axial planes are consistently NW dipping and a rarely preserved down dip stretching lineation suggests movement normal to regional strike. There is a distinct anticlockwise rotation of

the strike of F_3 fold axial planes across the Oceanic Exotic Terrane (Fig. 3.16 and Fig. 6.3b) and this, together with the local occurrence of F_4 fold axial planes forming obliquely to F_3 axial planes is further evidence for sinistral transpression (Sanderson & Marchini 1984).

6.2.3 *Contrasting metamorphic histories.*

Each formation within the imbricated thrust stack described above also displays distinctive metamorphic features. At the northern extent of the study area the Aracena Metamorphic Complex is represented by the granulite to amphibolite facies para- and orthogneisses of the Jabugo-Almonaster Zone. This high grade block may be related to similar high grade strike-parallel mega-boudins recently identified to the north of the Aracena Massif and which extend from Spain to Portugal (Quesada *pers. comm.*). The rocks of the Jabugo-Almonaster Zone have therefore been buried to relatively deep structural levels but are now thrust over the amphibolite/greenschist facies rocks of the Beja-Acebuches Amphibolites. The boundary between these two units is represented by a tectonic mélange which incorporates blocks of the high grade material.

Within the Beja-Acebuches Amphibolites metamorphism decreases rapidly from amphibolite facies on the northern margin to greenschist facies on the southern margin where the amphibolites are thrust over rocks of the Northern Metasedimentary Domain. Retrogression of the amphibolite facies rocks accompanied sinistral ductile shear probably operative during southwestward directed thrusting.

The Peramora Mélange Formation and the Cumbres de Los Ciries Formation underwent prograde syn-kinematic metamorphism to upper greenschist/lower amphibolite facies. This accompanied imbrication between the two lithologies, a process that occurred after early metamorphism of the formations. An important episode of low pressure/high temperature metamorphism followed in the immediate footwall of the Beja-Acebuches Amphibolites. Here, syn-kinematic cordierite and andalusite formed during the development of a narrow inverted metamorphic sole beneath the ophiolite. Garnet also formed as a syn- to post-kinematic mineral phase. This inverted metamorphic sole is observed south of both Aroche and Alajar but is not observed along strike to the east, south of Aracena or to the west in Portugal.

Syn-D_1/D_2 metamorphism in the La Giralda and Puerto Cañon Formations is of low greenschist facies. It is manifest both by the growth of mica orientated along cleavage planes and by high vitrinite reflectance values and is consistent with syn-deformational metamorphism at high structural levels. Metamorphic minerals indicative of low P/high T metamorphism are absent in these formations. These rocks are therefore unaffected by the low P/high T tectonothermal event observed in the structurally underlying Peramora Mélange and Cumbres de Los Ciries Formations.

6.2.4 *Geochemistry of the Peramora Mélange and other formations.*

Geochemically rocks of the Peramora Mélange Formation are similar to the Beja-Acebuches Amphibolites. Both blocks and matrix of the former give a signature that is consistent with MORB-type metabasalts. Only rocks of the mélange with a blue-green matrix were analysed and these suggest derivation from a basic provenance. As these mélanges occur in the footwall of the Beja-Acebuches Amphibolites, often juxtaposed in immediate tectonic contact, they are most simply interpreted as being derived from the overriding ophiolite either as volcaniclastic debris or as blocks released during imbrication and accretion accompanying underthrusting.

The Cumbres de Los Ciries Formation and the La Giralda Formation are more problematic than the metabasites as they display no definitive signature. However, averages of trace elements for these formations compare closely with averages obtained from the Geissen and Gramscatho greywackes that outcrop along strike around the Hercynian Arc (Floyd *et al. in press*) and suggest they may be derived from a Continental Arc/Active Margin. High Cr, Ni and V values from the La Giralda Formation suggest a basic input and the most likely source for this is the emerging ophiolite to the north.

6.2.5 *Critical features of the Oceanic Exotic Terrane: a summary.*

- A footwall tectono-sedimentary mélange (the Peramora Mélange Formation) principally composed of amphibolite blocks within a basic matrix that has been regionally metamorphosed prograde to upper greenschist/lower amphibolite facies. Basic blocks are geochemically similar to the Beja-Acebuches Amphibolites.

- A quartz-mica schist formation (the Cumbres de Los Ciries Formation) which contains rare exotic phacoids and has been metamorphosed prograde to upper greenschist facies.

- Distal sedimentary associations represented by the La Giralda Formation and the Cumbres de Los Ciries Formation. Proximal sediments are represented solely by the Peramora Mélange Formation.

- Exotic clasts in the matrix of the Alajar Formation. These include a block of serpentinite and blocks of marble. The latter may have sourced in the hangingwall marbles of the Ossa Morena Zone while no apparent source exists for the serpentinites.

- Granulite facies rocks, including wollastonite bearing marbles, occur within the hangingwall Aracena Metamorphic Complex. These are separated from the Beja-Acebuches Amphibolites by a tectonic mélange composed of blocks of high grade metamorphic material.

- Retrogressive greenschist facies metamorphism within the Beja-Acebuches Amphibolites occurred synchronously with prograde greenschist facies metamorphism in the footwall sedimentary units.

- An inverted low pressure/high temperature metamorphic sole is observed beneath the Beja-

Acebuches Amphibolites that is syn-sinistral ductile shear.

- Imbrication of formations of different metamorphic grade that were metamorphosed prior to imbrication.

- Anticlockwise rotation of F_3 fold axial planes towards the south.

- Age ranges of late Givetain to early Frasnian from the La Giralda and Puerto Cañon Formations on both northern and southern limbs of the Los Ciries Antiform.

6.3 The Iberian Pyrite Belt.

Consideration of the tectonic evolution of the Pyrite Belt is pertinent to any geotectonic reconstruction for the collision between the South Portuguese Zone and the Ossa Morena Zone. Existing models for its generation range from those that maintain that the South Portuguese Zone is an accretionary prism related to a northerly dipping subduction zone beneath the Ossa Morena Zone (Bard 1971, Carvalho 1972, Vegas & Muñoz 1976, Bard *et al.* 1973, 1979) to an oblique-slip mobile belt (Badham 1982, Badham & Halls 1975; Andrews *in press*). The most recent interpretation is given by Silva *et al.* (*in press*) who invoke a transpressive mechanism. This latter model is based on the following observations: (a) a late Devonian/early Carboniferous extensional phase with associated bi-modal volcanics and volcanogenic mineralisation, and (b) subsequent left lateral transpressive shortening causing basin infill (Culm-type deposits) and producing one penetrative cleavage associated with southwesterly verging open to tight folds. The sedimentary units of the Oceanic Exotic Terrane are thrust southwards over the Upper Devonian and Carboniferous rocks of the Iberian Pyrite Belt which has suffered a less complicated structural and metamorphic history. This model agrees broadly with the model presented below.

6.4 Models for tectonostratigraphic evolution in southern Iberia.

Andrews *et al.* 1990 propose several models for terrane amalgamation within the constraints outlined above.

1. Subduction of an ocean between the Ossa Morena Zone and the South Portuguese Zone during Lower Carboniferous continent/continent collision.

2. Extensional generation of an ocean basin between the Ossa Morena Zone and the South Portuguese Zone followed by late Devonian tectonic inversion and oblique collision with the concomitant obduction of the still hot Beja-Acebuches Amphibolites over the Middle-Upper Devonian, syn-rift sediments of the Oceanic Exotic Terrane. Obduction of the hot amphibolites produced an inverted metamorphic aureole. Sinistral transpressive collision evolved to transtension accompanied by crustal thinning and production of the bi-modal volcanics of the Pyrite Belt. The final phase was a renewal of shortening and the production of folds and thrusts.

3. Early Devonian generation of a small ocean basin within the Ossa Morena Zone followed

by oblique collision and obduction of the hot ophiolite over the sediments of the southern margin of the Ossa Morena Zone. The sediments of the Oceanic Exotic Terrane were deposited in a foreland basin in front of the advancing thrust nappe, being overridden, metamorphosed and deformed. Subsequent crustal thinning resulted in the generation of the Pyrite Belt volcanics and this was followed by renewed shortening in the Upper Carboniferous.

The first model infers that the Oceanic Exotic Terrane represents an accretionary prism deposited outboard of the Ossa Morena Zone. It suggests that the first two phases of deformation and metamorphism are subduction related while the third is related to collisional shortening. The Beja-Acebuches Amphibolites would thus represent fragments of ocean crust obducted during collision.

The second model suggests that the Oceanic Exotic Terrane sediments were deposited over the oceanic crust of the Beja-Acebuches Amphibolites and during subsequent continent-continent collision were underthrust and accreted to the obducting ophiolite. Migration of the deformation front resulted in, (a) transpression, corresponding to deformation phases D_1 and D_2 and, (b) transtension thus providing a mechanism for the generation of the Pyrite Belt volcanics. Tectonic inversion resulted in the third phase of deformation, normal to the continental margin.

The third model provides a mechanism for the generation of a sedimentary/tectonic mélange in front of the advancing thrust sheet of the Beja-Acebuches Amphibolites. It also accounts for the presence, within the mélange, of high grade material from the Ossa Morena Zone. Combined with transpression/transtension this model may also explain the different phases of deformation and the generation of the Pyrite Belt.

6.4.1 A model for the Ocean Exotic Terrane.

In the model presented below the tectono-stratigraphic units are interpreted in terms of a foreland basin setting. The Cumbres de Los Ciries Formation and the La Giralda Formation are distal representatives of foreland basin deposits while the Peramora Mélange Formation is considered to have accumulated closer to a thrust stack uplifting to the north. This interpretation allows for the fine grained nature of some of the formations identified and the presence of large exotic blocks in the Cumbres de Los Ciries Formation and Peramora Mélange Formation.

The model assumes that a small ocean basin opened to the north of the present day Aracena Massif, within the southern margin of the Ossa Morena Zone (Fig. 6.2, inset 1). Collision accompanied by subduction ensued with the subduction zone dipping northwards beneath the Ossa Morena Zone. Initial thrusting of the ocean crust may have occurred at the ocean ridge, as the model necessitates that hot ocean crust was obducted southwards onto the platformal sediments of the Ossa Morena Zone (Fig. 6.2A).

Obduction of the ophiolite onto Ossa Morena platformal sediments resulted in an inverted

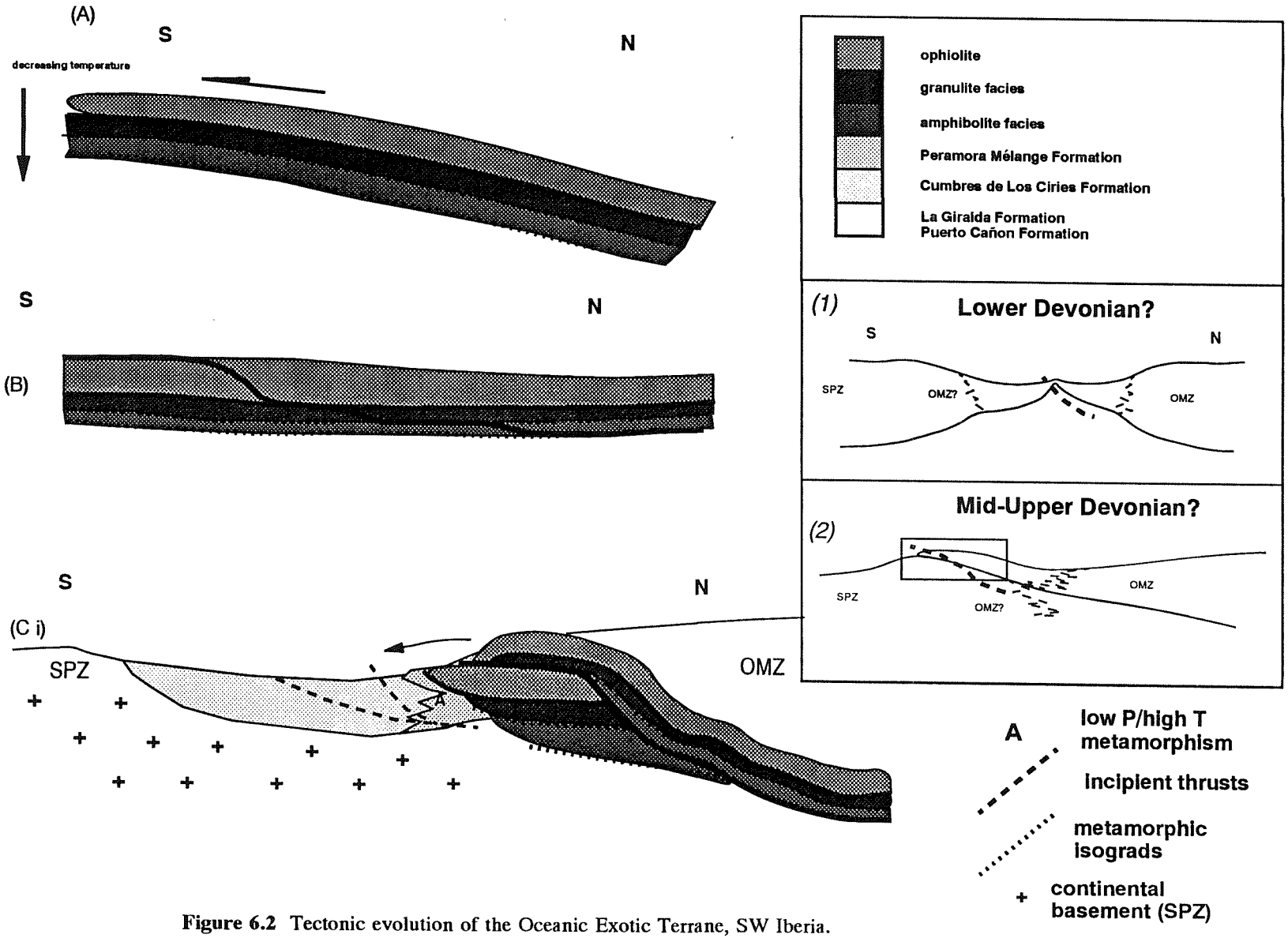

Figure 6.2 Tectonic evolution of the Oceanic Exotic Terrane, SW Iberia.

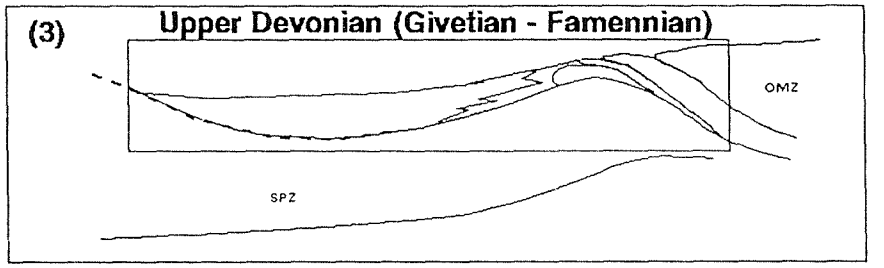
(3)
Upper Devonian (Givetian - Famennian)
OMZ
SPZ

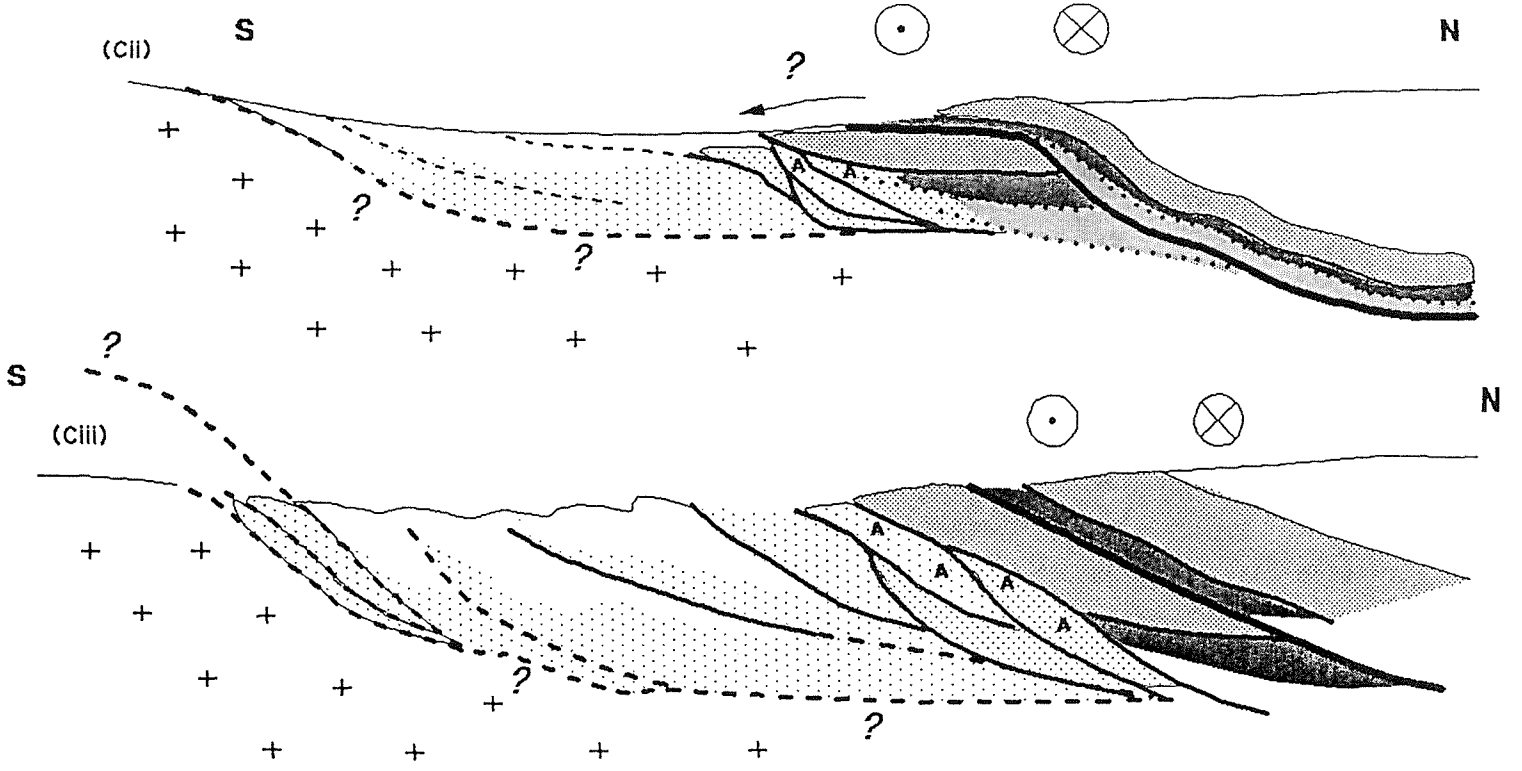
(Cii)
S
N
?
?
?
?
A
A
S
N
?
(Ciii)
A
A
A
A
?
?

metamorphic sole beneath the ophiolite (Fig. 6.A and inset 2). The temperature of the ocean crust must have been high which, together with possible frictional heating accompanying obduction, resulted in a granulite facies sole immediately beneath the ophiolite giving way to an amphibolite facies layer beneath. The ocean crust may itself have been recrystallised over amphibolite facies conditions during on-ridge metamorphism and/or the obduction process.

Continued compression and closure of the ocean basin in the hinterland resulted in the creation of a basal thrust below the metamorphic sole as the original thrust locked up. The new surface (Fig. 6.2B and inset 2) propagated through the amphibolite and granulite facies rocks and, as an out-of-sequence thrust, through the ophiolite itself resulting in piggy-back thrusting taking the ophiolite, together with the underlying granulite facies metasediments were thrust over a fragment of oceanic material. The thickened thrust stack (Fig. 6.2Ci) created downwarping of the underlying crust of the Ossa Morena Zone (?South Portuguese Zone) and created a foreland basin above continental basement (Fig. 6.2Ci). At this stage the ophiolite and the granulite facies metasediments of the Jabugo-Almonaster Zone may have become emergent.

Deposition of the Cumbres de Los Ciries Formation occurred within the foreland basin as distal deposits while the Peramora Mélange Formation was deposited by mass wastage from the ophiolite. The mature quartzites seen in the Alajar Formation may be the result of a periodic influx of quartz-rich sediments from the Ossa Morena Zone.

Oblique shortening continued, and both the Cumbres de Los Ciries Formation and the Peramora Mélange Formation were overridden by the advancing thrust stack, which retained residual heat. This resulted in the low pressure/high temperature, mid-upper greenschist facies metamorphism of the Northern Metasedimentary Domain immediately juxtaposed against the Beja-Acebuches Amphibolites ophiolite and, at a later stage, the syn-kinematic growth of andalusite and cordierite porphyroblasts. The presence of sector trilling in the cordierite porphyroblasts may indicate that these was a period of little active deformation prior to the recommencement of ductile deformation. The presence of exotic clasts, including marbles, within the matrix of the Cumbres de Los Ciries Formation and the Peramora Mélange Formation indicates that supply was from the immediate hangingwall rocks of the Peramora Mélange Formation and the Jabugo-Almonaster Zone.

Oblique shortening continued with the Beja-Acebuches Amphibolites and the granulites overriding the sediments of the Oceanic Exotic Terrane foreland basin. The La Giralda Formation and the Puerto Cañón sedimentary formations may have been deposited unconformably over the Cumbres de Los Ciries and Peramora Mélange Formations and these two former formations were caught up in the compressional cycle. Spores retrieved from samples of both the La Giralda and Puerto Cañón Formations suggests that deposition occurred during the Upper Givetian to Upper Famennian (Fig. 6.2Cii). The source of the sediments of the La Giralda Formation and Puerto Cañón Formation probably included the Beja-Acebuches Amphibolites as they contain a basic volcanic component. The

volcanic component. The very different nature of the La Giralda and Puerto Cañon Formations (structure, lithology and metamorphism) from the Cumbres de Los Ciries and Peramora Mélange Formations, might suggest (a) that these formations occupied higher structural levels and are therefore younger and, (b) that supply was from a variety of sources (either along stike or from the south). The absence of proximal deposits such as conglomerates can possibly be explained in this scenario as having been underthrust beneath the ophiolite.

Further shortening resulted in the imbrication of all the formations (Fig. 6.2Ciii). Imbrication and intense deformation occurred at the southern end of the Oceanic Exotic Terrane and this may correspond to the end of regional D_2 (Fig. 6.2Ciii). The stages represented in Fig. 6.2Ci, ii and iii may correspond to deformation events D_1 and D_2. At this time the Peramora Mélange Formation and the Cumbres de Los Ciries Formation were probably subject to middle to upper greenschist facies metamorphism with temperatures between 500- 600°C and pressures of 2 - 3kb (Chapter 5).

After this event basin inversion and extension within the Pyrite Belt gave rise to a bimodal volcanic association within a transtensile regime (de Graciausky *et al.* 1989, Butler 1989, Silva *et al in press*; Oliveira *in press*). Renewed compression during the Upper Carboniferous produced open to tight folds, folded thrust surfaces and backthrusting corresponding to D_3 in the Oceanic Exotic Terrane. The Los Ciries Antiform formed above such a blind backthrust (Dunne & Ferrill 1988); its fold axial plane dips in the opposite sense to the general direction of structural vergence. A component of sinistral strike-slip resulted in an anticlockwise rotation of the fold axial planes towards the SW and the local production of D_4 fold axes orientated clockwise of the regional strike.

Tectonic zones, such as is observed in the Oceanic Exotic Terrane, often occur at more than one scale and, although a regional strike-slip system may be operative, locally extensional or compressional tectonics may dominate (Reading 1980, 1986). Strike-slip displacements may mean that the present juxtaposition of units is far removed from their original pre- and syn-subduction relative positions. The model presented above requires that the Beja-Acebuches Amphibolites to the north of the Jabugo-Almonaster zone were removed during subsequent events. This may have been during strike-slip as the margin evolved, with the oceanic rocks to the north of the Oceanic Exotic Terrane being transported a considerable distance along strike or being further uplifted and removed by erosion. It may also have been faulted away during the extensional phase that resulted in the Pyrite Belt.

A change in the geochemistry of the Beja-Acebuches Amphibolites, from island arc in Portugal to MORB in the Acebuches area, may be explained by invoking an island-arc tectonic environment close to a destructive margin (Munha *et al.* 1986; Munha *et al.* 1989). An unstable migrating triple junction may account for different geochemical signatures in different parts of the belt, as well as the creation of an ocean crust that retained enough heat to produce a metamorphic sole upon obduction over basinal sediments.

This type of ridge-transform-transform triple junction may account for the local development of tectonic mélanges (Saleeby 1984, Hsü 1974) and may provide an alternative model for the generation of the Peramora Mélange Formation. Saleeby (1984), considers that 'ophiolitic mélange' may be generated as a primary deposit at a fracture zone possibly having formed along a transform junction between crustal blocks. Often mélange such as this forms as a structural response to small variations in the pole of relative motion between plates (Vogt *et al.* 1971). Fragments of ocean crust are obducted onto oceanic sediments producing imbricate slabs, mélanges and dynamothermal aureoles along thrust soles. Hot soles result if young ocean crust is obducted onto the overlying sediments. Serpentinite blocks are considered to represent vestiges of primary mantle sequences imbricated on the sea floor soon after formation eg. those associated with the Semail Ophiolite (Coleman 1981). In this latter example initial imbrication is not considered to represent a collisional suture. Thus ocean floor imbrication, mélange formation and basal metamorphism may occur on the ocean floor and the whole assemblage may be obducted at a later stage. In the context of SW Iberia however, this model fails to account for the incorporation of high grade metamorphic material within the mélange.

6.5 The Oman Ophiolite.

This example is used as an analogue for the Beja-Acebuches Amphibolites as there are many similarities between the two areas, as will be highlighted later. In Oman the ophiolite succession is better preserved than the Beja-Acebuches ophiolite of SW Iberia. The Semail ophiolite is more than 10km thick and includes mantle peridotites, high level gabbros, sheeted dyke complex, pillow lavas marine sediments (Searle & Malpas 1980, Pearce *et al.* 1981, Gass *et al.* 1984; Lippard *et al.* 1986) and comprises a well preserved sequence that may be analogous to the Beja-Acebuches Amphibolites. Similarities between the two areas include imbricated and folded allochthonous units beneath the ophiolite, mélange (both tectonic and sedimentary), and a basal metamorphic sheet (Fig. 6.5). Radiometric dates from amphiboles and biotites suggest that the ocean crust was formed less than 20 Ma before obduction (Searle & Malpas 1980, Lanphere 1981). Pearce *et al.* (1981) interpret the ophiolite as the remnant of a back-arc basin created and obducted within a relatively short time span during the Cretaceous.

One of the units identified, the Haybi Complex, is composed of a series of imbricated rocks which include an Upper Cretaceous sedimentary mélange. This consists of a series of olistostromes with volcanic and continental margin sedimentary blocks within an intensely sheared red mudstone - shale matrix. The mélange is overlain by a volcanic-limestone association interpreted as a series of ocean islands.

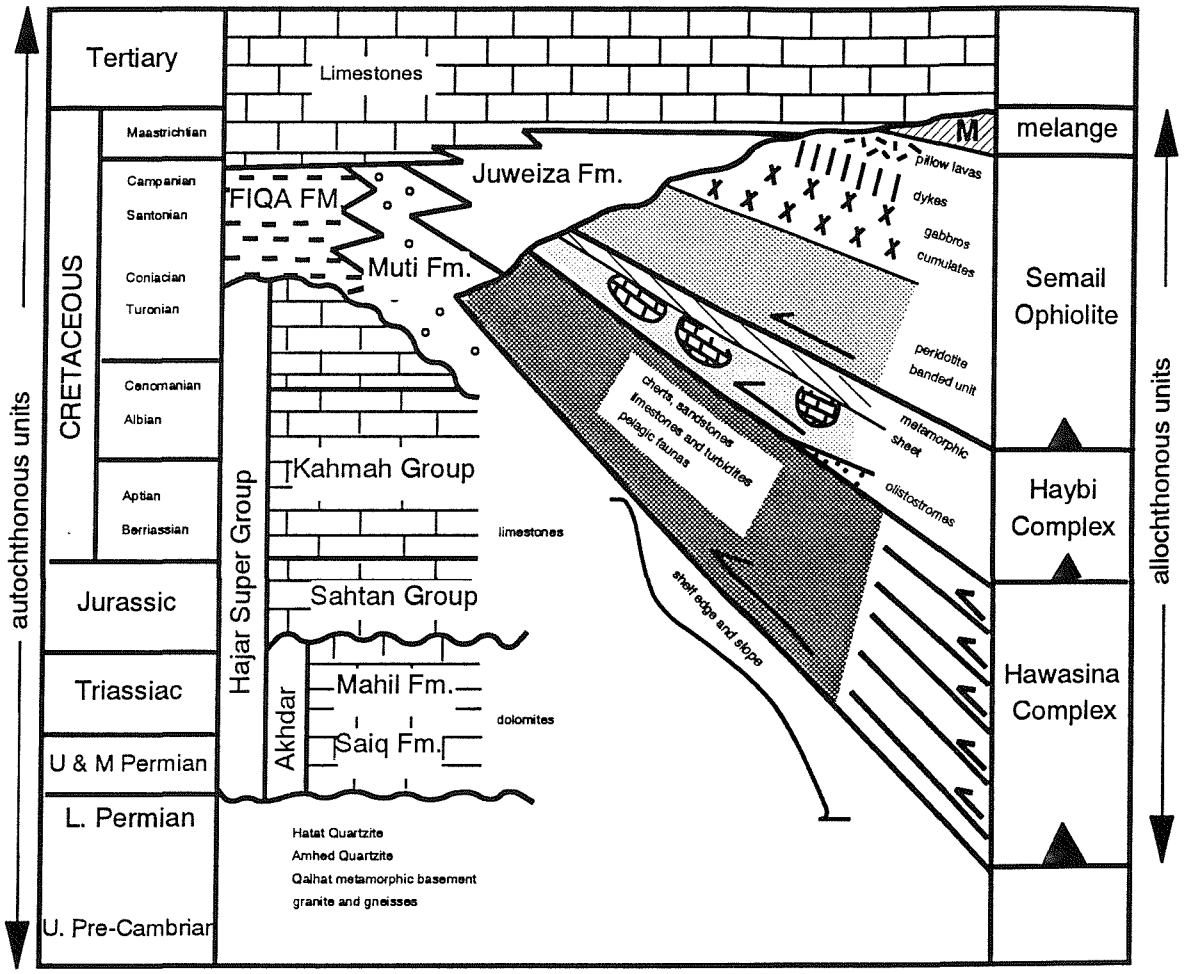

Figure 6.3 Stratigraphy and schematic cross section of the Semail Ophiolite, Oman (from Searle *et al.* 1980, Pearce *et al.* 1981)

Beneath the ophiolite itself are metamorphic rocks that are interpreted as representing a 'dynamothermal aureole'(Searle & Malpas 1980, Searle 1989). There are several similarities between this metamorphic sheet and the metamorphic sheet observed beneath the Beja-Acebuches Amphibolites:

1. the metamorphic rocks occupy a constant stratigraphic position at the base of the ophiolite.
2. there is a decreasing metamorphic grade beneath the ultrabasic material.
3. these metamorphic complexes generally have a narrow width which suggests a high thermal gradient.
4. deformation/metamorphism fabrics are similar within both the ophiolite and the basal metamorphic rocks.
5. imbrication and intense deformation of the metamorphic rocks results in a zone of repeated units and tectonic thickening.
6. mineral assemblages are consistent with high temperature rather than high pressure.
7. geochemistry suggests that the protolith was a tholeiitic volcanic rock, although a sedimentary or tuffaceous origin for some thin amphibolite bands may also be a possibility.

The metamorphic unit below the Semail ophiolite is composed of several lithotypes including banded amphibolites and is characterised by an S_2 transposed schistosity, while intercalated marbles and quartzites indicate a possible sedimentary origin for these rocks. Structurally beneath the amphibolites are greenschist facies metasediments that demonstrate features consistent with intense polyphase deformation. Some of the greenschist facies rocks are clearly sedimentary in origin as metapelites and actinolite-epidote schists are often interbanded with quartzites and marbles.

A possible heat source for the metamorphic aureole is the hot overriding ophiolite slab with heat enhancement by limited frictional heating associated with obduction (Searle 1989). Two alternative environments of generation are considered (Searle & Malpas 1980): the first, at or close to a spreading ridge or the second, within a marginal basin where high heat flow existed represented by igneous activity above a subduction zone. Such igneous rocks are interpreted as incipient island-arc volcanics that belonged to a Pacific-type arc-basin complex (Pearce *et al.* 1981).

Models for obduction of the Oman Ophiolite are structurally constrained by the differences in deformation seen above and below the Semail thrust which separates the Haybi Complex from the Semail Ophiolite, and involves processes of underthrusting of a continental margin beneath a back-arc basin together with accretion of imbricate thrust slices on to the base of the ophiolite. A gravitational model for emplacement is favoured (Coleman 1981, Searle and Malpas 1982, Lippard *et al.* 1984) on the basis of several field observations:

- The ophiolite is relatively intact with compressional features generally absent.
- The long thin nature of the ophiolite suggests movement by gravity down a regional surface slope.

- A thin basal sheet of serpentinite facilitates movement by providing a zone of low friction along which the ophiolite could move.

The geotectonic evolution of the Semail ophiolite therefore has many features in common with the model proposed here for the Beja-Acebuches Amphibolites and processes similar to those seen in Oman may have been operative in Iberia during Palaeozoic times. Important differences that exist between these two areas are (a) the Beja-Acebuches Amphibolites have been subjected to greater amounts of deformation which has obliterated ophiolite stratigraphy, (b) high grade rocks of the Jabugo-Almonaster Zone exist in the hangingwall while no such high grade rocks are recorded in Oman, and (c) strong sinistral transpression is observed in the SW Iberian Peninsula, a feature that is absent in Oman.

The evidence presented in this thesis supports existing hypothesis for creation and destruction of a small ocean basin that formed at the southern margin of the Ossa Morena Zone during the Middle-Upper Devonian (Munha *et al.* 1986, 1989, Oliveira *in press*, Silva *et al. in press*). Tectonostratigraphic evolution of the SW Iberian Peninsula was dominated by sinistral transpression resulting in the development of local areas of transtension and transpression and a migrating deformation front with ocean creation and subduction occurring towards the west. The length of the belt, which extends from the north of Sevilla to the Portuguese coast may indicate the presence of several rather than one sedimentary basin. Analogues for the types of sedimentary environment that may have existed within the Devonian Oceanic Exotic Terrane include the Semail Ophiolite of Oman.

Whilst allowing for subduction and metamorphism the models presented in section 6.4 also highlight that similar processes may have been operative in different areas connected around the Ibero-Armorican Arc. The geological evolution of both the southwestern Iberian Peninsula and the southwest of England displays many parallels (Barnes 1982, 1983, 1984; Barnes & Andrews 1982, 1984; Wilkinson & Knight 1989; Eden & Andrews 1990; Andrews *et al.* 1990). These include (a) observations that structural relationships between the dismembered ophiolites (Beja-Acebuches Amphibolites and the Lizard Complex) and the footwall sedimentary units are the same, (b) the fact that palynological ages obtained from the footwall basinal sediments is found to be Middle-Upper Devonian in both cases, (c) isotopic dates from the Lizard Complex suggest generation in the Middle-Upper Devonian. Obduction in both cases probably occurred in the Lower Carboniferous soon after generation, (d) an extensional phase (Pyrite Belt) and a late regional phase of shortening are recognised in both areas.

6.6 Summary.

1. The Beja-Acebuches Amphibolites represent a dismembered ophiolite and mark an important geosuture between the Iberian Terrane and the South Portuguese Terrane. This conclusion is supported by:

(a) A zone of ductile deformation (the South Iberian Shear Zone), marked by the development of mylonites and accompanied by a strong foliation and lineation.

(b) Identification of an oceanic mélange (the Peramora Mélange Formation) that exists in the footwall of the Beja-Acebuches Amphibolites.

(c) Granulite grade rocks of the Jabugo-Almonaster Zone within the hangingwall of the Ossa Morena zone which are separated from the Beja-Acebuches Amphibolites by a narrow horizon of tectonic mélanges composed of high grade blocks.

(d) The geochemistry of the amphibolites and the mélange. This correlates closely with MORB. The mélange may represent basic volcaniclastic material that was shed into a basin in front of the emergent ophiolite. It is composed of a recrystallised matrix with blocks and phacoids of amphibolitic material. One locality exposes sheeted igneous metabasalts and gabbros which represent a raft of sheeted dyke complex introduced into the deforming matrix.

(e) The metasediments of the Cumbres de Los Ciries Formation, which are structurally imbricated with the Peramora Mélange Formation, are composed of intensely sheared quartz-mica schists that may originally have been fine grained deep water muds. Within this formation are blocks of basic material and exotic serpentinites and marbles. The latter blocks may be derived from the high grade rocks of the Ossa Morena Zone in the hangingwall.

(f) The La Giralda Formation and the Puerto Cañón Formation, which are deep marine turbidites that accumulated in elongate basin(s) parallel to strike on the southern margin of the Beja-Acebuches Amphibolites.

2. Ophiolite obduction was accompanied by local (?) generation of an oceanic mélange. Facies changes within this mélange were rapid; south of Aroche facies range from chaotic blocks of amphibolite to blocks of metasediment, all contained within a fine grained recrystallised matrix. South of Alajar blocks and phacoids of serpentinite, marble and quartzite are contained within a fine grained recrystallised matrix of quartz-mica schists that resembles the matrix of the Cumbres de Los Ciries Formation along strike.

3. Several metasedimentary formations were imbricated together within a folded thrust stack. Each formation displays distinct structural and metamorphic characteristics suggesting deformation and metamorphism at different structural levels. These were juxtaposed during obduction of the Beja-Acebuches Amphibolites and/or subsequent late Carboniferous collision.

4. All contacts between formations are tectonic, with imbricated wedges of different lithologies causing considerable stratigraphic repetition. The contact between the Southern Metasedimentary Domain and the Central Metasedimentary Domain is marked by quartzite ultramylonites

and imbrication between arenites and silty mudstones of the Central Metasedimentary Domain and quartz-mica schists of the Southern Metasedimentary Domain.

5. Petrography, microstructural analysis, geobarometry and vitrinite reflectance studies indicate that each formation within the thrust nappe experienced different grades of metamorphism. The Beja-Acebuches Amphibolites suffered high grades of metamorphism on the northern boundary with the Ossa Morena Zone but this was retrogressed to middle-upper greenschist facies during shearing. The Peramora Mélange Formation experienced upper greenschist to lower amphibolite facies while the imbricated Cumbres de Los Ciries Formation may have experienced slightly lower grades of metamorphism. Vitrinite reflectance studies of spores and woody material from the La Giralda Formation show that it may have been taken to lower greenschist facies.

6. There is a thin sheet of low pressure/high temperature metamorphic rocks beneath the Beja-Acebuches Amphibolites which is observed to the south of Aroche and Alajar. This may be related to the emplacement of still hot oceanic material. High temperature/low pressure metamorphism affected all facies of the mélange formation and the Cumbres de Los Ciries Formation but is only recognised by mineral changes in the phyllosilicate rich facies. Syn-deformation metamorphic minerals include cordierite, andalusite and garnet.

7. Spores extracted from samples collected from both the La Giralda Formation and the Puerto Cañón Formation range in age between Upper Givetian and Lower Famennian. These compare with ages obtained further along strike, south of Almonaster la Réal (Giese *et al.* 1988) which come from rocks that correlate with the Santa Iria of Oliveira *et al.* (1986) and thus with rocks of the Puerto Cañón Formation.

8. The Alajar Formation exhibits similar structural and lithological features as the Cumbres de Los Ciries Formation. Large phacoids of pure quartzites represent dismembered beds of sandy material. Exotic phacoids, including a block of serpentinite and isolated marbles are found within the fine grained recrystallised matrix.

9. The Northern and Southern Metasedimentary Domains are characterised by intense polydeformation which has resulted in the imposition of a strong regional schistosity and a well developed mineral lineation. In contrast the Central Metasedimentary Domain has been strongly thrusted and folded but many original sedimentary features are retained suggesting that deformation occurred in this domain at higher structural levels. Three main phases of deformation are recognised throughout the region, although correlation across the tectonic boundaries is limited.

10. There is a significant rotation of structural elements towards the south with fold axial surfaces rotating anticlockwise. In the Beja-Acebuches Amphibolites Domain and the Northern Metasedimentary Domain the mineral stretching lineation is sub-horizontal whereas in the Southern Metasedimentary Domain a rarely preserved down dip stretching lineation is observed.

11. A model for the deposition of the sedimentary formations within a foreland basin setting is proposed. The Peramora Mélange Formation represents a chaotic deposit that accumulated at the front of the advancing thrust sheet of the Beja-Acebuches amphibolites while the Cumbres de Los Ciries Formation represents the distal deposit. Both formations were overthrust by the ophiolite with the concommitant imposition of a dynamothermal aureole. The metasediments of the La Giralda Formation and the Puerto Cañón Formation were also deposited within a foreland basin. Extension in the Pyrite Belt during the Lower Carboniferous was followed by compression in the Late Carboniferous giving rise to the third phase of deformation observed across the region.

6.7 Suggestions for further research.

Mulitidisciplinary research has highlighted a need to explore further several avenues of investigation:

6.7.1 *Lithological and sedimentological analysis*

The provenance of the sediments located within the Oceanic Exotic Terrane remains an important issue. Did the sediments accumulate in a series of sedimentary basins that formed along the southern margin of the Beja-Acebuches Amphibolites, or were they deposited in a single elongate basin? Sedimentary geochemistry may facilitate interpretation if samples from various localities are collected and analysed. Possible source areas could be sampled and compared with fresh samples of sedimentary rocks found in the depocentres. Such a study should include sedimentary petrography, however, the fine grained nature and maturity of the metasediments may complicate this latter technique. Sediments may originally have been transported from the west so sources in Portugal may provide suitable sites. Alternatively sources may have been transported west by sinistral strike-slip.

Isotope geochemistry and rare earth elements, in particular the immobile elements Sm and Nd may provide further information about provenance. However, as the Beja-Aracena metamorphic belt represents a deeply incised orogen that has experienced considerable strike-slip mobility, the source area may have been removed. Although the sediments are very mature they contain a rich population of zircons. Microprobe analysis of zircons from possible source areas and known sink areas may result in characterisation of a source. These results can be supplemented by radiometric dating of zircons to date the age of their crystallisation in the parent magma.

6.7.2 *Dating*

There remains a need for further, more systematic work in this area. Limited sampling both to the south of Aroche (Lake, in this study) and to the south of Almonaster la Réal (Giese *et al.* 1988) has demonstrated that there are abundant spores within the sediments. Dating of the sediments of the Cumbres de Los Ciries Formation (Pulo do Lobo Formation) would provide a constraint for the onset of sedimentation associated with oceanic obduction. Attempts thus far have yielded negative results both in Spain and in Portugal.

Absolute dating of the igneous rocks from the study area is, as yet, also poorly constrained. The latest results indicate a $^{40}Ar/^{39}Ar$ age for the Beja-Acebuches Amphibolites of ≈340 Ma (Quesada & Dallmeyer 1990) although the significance of this date is still open to debate. Dating of the Gil Marquez granite, which is recognised as a syn-to post tectonic intrusion (Crespo-Blanc 1989), may give an age for the cessation of deformation along the South Iberian Shear Zone.

6.7.3 *Metamorphism studies*

Analysis of the metamorphic components would quantitatively constrain a P-T-t path for each unit involved in terrane amalgamation and also begin to identify reactions associated with retrogression of mineral phases. Microprobe analysis of each mineral phase from the separate formations would provide a data base for quantitative analysis of temperatures and further constrain P-T conditions by providing data for geobarometry and geothermometry. Fluid inclusion analysis of inclusions from the various generations of quartz veins that cross cut each deformational fabric may also provide a more accurate estimate of pressure during tectonic evolution. Coupled with crush-leach studies of the fluids within the fluid inclusions this may provide an insight into fluid evolution associated with this major shear zone.

Further vitrinite reflectance, illite crystallinity and b_0 studies of the metasediments of the La Giralda and Puerto Cañón Formations on either side of the Los Ciries Antiform may also provide further constraints on metamorphic evolution. Do these values change significantly away from the suture zone and if so is there a consistent relationship?

6.7.4 *Structural studies*

Sinistral transpression was of considerable importance during terrane amalgamation. Further structural studies may lead to quantification of strain across the belt. Analysis of folds and thrusts may allow quantification of the final increments of strike normal shortening. Further microstructural studies, coupled with fluid inclusion studies, may provide additional constraints on structural levels of deformation of each unit involved. The structure of the Central Metasedimentary Domain in particular is important in any analysis of the effects of transpression and terrane amalgamation, as the domain is dominated by brittle/ductile features.

References:

ANDREWS, J.R., *in press.* The Iberian Pyrite Belt. An oblique-slip mobile belt. *Note and mem. Serv. Marroco.* **335.**

ANDREWS, J.R., CRESPO-BLANC, A., EDEN, C.P., LAKE, P.A., & OROZCO, M. 1990. The South Portuguese/Ossa Morena Zone terrane boundary and the evolution of the Ibero-Armorican Arc. *Abstract in: Terranes in the Circum-Atlantic Palaeozoic Orogens. Conference on Palaeozoic Orogens in Central Europe.* International Correlation Programme 233, Göttingen-Geissen 1990.

AOKI, K. 1984. Measurement of fluorescence spectra as a new technique for study of sedimentary zircons. *Journal of the Geological Society of Japan,* **90**, 659-662.

AOKI, K., LORENC, S., ZIMMERLE, W. 1987. Fluorescence spectra of volcanogenic zircon from a Miocene kaolin claystone in the Belchatow opencast lignite mine, SW Lódź (P.R. Poland). *N. Jb. Geol. Palaont. Mh.* 267-273.

APALATEGUI, O., BARRANCO, E., CONTRERAS, F., ROLDÁN, F.J. 1983. Mapa Geologico 1:50 000, Hoja Aroche 916. Serv. Publ. Minist. Industria y Energia, Madrid.

APALATEGUI, O., BARRANCO, E., CONTRERAS, F., DELGADO, M., ROLDÁN, F.J. 1983. Mapa Geologico 1:50 000, Hoja Aracena 917. Serv. Publ. Minist. Industria y Energia, Madrid.

APALATEGUI, O., EGUILEZ, L., QUESADA, C. *in press.* Ossa Morena Zone - Structure. in Dallmeyer, R.D., & Lecorché, J.P. (eds) Pre-Mesozoic Geology of Iberia. *Hercynia Special Issue.*

ARNOTT, R.J. 1983. Sedimentology of Upper Ordovician - Silurian sequences on New World Island, Newfoundland: separate fault-controlled basins? *Canadian Journal of Earth Sciences,* **20**, 345-354.

ARNOTT, R.J., M^{c}KERROW, W.S. & COCKS, L.R.M. 1985. The tectonics and depositional history of the Ordovician and Silurian rocks of Notre Dame Bay, Newfoundland. *Canadian Journal of Earth Sciences,* **22**, 607-618.

BADHAM, J.P.N. 1982. Strike-slip orogens; an explanation for the Hercynides. *Journal of the Geological Society of London,* **139**, 493-504.

BADHAM, J.N.P., & HALLS, C. 1975. Microplate tectonics, oblique collision and the evolution of the Hercynian orogenic systems. *Geology,* **3**, 373-376.

BARD, J.P. 1964. Note préliminaire sur l'age des terrains de l'Estrado cristalino affleurant au Nord - Ouest de la Province de Huelva (Espagne). *C.R. Acad. Sc. Paris* **t.258**, 2129-2130.

BARD, J.P. 1969. Le Metamorphisme Regional Progressif des Sierras d'Aracena en Andalousie Occidentale (Espagne). Sa Place Dans le Segment Hercynien Sub-Iberique. *thèse doctoral, Universite de Montpelier.*

BARD, J.P. 1970. Composition of hornblendes formed during the Hercynian progressive metamorphism of the Aracena metamorphic belt (South West Spain). *Contributions to Mineralogy and Petrology,* **28**, 117-134.

BARD, J.P. 1971. Sur l'alternance des zones metamorphiques et granitiques dans le segment sud -iberique. *Bol. Geol. Min. (Madrid),* **82**, (3/4) 324-345.

BARD, J.P. 1977. Significance tectonique des metatholeiites d'affinité abyssale de la ceinture metamorphique de basse pression d'Aracena (Huelva, Espagne). *Bulletin de la Societé Geologique de France,* **7**, t. **XIX, 2** 385-393.

BARD, J.P., CAPDEVILA, R., MATTE, P., RIBEIRO, A. 1973. Geotectonic model for the Iberian Variscan orogen. *Nature Physical Science,* **241**, 50-52.

BARD, J.P., AND MOINE, B. 1979. Acebuches Amphibolites in the Aracena Hercynian metamorphic belt (southwest Spain): geochemical variation and basaltic affinities. *Lithos,*. **12** 271-282.

BARKER, A.J. 1984. The geology between Gratangenfjord and Salangsdalen, South Troms, Norway, and its regional significance. *Unpublished Ph.D thesis*, University of Wales.

BARKER, A.J. 1986. The petrography and geochemistry of metabasites from the Gronfjellet Nappe, South Troms, Norway. *Nor. Geol. Unders. Bull.* **405**, 57-69.

BARKER, A.J. 1990. Introduction to metamorphic textures and microstructures, *Blackie, New York*, 170pp. ISBN 0-216-92685-8.

BARKER, C.E. & PAWLEWICZ, M.J. 1986. The correlation of vitrinite reflectance with maximum temperature in humic organic matter. in: Buntebarth, G. & Stegna, L. (eds) *Lecture notes in Earth Sciences, 5, Palaeogeothermics.* Springer-Verlag, Berlin, 79-93.

BARNES, R.P. 1982. The Geology of South Cornish Melanges. *Unpublished Ph.D. Thesis, University of Southampton.*

BARNES, R.P., 1983. The stratigraphy of a sedimentary mélange and associated deposits in south Cornwall. *Proceedings of the Geologists' Association, London,* **94**, 217-229.

BARNES, R.P., 1984. Possible Lizard-derived material in the underlying Meneage Formation. *Journal of the Geological Society,* **141**, 79-85.

BARNES, R.P., & ANDREWS, J.R. 1984. Hot or Cold Emplacement of the Lizard Complex? *Journal of the Geological Society, London,* **141**, 37-39.

BARNES, R.P., & ANDREWS, J.R. 1986. Upper Palaeozoic ophiolite generation and obduction in south Cornwall. *Journal of the Geological Society, London,* **143**, 117-124.

BECCALUVA, L., OHENENSTETTER, D., OHENENSTETTER, M. 1979. Geochemical discrimination between ocean floor and island arc tholeiites - applications to some ophiolites. *Canadian Journal of Earth Sciences,* **16**, 1874-1882.

BELL, T.H. 1978. Progressive deformation and reorientation of fold axes in a ductile mylonite zone: The Woodroffe Thrust. *Tectonophysics,* **44**, 285-320

BELL, T.H. 1981. Foliation development: the contribution, geometry and significance of progressive bulk inhomogenous shortening. *Tectonophysics*, **75**, 273-296.

BELL, T.H. 1985. Deformation and porphyroblast rotation in metamorphic rocks: a radical reinterpretation. *Journal of Metamorphic Geology,* **3**, 109-118.

BELL, T.H. & HAMMOND, R.L. 1984. Internal geometry of mylonite zones. *Journal of Geology,* **92**, 667-686.

BERTHÉ, D., CHOUKROUNE, P., JEGOUZO, P. 1979. Orthogneiss, mylonite, and non coaxial deformation of granites: the example of the South Armorican Shear Zone. *Journal of Structural Geology*, **1**, 31-42.

BINNS, R.A. 1965. The Mineralogy of Metamorphic Belts. George Allen & Unwin, London. 492pp.

BJORNERUD, M. 1989. Toward a unified conceptual framework for shear sense indicators. *Journal of Structural Geology*, **11**, 1045-1049.

BLAKE, M.C. JR., & JONES, D.L. 1974. Origin of the Fransiscan Melanges in northern California. *Special Publication of the Society of Economic Palaeontology and Mineralogy, Tulsa,* **19**, 345-357.12

BLUCK, B.J. 1985. The Scottish paratectonic Caledonides. *Scottish Journal of Geology,* **21**, 437-464.

BOOGÄRD, VAN DEN. 1963. Conodonts of Upper Devonian and Lower Carboniferous age from Southern Portugal. *Geologie en Minjbouw,* **42**, 248-259.

BOOGÄRD, VAN DEN. & SCHERMERHORN, J.L.G. 1980. Conodont fauna from Portugal and southwest Spain, Part 3 - Carboniferous conodonts from Sotiel Caronada. *Scripta Geologica*, **29**, 37-43.

BOOGARD, M.VAN DEN & SCHERMERHORN, J.L.G. 1981. Conodont fauna from Portugal and southwest Spain. Part 6 - A Lower Famennain conodont fauna at Monte Forno da Cal (south Portugal). *Scripta Geologica*, **63**, 1-16.

BOOGÄRD, VAN DEN. & VASQUEZ, M. 1981. Conodont fauna from Portugal and southwest Spain, Part 5 - Lower Carboniferous conodonts at Santa Olalla de Cala (Spain). *Scripta Geologica*, **61**, 1-8.

BORYTA, M. & CONDIE, K.C. 1990. Geochemistry and origin of the Archaean Beit Bridge complex, Limpopo Belt, South Africa. *Journal of the Geological Society,* **147**, 229-241.

BOYLE, A.P. 1986. Metamorphism of basic and pelitic rocks at Sulitjelma, Norway. *Lithos,* **19**, 113-128.

BUTLER, R.W.H. 1989. The influence of pre-existing basin structure on thrust system evolution in the Western Alps. in: Inversion Tectonics. M.A. Cooper & G.D. Williams (eds). *Geological Society Special Publication,* **44**, 105-123.

CABY, R. DOSTAL, J. & DUPUY, C. 1977. Upper Proterozoic volcanic greywackes from Northwestern Hoggar (Algeria). *New Zealand Journal of Geology and Geophysics,* **22**, 71-85.

CARRERAS, J. & CASAS, J.M. 1986. On folding and shear zone development: a mesoscale structural study on the transition between two different tectonic styles. *Tectonophysics,* **135**, 87-98.

CARRERAS, J., ESTADA, A., & WHITE, S. 1977. The effects of folding on the c-axis fabrics of a quartz-mylonite. *Tectonophysics,* **39**, 3-24.

CARVALHO, D. 1972. The metallogenic consequences of plate tectonics and the Upper Palaeozoic evolution of southern Portugal. *Estudos, Notas e Trabalhos do Servico de Fomento Mineiro (Porto),* **20(3/4)**, 297-320.

CARVALHO, D. 1976. Considerações sobre o vulcanismo da regiao de Cercal-Odemira. Suas relações a faixa piritosa. *Comun. Serv. Geol. Portugal,* **60**, 215-238.

CARVALHO, D., CORREIA, H.A.C., INVERNO, C.M.C. 1976. Contribuicao para o conheamento geologico do grupo de ferreira-ficalho. Suas relacoes con a faixa piritosa e grupo do pulo do lobo. *Memorias e Noticias,* **82**, 145-169.

CASTRO, P., QUESADA, C., MUNHA, J., 1987. Metamorphic regime in the Beja-Acebuches Variscan ophiolite (SW Iberia). Extended abstract, Intern. Conf. on the Tectonothermal evolution of the West African Orogens and Circum-Atlantic Terrane linkages, **IGCP Project 233**, 57-60.

CLAYTON, G. 1989. Vitrinite reflectance data from the Kinsale Harbour-Old Head of Kinsale area, southern Ireland, and its bearing on the interpretation of the Munster Basin. *Journal of the Geological Society,* **146**, 611-617.

COBBOLD, P.R. & QUINQUIS, H. 1980. Development of sheath folds in shear regimes. *Journal of Structural Geology,* **2**, 119-126.

CONDIE, K.C., MARTELL, C. 1983. Early Proterozoic metasediments from north-central Colorado: metamorphic setting and tectonic setting. *Bulletin of the Geological Society of America,* **94**, 1215-1224.

COLEMAN, R.G. 1981. Tectonic setting for ophiolite obduction in Oman. *Journal of Geophysical Research,* **86**, 2497-2508.

CRESPO-BLANC, A. 1989. Evolución geotectonica del contacto entra la zona de Ossa Morena y zona Surportuguesa en la sierras de Aracena y Aroche (Macizo Ibérico Meridional); un contacto major en la cadena hercínica europea. *tesis doctoral, Universidad de Sevilla.*

CRESPO-BLANC, A. & OROZCO, M. 1988. The Southern Iberian Shear Zone. A major boundary in the Hercynian Folded Belt. *Tectonophysics,* **148**, 221-227.

CRESPO-BLANC, A. *in press.* Geología del extremo septentrional de la zona Surportuguesa en la región de Aracena (Macizo Iberico Meridional). Discusión y cuestiones abiertas.

DALLMEYER, R.D. & QUESADA, C. (*in press*). in: Premesozoic Geology of the Iberian Peninsula, R.D Dallmeyer & E. Martinez (eds) Hercynia Special Issue.

DEER, W.A., HOWIE, R.A. & ZUSSMAN, J. 1966. An introduction to the rock forming minerals. Longman. 528pp.

DEWEY, J.F., 1982. Plate Tectonics and the Evolution of the British Isles. *Journal of the Geological Society of London,* **139**, 371-412.

DRIESSCHE, J. VAN DEN, & BRUN, J.P. 1987. Rolling structures at large shear strains. *Journal of Structural Geology,* **9**, 691-704.

DRURY, M.R., & HUMPHREYS, F,J. 1988. Microstructural shear criteria associated with grain boundary sliding during ductile deformation. *Journal of Structural Geology,* **10**, 83-89.

DUNNE, W.M. & FERRILL, D.A. 1988. Blind thrust systems. *Geology,* **16**, 33-36.

DUPUY, C., DOSTAL, J., & BARD, J.P. 1979. Trace Element geochemistry of Palaeozoic amphibolites from SW Spain. *Tschermakes Min. Petr. Mitt.,* **26**, 87-93.

EDEN, C.P. & ANDREWS, J.R. 1990. Middle to Upper Devonian melanges in SW Spain and their relationship to the Meneage Formation in South Cornwall. *Proceedings of the Ussher Society.*

ENGEL, W. & FRANKE, W. 1983. Flysch sedimentation: its relations to tectonism in the European Variscides. in Martin, H. & Eder, W. (eds). *Intracontinental Fold Belts.* 289-313.

FLOYD, P.A. & LEVERIDGE, B.E. 1987. Tectonic environment of the Devonian Gramscatho basin, South Cornwall: framework mode and geochemical evidence from turbiditic sandstones. *Journal of the Geological Society of London,* **4??**, 531-542

FLOYD, P.A. & WINCHESTER, J.A. 1975. Magma type and tectonic setting discrimination using immobile elements. *Earth and Planetary Science Letters,* **27**, 211-218.

FLOYD,P.A. & WINCHESTER,J.A. 1983. Element mobility associated with meta-shear zones within the Ben Hope amphibolite suite, Scotland. *Chemical Geology,* **39**, 1-15.

FLOYD, P.A. & WINCHESTER, J.A. 1978. Identification and discrimination of altered and metamorphosed volcanic rocks using immobile elements. *Chemical Geology,* **21**, 291-306.

FLOYD, P.A., SHAIL, R., LEVERIDGE, B.E., FRANKE,W. (*in press*) Geochemistry and provenance of Rhenohercynian synorogenic sandstones.

FRANKE, W. & ENGEL, W. 1982. Variscan sedimentary basins on the continent and relations with southwest England. *Proceedings of the Usshers Society,* **5**, 259-269.

FRANKE, W. & ENGEL, W. 1983. Tectonic settings of synorogenic sedimentation in the Variscan Belt of Europe. Intracontinental Fold Belts. H. Martin & F.W Elder (eds), Springer, Berlin.

GAPAIS, D., BALE, P., CHOUKROUNE, P., COBBOLD, P.R., MAHJOUB, Y., MARQUER, D. 1987. Bulk kinematics from shear zone patterns: some field examples. *Journal of Structural Geology,* **9**, 635-646.

GASS, I.G., LIPPARD, S,J., SHELTON, A.W. (EDS). 1984. Ophiolites and Oceanic Lithosphere. *Geological Society Special Publication,* **13**, pp413.

GIESE, U., REITZ, E., WALTER, R. 1988. Contributions to the stratigraphy of the Pulo do Lobo Succession in southwest Spain. *Communicações dos Serviços Geologicos de Portugal.* **74**, 79 -84.

GREENWOOD, A. 1967. in: P.H. Abelson (ed) Researches in Geochemistry, **2**, 542-567, Wiley & Sons, New York.

GROCOTT, J. 1980. Strain profile of a boundary within a large ductile shear zone. *Journal of Structural Geology,* **12**, 111-117.

HANMER, S.K. 1986. Asymmetrical pull-apart and foliation fish as kinematic indicators. *Journal of Structural Geology,* **8**, 111-122.

HANSEN, V.L. 1989. Structural and kinematic evolution of the Teslin suture zone, Yukon: record of an ancient transpressional margin. *Journal of Structural Geology,* **11**, 717-733.

HARTE, B. & HUDSON, N.F.C. 1979. Pelite facies series and the temperatures and pressures of Dalradian metamorphism in E. Scotland. in The Caledonides of the British Isles-reviewed. *Geological Society of London Special Publication,* **8**, 323-337.

HILLIER, S.J. & MARSHALL, J.A.E. 1989. A rapid technique to make polished thin sections of sedimentary organic matter concentrates. *Journal of Sedimentary Petrology,* **58**, 754-755.

HOBBS, B.E., MEANS, W.D., WILLIAMS, P.F. 1976. An Outline of Structural Geology. *Wiley International.* pp571.

HOLDSWORTH, R.E. 1990. Progressive deformation structures associated with ductile thrusts in the Moine Nappe, Sutherland, N. Scotland. *Journal of Structural Geology,* **12**, 443-452.

HOLM, P.E. 1982. Non-recognition of continental tholeiites using the Ti-Y-Zr diagram. *Contributions to Mineralogy and Petrology,* **79**, 308-310.

HOWELL, D.G. 1985. Tectonostratigraphic terranes of the circum-Pacific region. Houston, Texas - Circum-Pacific Council for Energy and Mineral Resources, Earth Sciences Series 1.

HSÜ, K.J. 1974. Melanges and their distinction from olistostromes. *Special Publication of the Society of Economic Palaeontology and Mineralogy, Tulsa,* **19**,321-333.

HUMPHRIES, S.E. & THOMPSON, G. 1978. Trace element mobility during hydrothermal alteration of oceanic basalt. *Geochimca, Cosmochimica Acta,* **42**, 193-204.

HUTTON, D.W. 1987. Strike-slip terranes and a model for the evolution of the British and Irish Caledonides. *Geological Magazine,* **124**, 405-425.

HUTTON, D.W. & SANDERSON, D.J. (eds) 1984. Variscan Tectonics of the North Atlantic Region. *Geological Society Special Publication,* **14**, pp270.

HUTTON, D.W. & DEWEY, J.F. 1986. Palaeozoic terrane accretion in the western Irish Caledonides. *Tectonophysics,* **5**, 1115-1124.

IGLESIAS, M. & CHOUKROUNE, P. 1980. Shear zones of the Iberian Arc. *Journal of the Geological Society,* **2**, 63-68.

JOHANNES, R. 1969. American Journal of Science, 267, 1083-1104.

JONES, M.E. & PRESTON, R.M.F. 1987 (eds). Deformation of Sediments and Sedimentary Rocks. *Geological Society Special Publication,* **29**.

JULIVERT, M. 1976. A cross section through the northern part of the Iberian Massif: its position within the Hercynian fold belt. *Krystalinileum,* **14**, 51-67.

JULIVERT, M. 1978. Palaeogeographic and tectonic evolution of the Iberian Massif during Carboniferous times. *Zdt. Geol. Ges,* **128**, 565-592.

JULIVERT, M., FONTBOTE, J.M., RIBEIRO, A. & NABAIS CONDIE, L.E 1974. Mapa tectónico de la Peninsula Ibérica y Baleares, escala 1:1 000 000. *Memoria explicativa*: 1-113, **IGME.**

JULIVERT, M., MARTINEZ, F.J., RIBEIRO, A. 1984. The Iberian segnment of the European Hercynian foldbelt. *Journal of Structural Geology,* **6**, 499-580.

KISCH, H.T. 1987. in Frey, M. (ed). Low Temperature Metamorphism. Blackie, New York.

KITAMURA, M. & YAMADA, H. 1987. Origin of sector trilling in cordierite in Daimonji hornfels, Kyoto, Japan. *Contributions to Mineralogy and Petrology,* **97**, 1-6.

KNELLER, B.C. & LESLIE, A.G. 1984. Amphibolite facies metamorphism in shear zones in the Buchan area of NE Scotland. *Journal of Metamorphic Geology,* **2**, 83-94.

KNIGHT, R.R.W. 1990. Aspects of the micropalaeontology of Devonian strata of North Devon. Unpublished Ph.D thesis, *University of Southampton.*

KNIPE, R.J. & LAW, R.D. 1987. The influence of crystallographic orientation and grain boundary migration on microstructural and textural evolution in an S-C mylonite. *Tectonophysics,* **135**, 155-169.

KOSTYUK, E.A. & SOBOLEV, V.S. 1969. Paragenetic types of calciferous amphiboles of metamorphic rocks. *Lithos,* **2**, 67-82.

LAKE, P.A. 1988. The palynology and structure of the Devonian/Carboniferous Pyrite Belt successions, South Iberia. Transfer Report, *University of Southampton.*

LAKE, P.A., OSWIN, W.M., MARSHALL, J.E.A. 1988. Palynological approach to terrane analysis in the South Portuguese Zone. *Trabajos de Geologia,* Universidad de Oviedo.

LANPHERE, M.A. 1981. K-Ar ages of metamorphic rocks at the base of the Somail ophiolite, Oman. *Journal of Geophysical Research,* **86**, 2777-2782.

LAW, R.D., CASEY, M., KNIPE, R.J. 1986. Kinematic and tectonic significance of microstructures and crystallographic fabrics within quartz mylonites from the Assynt and Eriboll regions of the Moine Thrust Zone, NW Scotland. *Transactions of the Royal Society of Edinburgh, Earth Sciences,* **77**, 99-125.

LEAKE, B. E. 1978. Nomenclature of amphiboles. *American Mineralogist,* **63**, 1023-1052.

LEGGETT, J.K., McKERROW, W.S., CASEY, D.M. 1982. The anatomy of a lower Palaeozoic accretionary forearc: the Southern Uplands of Scotland. in Leggett, J.K. (ed) Trench - Forearc Geology, *Geological Society of London Special Publication,* **10.**

LE MAITRE, R.W. 1976. The chemical variability of some common igneous rocks. *Journal of Petrology,* **17**, 589-637.

LI, Y,-H. 1981. Ultimate removal mechanism of elements from the ocean. *Geochimica et Cosmochimica Acta,* **45**, 1659-1664.

LIOU, J.G., MARUYAMA, S. & CHO, M. 1985. Phase equilibria and mineral parageneses of metabasalts in low-grade metamorphism. *Mineralogical Magazine,* 49, 321-333.

LIPPARD, S.J., SHELTON, A.W., GASS,I.G. 1986. The ophiolite of northern Oman. *Geological Society Memoirs,* **11.**

LISTER, G.S. & SNOKE, A.W. 1984. S-C Mylonites. *Journal of Structural Geology,* **6**, 617-638.

LISTER, G.S. & PRICE, G.P. 1978. Fabric development in a quartz feldspar mylonite. *Tectonophysics*, **49**, 37-78.

LOTZE, F. 1945. zur Gliederung der Varisciden der Iberishen Mesetas. *Geoth. Forsch.* **6**, 78-92.

LOTZE, F. 1956. Das Prakambrium Spaniens. *Nues Jahrbuch Geologische Palaontogische Monatshefte*, **8**, 373-380.

LUDDEN, J.N. & THOMPSON, G. 1979. An evaluation of the behaviour of rare earth elements during the weathering of sea floor basalt. *Earth and Planetary Science Letters*, **43**, 85-92.

MALAVIEILLE, J. 1987. Kinetics of compressional and extensional ductile shearing deformation in a metamorphic core complex of the northeastern Basin and Range. *Journal of Structural Geology,* **9**, 541-554.

MALAVIEILLE, J. & LACASSIN, R. 1988. "Bone-shaped" boudins in progressive shearing. *Journal of Structural Geology,* **10**, 335-345.

MATA, J. & MUNHA, J. 1986. Tectonic setting of magmatic activity in the southern branch of the Iberian Variscan Chain. *Maleo*, **2**, No.13:28.

MATTE, P. 1983. Two geotraverses across the Ibero-Armorican Variscan Arc of Western Europe. in Rast, N. & Delany, F.M. (eds). Profiles of Orogenic Belts. *Geodynamics Series*, **10.**

MATTE, P. 1986. Tectonics and Plate Tectonics Model for the Variscan Belt of Europe. *Tectonophysics*, **126**, 339-374.

MATTE, P., AND BURG, J.P., 1981. Sutures, thrusts and nappes in the Variscan Arc of western Europe: plate tectonic implications. in: McClay K.R. and Price N.J., (eds). Thrust and Nappe Tectonics. *Special Publication of the Geological Society of London.* **2**, 353-358.

M°CLENNAN, S.M., TAYLOR, S.R., M$_c$CULLOCH, M.T. & MAYNARD, J.B. 1990. Geochemical and Nd-Sr isotopic composition of deep-sea turbidites: Crustal evolution and plate tectonic associations. *Geochimica et Cosmochimica Acta*, **54**, 2015-2050.

MESCHEDE, M. 1986. A method of dicriminating between different types of mid-ocean ridge basalts and continental tholeiites with the Nb-Zr-Y diagram. *Chemical Geology,* **56**, 207-218.

MISCH, P.M. & RICE, J.M. 1975. Miscibility of tremolite and hornblende in progressive Skagit metamorphic suite, North Cascades, Washington. *Journal of Petrology*, **66**, 1-21.

MIYASHIRO, A. 1973. Metamorphism and Metamorphic Belts. George Allen & Unwin, London, 492pp.

MOOREHOUSE, S.J. & MOOREHOUSE, V.E. 1979. The Moine amphibolite suites of central and northern Sutherland, Scotland. *Mineralogical Magazine,* **43**, 211-225.

MULLEN, E.D. 1983. $MnO/TiO_2/P_2O_5$: a minor element discriminant for basaltic rocks of oceanic environment and its implications for petrogenesis. *Earth and Planetary Science Letters*, **62**, 53-62.

MUNHA, J.M. 1983a. Hercynian magmatism in the Iberian Pyrite Belt. in De Sousa, M.J.L. & Oliveira, J.T. (eds). The Carboniferous of Portugal. *Mem. Serv. Geol. Portugal,* **29**, 39-81.

MUNHA, J.M. 1983b. Low grade regional metamorphism in ther Pyrite Belt. *Comun. Serv. Geol. Portugal,* **t69**, fasc.1, 3-35.

MUNHA, J.M., OLIVEIRA, J.T., RIBEIRO, A., OLIVEIRA, V., QUESADA, C., KERRICH, R., 1986. Beja-Acebuches Ophiolite: Characterisation and Geodynamic Significance. *Malaeo. 2:(13) Abstract.*

MUNHA, J.M., OLIVEIRA, J.T., RIBEIRO, A., QUESADA, C., FONSECA, P., CASTRO, P. 1989. Accreted terranes in southern Iberia: the Beja-Acebuches ophiolite and related oceanic sequences. 28th International Geological Congress. Washington D.C.

NITSCH, K.H. 1970. Experimentelle Bestimmungder Oberen Stabilitätsgrenze von Stilpnomelan. *Abstract. Forschr. Mineral.*, **47**, 48-49.

O'BRIEN, D.K. & WENK, H.R. 1987. Preferred orientation of phyllosilicates in phyllonites and ultramylonites. *Journal of Structural Geology,* **9**, 719-730.

OGAWA, Y. 1985. Variety of subduction and accretion processes in Cretaceous to Recent plate boundaries around southwest and central Japan. *Tectonophysics,* **112**, 493-518.

OLIVEIRA, J.T. 1980. The Devonian - Carboniferous stratigraphy and geodynamics of southern Portugal: Some comments. *Rundgespräch "Subsidenz-Entwicklung" Tübingen, Stuttgart.*

OLIVEIRA, J.T., 1983. The Marine Carboniferous of South Portugal: A Stratigraphic and Sedimentological Approach. in: De Sousa, M.L.J. and Oliveira, J.T. (eds) The Carboniferous of Portugal. *Mem. Serv. Geol. Portugal.*

OLIVEIRA, J.T., *(in press)*. Stratigraphy and Syn-sedimentary tectonism in the South Portuguese Zone. in Dallmeyer, R.D. and Lecorché, J.P. (eds) *Hercynia Special Issue.*

OLIVEIRA, J.T., HORN, M. & PAPROTH, E. 1979. Preliminary note on the stratigraphy of the Baixo Alentejo Flysch Group, Carboniferous of Portugal, and on the palaeogeographic development compared to corresponding units in North West Germany. *Communicações dos Serviços Geologicos de Portugal,* **63**, 151-168.

OLIVEIRA, J.T., HORN, M. KULLMAN, J. & PAPROTH, E. 1985. Stratigraphy of the Upper Devonian and Carboniferous sediments of southwestern Portugal. *Dixième Congrés International de Stratigraphie et de Géologie du Carbonifére, Madrid 1983,* Compte rendu, **1**, 107-120.

OLIVEIRA, J.T., CUNHA, T., STREEL, M., VANGUESTAINE, M. 1986. Dating the Horta da Torre Formation, a New Lithostratigraphic Unit of the Ferreira-Ficalho Group, South Portuguese Zone. Geological Consequences. *Com. Serv. Geol. Portugal* **72**, (1/2): 129-135.

OSBORN, E.F. 1959. Role of oxygen in the crystallisation and differentiation of basaltic magma. *American Journal of Science,* **257**, 609-647.

OSWIN, W.M., 1986. Upper Devonian/Lower Carboniferous Volcanism and Mineralisation in the Area East of the Rio Tinto Mines, Iberian Pyrite Belt. *Unpublished Ph.D thesis, University of Southampton.*

PACHECO-SANTOS, J.F.H., MATA, J., GONÇALVES, F. & MUNHA, J. 1985. Hercynian magmatism in the Santa Susana region (Alcâcer do sal, South Portugal): Identification of Carboniferous convergent plate margin in the southern branch of the Iberian Hercynian chain. Resumen Reunión GOM.

PASSCHIER, C.W. 1984. The generation of ductile and brittle shear bands in a low angle mylonite zone. *Journal of Structural Geology,* **6**, 273-281.

PASSCHIER, C.W. & SIMPSON, C. 1986. Porphyroclast systems as kinematic indicators. *Journal of Structural Geology,* **8**, 831-843.

PEARCE, J.A. 1973. Tectonic setting of basic volcanic rocks determined using trace element analysis. *Earth and Planetary Science Letters,* **19**, 290-300.

PEARCE, J.A. 1975. Basalt geochemistry to investigate past environments on Cyprus. *Tectonophysics,* **25**, 41-67.

PEARCE, J.A. & CANN, J.R. 1973. Tectonic studies of basic volcanic rocks determined using trace element analysis. *Earth and Planetary Science Letters,* **19**, 290-300.

PEARCE, J.A., HARRIS, N.B.W., TINDLE, A.G. 1984. Trace element discrimination for the tectonic interpretation of granitic rocks. *Journal of Petrology,* **25**, 956-983.

PEARCE, J.A. & NORAY, M. 1979. Petrogenetic implications of Ti, Zr, Y and Nb variations in volcanic rocks. *Contributions to Mineralogy and Petrology,* **69**, 33-47.

PEARCE, J.A., ALABASTER, T., SHELTON, A.W., SEARLE, M.P. 1981. The Oman ophiolite as a Cretaceous arc-basin complex: evidence and implications. *Phil. Trans. Roy. Soc. Lond.* **A300**, 299-317.

PFEFFERKORN, H.W. 1968. Geologie des Gebeites zwischen Serpa und Mertola (Baixo Alentejo, Portugal). *Munst. Forsch. Geol. Palaont.*, **9**, 143pp

PICKERING, K.T. 1987. Deep marine foreland basin and forearc sedimentation: a comparative study from the Lower Palaeozoic Northern Appalachians, Quebec and Newfoundland. in: Marine Clastic Sedimentology. J.K. Legett & G.G. Zuffa (eds), 190-211. London.

PICKERING, K.T., AGAR, S. & OGAWA, Y. 1988a. Genesis and deformation of mud injections containing chaotic basalt-limestone-chert associations: examples from the southwest Japan forearc. *Geology*, **16**, 881-885.

PICKERING, K.T., BASSELL, M.G., SIVETER, D.J. 1988b. Late Ordovician - early Silurian destruction of the Iapetus Ocean: Newfoundland, British Isles and Scandinavia: a discussion. *Trans. R. Soc. Edin.*, **79**, 361-382.

PICKERING, K.T., HISCOTT, K.N. & HEIN, F.J. 1989. Deep Marine Environments. Unwin Hyman, 416pp.

PLATT, J.P. 1983. Progressive refolding in ductile shear zones. *Journal of Structural Geology*, **5**, 619-622.

PLATT, J.P. 1984. Secondary cleavage in ductile shear zones. *Journal of Structural Geology*, **6**, 439-442.

PLATT, J.P. 1986. Dynamics of orogenic wedges and the uplift of high pressure metamorphic rocks. *Geological Society of America Bulletin*, **97**, 1037-1053.

PLATT, J.P. & VISSIERS, R.L.M. 1980. Extensional structures in anisotropic rocks. *Journal of Structural Geology*, **2**, 397-410.

PLATT, J.P. & BEHRMANN, J.H. 1986. Structures and fabrics in a crustal scale shear zone, Betic Cordillera, southeast Spain. *Journal of Structural Geology*, **8**, 15-33.

PLINT, H.E. & JAMIESON, R.A. 1989. Microstructure, metamorphism and tectonics of the western Cape Breton Highlands, Nova Scotia. *Journal of Metamorphic Geology*, 7, 407-424.

POTTS, P.J., WILLIAMS THORPE, M.C., ISAACS, M.C. & WRIGHT, D.W. 1985. High precision instrumental neutron-activation analysis of geological samples employing simultaneous countine with both planar and coaxial detectors. *Chemical Geology*, **48**, 145-155.

PRESTVIK, T. 1982. Basic volcanic rocks and tectonic setting. A discussion of the Zr-Ti-Y discrimination diagram and its suitability for classification purposes. *Lithos*, **15**, 241-247.

PRODEHL, C. SOUSA, M.V., MUELLER, S. & MENDE, A.S. 1976. Deep seismic sounding experiments in central and southern Portugal. *XIVth General Assembly Europ. Seismol. Com. Berlin*: 261-266.

PUSCHMANN, H. 1967. Problem des Schichtlucken im der Devon der Sierra Morena (Spanien). *Geol. Rundschau,* **56**, 528-542.

PUTNIS, A. & HOLLAND, T.J.B. 1986. Sector trilling in cordierite and equilibrium overstepping in metamorphism. *Contributions to Mineralogy and Petrology,* **93**, 265-272.

QUESADA, C., *(in press).* The West African Orogens and Circum-Atlantic Correlations. in: Dallmeyer, R.D. and Lecorché, J.P. (eds) *Hercynia Special Issue.*

QUESADA, C., & IBARGUCHI, I.G. *(in press).* Oceanin Exotic Terranes. in: The West African Orogens & Circum-Atlantic Correlations, section 6A: Iberia. R.D. Dallmeyer & Lecorché (eds), Springer Verlag.

RAASE, P. 1974. Al & Ti contents of hornblende, indicators of pressure and temperature of regional metamorphism. *Contributions to Mineralogy and Petrology,* **45**, 231-236.

RAMSAY, J.G. 1980. Shear zone geometry - a review. *Journal of Structural Geology,* **2**, 83-99.

RAMSAY, J.G. & GRAHAM, R.H. 1970. Strain variations in shear belts. *Canadian Journal of Earth Sciences,* **6**, 786-813.

RAMSAY, J.G. & HUBER, M.I. 1988. The techniques of modern structural geology. Volume 2: Folds and fractures, Academic Press, 700pp.

READING, H.G. 1980. Characteristics and recognition of strike-slip fault systems. *Special Publication of the International Association of Sedimentology,* **4**, 7-26.

READING, H.G. 1986. Sedimentary Environments and Facies. Blackwell, 615pp.

RIBEIRO, A. & SILVA, J.B. 1983. Structure of the South Portuguese Zone. in A. Sousa & J.T. Oliveira (eds): The Carboniferous of Portugal. *Mem. Serv. Geol. Portugal.* **29**, 91-97.

RIBEIRO, A., OLIVEIRA, J.T., RAMALHO, M. & RIBEIRO, L. 1987. Carta Geológica de Portugal a escala 1:150 000. Noticia explictiva da folha, 48-D Bordeira. *Serviços geológicos de Portugal.*

RIBEIRO, A., QUESADA, C.O., DALLMEYER, R.D. *in press.* Geodynamic evolution of the Iberian Massif. in: Dallmeyer, R.D. and Lecorché, J.P. (eds) *Hercynia Special Issue.*

RIDING, R. 1974. Model of the Hercynian foldbelt. *Earth and Planetary Science Letters,* **24**, 125-135.

ROUTHIER, P., AYE, F., BOYER, C., LECOLLE, M., MOLIERE, P., PICOT, P. ROGER, G. 1980. La ceinture sud-iberique à amas sulfurés dans sa partie espagnole. Tableau gélogique et metallogénique. Synthese sur le type amas sulfurés volcano-sedimentaires. *Memoire Bureau de Rescherches Géologiques et Minères,* **94**, 26° Congrés International de Géologie, Paris, 1980.

SALEEBY, J.B. 1984. Tectonic significance of serpentinite mobilty and opholite melange. *Geological Society of America. Special Paper,* **198**, 153-168.

SANDERSON, D.J. & MARCHINI, W.R.D. 1984. Transpression. *Journal of Structural Geology,* **6**, 449-458.

SANTOS, J.F.H.P., MATA, J., GONÇALVES, F. & MUNHA, J. 1987. Contribução para o conhecimiento da região de Santa Susana: o complexo vulcano-sedimentar de Foca da Moura. *Commun. Serv. Geol. Portugal*, **73**, 29-48.

SAUNDERS, A.D. TARNEY, J., MARSH, NG., WOOD, D.A. 1980. Ophiolites as ocean crust or marginal basin crust: A geochemical approach. in: Pandyiotou A. (ed) Ophiolites: Proceedings of the International Ophiolite Symposium, Cyprus, 1979, 193-204.

SCHERMERHORN, L.J.G. 1971. An Outline Stratigraphy of the Iberian Pyrite Belt. *Bolletin Geológico y Minero* **T. LXXXII-III-IV**, 239-268.

SCHERMERHORN, L.T.G. 1975. Pumpellyite facies metamorphism in the Spanish Pyrite Belt. *Pétrologie,* **t.1**, 71-86.

SCHERMERHORN, L.T.G. 1975. Spilites, regional metamorphism and subduction in the Iberian Pyrite Belt: some comments. *Geologisch Minjbow (Den Haag),* **54**(1), 23-35.

SCHERMERHORN, L.J.T. & STANTON, W.I. 1969. Folded overthrusts at Aljustrel (south Portugal). *Geological Magazine,* **106**, 130-141.

SCHULTZ-DOBNICK, B. & WEDEPOHL, K.H. 1983. The chemical composition of sedimentary deposits in the Rhenohercynian belt of Central Europe. in Martin, H. & Eder, F.W. (eds). Intracontinental Fold belts. *Springer-Verlag, Berlin,* 211-229.

SEARLE, M.P. 1991. Symposium on the genesis and evolution of ocean lithosphere. Conference report. *Journal of the Geological Society of London*, **148**, 203-205.

SEARLE, M.P. & MALPAS, J. 1980. Structure and metamorphism of rocks beneath the Semail ophilite of Oman and their significance in ophiolite obduction. *Transactions of the Royal Society of Edinburgh, Earth Sciences,* **17**, 247-262.

SHAW, D.M. 1954. Trace elements in pelitic rocks. Part I. *Bulletin of the Geological Society of America*, **65**, 1151-1166.

SHAW, D.M. 1956. Geochemistry of pelitic rocks. Part III. Major elements and general geochemistry. *Bulletin of the Geological Society of America*, **67**, 919-934.

SHAIL, R.K. 1989. Gramscatho - Mylor facies relationships; Hayle, south Cornwall. *Proceedings of the Ussher Society,* **7**, 125-130.

SHIMAMOTO, T. 1989. The origin of S-C mylonites and a new fault-zone model. *Journal of Structural Geology,* **11**, 51-64.

SILVA, J.B., OLIVEIRA, J.T., RIBEIRO, A. *in press.* Structural Outline of the South Portuguese Zone. Dallmeyer, R.D. and Lecorché, J.P. (eds) *Hercynia Special Issue.*

SILVER, E.A., ELLIS, M.J., BREEN, N.A., SHIPLEY, T.H. 1985. Comments on the growth of accretionary prisms. *Geology*, **13**, 6-9.

SIMANCAS, J.F. 1983. Geologia de la extremidad oriental de la Zone Sudportuguesa. *Tésis Doctoral,* Universidad de Granada.

SIMANCAS, J.F. 1986. La deformación en el sector oriental de la Zone Sudportuguesa. *Bolletín Geológico y Minero*, **T. XCVII-II**, 148-159.

SIMPSON, C. 1983. Strain and shape fabric variations associated with ductile shear zones. *Journal of Structural Geology*, **5**, 61-71.

SIMPSON, C. 1985. Deformation of granitic rocks across the brittle-ductile transition. *Journal of Structural Geology*, **7**, 503-511.

SMITH, R.E. & SMITH, S.E. 1976. Comments on the use of Ti, Zr, Y, Sr, K, P and Nb in classification of basaltic magmas. *Earth and Planetary Science Letters*, **32**, 114-120.

SPEAR, F.S. 1981. Amphibole-plagioclase equilibrium: an empirical model for the relation albite + tremolite = edenite + 4quartz. *Contributions to Mineralogy and Petrology*, **77**, 355-364.

SPEAR,F.S. & CHENEY, J.T. 1989. A petrogenetic grid for the pelitic schists in the system SiO_2 - Al_2O_3 - FeO - MgO - K_2O - H_2O. *Contributions to Mineralogy and Petrology*, **101**, 149-164.

SUN, S.S. & NESBITT, R.W. 1979. Chemical heterogeneity of the Archaean mantle, composition of the earth and mantle evolution, *Earth and Planetary Science Letters*, **35**, 429.

TAIRA, A. 1985. Sedimentary evolution of the Shikoku subduction zone: the Shimanto Belt and Nankai Trough. in: Formation of Active Margins, N. Nash (ed), 835-851.

TAKAGI, H. & ITO, M. 1988. The use of asymmetric pressure shadows in mylonites to determine the sense of shear. *Journal of Structural Geology*, **10**, 347-360.

TANNER, P.W.G. 1989. The flexural-slip mechanism. *Journal of Structural Geology*, **11**, 635-655.

TARNEY, J., WOOD, D.A., SAUNDERS, A.D., CANN, J.R., VARET, J. 1980. Nature of mantle heterogeneity in the North Atlantic: evidence from deep sea drilling. *Phil. Trans. Roy. Soc. Lond.* **A297**, 179-202.

TAYLOR, S.R. & McCLENNAN, S.M. 1985. The Continental Crust: Its Composition and Evolution. *Blackwell Scientific Publications, London.* pp312.

TAYLOR, R. 1988. The stratigraphy, geochemistry and petrogenesis of the Troodos Extrusive Sequence, Cyprus. *Unpublished Ph.D thesis*, University of Southampton.

TEICHMULLER, M. 1987. Recent advances in coalification studies and their application to geology. in Scott, A.C. (ed). Coal and Coal Bearing Strata: Recent Advances. *Geological Society Special Publication*, **32**, 127-169.

THOMPSON, R.N. 1982. Magmatism of the British Tertiary volcanic province. *Scottish Journal of Geology*, **18**, 50-107.

TULLIS, J.A., CHRISTIE, J.M., GRIGGS, D.T. 1973. Microstructures and preferred orientation of deformed quartzites. *Bulletin of the Geological Society of America*, **84**, 297-314.

VERBEEK, E.R. 1978. Kink bands in the Somport slates, west-central Pyrenees, France and Spain. *Geol. Soc. Am. Bull.* **89**, 814-824.

VEGAS, R. 1981. Carboniferous subduction complex in the South Portuguese Zone coeval with basement reactivation and uplift in the Iberian Massif. *Leidse Geologische Mededelingen,*

VEGAS, R. & MUÑOZ, M. 1976. El contacto entre las zonas Surportuguesa y Ossa Morena en el SW de España. Una nueva interpretación. *Commun. Serv. Geol. Portugal,* **60**, 31-51.

VIERECK, L.G., FLOWER, M.F.J., HERTOGEN, J., SCHIMNCKE, H.U., JENNER, G.A. 1989. The genesis and significance of N-MORB sub-types. *Contributions to Mineralogy and Petrology,* **102**, 112-126.

VOGT, P.R., JOHNSON, G.L., HOLCOMBE, T.L., GILG, J.G., AVERY, O.E. 1971. Episodes of sea-floor spreading recorded by the North Atlantic basement. *Tectonophysics,* **12**, 211-234.

WALDRON, J.W.F., TURNER, D., STEVENS, K.M. 1988. Disruption and development of melanges, western Newfoundland: effects of high fluid pressures in an accretionary terrain during ophiolite emplacement. *Journal of Structural Geology,* **10**, 861-873.

WEDEPOHL, K.H. 1961. Distribution of elements in some major units of the earth's crust. *Geological Society of America Bulletin,* **72**, 175-192.

WENK, H.R. 1979. An albite-anothorthite assemblage in low-grade amphibolite facies rocks. *American Mineralogist,* **65**, 1294-1299.

WHITE, S.H. 1988. Internal structures in a shear zone. MSc course in structural geology, Imperial College.

WHITE, S.H., BURROWS, S.E., CARRERAS, J., SHAW, N.D., HUMPHREYS, F.J. 1980. On mylonites in ductile shear zones. *Journal of Structural Geology,* **2**, 175-187.

WHITE, S.H., BRETAN, P.G., RUTTER, E.H. 1986. Fault zone reactivation: kinematics and mechanisms. *Phil. Trans. Roy. Soc. Lond.* **A317**, 81-97.

WIGHTMAN, R. 1986. Constraints on crustal development and tectonics in the Archaean rocks of South India. *Unpublished Ph.D thesis,* Open University.

WILLIAMS, H. 1977. Ophiolitic melanges and its significance in the Fleur de Lys supergroup, northern Appalachians. *Canadian Journal of Earth Sciences,* **14**, 987-1003.

WILLIAMS, H. & HATCHER, R.D.Jr 1983. Appalachian suspect terranes. in: Contributions to the tectonics and geophysics of mountain chains. R.D. Hatcher, H. Williams, Zeitz, I. (eds) 33-53, *Geol. Soc. Am. Mem.* **158.**

WILKINSON, J.J., AND KNIGHT, R, R. 1989. Palynological evidence from the Porthleven area, south Cornwall: implications for the Devonian stratigraphy and Hercynian structural evolution. *Journal of the Geological Society,* **146**, 739-743.

WINCHESTER, J.A. & FLOYD, P.A. 1976. Geochemical magma type discrimination: application to altered and metamorphosed basic igneous rocks. *Earth and Planetary Science Letters,* **28**, 459-469

WINCHESTER, J.A. & FLOYD, P.A. 1977. Geochemical discrimination of different magma series and their differentiation products using immobile elements. *Chemical Geology,* **20**, 325-343.

WINKLER, H.G.F. 1979 Petrogenesis of metamorphic rocks. *Springer-Verlag, New York.* ISBN 3-540904131

WOOD, D.A., JORON, J.L., TREUIL, M. 1979. A reappraisal of the use of trace elements to classify and discriminate between magma series erupted in different tectonic settings. *Earth and Planetary Science Letters,* **45**, 326-336.

WOODCOCK, N.H. & FISCHER, M. 1986. Strike slip duplexes. *Journal of Structural Geology,* **8**, 725-735.

WRAFTER, J.P. & GRAHAM, J.R. 1989. Ophiolite detritus in the Ordovician sediments of South Mayo, Ireland. *Journal of the Geological Society of London,* **146**, 213-216.

WRONKIEWICZ, D.J. & CONDIE, K.C. 1987. Geochemistry of Archean shales from the Witwatersrand Supergroup, South Africa: Source-area weathering and provenance. *Geochimica et Cosmochimica Acta,* **51**, 2401-2416.

WRONKIEWICZ, D.J. & CONDIE, K.C. 1990. Geochemistry an mineralogy of sediments from the Ventersdorp and Transvaal Supergroups, South Africa: Cratonic evolution during the early Proterozoic, *Geochimica et Cosmochimica Acta,* **54**, 343-354.

YARDLEY, B.W.D. 1989. An introduction to metmorphic petrology. Longman, 248pp.

ZAMARREÑO, I. & DEBRENNE, F. 1977. Sedimentologie et biostratigraphie des constructions organogenes du Cambrien inferieur du Sud de l'Espagne. *2nd symposium International Coraux et Recifs Coral. Foss., Paris 1975, Mem. BRGM,* **89**, 49-61.

Appendix 1 Sample numbering and location

The sample numbering system of this study uses the numbering of 1-n according the year it was collected. Thus CE8021 was the twenty-first sample collected in 1988 whereas CE9021 was collected in the 1989 field season. Also listed in the tables below are the grid reference of each sample and which techniques were used to analyse the sample during the course of the study.

sample no.	location	rock type	Formation	Thin section	XRF bead	XRF pellet
7001	1160 9635	tuffaceous	OMZ	x	-	-
7004	1390 9555	amphibolite	BAA	x	x	x
7005	1385 9520	amphibolite	BAA	x	x	-
7006	1380 9550	amphibolite	BAA	-	x	x
7007	1430 9325	phyllite	AF	-	x	x
7009	1460 9315	amphibolite	BAA	x	-	x
7010	1415 9430	mica-schist	AF	-	x	x
7011	1405 9435	metabasite	BAA	x	-	-
7012	1410 9475	metased	AF	x	x	x
7013	1390 9515	phyllite	AF	-	x	x
7014	1270 9575	marble	OMZ	x	-	-
7015	1230 9540	quartzite	AF	x	-	-
7017	0525 9425	amphibolite	BAA	x	-	-
7018	0500 9410	phyllite	AF	x	x	x
7019	1460 9315	phyllite	AF	-	x	x
7020	1465 9300	phyllite	AF	x	x	x
7021	1480 9290	granite	OMZ	-	x	x
7022	1430 9270	metased	AF	-	x	x
7023	1430 9270	metabasite	AF	x	x	x
7024	1360 9210	metased	AF	x	x	x
7025	1410 9075	phyllite	AF	x	x	x
7028	1410 9430	phyllite	AF	x	-	-
7031	0440 9340	phyllite	AF	x	x	x
7032	0440 9335	phyllite	AF	x	-	-
7033	0435 9330	phyllite	AF	x	x	x
7034	0420 9275	ultramafic	AF	x	x	x
7035	0460 9150	metased.	AF	x	x	x
7036	0525 9395	metased.	AF	x	x	x
7037	0570 9530	quartzite	AF	x	x	x
7038	0570 9530	phyllite	AF	-	x	x
7039	0570 9530	phyllite	AF	-	x	x
7040	0560 9530	metabasite	BAA	x	x	-
7041	0470 9430	metabasite	BAA	x	x	x
7042	0430 9280	quartzite	AF	x	x	x
7043	0385 9240	quartzite	AF	-	x	x
7044	0370 9295	metased.	AF	x	-	x
7045	0520 9435	metabasite	BAA	x	x	x
7046	0510 9420	marble	OMZ	x	x	x
7047	0490 9395	amphibolite	BAA	x	x	x
7048	0485 9390	amphibolite	BAA	x	x	x
7049	0430 9275	quartzite	AF	x	-	-
7051	0430 9255	mica-schist	CLCF	x	-	-
7053	9915 9215	mica-schist	CLCF	x	-	-

sample no.	location	rock type	Formation	Thin section	XRF bead	XRF pellet
8001	7495 9705	dolerite	LCA	-	-	-
8002	7495 9705	metabasite	PMF	x	-	-
8004	7505 9705	metabasite	PMF	x	-	x
8005	7515 9705	qtz schist	CLCF	-	-	-
8006	7530 9740	qtz schist	CLCF	x	x	x
8007	7565 9755	qtz schist	CLCF	-	-	-
8008	7575 9770	qtz schist	CLCF	-	x	x
8009	7575 9770	qtz schist	CLCF	x	-	-
8010	7590 9810	pelite	LGF	-	-	x
8011	7590 9815	phyllite	LGF	-	-	-
8012	7610 9835	qtz schist	CLCF	-	x	x
8013	7490 9705	dolerite	LCA	-	-	-
8014	7490 9700	qtz schist	CLCF	x	x	x
8015	7485 9695	metabasite	PMF	-	-	-
8016	7485 9700	metabasite	PMF	-	-	-
8017	7470 9685	tuffaceous	LGF	-	-	-
8019	7465 9680	dolerite	LCA	-	-	-
8020	7460 9680	mica-schist	CLCF	-	-	-
8021	7455 9675	metabasite	PMF	x	x	x
8022	7390 9675	qtz schist	CLCF	x	-	-
8023	7385 9690	dolerite	LCA	-	-	-
8024	7345 9635	qtz schist	CLCF	-	-	-
8025	7315 9605	qtz schist	CLCF	-	-	-
8026	7300 9530	phyllite	LGF	-	-	x
8027	7295 9525	phyllite	LGF	-	-	-
8028	7285 9500	phyllite	LGF	-	-	x
8029	7390 9745	phyllite	LGF	-	-	-
8030	6976 9830	granite	Las Peñas	-	-	-
8031	7635 9905	vein qtz	LCA	-	-	-
8032	7635 9910	pelite	CLCF	-	x	x
8033	7630 9910	metabasite	CLCF	-	-	x
8034	7630 9915	diorite	BAA	-	-	-
8035	7625 9920	qtz schist	CLCF	-	-	x
8036	7640 9920	amphibolite	BAA	-	-	-
8037	7655 9915	amphibolite	BAA	x	-	-
8038	6795 9910	metabasite	CLCF	-	-	-
8039	6715 9865	mica-schist	CLCF	x	-	-
8040	7680 9995	aplite	BAA	-	-	x
8041	7675 9990	amphibolite	BAA	x	x	x
8042	7685 9995	schorl	BAA	x	-	-
8043	7650 9975	amphibolite	BAA	x	-	-
8044	7650 9960	acidic	BAA	-	-	-
8045	7680 0020	qtz/pyx	OMZ	-	-	-
8046	7680 0015	granite	OMZ	x	-	x
8047	7675 0035	metabasite	OMZ	x	-	x
8048	7670 0040	marble	OMZ	x	-	-
8049	7695 0075	gneiss	OMZ	x	-	-
8050	7740 0090	gneiss	OMZ	x	-	-
8051	7745 0115	granite	OMZ	x	-	x
8052	7695 0120	metabasite	OMZ	x	-	-
8053	7280 9925	gneiss	OMZ	x	-	-
8054	7965 0170	gneiss	OMZ	-	-	-
8055	7080 9860	qtz schist	CLCF	x	-	-
8056	7060 9860	qtz schist	CLCF	x	-	-
8057	7045 9865	granite	Las Peñas	x	-	-
8058	7040 9865	granite	Las Peñas	x	-	-
8059	7015 9875	vein quartz	Las Peñas	-	-	-
8060	7305 9545	phyllite	LGF	-	-	x
8061	7300 9530	arenite	LGF	x	-	x
8062	7290 9520	phyllite	LGF	-	-	x
8063	7280 9500	slate	LGF	-	-	-
8064	7270 9490	arenite	LGF	-	-	x
8065	7255 9485	phyllite	LGF	-	-	-
8066	7240 9475	arenite	LGF	x	-	x
8067	7245 9470	arenite	LGF	-	-	x
8068	7245 9470	vein quartz	LGF	-	-	-
8069	7250 9455	arenite	LGF	x	-	-
8070	7260 9450	arenite	LGF	x	-	-

sample no.	location	rock type	Formation	Thin section	XRF bead	XRF pellet
8071	7255 9425	phyllite	LGF	-	-	-
8072	7215 9410	slate	LGF	-	x	x
8073	7125 9345	phyllite	LGF	-	-	x
8074	7175 9335	arenite	LGF	-	x	x
8075	7610 9835	phyllite	LGF	-	-	-
8076	7610 9640	phyllite	LGF	-	-	x
8077	7610 9645	phyllite	LGF	x	-	x
8078	7615 9855	phyllite	LGF	-	-	x
8079	7645 9860	phyllite	LGF	-	-	x
8080	7645 9860	qtz schist	CLCF	-	x	x
8081	7665 9860	qtz schist	CLCF	x	x	x
8082	7485 9700	metabasite	PMF	x	x	x
8083	7630 9910	qtz schist	CLCF	x	x	x
8084	7640 9900	qtz schist	CLCF	-	x	x
8085	7670 9860	qtz schist	CLCF	-	-	-
8086	7675 9855	qtz schist	CLCF	-	x	x
8087	7685 9855	qtz schist	CLCF	x	-	-
8088	7155 9325	arenite	LGF	-	-	x
8089	7915 9310	arenite	LGF	-	x	x
8090	7135 9275	arenite	LGF	-	-	x
8091	7115 9240	phyllite	LGF	x	-	x
8092	7110 9185	phyllite	LGF	-	-	x
8093	7105 9170	phyllite	LGF	x	x	x
8094	7080 9140	arenite	LGF	x	-	x
8095	7085 9085	phyllite	LGF	-	-	-
8096	7085 9070	arenite	LGF	-	-	x
8097	7085 9050	arenite	LGF	-	-	x
8098	7065 9015	phyllite	LGF	-	-	-
8099	7060 9000	arenite	LGF	-	-	x
8100	7015 8980	arenite	LGF	-	-	x
8101	7000 8940	arenite	LGF	-	-	x
8102	7000 8940	phyllite	LGF	-	-	-
8103	7000 8935	phyllite	LGF	-	x	x
8104	7015 8880	phyllite	LGF	-	-	-
8105	7005 8830	arenite	LGF	x	x	x
8106	7005 8830	arenite	LGF	x	x	-
8107	7365 9645	metabasite	CLCF	x	x	x
8108	Paymogo	arenite	-	-	-	-
8109	6995 8625	qtz schist	CLCF	-	-	-
8110	6995 8625	qtz schist	CLCF	-	-	-
8111	6995 8625	qtz schist	CLCF	-	-	-
8112	6995 8625	qtz schist	CLCF	-	x	x
8113	6995 8625	phyllite	LGF	-	-	x
8114	7675 9990	granite	OMZ	-	x	x
8115	7665 9990	metabasite	OMZ	-	-	-
8116	7665 9985	metabasite	BAA	x	x	x
8117	7660 9980	acidic	BAA	x	-	x
8118	7660 9980	granite	BAA	x	-	x
8119	7650 9975	granite	BAA	x	-	-
8120	7650 9940	tuffaceous	CLCF	-	-	x
8121	7645 9965	granite	OMZ	x	-	x
8122	7295 0255	granite	OMZ	x	-	x
8123	7300 0250	metabasite	OMZ	-	-	x
8124	7275 0230	diorite	OMZ	x	x	x
8125	7275 0240	granite	OMZ	x	-	x
8127	7340 0660	arenite	OMZ	-	x	x
8128	7340 0660	granite	OMZ	-	-	x
8129	7645 9955	granite	OMZ	-	-	-
8130	7630 9915	amphibolite	BAA	x	-	-
8131	7635 9905	qtz schist	CLCF	-	-	-
8132	7630 9915	gabbro	BAA	-	-	-
8133	7630 9890	qtz schist	CLCF	-	x	x
8134	7630 9890	arenite	PCF	-	-	-
8135	7635 9885	phyllite	PCF	-	-	-
8136	7625 9865	tuffaceous	-	-	-	-
8137	7625 9855	arenite	LGF	-	x	-
8138	7615 9845	arenite	LGF	-	x	x
8139	7595 9825	slate	LGF	-	-	x
8140	7590 9820	tuff	LGF	x	-	x

sample no.	location	rock type	Formation	Thin section	XRF bead	XRF pellet
8141	7585 9815	arenite	LGF	-	-	-
8142	7540 9765	tuffaceous	LGF	-	-	-
8143	7475 9670	quartzite	CLCF	-	-	-
8144	7460 9660	metabasite	PMF	-	x	x
8145	7410 9690	metabasite	PMF	-	x	x
8146	7370 9660	mica-schist	CLCF	-	x	x
8147	7305 9630	arenite	LGF	-	-	x
8148	7005 9625	arenite	LGF	-	-	-
8149	7000 9620	phyllite	LGF	-	-	-
8150	7000 9620	arenite	LGF	x	-	-
8151	7290 9505	slate	LGF	x	x	x
8152	7285 9500	slate	LGF	-	-	x
8153	7280 9400	slate	LGF	-	-	-
8154	7275 9495	tuffaceous	LGF	x	-	x
8155	7265 9485	slate	LGF	-	x	x
8156	7255 9480	slate	LGF	-	x	x
8157	7250 9480	slate	LGF	-	-	-
8158	7260 9475	slate/phyllite	LGF	-	-	-
8159	7240 9480	slate	LGF	-	-	-
8160	7235 9480	phyllite	LGF	-	-	x
8161	7240 9475	arenite	LGF	-	-	-
8162	7440 9475	phyllite	LGF	-	-	x
8163	7246 9250	slate	LGF	-	x	x
8164	7450 9450	slate	LGF	-	-	-
8165	7260 9475	arenite	LGF	-	-	x
8166	7250 9450	slate	LGF	-	-	-
8167	7250 9450	slate	LGF	-	-	-
8168	7250 9445	slate	LGF	-	x	x
8169	7255 9435	slate	LGF	-	-	-
8170	7255 9425	slate	LGF	-	-	-
8171	7210 9410	tuffaceous	LGF	-	-	x
8172	7195 9410	slate	LGF	-	x	x
8173	7180 9390	slate	LGF	-	x	x
8174	7180 9390	tuffaceous	LGF	x	-	-
8175	7180 9390	tuffaceous	LGF	x	-	-
8176	7180 9390	arenite	LGF	x	-	-
8177	7180 9390	tuffaceous	LGF	x	-	-
8178	7190 9365	slate	LGF	-	x	-
8180	7190 9360	slate	LGF	-	x	x
8181	7145 9315	tuffaceous	LGF	x	x	x
8182	7145 9315	slate	LGF	-	-	-
8183	7145 9315	tuffaceous	LGF	-	-	x
8184	7155 9290	slate/psmte.	LGF	-	-	x
8185	7115 9290	slate	LGF	-	-	-
8186	7090 9135	slate	LGF	-	-	x
8187	7335 9630	quartzite	LGF	-	-	x
8188	7325 9620	arenite	LGF	-	-	-
8189	7320 9605	arenite	LGF	-	-	x
8190	7080 9080	phyllite	LGF	-	-	-
8191	7070 9030	slate	LGF	-	-	-
8192	7000 8725	quartzite	CLCF	x	-	x
8193	7005 8730	quartzite	CLCF	x	-	-
8194	7005 8830	arenite	LGF	-	-	x
8195	7035 8965	phyllite	LGF	x	-	-
8196	7000 8940	phyllite	LGF	-	-	-
8197	7145 9315	arenite	LGF	x	-	-
8198	7145 9315	arenite	LGF	x	-	-
8199	7145 9315	phyllite	LGF	x	x	x
8200	7145 9315	slate	LGF	-	x	x
8201	7640 9905	arenite	LGF	x	-	-

sample no.	location	rock type	Formation	Thin section	XRF bead	XRF pellet
9001	7680 9995	amphibolite	BAA	-	-	-
9002	7680 9995	amphibolite	BAA	-	-	-
9003	7680 9995	amphibolite	BAA	-	-	-
9004	7675 9990	amphibolite	BAA	x	-	-
9005	7675 9990	amphibolite	BAA	x	-	-
9006	7670 9980	amphibolite	BAA	-	-	-
9007	7665 9975	amphibolite	BAA	-	-	-
9008	7665 9970	amphibolite	BAA	-	-	-
9009	7665 9970	amphibolite	BAA	-	-	-
9010	7660 9975	amphibolite	BAA	-	-	-
9011	7665 9975	amphibolite	BAA	-	-	-
9012	7660 9970	amphibolite	BAA	-	-	-
9013	7655 9965	amphibolite	BAA	-	-	-
9014	7655 9970	amphibolite	BAA	-	-	-
9015	7655 9970	amphibolite	BAA	-	-	-
9016	7680 9995	granite	OMZ	-	-	-
9017	7680 9995	granite	OMZ	-	-	-
9018	7645 9950	amphibolite	BAA	-	-	-
9019	7645 9955	amphibolite	BAA	-	-	-
9020	7640 9950	amphibolite	BAA	-	-	-
9021	7640 9950	amphibolite	BAA	-	-	-
9022	7640 9945	amphibolite	BAA	-	-	-
9023	7640 9940	amphibolite	BAA	-	-	-
9024	7635 9935	amphibolite	BAA	-	-	-
9025	7635 9930	amphibolite	BAA	-	-	-
9026	7635 9925	amphibolite	BAA	-	-	-
9027	7635 9920	amphibolite	BAA	-	-	-
9028	7630 9915	amphibolite	BAA	-	-	-
9029	7630 9915	amphibolite	BAA	-	-	-
9030	7630 9910	amphibolite	BAA	-	-	-
9031	7630 9920	amphibolite	BAA	-	-	-
9032	7630 9920	amphibolite	BAA	-	-	-
9033	7495 9705	metabasite	PMF	x	-	-
9034	7505 9705	metabasite	PMF	x	x	x
9035	7490 9700	metabasite	PMF	x	-	-
9036	7490 9705	metabasite	PMF	x	x	x
9037	7490 9705	metabasite	PMF	x	-	-
9038	7465 9680	amphibolite	PMF	x	x	x
9039	7465 9680	metabasite	PMF	x	-	-
9040	7470 9685	metabasite	PMF	x	-	-
9041	7470 9680	metabasite	PMF	x	x	x
9042	7470 9680	metabasite	PMF	x	-	-
9043	7465 9680	metabasite	PMF	x	-	-
9044	7455 9675	metabasite	PMF	x	-	-
9045	7460 9680	metabasite	PMF	x	x	x
9046	7455 9680	metabasite	PMF	x	-	-
9047	7460 9690	metabasite	PMF	x	-	-
9048	7220 9875	metabasite	PMF	x	-	-
9049	7215 9875	metabasite	PMF	x	x	x
9050	7210 9890	metabasite	PMF	x	-	-
9051	7200 9910	metabasite	PMF	x	x	x
9052	7195 9910	metabasite	PMF	-	-	-
9053	7195 9915	metabasite	PMF	x	-	-
9054	7190 9910	metabasite	PMF	x	-	-
9055	7190 9910	metabasite	PMF	x	-	-
9056	7190 9915	metabasite	PMF	x	x	x
9057	7185 9895	metabasite	PMF	x	-	-
9058	-	pelite	Terena Fm.	-	-	-
9059	-	pelite	Terena Fm.	-	-	-
9060	8145 9705	mica-schist	CLCF	x	-	-
9061	8150 9705	mica-schist	CLCF	x	-	-
9062	7680 0015	metabasite	PMF	x	-	-
9063	8155 9725	metased	PMF	-	-	-
9064	8150 9700	mica-schist	PMF	-	-	-
9065	8125 9685	metabasite	PMF	-	-	-
9066	8125 9680	metabasite	PMF	-	-	-
9067	8120 9675	metabasite	PMF	x	-	-
9068	8105 9660	metabasite	PMF	x	-	-
9068a	8420 9685	metabasite	PMF	x	-	-
9069	8420 9685	amphibolite	PMF	x	x	x
9070	8415 9690	amphibolite	PMF	-	-	-

sample no.	location	rock type	Formation	Thin section	XRF bead	XRF pellet
9071	8430 9680	amphibolite	BAA	x	x	x
9072	8435 9665	amphibolite	BAA	x	-	-
9073	8435 9665	amphibolite	BAA	-	-	-
9074	8435 9660	amphibolite	BAA	x	-	-
9075	8435 9660	amphibolite	BAA	x	x	x
9076	8430 9650	amphibolite	BAA	x	-	-
9077	8430 9645	amphibolite	BAA	x	x	x
9078	8430 9645	amphibolite	BAA	-	-	-
9079	8430 9640	amphibolite	BAA	x	-	-
9080	8165 9735	amphibolite	BAA	x	x	x
9081	7375 9670	mica-schist	CLCF	-	-	-
9082	7365 9655	mica-schist	CLCF	-	-	-
9083	7365 9655	mica-schist	CLCF	-	-	-
9084	7360 9645	mica-schist	CLCF	-	-	-
9085	7355 9640	mica-schist	CLCF	x	-	-
9086	7355 9640	amphibolite	CLCF	x	-	x
9087	7350 9640	mica-schist	CLCF	x	-	-
9088	7350 9645	quartzite	CLCF	x	-	-
9089	7345 9640	amphibolite	CLCF	-	-	-
9090	7340 9635	mica-schist	CLCF	-	-	-
9091	7340 9630	mica-schist	CLCF	-	-	-
9092	7390 9695	metabasite	CLCF	x	x	x
9093	7390 9690	amphibolite	CLCF	x	-	-
9094	7385 9685	mica-schist	CLCF	-	-	-
9095	7425 9735	amphibolite	PMF	x	x	x
9096	7425 9730	metabasite	PMF	x	-	-
9097	7430 9735	metabasite	PMF	x	x	x
9098	7430 9735	metabasite	PMF	x	-	-
9099	7425 9735	quartzite	PMF	x	-	-
9100	7425 9730	metabasite	PMF	-	-	-
9102	7495 9705	metabasite	PMF	x	-	-
9103	7495 9705	quartzite	PMF	x	-	-
9104	7490 9685	amphibolite	PMF	x	x	x
9105	7330 9620	mica-schist	CLCF	-	-	-
9106	7335 9625	mica-schist	CLCF	-	-	-
9107	7325 9615	mica-schist	CLCF	-	-	-
9108	7315 9605	mica-schist	CLCF	-	-	-
9109	7315 9595	mica-schist	CLCF	-	-	-
9110	7315 9595	mica-schist	CLCF	-	-	-
9111	7315 9590	mica-schist	CLCF	-	-	-
9112	7315 9585	mica-schist	CLCF	-	-	-
9113	7315 9585	mica-schist	CLCF	-	-	-
9114	7315 9580	mica-schist	CLCF	-	-	-
9115	7315 9555	slate	LGF	-	-	-
9116	7315 9550	slate	LGF	-	-	-
9117	7325 9615	quartzite	CLCF	x	-	-
9118	8155 9715	amphibolite	BAA	x	x	x
9119	8155 9685	metased	PMF	x	-	-
9120	8155 9680	metased	PMF	x	-	-
9121	8140 9685	metased	PMF	x	-	-
9122	7310 9545	mica-schist	CLCF	-	-	-
9123	7305 9540	mica-schist	CLCF	-	-	-
9124	7305 9535	slate	LGF	-	-	-
9125	7300 9530	slate	LGF	-	-	-
9125	7295 9520	slate	LGF	-	-	-
9126	7295 9520	slate	LGF	-	-	-
9127	7290 9520	slate	LGF	-	-	-
9128	7290 9515	slate	LGF	-	-	-
9129	7285 9505	slate	LGF	-	-	-
9130	7325 9515	slate	LGF	-	-	-
9131	7320 9505	slate	LGF	-	-	-
9132	7150 9330	slate	LGF	-	-	-
9133	7145 9325	slate	LGF	-	-	-
9134	7145 9320	slate	LGF	-	-	-
9135	7970 9780	fault rock	PMF	x	-	-
9136	7910 9730	mica-schist	CLCF	x	-	-
9137	8010 9730	amphibolite	PMF	-	-	-
9138	7930 9755	mica-schist	CLCF	x	-	-
9139	8080 9725	quartzite	CLCF	x	-	-
9140	7470 9670	metabasite	PMF	x	-	-

sample no.	location	rock type	Formation	Thin section	XRF bead	XRF pellet
9141	7475 9665	amphibolite	PMF	x	x	x
9142	7550 9635	metased	PMF	x	-	-
9143	7550 9635	amphibolite	PMF	x	x	x
9144	7550 9635	amphibolite	PMF	x	x	x
9145	7550 9635	amphibolite	PMF	x	-	-
9146	7550 9635	amphibolite	PMF	x	x	x
9147	7550 9635	amphibolite	PMF	x	-	-
9148	7550 9635	amphibolite	PMF	x	x	x
9149	7495 9705	amphibolite	PMF	x	-	-
9150	7495 9705	amphibolite	PMF	x	-	x
9151	7495 9705	amphibolite	PMF	x	-	-
9152	7520 9695	amphibolite	PMF	x	-	-
9153	7530 9690	amphibolite	PMF	x	-	-
9154	7525 9690	amphibolite	PMF	x	x	x
9155	7545 9665	amphibolite	PMF	x	-	-
9156	7495 9695	amphibolite	PMF	x	x	-
9157	0610 9325	metabasite	AF	x	x	x
9158	0640 9270	marble	AF	x	-	-
9159	0640 9270	marble	AF	x	-	-
9160	0640 9270	marble	AF	-	-	-
9161	0640 9270	marble	AF	x	-	-
9162	0640 9270	quartzite	AF	x	-	-
9163	0640 9270	quartzite	AF	-	-	-
9164	0640 9270	marble	AF	x	-	-
9165	0640 9270	quartzite	AF	x	-	-
9166	0640 9270	granite	Gil Marquez	x	-	-
9167	0610 9300	metased	PMF(?)	x	-	-
9168	0610 9300	chert	PMF(?)	x	-	-
9169	0610 9300	metased	PMF(?)	x	-	-
9170	0610 9300	metased	PMF(?)	x	-	-
9171	8435 9660	amphibolite	BAA(EH)	x	x	x
9172	8435 9660	amphibolite	BAA(EH)	x	-	-
9173	8435 9660	amphibolite	BAA(EH)	x	x	x
9174	8435 9660	amphibolite	BAA(EH)	x	-	-
9175	8435 9660	amphibolite	BAA(EH)	x	x	x
9176	8435 9660	amphibolite	BAA(EH)	x	x	x
9177	8435 9660	amphibolite	BAA(EH)	x	-	-
9178	8435 9660	amphibolite	BAA(EH)	x	x	x
9179	8435 9660	amphibolite	BAA(EH)	x	-	-
9180	8435 9660	amphibolite	BAA(EH)	x	x	x
9181	8435 9660	amphibolite	BAA(EH)	x	-	-
9182	8435 9660	amphibolite	BAA(EH)	x	-	-
9183	8435 9660	amphibolite	BAA(EH)	x	x	x
9184	8435 9660	amphibolite	BAA(EH)	x	-	-
9185	8435 9660	amphibolite	BAA(EH)	x	-	-
9186	8435 9660	amphibolite	BAA(EH)	x	x	x
9187	8435 9660	amphibolite	BAA(EH)	x	-	-
9188	8435 9660	amphibolite	BAA(EH)	x	x	x
9189	8435 9660	amphibolite	BAA(EH)	x	x	x
9190	8435 9660	amphibolite	BAA(EH)	x	-	-
9191	8435 9660	amphibolite	BAA(EH)	x	x	x
9192	8435 9660	amphibolite	BAA(EH)	x	-	-
9193	8435 9660	amphibolite	BAA(EH)	x	-	-
9194	8435 9660	amphibolite	BAA(EH)	x	x	x
9195	8435 9660	amphibolite	BAA(EH)	x	-	-
9196	8435 9660	amphibolite	BAA(EH)	x	x	x
9197	8435 9660	amphibolite	BAA(EH)	x	-	-
9198	8435 9660	amphibolite	BAA(EH)	x	-	-
9199	8435 9660	amphibolite	BAA(EH)	x	x	x
9200	8435 9660	amphibolite	BAA(EH)	x	x	x
9201	7790 9770	mica-schist	CLCF	x	-	-
9202	7730 9725	mica-schist	CLCF	-	-	-
9203	7655 9765	arenite	PCF	x	-	-
9204	7655 9765	arenite	PCF	x	-	-
9205	7700 9760	arenite	PCF	x	-	-
9206	7695 9755	arenite	PCF	x	-	-
9207	7640 9770	arenite	PCF	-	-	-
9208	0420 9265	quartzite	AF	x	-	-
9209	0420 9265	quartzite	AF	x	-	-
9210	0425 9235	quartzite	AF	x	-	-

sample no.	location	rock type	Formation	Thin section	XRF bead	XRF pellet
9211	0425 9230	quartzite	AF	x	-	-
9212	0425 9230	quartzite	AF	x	-	-
9213	0425 9225	quartzite	AF	x	-	-
9214	0425 9220	quartzite	AF	x	-	-
9215	0430 9220	quartzite	AF	x	-	-
9216	0430 9220	quartzite	AF	-	-	-
9217	0420 9275	serpentinite	AF	-	-	-
9218	8130 9670	metased	PMF	x	-	-
9219	8130 9660	metased	PMF	x	-	-
9220	8105 9660	amphibolite	PMF	x	-	-
9221	8110 9660	amphibolite	PMF	x	x	x
9222	8105 9665	amphibolite	PMF	x	x	x
9223	8105 9665	amphibolite	PMF	x	-	-
9224	8105 9660	amphibolite	PMF	x	x	x
9225	8110 9665	amphibolite	PMF	x	-	-
9225	8110 9665	amphibolite	PMF	x	-	-
9227	8105 9660	amphibolite	PMF	x	x	x
9228	8105 9660	amphibolite	PMF	x	x	x
9229	8105 9660	quartzite	PMF	x	-	-
9230	8095 9655	amphibolite	PMF	x	-	-
9231	8090 9650	amphibolite	PMF	x	x	x
9232	7955 9770	amphibolite	PMF	x	-	-
9233	7955 9770	amphibolite	PMF	x	x	x
9234	7955 9770	metased	PMF	x	-	-
9235	7955 9770	amphibolite	PMF	x	x	x
9236	7955 9770	amphibolite	PMF	x	-	-
9237	7945 9775	amphibolite	PMF	x	x	x
9238	7945 9775	amphibolite	PMF	x	-	-
9239	7945 9775	metased	PMF	x	-	-
9240	7920 9760	amphibolite	PMF	x	x	x
9241	7915 9745	amphibolite	PMF	x	-	-
9242	7905 9740	metagabbro	PMF	-	-	-
9243	8025 9720	amphibolite	PMF	x	x	x
9244	8070 9710	mica schist	CLCF	x	-	-
9245	8075 9695	mica schist	CLCF	x	x	x
9246	8070 9720	mica schist	CLCF	x	-	-
9247	7770 9910	metabasic	Puerto Cañon	-	-	-
9248	7770 9910	metabasic	Puerto Cañon	x	-	-
9249	7770 9910	metabasic	Puerto Cañon	-	-	-
9250	7770 9910	metabasic	Puerto Cañon	-	-	-
9251	7755 9905	granite	Puerto Cañon	x	-	-
9252	7920 9720	mica-schist	CLCF	x	-	-
9253	7915 9725	mica-schist	CLCF	x	-	-
9254	7915 9720	mica-schist	CLCF	x	-	x
9255	7755 9905	amphibolite	Puerto Cañon	x	x	x
9256	7755 9905	granite	Puerto Cañon	x	-	-
9257	7755 9905	amphibolite	Puerto Cañon	x	x	-
9258	7755 9905	granite	Puerto Cañon	x	-	-
9259	7755 9905	metabasite	Puerto Cañon	x	-	-
9260	7755 9905	amphibolite	PMF	x	-	-
9261	7450 9675	amphibolite	PMF	x	-	-
9262	7470 9685	mica-schist	CLCF	x	-	-
9263	7505 9705	mica-schist	CLCF		-	-
9264	7175 9890	amphibolite	PMF	x	-	-
9265	7180 9895	amphibolite	PMF	x	-	-

Appendix 2 XRF preparation and results

X-ray fluorescence spectrometry played an important role in this study as representative samples of many differing lithologies were analysed for both major and trace elements. The laboratory preparation and analysis was carried out at Southampton University under the guidance of Dr. Ian Croudace.

A.2.1 Preparation

Hand samples weighing approximately 1kg were firstly washed then cut using a diamond saw to remove weathered surfaces. They were then passed through a jaw crusher which reduced each sample to grit sized fragments. Subsequent milling in a tungsten carbide Tema mill for ≈8 minutes reduced them to a fine powder which was separated into splits for the analysis of trace elements, as compressed powder pellets, as well as for major elements, as fused glass beads.

For the preparation of pressed powder briquettes approximately 10 grams of rock powder is placed in a plastic tube and an aqueous binder consisting of a 7% w/v solution of polyvinyl alcohol. The resultant mixture is tipped into a clean pellet die and pressed to around 12 tonnes. Once compressed the pellets were dried in a low temperature oven at ≈80°C.

Element	Line	Detection Limit (ppm)
Sb	Sb Kα	3
Sn	Sn Kα	5
Mo	Mo Kα	2
Nb	Nb Kα	2
Zr	Zr Kα	2
Y	Y Kα	2
Sr	Sr Kα	2
Rb	Rb Kα	2
U	U Lα	4
Th	Th Lα	3
Bi	Bi Lα	3
As	As Kβ	5
Pb	Pb Lβ	3
Ga	Ga Kα	1
Zn	Zn Kα	1
W	W Lβ	5
Cu	Cu Kα	2
Ni	Ni Kα	2
Cr	Cr Kα	3
V	V Kα	4
Ce	Ce Lβ	8
La	La Lα	5
Ba	Ba Lβ	8

Table A.2.1 Detection limits for routine measuring.

Fused glass beads were prepared as follows:

(a) the separated rock powder was dried at 110°C and cooled in a desiccator.

(b) 5g of powder was placed in a silica crucible and ignited for 1-2 hours at 1000°C.

(c) upon cooling the resultant mass reduction was noted and loss-on-ignition (LOI) calculated.

(d) 0.8g of powder was then mixed with 4g ®Spectroflux 100B, a mixture of 4:1 lithium metaborate and di-lithium tetraborate.

(e) fusion of the glass bead occurred at 1100°C for 10 minutes and the molten liquid was cast into a platinum mould for cooling assisted by a jet of air.

Samples were analysed by a PW 1400 X-ray Spectrometer with 3kW Rhodium Anode, using an 80 second count time. The theoretical detection limits for the trace elements are given in table

A.2.1 and demonstrate that all the elements analysed were above the detection limits.

A.2.2 Results

The results of XRF analysis are presented on the following pages. Several rock types were analysed for both major and trace elements and the samples are grouped according to lithology and hence formation. Results for the analysis of beads are shown as wieght % oxides for the major elements and as ppm for trace elements as determined from pressed powder pellets. The major elements have been corrected for LOI.

Some of the samples from the Beja-Acebuches Amphibolites collected at El Hurón were taken from loose blocks contained within the walls of the derelict buildings as these were very fresh.

Rock type	tuff	phyllite	arenite	arenite	arenite	slate	slate	slate	slate	slate	slate	slate	slate
SAMPLE	8074	8089	8093	8105	8137	8072	8155	8156	8163	8168	8172	8173	8178
SiO2	74.77	76.26	91.81	84.63	77.42	61.60	55.51	54.56	56.32	55.25	57.75	53.39	63.59
TiO2	0.69	0.82	0.33	0.35	0.59	1.09	1.11	1.21	1.05	1.03	1.02	1.07	0.88
Al2O3	11.74	14.77	3.48	3.48	9.85	22.07	27.56	29.08	24.92	25.36	23.03	25.75	18.62
Fe2O3	5.97	4.94	1.95	7.60	5.63	4.46	3.33	2.51	5.29	6.16	6.49	6.67	6.19
MnO	0.10	0.03	0.01	0.07	0.15	0.03	0.01	0.01	0.03	0.01	0.11	0.05	0.11
MgO	1.08	0.70	0.08	0.60	1.03	0.86	0.43	0.46	0.85	0.42	1.47	1.45	1.24
CaO	0.06	0.04	0.04	0.05	0.61	0.04	0.05	0.05	0.05	0.04	0.04	0.05	0.10
Na2O	0.60	0.08	0.03	0.04	0.45	0.29	0.56	0.64	0.49	0.41	0.53	0.34	0.75
K2O	1.97	0.61	0.59	0.01	0.22	4.85	6.09	6.34	5.46	5.59	5.33	5.74	3.91
P2O5	0.08	0.02	0.02	0.11	0.02	0.01	0.02	0.02	0.08	0.12	0.09	0.10	0.11
SUM	97.05	98.28	98.34	96.93	95.97	95.30	94.67	94.88	94.52	94.40	95.85	94.60	95.51
Na2O+K2O	2.57	0.69	0.62	0.05	0.67	5.14	6.65	6.98	5.95	6.00	5.86	6.09	4.66
Rb	109.4	52	46.2	0.7	15.8	13.9	264.5	282.6	243.7	245.6	220.6	239.9	-
Sr	65	24.7	22.4	2.9	43.4	114	163.2	156.3	127.1	111.2	82	107.8	-
Y	26.5	29.4	24.8	17	44.7	26.6	36.4	38.9	34.3	34.2	34.8	38.8	-
Zr	278.1	494.8	526.2	366.1	320.7	240.7	173.6	190.4	164.2	151.9	187.9	189	-
Nb	15.7	12.4	12.4	8.3	11.6	12.2	22.1	24.8	21.7	21	21.8	22	-
Th	11.7	9.1	8.6	4.1	9.2	9.5	20.7	20.9	19.5	19.2	16.6	18.1	-
U	1.9	2.8	3.1	1.9	2.2	1.1	3.7	3.7	2.4	2.7	3.7	3.2	-
Pb	17.1	7.1	9.6	4.5	13.8	14.9	28.2	25.9	21.2	30.4	29.5	117.3	-
Zn	67.8	34.4	25.5	59.8	61.8	64.7	32.6	23.6	131.3	61.6	119.2	135.7	-
Ni	51.3	28.1	35.8	39.4	74.8	36.4	16.7	23.4	50.4	41.7	43.1	90.4	-
Ga	18.4	8.9	8.8	5.4	13.1	13.5	35.8	36.7	32.6	33.3	30.1	34.7	-
Cr	72.4	122.7	40.6	55.2	91.8	118.9	148.4	160.7	133.5	136.1	121.6	145.3	-
V	82.8	100.3	32.8	52	52.9	167.8	233.8	273.5	218.2	224.4	180.6	219.4	-
Ba	410.6	513.9	117.2	217.9	133.1	855.8	975.8	1106.7	895.5	883.8	893.4	986.1	-
La	27.7	43	11.6	23.7	81.1	37.3	61.2	57.1	62.2	61.4	38.4	58.8	-
Ce	48.9	77.6	25.4	46.6	126.2	75.5	100.5	96.7	110.7	121.3	74.7	115.3	-
Ti	5556.24	6673.6	2809.76	4137.44	4811.04	9345.12	9637.04	10687.28	8853.6	8503.52	8197.44	9117.52	-
K	16404.52	5091.65	4914.97	80.48	1830.28	40455.38	50776.87	52815.22	45471.68	46606.65	44407.11	47866.26	32625.00
K/Rb	149.95	97.92	106.38	114.98	115.84	-	191.97	186.89	186.59	189.77	201.30	199.53	-
Cr/Nb	4.61	9.90	3.27	6.65	7.91	9.75	6.71	6.48	6.15	6.48	5.58	6.60	-
Ni/Nb	3.27	2.27	2.89	4.75	6.45	2.98	0.76	0.94	2.32	1.99	1.98	4.11	-

ROCK TYPE	slate	slate	phyllite	phyllite	phyllite	phyllite	schist	schist	schist	schist	pelite	schist	schist
SAMPLE	8180	8200	8103	8181	8199	8138	8006	8008	8012	8014	8032	8080	8081
SiO2	53.72	50.58	87.04	74.76	73.56	61.29	74.04	68.54	74.54	56.26	60.80	53.90	74.27
TiO2	0.98	0.99	0.50	0.69	0.69	1.11	0.59	0.66	0.77	0.93	0.87	0.96	0.71
Al2O3	24.30	24.21	5.52	11.02	11.98	20.93	11.96	15.31	12.41	18.86	20.05	23.77	12.81
Fe2O3	7.61	11.11	3.45	5.85	5.96	10.91	5.67	4.83	4.48	8.41	8.88	7.88	4.81
MnO	0.09	0.18	0.01	0.05	0.10	0.17	0.14	0.05	0.10	0.12	0.15	0.15	0.09
MgO	1.50	1.95	0.21	0.95	1.11	0.16	1.11	1.32	1.20	3.46	1.71	1.64	1.07
CaO	0.05	0.04	0.04	0.05	0.09	0.27	0.15	0.06	0.21	1.20	0.18	0.15	0.20
Na2O	0.36	0.29	0.12	1.02	0.71	0.35	1.86	0.43	1.10	2.08	0.37	0.63	0.51
K2O	5.36	4.76	0.93	1.66	2.00	1.90	1.57	3.09	2.08	2.89	3.61	5.19	2.76
P2O5	0.18	0.19	0.03	0.11	0.10	0.15	0.09	0.07	0.08	0.12	0.10	0.09	0.08
SUM	94.14	94.31	97.85	96.14	96.30	97.24	97.16	94.36	96.96	94.34	96.72	94.36	97.32
Na2O+K2O	5.72	5.05	1.04	2.67	2.72	2.25	3.43	3.52	3.18	4.97	3.98	5.82	3.27
Rb	223.5	191.9	40.5	70.1	80.9	92.4	62	149.7	96.9	112.3	182.2	78.9	107.8
Sr	98.8	74	20.9	51.1	48.5	78.6	56.2	60.2	61.7	104.2	94.5	49.3	54.4
Y	37.4	36.9	27.7	29.5	30.1	49.4	20.3	18.5	27.4	33	33	30.8	30.2
Zr	184.4	163.9	573.3	389.7	336.6	252.9	226.6	146.2	271.9	160.6	163.1	420	328.8
Nb	21.5	20.6	12	14.4	16.5	22.6	14.3	14.7	16.4	16.5	17.7	15.4	17
Th	18.4	19.6	7.7	10.5	9.9	18.5	8.6	8.7	9.6	12.1	12.9	9.9	12.1
U	5	3.7	3.4	4.4	3.8	4.7	2.8	2.7	1.8	3	2.8	1.5	2.1
Pb	33.7	10.5	10.4	20.3	12.6	14	10.3	18.1	10.5	8.4	24.8	12.6	15.3
Zn	122.6	128.3	28	87.8	94.5	123.5	70.3	59.8	65	97.4	116.3	58	68.2
Ni	48.4	81.2	13.4	43	57.9	59.6	20.3	22.7	46.9	74.2	72.4	43.9	44.2
Ga	33	30.6	7.8	13.7	16.3	26.1	14.4	22	16.9	25.5	27	13.9	17.5
Cr	119.6	122.8	47.7	61.4	69.2	138.2	61.5	104.2	73.3	139.1	246.4	127.9	75.9
V	190.4	190.1	50.7	75.7	79.9	125.7	73.5	143.7	80	258.9	150.7	195.9	85.5
Ba	935.7	846.7	192.2	341.3	379.6	294.5	300.7	445.3	385.7	406.9	613.9	914.8	537.2
La	48.8	50.8	58.5	33.8	29.2	66.2	18.9	11.5	28.5	37.5	44.5	42.6	32.9
Ce	105.8	112.9	65.9	72.9	56.7	116.5	38.2	25.6	60.7	79.4	78.7	92.8	56.7
Ti	8226.56	8012.32	3635.92	5518.16	5428.72	8764.32	5305.68	5985.92	6101.68	6497.04	7413.76	8116.72	6186.32
K	44671.09	39629.91	7717.54	13809.07	16702.00	15833.95	13111.89	25730.72	17339.17	24047.53	30112.72	43210.47	23008.13
K/Rb	199.87	206.51	190.56	196.99	206.45	171.36	211.48	171.88	178.94	214.14	165.27	547.66	213.43
Cr/Nb	5.56	5.96	3.98	4.26	4.19	6.12	4.30	7.09	4.47	8.43	13.92	8.31	4.46
Ni/Nb	2.25	3.94	1.12	2.99	3.51	2.64	1.42	1.54	2.86	4.50	4.09	2.85	2.60

ROCK TYPE	schist	schist	schist	metabas	schist	schist	schist	schist	schist	PMF	PMF	PMF	PMF
SAMPLE	8083	8084	8086	8107	8112	8133	8146	9092	9245	8021	8082	8144	8145
SiO2	57.71	71.99	85.97	51.05	82.44	77.92	64.68	48.8	48.21	47.47	48.54	49.83	50.06
TiO2	1.04	0.80	0.57	1.83	0.57	0.71	1.06	1.94	1.54	1.32	1.66	1.60	1.41
Al2O3	23.41	13.80	7.23	15.6	8.31	11.33	22.27	18.03	15.7	14.07	13.37	14.46	14.45
Fe2O3	7.77	5.40	2.43	11.37	3.65	3.93	5.26	14.04	11.5	10.61	12.60	12.18	11.17
MnO	0.10	0.14	0.05	0.2	0.03	0.06	0.03	0.18	0.18	0.18	0.20	0.20	0.17
MgO	1.44	1.14	0.55	6.62	0.73	0.64	0.91	6.8	6.72	8.31	9.47	7.07	8.20
CaO	0.29	0.23	0.10	10.32	0.06	0.05	0.08	10.29	11.79	12.02	8.00	9.87	7.94
Na2O	0.52	0.78	0.20	2.46	0.80	0.29	0.74	3.08	2.61	1.92	0.93	1.58	3.10
K2O	3.13	2.38	1.32	0.06	1.24	2.29	4.22	0.14	0.22	0.27	0.67	0.04	0.17
P2O5	0.09	0.06	0.04	0.21	0.04	0.06	0.05	0.22	0.13	0.10	0.15	0.11	0.11
SUM	95.53	96.72	98.44	99.72	97.87	97.27	99.30	103.52	98.60	96.28	95.60	96.94	96.78
Na2O+K2O	3.66	3.16	1.52	2.52	2.04	2.58	4.96	3.22	2.83	2.20	1.60	1.62	3.28
Rb	104.5	67.4	27.7	2.6	55.6	92.8	193.1	2.5	2.2	5.9	72.2	0	2.9
Sr	54.2	35	17.9	182.6	30.7	35.8	137.7	261	166.3	149.2	39.8	127.1	103.7
Y	31.2	31.5	14.5	44.2	26	36.9	32.1	35.8	34.8	33.5	27	39.4	35.6
Zr	295.6	690.9	290.7	148.9	339.9	408.5	197.2	160.6	143.3	82.6	343.9	103.9	89.5
Nb	17.8	13.8	8.6	6.6	12.5	14.6	20.6	6.5	6.5	4.3	13.3	5.3	4.8
Th	12	10.3	4.4	0.6	8.2	11.3	15.3	-	-	0.9	8.7	0.6	-
U	4.4	4.6	2.8	1.5	3.2	4.2	1.7	-	-	0.8	3.2	1	-
Pb	25.6	15	4.3	6.3	8.2	18.1	27.6	4.1	1.6	3.1	5.9	1.1	2.2
Zn	72.2	13.4	8	97.1	50.2	134.6	96.4	66.7	81	84.9	49.9	89.7	84.5
Ni	48.6	24.6	16.6	37.8	36.4	29.2	21.4	30.8	66.3	86.8	33.8	82.5	87.6
Ga	18.1	10.8	5.7	17.6	11.2	14.5	28.2	19.3	19	17.4	12.5	18.8	15.9
Cr	124.4	86.2	56.1	59.4	53.4	77.7	131.1	251.5	245.9	309.8	177.8	199.3	328.6
V	169.9	97.1	59.5	57.8	51.1	76.7	198.3	277.7	303	329.1	385.2	347.2	343.7
Ba	480.2	386.8	268.7	202.5	189.1	464.5	551.6	39	51.6	32.5	92.1	18.4	47
La	48.2	26.9	25.9	17.7	14.1	43.3	51.6	7.7	2.3	2.5	6.6	7.5	3.8
Ce	103.9	48.6	46.2	48.2	18.3	73.7	82.4	35.5	18.6	5.7	23.2	15.6	7.1
Ti	8884.56	6664.24	5019.04	4821.5	3948.08	6006.32	8752.72	17165.1	15668.5	11017.12	13204.64	12414.80	11359.52
K	26108.42	19848.92	11007.83	-	10346.40	19059.72	33801.10	-	-	2256.83	5558.73	325.11	1453.49
K/Rb	249.84	294.49	397.39	-	186.09	205.38	175.04	-	-	204.130483	382.51	-	-
Cr/Nb	6.99	6.25	6.52	-	4.27	5.32	6.36	-	-	72.05	13.37	37.60	68.46
Ni/Nb	2.73	1.78	1.93	-	2.91	2.00	1.04	-	-	20.19	2.54	15.57	18.25

ROCK TYPE	PMF	PMF	PMF	PMF	PMF	PMF	PMF	PMF	PMF	PMF	PMF	PMF	PMF
SAMPLE	9034	9036	9038	9041	9045	9049	9051	9056	9069	9086	9092	9095	9097
SiO2	48.02	50.14	48.7	48.96	49.2	48.74	48.36	49.4	49.29	49.35	48.8	45.63	55.41
TiO2	1.54	1.62	1.68	1.47	1.43	1.6	1.69	1.45	1.51	1.32	1.94	1.71	1.17
Al2O3	15.16	14.94	15.33	15.07	15.01	15.17	15.21	15.32	15.63	17.98	18.03	15.86	13.23
Fe2O3	12.28	11.02	11.84	11.08	11.02	12.34	12.44	11.49	10.93	10.22	14.04	13.01	8.4
MnO	0.22	0.18	0.21	0.2	0.19	0.19	0.22	0.2	0.18	0.18	0.18	0.21	0.15
MgO	8.73	7.77	9.02	7.82	8.19	7.79	7.93	7.68	8.47	8.17	6.8	8.42	4.34
CaO	10.57	10.61	9.75	12.16	11.51	11.83	10.22	10.55	11.24	10.05	10.29	12.43	15.22
Na2O	2.73	2.93	2.59	2.47	2.48	1.59	2.82	2.98	2.51	1.88	3.08	1.67	1.39
K2O	0.12	0.21	0.27	0.27	0.16	0.12	0.2	0.16	0.1	0.05	0.14	0.24	0.2
P2O5	0.12	0.15	0.16	0.13	0.11	0.13	0.13	0.11	0.14	0.1	0.22	0.12	0.13
SUM	99.49	99.57	99.55	99.63	99.30	99.50	99.22	99.34	100.00	99.30	103.52	99.30	99.64
Na2O+K2O	2.85	3.14	2.86	2.74	2.64	1.71	3.02	3.14	2.56	1.93	3.22	1.91	1.59
Rb	1.2	11.2	14.2	12.3	2.8	3.9	1.9	1.7	0.4	2.2	2.5	4.1	5.2
Sr	129.7	132	106.7	213	159.1	175.2	138.9	225.9	176.4	188	261	204.5	155.2
Y	37.6	38.4	36.2	34.8	33	37.7	41	34	34.9	26.9	35.8	41.5	27.7
Zr	93.5	100.2	109	88.9	84.6	97.6	108.8	87.6	107.9	87.8	160.6	97.2	74.1
Nb	5.2	4.9	7.1	5.1	4	5.4	5.2	4.7	5.3	4.5	6.5	5.2	5.1
Th	-	-	-	-	-	-	-	-	-	-	-	-	-
U	-	-	-	-	-	-	-	-	-	-	-	-	-
Pb	2.3	2.4	3	3.5	2.3	3.6	1.1	3.3	3.1	10.3	4.1	2.5	4.4
Zn	100.7	95.2	99.1	92.1	86.4	88.4	90.2	83.6	61.7	78.1	66.7	93.9	95.1
Ni	71	65.5	80.1	74.8	79.8	78.6	75.5	72.4	109.9	85.8	30.8	77.1	72.1
Ga	16.2	17.3	15.9	20.4	17.5	17.6	19.3	18.5	17.4	18.2	19.3	20.5	24.9
Cr	206.8	172	325.2	308.6	288.2	198.5	291	219.2	312.7	231.6	251.5	226.8	182.5
V	355.9	350.1	367	338	332.7	355.7	385.9	355	289.8	222.2	277.7	367.6	277.5
Ba	37.6	19.9	34	35.7	17.1	30.5	23.6	5.7	50.1	11.9	39	34.7	16.7
La	5.9	6.2	5.4	3.8	1.9	3.6	7.4	6.7	4.9	5.7	7.7	4.9	2.1
Ce	11.9	17.5	20.5	14.7	21.4	22.4	28.4	16.9	27.8	24.9	35.5	22.1	13.1
Ti	11900.16	12570.16	13327.36	11300.32	10929.76	11320.56	13004.32	10917.92	14328.6	10062.08	13732.08	13231.52	9982.80
K	1000.00	1750.00	2250.00	2250.00	1333.33	1000.00	1666.67	1333.33	-	416.67	1166.67	2000.00	1666.67
K/Rb	501.20	833.33	156.25	158.45	182.93	476.19	256.41	877.19	-	314.37	189.39	466.67	487.80
Cr/Nb	39.77	35.10	45.80	60.51	72.05	36.76	55.96	46.64	-	51.47	38.69	43.62	35.78
Ni/Nb	13.65	13.37	11.28	14.67	19.95	14.56	14.52	15.40	-	19.07	4.74	14.83	14.14

ROCK TYPE	amph	amph	amph	amph	amph	amph	amph	amph	amph	amph	amph	amph	amph
SAMPLE	7004	7006	7009	7045	7047	7048	8041	9071	9075	9077	9080	9118	9171
SiO2	49.44	48.79	51.96	45.21	50.75	48.01	45.37	51.14	49.92	54.42	50.98	49.4	49.77
TiO2	1.70	1.16	1.81	0.31	2.29	2.61	0.40	1.39	1.18	2.47	1.55	2.32	1.35
Al2O3	15.22	19.40	14.69	19.00	14.90	15.87	13.36	16.82	16.91	16.52	16.2	14.82	16.07
Fe2O3	11.18	8.47	12.31	6.52	9.21	14.36	8.25	9.47	9.36	10.68	10.21	13.63	9.7
MnO	0.19	0.15	0.19	0.13	0.16	0.30	0.15	0.16	0.14	0.16	0.2	0.25	0.16
MgO	6.76	6.50	1.47	9.47	6.49	5.52	10.57	6.85	7.6	4.8	6.98	6	8.19
CaO	10.62	10.37	10.02	14.31	9.97	6.05	8.89	9.23	10.88	4.17	8.39	9.05	11.59
Na2O	2.96	2.94	3.51	0.88	3.39	4.40	10.94	4.14	3.15	5.87	4.07	3.79	2.79
K2O	0.25	0.31	0.21	1.18	0.91	0.88	0.42	0.12	0.37	0.07	0.63	0.25	0.1
P2O5	0.19	0.14	0.16	0.00	0.33	0.41	0.00	0.21	0.13	0.52	0.2	0.3	0.13
SUM	98.48	98.25	96.34	97.02	98.38	98.40	98.34	99.53	99.64	99.68	99.41	99.81	99.85
Na2O+K2O	3.20	3.26	3.72	2.06	4.29	5.27	11.36	4.26	3.52	5.94	4.70	4.04	2.89
Rb	7	8	5	38	29	32	18.8	1.6	14.1	0.5	16.7	1.5	0.7
Sr	178	288	155	267	259	260	239.4	196.3	250.5	101.8	248.4	147.4	212.4
Y	40	30	40	8	64	66	11.8	45.1	24.4	46.5	38.2	60.7	32.2
Zr	134	111	113	21	129	262	13.3	524.5	95.1	180.8	154.6	226.5	96.4
Nb	7	5	6	3	16	9	3.6	8	5	8.7	5.8	7.7	5.4
Th	4	3	3	2	4	4	0	-	-	-	-	-	-
U	0	3	1	1	1	2	0.7	-	-	-	-	-	-
Pb	2	5	5	2	2	6	1.2	0.9	1.6	7.2	23.8	2.6	2.7
Zn	81	69	155	48	66	139	57.6	47.3	24.4	152.7	105.2	94.4	46.6
Ni	76	109	76	281	56	37	167.9	93.9	92.7	12.8	38.8	51.5	91.7
Ga	18	16	18	12	18	25	13.4	20.7	17.2	22.7	18.7	22	18.6
Cr	186	293	263	237	95	73	28.6	226	267.6	31.7	184.6	119.4	318.7
V	312	194	338	112	222	486	40.5	238.1	247.3	324.9	278.5	374.1	272.8
Ba	71	105	61	86	203	206	929.8	35.8	90.8	80.3	135.1	78.5	41.7
La	9	6	4	3	14	16	42	9.6	6.9	18.6	12.1	15.3	10.1
Ce	12	34	2	13	31	25	82.6	34.6	18	41.1	32.3	42	19.6
Ti	13531.20	9761.60	13715.20	2634.40	17578.40	20381.60	7469.92	11134.64	8895.76	20499.84	13158.00	19744.96	9904.00
K	2053.35	2623.90	1778.73	9858.56	7569.03	7292.69	3467.00	1000.00	3083.33	583.33	5250.00	2083.33	833.33
K/Rb	320.51	293.34	327.99	355.75	259.44	261.00	227.90	-	625.00	218.68	784.31	588.24	-
Cr/Nb	26.57	58.60	43.83	79.00	5.94	8.11	7.94	28.25	53.52	3.64	31.83	15.51	59.02
Ni/Nb	10.86	21.80	12.67	93.67	3.50	4.11	46.64	11.74	18.54	1.47	6.69	6.69	16.98

ROCK TYPE	amph	amph	amph	amph	amph	amph	amph	amph	amph	amph	amph	amph	amph
SAMPLE	9173	9175	9176	9178	9180	9183	9186	9188	9189	9191	9194	9196	9199
SiO2	49.69	48.6	48.53	48.02	49.15	48.66	49.56	48.82	48.87	49.45	49.02	48.56	47.44
TiO2	1.04	1.69	1.67	1.86	1.3	1.36	1.29	1.24	1.85	1.06	2.18	1.21	1.64
Al2O3	17.54	16.17	15.36	15.01	16.59	16.34	16.65	15.96	15.83	16.69	15.16	16.51	16.86
Fe2O3	8.48	11.11	12.04	12.85	9.92	10.36	9.35	10.88	11.51	9.61	12.29	10.63	12.14
MnO	0.14	0.18	0.17	0.18	0.16	0.18	0.14	0.18	0.17	0.15	0.14	0.15	0.16
MgO	8.42	7.62	7.38	7.43	8.12	8.43	8.17	8.54	7.17	8.6	6.72	8.61	7.9
CaO	11.18	11.18	11.41	11.05	11.59	11.69	10.96	11.09	11.05	11.33	10.96	11.3	10.39
Na2O	2.88	2.79	2.85	2.92	2.8	2.51	3.11	2.72	2.99	2.66	2.88	2.6	2.96
K2O	0.21	0.15	0.17	0.19	0.07	0.13	0.29	0.11	0.14	0.09	0.13	0.09	0.07
P2O5	0.1	0.2	0.2	0.19	0.13	0.11	0.13	0.13	0.23	0.09	0.26	0.11	0.17
SUM	99.68	99.69	99.78	99.70	99.83	99.77	99.65	99.67	99.81	99.73	99.74	99.77	99.73
Na2O+K2O	3.09	2.94	3.02	3.11	2.87	2.64	3.40	2.83	3.13	2.75	3.01	2.69	3.03
Rb	7.6	0.9	2.8	3.1	0.9	0.9	10.7	0.9	2	0.5	1	0.3	0.4
Sr	224	193.1	184.5	192.8	204.3	179.3	227.4	194.2	187.4	190.1	216	178.5	170.1
Y	21.5	38.1	38.1	37.5	23.2	28.1	26.5	27.3	38.5	22.9	48.8	27	36
Zr	88.8	137.9	138.3	128.4	98.4	90.4	101	91.6	152.3	79.4	182.8	85.5	117.3
Nb	3.9	7.1	6.9	6.1	5.6	5.1	4.8	5.2	6.7	4.4	8.2	4.9	5.2
Th	-	-	-	-	-	-	-	-	-	-	-	-	-
U	-	-	-	-	-	-	-	-	-	-	-	-	-
Pb	2.8	1	1.6	2	2.8	0.9	0	3	2.6	1.9	2	1.7	1.5
Zn	45.8	85.7	44.6	46.1	56	73	42.2	42.7	36.5	39.8	25.8	39.8	35.3
Ni	125.9	81.8	62.1	47.1	98.8	108.8	108	89.2	50.7	125.6	56.9	117.6	76.9
Ga	16.5	19.9	18.5	18.7	18.3	17.4	16.3	17.6	20.1	16.6	20.6	17.7	16.8
Cr	268.9	182.2	142.6	100.8	260	291.4	277.8	288.8	128.4	320.8	126.7	322.5	234.6
V	198.9	311.4	335.8	356.2	242.8	258.7	238.9	271.9	339.8	232.9	376.2	257.9	324.2
Ba	45.8	46.6	33.1	41.6	9.6	59	51.2	43.6	60.6	45.4	54.4	39.1	17.2
La	5.4	9	6.3	9.3	4.7	5.7	9.9	5.8	10.5	5	13.8	3.9	7.9
Ce	19.6	24.8	26.9	25.2	21.4	17.9	23.6	8.5	22.9	12.6	39.9	14.5	25.5
Ti	8385.68	13300.96	12986.40	14516.16	9726.64	10696.72	9984.96	9758.56	14441.04	8473.84	17066.80	9516.72	12538.00
K	1750.00	1250.00	1416.67	1583.33	583.33	1083.33	2416.67	916.67	1166.67	750.00	1083.33	750.00	583.33
K/Rb	-	230.26	-	505.95	510.75	648.15	-	225.86	-	583.33	-	-	-
Cr/Nb	68.95	25.66	20.67	16.52	46.43	57.14	57.88	55.54	19.16	72.91	15.45	65.82	45.12
Ni/Nb	32.28	11.52	9.00	7.72	17.64	21.33	22.50	17.15	7.57	28.55	6.94	24.00	14.79

ROCK TYPE	amph	amph	amph	PMF	PMF	PMF	PMF	PMF	PMF	PMF	PMF	PMF	PMF
SAMPLE	9200	9255	9257	9104	9141	9143	9144	9146	9148	9154	9156	9224	9228
SiO2	52.04	58.28	50.05	48.77	49.93	49.9	48.96	65.97	52.16	50.72	48.46	48.39	48.35
TiO2	1.42	0.51	1.75	1.6	1.36	1.71	1.57	0.88	1.49	2.06	1.09	1.07	1.71
Al2O3	15.43	21.08	17.21	15.11	14.31	16.82	14.34	9.56	14.86	15.26	15.86	15.9	17.33
Fe2O3	9.55	4.87	11.37	11.21	10.82	10.6	12.78	6.68	10.79	12.2	10.18	9.54	11.24
MnO	0.15	0.1	0.18	0.19	0.19	0.18	0.2	0.14	0.17	0.23	0.17	0.19	0.21
MgO	6.65	4.64	5.94	8.31	7.87	6.87	7.42	4.69	8.17	5.67	8.65	7.05	6.85
CaO	10.24	9.17	9.71	11.77	12.97	9.31	11.33	10.77	8.17	9	12.91	14.25	12.26
Na2O	3.84	2.92	3.84	2.34	1.61	3.18	2.27	0.91	3.44	3.51	1.9	2.36	3.26
K2O	0.2	1.22	0.84	0.12	0.21	0.67	0.44	0.34	0.25	0.59	0.15	0.26	0.28
P2O5	0.16	0.06	0.18	0.12	0.11	0.2	0.12	0.06	0.11	0.24	0.07	0.08	0.16
SUM	99.68	102.85	101.07	99.54	99.38	99.44	99.43	100.00	99.61	99.48	99.44	99.09	101.65
Na2O+K2O	4.04	4.14	4.68	2.46	1.82	3.85	2.71	1.25	3.69	4.10	2.05	2.62	3.54
Rb	3.5	33.3	-	1.7	7.1	17.7	21.7	11.3	8.80	27.4	-	6.9	4.6
Sr	218.2	416.8	-	143.3	202	212.5	170.4	161.5	155.5	174.9	-	162.4	170.6
Y	38.2	7.5	-	37.4	33.3	37.2	36.9	32.6	43.1	49.5	-	25.1	36.6
Zr	115.7	16.2	-	96.6	82.5	155.4	93	79.6	92	166.7	-	68.8	120.1
Nb	7.2	4.2	-	4.8	4.7	6.1	4.8	4.8	5.6	8.3	-	4.1	5.1
Th	-	-	-	-	-	-	-	-	-	-	-	-	-
U	-	-	-	-	-	-	-	-	-	-	-	-	-
Pb	3	5.5	-	11.7	2.5	3.7	2.6	3.1	4.2	2.6	-	1.9	4.9
Zn	60.7	35.4	-	98.5	77.2	89.3	90.6	95.5	89.5	73.7	-	61.8	82.7
Ni	58.3	29.8	-	72.6	69.5	53	46.5	78.7	80.3	31.6	-	88.2	71.3
Ga	17.6	20	-	15.9	18	18.2	18	22.3	15.2	18.4	-	15.6	18.5
Cr	185	106.1	-	215.8	203	232.6	159.9	294.8	268.6	66.1	-	253.6	248.8
V	253.7	125.6	-	359	324.5	267	355	314.9	344.7	322.6	-	252.2	313.8
Ba	79.2	101.7	-	0	24.6	55.8	50.1	44.2	27.1	89.4	-	36.5	43.8
La	10.5	2.6	-	5.3	3.7	9.5	0	3.6	1.3	10.2	-	4.5	5
Ce	35.9	22.8	-	33.8	11.2	24.7	14.5	17.7	12.5	17.6	-	18	17.2
Ti	10827.28	4350	-	11583.68	10704.00	12599.84	11820.24	10671.60	11277.36	15422.32	-	11118.3	11559.3
K	1666.67	-	-	1000.00	1750.00	5583.33	3666.67	2833.33	2083.33	4916.67	1250.00	-	-
K/Rb	-	-	-	476.19	-	246.48	315.44	168.97	250.74	236.83	179.44	-	-
Cr/Nb	25.69	-	-	44.96	43.19	38.13	33.31	61.42	47.96	7.96	-	61.85	48.78
Ni/Nb	8.10	-	-	15.13	14.79	8.69	9.69	16.40	14.34	3.81	-	21.51	13.98

ROCK TYPE	PMF	PMF	PMF	PMF	PMF	PMF	AF
SAMPLE	9231	9233	9235	9237	9240	9243	9157
SiO2	50.52	49.07	49.07	49.77	48.82	48.76	48.55
TiO2	1.83	1.44	1.49	1.69	1.2	1.51	1.23
Al2O3	15.05	16.82	17.11	16.28	19.42	16.28	16.5
Fe2O3	11.9	9.78	9.78	10.31	8.46	10.49	9.98
MnO	0.19	0.18	0.16	0.17	0.17	0.17	0.16
MgO	6.23	8.13	7.59	6.33	7.07	7.08	8.44
CaO	9.71	9.33	9.82	10.14	11.13	11.22	12.34
Na2O	3.59	3.05	3.15	3.33	2.84	2.49	2.16
K2O	0.28	0.49	0.42	0.66	0.35	0.19	0.25
P2O5	0.22	0.16	0.16	0.19	0.1	0.12	0.1
SUM	99.52	98.45	98.75	98.87	99.56	98.31	99.71
Na2O+K2O	3.87	3.54	3.57	3.99	3.19	2.68	2.41
Rb	1.9	17.4	14.2	23.6	10.1	1.8	4.2
Sr	200	214.2	237	210.7	190.6	135.7	157.6
Y	50.7	33.5	35.9	39.1	28.8	34.8	27.5
Zr	201.3	134.3	136.4	157.9	101.1	106.1	85
Nb	7.5	5.4	5.4	6.1	5	5.6	4.1
Th	-	-	-	-	-	-	-
U	-	-	-	-	-	-	-
Pb	5.5	4.7	5.5	4.8	2.7	4.1	2.7
Zn	88.4	71.2	75.1	74.5	60.7	72.7	67.1
Ni	40.7	74.4	83.5	60.3	94.6	74	95.6
Ga	20.2	19.6	18.8	19.6	17.6	16.4	16.6
Cr	139.6	195.4	185.9	186.6	199.2	398.8	319.3
V	280.3	235.2	247.6	273.5	197.9	306.5	241.6
Ba	117.8	110	100.5	150.7	89.5	34.9	38.5
La	14.2	4.8	11.5	10.1	5.8	3.8	2.1
Ce	40.7	31.5	20.1	31.3	8.3	8	15.5
Ti	19293.2	14074.8	14868	17536.7	12125.8	15460.7	9957.68
K	-	-	-	-	-	-	2083.33
K/Rb	-	-	-	-	-	-	-
Cr/Nb	18.61	36.19	34.43	30.59	39.84	71.21	77.88
Ni/Nb	5.43	13.78	15.46	9.89	18.92	13.21	23.32

ROCK TYPE	slate	slate	slate	slate	gr Mina Fe	gr Mina Fe	gr Mina Fe	gr Alba.	gr Alba.	gr Alba.	gr Alba.	gr Alba.
SAMPLE	SSOO6	HAB-3	HAB-4	PAS	GFO-1	GFO-2	GFO-3	ALBALA-1	ALBALA-2	ALBALA-3	ALBALA-4	ALBALA-5
SiO2	61.11	60.92	59.64	62.8	74.33	73.45	73.95	70.39	72.41	73.34	72.14	70.74
TiO2	0.7	0.87	0.84	1	0.04	0.33	1.17	0.39	0.21	0.14	0.23	0.31
Al2O3	19.91	19.04	18.72	18.9	14.26	13.37	13.81	15.04	14.66	14.96	15.14	15.42
Fe2O3	6.04	6.95	7.31	6.5	1.3	2.29	1.58	2.83	1.67	1.12	1.85	2.23
MnO	0.26	0.08	0.08	0.11	0.28	0.04	0.04	0.05	0.04	0.01	0.05	0.04
MgO	2.97	2.83	2.98	2.2	0.14	0.47	0.28	0.66	0.46	0.27	0.45	0.59
CaO	0.49	0.31	0.61	1.3	0.48	1.28	0.67	1.16	0.73	0.56	0.78	1.1
Na2O	1.94	2.29	1.59	1.2	6.33	3.67	3.32	3.55	3.37	3.87	3.94	3.59
K2O	3.4	4.2	3.91	3.7	2.37	4.75	4.53	4.36	4.44	4.55	4.45	4.75
P2O5	0.09	0.14	0.16	0.16	0.55	0.23	0.26	0.32	0.32	0.45	0.31	0.28
SUM	96.91	97.63	95.84	97.87	100.08	99.88	99.61	98.75	98.31	99.27	99.34	99.05
Na2O+K2O	5.34	6.49	5.50	4.90	8.70	8.42	7.85	7.91	7.81	8.42	8.39	8.34
Rb	134	166	168	160	304	265	416	257	283	320	286	272
Sr	78	32	60	200	21	108	78	106	55	36	55	93
Y	28	36	38	27	1	26	12	19	9	2	10	12
Zr	140	208	200	210	27	144	70	174	94	66	99	138
Nb	14	14	14	19	16	13	16	15	13	12	13	13
Th	12	13	12	14	2	17	7	11	7	6	8	12
U	206	16	4	3.1	3	11	3	8	10	12	5	3
Pb	221	18	16	20	9	32	22	25	23	22	27	28
Zn	193	129	137	85	63	52	52	66	55	73	59	59
Ni	66	43	51	55	39	30	32	28	26	26	28	26
Ga	26	27	26	20	27	21	24	24	23	24	23	22
Cr	105	110	126	110	18	28	20	35	23	18	18	24
V	136	143	178	150	3	17	9	27	10	5	12	22
Ba	607	695	655	650	40	256	128	405	210	150	222	361
La	30.4	32.31	36.43	38	2.17	26.89	9.84	-	-	-	-	-
Ce	69	64.6	67	80	3.82	57.41	21.17	-	-	-	-	-
Ti	4191.62	5209.58	5029.94	5988.02	239.52	1976.05	7005.99	2335.33	1257.49	838.32	1377.25	1856.29
K	28333.33	35000.00	32583.33	30833.33	19750.00	39583.33	37750.00	36333.33	37000.00	37916.67	37083.33	39583.33
K/Rb	496.03	211.44	210.84	193.95	192.71	-	149.37	141.37	130.74	118.49	129.66	145.53
Cr/Nb	7.50	7.86	9.00	5.79	1.13	2.15	1.25	2.33	1.77	1.50	1.38	1.85
Ni/Nb	4.71	3.07	3.64	2.89	2.44	2.31	2.00	1.87	2.00	2.17	2.15	2.00

ROCK TYPE	metabasite	metabasite	metabasite	metabasite	metabasite	greenschist	greenschist	greenschist	greenschist	amphibolite	amphibolite	amphibolite	amphibolite
SAMPLE	PU-1	PU-2	PU-3	PU-4	PU-5	ACE-1	ACE-2	ACE-3	ACE-4	ACE-5	ACE-6	ACE-7	ACE-8
SiO2	49.27	49.68	49.27	49.69	48.62	49.51	49.00	51.11	53.79	48.05	57.09	50.37	49.35
TiO2	1.91	1.55	2.01	1.88	1.85	1.89	1.43	1.46	1.47	1.47	1.95	1.96	1.18
Al2O3	14.83	13.74	15.85	13.83	15.19	14.72	14.56	18.21	14.30	16.34	15.61	14.63	17.90
Fe2O3	11.79	12.04	11.26	12.85	11.57	11.94	11.40	8.84	10.11	10.15	10.21	12.19	9.14
MnO	0.19	0.20	0.19	0.20	0.17	0.19	0.48	0.37	0.49	0.70	0.13	0.38	0.62
MgO	7.21	7.03	6.66	7.17	6.87	6.22	6.75	4.83	5.76	8.02	3.39	6.72	6.26
CaO	11.09	12.67	10.55	11.51	11.29	10.74	13.05	10.73	9.09	11.50	5.46	9.63	11.80
Na2O	2.07	1.71	2.23	1.48	2.29	2.83	1.96	3.45	3.12	2.28	4.95	2.51	2.66
K2O	0.22	0.12	0.40	0.26	0.16	0.32	0.15	0.36	0.70	0.23	0.06	0.15	0.25
P2O5	0.21	0.13	0.23	0.17	0.22	0.18	0.13	0.19	0.15	0.16	0.29	0.22	0.14
LOI	0.73	0.54	0.44	0.37	1.43	0.67	0.48	0.37	0.49	0.70	0.13	0.38	0.62
Pb	5.00	4.00	14.00	6.00	4.00	18.00	5.00	7.00	9.00	4.00	5.00	5.00	7.00
Rb	6.00	4.00	20.00	11.00	5.00	4.00	4.00	7.00	13.00	9.00	3.00	7.00	8.00
Sr	176.00	178.00	200.00	185.00	191.00	181.00	152.00	244.00	158.00	163.00	145.00	181.00	220.00
Y	34.00	31.00	33.00	33.00	30.00	33.00	27.00	29.00	27.00	25.00	36.00	36.00	25.00
Zr	120.00	83.00	137.00	103.00	115.00	115.00	76.00	114.00	103.00	97.00	184.00	140.00	79.00
Nb	7.00	4.00	6.00	6.00	9.00	4.00	4.00	5.00	5.00	5.00	8.00	6.00	5.00
Ga	17.00	18.00	20.00	20.00	18.00	19.00	19.00	19.00	19.00	16.00	21.00	20.00	18.00
Zn	86.00	79.00	86.00	90.00	81.00	93.00	73.00	70.00	75.00	67.00	77.00	76.00	66.00
Ni	76.00	47.00	46.00	54.00	83.00	48.00	50.00	39.00	28.00	90.00	76.00	40.00	30.00
Cr	262.00	106.00	191.00	144.00	214.00	244.00	120.00	165.00	83.00	215.00	13.00	137.00	241.00
Va	293.00	276.00	260.00	305.00	280.00	280.00	232.00	207.00	226.00	206.00	306.00	306.00	191.00
Ba	24.00	8.00	29.00	31.00	6.00	15.00	14.00	147.00	148.00	22.00	75.00	35.00	65.00
La	3.00	1.00	2.00	3.00	6.00	1.00	1.00	7.00	4.00	1.00	17.00	7.00	1.00
Ce	12.00	1.00	13.00	9.00	121.00	7.00	2.00	14.00	13.00	8.00	39.00	15.00	4.00
Ti	12000.00	8300.00	13700.00	10300.00	11500.00	11500.00	7600.00	11400.00	10300.00	9700.00	18400.00	14000.00	7900.00
Zr/TiO2	62.83	53.55	68.16	54.79	62.16	60.85	53.15	78.08	70.07	65.99	94.36	71.43	66.95
Zr/P2O5	571.43	638.46	595.65	605.88	522.73	638.89	584.62	600.00	686.67	606.25	634.48	636.36	564.29
Zr/Y	3.53	2.68	4.15	3.12	3.83	5.48	5.63	8.41	5.85	6.52	4.03	5.03	8.80
Ti/Y	352.94	267.74	415.15	312.12	383.33	348.48	281.48	393.10	381.48	388.00	511.11	388.89	316.00
Nb/Y	0.21	0.13	0.18	0.18	0.30	0.12	0.15	0.17	0.19	0.20	0.22	0.17	0.20
Ti/Cr	45.80	78.30	71.73	71.53	53.74	47.13	63.33	69.09	124.10	45.12	1415.38	102.19	32.78
Na2O+K2O	2.29	1.83	2.63	1.74	2.45	3.15	2.11	3.81	3.82	2.51	5.01	2.66	2.91

ROCK TYPE	amphibolite	amphibolite	granulite	granulite	migmatite	migmatite
SAMPLE	ACE-9	ACE-10	ACE-11	ACE-12	ACE-13	ACE-14
SiO2	44.47	40.32	49.09	49.69	46.01	50.48
TiO2	3.05	2.20	1.41	1.15	1.57	1.24
Al2O3	16.72	19.38	15.75	18.18	22.30	17.84
Fe2O3	13.97	12.30	10.00	9.64	8.21	7.47
MnO	0.81	0.14	0.16	0.15	0.11	0.11
MgO	7.12	2.56	7.69	5.89	6.04	7.27
CaO	11.53	21.23	12.28	10.85	12.74	9.18
Na2O	1.57	0.20	2.28	2.60	2.38	2.38
K2O	0.23	0.03	0.14	0.46	0.24	1.34
P2O5	0.06	0.36	0.15	0.09	0.03	0.08
LOI	0.81	1.06	0.51	1.04	0.67	1.73
Pb	6.00	8.00	2.00	4.00	3.00	5.00
Rb	6.00	6.00	3.00	12.00	4.00	34.00
Sr	286.00	813.00	181.00	368.00	389.00	210.00
Y	15.00	44.00	28.00	21.00	21.00	22.00
Zr	27.00	168.00	78.00	39.00	32.00	57.00
Nb	5.00	8.00	5.00	4.00	4.00	4.00
Ga	21.00	39.00	17.00	18.00	18.00	17.00
Zn	76.00	28.00	30.00	60.00	49.00	52.00
Ni	91.00	19.00	77.00	18.00	17.00	19.00
Cr	61.00	49.00	256.00	32.00	25.00	43.00
Va	516.00	272.00	213.00	239.00	242.00	292.00
Ba	82.00	11.00	29.00	115.00	57.00	215.00
La	1.00	6.00	6.00	1.00	1.00	4.00
Ce	1.00	25.00	15.00	4.00	2.00	8.00
Ti	2700.00	16800.00	7800.00	3900.00	3200.00	5700.00
Zr/TiO2	8.85	76.36	55.32	33.91	20.38	45.97
Zr/P2O5	450.00	466.67	520.00	433.33	1066.67	712.50
Zr/Y	19.07	18.48	6.46	17.52	18.52	9.55
Ti/Y	180.00	381.82	278.57	185.71	152.38	259.09
Nb/Y	0.33	0.18	0.18	0.19	0.19	0.18
Ti/Cr	44.26	342.86	30.47	121.88	128.00	132.56
Na2O+K2O	1.80	0.23	2.42	3.06	2.62	3.72

ROCK TYPE	pelite	pelite	pelite	pelite	pelite	pelite	pelite	pelite	pelite	pelite	pelite	pelite	pelite
SAMPLE	8010	8026	8028	8060	8061	8062	8064	8066	8073	8076	8091	8092	8154
Rb	154.5	33.1	209.7	169.2	72.1	80.5	96.7	79.8	204.7	38.5	39.5	46.5	45.5
Sr	80.8	11.9	117.8	171.3	38.4	40.4	50	88.5	123	139.7	18.7	20.4	23.3
Y	38.1	15.5	37.3	29.2	24.1	29.3	46.2	29.6	24.8	41.4	24.2	21.2	20.4
Zr	240.4	302.1	165.1	211.7	264.6	356.9	433.7	387.4	159.8	110.9	532.8	406.5	290.2
Nb	18.8	8.5	20.8	18.2	13.4	15.8	19.3	14.2	19.7	6.6	10.7	11.6	11.5
Th	14	3.5	16.9	13.1	7.4	11	14	10.6	16.7	0.5	7.9	7.2	6.1
U	1.8	0.8	4.4	4.8	2.3	2.2	3.4	3	2.8	0	3.1	2.2	1.5
Pb	6.1	3.5	28.5	15.2	10.3	11.9	13.1	26.5	29.5	4.7	12.6	10.6	7
Zn	94.2	9.9	145.3	85.1	49.6	85.6	82.3	81.7	115.2	90.9	39.5	10.5	46.6
Ni	56.6	19.9	77.3	42.8	41.4	50.1	36.4	36.6	51.3	60.6	30.7	37.2	36.1
Ga	24.2	5.1	29.9	26.1	12.7	16.6	16.6	15.2	31.9	18.2	7.5	10.3	9.2
Cr	94	34.1	127.4	63.8	69.7	55.4	68.9	64.8	58.3	75.9	83.8	58.9	48
V	129.5	26.4	205.3	68.9	67.1	43.7	46.8	67.8	68.2	75	104	54.8	45.5
Ba	696.1	119.1	773.7	301.3	292.1	180.7	170.7	311.6	323.4	327.5	396.6	269.4	182.5
La	43	14	59.9	27.1	24	17.9	29.5	19.9	31.5	62.3	36.6	23.2	21.9
Ce	84.4	25.1	106.2	53	45	34.4	55.3	33.9	51.2	92.7	65.3	58.5	40.5
MnO	4007	57.2	521	77.3	67.7	56.6	88.9	52.6	205	1591.9	343.7	47.3	126.8
TiO2	8902.7	3092.1	10378.1	5713.3	6222.1	4573.4	5120.4	6152.5	5588.8	9200.1	8367.4	5883.5	4577.4
Ti	7122.16	2473.68	8302.48	4570.64	4977.68	3658.72	-	4922	4471.04	7360.08	6693.92	4706.8	3661.92
Cr/Nb	5.00	4.01	6.13	3.51	5.20	3.51	3.57	4.56	2.96	11.50	7.83	5.08	4.17
Ni/Nb	3.01	2.34	3.72	2.35	3.09	3.17	1.89	2.58	2.60	9.18	2.87	3.21	3.14

ROCK TYPE	pelite	pelite	pelite	pelite	arenite	arenite	arenite	arenite	arenite	arenite	arenite	arenite	arenite
SAMPLE	8160	8162	8181	8187	8064	8090	8067	8093	8096	8097	8099	8100	8101
Rb	183.4	186.5	70.1	59.5	96.7	44.6	134.4	46.2	52.1	44.8	40.5	44.8	47.5
Sr	87.9	101.7	51.1	32.4	50	42	71.3	22.4	23.8	41.9	19.6	21	22.4
Y	31.3	37.4	29.5	30.9	46.2	28.1	18.1	24.8	28.6	27.1	24.7	20.9	24.6
Zr	222	335.8	389.7	459	433.7	549.5	286.2	526.2	495.7	548.4	532.6	406.6	529.6
Nb	21.2	25	14.4	13.4	19.3	11.8	16.9	12.4	13.1	11.8	10.6	11.8	11.6
Th	14.8	15.3	10.5	10.5	14	8.9	11.8	8.6	8.9	8.5	8.6	7.3	8.5
U	3.5	5.4	4.4	3.1	3.4	1.4	2.8	3.1	2.4	3.3	2.3	1	2.4
Pb	19.4	12.2	20.3	9.7	13.1	11.1	16.1	9.6	7.2	9.3	12.5	11.8	8.7
Zn	66.2	38.1	87.8	74.1	82.3	39.9	55.3	25.5	34.8	40.3	39.1	10.5	23.8
Ni	33.1	24.2	43	26.1	36.4	37	26.4	35.8	26.5	36.9	31.3	36.3	35.4
Ga	26.3	27	13.7	11	16.6	8.4	18.6	8.8	9.6	8.8	8.3	8.5	9.1
Cr	114.3	114.1	61.4	69.6	68.9	59.8	43.9	40.6	14.4	135.4	25.8	51.6	75.5
V	166	153	75.7	65.7	46.8	71.2	36.4	32.8	0	247.4	2.4	25.6	20
Ba	658.9	772.7	341.3	260.8	170.7	326.1	134.5	117.2	21.2	145.8	131.6	346.7	301
La	39.4	50.3	33.8	76.6	29.5	28.9	21.9	11.6	6.2	7.8	13.9	20.4	23.9
Ce	71.7	76.3	72.9	118.9	55.3	51.3	49	25.4	6.2	26.8	21.7	37.3	32.2
MnO	140.7	54.2	521.2	346	88.9	160.9	311	38.6	512.6	1634.1	191.6	202.8	243.9
TiO2	10354.8	12090.1	6897.7	6423.6	5120.4	6427.9	4363.5	3512.2	539.4	18037.9	797.6	4056.6	1732
Ti	8283.84	9672.08	5518.16	5138.88	4096.32	5142.32	3490.8	2809.76	431.52	14430.32	638.08	3245.28	1385.6
Cr/Nb	5.39	4.56	4.26	5.19	3.57	5.07	2.60	3.27	1.10	11.47	2.43	4.37	6.51
Ni/Nb	1.56	0.97	2.99	1.95	1.89	3.14	1.56	2.89	2.02	3.13	2.95	3.08	3.05

ROCK TYPE	arenite	arenite	arenite	qtz my.	arenite	slate	slate	slate	slate	tuff	tuff	phyllite	tuff
SAMPLE	8147	8165	8189	8192	8194	8139	8152	8155	8186	8074	8077	8079	8088
Rb	31.3	36.2	51.6	9.2	0.7	241.3	291.3	264.5	65	109.4	153.6	66.3	40.6
Sr	19	27.9	38.1	4.1	3.2	131	193.4	163.2	12.4	65	81.1	37.8	24.1
Y	26.1	28.6	21.8	10	14.5	41.1	43.4	36.4	25.1	26.5	43.3	27.4	28.1
Zr	490.2	928.1	363.1	372.8	300.3	183.1	195.4	173.6	342.7	278.1	221.9	498.8	562.7
Nb	10.9	11.9	12.2	7.1	7.2	21.8	26	22.1	17.3	15.7	22.2	12.7	11.2
Th	7.4	10	7.9	4.2	5.6	17.9	24	20.7	11.1	11.7	18	9.5	8.7
U	3.5	3.4	1.6	1.2	2.4	4.1	5.9	3.7	3.6	1.9	2.6	2.8	1.2
Pb	10.8	13.2	8.6	3.8	6.9	10.7	31.1	28.2	15.9	17.1	28.9	9.8	16.9
Zn	47.5	16.3	58.4	8.2	103.5	100.9	36.9	32.6	57.9	67.8	110.5	38.2	38
Ni	32.5	49.4	35.4	28.5	51.1	58	12.2	16.7	251.4	51.3	55.9	37.8	29.2
Ga	8.3	7.7	9.2	4	6.3	34.9	39.9	35.8	23.1	18.4	30.8	10.2	8.9
Cr	45.4	52.1	53.6	33.8	40.1	138.7	166.4	148.4	99	72.4	62.7	68	72.1
V	36.7	43.5	50.7	11.2	30.9	203.9	278.7	233.8	94.8	82.8	73.4	61.6	78.6
Ba	128.9	197.9	211.2	41.1	16	766.1	1002.6	975.8	248.3	410.6	316.2	100.1	377.1
La	23.8	34.3	41.1	10.2	26.3	55.8	75.3	61.2	29.6	27.7	83.6	25.3	32.6
Ce	42	64.2	57.4	18.2	41.9	119.1	147.5	100.5	82	48.9	72.5	44.4	64
MnO	342.1	81.4	328.5	85.3	389.8	730.9	45.1	57.4	2759.4	1014.5	776.1	1995.7	767.6
TiO2	4209.4	5880.9	5321.2	2293.1	2639.8	11377.3	13041	12046.3	9807.3	6945.3	7140.8	5825.4	6846.2
Ti	3367.52	4704.72	4256.96	1834.48	2111.84	9101.84	10432.8	9637.04	7845.84	5556.24	5712.64	-	5476.96
Cr/Nb	4.17	4.38	4.39	4.76	5.57	6.36	6.40	6.71	5.72	4.61	2.82	5.35	6.44
Ni/Nb	2.98	4.15	2.90	4.01	7.10	2.66	0.47	0.76	14.53	3.27	2.52	2.98	2.61

ROCK TYPE	tuff	tuff	tuff	tuff	tuff	tuff	tuff	schist
SAMPLE	8089	8094	8120	8140	8171	8183	8184	8113
Rb	52	42	28.4	148.6	96.7	145	38.8	49.2
Sr	24.7	25.4	215.6	78.6	79.9	57.2	15.8	19.1
Y	29.4	28.9	17.7	32.2	26.3	30.6	23.6	24.1
Zr	494.8	565.1	137.1	267.1	255.6	263.9	544.4	416.9
Nb	12.4	11.1	6.5	20.3	18.3	18.7	12.1	10.4
Th	9.1	7.8	5.3	14.4	10	14.4	7.9	8
U	2.8	2.8	1.1	2.9	3.9	2.3	1.4	1
Pb	7.1	17.3	7.8	6.9	18.1	22.6	11.5	7
Zn	34.4	37.1	54.1	76.6	59.6	79.4	36.6	41.4
Ni	28.1	28.5	46.3	40.6	30.2	32.8	39.6	34.4
Ga	8.9	8.5	16.5	25.3	18.1	25.3	8.7	7.6
Cr	122.7	15.7	61	80.5	113.7	82.7	55.4	65.7
V	100.3	2.4	66.8	105.3	66.4	98.6	42.9	54.3
Ba	513.9	70.6	281.5	610.3	437.7	609.6	148.2	192
La	43	9.9	32.5	4409	24.9	40.7	22.1	26.3
Ce	77.6	9.7	56.2	88.2	59.5	72.5	41.1	54
MnO	295.1	432.8	238.1	344.6	503.2	323.5	729.8	116.4
TiO2	8342	905.4	5799.8	7789.3	6004.5	6914.3	5327.8	5120.6
Ti	6673.6	724.32	4639.84	6231.44	4803.6	5531.44	4262.24	4096.48
Cr/Nb	9.90	1.41	9.38	3.97	6.21	4.42	4.58	6.32
Ni/Nb	2.27	2.57	7.12	2.00	1.65	1.75	3.27	3.31

ROCK TYPE	Rb	Sr	U	Ba	V	Cr	Ni	Nb	Ti	Zr	Y
average schist	0.73	0.26	0.81	0.67	2.80	3.69	2.03	0.52	2.65	1.48	1.35
average psammite	0.39	0.08	0.85	0.30	0.79	1.59	1.92	0.47	1.27	2.45	1.15
average silt	0.89	0.19	1.08	0.68	1.47	2.18	2.10	0.62	1.92	1.66	1.37
average slate	1.94	0.31	1.30	1.52	3.32	3.75	3.14	0.85	2.92	1.04	1.62
average tuff	0.71	0.20	0.78	0.77	1.34	2.23	1.90	0.58	1.79	1.83	1.29
average amphibolite	0.12	0.58	0.56	0.21	4.41	5.74	4.34	0.27	3.82	0.74	1.50
average matrix	0.19	0.42	0.87	0.20	4.20	5.33	2.84	0.31	3.52	0.78	1.55
average granite (USG stan	1.96	0.71	1.43	2.18	0.27	0.63	0.08	0.80	0.50	1.11	0.59
granite, Peru	1.09	0.68	-	-	0.65	0.09	0.65	-	-	0.51	1.77
granite (Himalayas)	3.33	0.18	-	0.44	0.17	0.00	-	0.12	-	0.26	0.64
M277	-	0.54	0.11	0.15	5.83	0.89	0.70	-	2.77	0.55	0.86
MK64	0.32	0.63	0.48	0.27	2.87	3.11	1.00	0.40	2.00	0.92	1.00
MK97	0.81	0.13	1.22	0.73	0.95	1.46	0.95	0.44	1.24	2.02	1.45
T&Mc	1.43	0.57	1.11	1.18	2.50	3.14	2.75	0.76	2.00	1.11	1.23
greywackes	0.61	-	0.79	0.76	1.40	2.94	10.00	-	-	-	-
sandstones	0.48	-	0.57	0.45	0.72	5.83	16.00	-	-	-	-
siltstones	1.09	-	0.89	0.65	1.60	3.71	7.75	-	-	-	-
shales (worldwide)	1.25	-	1.32	1.05	2.17	2.57	3.40	-	-	-	-
Rheno-hercynian belt	0.95	-	0.82	0.63	1.52	4.09	8.40	-	-	-	-
Oceanic island arc	0.27	1.03	0.29	0.67	3.13	1.40	1.10	0.20	1.96	0.52	0.68
continental arc+active mar	0.55	0.78	0.71	0.87	1.77	1.57	1.55	0.36	1.16	0.77	0.77
passive margin	0.45	0.21	1.14	0.46	0.73	0.83	0.75	0.28	1.24	1.59	1.09
ocean islands and seamoun	0.17	1.23	0.11	0.38	6.67	6.57	5.70	1.08	4.77	0.77	0.91
Giessen greywacke	0.61	0.67	0.96	1.14	1.65	2.63	1.95	0.28	1.34	1.08	0.91
Gramscatho greywacke	0.23	0.78	1.00	0.75	1.93	2.43	2.05	0.32	1.38	1.06	1.09
av NMORB	0.01	0.32	0.03	0.03	-	-	7.48	0.14	3.22	0.55	1.63
482/3 (Mid-Atlantic Ridge	-	0.27	-	-	3.07	10.60	10.15	0.04	1.78	0.27	1.14
BHVO-1	0.09	1.15	-	0.24	5.62	9.97	6.05	0.80	5.48	0.89	1.27
482/4 (Mid-Indian ridge)	0.01	0.41	-	0.03	4.82	8.66	5.75	0.80	3.14	0.59	1.59
482/11 (Yap Trench)	0.03	0.29	-	0.02	4.15	12.46	10.15	0.06	2.21	0.30	1.27
K10 (coastal Range ophiol	0.03	0.26	-	0.03	4.25	12.40	8.40	0.04	1.73	0.23	1.18
AVG SLATE	1.40	0.26	20.46	1.19	2.53	3.22	2.69	0.61	1.70	1.00	1.47
AVG GRANITE	2.93	0.20	2.02	0.26	0.16	0.63	1.68	0.60	1.02	0.42	0.59
AVG ALBALA	2.53	0.20	2.71	0.49	0.25	0.67	1.34	0.53	0.51	0.60	0.47

ROCK TYPE	La	Ce	Th	Pb	Zn	Ga
average schis	0.92	0.87	0.76	0.64	0.98	1.02
average psam	0.84	0.69	0.78	0.50	0.62	0.55
average silt	1.29	1.04	0.99	0.70	1.01	1.04
average slate	1.81	1.61	1.68	1.52	1.22	1.88
average tuff	14.43	0.95	0.99	0.77	0.84	0.98
average amp	0.34	0.41	0.42	0.16	0.86	1.05
average matr	0.35	0.52	0.61	0.37	1.03	1.05
average gran	3.33	2.66	4.86	2.45	0.63	1.06
granite, Peru	-	-	-	-	-	-
granite (Him	0.57	0.55	-	2.25	0.44	0.82
M277	0.33	0.28	0.08	-	-	1.35
MK64	0.83	0.83	0.65	0.65	1.34	0.88
MK97	1.43	1.30	1.53	0.80	0.75	0.76
T&Mc	1.27	1.25	1.36	1.00	-	-
greywackes	-	-	0.75	0.70	0.96	-
sandstones	-	-	0.62	0.45	0.68	-
siltstones	-	-	0.97	1.05	1.11	-
shales (world	-	-	1.12	1.00	1.34	-
Rheno-hercy	-	-	0.87	0.85	1.13	-
Oceanic islan	0.33	0.34	0.18	0.75	1.24	1.18
continental a	0.77	0.75	0.79	0.75	1.03	0.88
passive marg	0.73	0.88	0.76	0.55	0.69	0.47
ocean islands	0.33	0.38	0.09	-	1.72	-
Giessen grey	0.77	0.77	0.79	0.75	0.90	0.82
Gramscatho g	0.97	0.89	0.83	1.30	0.89	0.88
av NMORB	0.13	0.19	0.02	0.02	-	-
482/3 (Mid-A	0.04	0.07	-	-	-	-
BHVO-1	0.48	0.57	-	-	-	-
482/4 (Mid-I	0.14	0.20	-	-	-	-
482/11 (Yap	0.07	0.11	-	-	-	-
K10 (coastal	0.06	0.08	-	-	-	-
AVG SLATE	1.14	1.10	1.19	-	-	-
AVG GRANIT	0.43	0.43	0.81	-	-	-
AVG ALBAL	-	-	0.82	-	-	-

Appendix 3 High Precision Instrumental Nuetron Activation (INAA)

This method was used to analyse for Rare Earth Elements and other important trace elements to low limits of dectection. Samples were irradiated and counted simultaneously suing both planar and coaxial Ge dectectors. A planar detector is preferred for the determination of many REE from photopeaks in the 63-208 keV region whereas the coaxial detector is more suited to gamma energies about ca. 200 keV. The technique is described in detail by Potts *et al.* (1985).

A.3.1 Experimental preparation and procedure

Rock samples were crushed and milled in an agate Tema to ≈200 mesh and dried overnight at 110°C. 300mg aliquots were sealed into polyethylene vials and packed in batches of eleven into an outer polyethylene container. They were then irradiated in one of the core tubes at the Imperial College Reactor Centre, Silwood Park, Ascot for ≈24 hours in a nuetron flux of ≈1 x 10^{12} n $cm^{-2}s^{-1}$. The container contained two quality assurance standards (USGS BHVO-1 Hawaiian basalt and USGS BCR-1) and ten samples of the El Hurón amphibolites.

After irradiation, samples were allowed to cool for at least 5 days to allow the short lived isotopes to decay. In the ensuing four weeks each sample was counted twice with data collection simultaneously by planar and coaxial detectors.

Data were accumulated and analysed by a Canberra Ind. series 90 integrated data aquisition and analysis system incorporating a DEC® PDP 11/73 microcomputer.

The first set of 'short counts' was taken at 5-10 days after irradiation, each sample being counted for 6000-8000s. 2-4 weeks after irradiation the samples were counted again ('long counts') for between 6-10 hours each to improve the precision of the longer lived isotopes.

A.3.2 Results

The data presented below are given as raw data. Those given in bold are the isotopes which are considered most reliable as the gamma lines produced generally do not overlap.

10 samples were analysed by this technique:

9146, 9148, 9171, 9189, 9200, 9186, 9231, 9237, 9240, 9243, BHVO-1, BCR-1.

A.3.2 Detection limits

Isotope	Half life	Photo peak (%)	Decay intensity (keV)	Limit of detection ($\mu g\ g^{-1}$)			
				planar short 6000s	**coaxial short 5000s**	**planar long 7 hours**	**coaxial long 6 hours**
Nd^{147}	11.06 days	91.1	28.3	2.7		2.9	
		531	13.5		9		
Sm^{153}	1.948 days	103.2	28.3	0.06			
		69.7	5.3	0.2			
Eu^{152}	12.7 years	121.8	29.2	0.1		0.03	
Lu^{177}	6.71 days	113	6.6	0.08		0.2	
		208.4	11	0.06	0.04	0.14	0.08
Th(Pa)	27.4 days	98.4	15.5	0.7		0.3	
Yb^{175}	4.19 days	396.3	6.2	0	0.2		
Hf^{181}	42.5 days	133	43	0.5		0.13	
		136.3	6.1	2.9		1.2	
		482.2	86		0.6		0.1
Fe^{59}	45.1 days	1,099.2	56.5		0.05%		0.02%
		1,291.6	43.2		0.06%		0.01%
		192.3	3.1	0.05%	0.4%	0.2%	0.1%
		142.6	1	0.9%	1.4%	0.5%	0.4%
Na^{24}	15.03 hours	1,368.6	100		0.06%		
La^{140}	40.7 hours	1,596.2	95.5		0.3		
		328.7	18.5	2.9	0.9		
		815.8	22.3		1.3		
		487	43		1		
U(Np)	2.355 days	106.1	10.7	1.3	1.1		
Ce^{141}	32.38 days	145.4	48	2.9	2.2	1.2	0.9
Rb^{86}	18.6 days	1,076.6	8.8		11		6
Ta^{182}	115 days	67.7	41.3	0.16		0.04	
		100.1	14.1	0.3		0.08	
		152.4	7.2	0.8	1	0.3	
		222.1	7.6	1.3	0.4	0.5	0.3
		1,221.4	27.4		1		0.09
		1,231	11.6		2.4		0.2
		179.4	3.2	2.2		0.8	0.7
		84.7	2.7	2.1		0.4	
Yb^{169}	30.7 days	63.1	45	0.2		0.08	
		109.8	18	0.8		0.4	
		130.5	11.5	1		0.5	
		177.2	22	0.8	0.9	0.4	0.3
		198	36	0.5	0.4	0.4	0.2
Cs^{134}	2.06 years	795.8	85.4		0.5		0.14
		604.7	97.6		0.4		0.1
Sc^{46}	83.85 days	889.3	100		0.03		0.02
Tb^{160}	72.1 days	86.8	13.4	0.14		0.05	
		1,177.9	15.5		0.9		0.4
		876.4	30		0.3		0.1
Co^{60}	5.272 years	1,332.5	100		0.6		0.08

1st count. Standard BHVO

isotope	energy	9146	9148	9171	9189	9200	9186	9231	9237	9240	9243
Nd-147	91.1	-	11.44	16.14	14.9	17.43	-	24.91	15.68	10.08	9.94
Sm-153	103.2	2.31	3.38	3.94	4.48	4.79	3.1	6.7	4.92	3.65	4.01
U(Np)	106.1	0.9	-	-	0.86	2.36	-	2.24	2.01	-	-
Lu-177	113	0.35	0.55	0.48	0.71	0.59	0.43	0.8	0.61	0.45	0.56
Eu-152	121.8	0.95	1.14	1.4	1.42	1.38	1.17	2	1.49	1.24	1.47
Hf-181	133	1.23	2.08	2.52	3.6	3.09	2.32	5.33	4.07	2.72	2.9
Ce-141	145.4	-	-	23.68	24.59	37.16	14.59	36.72	28.15	17.23	15.96
Fe-59	192.3	7.19	11.05	10.12	11.28	9.79	9.44	11.9	10.81	8.81	11.37
Lu-177	208.4	0.42	0.62	0.6	0.72	0.69	0.51	0.98	0.73	0.51	0.69
Th(Pa)	311.9	-	-	-	1.66	2.27	-	2.15	1.35	0.73	-
Cr-51	320.1	213.13	266.35	344.74	127.88	180.89	303.28	142.82	158.63	211.39	468.12
La-140	328.7	3.48	4.16	8.43	9.12	14.63	4.59	11.68	10.01	5.52	4.83
Yb-175	396.3	2.29	3.47	3.31	3.8	3.81	2.75	5.08	3.93	2.87	3.68
Hf-181	482.2	1.55	2.41	2.18	3.67	3.11	2.32	4.83	3.41	2.52	2.55
Eu-152	778.9	-	-	-	1.44	-	-	1.4	-	-	-
La-140	815.8	3.5	3.66	8.17	8.93	14.65	4.13	11.24	9.46	5.7	4.5
Fe-59	1099.2	6.97	10.83	9.69	11.41	9.49	9.49	11.86	10.45	8.55	10.83
Fe59	1291.6	6.83	10.7	9.66	11.02	9.43	9.23	11.59	10.31	8.46	10.49
Na-24	1368.6	0.95	3.46	2.94	2.88	4.03	2.86	4.29	3.14	2.93	2.67
Eu-152	1408.1	0.88	1.04	1.36	1.45	1.39	1.16	1.79	1.62	1.14	1.29
La-140	1596.2	3.38	3.87	8.16	8.76	14.33	4.32	11.31	9.71	5.33	4.63

1st count. Standard BCR

isotope	energy	9146	9148	9171	9189	9200	9186	9231	9237	9240	9243
Nd-147	91.1	-	10.43	13.59	13.59	15.9	-	22.72	14.3	9.19	9.07
Th(Pa)	94.7	-	-	-	-	-	-	-	-	-	-
Th(Pa)	98.4	-	-	-	-	1.79	-	-	-	-	-
Sm-153	103.2	2.19	3.21	4.26	4.26	4.55	2.95	6.36	4.67	3.47	3.81
U(Np)	106.1	0.38	-	0.36	0.36	0.99	-	0.94	0.85	-	-
Yb-169	109.8	2.4	-	2.63	2.63	4.09	-	4.89	3.46	-	3.6
Lu-177	113	0.37	0.51	0.76	0.76	0.63	0.46	0.85	0.64	0.48	0.59
Eu-152	121.8	0.93	1.38	1.4	1.4	1.36	1.15	1.97	1.46	1.22	1.45
Yb-169	130.5	-	1.98	2.58	2.58	-	-	3.26	2.48	-	2.19
Hf-181	133	1.16	2.39	3.4	3.4	2.92	2.19	5.03	3.85	2.57	2.74
Ce-141	145.4	-	20.11	20.88	20.88	31.55	12.38	31.17	23.9	14.63	13.55
Fe-59	192.3	6.71	9.43	10.51	10.51	9.12	8.8	11.09	10.08	8.21	10.6
Lu-177	208.4	0.31	0.45	0.53	0.53	0.51	0.38	0.73	0.54	0.38	0.51
U(Np)	228.2	-	-	-	-	-	-	-	1.18	-	-
Th(Pa)	311.9	-	-	2	2	2.73	-	2.58	1.63	0.88	-
La-140	328.7	3.02	7.32	7.93	7.93	12.71	3.99	10.15	8.69	4.8	4.2
Yb-175	396.3	2.17	3.13	3.6	3.6	3.61	2.6	4.81	3.72	2.71	3.48
Au-198	411.8	-	-	-	-	-	9.61	0.24	-	-	-
Hf-181	482.2	1.58	2.23	3.75	3.75	3.18	2.37	4.94	3.49	2.58	2.61
Sb-122	564	-	-	-	-	-	-	-	-	-	-
La-140	815.8	3.14	7.33	8.01	8.01	13.14	3.71	10.08	8.49	5.12	4.04
Rb-86	1076.6	-	-	-	-	-	-	-	-	-	-
Fe-59	1099.2	6.84	9.52	11.2	11.2	9.32	9.32	11.64	10.26	8.4	10.63
Fe59	1291.6	6.83	9.66	11.02	11.02	9.43	9.23	11.59	10.31	8.46	10.49
Na-24	1368.6	0.97	3.01	2.95	2.95	4.12	2.92	4.39	3.22	3	2.73
Eu-152	1408.1	0.9	1.38	1.48	1.48	1.42	1.19	1.83	1.65	1.16	1.32
La-140	1596.2	3.06	7.4	7.95	7.95	13	3.92	10.26	8.81	4.84	4.2

2nd count. Standard BHVO

isotope	energy	9146	9148	9171	9186	9189	9200	9231	9237	9240	9243
Yb-169	63.1	2.61	4.11	3.59	2.9	4.18	4.18	5.71	4.22	3.16	4.1
Ta-182	67.7	0.11	0.19	0.23	0.13	0.25	0.51	0.33	0.25	0.14	0.17
Tm-170	84.3	0.22	0.32	0.29	0.25	0.3	0.31	0.35	0.28	0.25	0.32
Tb-160	86.8	0.61	0.91	0.85	0.67	0.96	1.02	1.41	1.02	0.77	0.96
Nd-147	91.1	7.36	10.34	12.26	9.89	13.73	15.97	22.16	15.42	10.47	12.89
Th(Pa)	94.7	-	-	-	-	1.9	2.73	2.56	1.24	-	-
Gd-153	97.5	2.31	-	4.71	2.28	13.52	20.06	19.35	10.92	3.7	3.64
Th(Pa)	98.4	0.22	0.3	0.21	-	0.43	1.08	0.58	0.42	0.54	-
Th(Pa)	98.4	0.1	0.13	0.09	-	0.19	0.48	0.26	0.19	0.24	-
Ta-182	100.1	0.11	0.15	0.1	-	0.21	0.52	0.28	0.2	-	-
Gd-153	103.2	-	6.12	-	-	6.3	6.74	8.65	6.16	-	7.12
Yb-169	109.8	2.49	3.8	3.34	2.75	3.76	3.72	5.21	3.98	2.99	3.74
Eu-152	121.8	0.87	1.13	1.43	1.14	1.39	1.42	2.03	1.56	1.19	1.35
Yb-169	130.5	2.26	3.57	3.25	2.51	3.68	3.66	5.12	3.8	2.89	3.44
Hf-181	133	2.42	2.27	2.34	2.14	3.5	3.11	4.99	3.57	2.47	2.61
Ce-141	145.4	7.67	11.11	20.66	12.24	21.32	33.59	31.92	24.93	14.76	12.98
Ta-182	152.4	-	-	-	-	-	0.61	0.25	-	-	-
Fe-59	192.3	6.78	10.51	9.58	9.11	10.8	9.23	11.27	10.13	8.28	10.35
Th(Pa)	311.9	-	0.23	0.75	0.32	1.79	2.78	2.6	1.49	0.74	0.28
Cr-51	320.1	201.77	259.95	336.82	284.19	120.69	176.07	137.19	152.32	200.49	437.63
Hf-181	482.2	1.42	2.36	2.44	2.2	3.59	3.24	5.08	3.67	2.46	2.71
Zr-95	756.7	-	-	-	-	-	-	-	-	-	-
Eu-152	778.9	0.83	1.17	1.49	1.17	1.47	1.4	2.07	1.54	1.33	1.37
Sc-46	889.3	29.49	44.37	38.78	34.76	38.06	35.06	37.83	32.38	26.34	42.46
Rb-86	1076.6	-	13.18	-	-	-	-	-	20.68	-	-
Fe-59	1099.2	6.85	10.73	9.65	9.22	11	9.47	11.64	10.31	8.46	10.45
Sc-46	1120.3	29.33	44.18	38.7	34.76	38.07	35.05	37.89	32.38	26.42	42.56
Co-60	1173.2	32.64	42.08	39.5	43.46	41.04	33.22	36.35	34.38	37.93	36.07
Tb-160	1177.9	0.59	0.87	0.83	0.72	0.94	1	1.43	1.02	0.8	0.96
Ta-182	1221.4	-	0.18	0.25	-	0.24	0.5	0.34	0.27	0.17	0.16
Ta-182	1231	-	-	-	-	-	0.52	-	-	-	-
Fe59	1291.6	6.83	10.7	9.66	9.23	11.02	9.43	11.59	10.31	8.46	10.49
Co-60	1332.5	32.84	42.16	39.63	43.45	41.23	33.3	36.56	34.42	37.95	36.15
Eu-152	1408.1	0.86	1.13	1.42	1.15	1.42	1.45	2.07	1.58	1.23	1.39

2nd count. Standard BCR

isotope	energy	9146	9148	9171	9186	9189	9200	9231	9237	9240	9243
Yb-169	63.1	2.24	3.52	3.08	2.49	3.58	3.59	4.9	3.62	2.71	3.52
Ta-182	67.7	0.12	0.2	0.24	0.14	0.26	0.54	0.35	0.26	0.15	0.18
Tm-170	84.3	0.4	0.57	0.51	0.44	0.54	0.55	0.63	0.51	0.44	0.56
Tb-160	86.8	0.57	0.84	0.78	0.62	0.89	0.94	1.3	0.94	0.71	0.88
Nd-147	91.1	6.98	9.81	11.64	9.39	13.03	15.15	21.02	14.63	9.94	12.23
Th(Pa)	94.7	-	-	-	-	1.86	2.68	2.51	1.22	-	-
Gd-153	97.5	0.41	-	0.83	0.4	2.4	3.55	3.43	1.93	0.66	0.65
Th(Pa)	98.4	0.23	0.31	0.22	-	0.45	1.12	0.6	0.44	0.56	-
Th(Pa)	98.4	0.77	1.06	0.74	-	1.52	3.83	2.06	1.5	1.91	-
Ta-182	100.1	0.11	0.154	0.11	-	0.21	0.53	0.29	0.21	-	-
Gd-153	103.2	-	5.1	-	-	5.25	5.62	7.21	5.13	-	5.94
Yb-169	109.8	2.21	3.38	2.97	2.44	3.34	3.31	4.63	3.53	2.66	3.32
Yb-169	109.8	7.59	11.57	10.17	8.37	11.46	11.33	15.87	12.1	9.1	11.38
Lu-177	113	1.42	1.96	1.62	1.45	1.51	1.25	2.03	1.62	1.33	2.03
Eu-152	121.8	0.85	1.1	1.39	1.11	1.35	1.38	1.97	1.51	1.16	1.31
Yb-169	130.5	2.16	3.41	3.1	2.4	3.51	3.5	4.89	3.63	2.76	3.29
Hf-181	133	1.46	2.33	2.41	2.2	3.6	3.21	5.14	3.68	2.54	2.69
Ce-141	145.4	7.08	10.26	19.08	11.31	19.68	31.02	29.48	23.02	13.63	11.99
Ta-182	152.4	-	-	-	-	-	0.59	0.24	-	-	-
Fe-59	192.3	6.86	10.62	9.69	9.21	10.93	9.34	11.4	10.24	8.38	10.46
Lu-177	208.4	0.38	0.51	0.49	0.41	0.56	0.56	0.75	0.58	0.48	0.53
Th(Pa)	311.9	-	0.25	0.81	0.34	1.93	3	2.8	1.61	0.79	0.3
Cr-51	320.1	245.19	315.88	409.3	345.35	146.67	213.96	166.71	185.1	243.63	531.79
Hf-181	482.2	1.48	2.47	2.56	2.3	3.75	3.38	5.31	3.84	2.57	2.83
Sb-124	564	-	-	-	-	-	-	-	-	-	-
Cs-134	604.7	-	1.2	-	0.94	-	-	-	0.81	0.65	-
Zr-95	756.7	-	-	-	-	161.06	-	-	-	-	-
Eu-152	778.9	0.86	1.22	1.55	1.22	1.53	1.46	2.15	1.6	1.38	1.43
Cs-134	795.8	-	1.18	-	1.1	-	-	-	0.98	0.67	-
Sc-46	889.3	30.86	46.45	40.59	36.5	39.83	36.7	39.6	33.9	27.57	44.45
Rb-86	1076.6	-	13.58	-	-	-	-	-	21.3	-	-
Fe-59	1099.2	6.84	10.72	9.64	9.21	10.99	9.46	11.63	10.3	8.45	10.44
Sc-46	1120.3	30.72	46.28	40.53	36.41	39.88	36.72	39.69	33.92	27.67	44.58
Co-60	1173.2	30.98	39.94	37.49	41.25	38.95	31.53	34.5	32.63	36	34.23
Tb-160	1177.9	0.49	0.73	0.7	0.6	0.79	0.84	1.2	0.86	0.67	0.81
Ta-182	1221.4	-	0.17	0.24	-	0.24	0.49	0.33	0.27	0.17	0.16
Ta-182	1231	-	-	-	-	-	0.56	-	-	-	-
Fe59	1291.6	6.83	10.7	9.66	9.23	11.02	9.43	11.59	10.31	8.46	10.49
Co-60	1332.5	31.19	40.05	37.64	41.27	39.16	31.63	34.73	32.7	36.05	34.34
Eu-152	1408.1	0.86	1.13	1.43	1.15	1.42	1.45	2.08	1.59	1.23	1.39

Appendix 4 Extraction of spore material and vitrinite reflectance procedures.

Organic material was isolated by firstly crushing the samples and placing about 25 grams into a 250ml plastic beaker together with 75ml of industrial grade HCl. This dissolved any fine grained carbonate material. After reaction the samples were washed until neutral and then 75ml of industrial grade 60% HF was added to digest the silicates. This took 3-4 days after which fresh HCl was added to deter formation of fluorides. Finally the samples were washed to neutrality and sieved using 30μm plastic mesh to collect the organic material. These were then examined in polished thin section using a preparatory technique devised by Hillier & Marshall (1988). The method allows a small amount of material to be used and viewed both in transmitted and incident light. A Zeiss UMSP (microspectrophotometer) microscope equipped with a x40 antiflex objective and calibrated using a diamond standard (of 5.23% reflectivity) was used to study the specimens extracted. Measurements were made under oil (R.I. 1.515) at 546nm, illuminated in white light. The mean random reflectivity (Rm) was calculated on the basis of up to 100 measurements on different vitrinite grains (Table 5.D). The results from the study are plotted as relative frequency histograms and extreme values were edited from the final data set to minimise deviation of the calculated mean. Comparison of Rm with other methods which determine low-temperature metamorphic grade is given in Fig. A.4.1.

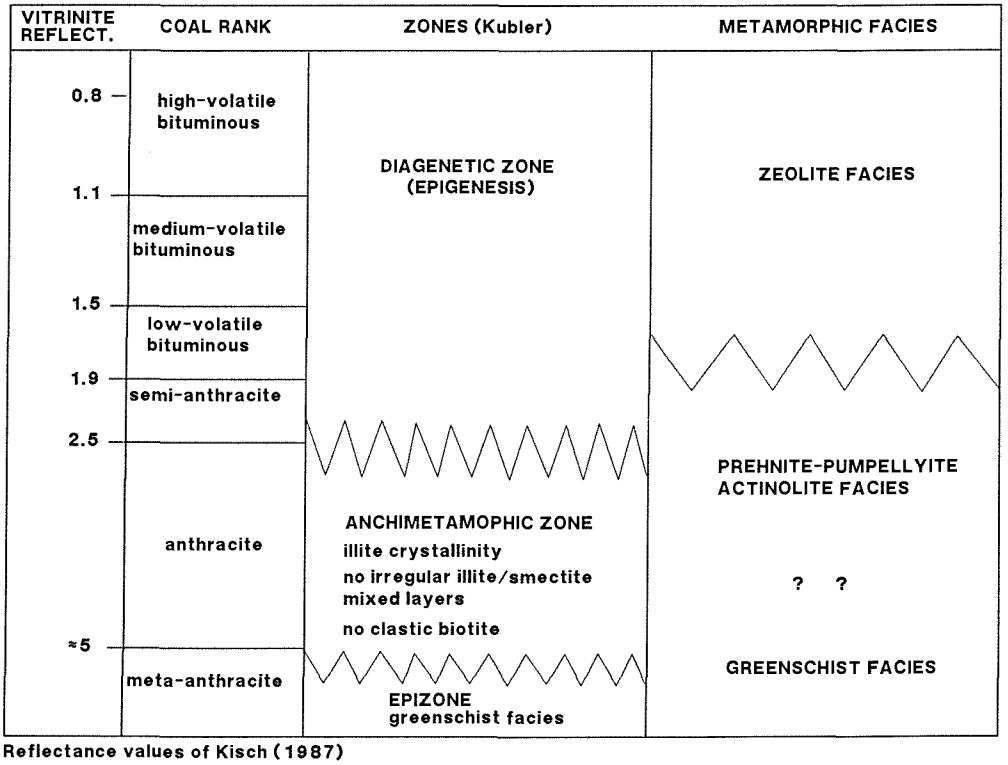

Reflectance values of Kisch (1987)

Appendix 5 Microprobe Analysis.

Microprobe analysis was carried out using a modified Cambridge Instrument Company Geoscan microprobe at Manchester University. This machine uses only energy dispersive spectrometer (EDS) analysis. The EDS comprises a Kevex Detector, Link Systems 860 Electronics. Link Systems ZAF - 4/FLS software is used to convert X - ray spectra obtained into chemical analysis. The instrument applies ZAF corrections.

A.5.1 Operating Conditions

15 kV electron beam accelerating voltage

75° X - ray take off angle

3nA specimen current on cobalt metal

2.5 kCPS output rate from cobalt metal with 18% detection system dead time.

counting time - 100s

Principle standards:

ELEMENT	STANDARD	ELEMENT	STANDARD
F	fluorite	Ti	rutile
Na	jadeite/albite	Mn	tephroite
Mg	periclase	Fe	fayalite
Al	corundum	Cr	metal
Si	woll/fosterite	Ni	"
P	apatite	Cu	"
S	pyrite	Zn	"
Cl	halite	Zr	"
K	orthoclase	Ba	barytes
Ca	wollastonite		

A.5.2 Results.

The results are presented as raw data in the form of weight % oxide and are presented with calculated mineral formulae based on a fixed number of oxygens appropriate for each mineral. Calculation of mineral formulae follows the method described by Deer *et al.* (1966), assuming all iron to be Fe^{2+}. Some of the amphibole analyses total to 100 wt% which is considered to be slightly high as H_2O in amphiboles usually accounts for up to 2 wt% of the total. These analyses are tabulated here as their Mg/Fe ratios provide an idea as to the amphibole composition. These analyses are not considered to be useful in the caluculation of temperatures and pressures.

sample 9074 (amphibolite)
weight % oxides

	feldspar	feldspar	feldspar	feldspar	feldspar	feldspar	ilmenite	ilmenite
SiO2	56.602	56.594	56.071	57.044	56.772	60.247	0.414	0.235
TiO2	0	0	0	0.087	0.027	0	49.686	50.617
Al2O3	28.338	27.811	27.858	27.886	28.002	24.748	0.076	0
FeO	0.185	0.283	0.239	0.237	0.221	0.418	47.344	47
MnO	0.04	0	0	0.038	0	0.052	1.949	0.888
MgO	0	0	0	0	0	0	0.277	0.191
CaO	10.118	9.752	9.952	9.514	9.629	5.956	0.294	0.077
Na2O	6.264	6.347	6.146	6.612	6.426	8.329	0.317	0.153
K2O	0.008	0.017	0.04	0.029	0.101	0.078	0.001	0
Cr2O3	0	0	0.116	0.111	0.115	0.048	0.085	0.245
NiO	0.489	0	0.054	0.248	0.431	0.046	0.48	0.636
Total	102.044	100.804	100.476	101.806	101.724	99.922	100.923	100.042
formula amounts calculated to O as below								
Si	2.504	2.526	2.514	2.525	2.518	6.722	0.112	0.063
Ti	0	0	0	0.003	0.001	0	10.094	10.296
Al	1.478	1.463	1.472	1.455	1.464	3.255	0.024	0
Fe	0.007	0.011	0.009	0.009	0.008	0.039	10.695	10.722
Mn	0.001	0	0	0.001	0	0.005	0.446	0.203
Mg	0	0	0	0	0	0	0.112	0.077
Ca	0.48	0.466	0.478	0.451	0.458	0.712	0.085	0.022
Na	0.537	0.549	0.534	0.568	0.553	1.802	0.166	0.02
K	0	0.001	0.002	0.002	0.006	0.011	0	0
Cr	0	0	0.004	0.004	0.004	0.004	0.018	0.052
Ni	0.017	0	0.002	0.009	0.015	0.004	0.104	0.138
O -2	24	24	24	24	24	24	6	6
mol% An	47.20	45.91	47.23	44.26	45.30	28.32	-	-
mol%Ab	52.80	54.09	52.77	55.74	54.70	71.68	-	-
XAn	0.47	0.46	0.47	0.44	0.45	0.28	-	-
XAb	0.53	0.54	0.53	0.56	0.55	0.72	-	-
ln(XAn/XAb)	-0.11	-0.16	-0.11	-0.23	-0.19	-0.93	-	-

sample 9074 (amphibolite)
weight % oxides

	amphibole	amphibole	amphibole
SiO2	53.25	52.62	52.62
TiO2	0.09	0.14	0.07
Al2O3	0.93	1.38	1.45
FeO	9.07	9.44	9.09
MnO	0.26	0.26	0.37
MgO	13.23	13.05	13.11
CaO	23.05	22.74	22.57
Na2O	0.5	0.54	0.54
K2O	0.05	0.04	0
Cr2O3	0.21	0.06	0
NiO	0	0.42	0.52
Total	100.64	100.69	100.34
formula amounts calculated to O as below			
Si	7.92	7.85	7.87
Ti	0.01	0.02	0.01
Al	0.16	0.24	0.26
Fe	1.13	1.18	1.14
Mn	0.03	0.03	0.05
Mg	2.94	2.9	2.92
Ca	3.68	3.64	3.62
Na	0.15	0.16	0.16
K	0.01	0.01	0
Cr	0.02	0.01	0
Ni	0	0.05	0.06
O -2	24	24	24
Aliv	0.08	0.15	0.13
Alvi	0.09	0.1	0.12
Na+K	0.16	0.16	0.16
Alvi+Ti	0.1	0.11	0.13
XNa(amp)	3.20	3.12	3.12

sample 9074 (amphibolite)
weight % oxides

	amphibole	amphibole	amphibole	amphibole	amphibole	amphibole	amphibole	amphibole	amphibole	amphibole	sphene	sphene
SiO2	52.76	52.48	46.84	45.93	46.32	46.38	46.19	53.12	52.28	46.74	20.493	30.294
TiO2	0.3	0.15	1.26	1.62	1.46	1.29	1.63	0.15	0.08	1.03	58.741	39.378
Al2O3	1.31	1.4	8.44	9.31	8.37	8.35	9.42	1.58	1.17	8.87	0.657	0.922
FeO	9.09	9.11	14.54	14.93	14.88	14.97	14.75	9.53	9.45	16.04	2.838	0.748
MnO	0.26	0.29	0.1	0.15	0.28	0.23	0.41	0.19	0.23	0.42	0.173	0.005
MgO	13.26	13.06	12.54	12.28	12.39	12.68	12.71	13.15	12.97	12.43	0	0.033
CaO	22.87	22.58	11.85	11.96	11.94	11.64	11.56	22.87	22.71	11.76	18.378	27.143
Na2O	0.49	0.43	1.53	1.73	1.55	1.76	1.84	0.64	0.37	1.92	0.158	0.246
K2O	0.01	0	0.14	0.12	0.12	0.03	0.05	0	0.05	0.08	0.065	0.053
Cr2O3	0.13	0.18	0.09	0.24	0.25	0.16	0.18	0.06	0.03	0.08	0.175	0.003
NiO	0	0.07	0.18	0	0.03	0	0.51	0.23	0.22	0	0.326	0.436
Total	100.48	99.75	97.51	98.27	97.59	97.49	99.25	101.52	99.56	99.37	102.004	99.261
formula amounts calculated to O as below												
Si	7.86	7.88	7.21	7.04	7.15	7.16	7.02	7.85	7.89	7.12	4.276	3.99
Ti	0.03	0.02	0.15	0.19	0.17	0.15	0.19	0.02	0.01	0.12	9.217	3.901
Al	0.23	0.25	1.53	1.68	1.52	1.52	1.69	0.27	0.21	1.59	0.162	0.143
Fe	1.13	1.14	1.87	1.91	1.92	1.93	1.87	1.18	1.19	2.04	0.495	0.082
Mn	0.03	0.04	0.01	0.02	0.04	0.03	0.05	0.02	0.03	0.05	0.031	0.001
Mg	2.95	2.92	2.88	2.81	2.85	2.92	2.88	2.9	2.92	2.82	0	0.007
Ca	3.65	3.63	1.95	1.96	1.97	1.93	1.88	3.62	3.67	1.92	4.108	3.831
Na	0.14	0.13	0.46	0.51	0.46	0.53	0.54	0.18	0.11	0.57	0.064	0.063
K	0	0	0.03	0.02	0.02	0.01	0.01	0	0.01	0.02	0.017	0.009
Cr	0.02	0.02	0.01	0.03	0.03	0.02	0.02	0.01	0	0.01	0.029	0
Ni	0	0.01	0.02	0	0	0	0.06	0.03	0.03	0	0.055	0.046
O -2	24	24	24	24	24	24	24	24	24	24	20	20
Aliv	0.14	0.12	0.79	0.96	0.85	0.84	0.98	0.15	0.11	0.88	-	-
Alvi	0.09	0.13	0.74	0.72	0.67	0.68	0.71	0.13	0.09	0.71	-	-
Na+K	0.14	0.13	0.48	0.54	0.49	0.53	0.55	0.18	0.12	0.58	-	-
Alvi+Ti	0.13	0.14	0.88	0.91	0.84	0.83	0.89	0.14	0.1	0.83	-	-
XNa(amp)	3.26	3.33	1.44	1.35	1.45	1.29	1.25	3.00	3.51	1.21	-	-

sample 9080 (amphibolite)
weight % oxides

	feldspar	feldspar	feldspar	feldspar	feldspar	feldspar
SiO2	59.36	59.93	59.678	59.689	58.835	58.908
TiO2	0	0	0	0.128	0.111	0.077
Al2O3	25.549	25.932	25.733	26.297	25.832	26.011
FeO	0.102	0.161	0.133	0.134	0.441	0.208
MnO	0.004	0	0.086	0.02	0	0.074
MgO	0	0	0	0.01	0	0
CaO	7.416	7.579	7.502	7.732	7.95	7.909
Na2O	7.652	7.926	7.977	7.754	7.593	7.647
K2O	0.1	0.001	0.051	0.018	0.061	0.015
P2O5	0	0.059	0	0	0	0
Cr2O3	0.157	0.087	0.042	0.025	0.036	0
Total	100.34	101.675	101.202	101.807	100.859	100.849

formula calculated to 24 Oxygens

Si	2.644	2.636	7.918	2.623	7.852	2.617
Ti	0	0	0	0.004	0.011	0.003
Al	1.341	1.344	4.024	1.362	4.063	1.362
Fe	0.004	0.006	4.015	0.005	0.049	0.008
Mn	0	0	0.01	0.001	0	0.003
Mg	0	0	0	0.001	0	0
Ca	0.345	0.357	1.066	0.364	1.137	0.377
Na	0.661	0.676	2.052	0.661	1.965	0.659
K	0.006	0	0.009	0.001	0.01	0.001
P	0	0.002	0	0	0	0
Cr	0.006	0.003	0.004	0.001	0.004	0
O -2	24	24	24	24	24	24
XAn	0.34	0.35	0.34	0.36	0.37	0.36
XAb	0.66	0.65	0.66	0.64	0.63	0.64
Ln(Xan/Xab)	-0.65	-0.64	-0.65	-0.60	-0.55	-0.56
An	34.29	34.56	34.19	35.51	36.65	36.39
Ab	65.71	65.44	65.81	64.49	63.35	63.61

sample 9080 (amphibolite)
weight % oxides

	amphibole	amphibole	amphibole	amphibole	amphibole
SiO2	45.92	41.73	45.26	48.15	47.7
TiO2	0.84	14.11	0.88	0.81	0.89
Al2O3	8.44	6.97	8.44	8.49	8.54
FeO	13.72	7.35	13.71	15.09	14.46
MnO	0.41	0.19	0.23	0.1	0.27
MgO	12.82	6.79	12.56	13.32	13.5
CaO	11.16	16.31	11.18	11.79	11.96
Na2O	1.36	1.75	0.98	1.09	1.06
K2O	0.36	0.14	0.36	0.38	0.41
P2O5	0	0	0	0	0
Cr2O3	0.13	0.23	0.15	0.2	0
Total	95.16	95.57	93.75	99.42	98.79

Si	7.22	6.55	7.22	7.26	7.23
Ti	0.1	1.66	0.11	0.09	0.1
Al	1.56	1.29	1.59	1.51	1.53
Fe	1.8	0.96	1.83	1.9	1.83
Mn	0.05	0.03	0.03	0.01	0.03
Mg	3	1.59	2.99	2.99	3.05
Ca	1.88	2.74	1.91	1.9	1.94
Na	0.42	0.53	0.3	0.32	0.31
K	0.07	0.03	0.07	0.07	0.08
P	0	0	0	0	0
Cr	0.02	0.03	0.02	0.02	0
O -2	24	24	24	24	24
Aliv	0.78	1.45	0.78	0.74	0.77
Alvi	0.79	-0.2	0.81	0.76	0.75
AlVI+Ti+4	0.89	1.5	0.91	0.86	0.85
Na+1+K+1	0.49	0.56	0.37	0.39	0.39
XNa(amp)	1.50	1.64	1.85	1.78	1.83

sample 9080 (amphibolite)
weight % oxides

	amphibole	amphibole	amphibole	amphibole	amphibole	amphibole	amphibole	amphibole	amphibole	amphibole	amphibole
SiO2	47.44	47.04	48.37	47.27	49.19	49.18	47.25	48.55	48.23	45.32	48.36
TiO2	0.81	0.94	0.78	0.81	0.69	0.74	0.8	0.73	0.87	1	0.9
Al2O3	8.86	8.94	8.22	8.67	7.71	7.2	8.59	7.38	8.37	10.2	8.18
FeO	14.64	14.47	13.95	14.78	12.64	12.6	13.18	12.74	13.4	15.03	13.77
MnO	0.31	0.32	0.23	0.22	0.29	0.29	0.18	0.34	0.25	0.37	0.34
MgO	12.81	13.03	13.6	13.13	15.04	14.76	13.35	14.71	13.97	12.47	13.83
CaO	11.46	11.55	12.11	11.86	11.49	11.52	10.66	11.66	11.88	11.25	11.82
Na2O	1.3	1.1	0.94	1.12	0.98	1.07	0.92	1.12	1.11	1.54	1.12
K2O	0.41	0.44	0.37	0.37	0.23	0.26	0.58	0.29	0.23	0.42	0.25
P2O5	0	0.1	0.02	0	0.04	0	0	0	0	0	0
Cr2O3	0.02	0.12	0	0.04	0.09	0.1	0.1	0.01	0	0.05	0.08
Total	98.06	98.05	98.59	98.27	98.39	97.72	95.61	97.53	98.31	97.65	98.65
formula calculated to 24 Oxygens											
Si	7.24	7.18	7.31	7.21	7.38	7.44	7.33	7.38	7.29	6.99	7.3
Ti	0.09	0.11	0.09	0.09	0.08	0.08	0.09	0.08	0.1	0.12	0.1
Al	1.59	1.61	1.46	1.56	1.36	1.28	1.57	1.32	1.49	1.85	1.46
Fe	1.87	1.85	1.76	1.89	1.59	1.59	1.71	1.62	1.69	1.94	1.74
Mn	0.04	0.04	0.03	0.03	0.04	0.04	0.02	0.04	0.03	0.05	0.04
Mg	2.92	2.97	3.07	2.99	3.37	3.33	3.09	3.33	3.15	2.87	3.11
Ca	1.87	1.89	1.96	1.94	1.85	1.87	1.77	1.9	1.92	1.86	1.91
Na	0.38	0.32	0.27	0.33	0.28	0.31	0.28	0.33	0.33	0.46	0.33
K	0.08	0.09	0.07	0.07	0.04	0.05	0.11	0.06	0.04	0.08	0.05
P	0	0.01	0	0	0	0	0	0	0	0	0
Cr	0	0.01	0	0.01	0.01	3	0.01	0.01	0	0.01	0.01
O -2	24	24	24	24	24	24	24	24	24	24	24
Aliv	0.76	0.82	0.69	0.79	0.62	0.56	0.67	0.62	0.71	1.01	0.7
Alvi	0.84	0.79	0.78	0.77	0.75	0.72	0.9	0.7	0.78	0.85	0.76
AlVI+Ti+4	0.93	0.9	0.87	0.86	0.83	0.81	0.99	0.79	0.88	0.96	0.86
Na+1+K+1	0.46	0.41	0.35	0.4	0.33	0.36	0.39	0.38	0.37	0.54	0.38
XNa(amp)	1.59	1.78	1.98	1.77	1.89	1.80	1.84	1.75	1.76	1.40	1.76

sample 9104 (Mélange - Rioja)
weight % oxides

	feldspar	feldspar	feldspar	feldspar	feldspar
SiO2	68.542	68.779	68.467	68.864	68.467
TiO2	0	0	0.04	0	0.003
Al2O3	19.235	19.438	19.263	19.627	19.475
FeO	0.178	0.227	0.231	0.278	0.238
MnO	0.142	0.019	0	0	0.009
MgO	0	0	0	0.028	0
CaO	0.279	0.299	0.393	0.288	0.406
Na2O	12.296	12.457	12.267	12.299	12.128
K2O	0.038	0	0	0.008	0
Cr2O3	0	0	0.126	0.085	0.036
NiO	0.168	0	0.029	0.359	0.241
Total	100.878	101.219	100.816	101.836	101.003
formula calculated on the basis of 24 Oxygens					
Si	2.984	2.982	2.981	2.973	2.977
Ti	0	0	0.001	0	0
Al	0.987	0.993	0.989	0.999	0.998
Fe	0.006	0.008	0.008	0.01	0.009
Mn	0.005	0.001	0	0	0
Mg	0	0	0	0.002	0
Ca	0.013	0.014	0.018	0.013	0.19
Na	1.038	1.047	1.036	1.029	1.022
K	0.002	0	0	0	0
Cr	0	0	0.004	0.003	0.001
Ni	0.006	0	0.001	0.012	0.008
An	1.24	1.32	1.71	1.25	15.68
Ab	98.76	98.68	98.29	98.75	84.32
XAn	0.01	0.01	0.02	0.01	0.16
XAb	0.99	0.99	0.98	0.99	0.84
ln(XAn/XAb)	-4.38	-4.31	-4.05	-4.37	-1.68

sample 9104 (Mélange - Rioja)
weight % oxides

	amphibole	amphibole	amphibole	amphibole	amphibole	amphibole
SiO2	62.44	50.9	52.94	53.09	57.55	53.35
TiO2	0.06	4.17	0	0.08	0.03	0.12
Al2O3	14.1	3.05	5.47	3.87	3.03	4447
FeO	4.66	11.69	12.72	13.09	11.76	12.95
MnO	0.02	0.1	0.11	0.38	0.24	0.21
MgO	5.13	13.55	13.7	14.72	13.79	14.57
CaO	4.78	14.23	12.1	12.09	11.24	11.93
Na2O	8.35	0.38	1.04	0.63	0.41	0.49
K2O	0.03	0.06	0.07	0.02	0.06	0.25
Cr2O3	0.02	0.1	0.07	0.19	0	0
NiO	0	0	0.41	0.44	0.19	0.04
Total	99.59	98.23	98.63	98.6	98.3	4540.91
Si	8.58	7.67	7.89	7.94	8.44	0.16
Ti	0.01	0.47	0	0.01	0	0
Al	2.28	0.54	0.96	0.68	0.52	15.69
Fe	0.54	1.47	1.58	1.64	1.44	0.03
Mn	0	0.01	0.01	0.05	0.03	0
Mg	1.05	3.04	3.04	3.28	3.01	0.07
Ca	0.7	2.3	1.93	1.94	1.77	0.04
Na	2.22	0.11	0.3	0.18	0.12	0
K	0	0.01	0.01	0	0.01	0
Cr	0	0.01	0.01	0.02	0	0
Ni	0.05	0.05	0.02	0	0.02	0
Mg/(Mg+Fe)	0.66	0.67	0.66	0.67	0.68	0.70
Na+K	2.22	0.12	0.31	0.18	0.13	0
ln(Ca/Na(M4)) amph		3.04	1.86	2.38	2.69	-

sample 9104 (Mélange - Rioja)
weight % oxides

	amphibole	amphibole
SiO2	54.54	52.68
TiO2	0.02	0.29
Al2O3	2.81	3.31
FeO	13.19	12.79
MnO	0.34	0.24
MgO	15.61	15
CaO	12.34	12.47
Na2O	0.57	0.42
K2O	0.04	0.14
Cr2O3	0.29	0.07
NiO	0	0.18
Total	99.75	97.59

formula calculated on the basis of 24 O

Si	8.04	7.95
Ti	0	0.03
Al	0.49	0.59
Fe	1.63	1.61
Mn	0.04	0.03
Mg	3.43	3.38
Ca	1.95	2.02
Na	0.16	0.12
K	0.01	0.03
Cr	0.03	0.01
Ni	0	0
Mg/(Mg+Fe)	0.68	0.68
Na+K	0.17	0.15
ln(Ca/Na(M4	2.50	2.82

sample 9136 (Quartz-mica schist - Rioja)
weight % oxides

	muscovite	garnet	garnet	garnet	garnet	andalusite
SiO2	45.762	37.128	36.872	37.283	36.944	36.942
TiO2	0.546	0.23	0.093	0.181	0.163	0
Al2O3	35.952	20.967	20.697	20.975	20.423	62.965
FeO	0.918	23.494	28.184	20.832	22.52	0.184
MnO	0.009	13.996	10.062	17.291	15.619	0.028
MgO	0.156	1.189	1.064	0.712	0.688	0
CaO	0	1.689	1.534	2.102	1.818	0.008
Na2O	0.756	0	0.15	0.02	0.064	0
K2O	9.603	0.015	0	0.009	0	0.018
Cr2O3	0.067	0.191	0.03	0	0.027	0.087
NiO	0	0	0	0	0.015	0.006
Total	93.769	98.899	98.686	99.405	98.281	100.238
fromula calculated on the basis of oxygen as below						
Si	6.7	6.055	6.061	6.074	6.097	4.777
Ti	0.06	0.028	0.011	0.022	0.02	0
Al	6.205	4.03	4.01	4.028	3.973	9.597
Fe	0.112	3.204	3.874	2.837	3.108	0.02
Mn	0.001	1.933	1.401	2.386	2.183	0.003
Mg	0.034	0.289	0.261	0.173	0.169	0
Ca	0	0.295	0.27	0.367	0.322	0.001
Na	0.215	0	0.048	0.006	0.021	0
K	1.794	0.003	0	0.002	0	0.003
Cr	0.008	0.026	0.004	0	0.004	0.009
Ni	0	0	0	0	0.002	0.001
O	24	24	24	24	24	24
Alm(Fe)	-	56.00	66.72	49.23	53.75	-
Spess(Mn)	-	33.79	24.13	41.40	37.76	-
Gross(Ca)	-	5.16	4.65	6.37	5.57	-
Pyr(Mg)	-	5.05	4.50	3.00	2.92	-

sample 9156 (Mélange - Peramora)
weight % oxides

	feldspar	feldspar	feldspar	feldspar	clinozoisite	clinozoisite	clinozoisite	clinozoisite	clinozoisite	epidote	epidote	epidote
SiO2	68.611	68.683	58.659	68.92	39.073	39.414	39.223	39.562	39.624	39.264	39.28	39.6
TiO2	0	0	0.051	0.029	0.139	0.122	0.136	0.201	0.118	0.305	0.175	0.04
Al2O3	20.195	20.285	25.689	19.969	27.551	28.812	28.663	27.288	29.43	26.175	28.03	27.592
FeO	0.129	0.287	0.637	0	7.354	6.2	6.048	6.97	5.875	8.795	6.922	7.607
MnO	0.001	0	0.109	0.017	0.034	0.24	0.029	0.064	0.099	0.061	0.087	0.113
MgO	0.046	0.067	0.453	0	0	0.006	0	0	0	0	0	0.056
CaO	0.883	0.879	8.275	0.753	23.436	23.236	23.749	23.923	24.121	23.585	23.915	23.785
Na2O	12.155	12	7.378	12.296	0.034	0.043	0.02	0.003	0	0	0.177	0.124
K2O	0.048	0.024	0.066	0.012	0.023	0.089	0.036	0.031	0	0.28	0.11	0.017
Cr2O3	0	0	0.045	0	0.065	0.196	0.037	0.16	0.04	0.182	0.136	0.136
NiO	0.141	0.438	0	0	0	0	0	0	0	0.083	0.1	0
Total	102.209	102.663	101.362	101.996	97.709	98.358	97.941	98.202	99.307	98.73	98.932	99.07
formulae calculated on the basis of oxygens given below												
Si	2.951	8.836	2.604	2.965	1.972	5.891	3.188	3.226	3.173	3.226	3.186	3.21
Ti	0	0	0.002	0.001	0.005	0.014	0.008	0.012	0.007	0.019	0.011	0.002
Al	1.024	3.076	1.344	1.013	1.639	5.076	2.746	2.623	2.778	2.535	2.679	2.637
Fe	0.005	0.031	0.024	0	0.31	0.775	0.411	0.475	0.393	0.604	0.47	0.516
Mn	0	0	0.004	0.001	0.001	0.03	0.002	0.004	0.007	0.004	0.006	0.008
Mg	0.003	0.13	0.03	0	0	0.001	0	0	0	0	0	0.007
Ca	0.041	0.121	0.394	0.035	1.268	3.721	2.068	2.091	2.07	2.076	2.078	2.066
Na	1.014	2.994	0.635	1.026	0.003	0.013	0.003	0.001	0	0	0.018	0.019
K	0.003	0.004	0.004	0.001	0.001	0.017	0.004	0.003	0	0.003	0.011	0.002
Cr	0	0	0.002	0	0.003	0.023	0.002	0.01	0.003	0.012	0.009	0.009
Ni	0.005	0.05	0	0	0	0	0	0	0	0	0	0
O	24	24	24	24	13	13	13	13	13	13	13	13
An	3.89	3.88	38.29	3.30	-	-	-	-	-	-	-	-
Ab	96.11	96.12	61.71	96.70	-	-	-	-	-	-	-	-
XAn	0.04	0.04	0.38	0.03	-	-	-	-	-	-	-	-
XAb	0.96	0.96	0.62	0.97	-	-	-	-	-	-	-	-
ln(XAn/XAb)	-3.21	-3.21	-0.48	-3.38	-	-	-	-	-	-	-	-

sample 9156 (Mélange - Peramora)
weight % oxides

	epidote	amphibole	amphibole	amphibole	amphibole
SiO2	39.316	53.87	54.9	54.34	52.72
TiO2	0.099	0.21	0.29	0	0.23
Al2O3	27.633	2.94	2.62	3.41	3.78
FeO	7.371	14.04	13.7	13.82	14.39
MnO	0.218	0.24	0.27	0.27	0.41
MgO	0	14.61	14.93	14.93	13.77
CaO	23.394	12.23	11.99	12.37	11.84
Na2O	0	0.17	0.52	0.59	0.69
K2O	0.031	0.12	0.04	0.23	0.08
Cr2O3	0.011	0.1	0.06	0	0.12
NiO	0.352	0	0	0	0
Total	98.425	98.53	99.32	99.96	98.03
formulae calculated on the basis of oxygens below					
Si	3.207	8.06	8.12	8.01	7.96
Ti	0.006	0.02	0.03	0	0.03
Al	2.657	0.52	0.46	0.59	0.67
Fe	0.503	1.76	1.69	1.7	1.82
Mn	0.015	0.03	0.03	0.03	0.05
Mg	0	3.26	3.29	3.28	3.1
Ca	2.045	1.96	1.9	1.95	1.92
Na	0	0.05	0.15	0.17	0.2
K	0.003	0.02	0.01	0.04	0.01
Cr	0.001	0.01	0.01	0	0.01
Ni	0.023	0	0	0	0
O	13	24	24	24	24
Mg/(Mg+Fe)	-	0.65	0.66	0.66	0.63
Na+K	-	0.07	0.16	0.21	0.21
Ln(Ca/Na(M	-	3.67	2.54	2.44	2.26

sample 9176 (amphibolite El Huron)
weight % oxides

	feldspar	feldspar	feldspar	feldspar	feldspar	feldspar	feldspar	feldspar
SiO2	56.066	55.844	54.543	54.151	54.371	54.485	54.66	57.456
TiO2	0.026	0.071	0.031	0.003	0	0	0	0
Al2O3	25.858	26.05	26.159	26.29	24.841	26.484	25.71	22.192
FeO	0.179	0.37	0.245	0.132	0.124	0.582	0.49	0.305
MnO	0.033	0	0.176	0	0.059	0	0	0.019
MgO	0	0	0	0	0	0	0	0.131
CaO	8.184	8.59	9.093	9.247	7.938	9.144	8.293	5.461
Na2O	7.012	6.816	6.514	5.975	6.393	6.405	6.67	8.099
K2O	0.045	0.081	0.006	0.115	0.143	0	0.004	0.206
Cr2O3	0	0.032	0	0.02	0	0	0	0.094
NiO	0.006	0.022	0.062	0.062	0.025	0.031	0.119	0
Total	97.409	97.876	96.829	95.995	93.894	97.131	95.946	93.963
formulae calculated on the basis of oxygens given below								
Si	10.331	10.263	10.155	7.609	10.371	7.588	10.27	10.902
Ti	0.004	0.01	0.004	0	0	0	0	0
Al	50616	5.643	50741	4.355	5.597	4.348	5.694	40963
Fe	0.028	0.057	0.038	0.016	0.02	0.068	0.008	0.048
Mn	0.005	0	0.028	0	0.01	0	0	0.003
Mg	0	0	0	0	0	0	0	0.037
Ca	1.616	1.692	1.814	1.392	1.626	1.365	1.67	1011
Na	2.505	2.429	2.352	1.628	2.369	1.73	2.43	2098
K	0.011	0.019	0.001	0.021	0.035	0	0.001	0.05
Cr	0	0.005	0	0.002	0	0	0	0.015
Ni	0.001	0.003	0.009	0.007	0.004	0.003	0.018	0
O -2	24	24	24	24	24	24	24	24
An	39.21	41.06	43.54	46.09	40.70	44.10	40.73	32.52
Ab	60.79	58.94	56.46	53.91	59.30	55.90	59.27	67.48
XAn	0.39	0.41	0.44	0.46	0.41	0.44	0.41	0.33
XAb	0.61	0.59	0.56	0.54	0.59	0.56	0.59	0.67
ln(XAn/XAb)	-0.44	-0.36	-0.26	-0.16	-0.38	-0.24	-0.38	-0.73

sample 9176 (amphibolite El Huron)
weight % oxides

	amphibole	amphibole	amphibole
SiO2	34.21	45.69	45.64
TiO2	2.58	0.96	1.18
Al2O3	19.94	8.41	8.71
FeO	22.89	16.38	15.59
MnO	0.31	0.22	0.23
MgO	6.32	11.27	11.66
CaO	0	1.4	11.28
Na2O	0.14	1.6	1.51
K2O	8.07	0.12	0.02
Cr2O3	0.02	0	0
NiO	0	0.08	0.09
Total	94.48	86.13	95.91
Si	5.8	7.75	7.17
Ti	0.33	0.12	0.14
Al	3.98	1.68	1.61
Fe	3.24	2.32	2.05
Mn	0.04	0.03	0.03
Mg	1.59	2.85	2.73
Ca	0	0.25	1.9
Na	0.05	0.52	0.46
K	1.74	0.03	0
Cr	0	0	0
Ni	0	0.01	0.01
O -2	24	24	24
Aliv	2.2	0.25	0.83
Alvi	1.78	1.43	0.79
Na+K	1.79	0.55	0.46
Alvi+Ti	2.1	1.55	0.93
LnCa/Na(M4	0.00	-0.73	1.42

sample 9176 (amphibolite El Huron)
weight % oxides

	amphibole	amphibole	amphibole	amphibole	amphibole	amphibole	amphibole	amphibole	amphibole	amphibole	amphibole
SiO2	45.35	45.94	52.07	45.84	44.45	44.81	45.15	49.66	49.16	49.16	44.06
TiO2	1.05	1.1	0.4	1.14	0.73	1.04	1.3	0.25	0.21	0.29	1.17
Al2O3	8.32	8.03	12.13	7.98	9.01	8.57	8.54	1.32	1.74	1.43	7.88
FeO	16.21	15.74	8.13	16.19	15.87	16.47	16.08	10.11	10.45	10.45	15.37
MnO	0.33	0.27	0.21	0.18	0.33	0.08	0.23	0.31	0.22	0.27	0.23
MgO	11.46	11.65	8.39	11.76	11.1	11.24	11.09	11.83	11.48	11.56	11.04
CaO	11.35	11.51	9.72	11.44	11.22	11.21	11.28	20.85	21.06	20.83	10.87
Na2O	1.42	1.53	3.78	1.43	1.54	1.46	1.16	0.35	0.59	0.49	1.3
K2O	0.17	0.17	0.07	0.11	0.12	0.1	0.12	0.08	0	0.01	0.14
Cr2O3	0	0	0	0	0	0	0	0.02	0	0	0
NiO	0.04	0.06	0	0.09	0	0.06	0.04	0.13	0.05	0.06	0.11
Total	95.7	96	94.9	96.16	94.37	95.04	94.99	94.91	94.96	94.55	92.17
formulae calculated on the basis of oxygens given below											
Si	7.18	7.23	7.82	7.21	7.13	7.15	7.18	7.88	7.82	7.85	7.22
Ti	0.12	0.13	0.05	0.14	0.09	0.12	0.16	0.03	0.03	0.03	0.14
Al	1.55	1.49	2.15	1.48	1.7	1.61	1.6	0.25	0.33	0.27	1.52
Fe	2.15	2.07	1.02	2.13	2.13	2.2	2.14	1.34	1.39	1.4	2.11
Mn	0.04	0.04	0.03	0.02	0.04	0.01	0.03	0.04	0.03	0.04	0.03
Mg	2.71	2.73	1.88	2.76	2.66	2.67	2.63	2.8	2.72	2.75	2.7
Ca	1.93	1.94	1.56	1.93	1.93	1.92	1.92	3.55	3.59	3.56	1.91
Na	0.44	0.47	1.1	0.44	0.48	0.45	0.36	0.11	0.18	0.15	0.41
K	0.03	0.03	0.01	0.02	0.02	0.02	0.02	0.02	0	0	0.03
Cr	0	0	0	0	0	0	0	0	0	0	0
Ni	0	0.01	0	0.01	0	0.01	0.01	0.02	0.01	0.01	0.01
O -2	24	24	24	24	24	24	24	24	24	24	24
Aliv	0.82	0.77	0.18	0.79	0.87	0.85	0.82	0.12	0.18	0.15	0.78
Alvi	0.73	0.72	1.97	0.69	0.83	0.76	0.79	0.13	0.14	0.12	0.75
Na+K	0.47	0.5	1.11	0.46	0.5	0.47	0.38	0.12	0.18	0.15	0.44
Alvi+Ti	0.86	0.85	2.01	0.83	0.92	0.88	0.94	0.16	0.17	0.15	0.89
LnCa/Na(M4	1.48	1.42	0.35	1.48	1.39	1.45	1.67	3.47	2.99	3.17	1.54

sample 9179 (Amphibolite - El Huron)
weight % oxides

	feldspar	feldspar	feldspar	feldspar	feldspar	sphene	sphene	sphene	sphene	sphene	sphene	ilmenite
SiO2	55.64	56.174	57.682	57.709	57.373	30.005	30.253	30.658	30.475	30.73	24.754	4.044
TiO2	0.041	0	0.109	0	0	38.771	40.246	39.779	39.748	40.236	42.342	45.608
Al2O3	26.478	26.723	27.319	27.387	27.593	1.099	0.861	0.888	0.773	0.844	0.94	0.217
FeO	0.077	0	0.358	0.315	0.135	0.793	0.669	0.69	0.665	0.628	10.667	44.597
MnO	0.194	0.055	0.033	0.042	0	0.076	0.094	0.102	0.197	0.109	0.817	1.302
MgO	0	0	0	0	0	0.141	0.019	0.11	0	0.038	0	0.262
CaO	8.853	9.033	9.36	9.179	9.343	27.116	27.818	28.362	28.052	28.17	21.499	3.306
Na2O	6.39	6.504	6.808	6.834	6.831	0.097	0	0.048	0	0.029	0.054	0.074
K2O	0.027	0.044	0.078	0.083	0.05	0	0	0.044	0	0.056	0	0.012
P2O5	0	0	0	0	0	0.073	0.114	0.059	0.103	0.191	0.248	0
Cr2O3	0.069	0	0	0	0.035	0.093	0	0.208	0	0.121	0.125	0.171
Total	97.769	98.533	101.747	101.549	101.36	98.264	100.074	100.948	100.013	101.152	101.446	99.593
formulae calculated from oxygen given below												
Si	2.556	2.558	2.552	2.556	2.545	3.984	3.947	3.972	3.981	3.967	5.344	1.081
Ti	0.001	0	0.004	0	0	3.872	3.949	3.876	3.905	3.906	6.874	9.171
Al	1.434	1.435	1.425	1.43	1.443	0.172	0.132	0.136	0.119	0.128	0.239	0.068
Fe	0.003	0	0.013	0.012	0.005	0.088	0.073	0.075	0.073	0.068	1.926	9.972
Mn	0.008	0.002	0.001	0.002	0	0.009	0.01	0.011	0.022	0.012	0.149	0.295
Mg	0	0	0	0	0	0.028	0.004	0.021	0	0.007	0	0.104
Ca	0.436	0.441	0.444	0.436	0.444	3.858	3.889	3.937	3.927	3.896	4.973	0.947
Na	0.569	0.574	0.584	0.587	0.588	0.025	0	0.012	0	0.007	0.023	0.038
K	0.002	0.003	0.004	0.005	0.003	0	0	0.007	0	0.009	0	0.004
P	0	0	0	0	0	0.008	0.013	0.006	0.011	0.021	0.045	0
Cr	0.002	0	0	0	0.001	0.01	0	0.021	0	0.012	0.021	0.036
O	24	24	24	24	24	20	20	20	20	20	20	6
An	43.38	43.45	43.19	42.62	43.02	-	-	-	-	-	-	-
Ab	56.62	56.55	56.81	57.38	56.98	-	-	-	-	-	-	-
XAn	0.43	0.43	0.43	0.43	0.43	-	-	-	-	-	-	-
XAb	0.57	0.57	0.57	0.57	0.57	-	-	-	-	-	-	-
ln(XAn/XAb)	-0.27	-0.26	-0.27	-0.30	-0.28	-	-	-	-	-	-	-

sample 9179 (Amphibolite - El Huron)
weight % oxides

	amphibole	amphibole	amphibole	amphibole	amphibole	amphibole	amphibole	amphibole	amphibole	amphibole
SiO2	45.77	46.25	47.37	46.87	46.98	47.71	47.11	53.06	53.17	52.98
TiO2	1.43	1.2	1.27	1.41	0.99	1.13	1	0.14	0.52	0.25
Al2O3	8.21	7.99	8.66	8.27	8.32	8.11	7.56	1.13	1.26	1.42
FeO	15.7	15.08	16.38	16.02	16.04	15.92	15.42	9.88	10.57	10.47
MnO	0.32	0.27	0.25	0.23	0.21	0.32	0.22	0.21	0.19	0.27
MgO	11.78	12.12	12.2	12.17	12.38	12.69	12.33	12.77	12.79	12.6
CaO	11.44	11.46	11.78	11.39	11.82	11.37	11.78	22.71	22.94	22.38
Na2O	1.46	1.33	1.58	1.65	1.65	1.58	1.53	0.29	0.68	0.44
K2O	0.14	0.18	0.17	0.07	0.14	0.09	0.15	0.06	0.08	0.08
P2O5	0	0	0	0	0	0	0	0	0	0
Cr2O3	0.09	0.02	0.19	0.02	0.7	0.11	0.16	0.2	0.11	0.04
Total	96.34	95.9	99.85	98.1	99.23	99.03	97.26	100.45	102.31	100.93
formulae calculated from oxygen given below										
Si	7.18	7.25	7.17	7.21	7.16	7.25	7.3	7.92	7.84	7.89
Ti	0.17	0.14	0.14	0.16	0.11	0.13	0.12	0.02	0.06	0.03
Al	1.52	1.48	1.54	1.5	1.5	1.45	1.38	0.2	0.22	0.25
Fe	2.06	1.98	2.07	2.06	2.05	2.02	2	1.23	1.3	1.3
Mn	0.04	0.04	0.03	0.03	0.03	0.04	0.03	0.03	0.02	0.03
Mg	2.75	2.83	2.75	2.79	2.81	2.88	2.85	2.84	2.81	2.8
Ca	1.92	1.93	1.91	1.88	1.93	1.85	1.95	3.63	3.62	3.57
Na	0.45	0.4	0.46	0.49	0.49	0.46	0.46	0.08	0.19	0.13
K	0.04	0.03	0.01	0.03	0.02	0.03	0.01	0.02	0.01	0
P	0	0	0	0	0	0	0	0	0	0
Cr	0.01	0	0.02	0	0.08	0.01	0.02	0.02	0.01	0
O	24	24	24	24	24	24	24	24	24	24
Aliv	0.75	0.83	0.79	0.84	0.75	0.7	0.08	0.16	0.11	0
Na+1+K+1	0.47	0.44	0.5	0.51	0.51	0.48	0.49	0.1	0.21	0.14
Alvi	0.7	0.73	0.71	0.71	0.66	0.71	0.68	0.12	0.06	0.14
Alvi+Ti+4	0.86	0.87	0.86	0.87	0.77	0.84	0.79	0.14	0.11	0.17
ln(Ca/Na(M4	1.45	1.57	1.42	1.34	1.37	1.39	1.44	3.81	2.95	3.31

sample 9187 (amphibolite - El Huron)
weight % oxide

	feldspar	feldspar	feldspar	feldspar	feldspar	feldspar	ilmenite	ilmenite	ilmenite	ilmenite	ilmenite	ilmenite
SiO2	54.251	54.43	56.552	54.491	54.505	55.655	12.911	10.867	0.646	0.793	17.585	14.581
TiO2	0.08	0.042	0.001	0	0.057	0.122	60.635	49.282	53.654	51.958	37.496	47.347
Al2O3	29.093	28.985	27.765	28.986	29.195	28.834	1.595	0.988	0.286	0.09	3.548	0.686
FeO	0.222	0.293	0.148	0.097	0.184	0.179	16.425	30.695	44.363	45.62	29.834	26.722
MnO	0.026	0	0	0	0.003	0	0.73	1.101	0.9	0.787	0.895	0.805
MgO	0	0	0	0	0.065	0	1.968	0.461	0.273	0.119	5.187	0.041
CaO	11.371	11.251	9.865	11.545	11.35	11.015	7.137	8.563	0.388	0.597	6.821	12.405
Na2O	5.289	5.409	6.448	5.221	5.29	5.729	0.169	0.253	0.332	0.297	0.685	0.058
K2O	0.115	0.014	0.032	0.012	0.057	0.009	0.067	0	0.053	0	0	0.006
Cr2O3	0.038	0.065	0.116	0.089	0.049	0.07	0.114	0.054	0.036	0.284	0.199	0.091
NiO	0	0	0	0	0	0.273	0.358	0	0	0.486	0.301	0
Total	100.485	100.489	100.927	100.441	100.755	101.886	102.109	102.264	100.931	101.031	102.551	102.742
formulae calculated from oxygen given below												
Si	2.442	2.449	2.523	2.541	2.445	2.47	0.533	0.485	0.032	0.039	0.755	0.633
Ti	0.003	0.001	0	0	0.002	0.004	1.882	1.655	1.992	1.945	1.211	1.547
Al	1.544	1.537	1.46	1.537	1.544	1.508	0.078	0.052	0.016	0.005	0.18	0.035
Fe	0.008	0.011	0.006	0.004	0.007	0.007	0.567	1.146	1.831	1.899	1.071	0.971
Mn	0.001	0	0	0	0	0	0.026	0.042	0.038	0.033	0.033	0.03
Mg	0	0	0	0	0.004	0	0.121	0.031	0.02	0.009	0.332	0.003
Ca	0.549	0.542	0.472	0.556	0.545	0.524	0.316	0.41	0.021	0.032	0.314	0.577
Na	0.462	0.472	0.558	0.455	0.46	0.493	0.014	0.022	0.032	0.029	0.057	0.005
K	0.007	0.001	0.002	0.001	0.003	0.001	0.004	0	0.003	0	0	0
Cr	0.001	0.002	0.004	0.003	0.002	0.002	0.004	0.002	0.001	0.011	0.007	0.003
Ni	0	0	0	0	0	0.01	0.012	0	0	0.019	0.01	0
O	24	24	24	24	24	24	6	6	6	6	6	6
An	54.30	53.45	45.83	55.00	54.23	51.52	-	-	-	-	-	-
Ab	45.70	46.55	54.17	45.00	45.77	48.48	-	-	-	-	-	-
XAn	0.54	0.53	0.46	0.55	0.54	0.52	-	-	-	-	-	-
XAb	0.46	0.47	0.54	0.45	0.46	0.48	-	-	-	-	-	-
ln (XAn/Xab	0.17	0.14	-0.17	0.20	0.17	0.06	-	-	-	-	-	-

sample 9187 (amphibolite - El Huron)
weight % oxide

	amphibole	amphibole	amphibole	amphibole	amphibole	amphibole	amphibole
SiO2	48.02	48.22	48.79	48.36	47.47	52.47	47.78
TiO2	0.85	1.06	1.11	1.13	1.02	0.74	0.98
Al2O3	8.57	8.33	7.98	8.12	8.99	23.2	8.84
FeO	12.9	12.66	12.33	12.75	12.93	5.32	12.74
MnO	0.19	0.18	0.31	0.17	0.21	0	0.34
MgO	14.56	14.67	14.77	14.56	14.15	3.63	14.44
CaO	11.52	11.6	11.47	11.9	11.48	10.73	11.84
Na2O	1.39	1.29	1.39	1.39	1.5	4.25	1.44
K2O	0.02	0.02	0.14	0.11	0.12	0.13	0.04
Cr2O3	0.08	0.14	0.06	0	0.14	0	0.25
NiO	0.27	0.01	0	0	0	0	0.02
Total	98.37	98.18	98.35	98.49	98.01	100.47	98.71
formulae calculated from oxygen given below							
Si	7.25	7.26	7.33	7.28	7.19	7.29	7.19
Ti	0.1	0.12	0.13	0.13	0.12	0.08	0.11
Al	1.53	1.48	1.41	1.44	1.61	3.8	1.57
Fe	1.63	1.59	1.55	1.61	1.64	0.62	1.6
Mn	0.02	0.02	0.04	0.02	0.03	0	0.04
Mg	3.28	3.29	3.31	3.27	3.19	0.75	3.24
Ca	1.86	1.87	1.85	1.92	1.86	1.6	1.91
Na	0.41	0.38	0.41	0.41	0.44	1.15	0.42
K	0	0	0.03	0.02	0.02	0.02	0.01
Cr	0.01	0.02	0.01	0	0.02	0	0.03
Ni	0	0.03	0	0	0	0	0
O	24	24	24	24	24	24	24
Aliv	0.75	0.74	0.67	0.72	0.81	0.71	0.81
Na+1+K+1	0.41	0.38	0.43	0.43	0.46	1.17	0.43
Alvi	0.78	0.74	0.74	0.72	0.8	3.1	0.75
Alvi+Ti+4	0.87	0.86	0.87	0.85	0.91	3.17	0.87
Ln(Ca/Na(M	1.51	1.59	1.51	1.54	1.44	0.33	1.51

sample 9200 (amphibolite - El Huron)
weight % oxide

	feldspar	feldspar	feldspar	feldspar	feldspar	feldspar	feldspar	feldspar	feldspar	sphene	sphene
SiO2	56.475	58.431	57.237	58.037	57.647	57.607	59.065	57.266	56.458	42.142	30.39
TiO2	0.061	0	0.081	0.015	0.22	0.048	0	0.11	0	28.053	39.493
Al2O3	27.119	26.143	26.922	26.628	26.475	26.803	25.832	27.407	26.736	1.397	0.805
FeO	0.267	0.207	0.275	0.043	0.34	0.07	0.419	0.396	0.306	2.632	0.703
MnO	0.015	0.02	0.061	0.028	0.034	0	0	0.014	0.004	0.032	0.035
MgO	0	0	0	0.02	0.128	0.033	0	0	0	0.48	0
CaO	9.374	8.432	9.138	8.759	8.582	8.799	7.846	9.507	8.969	20.938	27.544
Na2O	6.326	7.087	6.658	7.147	6.995	7.296	7.564	6.537	6.498	0.038	0.119
K2O	0.054	0.017	0.137	0.048	0.129	0.057	0	0.115	0.156	0.23	0.07
Cr2O3	0.085	0.037	0	0.107	0.008	0.124	0.013	0.033	0.046	0.18	0.074
NiO	0	0	0.37	0.166	0.031	0.115	0	0	0	0.105	0.14
Total	99.776	100.374	100.879	100.998	100.589	100.952	100.739	101.385	99.173	96.227	99.373
formulae calculated from the oxygen given below											
Si	2.545	2.608	2.557	2.581	7.728	2.567	2.626	2.545	2.559	6.533	3.996
Ti	0.002	0	0.003	0	0.022	0.002	0	0	0	3.271	3.906
Al	1.44	1.375	1.417	1.396	4.183	1.408	1.354	1.436	1.428	0.255	0.125
Fe	0.01	0.008	0.01	0.002	0.038	0.003	0.016	0.015	0.012	0.314	0.077
Mn	0.001	0.001	0.002	0.001	0.004	0	0	0.001	0	0.004	0.004
Mg	0	0	0	0.001	0.026	0.002	0	0	0	0.111	0
Ca	0.453	0.403	0.437	0.417	1.233	0.42	0.374	0.453	0.436	3.478	3.881
Na	0.553	0.613	0.577	0.616	1.818	0.63	0.652	0.536	0.571	0.011	0.03
K	0.003	0.001	0.008	0.003	0.022	0.003	0	0.007	0.009	0.046	0.012
Cr	0.003	0.001	0	0.004	0.001	0.004	0	0.001	0.002	0.022	0.008
Ni	0	0	0.013	0.006	0.003	0.004	0	0	0	0.013	0.015
O	24	24	24	24	24	24	24	24	24	20	20
An	45.03	39.67	43.10	40.37	40.41	40.00	36.45	45.80	43.30	-	-
Ab	54.97	60.33	56.90	59.63	59.59	60.00	63.55	54.20	56.70	-	-
XAn	0.45	0.40	0.43	0.40	0.40	0.40	0.36	0.46	0.43	-	-
XAb	0.55	0.60	0.57	0.60	0.60	0.60	0.64	0.54	0.57	-	-
ln(Xan/XAb)	-0.20	-0.42	-0.28	-0.39	-0.39	-0.41	-0.56	-0.17	-0.27	-	-

sample 9200 (amphibolite - El Huron)
weight % oxide

	amphibole	amphibole	amphibole	amphibole	amphibole	amphibole	amphibole	amphibole	amphibole
SiO2	46.73	49.54	47.35	57.65	46.59	47.55	42.14	46.78	46.55
TiO2	1.17	0.85	1.11	0.22	1.35	1.1	28.06	1.37	1.18
Al2O3	8.42	5.56	7.04	26.47	8.48	7.37	1.4	8.43	8.21
FeO	15.5	14.39	15	0.34	15.53	15.32	2.63	15.34	16.38
MnO	0.24	0.27	0.29	0.03	0.19	0.35	0.03	0.28	0.38
MgO	12.53	13.66	12.59	0.13	12.29	12.24	0.48	12.61	11.96
CaO	11.49	11.63	11.62	8.58	11.41	11.35	20.94	11.48	11.3
Na2O	1.68	0.73	1.08	6.99	1.66	1.02	0.04	1.53	1.25
K2O	0.17	0.2	0.16	0.13	0.12	0.08	0.23	0.08	0.35
Cr2O3	0.18	0.2	0.06	0.01	0.02	0.06	0.18	0.11	0.14
NiO	0.03	0.45	0.05	0.03	0.31	0.05	0.1	0	0.04
Total	98.14	97.48	96.35	100.58	97.95	96.49	96.23	98.01	97.74
formulae calculated from the oxygen given below									
Si	7.18	7.59	7.38	7.73	7.18	7.39	6.53	7.18	7.21
Ti	0.14	0.1	0.13	0.02	0.16	0.13	3.27	0.16	0.14
Al	1.53	1	1.29	4.18	1.54	1.35	0.26	1.52	1.5
Fe	1.99	1.84	1.95	0.04	2	1.99	0.34	1.97	2.12
Mn	0.03	0.04	0.04	0	0.02	0.05	0	0.04	0.05
Mg	2.87	3.12	2.92	0.03	2.82	2.84	0.11	2.89	2.76
Ca	1.89	1.91	1.94	1.23	1.88	1.89	3.48	1.89	1.88
Na	0.5	0.22	0.33	1.82	0.49	0.31	0.01	0.45	0.37
K	0.03	0.04	0.03	0.02	0.02	0.01	0.05	0.02	0.07
Cr	0.02	0.02	0.01	0	0	0.01	0.02	0.01	0.02
Ni	0	0.06	0.01	0	0.04	0.01	0.01	0	0
O	24	24	24	24	24	24	24	24	24
Aliv	0.82	0.41	0.62	0.27	0.82	0.61	1.47	0.82	0.79
Na+1+K+1	0.53	0.26	0.36	1.84	0.52	0.32	0.06	0.47	0.44
Alvi	0.7	0.59	0.67	3.91	0.71	0.74	-1	0.7	0.71
AlVI+Ti+4	0.84	0.69	0.8	3.93	0.87	0.87	2.06	0.86	0.85
ln(Ca/Na(M4	1.33	2.16	1.77	-0.39	1.34	1.81	5.85	1.44	1.63

sample 9221 (Mélange - Peramora)
weight % oxide

	feldspar	feldspar	feldspar	feldspar	feldspar	feldspar	feldspar	feldspar	feldspar	chromite	chromite	chromite
SiO2	53.745	48.59	47.826	48.765	49.505	51.353	49.987	51.279	50.921	0.42	0.418	0.374
TiO2	0.018	0	0	0	0	0.019	0.021	0.014	0.105	0.432	0.326	0.294
Al2O3	28.593	32.246	33.522	31.472	32.308	30.365	31.673	28.89	32.129	18.417	27.381	27.808
FeO	0.229	0.209	0.085	0.346	0.062	0.01	0.093	0.561	0.07	39.267	33.072	35.11
MnO	0.011	0	0	0.05	0.063	0	0	0.116	0.107	1.059	1.005	1.023
MgO	0	0	0	0	0	0	0	0.436	0.109	0.724	1.643	1.713
CaO	11.291	15.66	16.196	15.033	14.848	13.159	14.405	12.877	14.485	0.053	0.023	0.027
Na2O	5.254	2.937	2.245	2.8	3.067	4.173	3.331	4.067	3.566	0.933	1.131	1.362
K2O	0.005	0.021	0	0	0	0.044	0.002	0.025	0.014	0	0.019	0.035
P2O5	0	0	0	0	0	0	0	0	0	0	0	0
Cr2O3	0	0.022	0	0.062	0	0.14	0.168	0	0.04	31.056	30.527	31.863
Total	99.146	99.685	99.874	98.528	99.853	99.263	99.68	98.265	101.546	92.361	95.545	99.609
formulae calculated from oxygen given below												
Si	2.45	2.234	2.189	2.263	2.261	2.351	2.286	7.129	2.287	0.095	0.113	0.098
Ti	0.001	0	0	0	0	0.001	0.001	0.001	0.004	0.073	0.066	0.058
Al	1.537	1.747	1.809	1.721	1.74	1.638	1.707	4.734	1.701	4.884	8.73	8.563
Fe	0.009	0.008	0.003	0.013	0.002	0	0.004	0.065	0.003	7.389	7.482	7.671
Mn	0	0	0	0.022	0.002	0	0	0.014	0.004	0.202	0.23	0.226
Mg	0	0	0	0	0	0	0	0.09	0.007	0.243	0.662	0.667
Ca	0.552	0.771	0.806	0.747	0.727	0.645	0.706	1.918	0.679	0.013	0.007	0.008
Na	0.465	0.262	0.199	0.252	0.272	0.37	0.295	1.096	0.311	0.407	0.593	0.69
K	0	0.001	0	0	0.001	0.003	0	0.004	0.001	0	0.007	0.012
P	0	0	0	0	0	0	0	0	0	0	0	0
Cr	0	0.001	0	0.002	0	0.005	0.006	0	0.001	5.525	6.529	6.582
O	24	24	24	24	24	24	24	24	24	32	32	32
An	54.28	74.64	80.20	74.77	72.77	63.55	70.53	63.64	68.59	-	-	-
Ab	45.72	25.36	19.80	25.23	27.23	36.45	29.47	36.36	31.41	-	-	-
XAn	0.54	0.75	0.80	0.75	0.73	0.64	0.71	0.64	0.69	-	-	-
XAb	0.46	0.25	0.20	0.25	0.27	0.36	0.29	0.36	0.31	-	-	-
Ln(XAn/XAb	0.17	1.08	1.40	1.09	0.98	0.56	0.87	0.56	0.78	-	-	-

sample 9221 (Mélange - Peramora)
weight % oxide

	chromite	chromite	chromite	amphibole	amphibole	amphibole	amphibole	amphibole	amphibole	amphibole	amphibole	amphibole
SiO2	0.498	11.428	1.154	44.77	45.16	43.68	49.83	44.96	45.4	48.8	53.51	52.83
TiO2	0.098	0.597	1.137	0.77	0.56	0.85	0.23	0.55	0.62	0.43	0.04	0.02
Al2O3	26.852	12.134	17.174	10.68	12.75	11.89	19.29	12.12	10.65	8.38	0.43	0.75
FeO	36.704	32.118	43.395	13.05	12.97	13.5	6.96	12.69	13.77	12.69	7.37	7.66
MnO	1.199	1.404	1.673	0.14	0.33	0.11	0.19	0.3	0.27	0.26	0.34	0.27
MgO	1.571	1.17	0.514	11.58	10.71	10.86	6.47	11.65	12.16	13.41	13.79	13.48
CaO	0.1	1.744	0.567	11.97	12.18	12.36	11.55	12.23	12.22	12.23	24.1	23.94
Na2O	1.254	2.029	1.006	1.58	2.31	1.59	3.72	1.88	1.71	1.19	0.3	0.29
K2O	0	0.107	0.068	0.48	0.55	0.52	0.23	0.51	0.45	0.34	0.02	0
P2O5	0	0	0	0.02	0	0.04	0	0	0	0	0	0
Cr2O3	30.991	35.477	30.809	1.93	0.98	1.75	0.22	0	0.11	0.14	0	0.04
Total	99.267	98.208	97.497	96.97	98.5	97.15	98.69	96.89	97.36	97.87	99.9	99.28
formulae calculated from oxygen given below												
Si	0.132	3.019	0.333	6.94	6.88	6.79	7.2	6.93	7	7.39	7.98	7.94
Ti	0.02	0.119	0.246	0.09	0.06	0.1	0.03	0.06	0.07	0.05	0	0
Al	8.388	3.779	5.834	1.95	2.29	2.18	3.28	2.2	1.94	1.5	0.07	0.13
Fe	8.135	7.097	10.461	1.69	1.65	1.75	0.84	1.64	1.78	1.61	0.92	0.96
Mn	0.269	0.314	0.409	0.02	0.04	0.01	0.02	0.04	0.04	0.03	0.04	0.03
Mg	0.621	0.461	0.221	2.68	2.43	2.52	1.39	2.68	2.8	3.03	3.06	3.02
Ca	0.028	0.494	0.175	1.99	1.99	2.06	1.79	2.02	2.02	1.98	3.85	3.85
Na	0.645	1.04	0.562	0.47	0.68	0.48	1.04	0.56	0.51	0.35	0.09	0.08
K	0	0.036	0.025	0.09	0.11	0.1	0.04	0.1	0.09	0.07	0	0
P	0	0	0	0	0	0.01	0	0	0	0	0	0
Cr	6.494	7.411	7.021	0.24	0.12	0.22	0.03	0	0.01	0.02	0	0
O	32	32	32	24	24	24	24	24	24	24	24	24
Aliv	-	-	-	1.06	1.12	1.21	0.8	1.07	1	0.61	0.02	0.06
Alvi	-	-	-	0.89	1.17	0.96	2.48	1.13	0.94	0.88	0.05	0.07
Na+1+K+1	-	-	-	0.57	0.79	0.58	1.09	0.66	0.6	0.42	0.09	0.08
AlVI+Ti+4	-	-	-	0.98	1.23	1.06	2.51	1.2	1.01	0.93	0.06	0.07
ln(Ca/Na(M4	-	-	-	1.44	1.07	1.46	0.54	1.28	1.38	1.73	3.76	3.87

sample 9221 (Mélange - Peramora)

weight % oxide

	amphibole	amphibole
SiO2	46.28	51.28
TiO2	0.68	0.01
Al2O3	0.61	28.89
FeO	14.19	0.56
MnO	0.21	0.12
MgO	12.47	0.44
CaO	11.94	12.88
Na2O	1.77	4.07
K2O	0.37	0.02
P2O5	0	0
Cr2O3	0.08	0
Total	88.6	98.27
formulae calculated from oxygen given below		
Si	7.93	7.13
Ti	0.09	0
Al	0.12	4.73
Fe	2.03	0.07
Mn	0.03	0.01
Mg	3.18	0.09
Ca	2.19	1.92
Na	0.59	1.1
K	0.08	0
P	0	0
Cr	0.01	0
O	24	24
Aliv	0.07	0.87
Alvi	0.05	3.86
Na+1+K+1	0.67	1.1
AlVI+Ti+4	0.14	3.86
ln(Ca/Na(M4	1.31	0.56

sample 9231 (Mélange - Peramora)
weight % oxide

	feldspar	feldspar	feldspar	feldspar	feldspar	ilmenite	ilmenite
SiO2	60.786	60.718	59.88	59.766	60.584	0.391	0.438
TiO2	0.001	0.037	0	0.091	0	55.585	61.522
Al2O3	24.824	24.897	24.79	25.077	23.832	0.105	0.113
FeO	0.249	0.172	0.257	0.271	0.246	41.228	33.986
MnO	0.035	0	0.047	0.083	0	2.181	1.538
MgO	0	0	0	0	0	0.189	0.028
CaO	6.055	6.506	6.681	6.912	5.839	0.189	0.194
Na2O	8.753	8.271	8.161	8.087	8.382	0.202	0.25
K2O	0	0.087	0.107	0.107	0.034	0.022	0.051
P2O5	0	0	0	0	0	0	0
Cr2O3	0	0	0.054	0	0	0.022	0.074
Total	100.703	100.688	99.977	100.394	98.917	100.114	98.194
formulae calculated by oxide values given below							
Si	2.692	2.684	2.676	2.662	2.724	0.103	0.113
Ti	0	0.001	0	0.003	0	10.995	11.936
Al	1.296	1.297	1.306	1.316	1.263	0.032	0.034
Fe	0.009	0.006	0.01	0.01	0.009	9.069	7.332
Mn	0	0	0.002	0.003	0	0.486	0.336
Mg	0.287	0	0	0	0	0.074	0.011
Ca	0.751	0.308	0.32	0.33	0.281	0.053	0.053
Na	0	0.709	0.707	0.689	0.731	0.103	0.125
K	0	0.005	0.006	0.006	0.002	0.007	0.017
P	0	0	0	0	0	0	0
Cr	0	0	0.002	0	0	0.004	0.015
O	24	24	24	24	24	6	6
An	99.00	30.29	31.16	32.38	27.77	-	-
Ab	0.00	69.71	68.84	67.62	72.23	-	-
XAn	1.00	0.30	0.31	0.32	0.28	-	-
XAb	0.00	0.70	0.69	0.68	0.72	-	-
ln(XAn/XAb)	0.00	-0.83	-0.79	-0.74	-0.96	-	-

sample 9231 (Mélange - Peramora)
weight % oxide

	amphibole	amphibole	amphibole	amphibole
SiO2	51.05	49.95	48.07	47.63
TiO2	0.58	0.78	1.28	1.21
Al2O3	5.34	5.17	6.4	8.19
FeO	14.78	15.77	16.82	16.91
MnO	0.23	0.21	0.29	0.19
MgO	13.19	12.86	12.22	11.04
CaO	11.75	11.9	11.43	11.38
Na2O	0.76	0.85	1.45	0.98
K2O	0.15	0.22	0.23	0.45
P2O5	0.12	0.04	0	0.01
Cr2O3	0.08	0.14	0	0
Total	98.03	97.89	98.19	97.99
Si	7.74	7.65	7.41	7.34
Ti	0.07	0.09	0.15	0.14
Al	0.95	0.93	1.16	1.49
Fe	1.87	2.02	2.17	2.18
Mn	0.03	0.03	0.04	0.03
Mg	2.98	2.94	2.81	2.54
Ca	1.91	1.95	1.89	1.88
Na	0.22	0.25	0.43	0.29
K	0.03	0.04	0.05	0.09
P	0.02	0.01	0	0
Cr	0.01	0.02	0	0
O	24	24	24	24
Aliv	0.26	0.35	0.59	0.66
Na+1+K+1	0.25	0.3	0.48	0.38
Alvi	0.69	0.58	0.57	0.83
AlVI+Ti+4	0.76	0.67	0.72	0.97
ln(Ca/Na(M4	2.16	2.05	1.48	1.87

sample 9231 (Mélange - Peramora)
weight % oxide

	amphibole	amphibole	amphibole	amphibole	amphibole	amphibole	amphibole	amphibole	amphibole	amphibole	amphibole	amphibole
SiO2	50.41	48.23	48.46	56.37	49.31	47.77	44.43	45.79	48.03	49.29	48.62	47.63
TiO2	0.92	1.48	1.31	0.38	1.29	0.97	1.3	1.45	1.39	0.88	1.02	1.39
Al2O3	5.13	6.75	6.5	17.09	6.51	7.61	8.42	8.51	7.22	21.22	6.95	7.78
FeO	15.3	16.56	16.59	6.39	15.81	16.28	17.25	16.92	16.67	5.19	15.8	16.71
MnO	0.14	0.22	0.13	0.23	0.39	0.22	0.23	0.28	0.15	0	0.25	0.3
MgO	13.31	11.62	11.89	4.79	12.43	11.57	10.22	10.97	11.88	2.74	12.18	11.78
CaO	11.87	1.66	11.5	7.79	12.08	11.01	12.37	11.59	11.58	4.49	11.98	11.75
Na2O	0.83	1.09	1.22	6.05	0.92	0.88	1.25	1.51	1.22	5.87	1.25	1.28
K2O	0.23	0.28	0.31	0.22	0.25	0.6	0.48	0.4	0.31	1.21	0.3	0.33
P2O5	0	0	0	0	0.07	0.17	1	0	0.05	0	0	0.06
Cr2O3	0.15	0.14	0.24	0	0.19	0.05	0.03	0.02	0.24	0.1	0.33	0.15
Total	98.29	88.03	98.15	99.31	99.25	97.13	96.98	97.44	98.74	90.99	98.68	99.16
formulae calculated by oxide values given below												
Si	7.66	7.98	7.45	7.93	7.47	7.4	7.02	7.15	7.35	7.52	7.42	7.27
Ti	0.1	0.18	0.15	0.04	0.15	0.11	0.15	0.17	0.16	0.1	0.12	0.16
Al	0.92	1.31	1.18	2.83	1.16	1.39	1.57	1.57	1.3	3.82	1.25	1.4
Fe	1.95	2.29	2.13	0.75	2	2.11	2.28	2.21	2.13	0.66	2.02	2.13
Mn	0.02	0.03	0.02	0.03	0.05	0.03	0.03	0.04	0.02	0	0.03	0.04
Mg	3.02	2.86	2.73	1	2.81	2.67	2.41	2.55	2.71	0.62	2.77	2.68
Ca	1.93	0.29	1.89	1.17	1.96	1.83	2.09	1.94	1.9	0.73	1.96	1.92
Na	0.25	0.35	0.36	1.65	0.27	0.27	0.38	0.46	0.36	1.74	0.37	0.38
K	0.04	0.06	0.06	0.04	0.05	0.12	0.1	0.08	0.06	0.24	0.06	0.07
P	0	0	0	0.01	0.03	0	0.17	0	0.01	0	0	0.01
Cr	0.02	0.02	0.03	0	0.02	0.01	0	0	0.03	0.01	0.04	0.02
O	24	24	24	24	24	24	24	24	24	24	24	24
Aliv	0.34	0.02	0.55	0.07	0.53	0.6	0.98	0.85	0.65	0.48	0.58	0.73
Na+1+K+1	0.29	0.41	0.42	1.69	0.32	0.38	0.48	0.54	0.42	1.97	0.43	0.44
Alvi	0.58	1.29	0.63	2.77	0.63	0.79	0.58	0.72	0.65	3.34	0.67	0.67
AlVI+Ti+4	0.69	1.47	0.78	2.81	0.78	0.91	0.74	0.89	0.81	3.44	0.79	0.83
ln(Ca/Na(M4	2.04	-0.19	1.66	-0.34	1.98	1.91	1.70	1.44	1.66	-0.87	1.67	1.62

sample 9231 (Mélange - Peramora)
weight % oxide

	amphibole	amphibole	amphibole	amphibole	amphibole	amphibole	amphibole	amphibole
SiO2	45.05	48.36	47.02	46.78	50.19	47.34	48.04	48.61
TiO2	1.13	1.06	1.26	1.31	0.69	1.17	1.18	1.02
Al2O3	9.07	6.79	7.56	8.87	4.86	8.22	6.75	6.02
FeO	17.46	15.35	17.15	17.58	15.5	17.7	16.66	15.86
MnO	0.23	0.08	0.34	0.36	0.28	0.18	0.31	0.21
MgO	10.5	12.11	11.45	11.02	12.99	11.16	11.87	12.26
CaO	11.54	11.98	11.69	11.52	11.84	11.53	11.88	11.66
Na2O	1.34	0.97	1.31	1.6	0.63	1.29	1.28	0.86
K2O	0.49	0.22	0.32	0.39	0.15	0.41	0.34	0.29
P2O5	0	0	0.23	0.05	0	0.07	0	0
Cr2O3	0.09	0.22	0.09	0.12	0.35	0.12	0.1	0.05
Total	96.9	97.14	98.42	99.6	97.48	99.19	98.41	96.84
formulae calculated by oxide values given below								
Si	7.08	7.47	7.28	7.15	7.7	7.25	7.39	7.54
Ti	0.13	0.12	0.15	0.15	0.08	0.13	0.14	0.12
Al	1.68	1.24	1.38	1.6	0.88	1.48	1.22	1.1
Fe	2.29	1.98	2.22	2.25	1.99	2.27	2.14	2.06
Mn	0.03	0.01	0.04	0.05	0.04	0.02	0.04	0.03
Mg	2.46	2.79	2.64	2.51	2.97	2.55	2.72	2.84
Ca	1.94	1.98	1.94	1.89	1.95	1.89	1.96	1.94
Na	0.41	0.29	0.39	0.48	0.19	0.38	0.38	0.26
K	0.1	0.04	0.06	0.08	0.03	0.08	0.07	0.06
P	0.04	0	0	0.01	0	0.01	0	0
Cr	0.01	0.03	0.01	0.01	0.04	0.01	0.01	0.01
O	24	24	24	24	24	24	24	24
Aliv	0.92	0.53	0.72	0.85	0.3	0.75	0.61	0.46
Na+1+K+1	0.51	0.33	0.46	0.55	0.22	0.46	0.45	0.32
Alvi	0.76	0.7	0.65	0.75	0.58	0.73	0.62	0.64
AlVI+Ti+4	0.89	0.82	0.8	0.9	0.66	0.87	0.75	0.76
ln(Ca/Na(M4	1.55	1.92	1.60	1.37	2.33	1.60	1.64	2.01

sample 9234 (Mélange - Peramora)
weight % oxide

	feldspar	feldspar	ilmenite	ilmenite	ilmenite
SiO2	59.701	54.308	0.609	16.893	3.558
TiO2	0	0.101	52.465	39.504	51.385
Al2O3	25.919	28.73	0.151	6.17	0.465
FeO	0.106	0.324	40.821	26.143	35.575
MnO	0	0.006	2.695	1.314	3.937
MgO	0.032	0	0.248	0.759	0.13
CaO	7.317	10.807	0.472	6.868	2.99
Na2O	8.07	5.555	0.325	1.399	0.104
K2O	0.076	0.083	0.004	0.245	0
P2O5	0	0	0.073	0	0
Cr2O3	0.088	0.076	0.031	0.102	0.015
Total	101.309	99.99	97.894	99.397	98.159
formulae calculated on the basis of oxygen value given below					
Si	2.636	7.366	0.165	3.94	0.934
Ti	0	0.01	10.682	6.929	10.15
Al	1.349	4.593	0.048	1.696	0.144
Fe	0.004	0.037	9.242	5.099	7.185
Mn	0	0.001	0.618	0.26	0.876
Mg	0.002	0	0.1	0.264	0.051
Ca	0.346	1.571	0.137	1.716	0.841
Na	0.691	1.461	0.171	0.633	0.053
K	0.004	0.014	0.001	0.073	0
P	0	0	0.017	0	0
Cr	0.003	0.008	0.007	0.019	0.003
O-2	24	24	6	6	6
An	33.37	51.81	-	-	-
Ab	66.63	48.19	-	-	-
XAn	0.33	0.52	-	-	-
XAb	0.67	0.48	-	-	-
ln(XAn/Xab)	-0.69	0.07	-	-	-

sample 9234 (Mélange - Peramora)
weight % oxide

	amphibole	amphibole	amphibole	amphibole	amphibole	amphibole
SiO2	51.52	54.13	51.11	45.95	46.71	51.31
TiO2	0.28	0.27	0.36	0.65	0.61	1.01
Al2O3	5.79	3.4	5.7	9.2	9.97	3.71
FeO	11.49	10.03	11.23	12.65	12.24	10.5
MnO	0.23	0.34	0.17	0.26	0.34	0.27
MgO	16.35	17.95	15.95	13.16	13.44	17.02
CaO	12.16	11.62	11.94	11.03	11.46	11.27
Na2O	0.86	0.51	0.75	1.16	1.38	0.58
K2O	0.04	0	0.11	0.23	0.16	0.05
P2O5	0	0	0	0	0	0
Cr2O3	0.29	0.2	0.14	0.16	0	0.01
Total	99.01	98.45	97.46	94.45	96.31	95.73
Si	7.63	7.96	7.67	7.22	7.18	7.81
Ti	0.03	0.03	0.04	0.08	0.07	0.12
Al	1.01	0.59	1.01	1.7	1.8	0.67
Fe	1.42	1.23	1.41	1.66	1.57	1.34
Mn	0.03	0.04	0.02	0.03	0.04	0.03
Mg	3.61	3.93	3.57	3.08	3.08	3.86
Ca	1.93	1.83	1.92	1.86	1.89	1.84
Na	0.25	0.15	0.22	0.35	0.41	0.17
K	0.01	0	0.02	0.05	0.03	0.01
P	0	0	0	0	0	0
Cr	0.03	0.02	0.02	0.02	0	0
O-2	24	24	24	24	24	24
Mg/(Mg+Fe)	0.72	0.76	0.72	0.65	0.66	0.74
Na+K	0.26	0.15	0.24	0.4	0.44	0.18
Aliv	0.37	0.04	0.33	0.78	0.82	0.19
Alvi	0.64	0.55	0.68	0.92	0.98	0.47
Alvi+Ti	0.67	0.58	0.72	1	1.05	0.59
ln(Ca/Na(M4	2.04	2.50	2.17	1.67	1.53	2.38

sample 9234 (Mélange - Peramora)
weight % oxide

	amphibole	amphibole	amphibole	amphibole	amphibole
SiO2	49.22	50.35	52.21	49.13	50.85
TiO2	0.02	0.21	0.27	0.5	0.12
Al2O3	6.18	4.25	2.94	6.06	4.36
FeO	11.5	10.26	9.56	11.21	10.35
MnO	0.18	0.21	0.17	0.15	0.19
MgO	15.28	16	17.07	15.32	16.46
CaO	11.58	11.43	11.32	11.64	11.61
Na2O	1.03	0.59	0.45	0.97	0.68
K2O	0.17	0.08	0.06	0.16	0.08
P2O5	0	0	0	0	0
Cr2O3	0.07	0	0.21	0.09	0.12
Total	95.23	93.38	94.258	95.23	94.82
formulae calculated on the basis of oxygen value given below					
Si	7.59	7.85	2.24	7.57	7.81
Ti	0	0.02	8.65	0.06	0.01
Al	1.12	0.78	0.15	1.1	0.79
Fe	1.48	1.34	0.34	1.45	1.33
Mn	0.02	0.03	0.01	0.02	0.02
Mg	3.52	3.72	1.09	3.52	3.77
Ca	1.92	1.91	0.52	1.92	1.91
Na	0.31	0.18	0.04	0.29	0.2
K	0.03	0.02	0	0.03	0.02
P	0	0	0	0	0
Cr	0.01	0	0.01	0.01	0.01
O-2	24	24	24	24	24
Mg/(Mg+Fe)	0.70	0.74	0.76	0.71	0.74
Na+K	0.34	0.2	0.04	0.32	0.22
Aliv	0.41	0.15	5.76	0.43	0.19
Alvi	0.72	0.63	-6	0.67	0.6
Alvi+Ti	0.72	0.65	3.04	0.73	0.62
ln(Ca/Na(M4	1.82	2.36	2.56	1.89	2.26

sample 9238 (Mélange - Rioja)
weight % oxide

	feldspar	feldspar	feldspar	feldspar
SiO2	59.493	59.426	58.152	59.431
TiO2	0.104	0.074	0.109	0
Al2O3	25.913	25.629	26.919	25.222
FeO	0.11	0.303	0.39	0.209
MnO	0	0.032	0.019	0.004
MgO	0	0	0	0
CaO	7.548	7.604	8.903	7.112
Na2O	7.685	7.707	6.986	7.715
K2O	0.115	0.102	0.061	0.111
P2O5	0	0	0.003	0
Cr2O3	0.122	0	0.067	0.066
Total	101.09	100.877	101.609	99.87
formula amount calculated from oxygen value given below				
Si	2.632	2.638	2.572	7.974
Ti	0.003	0.002	0.004	0
Al	1.351	1.341	1.404	3.989
Fe	0.004	0.011	0.014	0.023
Mn	0	0.001	0.001	0
Mg	0	0	0	0
Ca	0.358	0.362	0.422	1.022
Na	0.659	0.663	0.599	2.007
K	0.006	0.006	0.003	0.019
P	0	0	0	0
Cr	0.004	0	0.002	0.007
O-2	24	24	24	24
An	35.20	35.32	41.33	33.74
Ab	64.80	64.68	58.67	66.26
XAn	0.35	0.35	0.41	0.34
XAB	0.65	0.65	0.59	0.66
Ln(XAn/XAb	-0.61	-0.61	-0.35	-0.67

sample 9238 (Mélange - Rioja)
weight % oxide

	amphibole	amphibole	amphibole	amphibole	amphibole	amphibole	amphibole
SiO2	45.57	48.29	48.08	46.82	45.59	48.74	46.57
TiO2	0.71	0.21	0.62	0.71	0.63	0.51	0.71
Al2O3	9.51	7.82	7.59	8.6	9.4	6.64	7.97
FeO	16.12	15.32	15.36	15.86	16.71	15.15	15.47
MnO	0.31	0.38	0.23	0.26	0.21	0.19	0.31
MgO	11.67	12.91	13.01	12.26	11.76	13.19	12.19
CaO	11.84	11.94	11.99	11.87	11.94	12.33	11.75
Na2O	1.41	1.19	1.15	1.34	1.44	1.1	1.29
K2O	0.53	0.27	0.42	0.56	0.5	0.36	0.42
P2O5	0	0.06	0	0	0	0	0
Cr2O3	0.07	0.95	0	0.04	0.05	0.16	0
Total	97.74	99.34	98.45	98.32	98.23	98.37	96.68
Si	7.07	7.31	7.34	7.2	7.06	7.44	7.27
Ti	0.08	0.02	0.07	0.08	0.07	0.06	0.08
Al	1.74	1.4	1.37	1.56	1.71	1.19	1.47
Fe	2.09	1.94	1.96	2.04	2.16	1.94	2.02
Mn	0.04	0.05	0.03	0.03	0.03	0.02	0.04
Mg	2.7	2.91	2.96	2.81	2.72	3	2.84
Ca	1.97	1.94	1.96	1.96	1.98	2.02	1.96
Na	0.42	0.35	0.34	0.4	0.43	0.33	0.39
K	0.11	0.05	0.08	0.11	0.1	0.07	0.08
P	0	0.01	0	0	0	0	0
Cr	0.01	0.11	0	0.01	0.01	0.02	0
O-2	24	24	24	24	24	24	24
Mg/(Mg+Fe)	0.56	0.60	0.60	0.58	0.56	0.61	0.58
Na+K	0.53	0.4	0.42	0.51	0.53	0.4	0.47
Aliv	0.93	0.69	0.66	0.8	0.94	0.56	0.73
Alvi	0.81	0.71	0.71	0.76	0.77	0.64	0.73
Na+1+K+1	0.53	0.4	0.42	0.51	0.53	0.4	0.48
Alvi+Ti+4	0.9	0.73	0.78	0.84	0.85	0.69	0.82
lnCa/NaM4	1.55	1.71	1.75	1.59	1.53	1.81	1.61

sample 9238 (Mélange - Rioja)
weight % oxide

	amphibole
SiO2	50.81
TiO2	0.37
Al2O3	5.06
FeO	13.66
MnO	0.29
MgO	14.6
CaO	12.24
Na2O	0.79
K2O	0.17
P2O5	0
Cr2O3	0.22
Total	98.21

formula amount calculated from oxygen value given below

Si	7.68
Ti	0.04
Al	0.9
Fe	1.73
Mn	0.04
Mg	3.29
Ca	1.98
Na	0.23
K	0.03
P	0
Cr	0.03
O-2	24
Mg/(Mg+Fe)	0.66
Na+K	0.26
Aliv	0.32
Alvi	0.58
Na+1+K+1	0.26
Alvi+Ti+4	0.62
lnCa/NaM4	2.15

sample 9264 weight % oxide								sample 9264 weight % oxide				
	feldspar	feldspar	clinozoisite	clinozoisite	clinozoisite	clinozoisite	clinozoisite		amphibole	amphibole	amphibole	amphibole
SiO2	67.303	56.519	39.242	39.068	39.098	38.016	38.032	SiO2	54.04	52.27	52.05	50.82
TiO2	0.109	0	0.089	0.285	0.239	0.059	0.13	TiO2	0.12	0.09	0.06	0.24
Al2O3	19.274	27.965	28.412	28.349	28.727	28.037	28.541	Al2O3	3.12	2.84	3.05	5.67
FeO	0.573	0.125	6.035	5.207	5.57	5.451	5	FeO	14.22	13.08	13.22	14.89
MnO	0.022	0.012	0	0.011	0.048	0.094	0.266	MnO	0.37	0.4	0.14	0.26
MgO	0.111	0	0	0	0	0	0	MgO	14.73	14.57	14.22	12.61
CaO	1.052	9.909	23.52	23.558	23.945	22.948	23.016	CaO	12.44	11.98	11.67	11.75
Na2O	11.686	6.328	0	0.11	0.049	0.1	0.086	Na2O	0.51	0.44	0.44	0.74
K2O	0.018	0.019	0	0	0.004	0.037	0.072	K2O	0.09	0.05	0.07	0.11
Cr2O3	0.121	0.097	0.174	0.147	0	0.045	0.054	Cr2O3	0	0	0.03	0.02
NiO	0.119	0	0.574	0.028	0	0	0.469	NiO	0	0.1	0.13	0
Total	100.388	100.974	98.046	96.763	97.68	94.787	95.666	Total	99.64	95.82	95.08	97.11
formulae calculated from oxygen values below												
Si	2.955	2.519	5.895	5.912	5.874	5.883	5.838	Si	8.02	8.04	8.06	7.77
Ti	0.004	0	0.01	0.032	0.027	0.007	0.015	Ti	0.01	0.01	0.01	0.03
Al	0.997	1.469	5.031	5.056	5.087	5.114	5.164	Al	0.54	0.52	0.56	1.02
Fe	0.021	0.005	0.785	0.695	0.7	0.705	0.642	Fe	1.76	1.68	1.71	1.9
Mn	0.001	0	0	0.001	0.006	0.012	0.035	Mn	0.05	0.05	0.02	0.03
Mg	0.007	0	0	0	0	0	0	Mg	3.26	3.34	3.28	2.87
Ca	0.049	0.473	3.786	3.82	3.855	3.805	3.785	Ca	1.98	1.97	1.94	1.92
Na	0.995	0.547	0	0.032	0.014	0.03	0.026	Na	0.15	0.13	0.13	0.22
K	0.001	0.001	0	0	0.001	0.007	0.014	K	0.02	0.01	0.01	0.02
Cr	0.004	0.003	0.021	0.018	0	0.006	0.007	Cr	0	0	0	0
Ni	0.004	0	0.069	0.003	0	0	0.058	Ni	0	0.01	0	0.02
O	24	24	13	13	13	13	13	O	24	24	24	24
An	4.69	46.37	-	-	-	-	-	Mg/(Mg+Fe)	0.65	0.67	0.66	0.60
Ab	95.31	53.63	-	-	-	-	-	Na+K	0.17	0.14	0.14	0.24
XAn	0.05	0.46	-	-	-	-	-	ln(Ca/Na(M4	2.58	2.72	2.70	2.17
XAb	0.95	0.54	-	-	-	-	-					
ln(XAb/XAn)	-3.01	-0.15	-	-	-	-	-					

sample 9264
weight % oxide

	amphibole	amphibole	amphibole	amphibole	amphibole	amphibole	amphibole
SiO2	44.28	51.55	52.39	52.21	48.85	52.06	51.74
TiO2	0.23	0.11	0.19	0.06	0.14	0.09	0.07
Al2O3	22.22	3.86	3.49	3.46	11.21	3.9	3.26
FeO	10.59	13.64	14.01	13.85	12.49	14.12	13.87
MnO	0.23	0.33	0.27	0.28	0.18	0.25	0.22
MgO	5.48	13.99	13.8	13.84	10.69	13.8	14.21
CaO	13.55	12.15	12.17	12.11	12.86	12.04	12.35
Na2O	2.31	0.43	0.39	0.37	1.05	0.39	0.81
K2O	0.19	0.11	0.06	0.11	0.12	0.11	0.42
Cr2O3	0.02	0.16	0.06	0.04	0.07	0.12	0
NiO	0.03	0.24	0	0.03	0	0.04	0.36
Total	99.13	96.57	96.83	96.36	97.66	96.92	97.31
formulae calculated from oxygen values below							
Si	6.55	7.92	7.98	8.01	7.36	7.94	7.91
Ti	0.03	0.01	0.02	0.01	0.02	0.01	0.01
Al	3.87	0.7	0.63	0.63	1.99	0.7	0.59
Fe	1.31	1.75	1.79	1.78	1.57	1.8	1.77
Mn	0.03	0.04	0.04	0.04	0.02	0.03	0.03
Mg	1.21	3.2	3.14	3.16	2.4	3.14	3.24
Ca	2.15	2	1.99	1.99	2.08	1.97	2.02
Na	0.66	0.13	0.12	0.11	0.31	0.12	0.24
K	0.04	0.02	0.01	0.02	0.02	0.02	0.08
Cr	0	0.02	0.01	0.01	0.01	0.01	0
Ni	0	0	0.03	0	0	0	0.04
O	24	24	24	24	24	24	24
Mg/(Mg+Fe)	0.48	0.65	0.64	0.64	0.60	0.64	0.65
Na+K	0.7	0.15	0.13	0.13	0.33	0.14	0.32
ln(Ca/Na(M4	1.18	2.73	2.81	2.90	1.90	2.80	2.13

sample 9265 (Mélange - Peramora)
weight % oxide

	feldspar	feldspar	feldspar	feldspar	feldspar	feldspar	feldspar	feldspar	feldspar	clinozoisite	clinozoisite	clinozoisite
SiO2	60.911	66.884	70.445	69.132	70.199	70.216	70.294	70.762	70.195	43.082	40.151	40.438
TiO2	0	0.148	0	0.006	0.059	0.61	0.007	0.017	0	0.07	0.072	0.141
Al2O3	19.938	19.966	20.082	19.774	20.856	20.054	20.39	20.002	19.726	27.816	28.417	29.541
FeO	4.418	1.803	0.067	0.058	0.162	0.303	0.289	0.242	0.079	5.631	7.229	6.103
MnO	0.047	0.021	0.02	0.106	0.105	0.017	0.048	0	0.008	0.105	0.097	0.056
MgO	2.823	1.155	0	0	0.126	0	0.066	0	0	0	0	0
CaO	0.547	0.504	0.417	0.817	0.86	0.618	0.708	0.41	0.405	22.493	23.762	24.349
Na2O	5.626	11.858	12.654	12.199	12.236	12.331	12.339	12.747	12.559	0.621	0.133	0
K2O	5.871	0.174	0.023	0	0	0.055	0	0.018	0.014	0.02	0.023	0.029
Cr2O3	0	0.086	0.005	0.009	0.005	0	0.021	0.087	0.04	0.038	0.214	0.164
NiO	0.01	0	0.127	0.018	0	0.071	0.252	0	0.243	0	0.107	0.314
Total	100.191	102.599	103.84	102.119	104.608	104.275	104.414	104.285	103.269	99.876	100.205	101.135
formulae calculated from oxygen values given below												
Si	8.363	8.687	2.977	2.972	2.947	2.973	2.96	2.979	2.984	6.263	5.922	5.881
Ti	0	0.014	0	0	0.002	0.002	0	0.001	0	0.008	0.008	0.015
Al	3.226	3.057	1	1.002	1.032	1.001	1.012	0.993	0.988	4.766	4.94	5.064
Fe	0.507	0.196	0.002	0.002	0.006	0.011	0.01	0.009	0.003	0.685	0.892	0.742
Mn	0.005	0.002	0.001	0.004	0.004	0.001	0.002	0	0	0.013	0.012	0.007
Mg	0.578	0.224	0	0	0.008	0	0.004	0	0	0	0	0
Ca	0.081	0.07	0.019	0.038	0.039	0.028	0.032	0.018	0.018	3.504	3.755	3.794
Na	1.498	2.986	1.037	1.017	0.996	1.012	1.007	1.041	1.035	0.175	0.038	0
K	1.028	0.029	0.001	0	0	0.003	0	0.001	0.001	0.024	0.004	0.005
Cr	0	0.009	0	0	0	0	0.001	0.003	0.001	0.002	0.025	0.019
Ni	0.001	0	0.004	0.001	0	0.002	0.009	0	0.008	0.004	0.013	0.037
O	24	24	24	24	24	24	24	24	24	13	13	13
An	5.13	2.29	1.80	3.60	3.77	2.69	3.08	1.70	1.71	-	-	-
Ab	94.87	97.71	98.20	96.40	96.23	97.31	96.92	98.30	98.29	-	-	-
XAn	0.05	0.02	0.02	0.04	0.04	0.03	0.03	0.02	0.02	-	-	-
XAb	0.95	0.98	0.98	0.96	0.96	0.97	0.97	0.98	0.98	-	-	-
ln(XAn/XAb)	-2.92	-3.75	-4.00	-3.29	-3.24	-3.59	-3.45	-4.06	-4.05	-	-	-

sample 9265 (Mélange - Peramora)
weight % oxide

	clinozoisite	clinozoisite	clinozoisite	amphibole	amphibole	amphibole	amphibole	amphibole
SiO2	40.133	40.035	40.572	54.9	54.23	54.05	54.46	54.31
TiO2	0.081	0.188	0.069	0.07	0.32	0.12	1.19	0.05
Al2O3	28.73	29.306	29.869	3.59	3.29	4.11	3.02	3.64
FeO	6.181	6.068	5.852	14.33	14.03	13.88	13.81	13.9
MnO	0	0.163	0.169	0.25	0.09	0.32	0.19	0.3
MgO	0	0	0.048	15.34	14.84	14.75	14.89	14.84
CaO	23.75	24	24.149	12.57	12.48	12.23	12.97	12.52
Na2O	0.32	0.077	0.078	0.34	0.44	0.61	0.48	0.33
K2O	0.084	0.074	0.033	0.11	0.16	0.17	0.1	0.07
Cr2O3	0.044	0.039	0.093	0.14	0.05	0.18	0.09	0.15
NiO	0.038	0	0.259	0.36	0.22	0	0	0.31
Total	99.361	99.95	101.191	102	100.15	100.42	101.2	100.42
formulae calculated from oxygen values given below								
Si	5.936	5.875	5.885	7.95	7.98	7.93	7.94	7.98
Ti	0.009	0.021	0.007	0.01	0.04	0.01	0.13	0
Al	5.009	5.069	5.107	0.61	0.57	0.71	0.52	0.63
Fe	0.765	0.745	0.71	1.74	1.73	1.7	1.68	1.71
Mn	0	0.02	0.021	0.03	0.01	0.04	0.02	0.04
Mg	0	0	0.01	3.31	3.26	3.22	3.23	3.25
Ca	3.764	3.816	3.753	1.95	1.97	1.92	2.03	1.97
Na	0.092	0.022	0.022	0.08	0.1	0.14	0.11	0.07
K	0.016	0.014	0.006	0.02	0.03	0.03	0.02	0.01
Cr	0.005	0.005	0.011	0.02	0.01	0.03	0.01	0.02
Ni	0.005	0	0.03	0.04	0.03	0	0	0.04
O	13	13	13	24	24	24	24	24
Mg/(Mg+Fe)	-	-	-	0.66	0.65	0.65	0.66	0.66
Na+K	-	-	-	0.1	0.13	0.17	0.13	0.08
Aliv	-	-	-	0.05	0.02	0.07	0.06	0.02
ln(Ca/Na(M4	-	-	-	3.19	2.98	2.62	2.92	3.34

APPENDIX 6 Abbreviations

A.6.1 Structure

Structural symbols are designated according to which structural domain they refer to. This scheme is adopted firstly to avoid confusion of correlation between the domains identified and secondly to highlight the difficulty there pertains in trying to correlate across structural boundaries. The scheme adopted is tabulated below:

S_{A1} S_{A2}	Beja-Acebuches Amphibolites Domain first and second schistosity.
S_{N1} S_{N2} S_{N3}	Northern Metasedimentary Domain first, second and third cleavages.
S_{C1} S_{C2} S_{C3}	Central Metasedimentary Domain cleavages one to three.
S_{S1} S_{S2}	Southern Metasedimentary Domain first and second schistosity.
S_{AL1} S_{AL2}	Alajar Domain first and second schistosity.
	thrust
	overturned beds
	F_3 fold axial surface
	discrete shear zones with direction of dip
	F_3 fold axial plunge
	mineral lineation
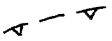	inferred thrust
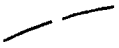	lithological boundary
	S_1 cleavage
	S_2 cleavage
	S_3 cleavage

A.6.2 Mineral abbreviations

chl - chlorite
qtz - quartz
hbl - hornblende
alm - almandine
gt - garnet
bte - biotite
cde - cordierite
and - andalusite
mus - muscovite
act - actinolite
actc hbl - actinolitic hornblende
als - alumino silicate
plag - plagioclase
cd - chloritoid

diop - diopside
cpx - clinopyroxene
clz - clinozoisite
ep - epidote
ab - albite
ilm - ilmenite
sps - spessartine
sph - sphene
tc - talc
zo - zoisite
gt - garnet
ortho - orthoclase
cte - calcite
serp - serpentine
magnes - magnesite

A.6.3 Formations and structural domains

CLCF - Cumbres de Los Ciries Formation
PMF - Peramora Mélange Formation
BAA - Beja-Acebuches Amphibolites
AF - Alajar Formation
OMZ - Ossa Morena Zone
JAZ - Jabugo Almonaster Zone
NMSD - Northern Metasedimentary Domain
CMSD - Central Metasedimentary Domain
SMSD - Southern Metasedimentary Domain
AD - Alajar Domain